Mahmoud Elsanhoury

Towards Precision Positioning For Smart Logistics Using Ultra Wide-Band Systems and LEO Satellite-Based Technologies

ACTA WASAENSIA 534

Vaasan yliopisto
UNIVERSITY OF VAASA

ISBN 978-952-395-145-7 (print)
978-952-395-146-4 (online)

ISSN 0355-2667 (Acta Wasaensia 534, print)
2323-9123 (Acta Wasaensia 534, online)

URN https://urn.fi/URN:ISBN:978-952-395-146-4

Hansaprint Oy, Turenki, 2024.

ACADEMIC DISSERTATION

To be presented, with the permission of the Board of the School of Technology and Innovations of the University of Vaasa, for public examination on the 3^{rd} of October, 2024, at noon.

Article based dissertation, School of Technology and Innovations at the University of Vaasa, in the field of Telecommunications engineering (Computer Science).

Author
Mahmoud Elsanhoury

https://orcid.org/0000-0002-9195-4613

Supervisors
Professor Mohammed Elmusrati
University of Vaasa. School of Technology and Innovations, Computer Science

Professor Heidi Kuusniemi
University of Vaasa. School of Technology and Innovations, Director of Digital Economy Platform

Doctor Janne Koljonen
University of Vaasa. School of Technology and Innovations, Automation Technology

Custos
Professor Mohammed Elmusrati
University of Vaasa. School of Technology and Innovations, Computer Science

Reviewers
Professor Salama Ikki
Lakehead University, Canada. Electrical Engineering Department.

Professor Simo Särkkä
Aalto University. Department of Electrical Engineering and Automation.

Opponents
Professor Jari Nurmi
Tampere University. Faculty of Information Technology and Communication Sciences.

Professor Simo Särkkä
Aalto University. Department of Electrical Engineering and Automation.

TIIVISTELMÄ

Nykyaikainen teknologinen aikakausi nojaa vahvasti älyjärjestelmiin ja -toimintoihin, kuten älykkääseen valmistukseen, älykkääseen logistiikkaan ja älykkääseen merenkulkuun. Ne ovat Teollisuus 4.0:n ja esineiden internetin (IoT) sovellusten ja palveluiden keskeisiä elementtejä, erityisesti älylogistiikka tai logistiikka 4.0, joka palvelee teollisuutta ja materiaalitoimitusketjuja. Älylogistiikan keskeinen perusta on muun muassa liikkuvien laitteiden ja henkilöstön tarkka paikannus teollisuusympäristöissä. Lisäksi navigointisovellusten ja sijaintitietoisten palvelujen luotettavuus on riippuvainen tarkasta paikannuksesta sekä siviiliettä teollisuuskäytössä, sisä- ja ulkotiloissa. Tässä väitöskirjassa esitän tiettyjen teknologioiden, anturien ja algoritmien käyttöä tarkkaan paikantamiseen sisä- ja ulkotiloissa. Ultra wideband (UWB) -järjestelmät ovat äskettäin nousseet luotettavaksi paikannusteknologiaksi monimutkaisissa sisätilaolosuhteissa. Ehdotamme UWB:n käyttöä yhdessä inertia-antureiden (IMU) kanssa integroituna monianturifuusiojärjestelmänä tarkkaan sisätilapaikannukseen. Toteuttamamme UWB/IMU-järjestelmä tarjosi 4,7 senttimetriä keskimääräisenä absoluuttisena tarkkuutena (MAE) tiheässä teollisuusympäristössä (Technobothnian laboratoriossa) Vaasan yliopiston kampuksella Suomessa. Toisaalta paransimme ulkona tapahtuvaa ajoneuvojen paikannusta globaalien satelliittinavigointijärjestelmien (GNSS) kaupallisia vastaanottimia käyttämällä useilla älypuhelinmalleilla, ja tämä parannus sai tunnustusta Googlen kansainvälisessä kilpailussa kolmen parhaan tuloksen joukossa. Fuusiopohjainen GNSS/IMU-paikannustarkkuus parani 2,291 metrin virheeseen reiteillä, jotka kulkivat puiden reunustamien teiden ja avointen valtateiden kautta. Lisäksi ehdotimme uutta satelliittipohjaista paikannusmenetelmää matalan maan kiertoradan (LEO) satelliiteilla, joita voidaan hyödyntää varateknologiana aina, kun tyypillisesti ensisijaisena toimiva GNSS-teknologia ei ole käytettävissä vaikeissa ympäristöissä ja olosuhteissa. Uuden LEO-pohjaisen paikannustekniikan patentoitu toimintaperiaate hyödyntää LEO-satelliittien MIMO-antenneista tulevia keiloja. Tulevaisuuden massiivisten LEO-konstellaatioiden keilamallien yhdistämisen ansiosta uusi keilapohjainen paikannusmenetelmä voi toimia luotettavana vaihtoehtona ulkotiloissa silloin, kun GNSS ei ole saatavilla. LEO/IMU-fuusion tulokset ajoneuvoskenaarioissa tuottivat vaikuttavan 9,15 metrin paikannustarkkuuden keskimääräisenä absoluuttisena tarkkuutena, mikä oli parempi kuin GNSS-tarkkuus (26,6 metriä) käyttäen vastaavia kaupallisten vastaanottimien datajoukkoja älypuhelimista.

Avainsanat: älykäs logistiikka, sisäpaikannus, ulkopaikannus, ultralaajakaista (UWB), globaali satelliittinavigointijärjestelmä (GNSS), matala maakiertorata (LEO) -satelliitti, monituloinen monilähtö (MIMO)

ABSTRACT

The modern technological era relies heavily on smart systems and smart operations such as smart manufacturing, smart logistics, and smart shipping. They are the core ingredients of Industry 4.0 and the internet of things (IoT) applications and services, especially smart logistics or Logistics 4.0 that empowers industry and material supply chains. Precise positioning estimation of movable assets such as robots and personnel in industrial environments is a crucial foundation of smart logistics. Moreover, the integrity and reliability of navigation applications and location-aware services are dependent on precise positioning systems for both civilian and industrial use cases, indoors and outdoors. In this doctoral dissertation, we propose the use of certain technologies, sensors, and algorithms to achieve precise positioning estimations for indoor and outdoor environments. Ultra wideband (UWB) systems have recently emerged as a reliable positioning technology for complex indoor conditions. We propose the use of UWB in addition to inertial motion units (IMUs) as an integrated multisensor fusion system for precise indoor positioning. Our implemented UWB/IMU system provided a mean absolute accuracy (MAE) of 4.7 centimeters in a dense industrial environment (Technobothnia laboratory) at the University of Vaasa campus, Finland. On the other hand, we enhanced the outdoor vehicular positioning estimations with global navigation satellite systems (GNSSs) commercial-grade receivers in several smart phone models. That enhancement was recognized by Google among the third best results in an international competition. The fusion based GNSS/IMU positioning accuracy was enhanced to 2.291 meter error for mixed routes passing by tree-lined roads and open highways. Furthermore, we proposed a novel satellite-based positioning methodology from low Earth orbit (LEO) satellites, which can be harnessed as a back-up technology whenever the primary GNSS technology is denied in harsh environments and conditions. The patented operating principle of the new LEO-based positioning technique is leveraging the use of beamforming loops that are incident from multiple-input multiple-output (MIMO) antennas onboard LEO satellites. With the inference of massive MIMO beam identifiers and the congregation of beam patterns from mega sizes of future LEO constellations, the new beam-based positioning methodology can be used as a reliable alternative system in outdoor GNSS-denied venues. The results of fusing LEO/IMU for vehicular scenarios yielded a staggering positioning accuracy MAE of 9.15 meters that outperformed GNSS accuracy (MAE = 26.6 meters) using the same datasets of commercial receivers in smart phones.

Keywords: smart logistics, indoor positioning, outdoor positioning, ultra wideband (UWB), global navigation satellite system (GNSS), low Earth orbit (LEO) satellites, multiple-input multiple-output (MIMO)

أَخي لَن تَنالَ العِلمَ إِلّا بِسِتَّةٍ
سَأُنبيكَ عَن تَفصيلِها بِبَيانِ
ذَكاءٌ وَحِرصٌ وَاِجتِهادٌ وَبُلغَةٌ
وَصُحبَةُ أُستاذٍ وَطولُ زَمانِ

~ الإمامُ الشَافِعيّ

An ancient Arabic poem by Imam Mohamed Bin Idriss Al-Shafie
which can be translated as:

The fruit of wisdom rises from a rose that is sublime.
A rose that's only harvested by keen and relentless minds.
Nurtured by passionate care, provided wealth to climb.
Guided by a mentor's shadow, and often needs its time.

~ Translated and composed by: Bassam Salem

ACKNOWLEDGEMENTS

This doctoral dissertation was developed throughout the years of my PhD studies at the University of Vaasa, Finland, between 2018 and 2024. This article compilation study was financially supported via several research projects handled by University of Vaasa, such as: INTENS, TULEVA, TosiPaikka, INCUBATE, KvarkenSpace, RESILIENT, and Global Pilots FAPISAT, in addition to the private grants from: NOKIA foundation (2022), and Riitta Ja Jorma foundation (2023 and 2024).

First and foremost, Alhamdolellah. I wish to thank my former supervisor, Professor Seppo Niemi, for his support through the years we spent together (2018–2020), as I truly appreciate his decency, his counsel, and the sparking initiation of my doctoral studies. I wish him a nice retirement time with his family, for the years to come.

Then, I would like to thank Dr. Janne Koljonen for his weekly support and coaching that he offered me during my years of studies, ever since the MSc. degree in 2015. With professionalism and a good scientific mindset, Janne helped me on weekly basis to overcome many scientific dilemmas that we faced in our research activities, we learnt much Finnish language together, and cooperated in teaching as well.

To my manager and co-supervisor, Professor Heidi Kuusniemi, I cannot describe my gratitude to your unwavering support and your belief in my potential. I really thank you very much for your professionalism, decency, and mentorship, I am proud of those years I spent among your team, and I will cherish this to the rest of my life.

To my supervisor, my wise mentor, and should I say– my elder brother, Professor Mohammed Elmusrati, a mere ”thank you” is not enough, Allah alone knows how much gratitude and appreciation I hold for you. You have been always my main supporter ever since we first met in 2015, at the inauguration of my MSc. degree studies. I was a totally different person before meeting you, but you have clearly left your fingerprint on my evolved character version. Thank you for the wise counsels in science and life, thank you for bearing my calls and messages on daily basis, thank you for your patience on my absurdity, thank you for the valuable advice that shortened and smoothed the complex ways for me. Jazakom Allah Khayran.

Special thanks to the respected reviewers: Prof. Simo Särkka, and Prof. Salama Ikki, and the respected opponent: Prof. Jari Nurmi. Thanks for being part of this. I extend my appreciation and thanks to the Dean, Professor Raine Hermans, for his continuous support. Nevertheless, I feel grateful, thankful, and appreciative to my mentor and the worldwide renowned scholar, Professor Moustafa Amin Youssef, for the great support, collaboration, and mentorship he provided to me over the years.

My time at the University of Vaasa -as a student- is coming to an end. As much as it is hard to say that but I am also very proud of what have been accomplished here. First, the MSc. degree and what it enclosed: teaching at universities of Vaasa and NOVIA, cross-border collaboration with Umeå University, research, and networks.

Then, the PhD period that included: receiving grants and awards, selected as one of the Top-10 young scientists in Finland, to represent Finland at the GYSS summit in Singapore, winning the NASA Space App challenge, filing and registering a LEO-MIMO patent application, that led to the ”innovation of the year” award, also winning the EUNICE competition in Spain using the patent entrepreneurial idea, receiving a world-class GNSS training at the TUMSAT University in Tokyo, and much of frequent travelling between many countries: Sweden, Turkey, Belgium, Germany, Singapore, Japan, Saudi Arabia, Portugal, Italy, Spain, Egypt, and others.

To my colleagues, friends, and acquaintances, in Finland, Egypt, and over the seas: Thank you for providing me with your companionship, and your heartfelt thoughts, those are really very invaluable to me. Special thanks to the Muslim community in Vaasa, which provided very close relations and some genuine feel-at-home gestures.

To my big family, my lovely parents who are the main pillar, my greatest supporters, the beacon and backbone of our greater family. To my four brothers who are keeping me checked, smiling, and happy. To every member of my family-in-law whom are all very decent, kind, nice, and respectful. To all of them: Thank You, and love you!

To my son, Faris, also the expected and future offspring insha'Allah: you, Faris, are a great blessing and a gift to our life. Thank you Faris, and Thank you my kids.

Finally, to my lovely wife, who endured all those years with me in this journey, she has been my best companion ever, in times of hardships and also in times of glory. I truly could not survive without her and her support, she kept me alive and well. With her great patience, everlasting positive attitude, and the inherited decency, I could not be much happier than to just be with her. Thank you, my dear!

In the end, I hope the reader finds this document insightful and beneficial, meeting or exceeding your expectations. Thank you for stopping by!

Vaasa – Finland, August 25^{th}, 2024.

Mahmoud Essam Elsanhoury

تَمَّتْ بِحَمْدِ اللَّهِ وَتَوْفِيقِهِ

CONTENTS

List of Figures

List of Tables

ABBREVIATIONS

3D	Three dimensional
6-DOF	Six degrees of freedom
AOD	Angle of departure
AOA	Angle of arrival
ALG. A	Algorithm A
ALG. B	Algorithm B
BLE	Bluetooth low energy
CDF	Cumulative distribution function
CKF	Cubature Kalman filter
CoG	Center of gravity
DGNSS	Differential global navigation satellite system
DL	Downlink
DLL	Delay-lock loop
DR	Dead reckoning
DS-UWB	Direct sequence ultra wideband
ECEF	Earth-centered Earth-fixed
EKF	Extended Kalman filter
ENU	East north up
ETA	Estimated time of arrival
FCC	Federal communication commission
FiRA	Fine ranging alliance
FKF	Federated Kalman filter
FGO	Factor graph optimization
FH-UWB	Frequency hopping ultra wideband
GEO	Geostationary Earth orbit
GDOP	Geometric dilution of precision
GN	Gauss Newton
GNSS	Global navigation satellite system
GPS	Global positioning system
GPR	Ground penetrating radar
GSDC	Google smartphone decimeter challenge
IMU	Inertial motion unit

INS	Inertial navigation system
IoT	Internet of things
IR-UWB	Impulse radio ultra wideband
IPS	Indoor positioning systems
ITU	International telecommunication union
ID	Identifier
KF	Kalman filter
kNN	k nearest neighbour
LASER	Light amplification by stimulated emission of radiation
LC	Loosely coupled
LEO	Low Earth orbit
LEO-PNT	Low Earth orbit positioning, navigation, and timing
LiDAR	Light detection and ranging
LO	Local oscillator
LOS	Line of sight
LR	Linear regression
MAC	Medium access control
MAE	Mean absolute error
MB-UWB	Multiband ultra wideband
MEO	Medium Earth orbit
MIMO	Multiple-input multiple-output
ML	Machine learning
MSE	Mean square error
NB	Narrowband
NIST	National institute of standards and technologies
NLOS	Non line of sight
OFDM	Orthogonal frequency division multiplexing
PAN	Personal area network
PDR	Pedestrian dead reckoning
PF	Particle filter
PLL	Phase-lock loop
PN	Pseudorandom number
PPP	Precise point positioning
PPK	Post processed kinematic

PSD	Power spectral density
PNT	Positioning, navigation, and timing
PS	Power spectral density
PVT	Position, velocity and timing
QPSK	Quadrature phase-shift keying
RADAR	Radio detection and ranging
ReLS	Regularized least square
RF	Radio frequency
RFID	Radio frequency identification
RMSE	Root mean square error
RSS	Received signal strength
RSSI	Received signal strength index
RTK	Real-time kinematic
RTLS	Real-time location system
RTS	Rauch-Tung-Striebel
RTT	Round trip time
SBAS	Satellite-based augmentation system
SF-UWB	Swept frequency ultra wideband
SFH-UWB	Stepped frequency hopping ultra wideband
SNR	Signal to noise ratio
SMC	Sequential Monte Carlo
SoO	Signal of opportunity
SV	Satellite vehicle
TC	Tightly coupled
TDOA	Time difference of arrival
TLE	Two line element
TOA	Time of arrival
TOF	Time of flight
TOT	Time of transmission
TWR	Two way ranging
UWB	Ultra wideband
UKF	Unscented Kalman filter
UT	User terminal
UTC	Ultra tightly coupled

VCO	Voltage-controlled oscillator
VMM	Visual map matching
WiP	Work in progress
WGS	World geodetic system
WLS	Weighted least square

LIST OF PUBLICATIONS

This doctoral dissertation is a culmination of research work done between 2021 and 2024, and it has been compiled based on the following publications:

[P1] **Elsanhoury, M.**, Mäkelä, P., Koljonen, J., Välisuö, P., Shamsuzzoha, A., Mantere, T., Elmusrati, M., Kuusniemi, H. (2022). Precision Positioning for Smart Logistics using Ultra-wideband Technology-based Indoor Navigation: A Review. IEEE Access, 10, 44413-44445. doi:10.1109/ACCESS.2022.3169267 [1]

[P2] **Elsanhoury, M.**, Nieminen, J., Välisuo, P., Siemuri, A., Koljonen, J., Elmusrati, M., Kuusniemi, H. (2023). Indoor Asset Tracking in Dense Industrial Environments Using Low-cost Wireless Technologies. Proceedings of Work-in-Progress in Hardware and Software for Location Computation (WIPHAL 2023) Castellon, Spain. doi:10.5281/zenodo.8160442 [1]

[P3] **Elsanhoury, M.**, Nieminen, J., Välisuo, P., Siemuri, A., Koljonen, J., Elmusrati, M., Kuusniemi, H. (2023). Precise Indoor Positioning System for Mobile Robots via Smoothed UWB/IMU Sensor Fusion. 13th International Conference on Indoor Positioning and Indoor Navigation (IPIN), Nuremberg, Germany, © 2023 IEEE, pp. 1-6, doi: 10.1109/IPIN57070.2023.10332542 [2]

[P4] **Elsanhoury, M.**, Siemuri, A., Nieminen, J., Välisuo, P., Koljonen, J., Elmusrati, M., Kuusniemi, H. (2023). Emerging Wireless Technologies for Reliable Indoor Navigation in Industrial Environments. Proceedings of the 36th International Technical Meeting of the Satellite Division of The Institute of Navigation (ION GNSS+ 2023), Denver, Colorado, September 2023, pp. 1706-1714. doi: /10.33012/2023.19225 [2]

[P5] **Elsanhoury, M.**, Koljonen, J., Välisuo, P., Elmusrati, M., Kuusniemi, H. (2021). Survey on Recent Advances in Integrated GNSSs Towards Seamless Navigation Using Multi-Sensor Fusion Technology. Proceedings of the 34th International Technical Meeting of the Satellite Division of The Institute of Navigation (ION GNSS+ 2021), St. Louis, Missouri, September 2021, pp. 2754-2765. doi:10.33012/2021.17961 [2]

[P6] Siemuri, A., **Elsanhoury, M.**, Välisuo, P., Kuusniemi, H. Elmusrati, M. (2022). Application of Machine Learning to GNSS/IMU Integration for High Precision Positioning on Smartphones. Proceedings of the 35th International Technical Meeting of the Satellite Division of The Institute of Navigation (ION GNSS+ 2022), Denver, Colorado, September 2022, pp. 2256-2264. doi:10.33012/2022.18375 [2]

[P7] Ferre, R. M., Lohan, E. S., Kuusniemi, H., Praks, J., Kaasalainen, S., Pinell, C., **Elsanhoury, M.** (2022). Is LEO-Based Positioning with Mega-Constellations the Answer for Future Equal Access Localization?. © 2022 IEEE Communications Magazine, vol. 60, no. 6, pp. 40-46, June 2022, doi: 10.1109/MCOM.001.2100841 [2]

[P8] Prol, F. S., Ferre, R. M., Saleem, Z., Välisuo, P., Pinell, C., Lohan, E. S., **Elsanhoury, M.**, Elmusrati, Mohammed., Islam, S., Çelikbilek, K., Selvan, K., Yliaho, J., Rutledge, K., Ojala, A., Ferranti, L., Praks, J., Bhuiyan, M. Z., Kaasalainen, S., Kuusniemi, H. (2022). Position, Navigation, and Timing (PNT) Through Low Earth Orbit (LEO) Satellites: A Survey on Current Status, Challenges, and Opportunities. IEEE Access, vol. 10, pp. 83971-84002, 2022, doi: 10.1109/ACCESS.2022.3194050 [1]

[P9] **Elsanhoury, M.**, Koljonen, J., Elmusrati, M., Kuusniemi, H. (2024). A Novel Beam-Based Positioning Paradigm Via Opportunistic Signal of Future Massive MIMO LEO Satellite Constellations. 2024 International Conference on Localization and GNSS (ICL-GNSS), Antwerp, Belgium, © 2024 IEEE. [2]

[P10] **Elsanhoury, M.**, Koljonen, J., Prol, F., Elmusrati, M., Kuusniemi, H. (2024). Massive MIMO Beam ID-Based Positioning Method With Low Earth Orbit Satellite Mega-Constellations. [*Submitted to a journal:*] IEEE Transactions on Geoscience and Remote Sensing. [3]

---

[1] Open Access articles, reprinted under a Creative Commons (CC BY) 4.0 license
[2] Reprinted with kind permissions from the copyright owners.
[3] Submitted to the publisher, currently under review.

AUTHOR'S CONTRIBUTION

Mahmoud Elsanhoury is the primary author in Publications **[P1]–[P5] and [P9]–[P10]**, and a coauthor in Publications **[P6]–[P8]** only. Publications on indoor positioning systems are **[P1]–[P4]**, while publications on outdoor positioning systems are **[P5]–[P10]**. Detailed contributions from the author(s) are described below each publication title.

Publication [P1]: "Precision Positioning for Smart Logistics using Ultra-wideband Technology-based Indoor Navigation: A Review"

Mahmoud Elsanhoury: Literature Review, Conceptualization, Investigation, Algorithms Development, Analysis, Python and/or MATLAB Coding, Illustrations and Sketching, Writing the First Draft, Writing - Format and Editing, Manuscript Smoothing, Corresponding Author, Project Coordination. **Petteri Mäkelä:** Literature Review, Investigation, Analysis, Python and/or MATLAB Coding, Writing and Editing, Project Coordination. **Janne Koljonen:** Validation, Analysis, Manuscript Smoothing, Mentorship, Publishing Guidance. **Petri Välisuö:** Literature Review, Investigation, Algorithms Development, Analysis, Python and/or MATLAB Coding, Illustrations and Sketching, Writing the First Draft, Writing - Format and Editing, Manuscript Smoothing, General Supervision, Project Coordination, Publishing Guidance. **Ahm Shamsuzzoha:** Literature Review, Investigation, Analysis, Writing and Editing, Publishing Guidance. **Timo Mantere:** Funding Acquisition, Project Management. **Mohammed Elmusrati:** General Supervision, Mentorship, Publishing Guidance, Conceptualization. **Heidi Kuusniemi:** Funding Acquisition, Project Management, General Supervision, Mentorship, Publishing Guidance, Manuscript Smoothing.

Publication [P2]: "Indoor Asset Tracking in Dense Industrial Environments Using Low-cost Wireless Technologies"

Mahmoud Elsanhoury: Literature Review, Conceptualization, Investigation, Algorithms Development, Software Development, Hardware Realization, Troubleshooting, Analysis, Python and/or MATLAB Coding, Illustrations and Sketching, Data Collection and Processing, Writing the First Draft, Writing - Format and Editing, Manuscript Smoothing, Corresponding Author, Project Coordination. **Jyri Nieminen:** Software Development, Hardware Realization, Data Collection and Processing, Troubleshooting. **Petri Välisuö:** Software Development, Hardware Realization, Data Collection and Processing, Troubleshooting, General Supervision, Project Coordination, Publishing Guidance. **Akpo Siemuri:** Algorithms Development, Data Processing, Conference Presentation. **Janne Koljonen:** Manuscript Smoothing, Mentorship, Publishing Guidance. **Mohammed Elmusrati:** General Supervision, Funding Acquisition, Conceptualization, Mentorship, Publishing Guidance. **Heidi Kuusniemi:** Funding Acquisition, Project Management, General Supervision, Conceptualization, Mentorship, Publishing Guidance, Manuscript Smoothing.

Publication [P3]: "Precise Indoor Positioning System for Mobile Robots via Smoothed UWB/IMU Sensor Fusion"

Mahmoud Elsanhoury: Literature Review, Conceptualization, Investigation, Algorithms Development, Software Development, Hardware Realization, Troubleshooting, Analysis, Python and/or MATLAB Coding, Illustrations and Sketching, Data Collection and Processing, Writing the First Draft, Writing - Format and Editing, Manuscript Smoothing, Corresponding Author, Project Coordination, Conference Presentation. **Jyri Nieminen:** Software Development, Hardware Realization, Data Collection and Processing, Troubleshooting. **Petri Välisuö:** Software Development, Hardware Realization, Data Collection and Processing, Troubleshooting, General Supervision, Project Coordination, Publishing Guidance. **Akpo Siemuri:** Algorithms Development, Data Processing. **Janne Koljonen:** Manuscript Smoothing, Mentorship, Publishing Guidance. **Mohammed Elmusrati:** General Supervision, Funding Acquisition, Conceptualization, Mentorship, Publishing Guidance. **Heidi Kuusniemi:** Funding Acquisition, Project Management, General Supervision, Conceptualization, Mentorship, Publishing Guidance, Manuscript Smoothing.

Publication [P4]: "Emerging Wireless Technologies for Reliable Indoor Navigation in Industrial Environments "

Mahmoud Elsanhoury: Literature Review, Conceptualization, Investigation, Algorithms Development, Software Development, Hardware Realization, Troubleshooting, Analysis, Python and/or MATLAB Coding, Illustrations and Sketching, Data Collection and Processing, Writing the First Draft, Writing - Format and Editing, Manuscript Smoothing, Corresponding Author, Project Coordination. **Akpo Siemuri:** Algorithms Development, Data Processing. **Jyri Nieminen:** Software Development, Hardware Realization, Data Collection and Processing, Troubleshooting. **Petri Välisuö:** Software Development, Hardware Realization, Data Collection and Processing, Troubleshooting, General Supervision, Project Coordination, Publishing Guidance. **Janne Koljonen:** Manuscript Smoothing, Mentorship, Publishing Guidance. **Mohammed Elmusrati:** General Supervision, Funding Acquisition, Conceptualization, Mentorship, Publishing Guidance. **Heidi Kuusniemi:** Funding Acquisition, Project Management, General Supervision, Conceptualization, Mentorship, Publishing Guidance, Manuscript Smoothing, Conference Presentation.

Publication [P5]: "Survey on Recent Advances in Integrated GNSSs Towards Seamless Navigation Using Multi-Sensor Fusion Technology "

Mahmoud Elsanhoury: Literature Review, Conceptualization, Investigation, Analysis, Illustrations and Sketching, Writing the First Draft, Writing - Format and Editing, Manuscript Smoothing, Corresponding Author, Project Coordination, Conference Presentation. **Janne Koljonen:** Manuscript Smoothing, Mentorship, Publishing Guidance. **Petri Välisuö:** Project Coordination, Publishing Guidance. **Mohammed Elmusrati:** General Supervision, Funding Acquisition, Conceptualization, Mentorship, Publishing Guidance. **Heidi Kuusniemi:** Funding Acquisition, Project Management, General Supervision, Conceptualization, Mentorship, Publishing Guidance, Manuscript Smoothing.

Publication [P6]: "Application of Machine Learning to GNSS/IMU Integration for High Precision Positioning on Smartphones "

Akpo Siemuri: Participation in Google Competition (Bronze Medal), Literature Review, Conceptualization, Investigation, Analysis, Algorithms Development, Data Processing, Python and/or MATLAB Coding, Illustrations and Sketching, Validation, Troubleshooting, Writing the First Draft, Writing - Format and Editing, Manuscript Smoothing, Corresponding Author, Project Coordination, Conference Presentation. **Mahmoud Elsanhoury:** Participation in Google Competition (Bronze Medal), Literature Review, Conceptualization, Investigation, Analysis, Algorithms Development, Data Processing, Python and/or MATLAB Coding, Validation, Troubleshooting, Writing - Format and Editing, Manuscript Smoothing. **Petri Välisuö:** Project Coordination, Analysis, Algorithms Development, Publishing Guidance. **Heidi Kuusniemi:** Funding Acquisition, Project Management, General Supervision, Conceptualization, Mentorship, Publishing Guidance, Manuscript Smoothing. **Mohammed Elmusrati:** General Supervision, Funding Acquisition, Conceptualization, Mentorship, Publishing Guidance.

Publication [P7]: "Is LEO-Based Positioning with Mega- Constellations the Answer for Future Equal Access Localization? "

Mahmoud Elsanhoury: Conceptualization, sketching, illustrations, discussion and writing the whole section about "Massive MIMO for LEO-based positioning".

Publication [P8]: "Position, Navigation, and Timing (PNT) Through Low Earth Orbit (LEO) Satellites: A Survey on Current Status, Challenges, and Opportunities "

Mahmoud Elsanhoury: Conceptualization, sketching, illustrations, discussion and writing the whole sections about "Kalman filters" and "Sensor fusion".

Publication [P9]: "A Novel Beam-Based Positioning Paradigm Via Opportunistic Signal of Future Massive MIMO LEO Satellite Constellations "

Mahmoud Elsanhoury: Literature Review, Conceptualization, Investigation, Algorithms Development, Software Development, Troubleshooting, Analysis, Python and/or MATLAB Coding, Illustrations and Sketching, Data Collection and Processing, Writing the First Draft, Writing - Format and Editing, Manuscript Smoothing, Corresponding Author, Project Coordination, Writing Patent Application, Pitching to Potential Incubators. **Janne Koljonen:** Literature Review, Conceptualiza-

tion, Investigation, Algorithms Development, Software Development, Troubleshooting, Analysis, MATLAB Coding, Figure Plots, Data Collection and Processing, Writing the First Draft, Writing - Format and Editing, Manuscript Smoothing, Mentorship, Publishing Guidance. **Mohammed Elmusrati:** Discovery of this Novel Idea, General Supervision, Funding Acquisition, Conceptualization, Mentorship, Publishing Guidance, Conceptualization. **Heidi Kuusniemi:** Funding Acquisition, Project Management, General Supervision, Conceptualization, Mentorship, Publishing Guidance, Manuscript Smoothing.

Publication [P10]: "Massive MIMO Beam ID-Based Positioning Method With Low Earth Orbit Satellite Mega-Constellations "

Mahmoud Elsanhoury: Literature Review, Conceptualization, Investigation, Algorithms Development, Software Development, Troubleshooting, Analysis, Python and/or MATLAB Coding, Illustrations and Sketching, Data Collection and Processing, Writing the First Draft, Writing - Format and Editing, Manuscript Smoothing, Corresponding Author, Project Coordination, Reviewing the Patent Application, Pitching to Potential Incubators. **Janne Koljonen:** Literature Review, Conceptualization, Investigation, Algorithms Development, Software Development, Troubleshooting, Analysis, Python and/or MATLAB Coding, Figure Plots, Data Collection and Processing, Writing the First Draft, Writing - Format and Editing, Manuscript Smoothing, Mentorship, Publishing Guidance. **Fabricio S. Prol:** Literature Review, Satellite Data Generation, Python and/or MATLAB Coding, Figure Plots, Writing - Format and Editing, Manuscript Smoothing. **Mohammed Elmusrati:** Discovery of this Novel Idea, General Supervision, Funding Acquisition, Conceptualization, Mentorship, Publishing Guidance. **Heidi Kuusniemi:** Funding Acquisition, Project Management, General Supervision, Conceptualization, Mentorship, Publishing Guidance, Manuscript Smoothing.

OTHER PUBLICATIONS (NOT INCLUDED IN THE DISSERTATION)

The following publications were also held by the author during the doctoral studies. Nevertheless, these publications are not included in the dissertation as their topics were already covered completely or partially by the main selected publications of the dissertation.

- Kuusniemi, H., Mäkelä, P., Välisuö, P., Basher, A., Siemuri, A., Selvan, K., **Elsanhoury, M.**, Boutellier, J., Ferranti, L. (2021). Precision Positioning Technology. Forum for Intelligent Machines ry, Finland. https://www.fima.fi/reports/precision-positioning-technology

- Siemuri, A., **Elsanhoury, M.**, Selvan, K., Välisuo, P., Kuusniemi, H., Elmusrati, M. (2023). Seamless Navigation for Indoor-Outdoor Positioning Using GNSS-Aided UWB/WiFi/IMU System. Proceedings of the 36th International Technical Meeting of the Satellite Division of The Institute of Navigation (ION GNSS+ 2023), Denver, Colorado, September 2023, pp. 2616-2623. doi:10.33012/2023.19323

- **Elsanhoury, M.**, Çuhac, C., Koljonen, J., Elmusrati, M. (2023). Nonlinear Estimation of Incident Solar Irradiance on Finland Using Discrete-time Extended Kalman Smoothers. Technical Research Journal issued by the College of Industrial Technology, Musrata, Libya. https://jtr.cit.edu.ly/jorview.php?jviewid=2&&pviewid=8

- Koljonen, J., **Elsanhoury, M.**, Elmusrati, M., Niemi, Seppo. (2024). Advancing Sustainable Maritime with AI/ML Enhanced Hardware-in-the-Loop Testing. 2024 International Workshop on Artificial Intelligence and Machine Learning for Energy Transformation (AIE), Vaasa, Finland, 2024, pp. 1-6, doi: 10.1109/AIE61866.2024.10561409.

- Mostafa, S., **Elsanhoury, M.**, Yliaho, J., Koljonen, J., Kuusniemi, H., Elmusrati, M., Harras, K., Youssef, M. (2024). Leveraging Low Earth Orbit Satellites for Future Ubiquitous Positioning (Vision Paper). Proceedings of the 32nd ACM SIGSPATIAL International Conference on Advances in Geographic Information Systems (ACM SIGSPATIAL 2024). *[Accepted Article]*.

1 INTRODUCTION

Positioning systems are the backbone of navigation services and smart use cases in the modern era of smart logistics and internet of things (IoT) applications. Reliable precise positioning systems are essential for resource management optimization in addition to cost- and time-saving of complex operations. Logistics is an important driver for the competitiveness of industries and material supply. The development of smart logistics, powered by precise positioning and communication technologies can significantly improve the efficiency of logistics.

Nowadays, smart logistics play a major role in Industry 4.0. They help corporations with crucial operations including: predicting the demands, planning the sales, and managing the inventory (N. Zhang, 2018), (Tang, 2020). Smart logistics, also known as 'Logistics 4.0', can accelerate the execution of all logistical processes through the application of intelligent tools, technologies, and methodologies for planning and control. Realization of smart technologies helps in acquiring accurate information to track material flow for various purposes. By using smart positioning technologies, tools, and equipment, global supply and logistics chains are improved and made more efficient (Humayun, Jhanjhi, Hamid, & Ahmed, 2020). These positioning technologies can significantly enhance visibility, optimize product routing, streamline inventory control, and asset restock (Issaoui, Khiat, Bahnasse, & Ouajji, 2019).

In recent years, the attention towards precise positioning and navigation systems has grown exponentially due to the rapid development and affordability of smart devices and the technological infrastructure. Achieving precise localization has been a major concern in the scientific community due to its direct relationship with the reliability of navigational applications and location-based services. Whether in an indoor or outdoor environments; precise location information of people and assets is an essential element in numerous use cases: smart logistics (Wu, Shen, Zhao, Li, & Huang, 2022), tracking medical equipment in healthcare centres (Pospelova et al., 2022), tracking individuals in crowded venues (Alarifi et al., 2016), ship-building and offshore industry (Park et al., 2021), and construction industry (Woo et al., 2011).

Existing positioning systems come from various: technologies, core techniques, shapes, and for various application avenues. The reliability of a given positioning system can be assessed depending on the utilized technology, sensor, technique, algorithm, and the relevant performance metric. In every environment and/or scenario, the performance of the positioning systems in a given application domain should be assessed based on a preset group of metrics that are directly proportional to the designed objectives and the expected outcomes of the positioning system. Moreover, the selection of the appropriate positioning system and performance metrics depends mainly on the environments of operation whether they are: indoors or outdoors.

In indoor environments, many technologies exist with the majority are based on wireless communication systems (Alarifi et al., 2016). There is no single indoor technology that can fit all usages and applications, consequently, the indoor positioning sector is a wide open topic for innovations. While in outdoor environments, the satellite-based positioning systems are the most commonly used technologies in today's world owing to their numerous advantages and reliable performance (Teunissen & Montenbruck, 2017).

The varying nature of both indoor and outdoor environments requires the continuous developments of positioning technologies to enhance system precision, accuracy, and reliability. For instance, when it comes to wireless technologies, the complex surroundings impose several types of signal impairments such as: shadowing and multipath effects, which in turn reflect in the performance behaviour of positioning systems. Hence, special maintenance solutions should be arranged in order to mitigate such inevitable impairments. Those enhancements can be from the perspectives of soft-

ware and/or hardware components of the positioning system. Certainly and expectedly, the slightest changes in the positioning system's technological components will incur positive and/or negative changes in the budgets of: time, power, and costs.

It is the mission of this dissertation to investigate the potential of developing precise positioning systems for indoor and outdoor venues by indulging in trade-offs and compromises between the positioning accuracy and system budgets. Noteworthy, the seamless integration of indoor and outdoor positioning systems was studied separately and individually in other publications held by the author, however, it had not been the focus of this thesis.

1.1 Scope and objectives

The main scope of this dissertation is to develop precise positioning systems for smart logistics in both environments: indoors and outdoors. By investigating and leveraging the existing positioning technologies and algorithms, we endeavor to recommend the best fitting technology ingredients to facilitate smart operations, indoors and outdoors.

The specific objectives are as follows:

1. To study and review the state-of-the-art literature in precise indoor and outdoor positioning scenarios.

2. To focus on literature studies that are concerned with developing precise positioning systems in challenging environments.

3. To identify and select the best fitting positioning technologies and algorithms in the corresponding environmental scenarios: indoors and outdoors.

4. To develop proprietary implementations for achieving precise positioning estimations in both environments.

5. To consider the feasibility of fusing multiple positioning technologies for maximizing system integrity.

6. To continuously seek alternatives or secondary positioning technologies as back-ups for the primary precise positioning system in every scenario.

Eventually, we selected ultra wideband (UWB) technology to render the precise indoor positioning system (IPS), in addition to validating a set of positioning algorithms and techniques to be used for maximizing the positioning accuracy. Besides, we also investigated other alternative technologies for indoor positioning.

For outdoors, we enhanced the positioning accuracy of global navigation satellite systems (GNSS) in vehicular navigation using a unique sequence of algorithmic treatment, multisensor fusion, and positioning techniques. Likewise, we sought a new back-up technology to GNSS, which is based on exploiting the advantages of low Earth orbit (LEO) satellites and the multiple-input multiple-output (MIMO) antenna beamforming capabilities.

1.2 Main research questions

This dissertation is compiled based on publications [P1]–[P10], in which the following research questions RQ1–RQ4 were studied and investigated.

RQ1: What are the advantages of precise positioning systems in indoor and outdoor environments?

Precise positioning systems offer significant advantages in both indoor and outdoor navigation applications, which revolutionize logistics and IoT implementations. They enable real-time tracking of assets with very high accuracy that is vital for optimizing inventory management and asset utilization across diverse environments. Fleet management benefits from precise location data, facilitating route optimization and scheduling for reduced costs and enhanced delivery efficiency, in situations of navigating urban streets or warehouse aisles. Those benefits significantly impact the supply chain which entice proactive problem solving and handling to tackle delays and disruptions whether indoors or outdoors. In addition, Geo-fencing and zone monitoring features can rely on precise positioning systems to automate processes and support security measures, ensuring seamless navigation transitions between indoor and outdoor spaces. Smart delivery gains precision guidance, improving efficiency and customer satisfaction, whether delivering parcels to urban residences or navigating warehouse complexes.

Furthermore, integration with IoT sensors enhances data collection for monitoring goods condition and compliance, which are very crucial in both indoor and outdoor environments. Predictive analytics and optimization algorithms can be based on precise positioning data to refine decision-making (indoors or outdoors), and ensure resource allocation that aligns with dynamic navigation demands. In fact, precise positioning systems drive efficiency and responsiveness in smart logistics and IoT applications, they also support achieving enhanced customer satisfaction and competitive advantage across indoor and outdoor navigation landscapes.

RQ2: How to build precise positioning systems for dense indoor environments?

Building precise positioning systems for dense indoor environments is very challenging as the indoor conditions are always very complex by default. It involves the selection of appropriate sensors that are capable of providing accurate positioning data. Also, can include the integration of sensor data using fusion techniques, and certainly requires the development of localization algorithms that are customized for indoor conditions.

Information about the use case environment are to be studied and investigated prior to design and implementation, while sensors are calibrated and algorithms fine-tuned to optimize the system performance. Infrastructure elements such as access points or beacons should be pragmatically deployed to provide reference points for localization. Then, in order to assess the developed system, testing and validation are conducted to check the accuracy and reliability of the overall integrated system with attention given to user interface design, integration with other systems, and privacy and security considerations.

Publications [P1]–[P4] focused on and thoroughly discussed the methodologies and the required equipment and technologies to build precise indoor positioning systems amid dense challenging indoor environments.

RQ3: How to achieve precise positioning estimations for outdoor environments?

Satellite-based technologies such as GNSS technologies are the most commonly used positioning technologies for outdoor environments. Achieving precise positioning estimations outdoors through satellite-based methods involves several crucial steps similar to the steps found in question **RQ2**. Firstly, selecting high-quality GNSS receivers with multi-constellation support (multi GNSS) is very essential to improve the integrity of the system. Installing the GNSS antenna in an optimal location with a clear view of the sky is paramount to maximize signal reception and minimize nearby interference and/or channel fading. Therefore, the primary acquisition and tracking loops of raw GNSS signals can be leveraged by gathering satellite signal information from multiple sources or constellations.

Then, the post-processing techniques like differential GNSS, real-time kinematic (RTK), or precise point positioning (PPP) can be applied to improve accuracy through correction data or precise orbit and clock corrections. For RTK, establishing a base station is necessary to transmit correction data to the user terminals. Subsequently, data processing using GNSS software computes precise position solutions by applying corrections and resolving integer ambiguities. Moreover, additional positioning algorithms and techniques (e.g. sensor fusion) can be introduced to the post-processed raw GNSS data in order to further-tine the output positioning estimations. For final assessment of the system, validation tests are conducted to verify accuracy against ground truth data in various motion and road scenarios. Continuous monitoring and maintenance can ensure optimal system performance and reliability over longer time intervals, which fortify the integrity of the developed system.

Publications [P5]–[P6] introduced a sensor fusion-based method on enhancing GNSS positioning estimations for low-grade commercial GNSS receivers found in various smart phones. This solution was recognized in an international decimeter competition.

RQ4: Are there any outdoor satellite-based backup technologies to GNSS?

As a well-established fact, GNSS positioning technologies are the most reliable, most common, and most accurate systems for outdoor environments, so far. However, in many conditions and scenarios, GNSS systems suffer challenging factors that affect their integrity such as: signal vulnerabilities, channel fading, and dense structures. This research question is very important to be addressed in order to tackle much of those GNSS shortcomings by finding a new backup technology to GNSS in such situations.

For other satellites than GNSS, we are left with the LEO satellite constellations that are residents in orbital altitudes much closer to Earth's surface. As reported in recent scientific researches, the configurations of LEO satellites can leverage outdoor positioning technologies in many ways since they are more dense in numbers, more closer to Earth with stronger signal reception, and possess more capability to penetrate obstacles.

Publications [P7]–[P10] discussed a new satellite-based method that passively exploits radio signals incident from LEO satellite constellations to provide a reliable backup technology to GNSS positioning systems. It is very important to note that: the newly developed LEO-based positioning method is not intended as an alternative technology that replaces GNSS, however, it is intended to be a backup technology when GNSS signals are denied or unavailable.

1.3 Summary of publications

This section briefly summarizes all the ten publications **[P1–P10]** of this compilation dissertation. An outline illustration depicting the scientific components of every publication is shown in Figure 1.

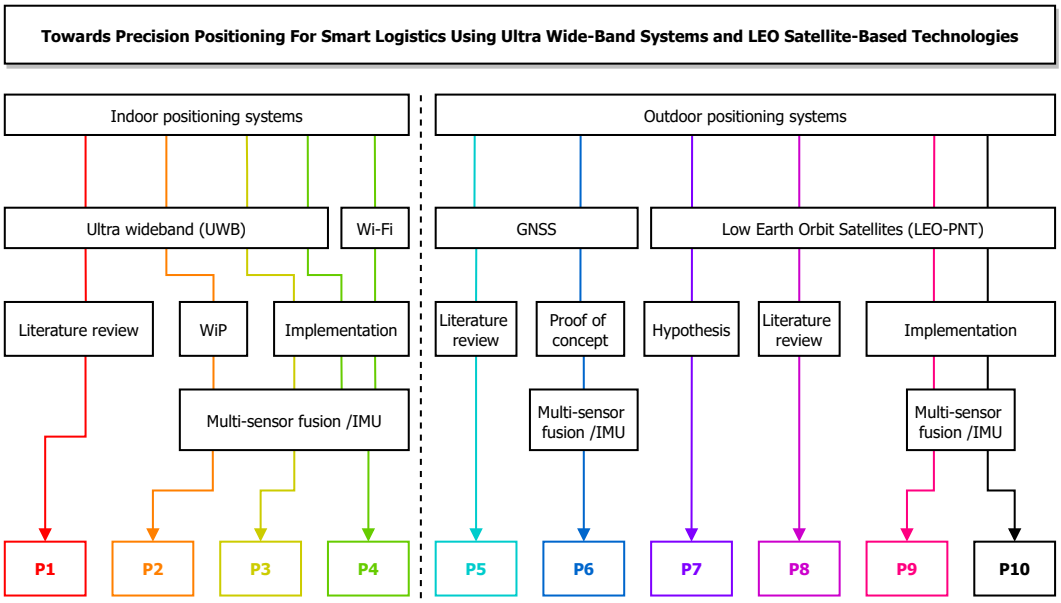

Figure 1. Scientific components of all publications [P1–P10].

Publication [P1]: Precision Positioning for Smart Logistics using Ultra-wideband Technology-based Indoor Navigation: A Review.

Publication P1 was compiled as a comprehensive literature review that focused on the most common implementations of indoor positioning systems, their structure and applications. It paved the way not only to understanding the requirements of precision positioning systems but also understanding the core concepts of smart logistics and smart operations. In publication P1, although the focus technology was UWB system, the whole precision positioning topic was dissected thoroughly by investigating the following aspects: the existing positioning and ranging methodologies, positioning algorithms, positioning technologies, sensor fusion and machine learning methods for improving the positioning estimations.

Publication [P2]: Indoor Asset Tracking in Dense Industrial Environments Using Low-cost Wireless Technologies.

Post to getting a solid understanding about UWB indoor positioning systems and sensor fusion schemes, a proposed low-cost fusion-based UWB system was coined and outlined. Publication P2 was compiled as a work-in-progress (WiP) article to introduce the elements, the structure, and the environment of the proposed UWB system. Also in which, the rationale, the algorithms, and the methodologies were discussed.

Publication [P3]: Precise Indoor Positioning System for Mobile Robots via Smoothed UWB/IMU Sensor Fusion.

Publication P3 is the main implementation contribution article that shows all the carried out procedures to build a sustainable precise indoor positioning system at the University of Vaasa's main laboratory environment. The accuracy level of the tested system was below 10 centimeter error. The developed system comprised UWB as the primary technology while being assisted with inertial sensors to form the fusion-based integration scheme. Inside the challenging dense lab environment, a complete experimental setup was deployed in the given region of interest along with configuring a millimeter-accurate autonomous patrolling robot to provide the ground truth trajectory. In addition to developing an embedded system that retrieves all sensors measurements in one data pool, all algorithmic details were discussed in publication P3. Hardware and software ports for other positioning technologies (e.g. Bluetooth and Wi-Fi) were also facilitated in the designed system for later use.

Publication [P4]: Emerging Wireless Technologies for Reliable Indoor Navigation in Industrial Environments.

Further experiments were carried out to fine-tune and improve the final accuracy of the fusion-based UWB system, whose newer results were documented in Publication P4. In addition, another IPS technology was investigated and tested to check the feasibility of such system in the future. Although the Wi-Fi positioning system was out of scope for this dissertation, the evaluated results encouraged developing such system for human tracking but with different ranging technique. That is, the Wi-Fi time based ranging technique(s) instead of Wi-Fi received power level technique.

Publication [P5]: Survey on Recent Advances in Integrated GNSSs Towards Seamless Navigation Using Multi-Sensor Fusion Technology.

This is the first article of this compilation to discuss outdoor satellite-based positioning technologies. Publication P5 focused on surveying the most commonly used multisensor fusion schemes for GNSS applications. Within, a very compact review of the available and trending fusion-based GNSS schemes in academic and industrial research and implementations. Also, it discussed the utilization of the same algorithmic set that was used in the indoor positioning use case (i.e. publications [P3] and [P4]).

Publication [P6]: Application of Machine Learning to GNSS/IMU Integration for High Precision Positioning on Smartphones.

GNSS technologies are known to be the most accurate, versatile, and widely used outdoor positioning systems in the majority of every day activities and applications. In publication P6, a global competition was attempted to improve the smart phones positioning accuracy in road driving. As a proof of concept, a set of procedure steps were carried out in order to improve the given dataset of 30+ smart phone devices measurements using fusion-based integration schemes. The final positioning results were very promising and encouraging to pursue further implementations in the satellite-based positioning domain.

Publication [P7]: Is LEO-Based Positioning with Mega-Constellations the Answer for Future Equal Access Localization?.

GNSS technologies have numerous benefits, however, GNSS can suffer limitations and impairments. A growing demand arises for developing a new outdoor technology that is as precise as GNSS, to work collaboratively with GNSS or at best to be active when GNSS service is denied. Publication P7 is the first article of this compilation to address the topic of satellite-based positioning from non GNSS constellations. In publication P7, a scientific hypothesis was discussed to utilize LEO satellites in providing positioning and navigation solutions for ground users, as a backup technology to GNSS. Furthermore, a new paradigm emerged to employ the spatial information and the geometrical shapes of the massive antenna beams incident from LEO satellites, in order to provide a seamless

positioning technique that is reliable and very numerous in benefits. This article can be considered as the starting point of research for the LEO positioning, navigation, and timing (LEO-PNT) topic in this dissertation.

Publication [P8]: Position, Navigation, and Timing (PNT) Through Low Earth Orbit (LEO) Satellites: A Survey on Current Status, Challenges, and Opportunities.

Due to the newness of the topic, LEO-PNT has a shallow literature compared to other positioning technologies such as GNSS. Thus, publication P8 presented a thorough survey and a comprehensive academic tutorial to understand the technical aspects and the feasible expected use cases of LEO-PNT. In this review, sophisticated details were documented regarding the following aspects: the space segment, the user segment, the control segment, the receiver design, the constellations design, the algorithmic toolboxes, and the potential fusion schemes.

Publication [P9]: A Novel Beam-Based Positioning Paradigm Via Opportunistic Signal of Future Massive MIMO LEO Satellite Constellations.

The technical concerns of the novel LEO-PNT method addressed in publication P7, were further nourished, fortified, and articulated in publication P9. In addition, a preliminary simulation environment was established to model the statistic attributes of LEO satellite constellations with minimal amounts of beamforming loops, to validate the concept statistically. Moreover, a subset positioning technique variant was coined to improve the overall accuracy of the beam-based method. Through the identification of the beam number, and by knowing the exported beam patterns from given constellations; the positioning problem can be solved geometrically using information from the beam shapes and the orbital satellite position in real-time. The method is totally passive, can operate in all climate modes even in blocked sights, and does not require time synchronizations nor sophisticated receiver design.

Publication [P10]: Massive MIMO Beam ID-Based Positioning Method With Low Earth Orbit Satellite Mega-Constellations.

Following the preliminary study reported in publication P9, the simulation environment was further enhanced in publication P10 to resemble more realistic scenarios. By generating real data configurations of mega LEO satellite constellations, the novel LEO-PNT method was proven to be reliable in real-world scenarios. The method was validated using a similar scheme and algorithmic approach that was adopted throughout the dissertation. Three scenarios were tested: 1) stationary user, 2) linear motion with constant acceleration, 3) nonlinear motion from a real vehicle driving data, and 4) same nonlinear motion dataset from scenario 3 but with using huge massive MIMO beamforming patterns. The results were very promising and sufficient to account this LEO-based passive method as a reliable backup technology for GNSS in harsh environments. Consequently, the proposed LEO-PNT idea was filed for intellectual property rights (as patent) by the University of Vaasa.

1.4 Scientific contribution

The scope, objectives, and research questions addressed by this thesis have been discussed thoroughly in Sections 1.1 and 1.2. The mission, research gaps, agitated questions around the topics, and their implementations are elaborated in the corresponding subsequent chapters. The scientific contributions are highlighted and discussed in Chapter 7 (Conclusion). Nevertheless, they are briefly stated below as follows:

1. A trending state-of-the-art literature review focused on UWB positioning systems.
2. The development of a precise low-cost indoor positioning system that provides accurate navigation solutions in dense industrial environments.
3. The enhancement of GNSS vehicular positioning estimations for commercial-grade receivers in smart phones.
4. Comprehensive literature reviews focused on LEO satellite positioning systems and their recent milestones.
5. Developing a novel LEO-based positioning methodology from LEO satellites and massive MIMO antenna beamforming to provide accurate positioning estimations outdoors. The method that was submitted by the University of Vaasa as an IPR patent application on 12/5/2023.

1.5 Dissertation outline

The rest of dissertation chapters are arranged as follows:

Chapter 2 highlights the importance of developing positioning systems and their role in vital human activities in every day life. In addition, it addresses the deep technical information such as: positioning technologies, ranging methods, positioning algorithms, integration techniques, performance metrics, and accuracy enhancement methods.

Chapter 3 introduces the smart logistic operations and the demand for precise positioning systems. Also, it discusses the merits and challenges of indoor positioning systems with a special focus on UWB technologies and the associated technical aspects.

Chapter 4 shows the implemented indoor positioning system using UWB as the primary technology, and the inertial sensors as the assisting fusion-based sensor. Within this chapter, all the procedures of building a precise UWB-based IPS are discussed in details. Exempli gratia: methodologies, positioning sensor nodes, algorithms, hardware and software configurations, calibration of sensors, route design, and experimental setup.

Chapter 5 discusses the aspects and developments of precise outdoor positioning systems using satellite-based technologies, starting with GNSS. Also, a methodology to achieve precise outdoor positioning using the fusion-based GNSS technology, is presented. The chapter highlights the implementation of the proposed method in a global decimeter challenge in order to enhance smart phones capabilities for outdoor positioning.

Chapter 6 introduces the adoption of LEO satellites in positioning and navigation applications, known as LEO-PNT. In this chapter, a novel methodology is presented to utilize mega LEO satellite constellations in the context of providing a passive positioning and navigation solution to ground users in situations when GNSS signals are denied or impaired. A proof of concept is conducted, followed by a realistic implementation and validation of the new proposed method.

Chapter 7 summarizes the conclusions, the results, and the insights from all articles, in addition to listing all scientific contributions and novelties found in the dissertation. A special section is allocated for the expected future research that can be developed based on the findings of this thesis.

2 PRECISE POSITIONING SYSTEMS

In recent years, the importance of positioning and navigation systems has grown significantly due to the rapid development and affordability of smart devices. Achieving precise localization has been a major concern in the scientific community due to its direct relationship with the reliability of navigational applications and location-based services. In addition to numerous other factors such as: operation and maintenance costs, power budgets, service availability, system integrity, and many others.

Publications **[P1]** and **[P5]** address those concerns thoroughly with key metrics by investigating the existing literature for ways to compromise precise positioning with minimal costs and resources.

2.1 Motivation and prospective applications

Precise location information of people and assets is an essential element for IoT applications and smart logistics (Song, Yu, Zhou, Yang, & He, 2021). The various positioning technologies have been widely adopted by researchers and industrial companies alike during the past decade due to their broad range of applications including: smart logistics (Wu, Shen, Zhao, Li, & Huang, 2022), tracking medical equipment in healthcare centres (Pospelova et al., 2022), tracking individuals in crowded venues (Alarifi et al., 2016), ship-building and offshore industry (Park et al., 2021), and construction industry (Woo et al., 2011).

2.2 Preface on smart logistics and manufacturing

Logistics are important drivers for the competitiveness of industries and material supply. The development of smart logistics, powered by precise positioning and communication technologies can significantly improve the efficiency of logistics. Nowadays, smart logistics are considered a fundamental pillar of Industry 4.0. They enable companies to perform several critical activities, such as demand forecasting, sales planning and inventory management (Tang, 2020; N. Zhang, 2018). Smart logistics or 'Logistics 4.0' promotes the acceleration of all logistics processes through planning and controlling with smart tools, technologies and methods. The use of smart technologies helps to gather the necessary information to monitor and control the material flow and for many other purposes. Through intelligent positioning technologies, tools and equipment, global supply and logistics chains are becoming increasingly efficient and effective (Humayun, Jhanjhi, Hamid, & Ahmed, 2020). Such positioning technologies significantly contribute to end-to-end visibility, improvement in product routing as well as control and replenishment of inventories and mobile assets (Issaoui, Khiat, Bahnasse, & Ouajji, 2019). A generic supply of logistics chain is displayed in Figure 2, which is divided into inbound and outbound supply, and logistics chains.

Smart logistics are considered fairly complex phenomena that can be applied in geographically dispersed areas for tracking materials and goods with relatively low costs. Such a phenomenon is generally characterized by the introduction of new technologies such as: IoT, 5G, sensors, radio frequency identification (RFID) tags, smart products, actuators and intelligent machines (Issaoui, Khiat, Bahnasse, & Ouajji, 2019; Y. Su & Fan, 2020). Smart logistics have the ability, reliability, traceability and authenticity of the information, which are useful to establish intelligent contractual

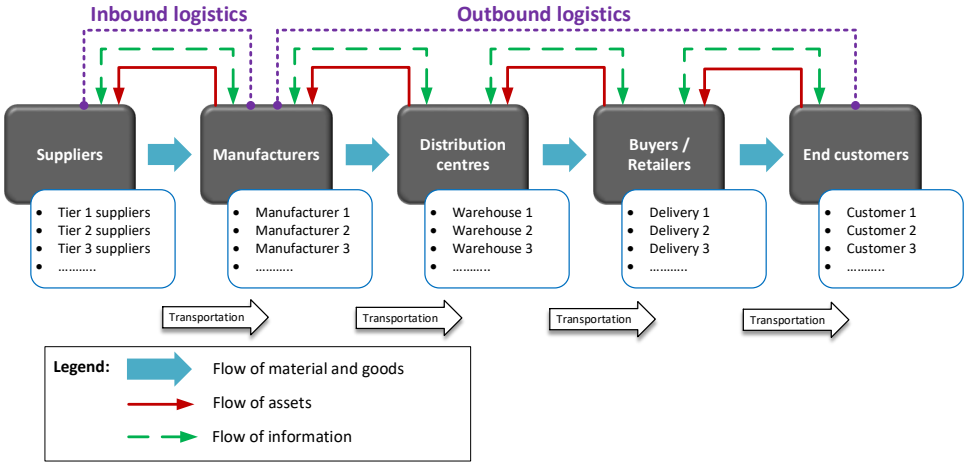

Figure 2. Various stakeholders and the flow of material, assets and information in a generic supply and logistics chain.

relationships among the stakeholders of the supply chains. Moreover, smart logistics include considerable potential for improving the logistics process through the application of communication and information technologies at all levels of the value chain. Figure 3 displays the fundamental elements and functionalities of the smart supply and logistics chain, showing all the way from the supplier till the end-user through smart transportation, smart manufacturing, smart warehousing, and smart delivery stages.

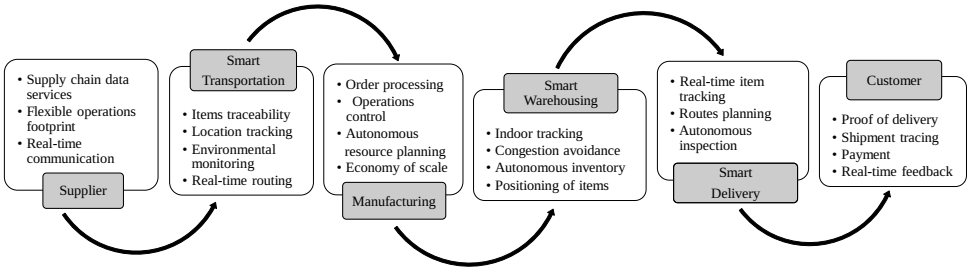

Figure 3. Fundamental elements and functionalities of smart supply and logistics chain.

Figure 3 also shows several activities at each stage in the smart supply and logistics chain. For instance, at the transportation stage, activities such as traceability of items, location tracking and real-time routing are carried out and monitored for smoother operations. Tracking logistic items is an essential issue in today's supply chain and inventory management. In addition, finding items in both indoor and outdoor environments is very crucial in any supply chain and logistics management (Issaoui, Khiat, Bahnasse, & Ouajji, 2020). Owing to the autonomous systems trend, most logistic systems nowadays are operated without the direct involvement of human workforce. In such

a changing environment, smart logistics can be helpful to deliver items through the available precise positioning technologies (Lu, Xu, Zhong, & Wang, 2017; Nantee & Sureeyatanapas, 2021).

Although several technologies are available to provide outdoor positioning for logistics, not every technology is suitable for indoor positioning. In indoor environments such as: warehouses and factory floors, the precision positioning of components, parts and products can be achieved through e.g.: UWB, Wi-Fi, 5G, 3D imaging, sensors and imaging radio signals (Horsmanheimo et al., 2019; Mazhar, Khan, & Sällberg, 2017; Tao & Zhao, 2018). The application of such technologies helps to track indoor logistic assets, which in turn can help in minimizing the time required to locate items and avoid delays caused by the incorrect localization. A precision positioning technique enables the automatic delivery of goods using unmanned ground vehicles and unmanned aerial vehicles (UAVs) to designated locations while reducing environmental influences.

2.3 Role of positioning systems in Industry 4.0

Due to the recent advancements in positioning technologies, a growing interest has surged to utilize location data in logistics and manufacturing. Location data of assets and materials can be used to improve the efficiency, safety and security of manufacturing operations. Real-time tracking of machines and materials yields new possibilities to improve the production processes and track the material flows.

The authors of (Rácz-Szabó et al., 2020) divided logistics units into six identification layers: (0) raw material (items), (1) package, (2) transport unit, (3) unit load (pallet), (4) container and (5) transportation unit (e.g. truck, ship and train). GNSSs are typically used for tracking large containers and transport equipment (the highest layers) in outdoor venues. On the other hand, the smaller cargo units (layers 1-3) are typically handled indoors, which can be tracked using indoor positioning technologies such as: UWB or others. To some extent, UWB is still a relatively expensive and power-consuming technology. But, RFID is a more available technology to track the materials of lower level layers and items.

Real-time location tracking is increasingly attracting global logistics companies due to the need for visibility. Especially, the application of IPSs in logistics and manufacturing has increased recently (Silvia, Martina, Fabio, & Alessandro, 2018). In the case of an indoor environment (e.g. a warehouse), an IPS contributes to tasks such as: minimizing the time spent to look for the right pallet, optimizing routes and preventing accidents. In the case of smart logistics, companies generally use RFID technology, which can track the inventory and identify goods (Bernardini et al., 2021; Lu, Xu, Zhong, & Wang, 2017; Motroni, Buffi, & Nepa, 2021). However, the limited power source of RFID tags minimizes their operational range to a couple of metres. Therefore, they are mainly used for identification rather than positioning purposes. Similarly, Bluetooth and Wi-Fi are also used for indoor positioning, but their operating ranges are no more than 3-5 m (Montoliu, Sansano, Gascó, Belmonte, & Caballer, 2020).

To obtain accurate positioning of logistics items, companies are recently exploring UWB-based positioning systems, which enable real-time positioning of goods, assets and people with an accuracy level of 5 to 30 cm. It can provide out-of-the-box localization with higher ranging accuracy than Wi-Fi, Bluetooth, or other active radio solutions (Ridolfi, Vandermeeren, et al., 2018; Zou, 2011).

In the case of autonomous robots operating in indoor environments (e.g. warehouses), accurate positioning is essential for indoor navigation. For outdoor smart logistics (e.g. smart delivery or shipping) that require reliable positioning and navigation systems, GNSSs are foreseen to be the best

integrated positioning solutions for outdoor tasks. While GNSS-based localization is mostly reliable in outdoor operations, it is unreliable in indoor environments, hence, localization by UWB technology can accelerate the adoption and ubiquity of distributed robotics systems. Nowadays, UWB-based technology is commonly used in indoor robotic applications from home cleaning to warehouse transportation, including the rapidly emerging autonomous last-mile delivery solutions (Silvia, Martina, Fabio, & Alessandro, 2018).

In the case of intelligent manufacturing, it is essential to track the parts along the production chain to take the right decisions. Real-time tracking of both stationary and moving parts in the production floor ensures safer operation with a reduced lead time (Cheng, Kuo, Lam, & Petering, 2021; Helo & Shamsuzzoha, 2020). In addition to parts, it is also important to track workers' movement on the production floor to enhance operational flexibility. For indoor smart manufacturing, UWB-based location technology is a prominent candidate due to its inherent accuracy and reliability (Barbieri, Brambilla, Trabattoni, Mervic, & Nicoli, 2021; Krishnan & Santos, 2021).

2.4 Existing positioning solutions

Modern positioning solutions are numerous and various. Most of nowadays positioning systems are based on one or more of the following technological foundations: space systems, acoustic systems, optical systems, wireless radio systems, inertial systems, and passive systems.

A comprehensive survey by Asaad and Maghdid stated some examples on: the main technological basis of modern positioning systems, the most commonly used positioning sensors, their techniques, the use case environments, the tagged devices or objects, and the performance metrics that can assess those positioning systems. Figure 4 summarizes most of the utilized elements in modern positioning systems.

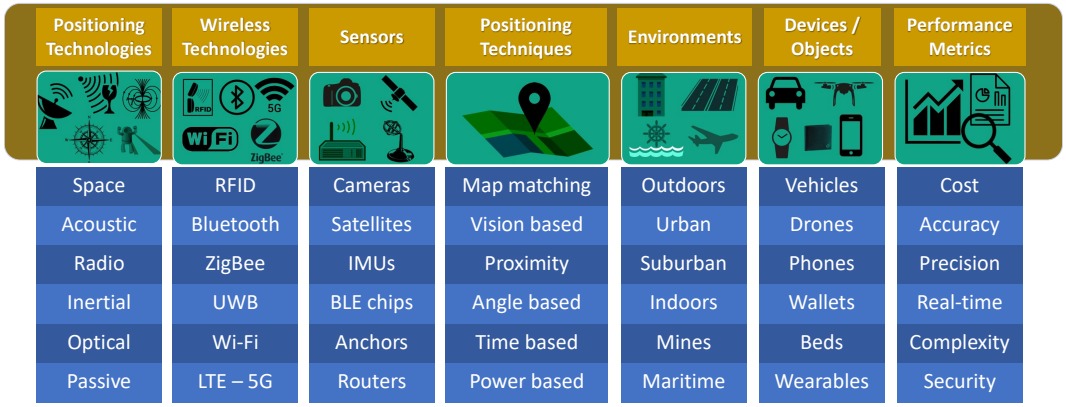

Figure 4. Summarized elements of existing positioning systems, adapted from (Asaad & Maghdid, 2022).

Recently, the utilization of wireless positioning technologies witnessed a positive surge; owing to their advantages in performance metrics, their established infrastructure, and their popularity. Such as: GNSS, Bluetooth, Wi-Fi, UWB, ZigBee, and 5G.

A given positioning system may accommodate a single or several elements of the following: sensors, techniques, technologies, and devices, and can be used in multiple environments. The elements highlighted in Figure 4 are further discussed in more details in the subsequent sections.

2.5 Performance metrics of positioning systems

In publications **[P1]** and **[P5]**, the performance metrics of both indoor and outdoor positioning systems were discussed, e.g. in UWB and GNSS, respectively.

The performance of localization technologies can be assessed using a pyramid-like scheme with system accuracy as the baseline, integrity as the second metric, continuity as the third, and availability as the peak paramount (N. Zhu, Marais, Bétaille, & Berbineau, 2018), see Figure 5. System accuracy is the degree of conformance of the estimated positioning values to the ground truth. The integrity of localization systems, as defined by N. Zhu et al., is the trustworthiness of the information provided by the navigation engine. Continuity is the probability of the system to maintain the desired service level within the operation period, while availability is the percentage of time in which the navigation engine is up-running for positioning and can be used by its intended users.

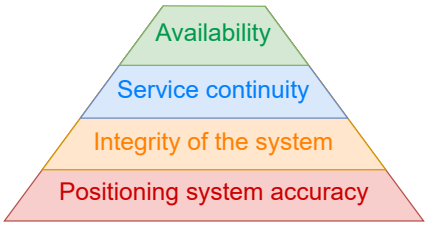

Figure 5. Performance metrics of positioning systems.

Accuracy of the estimated position is one of the most important performance metrics for positioning systems. Accuracy is often reported as the error distance between the estimated and actual locations. While, a location precision is reported in percentages of position information, which should be within the acceptable range(s) of accuracy. The most commonly used metrics of accuracy and location precision are the root mean square error (RMSE), the mean absolute error (MAE), the distance mean square error, and circular error probability.

The accuracy of the location estimate depends on the accuracy of individual measurements and the mutual geometry of the system network nodes (e.g. tag and anchors). In the time of arrival (TOA) and time difference of arrival (TDOA) methods, the accuracy of the position is expressed as the product of a geometric factor and a range measurement error factor.

In addition to the above mentioned metrics, there are other performance metrics presented in literature, such as scalability, cost, coverage, availability, and privacy (Alarifi et al., 2016). The scalability of IPS describes how many tags the system can support per time unit per geographic area. The cost measures the physical limitations and requirements associated with the implementation of a particular technology in terms of technical and financial resources. Money, power consumption and hardware dimensions are examples of cost metrics. Privacy is a concern in network-centric systems, where the location estimation takes place in the server. In the self-positioning model the device estimates its own position, and no one else may know where the device is.

Coverage as a metric, describes the coverage area or range of the positioning technology, and the ”Availability” describes how often a system is found to be available for positioning by its intended users. Data privacy is a challenge for positioning systems since it is very crucial to secure the positioning data of users and assets especially in sensitive applications, however, it is not yet adopted as a performance metric.

2.6 Positioning techniques

Mainly and commonly, the positioning solution can be determined via multiangulation or multilateration techniques. When using multiangulation, the unknown position of the movable tag (user) can be evaluated from known anchors positions geometrically by observing the angle of the received signal. While in multilateration, the pseudoranges between the anchors and the tags are obtained by measuring the time of flight (TOF) of the signal and then multiplying it by the value of the speed of light or by applying a channel attenuation model to the received signal strength (RSS) observations. Figure 6 shows the difference between multilateration and multiangulation techniques and how the positioning process is carried out.

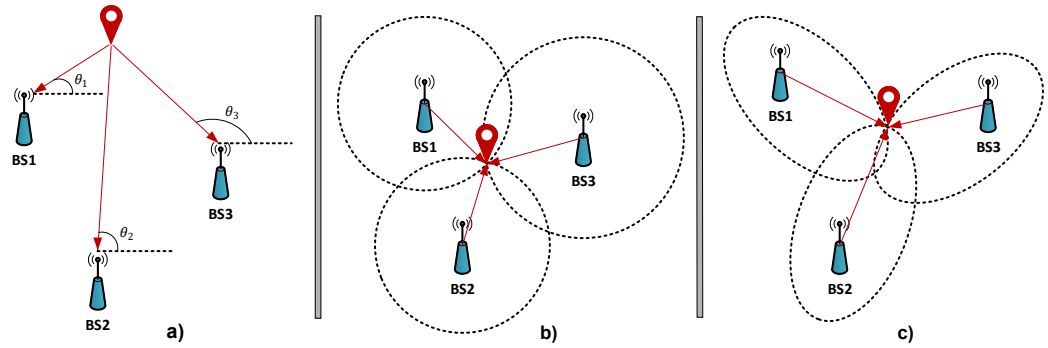

Figure 6. (a) Multiangulation and (b & c) multilateration ranging techniques between the wireless base stations (anchors) of positioning systems.

2.6.1 Multi-angulation

In multiangulation techniques, the position of an object can be estimated from the angle of arrival (AOA) or the angle of departure (AOD) of the signal. Each angle measurement defines a line between the base station and a mobile device. The object's location is determined from the intersection of these lines, as illustrated in Figure (6a). The solution would not be unique, in general.

In the AOA method, the tag transmits a signal using a single antenna, and the anchor (base station) receives the signal with an antenna array. The signal direction is determined from different propagation delays of the signal between multiple antennas of the receiver antenna array and the single transmitter antenna.

In the AOD method, there is a single antenna at the receiver and multiple antennas arranged in an array at the transmitter. Usually, the anchor (beacon) transmits the signal, and the tag receives it. The signal direction is determined from different propagation delays of the signal between multiple antennas of the transmitter antenna array and the single receiving antenna.

The advantage of AOA or AOD observables is the non compulsory time-synchronization of the anchor clocks. However, the antennas have to be precisely calibrated to the correct orientation angles. The AOA can be measured with various techniques, but currently, antenna arrays are mostly used in positioning systems.

In UWB, there exists a significant advantage of using phase difference-based AOA estimation. Due to the short duration of the pulse, the UWB receiver can separate the direct signal from the reflected signal better than the receiver of the narrowband signal (Dotlic, Connell, Ma, Clancy, & McLaughlin, 2017).

2.6.2 Multi-lateration

Multilateration methods can be categorized to two types: time-based and power-based multilateration.

In time-based multilateration techniques, the positioning is carried out by measuring the time taken for a radio frequency (RF) signal transmitted by an emitter to reach a receiver, that is, TOF. Due to the inevitable signal propagation delay, the time interval is multiplied by the speed of light to obtain the distance between the emitter and the receiver.

Multilateration based systems determine the position of mobile users based on the range (or pseudo range) from the mobile transceiver to at least three (3D) anchors at known locations using several strategies.

The following strategies are commonly used for estimating the TOF needed for multilateration:

- Time of arrival (TOA): The multilateration is performed as in Figure (6b), whereas the TOA of the signal is measured and subtracted from the known transmission time. The arrival timestamps are obtained by either using a precise clock (synchronous TOA) or by solving them together with the tag position by using at least $N + 1$ anchors, where N is the number of spatial dimensions. The latter method is used in GNSS systems and is known as the pseudorange method. The clock synchronisation accuracy of the sub-nanosecond range is not feasible for moving targets (Carbone et al., 2013; Soganci, Gezici, & Poor, 2011), and therefore, the pseudorange method is typically used.
- Round trip time (RTT): The RTT of signal propagation between two objects is measured, and the processing time is reduced to obtain double TOF. This method is also called two-way ranging (TWR) or two-way TOA (TW-TOA), see Figure 7. The measurement is repeated between a tag and at least N anchors. This method is sometimes called asynchronous TOA. (Shule, Almansa, Queralta, Zou, & Westerlund, 2020)
- Time of transmission (TOT): The arrival time of the signal sent by a tag is observed by at a minimum of $N + 1$ anchors, and the TOT is solved together with the position of the tag.
- Time difference of arrival (TDOA): The signal transmitted by the tag is received by at least $N + 1$ anchors, which calculate the time differences of arrival times between anchors, avoiding the need for absolute time synchronization in a tag. In TDOA, due to incorporating time

differentials, the approximated shape of an anchor range is considered hyperbolic, as seen from Figure (6c).

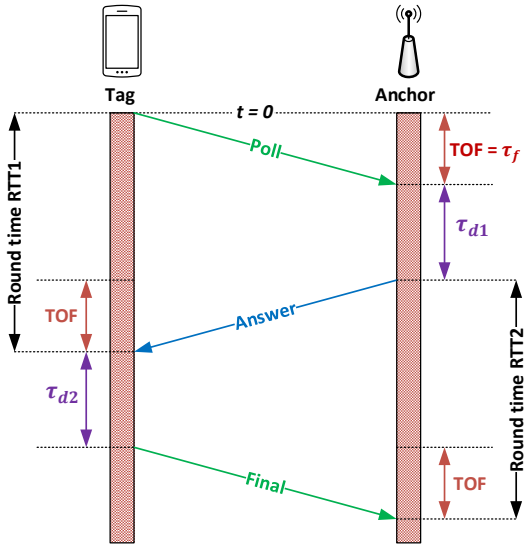

Figure 7. The DS-TWR method estimates signal TOF and cancels the effects of clock offsets and drifts.

The double-sided two-way ranging (DS-TWR) method employed in many IPSs (shown in Figure 7) can be represented by Equation (2.1).

$$\tau_f = \frac{1}{4}\left(\tau_{RTT1} - \tau_{d1} + \tau_{RTT2} - \tau_{d2}\right) \tag{2.1}$$

where τ_{RTT1} is the RTT measured by the tag, and τ_{RTT2} is that measured by the anchor. The terms τ_{d1} and τ_{d2} are the reply times of the anchor and the tag, respectively. τ_{RTT1} and τ_{d2} are measured using the tag oscillator, and both measurements are biased by the oscillator offset of the tag. Similarly, τ_{RTT2} and τ_{d1} are biased by the oscillator offset of the anchor. Double-sided TWR cancels these oscillator offsets.

Another type of multilateration techniques is the RSS method. The measurement of RSS is straightforward and is performed in most radio receivers. The general rule of thumb in this method is that the RSS decreases as the receiver–transmitter distance increases. This phenomenon can be used to estimate the location of a mobile device from the RSS measurements either by trilateration or location fingerprinting.

In fact, radio signal attenuation is not only affected by the distance between the transmitter and receiver but also by multipath interference and any obstructions on the line of sight (LOS) of signal path. Thus, IPSs seldom compute the object position by using geometric range estimates derived from RSS only (Pittet, Renaudin, Merminod, & Kasser, 2008). Instead, RSS-based IPSs use location fingerprinting more often, which involves recording RSS heat maps of the region of interest and transfer them via learning algorithms to the positioning engine.

Therefore, performing and applying the positioning ranging techniques cannot sufficiently achieve the accurate positioning estimations on their own, rather, positioning algorithms should be used for post-processing the results of the positioning techniques, which are presented and discussed in Section 2.7.

2.6.3 Passive positioning (device free)

To this point, all the discussed positioning techniques are considered active methods, where the nodes (anchors) and users (tags) are transmitting and receiving signals. However, the positioning estimation can also be determined by passive methods in which the communication system attributes of a positioning network are being monitored and observed passively (Blazek, Jiranek, & Bajer, 2019; Youssef, Mah, & Agrawala, 2007).

For example, both magnitude and phase of the channel state can be monitored, in addition to signal reflections from walls to infer the position of the target without bearing any devices (Kaltiokallio, Bocca, & Patwari, 2012). Also, device-free positioning can be achieved via special arrangement; where a tag listens passively to the positioning messages sent by the anchors simultaneously (Corbalán, Picco, & Palipana, 2019). These methods are also known as device-free positioning since there are no requirements for specific hardware held by the target user. But, passive monitoring is not as accurate as active positioning, besides, the simultaneous positioning message method requires special hardware.

Passive and device-free methods are still under research. Although, their performance is lagging behind the active positioning methods and they are more prone to environmental changes and variation, some use cases can benefit from the passive nature of this positioning method e.g. privacy-centric applications as in (Kaltiokallio, Bocca, & Patwari, 2012).

2.7 Positioning algorithms

The user location can be estimated via processing the observables (i.e. observed measurements) inbound from the various positioning techniques, as discussed in Section 2.6. However, when the position is estimated using the measurements of a single time epoch, it yields a static positioning value, whereas the previous or future measurements are not accounted. Hence, the dynamic positioning solutions become a nonlinear differential matter. The most common approach to solve a nonlinear system of equations is to use optimization methods such as: the iterative Gauss-Newton methods, or Bayesian filters such as: Kalman filter (KF) or Particle filters (PF). Alternatively, the position can be estimated using closed-form solutions or methods based on likelihoods or uncertainty probability.

Static positioning is not an optimal solution in most situations as it does not account for the dynamic state model of the target. Commonly, a Kalman or Particle filter provide a better position estimate, as they use the time series of the measurements for computing the current state estimate by comparing to a previously specified kinematic model.

In this section, the technical aspects and mathematical formulas of the most commonly used positioning algorithms in navigation and location-based applications, are highlighted.

2.7.1 Gauss-Newton methods

The over-determined system of equations can be solved using optimization methods such as Gauss-Newton (GN) algorithms. The linearization of GN algorithms is based on Taylor-series expansion, it is also called the Taylor algorithm. In this algorithm, the final user position is determined using an iterative process starting from an approximate position or an initial assumption. The main step of GN algorithm is to penalize the squared error cost-function, that is, the least square (LS) method (Hostettler & Särkkä, 2020).

Assume the general form of linear models is denoted as in Equation (2.2):

$$\mathbf{y} = \mathbf{G}\,\mathbf{x} + r, \tag{2.2}$$

where $\mathbf{y}$ is the observation vector, $\mathbf{x}$ is the state vector, $\mathbf{G}$ is the parameter matrix, and r is the residual (error) vector. The cost function of the LS algorithm can be formulated as in Equation (2.3):

$$J_{LS}(\mathbf{x}) = (\mathbf{y} - \mathbf{G}\mathbf{x})^T(\mathbf{y} - \mathbf{G}\mathbf{x}). \tag{2.3}$$

The true distance between the anchor *i* and the tag is as given in Equation (2.4):

$$d_i = \sqrt{(x_i - x_u)^2 + (y_i - y_u)^2 + (z_i - z_u)^2}, \tag{2.4}$$

where (x_i, y_i, z_i) is the position of the *i*-th anchor and (x_u, y_u, z_u) is the position of the tag. By linearizing Equation (2.4) using Taylor-series expansion (C.-S. Chen, 2017) and omitting the second-order and higher terms by performing partial derivative $\frac{\partial J_{LS}(\mathbf{x})}{\partial \mathbf{x}}$, the LS solution to the position estimation problem is obtained from Equation (2.5): (Hartikainen, Solin, & Särkkä, 2011)

$$\hat{\mathbf{X}}_{\mathbf{LS}} = (\mathbf{G}^{\mathbf{T}}\mathbf{G})^{-1}\mathbf{G}^{\mathbf{T}}\mathbf{y}. \tag{2.5}$$

The ordinary LS method described above assumes that the behaviour of error variance in each measurement is unchanged. Hence, the method of weighted least squares (WLS) can be used when the error variances of the measurements are changing over time. WLS method weighs the observations by the reciprocal of the error variance $w_i = 1/\sigma_i^2$ for the given observation. The weight matrix is calculated using Equation (2.6):

$$\mathbf{W} = \begin{bmatrix} \omega_1 & 0 & 0 & 0 \\ 0 & \omega_2 & 0 & 0 \\ \vdots & \vdots & \ddots & \vdots \\ 0 & 0 & \dots & \omega_L \end{bmatrix}. \tag{2.6}$$

The WLS cost function penalizes the weighted squared error using the **W** matrix, as shown in Equation (2.7).

$$J_{WLS}(\mathbf{x}) = (\mathbf{y} - \mathbf{G}\mathbf{x})^T \mathbf{W}^{-1} (\mathbf{y} - \mathbf{G}\mathbf{x}). \tag{2.7}$$

Thus, the WLS estimation solution is obtained from Equation (2.8):

$$\hat{\mathbf{X}}_{\mathbf{WLS}} = (\mathbf{G}^{\mathbf{T}} \mathbf{W}^{-1} \mathbf{G})^{-1} \mathbf{G}^{\mathbf{T}} \mathbf{W}^{-1} \mathbf{y}. \tag{2.8}$$

A special case of the WLS algorithm is the regularized least square (ReLS) estimator, which includes some additional information on the expected statistical behaviour of the density function. ReLS proceeds by incorporating the initial guesses for the mean (**m**) and the covariance (**P**) vectors, as presented in Equations (2.9) and (2.10).

$$J_{ReLS}(\mathbf{x}) = (\mathbf{y} - \mathbf{G}\mathbf{x})^T \mathbf{W}^{-1} (\mathbf{y} - \mathbf{G}\mathbf{x}) + (\mathbf{x} - \mathbf{m})^T \mathbf{P}^{-1} (\mathbf{x} - \mathbf{m}). \tag{2.9}$$

$$\hat{\mathbf{X}}_{\mathbf{ReLS}} = (\mathbf{G}^{\mathbf{T}} \mathbf{W}^{-1} \mathbf{G} + \mathbf{P}^{-1})^{-1} (\mathbf{G}^{\mathbf{T}} \mathbf{W}^{-1} \mathbf{y} + \mathbf{P}^{-1} \mathbf{m}). \tag{2.10}$$

In fact, the ReLS estimator method paved the way for the emergence of Kalman filters, as they both share similar optimization approaches in terms of minimizing the cost function, however, Kalman filters are considered a type of Bayesian estimators. More details are discussed in Section 2.7.4.

2.7.2 Dead reckoning

Dead reckoning (DR) is widely used in positioning and navigation applications even before the invention of modern localization systems. Nowadays, the most common implementation of DR is the pedestrian dead reckoning (PDR) algorithm which is employed by numerous location-based applications.

The operating principle of the DR algorithm is simple and intuitive. Basically, the kinematics of a mobile user are approximated to a line motion course, where the previous known velocity and heading attitudes (from the past) are considered to be also valid in the future (posterior) estimates. Thus, by knowing the location of the starting point (initial state) in a certain coordinate system, the new position estimation can be roughly inferred over time.

A set of mathematical representations of the DR algorithm is shown in Equations (2.11).

$$\begin{aligned} D_k &= \sqrt{(p^x_{k-2} - p^x_{k-1})^2 + (p^y_{k-2} - p^y_{k-1})^2}, \\ \phi_k &= \arctan2\left(\frac{p^y_{k-2} - p^y_{k-1}}{p^x_{k-2} - p^x_{k-1}}\right), \\ p^x_k &= p^x_{k-1} + D_k \cos(\phi_k), \\ p^y_k &= p^y_{k-1} + D_k \sin(\phi_k). \end{aligned} \tag{2.11}$$

where p^x_k and p^y_k are the x-y positions at time instant k, D_k and ϕ_k are the calculated Euclidean

distance and the heading angle from the previous two x-y positions, respectively.

This technique was heavily used by navigating vessels and nomad travellers in the pre-GNSS era, without considering other kinematic variables or dynamics arising from external factors. In modern navigation applications, the DR algorithm could be used as a standalone positioning system or to fix the null and invalid values arriving from motion sensor readings by incorporating the previous non-null values and the heading angle into the DR estimation of the current missing epoch.

2.7.3 Bayesian filters

The Bayesian algorithm is a class of probabilistic filtering algorithms used for state estimation in systems with uncertain observations and dynamics. Recursive Bayesian state estimation, or a Bayes filter is an abstract concept for tracking object's position in kinematic cases by combining a dynamic state model with observations. Bayesian filters recursively update the posterior belief to the current state, as in Equation (2.12):

$$\mathrm{Bel}(x_k) = p(x_k|\, y_{0..k-1}). \tag{2.12}$$

where x_k is the current state vector and y_k are the observations vector.

Practical implementations require the definition of dynamic and perceptual models, and the representation of beliefs. Depending on the implementation, the properties of Bayes filters can differ (Fox, Hightower, Liao, Schulz, & Borriello, 2003). The most common implementations are different variations of Kalman Filters, Particle Filters and factor graph optimizations.

The prediction is based on the predict and update steps. In the predict step, the belief is updated using the system dynamic model as in Equations (2.13) and (2.14):

$$\mathrm{Bel}^{-}(x_k) = \int p(x_k|\, x_{k-1})\, \mathrm{Bel}(x_{k-1})\, \mathrm{d}x_{k-1}, \tag{2.13}$$

In the update step, the predicted belief is updated using the sensor information y_k (measurements):

$$\mathrm{Bel}^{+}(x_k) = \frac{p(y_k|x_k)}{p(y_k)}\ \mathrm{Bel}^{-}(x_k). \tag{2.14}$$

The history of Bayesian filters dates back to the 1960s when Rudolf E. Kálmán developed the Kalman filter that revolutionized various fields. Bayesian filters (e.g. Kalman) provided a computationally efficient solution for state estimation problems in linear dynamic systems with Gaussian noise (Kalman, 1960). Another significant development was implemented in the 1990s with the introduction of particle filters as an estimation method for nonlinear and non-Gaussian state-space estimation problems (Doucet, Gordon, & Krishnamurthy, 2001).

Bayesian filters provide a principled framework for state estimation by incorporating prior knowledge, sensor measurements, and system dynamics (Särkkä, 2013). They offer robustness to uncertainties and nonlinearity inherent in real-world systems. Their flexibility and interpretability made them very efficient in fields where the accurate estimation of system states is critical.

Consequently, Bayesian filters are embedded in numerous applications within the fields of: robotics, signal processing, finance, navigation, healthcare, and more (Bongard, 2008). For example, in robotics, Bayesian filters are used for localization, mapping, trajectory prediction, and motion planning. In finance, their applications are in: stock price prediction, portfolio optimization, and risk management. In healthcare, Bayesian filters are used for patient monitoring, diagnosis, and predictive modeling (Bongard, 2008).

2.7.4 Kalman filters

The Kalman filter is a recursive Bayesian filter that estimates the state of a linear dynamic system from a series of noisy measurements. It recursively updates its estimates based on new measurements, incorporating both the predictions from the system dynamics and the observed measurements, while considering the uncertainty associated with both the state and the measurements. The Kalman filter maintains a probability distribution over the state variables and updates this distribution using Bayesian inference.

While Kalman filters involve elements of Gauss-Newton optimization methods, such as minimizing the regularized least squared error (see Equations (2.9) and (2.10)) between the predicted and the observed states, they perform within the framework of Bayesian inference rather than optimization methods. The Kalman filter explicitly models the probability distributions of the state variables and updates these distributions using Bayes' theorem, which is the climax of Bayesian filtering techniques.

In contrast, Gauss-Newton methods are optimization techniques used to find the minimum of a function, e.g. typically the least squares function. It is not inherently Bayesian and does not explicitly model probability distributions. Thus, the Kalman filter is primarily considered a Bayesian filter rather than a Gauss-Newton method, although it does involve elements of both. In other words, despite the fact that a Kalman filter shares some similarities with optimization methods like Gauss-Newton in minimizing errors, it is fundamentally a Bayesian filter due to its reliance on Bayesian inference for state estimation.

The linear Kalman algorithm predicts future states in linear state-space systems whose noise models are additive white Gaussian in nature (Kalman, 1960). The algorithm is based on predicting the prior knowledge (the mean $m_{\bar{k}}$ and covariance $P_{\bar{k}}$) to estimate the posterior states by evaluating the filter gain (i.e. Kalman gain K_k) and the measurement residuals error (V_k and S_k) to infer the new state (m_k) and covariance (P_k) vectors and use them as input to the next iteration (Darbellay, 1999; Faragher, 2012; Hartikainen, Solin, & Särkkä, 2011; Kalman, 1960). The output state-space estimation ve

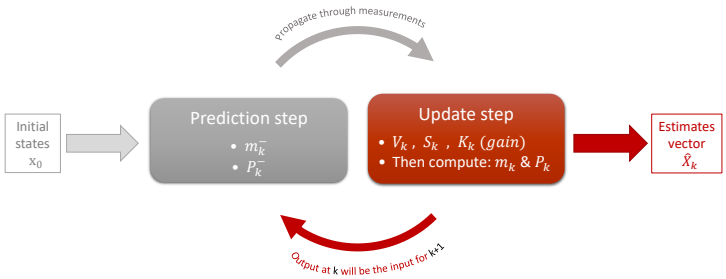

Figure 8. Steps of the Kalman filter algorithm.

For example, in case the linear Kalman filter is employed for positioning estimations, the vector-form Kalman algorithm becomes as follows:

The state vector of the linear Kalman filter may comprise the position, the velocity, and acceleration of the moving object, as shown in Equation (2.15):

$$\mathbf{x} = \begin{bmatrix} p^x & v_x & a_x & p^y & v_y & a_y \end{bmatrix}^T. \tag{2.15}$$

where p^x, p^y are the Cartesian positions, v_x, v_y are the velocities, and a_x, a_y are the accelerations.

Depending on the observation gauges, the measurement vector could comprise either the positions $[p^x, p^y]$, or the velocities $[v_x, v_y]$, or the accelerations $[a_x, a_y]$.

The model equations of motion could be selected by the IPS designer based on many factors that affect the given use cases. Commonly, the Newtonian equations of motion are considered for predicting the iterative position, velocity, and acceleration, as shown in Equations (2.16)–(2.18):

$$x_{k+1} = x_k + \Delta t \dot{x}_k + \frac{\Delta t^2}{2} \ddot{x}_k + \frac{\Delta t^3}{6} \dddot{x}_k, \tag{2.16}$$

$$\dot{x}_{k+1} = \dot{x}_k + \Delta t \ddot{x}_k + \frac{\Delta t^2}{2} \dddot{x}_k, \tag{2.17}$$

$$\ddot{x}_{k+1} = \ddot{x}_k + \Delta t \dddot{x}_k, \tag{2.18}$$

Where Δt is the time step. Considering the Newtonian equations of motion as the kinematic model for Kalman filter, the dynamic model can be written as in Equation (2.19):

$$\begin{bmatrix} x_{k+1} \\ \dot{x}_{k+1} \\ \ddot{x}_{k+1} \\ y_{k+1} \\ \dot{y}_{k+1} \\ \ddot{y}_{k+1} \end{bmatrix} = \begin{bmatrix} 1x_k + \Delta t \dot{x}_k + \frac{\Delta t^2}{2} \ddot{x}_k + \frac{\Delta t^3}{6} \dddot{x}_k \\ 0x_k + 1\dot{x}_k + \Delta t \ddot{x}_k + \frac{\Delta t^2}{2} \dddot{x}_k \\ 0x_k + 0\dot{x}_k + 1\ddot{x}_k + \Delta t. \dddot{x}_k \\ 1y_k + \Delta t \dot{y}_k + \frac{\Delta t^2}{2} \ddot{y}_k + \frac{\Delta t^3}{6} \dddot{y}_k \\ 0y_k + 1\dot{y}_k + \Delta t \ddot{y}_k + \frac{\Delta t^2}{2} \dddot{y}_k \\ 0y_k + 0\dot{y}_k + 1\ddot{y}_k + \Delta t \dddot{y}_k \end{bmatrix}. \tag{2.19}$$

The state transition matrix **F** becomes as in Equation (2.20):

$$\mathbf{F} = \begin{bmatrix} 1 & \Delta t & \frac{\Delta t^2}{2} & 0 & 0 & 0 \\ 0 & 1 & \Delta t & 0 & 0 & 0 \\ 0 & 0 & 1 & 0 & 0 & 0 \\ 0 & 0 & 0 & 1 & \Delta t & \frac{\Delta t^2}{2} \\ 0 & 0 & 0 & 0 & 1 & \Delta t \\ 0 & 0 & 0 & 0 & 0 & 1 \end{bmatrix}. \tag{2.20}$$

Depending on the observed quantities, the measurements matrix H can be formulated accordingly. For example, if the Cartesian positions $[x, y]$ and accelerations $[\ddot{x}, \ddot{y}]$ are measured and imported to

the Kalman algorithm, then the measurement matrix $\mathbf{H}$ becomes as in Equation (2.21):

$$\mathbf{H} = \begin{bmatrix} 1 & 0 & 0 & 0 & 0 & 0 \\ 0 & 0 & 1 & 0 & 0 & 0 \\ 0 & 0 & 0 & 1 & 0 & 0 \\ 0 & 0 & 0 & 0 & 0 & 1 \end{bmatrix}. \tag{2.21}$$

Consequently, the iterative state-space Kalman filter algorithm for positioning proceeds as in Equation (2.22):

$$\begin{aligned} \mathbf{x_{k+1}} &= \mathbf{F_k}\,\mathbf{x_k}, \\ \mathbf{y_k} &= \mathbf{H_k}\,\mathbf{x_k}. \end{aligned} \tag{2.22}$$

where $\mathbf{x_{k+1}}$ is the new updated state vector, $\mathbf{x_k}$ is the current state vector, and $\mathbf{y_k}$ is the current generated measurement vector. $\mathbf{F_k}$ is the state transition matrix, and $\mathbf{H_k}$ is the measurement matrix.

2.7.5 Extended Kalman filter

The extended Kalman filter (EKF) is an adapted version of the ordinary linear Kalman filter to estimate states in nonlinear dynamic systems (Bar-Shalom, Li, & Kirubarajan, 2001). All types of Kalman filters have to venture through two major steps: 1) prediction step, where the next state of the system is predicted given the previous measurements fed to the system, and 2) update step, where the current state of the system is estimated given the measurement performed at the active time step (Bar-Shalom, 1989; Hartikainen, Solin, & Särkkä, 2011). Then, the Kalman filter algorithm is used to satisfy the equations of state-space estimation in Equations (2.23) as follows:

$$\begin{aligned} x_k &= f(x_{k-1},\ k-1) + q_{k-1}, \\ y_k &= h(x_k,\ k) + r_k. \end{aligned} \tag{2.23}$$

where x_k and y_k are the state and measurement vectors of the system at time step *k* and q_{k-1} and r_k are the process and measurement noises at time step *k-1*, where $q_{k-1} \sim N(0, Q_{k-1})$ and $r_k \sim N(0, R_k)$, $f(.)$ and $h(.)$ are the nonlinear functions of model dynamics and measurement, respectively.

The state transition matrix $\mathbf{F}$ and the measurement matrix $\mathbf{H}$ in the linear Kalman filter (see Table 2) are replaced in EKF by the nonlinear state transition function $f(.)$ and nonlinear measurement function $h(.)$, respectively.

The nonlinearity in the EKF algorithm arises from either the state transition function $f(.)$ or the measurements function $h(.)$, or both. Hence, the Jacobean transform is considered for linearizing either functions by taking the partial derivative with respect to the state vector e.g.: $\frac{\partial f(x,k)}{\partial x_k}$ and $\frac{\partial h(x,k)}{\partial x_k}$.

The vector notation approximation resulted from mapping the given nonlinear space through an approximated Gaussian distribution allowed the state-space estimation procedures under nonlinear conditions. The complete Kalman algorithm for nonlinear systems is demonstrated in Table 2, adapted from (Hartikainen, Solin, & Särkkä, 2011).

Table 2. EKF algorithm for nonlinear systems.

0 Initialization	for $k = 0$ set $\hat{X}_0, P_0^-, Q_0, R_0$	
1 Prediction step	Prior estimate of the state:	$m_k^- = f(m_{k-1}, k-1)$
	Prior estimate of the covariance:	$P_k^- = F_x(m_{k-1}, k-1)P_{k-1}{F_x}^T(m_{k-1}, k-1) + Q_{k-1}$
2 Update step	Measurement residual update:	$V_k = y_k - h(m_k^-, k)$
	Measurement covariance update:	$S_k = H_x(m_k^-, k)\ P_k^-\ {H_x}^T(m_k^-, k) + R_k$
	Kalman gain calculation:	$K_k = P_k^-\ {H_x}^T(m_k^-, k)\ S_k^{-1}$
	Updating the posterior state:	$m_k = m_k^- + K_k V_k$
	Updating the posterior covariance:	$P_k = P_k^- - K_k S_k K_k^T$
	Return to step 1, repeat until k iterations are consumed.	
Output	Estimated state vector: $\hat{X}$	

whereas $m_{\bar{k}}$ and $P_{\bar{k}}$ are the predicted mean and covariance of the state, respectively, at time step *k* before checking the measurement, and m_k and P_k are the estimated mean and covariance of the state at the time step *k* after checking the measurement. y_k is the measurements vector of the system at the time step *k*. S_k is the measurement prediction covariance at the time step *k*. K_k is the filter gain (i.e. the prediction correction coefficient at the time step *k*). $f(.)$ and $h(.)$ are the nonlinear functions of the model dynamics and the measurements, respectively.

Another adaptation for Kalman filters to operate on nonlinear spaces is the sigma-point approximations, as shown in Figure 9. Where the sigma-point Gaussian transformation proceeds by mapping a set of selected points (samples or sigma points) from the given space (i.e. the nonlinear function) to form an approximation of a newly constructed Gaussian space that resembles those sigma points.

In other words, while the EKF approximation relies only on one point (i.e. the mean), the sigma-point Kalman filters use more than one point including the distribution mean.

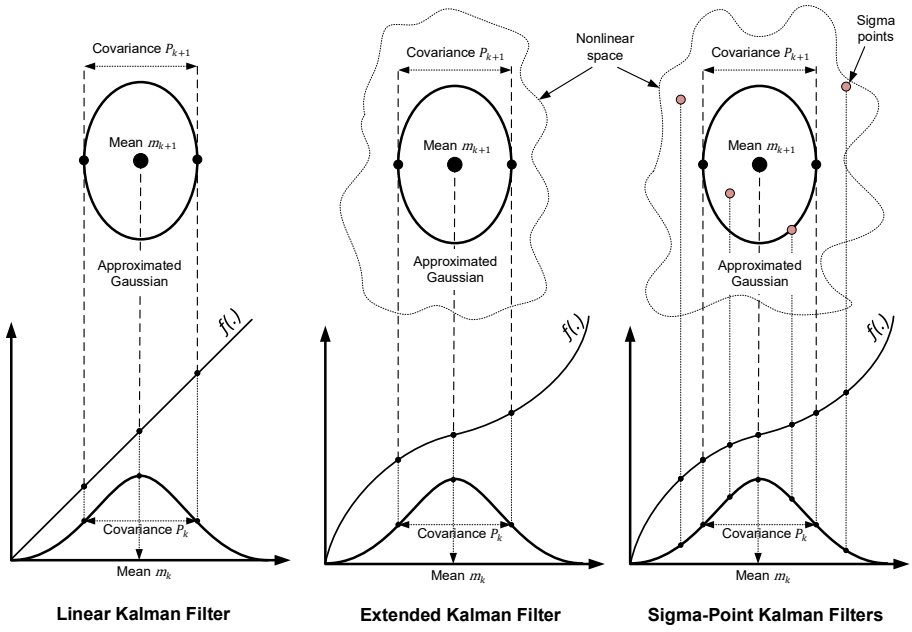

Figure 9. Types of Kalman filters in linear and nonlinear space estimations.

Types of sigma-point Kalman filters are: the unscented Kalman filter (UKF) and the Cubature Kalman filter (CKF), depending on the weighing principle of selecting the sigma points. In UKF, the algorithm selects additional weighted points (i.e. sigma points) in addition to the mean point for more accurate transformation, this procedure is called the unscented transform (Hartikainen, Solin, & Särkkä, 2011; Julier & Uhlmann, 2004; Sarkka, 2007). Thus, UKF occasionally outperforms EKF in severely nonlinear systems, while EKF performs sufficiently well in systems with modest nonlinearities (Ullah, Shen, Su, Esposito, & Choi, 2020).

2.7.6 Particle filters

Particle Filter (PF) is another type of Bayesian filters for state-space estimations. PF is one of the popular choices for positioning estimations because it can be used for solving the dynamic system problem shown in Equation (2.23) without requiring the dynamic systems to be either linearized or Gaussian systems. However, it is also possible to implement a PF that assumes Gaussian posterior distribution if a bootstrap or a restricted version is used (Vemula, Bugallo, & Djuric, 2007). The reasons for using PF are that the conditions of linearity and Gaussian noise do not hold very often, and linearization is only possible if the model is well known (Kitagawa, 1998; Vemula, Bugallo, & Djuric, 2007).

PF estimates the posterior belief $\mathrm{Bel}(x_k)$ of the dynamic system model through a sequential Monte Carlo (SMC) algorithm. The SMC is a similar algorithm to EKF without resorting to neither linearization nor Gaussian noise assumption. The posterior distribution can be any quantity that is representable by discrete samples (i.e. particles). Increasing the number of particles makes it possible to describe more complex distributions, but it increases the computational costs as well.

The algorithm is straightforward to implement, consisting of the following steps:

1. **Initialization**: N particles are initialized according to the *a priori* knowledge described as probability distribution $p(x_{k-1})$. This distribution can be any empirical distribution which can be represented with particles, or uniform distribution.
2. **Estimation loop**
   (a) **Predict**: All particles are moved based on the current dynamic system model by sampling new particles, $x_k^i, i \in [1, N]$, from the distribution obtained by the convolution of *a priori* distribution and the process model: $\int p(x_k|x_{k-1}, u_k)p(x_{k-1})\mathrm{d}x_{k-1}$. The process model includes the inputs vector, u_k, and the process noise.
   (b) **Update**: The weights of particles are updated according to the belief of the observations, $w_k^i = p(y_k|x_k^i)$ assuming that each particle, x_k^i, represents the correct location. Finally, the weights are normalized so that their sum is unity = 1.
   (c) **Resample**: New set of particles is generated by sampling the existing set of particles using the normalized weights, so that particles with higher weights are selected more probably than the others.
   (d) **Estimate**: The position estimate is obtained as a weighted average of the posterior distribution represented by particle locations and weights.

Researchers assessing the performance of PF had found it to be more accurate than other conventional estimation methods (e.g. other Bayesian filters) owing to its adaptability to work with nonlinear non-Gaussian systems (Angelis, Moschitta, & Carbone, 2016).

However, PF suffers from shortcomings such as: the increased computational cost when massive amount of particles is used, sample degeneracy and deficiency caused by the reduction in particle diversity (X. Fu & Jia, 2010; Tian, Wang, & Salcic, 2019b; Y. Zhang, Tan, & Zhao, 2020). A PF might also perform poorly in the kidnapped robot case when the robot is suddenly transferred to another location without allowing it to make measurements during the transfer. In this case, there might not be any particle near the actual position of the robot, and the robot might take a long time to find its new location. Counter intuitively, a PF does not also perform well when the measurement noise figure is very modest (Thrun, Fox, Burgard, & Dellaert, 2001).

2.7.7 Factor graph optimization

Factor Graph Optimization (FGO) is a relatively new positioning algorithm among Bayesian filters. Some earlier publications from 2012 proposed utilizing FGO for multipath mitigation of GNSS positioning (Sünderhauf & Protzel, 2012) and for multi-sensor fusion of the global positioning system (GPS), inertial motion units (IMU), and stereo vision (Indelman, Williams, Kaess, & Dellaert, 2012).

FGO models the previous states as nodes, and measurements as factors. Like EKF and PF, FGO assumes Gaussian noise and utilizes the Bayesian filtering principle for solving the position estimation. Distinctly, the FGO does not assume the Markov condition, but it uses information from previous states in addition to utilizing the latest state only. FGO solves the position by optimizing the factor graph model with an iterative solver, therefore requiring more resources than EKF or PF. However, it is still solvable in real-time, for example, by combining the expectation-maximization and nonlinear optimization methods (Pfeifer & Protzel, 2019; Wen, Pfeifer, Bai, & Hsu, 2021).

FGO is a graphical model representation consisting of linked state variables x_n, and constraint functions or factors $f_{m,k,L}$, see Figure 10. Each constraint is linked to one or more variables, and each variable can have zero or more constraints. The variables and constraints form a sparse graph representing the factorization of a complete probability density function to be solved iteratively with the message-passing algorithm (Pearl, 1987).

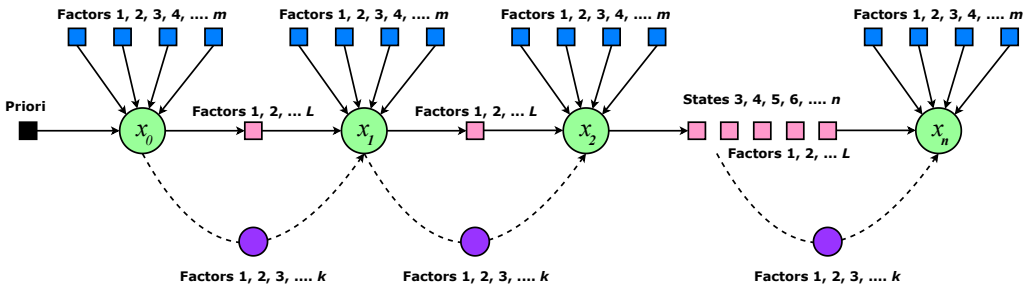

Figure 10. Factor graph optimization algorithm.

Even though FGO shares the unimodal Gaussian model with EKF, it can be more reliable in urban canyon environments for GNSS positioning use cases (W. Li, Cui, & Lu, 2018). FGO is a general representation in a user-friendly graphical form, which can model the behavior of a KF. However, it can also extend a conventional KF by utilizing historical measurements with an arbitrary batch size. For these reasons, FGO can be more accurate than KF variants, especially in non-line-of-sight (NLOS) situations (Pfeifer & Protzel, 2019; Wen, Pfeifer, Bai, & Hsu, 2021).

Recently, FGO has raised plenty of interest in positioning research, and it has been also applied to indoor navigation, including UWB positioning (Pfeifer & Protzel, 2019; Song & Hsu, 2021). Besides, FGO can be useful in indoor positioning where multipath propagation causes channel impairments or in complex multi-sensor fusion situations. One disadvantage of FGO is that it is more computationally intensive than recursive KF variants.

2.7.8 RTS smoother

The Rauch-Tung-Striebel (RTS) smoother is a recursive Bayesian filter that smooths the linearized state-space estimates by considering the maximum likelihood of the probability density function (mean and covariance). The smoothing process is carried out retroactively (Hartikainen, Solin, & Särkkä, 2011; Rauch, Tung, & Striebel, 1965).

The prior and posterior RTS states $\hat{X}_k|k-1, \hat{X}_k|k$ and their covariances $\hat{P}_k|k-1, \hat{P}_k|k$ which were obtained from the EKF fusion filter, are fed to the RTS smoother to calculate the smoothed state estimates $\hat{X}_k|n$, and covariance $\hat{P}_k|n$. The RTS smoother formulas are described in Equations (2.24) (Hartikainen, Solin, & Särkkä, 2011; Rauch, Tung, & Striebel, 1965).

$$\begin{aligned} \hat{X}_k|_n &= \hat{X}_k|_k + C_k(\hat{X}_{k+1}|_n - \hat{X}_{k+1}|_k), \\ P_k|_n &= P_k|_k + C_k(\hat{X}_{k+1}|_n - \hat{X}_{k+1}|_k)C_k^T. \end{aligned} \tag{2.24}$$

where $C_k = P_k|_k F_{k+1}^T P_{k+1}^{-1}|_k$, and $\hat{X}_k|_k$ is the a-posterior state estimate of time instant k and $\hat{X}_{k+1}|_k$ is the a-prior state estimate of time instant $k+1$ which also applies to the covariance.

Usually, RTS smoothers are used to fine-tune the predicted estimations resulting from the state-space process. In other words, they support in removing the fast fluctuations and instabilities in the estimated positioning routes.

2.8 Non-line-of-sight situations

NLOS situations occur when the wireless signal suffers a partial or total obstacle blockage that either prevents the signal from arriving at the receivers' end, or allows a small part of the signal to arrive in the form of bounced and reflected signal replicas from nearby structures. In most NLOS scenarios, only the reflected signal is received, while the direct path signal is missing, as shown in Figure 11. The use of reflected signals can cause a significant bias to the positioning estimation process.

Several methods have been developed to reduce the inaccuracies imposed by NLOS situations. The authors of (Guvenc, Chong, & Watanabe, 2007; Khodjaev, Park, & Malik, 2009) categorized these methods as NLOS identification and NLOS error mitigation techniques. The signal can be identified as an NLOS signal, for example, by analyzing the channel statistics parameters such as: the mean delay, the excess delay, the amplitude and the signal to noise ratio (SNR). When the faulty observable is identified, it can be excluded from further analysis to improve the positioning accuracy.

Various techniques and solutions can be used for mitigating NLOS errors such as: outlier detection,

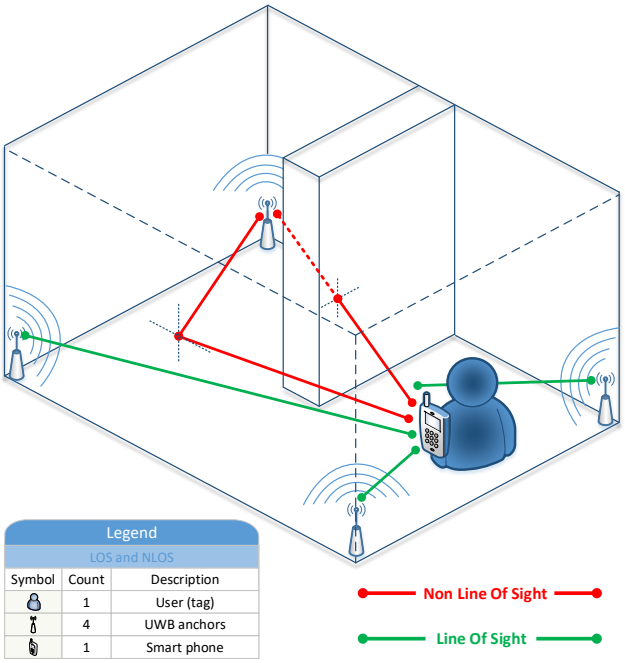

Figure 11. NLOS and LOS situations in IPSs e.g. UWB.

PF, machine learning (ML), and WLS. In some NLOS scenarios, the probability distribution of the position can be multimodal (Haggenmiller, Krogius, & Olson, 2019), it was found that the ranging measurements can be affected by non-Gaussian noise even in LOS situations (Angelis, Moschitta, & Carbone, 2016). Therefore, PF can be more competitive in some realistic indoor environment than LS or EKF.

Recently, both sensor fusion and ML techniques have been extensively applied for NLOS identification and error mitigation, which are discussed in Sections 2.9 and 2.10. It is relatively simple to fuse information from many sources into the PF estimations to compensate for NLOS issues. For example, some researchers used inertial navigation systems (INSs) for multi-sensor schemes (Tian, Wang, & Salcic, 2019b, 2020; Y. Zhang, Tan, & Zhao, 2020) by mixing with an EKF as a pre-processor of PF information (Y. Zhang, Tan, & Zhao, 2020). The PF positioning algorithm can also include other models, such as probabilistic uncertainty model (Tian, Wang, & Salcic, 2020) or a model to predict the wireless signal obstruction caused by pedestrians own bodies (Tian, Wang, & Salcic, 2019a).

In indoor UWB systems, a commercial solution was coined by Qorvo (Decawave) (Decawave, 2016) for systems that contain the DW1000 chips. This embedded resolution comprises the use of additional registers to assign a level of confidence to the received timestamps. Afterwards, it post-processes the accumulators to allow the identification of a falsely detected first path, hence, identifying NLOS situation epochs.

2.9 Multi-sensor fusion techniques

One way to mitigate the effect of NLOS situations on positioning estimation is to use mulitsensor fusion techniques, as suggested by numerous literature in publications **[P1]–[P5]** and demonstrated

in Figure 16.

Sensor fusion is a computational procedure that combines the observed measurements from multiple sources (sensors) such that the output information after fusion is maximized. Fusion systems import measurements from multiple sensors then apply estimation or inference to get the desired quantity of interest (Hostettler & Särkkä, 2020).

As sensor technologies have become more sophisticated, multisensor fusion has been trending recently for precise point positioning. The reliance on multiple measurement devices in positioning applications can result in less uncertainties, and greater reliability and accuracy than depending on a single measurement sensor (Guo et al., 2020). Numerous tracking systems can be fused with an IPS system to produce more accurate and reliable estimations. Common examples of these systems are: GNSSs, INSs, visual map matching (VMM), IMUs, and computer vision systems.

The optimal positioning estimations resulting from fusing multiple positioning methods should follow a unified framework. An example of fusion framework is illustrated in Figure 12, where the data from a set of sensors are processed locally using dedicated estimators (algorithms). Then, the product is weighed and combined globally with other sensors (i.e. fused) using a suitable fusion scheme (e.g. federated Kalman filter, see Figure 13) to produce the final optimal solution.

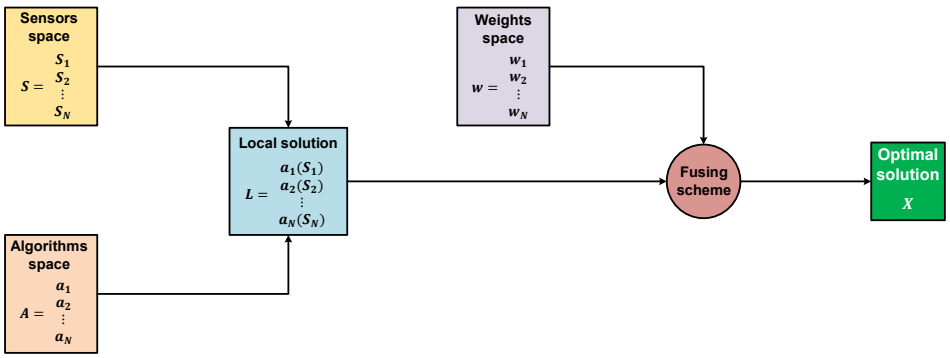

Figure 12. Sensor fusion framework, adapted from (Guo et al., 2020).

In other words, a multisensor fusion system consists of: 1) one or more sensor(s) that measure an observable quantity, 2) the model(s) that relate the observed quantity to the quantity of interest, and 3) the estimation algorithm(s) that estimate the quantity of interest by combining the model and the measured data (Hostettler & Särkkä, 2020).

A mulitsensor fusion technique can adopt the architecture of either three distinct schemes: a) loosely coupled (LC), b) tightly coupled (TC), and c) ultra tightly coupled (UTC).

As stated by Srinivas and Kumar, LC is the simplest type among the three architectures which provides the essential redundancy based on the received duplicated information from many visible anchors to achieve high accuracy e.g. as in GNSSs (Srinivas & Kumar, 2017). While in TC, the multisensors are affected by each other's sensor readings, that is, the tightly coupled data from one or more sensor(s) will be highly correlated. TC is widely adopted because it provides better accuracy and it is less susceptible to jamming, in addition to maintaining navigation in situations of few visible anchors in IPSs or satellites in GNSSs. In UTC, for example, the tracking loop of GNSSs is assisted

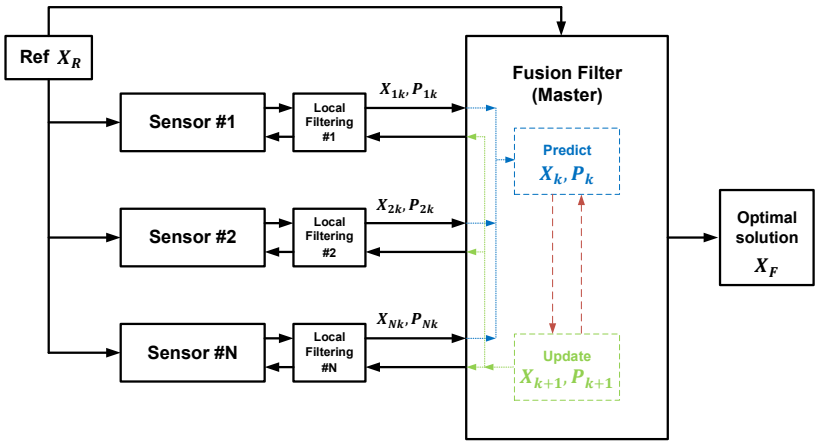

Figure 13. Structure of the federated Kalman filter (FKF).

with an accompanying software defined radio (SDR) loop that matches and smooths between the locally generated signal and the actual received signal.

2.10 Machine learning methods

While conventional multiangulation, multilateration, and dynamic state models have been the most commonly used methods for positioning estimation, some ML models have become increasingly popular due to their advances in navigation systems. They are used for positioning when simpler models cannot work efficiently due to e.g.: severe nonlinearities, abrupt changes in environmental conditions, heterogeneous information sources, skewed noise distribution or non-convexity).

Typical reasons for using ML methods are to increase robustness, allow adaptation to changes, implement a collaborative or model-free positioning system, use heterogeneous information sources or select the most useful features for positioning. These methods allow the use of ad-hoc observations not originally intended for positioning, such as optical images from Cameras and RSSs from Wi-Fi base stations.

Nowadays, traditional positioning algorithms are often supplemented with ML methods in order to achieve better performance. More details about the recent advances in ML based positioning system can be found in publication **[P1]**. The following ML algorithms were the ones used for implementing the methods proposed in publications **[P3]** and **[P6]**.

2.10.1 Linear Regression

Linear regression (LR) modelling is a statistical method that is used for predictive analysis. It is one of the most common types of supervised machine learning algorithms to compute the linear relationship between dependent variables and independent features (Kumari & Yadav, 2018). Generally, the LR function is represented as seen in Equations (2.25) and (2.26).

$$Y = m + Xb. \tag{2.25}$$

Where Y denotes the output vector of observed values or quantities, m is the intercept value, b is the slope, and X is the input vector of variables of interest or the regressor vector. Assuming a linear relationship between X and Y, then the offsets can be predicted using Equation (2.26) as follows:

$$y_i = m + \sum_{j=1}^{n} x_{i,j}\beta_j + \epsilon. \tag{2.26}$$

where $i = 1, 2 \ldots n$, and $y_i \in Y$ is the dependent variable, $x_{i,j} \in X$ are the independent variables (multiple inputs, $j = 1, 2 \ldots k$), and ϵ is the prediction error.

The model achieves the most improved regression fit by finding the best fitting m and β_j values, where m is the intercept and β_j is the coefficient of $x_{i,j}$. The mean squared error (MSE) is used as the cost (or loss) function L, in order to compute the error, which is the difference between the predicted value $\hat{y}$ and the true value y. The loss function $L(\Theta)$ can be written as in Equation (2.27):

$$L(\Theta) = \frac{1}{n}\sum_{i=1}^{n}(\hat{y_i} - y_i)^2. \tag{2.27}$$

The LR algorithm can be employed for positioning and navigation systems in various ways such as: trajectory prediction by forecasting the paths of moving objects, correcting errors in received signals or observation values, in sensor fusion schemes by integrating data from various sensors for an enhanced state estimation process, and as a learning algorithm that studies complex relationships for adaptive navigation e.g. like in autonomous vehicles.

2.10.2 K-Nearest Neighbour

k nearest neighbour (kNN) is a supervised machine learning algorithm that is used to solve both classification and regression problem statements. kNN classification operates by computing the distance between various feature values. The concept behind it is that if the majority of the k nearest neighboring samples in the feature space share a specific category, then the given sample is likely to belong to that category as well (L. Zhu, Spachos, Pensini, & Plataniotis, 2021). The most commonly used kNN distance measurements are done via the Euclidean or the Manhattan formulas, as found in Equations (2.28) and (2.29), respectively.

Euclidean distance:

$$d(x, y) = \sqrt{\sum_{k=1}^{n}(x_k - y_k)^2}, \tag{2.28}$$

Manhattan distance:

$$d(x, y) = \sum_{k=1}^{n} \mid x_k - y_k \mid. \tag{2.29}$$

kNN can help define trajectories (e.g. lane and road detection for outdoors) from dense maps, which is carried out by means of feature extraction and classification methods to enhance the positioning accuracy. This involves extracting features related to lane markings such as color, texture, and spatial relationships with path features. Labeled training data should include examples of path regions with annotated lane markings.

After feature representation and parameter selection, the kNN algorithm is trained to classify regions into path and non-path ways, also can be trained to identify lane markings within road regions. This combined approach enables the detection of both roads and lane markings from map data, facilitating tasks such as navigation systems, autonomous driving, and transportation planning. However, the effectiveness of the method depends on the data quality of training data, feature selection, and parameter tuning.

More examples on ML algorithms that are used in the context of indoor and/or outdoor positioning can be found in publication **[P1]**, Table 10.

3 INDOOR ULTRA WIDEBAND POSITIONING

In this chapter, the prospective design, the building blocks, and the development of UWB IPS are discussed which were realized inside the industrial laboratory of Technobothnia in Vaasa, Finland.

Between 2021 and 2022, a scrutinized comprehensive literature review (publication **[P1]**) was conducted, focusing on UWB and the methods of mitigating NLOS situations using multi-sensor fusion techniques and machine learning algorithms. Moreover, in publication **[P1]**, all the literature was summarized into compact tables mentioning the year of publications, the IPS technologies used, the multi-sensor technique (if any), the ML algorithm (if any), and general information on the findings and their novelties.

In 2023, the implementation for UWB multi-sensor fusion system was realized to provide precise positioning to movable assets e.g. humans and robots. The experiments were carried out in a dense environment inside one of the campus industrial laboratories, Technobothnia lab, Vaasa. All realization procedures and details are elaborated in publications **[P2]**, **[P3]**, and **[P4]**.

3.1 Background on UWB

UWB is a wireless short-range radio technology whose communication channel propagates information over a wide spectrum by modulating either a carrier-based waveform or a carrier-less baseband signal in the form of short-width pulses (Wilzeck, Guirao, & Dimitrov, 2018). According to the Federal Communication Commission (FCC) and the International Telecommunication Union (ITU), an UWB signal should have a spectrum that occupies a bandwidth greater than 20% of the central frequency or a bandwidth of at least 500 MHz. A typical UWB radio frequency signal occupies the 500 MHz ultra bandwidth, which facilitates the transmission of large data sizes using lower energy consumption than other technologies (Alarifi et al., 2016; Dabove, Pietra, Piras, Jabbar, & Kazim, 2018; Sabath, Mokole, & Samaddar, 2005).

To distinguish between narrowband (NB), wideband (WB) and UWB (as shown in Table 3), the FCC classification scheme adopts the fractional bandwidth calculation, B_F, a dimensionless indicator that can be calculated using Equation (3.1) as follows: (Muqaibel, Safaai-Jazi, & Riad, 2004; Sabath, Mokole, & Samaddar, 2005)

$$B_F = 2\left(\frac{f_h - f_l}{f_h + f_l}\right). \tag{3.1}$$

Table 3. Band types according to the spanned bandwidths.

Band Type	**Fractional Bandwidth** B_F	**Band Ratio** $b_r = \frac{f_h}{f_l}$
Narrowband (NB)	$0.00 < B_F \leq 0.01$	$0.00 < b_r \leq 1.01$
Wideband (WB)	$0.01 < B_F \leq 0.25$	$1.01 < b_r \leq 1.29$
Ultra-Wideband (UWB)	$0.25 < B_F < 2.00$	$b_r \geq 1.29$

Earlier in 2002, the FCC described UWB technology as an emerging technology that will hold leap advances for various applications (Federal Communications Commission, 2002), such as imaging systems, ground-penetrating radars (GPRs), wall-imaging systems, medical systems, surveillance systems, vehicular sensing systems, communications and measurements systems (Matin, 2010). UWB can transmit high data rates using tiny pulses of the spectrum spread over wider frequency bands with lower power spectral densities (PSDs), which leverages the signal with higher penetration capability compared to most RF waves. Moreover, some types of UWB signals (e.g. the impulse radio IR-UWB) do not require sinusoidal carrier waves, which in turn reduces the overall power required for transmission. More details are found in Section 3.2.

The combined advantages of an UWB signal makes it a prominent candidate for real-time applications such as: 1) tracking and navigation, 2) sensor network communications, 3) ranging and imaging, and 4) extremely high-data-rate short-range communication (e.g. wireless UWB).

Recently in the past few years, UWB has been widely adopted in personal area networks (PANs), precise indoor positioning, indoor tracking and navigation systems. UWB positioning relies on the unique radio frequency characteristics associated with the UWB signal to provide accurate estimates for indoor locations based on the TOA, AOA and TDOA techniques. The typical UWB positioning signal takes the form of a low-power short-pulse transmission with large bandwidth (Alarifi et al., 2016; Dabove, Pietra, Piras, Jabbar, & Kazim, 2018; Sabath, Mokole, & Samaddar, 2005), making it robust, precise, and secure for indoor positioning solutions.

UWB was first commissioned by the FCC for public use in 2002. Before that, it was only used by the US military for classified applications (Nekoogar, 2005).

3.2 Why UWB over other technologies?

UWB technology for IPSs has numerous advantages and challenges as well. The structure of an IR-UWB signal is based on the transmission of short pulses within a large bandwidth ranging between 3.1 and 10.6 GHz, which results in UWB superiority over NB signals. Owing to the large bandwidth and the short duty cycle, UWB possesses a larger capacity and higher data rates, which make it a suitable candidate for RF-based IPS implementation. Moreover, UWB lies in the unlicensed spectrum, hence, can be used by everyone without prior notification nor consent. Additionally, the pulse nature of the UWB signal increases its penetration capability to propagate through obstacles. Consequently, UWB tags mounted on mobile targets do not require a direct LOS with their anchors. A graphical illustration for some UWB advantages is shown in Figure 14.

However, some scenarios found in dense environments might have negative effects on the UWB signal, causing multipath deterioration and interference with neighbouring frequencies in the spectrum (Alarifi et al., 2016). In addition, the low transmission power can be ineffective in large-sized indoor spaces, as it disallows the signal from travelling to longer distances due to path loss attenuation. Hence, additional UWB anchors are required, which increases costs and complexity (Nekoogar, 2005).

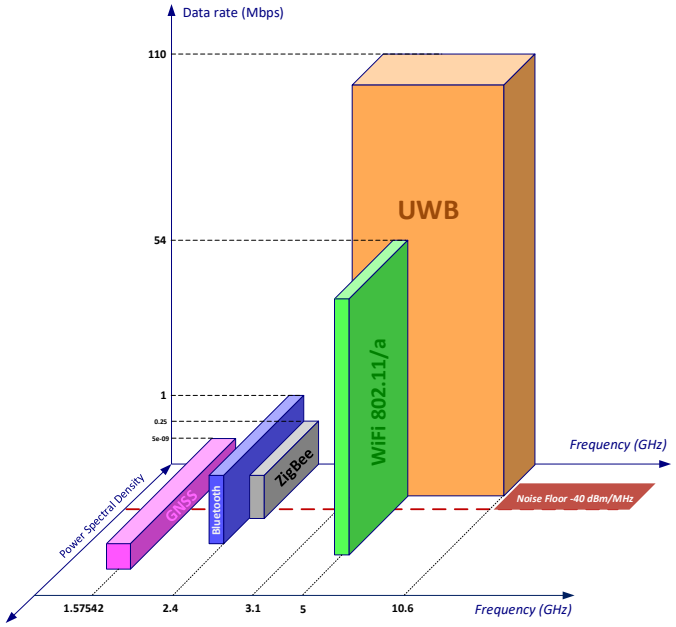

Figure 14. Comparison between the attributes of UWB and other positioning technologies (the dimensions of the shapes are only indicative).

3.2.1 Advantages

In more details, UWB offers numerous benefits over narrowband signals, which widens the range of affected applications. First, UWB is an unlicensed free spectrum that can be used without prior licensing. The UWB spectrum was made free for commercial use in 2002, but before that, it was restricted to military operators, mainly the US Department of Defense, for classified applications (Nekoogar, 2005).

UWB has a larger bandwidth than other positioning techniques ranging from 3.1 to 10.6 GHz (Lee, Su, & Shen, 2007; Matin, 2010), which provides it with the superiority in many aspects. For example, based on Shannon's law, the large UWB bandwidth provides large capacity for an RF signal, which implies a high data rate transmission that can support real-time applications, such as instant video streaming (Matin, 2010; Nekoogar, 2005). Owing to their large bandwidth, UWB communication systems are highly robust, operating at higher data rates (110 Mbps) than other RF technologies, making it the highest data rate achieved so far in the precise positioning realm.

Another benefit of the large bandwidth is the UWB system's capability of operating in low SNR communication channels (Nekoogar, 2005), which bestows immunity against multipath degradation. The high level of multipath resolution is mainly attributed to the nature of pulse-based RF communication, which occupies the entire bandwidth for each pulse. Unlike other carrier-based communications (Yin, Jiang, Yang, Zhao, & Chen, 2019), UWB systems do not require a clear LOS, but the UWB communication is feasible under NLOS conditions. However, in positioning applications, NLOS situations might produce erroneous sensor readings, which can disturb the positioning estimation process.

Additionally, the short-pulse low-power nature of UWB signals is another major advantage of UWB,

making it a suitable candidate for indoor positioning applications that conserves power.

3.2.2 Challenges

Although UWB technology offers numerous benefits for indoor positioning applications, the technology faces several challenges and limitations that might affect its performance. UWB technology is known for its coexistence with other RF systems, but this is not permanently true. The technical report published by the US National Institute of Standards and Technologies (NIST) (Miller, 2003) stated that UWB can cause interference to nearby spectrum and vice versa. Examples of the potentially affected RF technologies are the: GPS, 3G, and WiMAX communication systems (Alarifi et al., 2016; Miller, 2003), due to the misconfiguration of wireless transceiver devices. Thus, many countries and regional authorities have imposed regulations to mitigate the possible interference, which are discussed in Section 3.3.

The low power transmission of UWB is considered an advantage, yet it constrains the overall power consumption for the transmitter and receiver. For example, the low-power UWB signal can either travel short distances at a high data rate or long distances at a low data rate (Santhanam, 2011); hence, the range of the UWB anchor will be limited. This can only be compensated by using more UWB anchors, which affects the scalability (Ridolfi, de Velde, Steendam, & Poorter, 2018; Ridolfi, Vandermeeren, et al., 2018) and increases the system complexity and computational load, which in turn jeopardizes the system integrity and robustness. Additionally, the processing of wide-band signals usually leads to high power consumption (Khurshid & Khokhar, 2013). The high power consumption can be mitigated using a multiband approach in which the signal is split into sub-bands. The sub-band processing method is briefly discussed in Section 3.4.

Another advantage that creates a challenging situation is the short pulse nature of UWB signals. The coding of short width pulses requires longer synchronisation times, limiting the data capacity. Moreover, the short-width pulses increase the number of multipath components (Miller, 2003), which also compromises the overall system performance. Researchers have proposed a solution for this issue by devising special schemes and protocols to avoid repeated synchronisation (Miller, 2003). In addition, (Irene & Rajesh, 2018) proposed the use of MIMO systems to mitigate the effect of short communications.

One last challenge of UWB is its limited usage outdoors. According to various countries' regulations, fixed UWB transmitters operating outdoors are not allowed (FCC Federal Register, 2002; Harmonised European Standard, 2016a), refer to Section 3.3 for more details.

3.3 UWB licensing regulations

The license of UWB bandwidth is free for indoor applications, yet the regulations for UWB devices are country- or region-specific. The regulations are very essential to define the technical requirements and certification procedures for legal and safe operation (CETECOM, 2019), and more importantly, to minimize the potential interference to licensed services (Wilzeck, Guirao, & Dimitrov, 2018). These regulations prescribe the boundaries and safety limits of the operating frequency, power levels, emissions, energy disruptions, service times and antenna locations.

For example, the regulations for UWB devices in the United States are published by FCC in 2002 under the "Code of Federal Regulations Part 15, subpart F" (FCC Federal Register, 2002), while

those in the EU region are issued by the Harmonised European Standard in 2016 (the process started in 2006) under the radio equipment directive "ETSI EN 302 065 – 1 to 5" (Harmonised European Standard, 2016a).

Additionally, these official UWB regulations distinguish between the different types and usages of UWB devices, and each type and usage has its own regulation. For example, the FCC has set specific rules for each category of UWB devices and their respective application, such as indoor UWB systems, handheld UWB devices, GPRs and wall imaging systems, surveillance and transportation systems (e.g. UWB on-board aircrafts and UWB installed on rail vehicles) (Wilzeck, Guirao, & Dimitrov, 2018).

According to the FCC, the bandwidth of the UWB systems belonging to the indoor and the handheld categories must be kept between 3100 MHz and 10600 MHz (FCC Federal Register, 2002). The indoor UWB systems may not be used outdoors, and they must be designed so that they are capable of operating only indoors. The emissions from UWB devices may not be intentionally directed outside of a building to perform an outside function. Also, the use of outdoor mounted antennas is prohibited. The device may only transmit when sending information to an associated receiver.

An UWB device belonging to the handheld category must be relatively small. These devices are primarily kept in hand while being operated, and they do not employ a fixed infrastructure (FCC Federal Register, 2002). Antennas may be mounted only on the handheld UWB device. The use of antennas mounted on outdoor infrastructure is prohibited.

Part 1 of the EU regulation "ETSI EN 302 065" contains requirements for generic UWB applications, and it applies to fixed (indoor only), mobile or portable applications (Harmonised European Standard, 2016a). The UWB transmitter conforming to that document may not be installed at a fixed outdoor location, for use in flying models, aircraft and other forms of aviation. Allowed operation frequency band is from 3.1 to 4.8 GHz and from 6.0 to 9.0 GHz.

Requirements for UWB location tracking are defined in Part 2 of the EU regulation "ETSI EN 302 065" document, which covers three types of UWB location tracking system, of which two are applicable for smart logistics applications (Harmonised European Standard, 2016b):

- LT1 systems: These systems, operating in the 6 GHz to 9 GHz region, are intended for general location tracking of people and objects. They operate on an unlicensed basis. The transmitting terminals in these systems are mobile (indoors or outdoors), or fixed (indoors only). Fixed outdoor LT1 transmitters are not permitted.
- LT2 systems: These systems, operating in the 3.1 GHz to 4.8 GHz region, are intended for person and object tracking and industrial applications at well-defined locations. The transmitting terminals in these systems may be located indoors or outdoors, and may be fixed or mobile. They operate at fixed sites and may be subject to registration and authorization.

The regulation documents contain additional points describing the operation peak powers and tabulated emission limits for UWB devices, which vary regionally (e.g. US and EU).

Both the ETSI and the FCC regulations allow the use of UWB indoor location tracking, which is very important for many industrial and smart logistics applications. However, the unlicensed outdoor use of UWB is limited to handheld or mobile devices. Because the FCC or LT1 of ETSI do not allow fixed outdoor transmitters, development of UWB outdoor positioning systems becomes difficult. Without transmitter anchors, it is not possible to use TW-TOA and multilateration for position determination. In addition, TDOA scheme with wireless clock synchronization is inapplicable, since

the anchors must transmit synchronization messages to each other. Thus, the only possible way to implement outdoor UWB location system, operating under the provision of FCC or ETSI LT1, is to use TDOA approach with a wired clock synchronization. However, implementing the wired clock synchronization is complex and expensive.

LT2 of ETSI allows the fixed outdoor transmitters in the EU, but the LT2 systems are subject to registration and authorization. In addition, local coordination with possible interference victims has to be performed, and the possible permission would be granted only to a specific site (Harmonised European Standard, 2016b). In the meantime, developing an UWB-based positioning system for outdoor environment is very difficult.

In June 2020, the fine-ranging alliance (FiRa), the largest UWB consortium, was founded to pave the way for the widespread adoption of UWB-driven applications. Some well-known company members of the FiRa alliance are: NXP, Samsung, Qorvo, Qualcomm, Cisco, Apple and BOSCH. The FiRa consortium is committed to providing seamless user experience through secured fine ranging and positioning capabilities of interoperable UWB technologies (FiRa, 2021).

3.4 UWB types and signal attributes

The earliest attempt of UWB standardization within IEEE standards was made by the WiMedia alliance workgroup in IEEE 802.15.3a-2003. This workgroup was responsible for standardizing the physical and medium access control (MAC) layers of UWB indoor signals for wireless PANs.

The detailed technical aspects of an UWB signal are described in the currently active UWB standard (802.15.4z-2020), which was developed by the ”LAN/MAN Standards Committee” of the IEEE Computer Society (IEEE Computer Society, 2020).

UWB signals can be generated using different techniques, the most popular is the impulse radio (IR) method. However, there are other methods that can be adopted in UWB systems. Wilzeck et al. classified the types of UWB signals into the following six categories: (Wilzeck, Guirao, & Dimitrov, 2018)

3.4.1 Impulse radio ultra wideband

The IR-UWB signal modulates the baseband signal through short pulses ($\approx$ few nanoseconds duration), which have a low duty cycle to transfer information. The frequency spectrum characteristics of IR-UWB can be controlled by varying the pulse shape, phase, amplitude and duration to formulate the spectrum envelope of the signal. IR-UWB can be either carrier-based, which requires an external high-frequency sinusoidal carrier signal and a mixer, or carrier-less, which can operate without a local oscillator (LO) in the transceivers, only using the baseband signal. The IR-UWB is typically the most adopted system and is standardized in the IEEE 802.15.4z UWB standard.

3.4.2 Direct sequence ultra wideband:

Direct sequence spread spectrum (DSS) version of the IR-UWB forms the DS-UWB, which treats the signal by a pseudorandom number (PN) code before the amplitude modulation of a train of short

pulses. The new bandwidth of the transmitted signal is affected by a spread code, which is typically much higher than the symbol rate, and the chip interval is longer than the pulse width.

3.4.3 Multiband ultra wideband:

The orthogonal frequency division multiplexing (OFDM) version of the IR-UWB can be considered to form the MB-UWB, in which the total bandwidth is divided into multiple frequency sub-bands (minimum 500 MHz each) to occupy the spectrum efficiently. The MB-OFDM approach utilizes the quadrature phase-shift keying (QPSK) modulation with 128 subcarriers and five-band groups containing two or three bands each (14 sub-bands in total). The MB-OFDM recently received approval from ISO/IEC and ETSI.

3.4.4 Frequency hopping ultra wideband

Frequency hopping ultra wideband (FH-UWB) is a non-conventional carrier-based method in which the transmission occurs through fixed frequency hops over a broad bandwidth and using variant frequency carriers. The hopping sequence is determined by a spreading code or a PN sequence set by the user in which a narrow-band transmission occurs periodically, which can be smaller than (fast hopping), greater than (slow hopping) or equal to the symbol rate. The total spectrum bandwidth is determined by the range of hopping frequencies and not the symbol rate.

3.4.5 Stepped frequency hopping ultra wideband

Stepped frequency hopping ultra wideband (SFH-UWB) is a particular case of FH-UWB, in which the hopping frequencies are selected by the spreading code to form linearly increasing discrete steps until the desired bandwidth is achieved. Then, the hopping frequency is reset to the starting sequence, and the process is repeated.

3.4.6 Swept frequency ultra wideband

Swept frequency ultra wideband (SF-UWB) is also known as ‘Chirp signalling’. It is the frequency variation of the FH-UWB, in which the carrier frequencies of the UWB waveform are generated by a voltage-controlled oscillator (VCO) using a continuous variable speed. The symbols are modulated on the slope (chirp) using M-ary modulation and then transmitted sequentially or superimposed.

3.5 Architecture of UWB indoor positioning systems

A typical UWB indoor positioning system includes at least four fixed UWB sensors (anchors), at least one mobile UWB target(s) (tag(s)), location server and system interface. The location server stores and processes the sensors data, and the system interface (e.g. smartphone, computer or tablet) is for viewing the positioning results, as illustrated in Figure 15. It is noteworthy to state that a planar

two-dimensional positioning requires at least three anchors to solve the coordinate equations of the tag, while three-dimensional positioning requires at least four anchors.

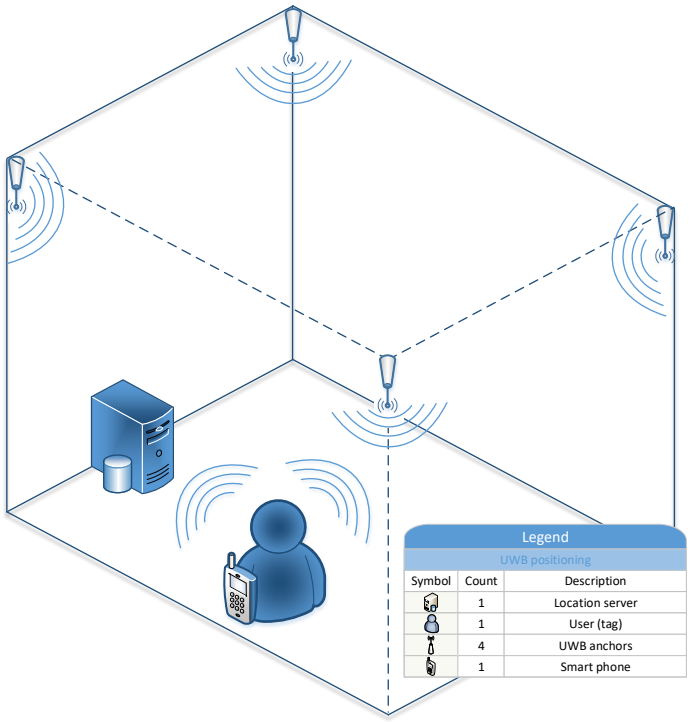

Figure 15. Elements of UWB positioning systems.

Additional optional units can be added to the previous structure to obtain a real-time location system (RTLS). For example, the location server is optional in small-scale systems but crucial in large-scale systems. There could be additional front-end and back-end units for complex indoor environments such as: navigation framework, network gateways, user interface and facilities for IoT integration or other accompanying multi-sensor technologies.

The process of UWB precise positioning commences with the relative positioning between the UWB anchors in which a single initiator anchor is specified as a reference point or origin (0,0). In an auto-positioning feature such as Decawave's (Qorvo) RTLS application, the system automatically measures the relative distances between all anchors and thus infer their positions in the specified coordinate system. A block diagram depicting an example of a complete process of UWB precise positioning is illustrated in Figure 16.

After fixing the coordinate system, the UWB system starts ranging to the mobile UWB tag(s) within the indoor environment before sending the measured raw data to the positioning framework for additional processing. The positioning algorithm, which is pre-specified by the user, uses the raw measurements and a kinematic model to carry out the positioning estimation. Precise position can be achieved when when the ranging method and the positioning algorithm are both fitting to the application and the properties of the environment. In other words, some scenarios of finely selected ranging techniques and positioning algorithms would suffice to have precise positioning without

going further for post processing algorithms, as shown from the bottom arrow of Figure 16.

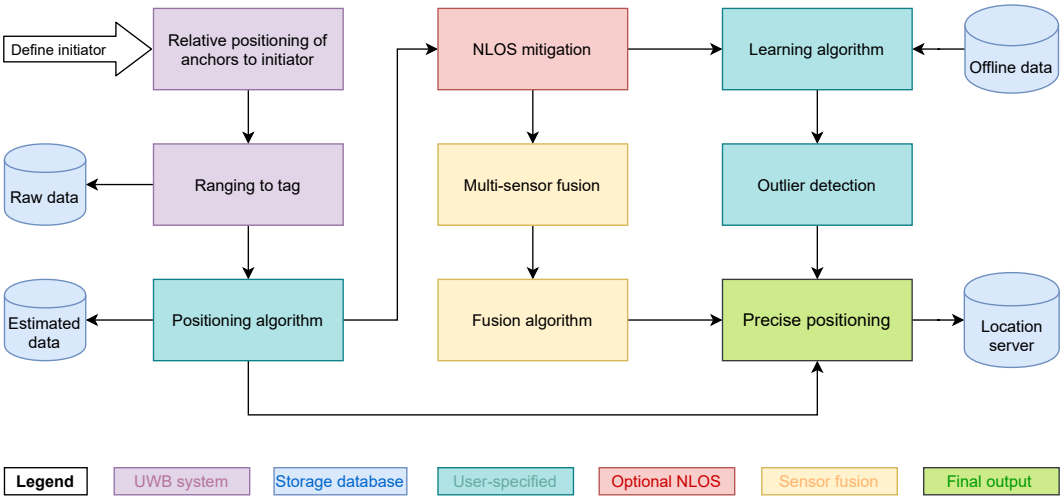

Figure 16. Suggested building blocks of the UWB precise positioning process, based on the surveyed UWB literature.

Many applications in various environments require specific NLOS mitigation methods to improve the performance. This dissertation focuses on two NLOS mitigation approaches, the multi-sensor fusion schemes and ML algorithms. Both approaches were discussed in Sections 2.9 and 2.10.

In the multi-sensor fusion approach, an additional accompanying technology is used to aid the UWB system with a fusion algorithm that fuses data obtained from all sensors based on their weights and shares.

In contrast, the ML approach is applied by the help of large offline data to train a learning algorithm to identify the outliers caused by the NLOS conditions. Finally, the overall efficiency of the system is determined by the combined metrics of all phases (ranging, algorithms, fusion, and ML), in addition to the degree of relevance of the final positioning results to the ground truth.

3.6 Commercial products of UWB technology

The growing demand for location-based services in an indoor environment has increased the size of the UWB market during recent years. In addition, the recent advances in UWB technology have provided opportunities for new commercial applications.

The major manufacturers providing UWB chips for open markets are Qorvo and NXP. Qorvo entered the UWB market by acquiring the Irish semiconductor company Decawave in January 2020 (Qorvo, 2020). Decawave has been one of the major providers of UWB technology during the past 15 years, along with some other companies as: Ubisense and BeSpoon (Jiménez Ruiz & Seco Granja, 2017).

Decawave's UWB technology has been very popular and its chips have been used extensively in research (Barbieri, Brambilla, Trabattoni, Mervic, & Nicoli, 2021; Cimdins, Schmidt, & Hellbrück, 2020; Dotlic, Connell, Ma, Clancy, & McLaughlin, 2017; J. Kulmer et al., 2017; Tian, Wang, & Salcic, 2020) and commercial IPS (Eliko, 2021; Exafore, 2021; Pozyx, 2021; Sewio, 2021).

NXP launched its UWB precision chips in February 2020. Currently, NXP provides Trimension UWB modules for IoT, industrial, mobile and automotive market segments (NXP, 2022). Trimension UWB modules can be used, for example: as tags or anchors in IPS systems, in mobile devices and in secure car access applications.

One of the most important markets for UWB is mobile smart phones. In 2019, Apple launched iPhones having an UWB chip called U1 (Apple, 2019). Samsung released its first high-end mobile phones with UWB technology in 2020. Samsung was one of the founders of the FiRa consortium together with NXP and others (Samsung, 2019). UWB technology provides new opportunities for mobile phone use cases such as: secure access control, location-based services and device-to-device communications. To support third-party application development, Apple has released its "nearby interaction" framework for developers and chipset manufacturers who are developing UWB-based applications (Apple, 2021).

The automotive industry is creating UWB applications for secure access control and localization. For example, Bosch's Keyless management system utilizes UWB in mobile phones for secure access control (Bosch, 2021). Whereas the vehicle's access and starting are controlled via a digital key on a mobile phone that is triggered by the precise localization of the phone.

4 PRECISE INDOOR POSITIONING USING UWB/IMU IN DENSE ENVIRONMENTS

As the world heads towards Industry 4.0 and the reign of IoT and internet of everything (IoE), smart manufacturing and warehousing are becoming dependent on asset tracking technologies. Asset tracking is considered the backbone for smart logistics, smart delivery, smart shipping, and automated manufacturing. Industrial operators strive to keep real-time track of human resources, and robotic equipment especially inside large industrial environments. Hence, indoor positioning and navigation are essential factors for asset tracking in dense industrial venues. Prior to building reliable indoor navigation systems, a reliable positioning technology should be identified, investigated and assessed. In this chapter, the practical implementations of the proposed IPS using UWB/IMU sensor fusion scheme are discussed, to provide precise positioning estimations for indoor logistics. The experiments were held in Technobothnia laboratory, Vaasa, Finland. The scientific contributions of this chapter were discussed in publications **[P2]**, **[P3]**, and **[P4]**.

4.1 Preface on Technobothnia laboratory

One of the main facilities inside the University of Vaasa campus is the reputable industrial venue of Technobothnia (see Figure 17), a modern technical laboratory that serves at least three universities besides several corporations in the Ostrobothnia region. Technobothnia consists of several laboratories that resemble many kinds of technological sciences e.g. industrial robotics, smart operations, mobile robots, chemistry labs, heavy-duty 3D printing machines, telecommunications equipment, etc. The visiting traffic of Technobothnia is high, hence, an IPS will be very beneficial to both human operators and robot assets that are roaming the lab. However, the allocated resources are limited to low-cost IPS systems that are based on wireless technologies e.g. UWB, Wi-Fi, and Bluetooth low energy (BLE).

Figure 17. Technobothnia laboratory: a dense industrial environment on the University of Vaasa campus, Finland.

4.2 Methodologies and the fusion technique

Since the Technobothnia environment is very dense and challenging, the solution had to be through the sensor fusion techniques to keep the overall cost under the budget limits allocated for the IPS. As discussed briefly in Chapter 3 and thoroughly in publication **[P1]**, building a low-cost precise positioning system is feasible by employing one or more assisting resources to aid the primary IPS technology (Guo et al., 2020). Thus, a reliable IPS is not necessarily dependent on a single technology, instead, multiple technologies could be fused together to complement the desired performance metrics and achieve reliable positioning estimations.

For the implementation, an UWB system and an IMU were employed as the elements of the precise IPS in Technobothnia, with UWB as the primary technology, and IMU as the assisting sensor fusion unit. The role of IMU is to correct the biased, missing, and null values caused by NLOS conditions especially in this dense environment. Therefore, a loosely-coupled UWB/IMU integrated scheme was used for developing the precise IPS. A floor plan of the experiment area at Technobothnia laboratory is illustrated in Figure 18. The methodological foundations for Wi-Fi and BLE positioning systems were also laid in Technobothnia for future IPSs that shall track assets within 2-5 meters of accuracy.

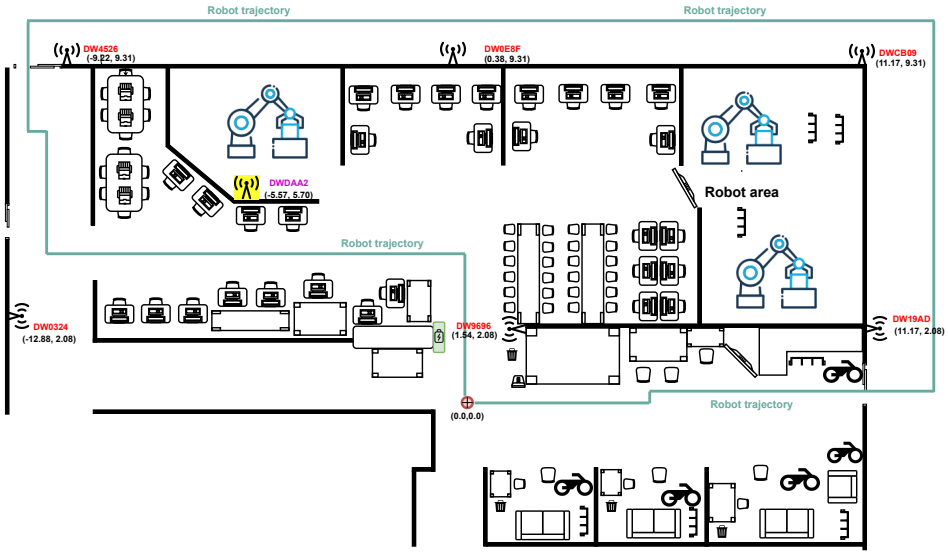

Figure 18. Floor plan of Technobothnia laboratory with the planned robot trajectory. The highlighted location (yellow) is for the tentative seventh UWB anchor. The robot's docking station is marked in Green.

4.3 Positioning sensors

A 12-anchor Decawave lab kit MDEK1001 (Decawave, 2017) was utilized to realize the UWB sensors in Technobothnia. The planned setup consisted of one movable tag, and 6 evenly distributed anchors to cover the experimental area of 28×15 square meters. A seventh anchor (DAA2) was

inserted during the experiments to investigate the performance of using six versus seven anchors. The default settings of the Decawave kit were programmed to provide raw distance measurements between the moving tag and a maximum of four anchors only (a limitation from Decawave) using TWR-TOA technique. In addition, a built-in filter was providing the final EKF estimates of the tag position (Decawave, 2017).

The IMU sensor (XSENS MTI-630) was used to obtain the inertial data of the mobile robot e.g.: orientation, rate of turn, acceleration, and magnetism. The IMU sensor provided another layer of information about the movement of the robot inside the dense environment, thus, accounting for the NLOS situations and helping in inferring the missing data to improve the output fusion-based positioning estimations.

Both UWB and IMU sensors were placed onboard an autonomous mobile robot developed by OMRON (as shown in Figure 19), the robot which possesses numerous positioning sensors e.g.: light amplification by stimulated emission of radiation (LASER), ultrasound, radio detection and ranging (RADAR), IMU, and light detection and ranging (LiDAR). The positioning data obtained from the OMRON robot had a millimeter accuracy with a confidence score of more than 90% most of the time (as stated by the built-in robot controller system). Hence, the OMRON trajectory data acted as the reference ground truth to the UWB/IMU fusion system.

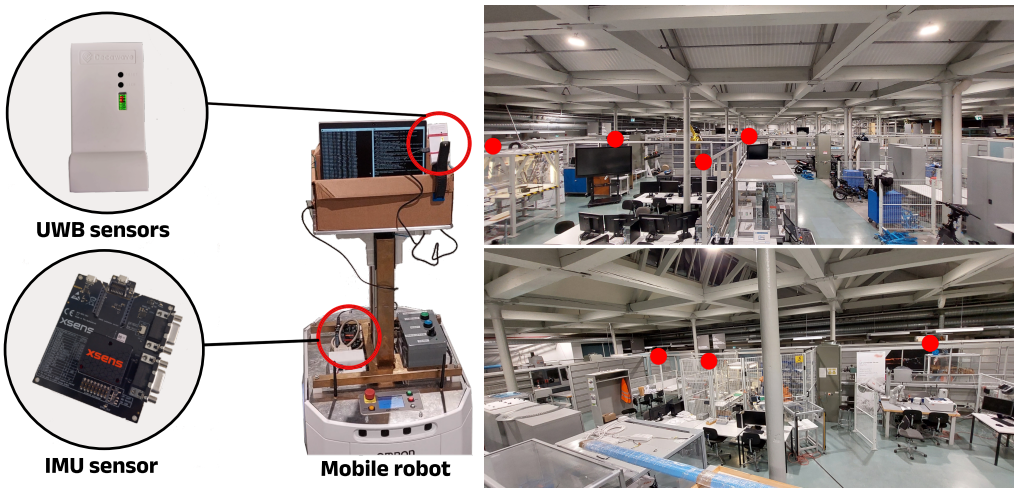

Figure 19. Elements of the designed IPS showing UWB anchors and tag (Decawave), IMU sensor (XSENS), the fusion software (on laptop), and the mobile robot (OMRON). The red dots refer to the locations of fixed UWB anchors in Technobothnia.

The planned robot trajectory was sketched to be a multi-modal route i.e. mixed paths of clear and obscured LOS between the user tag and the fixed UWB anchors, to test the reliability of the system in complex environments.

4.4 Implemented IPS algorithms

A set of algorithms was applied to sensor readings locally (per sensor) and globally (fusion) to achieve more accurate positioning estimations. Figure 20 illustrates the journey of the sensors data in the system through algorithms until obtaining the final positioning estimations.

First, the DR algorithm was utilized to fix the blank and null values arriving from UWB sensor readings. That was carried out by incorporating the previous non-null values fused with the heading angle, into the DR estimation algorithm of the current missing epoch, as illustrated in Equations (2.11). The IMU readings were propagated directly to the state-space estimation vectors of the measurements data. Afterwards, the refined UWB measurements were passed to the fusion EKF filter that combined both UWB and IMU information.

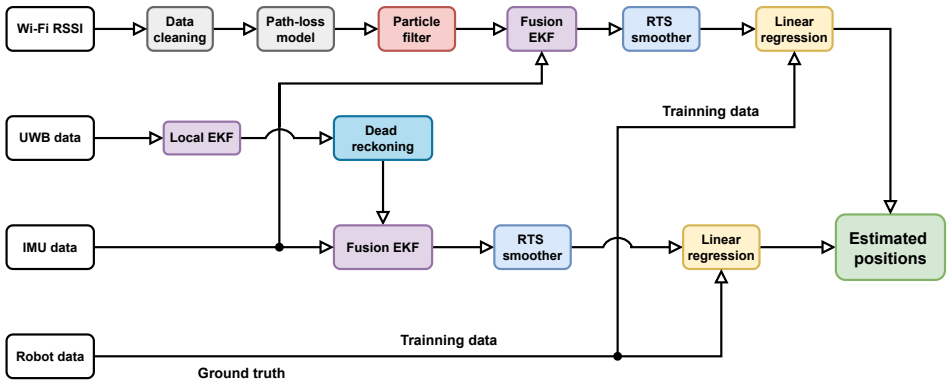

Figure 20. Data flow of measurements through the implemented algorithms to achieve optimum positioning estimations from three sensors: UWB, and RSS index (RSSI) based methods e.g.: Wi-Fi and BLE.

For the EKF fusion filter, the state-space vector $\mathbf{x_k}$ comprised the x-y positions, velocities, and accelerations (i.e. a 2-D Wiener dynamic model). While, the measurements vector $\mathbf{y_k}$ included the UWB x-y positions inbound from Decawave anchors, besides the x-y accelerations and (tentatively) the heading angles inbound from the IMU sensor. As shown in Equations (4.1).

$$\begin{aligned} \mathbf{x_k} &= [x \;\; \dot{x} \;\; \ddot{x} \;\; y \;\; \dot{y} \;\; \ddot{y}]^T, \\ \mathbf{y_k} &= [x_{UWB} \;\; \ddot{x}_{IMU} \;\; y_{UWB} \;\; \ddot{y}_{IMU}]^T. \end{aligned} \tag{4.1}$$

The output of the UWB/IMU-EKF method becomes the input to the RTS smoother to remove the excess fluctuations and retroactively smoothen the robot trajectory, using the formulas found in Equations (2.24).

Although the early results (see Figure 24) showed that the RTS algorithm made significant enhancements to the positioning estimations, a LR model was implemented to further refine and optimize the final estimations. In the hypothesis function for the multivariate LR, it was assumed that the independent features are the Cartesian $[x, \; y]$ position values of both OMRON robot and UWB, which are

represented by X in Equation (2.25). And, the offsets between the OMRON robot (which provides the ground truth data) and UWB represented by Y in Equation (2.25), is the dependent variable. Eventually, Equation (2.26) is applied to get the refined final positioning estimations, that is, the UWB/IMU EKF-RTS-LR method.

4.5 Experimental setup

The preparations for testing the hypothetical UWB/IMU fusion positioning technique were held in Technobothnia by developing a new customized embedded system that comprised the essential software and hardware peripherals. Then, the devices and the targeted environment were setup for experimentation.

Although Wi-Fi and BLE scanners were developed and reserved for Technobothnia's future use, the Wi-Fi fusion based positioning was attempted via RSSI data and IMU measurements. Using the same algorithmic suit EKF-RTS-LR, the results of Wi-Fi/IMU are discussed tacitly in Section 4.6.2, and thoroughly in publication **[P4]**. The results of the loosely coupled sensor fusion scheme UWB/IMU EKF-RTS-LR, which is the primary positioning system, are shown in Section 4.6.1.

4.5.1 Hardware and software

The hardware part consisted of a distributed set of UWB anchors (Decawave) with fixed positions around the coverage area, the IMU sensor (XSENS) mounted on the mobile robot, and the robot itself (OMRON), as shown in Figure 19.

The software part comprised numerous code files that record and communicate real-time data to a storage server, NodeRed. Every sensor point (UWB, IMU, and robot) has a dedicated software scanner that collects the desired tensors of data with the appropriate settings for their units. Afterward, the scanner passes them over to the NodeRed server via web sockets. Eventually, they are stored in a local web server, as illustrated in Figure 21.

4.5.2 Calibration and configuration

All sides of the coverage area including the locations of the fixed UWB anchors were LASER-metered using a highly accurate LASER ranger, the measurements were repeated several times until they were sufficiently verified (i.e. standard deviation was ≤ 0.01 m). The sensors of the OMRON robot were calibrated with localization accuracy exceeding 90% score (as stated by the built-in robot positioning system called "Mobile Planner"), as seen from Figure 23.

In addition, a new high-detail map of the surrounding environment with updated furniture positions was surveyed, as shown in Figure 22.

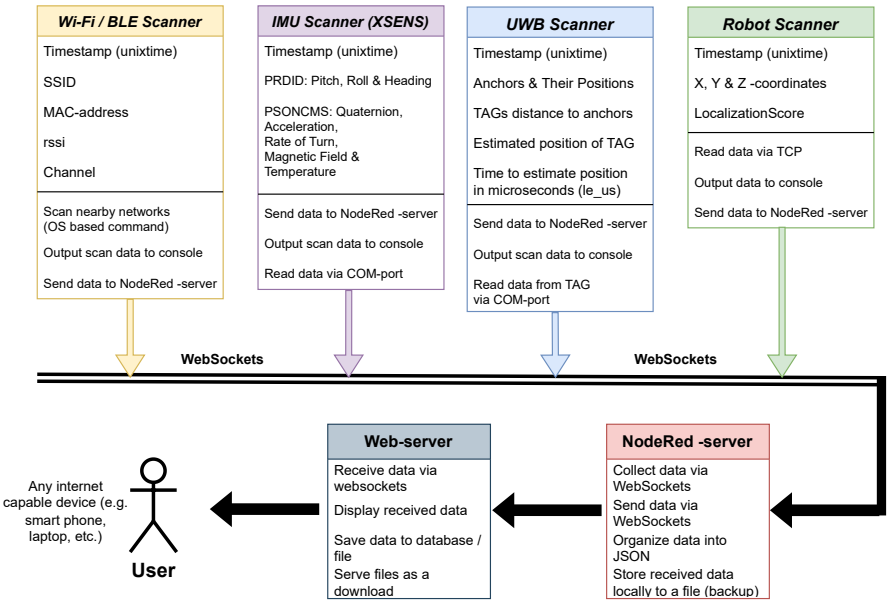

Figure 21. Block diagram showing the scheme of sensors data collection.

Figure 22. A cropped snapshot from the robot's internal software showing the floor plan of the laboratory after calibrating the map several times. The highlighted dense space is the target lab area where the experiment took place.

Figure 23. Calibration of IMU, surveying new OMRON map, and LASER-metering the coverage area.

UWB and IMU sensors were calibrated and configured to produce the appropriate units and positioning output, furthermore, the origin points of all sensors were aligned into a single point explicitly marked on the laboratory floor and programmed into sensor configurations.

All sensors (UWB, IMU, and robot) were configured to a sample rate of 10 Hz (Ts = 0.1 second) which was feasible across all sensors. However, increasing the sample rate frequency is directly proportional to increasing the fluctuations in sensor readings. On the other hand, decreasing the sample rate will mitigate the fluctuations but not in favor of sensitive operations that require such degree of semi-continuous positioning estimations for real-time applications.

4.5.3 Route design

On the robot's software controller (Mobile Planner), specific routes were designed to allow the robot to patrol the coverage area in various situations: 1) clear LOS between the UWB anchors and the robot, 2) poor LOS, 3) visibility through concrete and metal structures, and 4) with the fewest number of anchors (three) visible to the robot. Consequently, six UWB anchor locations were selected to provide evenly distributed coverage for the robot, while a seventh location was reserved for a feasibility test.

With all concerns addressed, sensors calibrated, and systems configured, the environment and sensors became ready for testing.

4.6 Results

The final results of the UWB IPS shown in Figure 24 and Table 5 are the same results from publication **[P3]**. In addition, a dedicated graph for every step (raw UWB data, EKF fusion, RTS smoothing, and LR filtration) is rendered to analyze and assess the proposed UWB IPS for both configurations scenarios (6 Vs 7 anchors). Moreover, a cumulative distribution function (CDF) curve is sketched per algorithm to investigate the performance of the system over time. Tables 4 and 5 show MAE, RMSE, and the 95% percentile values for all algorithms in both scenarios.

4.6.1 UWB/IMU with EKF-RTS-LR

Figure 24 reveals noticeable errors around the start and the stop positions which cause maximum fluctuations in the data. Higher accuracy is achieved by backing the EKF fusion algorithm with RTS smoother algorithm, which yielded significantly higher accuracy than the performance of the EKF fusion algorithm alone. Simultaneously, it has a higher accuracy than the raw UWB measurements, as also asserted by the numerical values of MAE, RMSE, and 95-percentile (p95%) errors.

The LR model was pre-trained using several positioning datasets recorded by the OMRON robot from the same environment but different values. Hence, the best positioning accuracy for the UWB/IMU configuration is achieved by smoothing the output of the EKF-RTS algorithm with LR algorithm. This procedure not only enhanced the performance of the UWB IPS but also resulted in significantly accurate positioning results, as seen from Figure 24 and Tables 4 and 5.

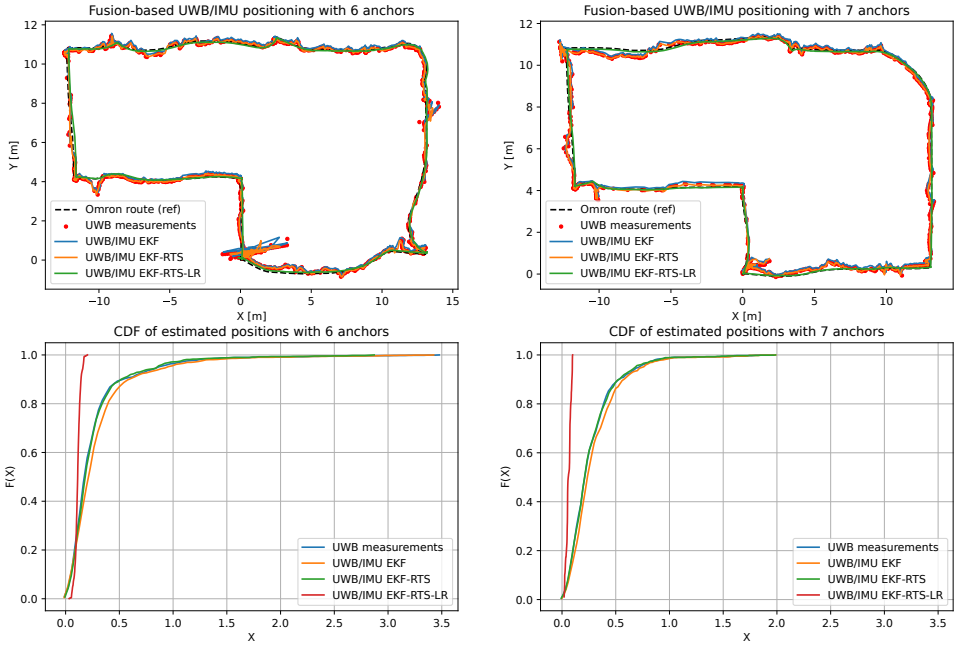

Figure 24. Subplots showing the final positioning results from both configuration scenarios (6 Vs 7 anchors). The lower subplots show the corresponding CDF curves for all algorithms in each scenario.

Table 4. UWB IPS positioning errors [in meters] from six UWB anchors.

	UWB raw EKF data	**UWB/IMU EKF fusion**	**UWB/IMU EKF-RTS**	**UWB/IMU EKF-RTS-LR**
MAE	0.240	0.259	0.232	0.078
RMSE	0.417	0.445	0.389	0.088
p95%	0.278	0.243	0.267	0.141

The LR filtration step yielded the best positioning accuracy in the 6-anchor configuration data with MAE = 7.8 cm, and RMSE = 8.8 cm compared to the second best records of 23.2 cm, and 38.9 cm (obtained with RTS MAE and RTS RMSE), respectively. Furthermore, the long term performance

Table 5. UWB IPS positioning errors [in meters] from seven UWB anchors.

	UWB raw EKF data	UWB/IMU EKF fusion	UWB/IMU EKF-RTS	UWB/IMU EKF-RTS-LR
MAE	0.221	0.235	0.218	0.047
RMSE	0.323	0.344	0.319	0.055
p95%	0.413	0.340	0.386	0.096

of the UWB/IMU EKF-RTS-LR algorithm is the highest ever in the 6-anchors configuration, by achieving 95% percentile value of 14.1 cm (could have been better if the stationary fluctuations were mitigated) and the most steep curve in the CDF plot, meaning that the LR smoothed solution is the best candidate for continuous accurate navigation services with relatively high standards for an IPS in this dense environment.

On the other hand, the UWB IPS results from the 7-anchor configuration are found to be more promising in most performance metrics as shown by the 2nd and the 4th subplots of Figure 24, and the values from Table 5. Similar to the 6-anchor configuration, the RTS smoothed EKF fusion results are coping with the raw UWB measurements most of the time, but outperform them in few occasions, that is why the CDF curve, MAE, RMSE, and p95% error values of both algorithms are nearly identical.

Finally, the ultimate method that comprises UWB/IMU EKF-RTS-LR possesses the best performance metrics in the 7-anchor configuration too, which was an expected behaviour from the algorithm, the more the merrier. The LR filtration step had leveraged the overall methodology to achieve MAE = 4.7 cm, and RMSE = 5.5 cm only, which is the most precise positioning accuracy ever achieved in the Technobothnia lab environment. The second most precise results were again from the RTS smoother of MAE = 21.8 cm, and RMSE = 31.9 cm. In addition, the long term performance of the UWB/IMU EKF-RTS-LR algorithm in the 7-anchors configuration is found to be also the highest with p95% = 9.6 cm and the steepest CDF plot among all other algorithms.

It is noteworthy to state that more recent UWB datasets yielded MAE = 3.7 cm, and RMSE = 4.5 cm, as outlined in publication **[P4]**.

In summary, the LR smoothed EKF-RTS-LR fusion algorithm can help to achieve the most precise positioning estimations inside Technobothnia laboratory, since it has demonstrated significantly better MAE, RMSE, and p95% values than all other algorithms, meaning that it does not only have the capability to achieve the most accurate positioning but will also score acceptable levels of continuity, availability and integrity.

4.6.2 Wi-Fi/IMU with EKF-RTS-LR

The Wi-Fi IPS is out of the scope for this doctoral dissertation, however, the fusion-based Wi-Fi/IMU PF-EKF-RTS-LR results were shown for documentation and insights. The Wi-Fi IPS performance could be acceptable in some scenarios for human resource positioning but it cannot be considered as a precise IPS under any circumstances for robots, as shown in Figure 25 and Table 6.

Table 6. Wi-Fi IPS positioning errors [in meters] from six Wi-Fi routers.

	Wi-Fi Particle Filter values	Wi-Fi/IMU EKF fusion	Wi-Fi/IMU EKF-RTS	Wi-Fi/IMU EKF-RTS-LR
MAE	6.862	6.863	6.854	4.515
RMSE	8.304	8.318	8.308	5.812

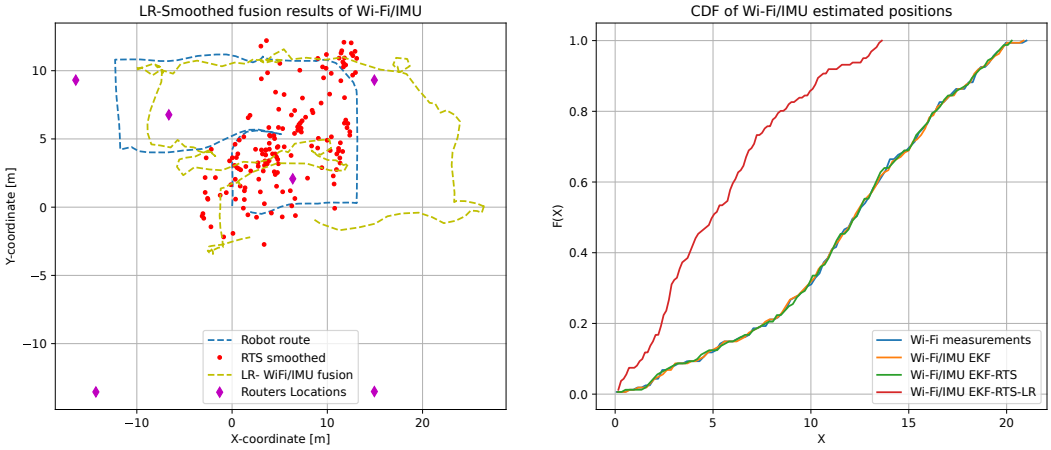

Figure 25. Result plots of the Wi-Fi IPS.

In short, the Wi-Fi IPS consisted of six routers (R0–R5) which were initially distributed by the IT department for non-positioning purposes i.e. just for normal internet coverage. That issue caused some problems of its own such as: 1) inconsistent path-loss readings that may be originated from 2) incompatible routers for positioning applications. More possibilities for the Wi-Fi inaccuracy could be 3) erroneous software scanner which holds the RSSI values for too long time before refreshing to new readings, 4) the extremely dense environment makes it super-challenging for Wi-Fi positioning in particular. In this occasion, PF was utilized instead of EKF for Wi-Fi sensors on a local scale. Since the designed Wi-Fi IPS uses RSSI measurements, therefore, PF was found to be more efficient than EKF in positioning estimations based on the very noisy RSSI values coming from routers R0–R5.

4.6.3 Commentary on the results

From Figures 24 and 25, all red curves in the given CDF sub-plots are having the most steepest slopes amongst their counterparts, meaning that the LR-smoothed EKF-RTS fusion method can yield the best and most accurate results even in dense industrial situations. That is, a very fitting solution to combating NLOS conditions with low-cost technologies. The method is proven to be reliable for both IPSs (UWB and Wi-Fi) to facilitate technical operations with precise location information using UWB/IMU, and ensure an acceptable level of performance for human resources tracking using Wi-Fi/IMU. Furthermore, both IPSs could be further enhanced in the future.

Thus, from the perspective of precise positioning aspects, the recommended IPS configuration is to cover the given lab region with seven UWB anchors aided by an IMU sensor per every UWB movable tag (user). And, their output data should be treated by the EKF-RTS-LR algorithm to achieve precise positioning estimations for mobile robot activities in dense industrial environments as found in Technobothnia lab, Finland.

In terms of assessment using other performance metrics, the integrity of the developed UWB/IMU IPS is well proven because the information provided by the positioning engine is trustworthy. Both service continuity and system availability metrics can be categorized into two parts: the onsite part (inside the lab environment), and the online part (providing the IPS service to end users via online platforms). For the onsite part, the developed UWB/IMU IPS performed well with regard to service continuity and system availability, all system components are capable for working in real-time with-

out known disruptions for local operations inside the environment. On the other hand, for the online part, both service continuity and system availability are subject to swings in connectivity concerns and/or service level disruptions. Could be based on several factors e.g. server errors, storage system capacity issues, web socket failures, and internet outages.

5 OUTDOOR SATELLITE-BASED POSITIONING SYSTEMS

Positioning and navigation technologies for outdoor environments are very essential for smart logistics and location-based applications that operate outdoors. Since the advent of GNSSs, the majority of outdoor navigation activities are carried out with the aid of GNSS satellites. However, other non-GNSS positioning methods exist with acceptable levels of performance. For example, as described in (Aly, Basalamah, & Youssef, 2017), the traces of outdoor radio signals in addition to pinpointing some unique virtual landmarks; yield the *DejaVu* positioning system which can be embedded in smart phones to retrieve the user locations with acceptable accuracy levels. Other positioning methods such as IMU, INS, and RFID can operate outdoors in some specific scenarios.

Yet, GNSS satellite-based positioning methods are known to have the unmatched, peak performance for outdoor positioning and navigation activities. Recently, a new satellite-based positioning method has emerged to seize the opportunity of having massive LEO satellite constellations in addition to mitigating some of GNSS shortcomings. Between the years 2021 and 2023, research activities were conducted for both outdoor satellite based positioning methods (i.e. GNSS and LEO) which are discussed in Chapters 5 and 6, respectively.

Publications **[P5]–[P10]** are concerned with leveraging smart logistics by achieving precise satellite-based positioning techniques for outdoor environments. GNSS publications are **[P5]**–**[P6]**, while LEO satellite publications are **[P7]**–**[P10]**.

5.1 GNSS positioning technologies

GNSSs are the most commonly used systems for outdoor positioning and navigation. They are key elements for location-based services that play a fundamental role in today's smart cities and the futuristic IoT applications. With the quantitative and diverse growth of GNSSs constellations, the positioning, navigation and timing (PNT) capabilities were strengthened to new frontiers. The advent of GPS marked the first commissioning of GNSS technologies during the 1990s when GPS was made available for civilian use (Ceruzzi, 2018). Since the 1990s and till present times, GPS was commercialized leading to the development of consumer GPS receivers and applications in various industries such as: transportation, surveying, and agriculture.

A typical GNSS system consists of three main segments: 1) space segment: where the satellite vehicles that form GNSS constellations reside permanently by orbiting Earth over $\geq 20,000$ kilometers above sea level, within the medium Earth orbit (MEO) and the geostationary Earth orbit (GEO) bands, 2) control segment: also known as ground stations that control the space segment, and 3) user segment: which represent the users who have GNSS receivers. Moreover, the space segment may contain an additional constellation called the "Differential GNSS or DGNSS", which provides satellite-based augmentation system (SBAS) to GNSS receivers. Figure 26 shows an outline of GNSS components.

Examples of existing GNSS constellations are: GPS, GLONASS, Beidou, Galileo, and recently the Korean KPS is scheduled to be launched into orbit before 2035 (Si-soo, 2021). And, examples of currently existing DGNSS in orbit are: WAAS, EGNOS, and QZSS (*GNSS Augmentation - Navipedia*, 2024).

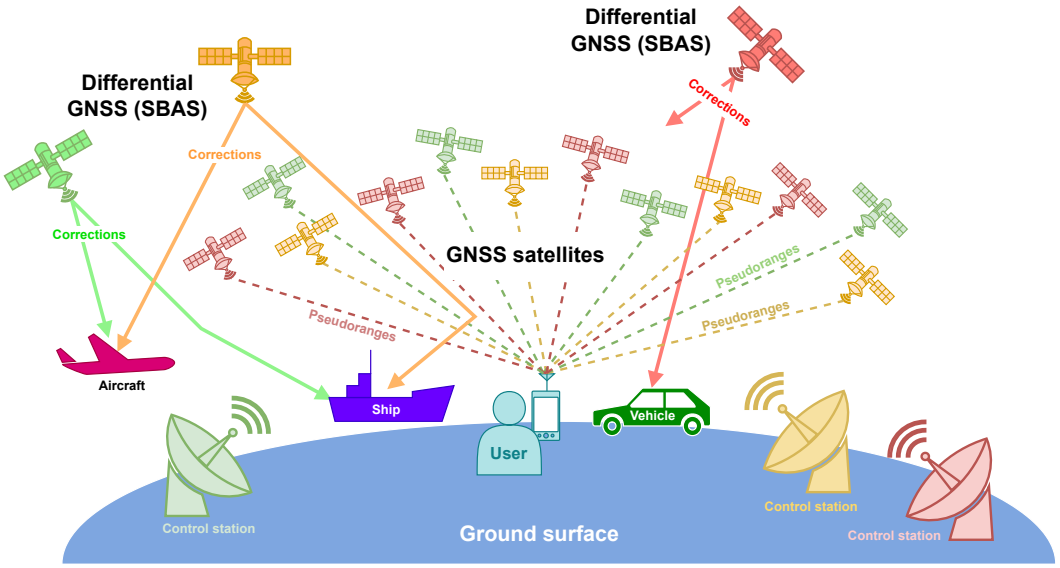

Figure 26. An overview showing the components of GNSS positioning systems. The coloring code refers to different GNSS constellations.

5.2 Operating principle of GNSSs

The basic positioning principle of GNSS relies on multilateration, where the receiver determines its distance from the pseudoranges of multiple satellites (with known positions) by measuring the time taken for radio signals to travel between GNSS satellites in space and receivers on ground surface.

5.2.1 System components

GNSSs operate by the collaboration between the three fundamental segments that are forming the system, as follows: (El-Rabbany, 2006; Misra & Enge, 2011)

1. **Satellite segment:** A constellation of satellite vehicles orbiting the Earth and continuously transmitting radio signals containing information about their orbital positions (ephemeris) and the current time stamp.
2. **Control segment:** A series of ground control stations that are responsible for monitoring and managing the satellite vehicles in orbit by: tracking their health, adjusting the orbits, providing data corrections for accuracy, and monitors signal integrity to ensure reliable positioning and timing information for users.
3. **User segment:** The receivers on the ground that are equipped in smartphones or vehicular GPS devices, receive the transmitted satellite signals and use the provided information to calculate their own position, velocity, and time using multilateration technique (discussed in Section 2.6).

Noteworthy, other peripheral components can exist to aid the main three segments of GNSS such as: the differential GNSS constellations, which are known as DGNSS or SBAS. As illustrated in Figure

26, DGNSS orbit the Earth via much higher altitudes than GNSS, to provide the essential clock and orbit corrections for vehicular users (e.g.: cars, ships, aircrafts), which improve the final positioning accuracy for such sensitive use cases.

5.2.2 Steps of GNSS positioning

GNSS signal reception precedes the GNSS positioning process. It has two main phases:

1. **Signal Acquisition:** Involves detecting and identifying the GNSS satellite signals from the channel background noise. This typically begins with a coarse acquisition search, where the receiver scans a wide range of frequencies and code phases to identify potential GNSS signals. Once a potential signal is detected, a fine acquisition search is performed to precisely lock onto the satellite signal of a given GNSS constellation.
2. **Signal Tracking:** Involves maintaining the phase coherence with GNSS satellite signals and continuously updating parameters such as: phase, frequency, and timing. Different tracking techniques, such as delay-lock loop (DLL) and phase-lock loop (PLL), are used to track the carrier and code phases. Also, during tracking, the receiver demodulates the received data payload to retrieve the navigation data broadcasted by GNSS satellites i.e. the ephemeris and clock corrections. The receiver processes the demodulated navigation data to extract precise satellite positions and timing information essential for accurate pseudorange estimation, hence, more accurate positioning.

Acquisition and tracking are essential processes for receiving and processing satellite signals to determine a receiver's position, velocity, and time. These processes are the core roles of GNSS receivers, which can bestow more precise positioning and better navigation capabilities.

After conducting GNSS signal acquisition and tracking stages, the receiver proceeds with the following steps in order to perform GNSS positioning:

- **Pseudorange measurements:** Once the receiver has acquired and tracked the signals from multiple satellites, it collects the measurements from each satellite. These measurements contain information about the distance between the receiver and each satellite, known as the pseudorange or carrier phase.
- **Satellite ephemeris and clock correction:** The receiver needs precise information about the positions and clocks of the satellites at the time of signal transmission. This data, known as ephemeris and clock corrections, is obtained from the satellite navigation message broadcast by GNSS satellites or through augmentation systems.
- **Geometrical evaluation:** Using the pseudorange measurements collected from multiple satellites and the precise satellite positions obtained from ephemeris data, the receiver calculates its position using geometric principles such as multilateration. By intersecting the spheres (or hyperbolas in the case of carrier phase measurements) centered at each satellite with radius equal to the measured pseudorange, the receiver position can be determined.
- **Error mitigation and optimization:** GNSS positioning is affected by various sources of errors such as: atmospheric effects, multipath, clock errors, and satellite geometry. To mitigate these errors and optimize the positioning solution, advanced techniques can be adopted such as: atmospheric modelling, RTK positioning, or precise point positioning.

- **Position estimation:** Finally, with the measurements processed, errors mitigated, and optimal positioning techniques applied, the GNSS receiver calculates its position in three-dimensional space (latitude, longitude, and altitude), along with velocity and time if needed. Also, the positioning solutions can be further optimized by using the positioning algorithms described in Section 2.7 and fusion techniques found in Section 2.9.

Overall, the positioning process in GNSS involves a combination of signal processing, measurement collection, geometric calculations, error mitigation, and optimization techniques to determine the accurate position of the receiver.

5.3 Advantages and challenges of GNSSs

The advantages of GNSSs are immense and outnumber the challenges significantly to a great extent. However, some GNSS shortcomings are inevitably existing.

5.3.1 Advantages

GNSSs possess numerous advantages such as:

- **Global coverage:** GNSSs offer a unique global coverage, which enable users to localize their positions anywhere on Earth provided that their GNSS receivers have an unobstructed line of sight to satellites (El-Rabbany, 2006). This global reach is essential for applications ranging from maritime navigation to precision agriculture, which provide users the necessary access for positioning and timing information regardless of their location.

- **High accuracy:** Throughout the past decades, the advances in GNSS technologies have significantly improved positioning accuracy, reaching the sub-meter and even centimeter-level accuracy (Teunissen & Montenbruck, 2017) in some cases. In addition, the differential techniques such as RTK positioning and carrier-phase processing, further enhance the GNSS accuracy for more sophisticated applications such as: land surveying, construction, and geodetic monitoring.

- **Availability:** GNSS satellites not only orbit the Earth constantly but also operate continuously, which provides positioning and timing information around the clock, irrespective of weather conditions or time of the day (Misra & Enge, 2011). This uninterrupted availability is vital for critical applications that rely on GNSS for navigation and timing synchronization such as: defense, emergency response, and transportation systems.

- **Versatility:** GNSS technologies are very versatile, with applications spanning various industries, activities, and customer segments. From guiding autonomous vehicles and optimizing logistics to facilitating search and rescue operations and supporting scientific research, GNSSs play an important role in enhancing efficiency, safety, and productivity for everyday life activities across diverse sectors.

5.3.2 Challenges

Some challenges affect the operation and performance of GNSSs, such as:

- **Signal degradation:** GNSS signals are susceptible to degradation due to various factors: atmospheric effects, ionospheric disturbances, multipath reflections, and signal blockages (El-Rabbany, 2006; Misra & Enge, 2011). These factors can lead to reduced accuracy or loss of signal acquisition and tracking, particularly in urban environments or areas with dense foliage, which require the development of advanced signal processing algorithms to mitigate their impact. One of the major impacts of signal degradation is the disability of GNSS to operate in indoor environments due to the fading and attenuation effects.

- **Vulnerability to interference:** GNSS signals are vulnerable to interference from both natural sources, such as solar activity and ionospheric disturbances, and human-made sources, including intentional jamming and nearby spectrum interference (Morales Ferre, Richter, De La Fuente, & Simona Lohan, 2019; Morales-Ferre, Richter, Falletti, de la Fuente, & Lohan, 2020). Jamming attacks impose significant threats to critical infrastructure and military operations, therefore, defensive measures for anti-jamming and signal authentication techniques, are required.

- **Urban canyon effects:** In urban environments characterized by large buildings and narrow streets, GNSS signals might suffer multipath reflections and signal blockages, leading to degraded accuracy and reliability (Morales Ferre, Richter, De La Fuente, & Simona Lohan, 2019). Augmentation systems, such as ground-based reference stations and SBAS, can mitigate urban canyon effects by providing additional correction data to GNSS receivers.

- **Cost and complexity:** Developing and maintaining GNSS infrastructure, including satellites, ground stations, and user equipment, incur significant costs and technical challenges. Moreover, ensuring the interoperability among different GNSS systems and addressing regulatory and policy issues add extra layers of complexity to the GNSS ecosystem, hence, collaboration and coordination among GNSS operators and stakeholders, are required.

- **Security and privacy concerns:** GNSS signals are vulnerable to spoofing attacks, where malicious actors transmit counterfeit signals to deceive GNSS receivers and manipulate positioning information (Morales-Ferre, Richter, Falletti, de la Fuente, & Lohan, 2020). Addressing security and privacy concerns requires the implementation of robust encryption, authentication, and integrity verification mechanisms to safeguard GNSS integrity and protect user privacy (Morales Ferre, Richter, De La Fuente, & Simona Lohan, 2019).

Dynamic positioning in urban environments is very challenging where GNSS satellites can experience frequent blockages, their carrier-phase reliability decrease or become insufficient in number of usable satellites (Aly, Basalamah, & Youssef, 2017). Hence, the mitigation of multipath effects is very essential for the integrity of GNSS positioning systems, as discussed in the subsequent sections.

Furthermore, LEO satellite based positioning systems emerged as a potential solution to the problems of jamming and spoofing, the topic which is discussed thoroughly in Chapter 6.

5.4 Mitigation of GNSS errors

GNSS standalone systems are providing acceptable level of integrity to many technologies especially in open-sky environments. Yet, they are not solely suitable for precise positioning and seamless navigation due to numerous factors such as: multipath fading, attenuation in dense environments, and signal obstruction in GNSS-denied conditions and urban environments. Mitigation solutions to GNSSs multipath shortcomings can be developed on various levels, as described in Figure 27. Examples are: antenna design, signal processing, receiver design, statistical methods, multi GNSSs, multisensor fusion GNSSs, and others.

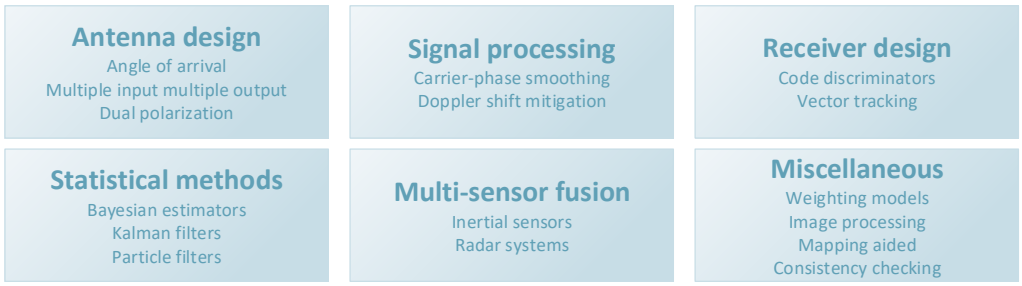

Figure 27. Summary of approaches for multipath mitigation in GNSSs, adapted from (N. Zhu, Marais, Bétaille, & Berbineau, 2018).

GNSS performs well in non-urban environments mainly due to the user visibility from numerous satellites (at least 4 satellites from the same GNSS constellation) in addition to the SBAS which provides GNSS with the essential clock corrections and the required redundancy. In urban canyon environments, satellites visibility becomes a challenge, hence, additional measures are required to maintain seamless navigation. Conventional GNSS stand-alone methodologies may fail to provide the required seamless navigation, therefore, researchers developed additional techniques to assist GNSSs. In this section three resolutions to GNSS challenges are highlighted: 1) multi GNSS, 2) multisensor fusion GNSS, and 3) LEO satellite based positioning.

5.4.1 Multi-GNSSs

Multi-GNSS refers to the use of signals from multiple GNSS constellations simultaneously to improve positioning accuracy, availability, and reliability. It works by the integration of all received GNSS signals from all visible GNSS satellite constellations. By utilizing signals from multiple constellations, multi-GNSS receivers shall have access to a larger number of satellites in view at any given time. This increases the number of available measurements, improves geometric dilution of precision (GDOP), and enhances positioning accuracy and availability, especially in challenging environments with obstructed sky views (K. Su, Jin, & Hoque, 2019).

Multi-GNSS enhances system redundancy and resilience by providing backup signals from different constellations. If signals from one constellation are obstructed or degraded due to factors like atmospheric conditions or satellite outages, the receiver can switch to signals from other constellations to maintain positioning capability (Montenbruck, Steigenberger, & Hauschild, 2014). By combining

measurements from multiple constellations, multi-GNSS receivers can mitigate errors and improve positioning accuracy. Differential corrections can be applied across multiple constellations to further enhance accuracy, while algorithms can optimize the use of available signals to improve reliability in challenging environments.

Moreover, multi-GNSS provides global coverage, as different constellations have varying satellite distributions and coverage areas. This ensures that positioning capability is available worldwide, regardless of the user's location.

In fact, multi-GNSS technology leverages signals from multiple satellite constellations to enhance positioning performance, reliability, and global coverage, making it a valuable tool for various applications such as navigation, surveying, timing, and transportation.

5.4.2 Multisensor fusion GNSSs

Similar to what was discussed earlier in Section 2.9, numerous positioning and/or tracking systems can be fused with GNSSs to provide more accurate and reliable estimations. Common examples of these systems are: INSs, IMUs, remote sensing devices (e.g. RADARS and LiDARS), and computer vision devices (e.g. cameras) as shown in Figure 28. A more detailed literature review on multisensor GNSSs is presented in publication **[P5]**.

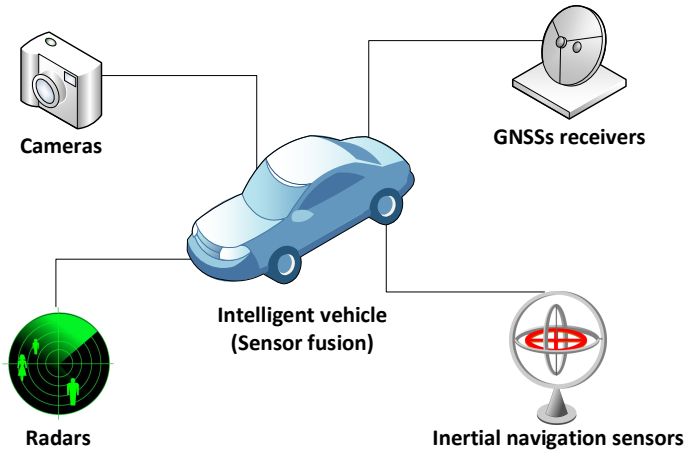

Figure 28. A multisensor GNSS-based system in intelligent vehicles.

INSs are very reliable positioning systems as they cannot be influenced by external factors. However, they can accumulate biases, drifts and errors over time (Liu, Pu, Sun, & He, 2019; Wang & Li, 2017). An IMU differs from an INS, as it is a standalone device not an integrated dynamic system as in the case of INSs. However, IMU units are considered the main building block of INSs (Christ & Wernli, 2014). IMUs can still be utilized independently in fusion-based localization endeavors, but INSs have been widely adopted in multisensor fusion systems throughout the recent literature.

When it comes to multisensor fusion schemes of GNSS/INS or GNSS/IMU, the main role of the primary positioning technology (i.e. GNSS) is to refine the inertial errors by tightening the position

estimate to the absolute coordinate system. In contrast, the inertial device provides more accurate delta position updates in a short term.

Globally, GNSS/INS fusion is a very popular implementation due to the numerous advantages of this integration over utilizing each system solely (Jie, Shaoshan, Yu, & Chongyu, 2006). Both systems have complementary data to provide, a GNSS estimates the position, velocity and timing (PVT) measurements while INS provide the detailed information about the attitude which yield a six degree of freedom (6-DOF) system (Srinivas & Kumar, 2017). The data rate of an INS is higher than a GNSS which produces better resolution for navigation. In addition, the multisensor fusion feature can leverage GNSSs to achieve seamless navigation in GNSS-denied environment. Consequently, the GNSS/INS multisensor fusion is appropriate for aerial, terrestrial and extraterrestrial navigation on Earth and in Space.

Another commonly used methods that can assist GNSSs in multisensor schemes are the remote sensing methods. Remote sensing is the process of mapping the target environment by sending pilot signals and analyzing the physical characteristics of the reflected signal. Pilot signals can be of different wavelengths, frequencies and types. RADAR systems are a type of remote sensing systems that utilizes low frequency radio signals as pilots, then detects the range of targets by analyzing the frequency of the rebounded fraction of the sent signal. LiDAR is another type of remote sensors that employs high frequency light LASERs in the same manner as RADARs.

Moreover, special types of Cameras can be considered as remote sensing systems when their functionalities are to map the topography of the surroundings, observe the heat maps of territories and so forth. Other types of remote sensing can be acoustical as the sonar systems, or can be ultra/infra sonic systems, depending on the target application. RADARs and LiDARs are very common types of localization techniques that can be used as standalone systems. They can be used in multisensor fusion systems with other technologies such as GNSSs.

As discussed in Section 2.9, every multisensor scheme should be treated with fusion algorithms that combine all sensor information in one fusion framework. Examples on those algorithmic methodologies of GNSS multisensor fusion systems are found under ”Statistical methods” in Figure 27.

5.5 Enhancing outdoor smart phone positioning

GNSS measurements can be impaired by external factors (e.g. multipath and interference). Hence, the integration of GNSS with IMU data becomes very beneficial. In multisensor fusion schemes, GNSS/IMU integration becomes advantageous by complementing both systems to enable accurate positioning results in dense and challenging regions. The research documented in publication **[P6]** shows the proposed multisensor GNSS/IMU fusion method during the participation in the Google Decimeter Challenge in 2022 (Howard et al., 2022).

5.5.1 Preface on the Google Decimeter Challenge

The Google Smartphone Decimeter Challenge (GSDC), initiated by the Android GPS team in Google Corporation, seeks to enhance smartphone positioning accuracy, particularly in urban environments where GNSS signals can be obstructed. The challenge aims to develop machine learning models that can improve GPS data resolution to the decimeter or even centimeter level, enabling advanced navigation services such as lane-level accuracy for carpool lane estimated time of arrival (ETA). The

competition, which began in 2021 and the participation took place in the 2022 edition, encourages research in smartphone GNSS positioning accuracy and leverages navigation data to achieve better smart phone localization performance. The GSDC ultimate goal is to enhance navigation methods and mobile internet applications by providing more precise geospatial information. (Howard et al., 2022; Leaderboard, 2022).

5.5.2 Problem statement and objectives

As stated on the GSDC web page, the problem statement of the competition can be described as follows: "*GNSS chipsets provide raw measurements, which can be used to compute the smartphone's position. Current mobile phones only offer 3-5 meters of positioning accuracy. For advanced use cases, the results are not fine enough nor reliable. Urban obstructions create the largest barriers to GPS accuracy. The data in this challenge includes only traces collected on open-sky and light urban roads. These highways and main streets are the most widely used roads and will test the limits of smartphone positioning*", (Howard et al., 2022).

The main goal of the GSDC was to "*compute smartphones location down to the decimeter or even centimeter resolution which could enable services that require lane-level accuracy such as HOV lane ETA estimation. You'll develop a model based on raw location measurements from Android smartphones collected in open-sky and light urban roads using datasets collected by the host.*"

5.6 Strategy for enhancing smart phone positioning

Inspired by the rationale of multisensor fusion GNSS/IMU schemes discussed in (C.-S. Chen, 2017; W. Li, Cui, & Lu, 2018) and the ML optimization method developed in (Watson & Gross, 2018), the same post-processing algorithmic approach was selected, since a similar environment was given in a similar context.

First, the RTK-GNSS technique that is a commonly used method for high-precision positioning (Takasu & Yasuda, 2009; Tim, 2021) was checked for adoption. However, RTK was found difficult to implement in smartphones due to the limitations of their antennas making them unable to solve the integer ambiguities in the carrier phase measurements.

Hence, a robust position estimation method was developed in which the post-processed kinematic (PPK) positioning data from smartphones GNSS observations (Takasu & Yasuda, 2009) were post-processed. In the PPK technique, the carrier phase is used to compute the user position by making use of differential corrections. In other words, the GNSS carrier-phase information were post-processed using PPK technique, that is, the MAP-PPK method.

The same algorithmic suit that was used in the UWB/IMU multisensor fusion scheme (discussed in Chapter 4), was utilized again in this context. That is, a loosely coupled integration scheme of GNSS data and IMU measurements was implemented for precise positioning estimation. The algorithms utilized are KF algorithm (as a fusion algorithm) and RTS smoother (to fine-tune the positioning trajectory).

In addition, a ML model is used to predict the driving paths (highways, tree-lined streets, or downtown areas) for adaptive positioning.

5.7 Methodologies and experimental setup

The competition datasets consisted of 206 traces collected by GNSS Android APIs (managed by Google Team) from various phone manufacturers (G. M. Fu, Khider, & van Diggelen, 2020). The training and test data were recorded while driving on some highways of the US San Francisco Bay Area, Summer of 2020, as shown in Figure 29. However, most of the ground truth data that was collected by a NovAtel SPAN system, was kept custodial by the competition organizers for results validation. Furthermore, GSDC datasets exhibited the WLS solutions for the GNSS positioning estimations in the Earth-centered Earth-fixed (ECEF) coordinates.

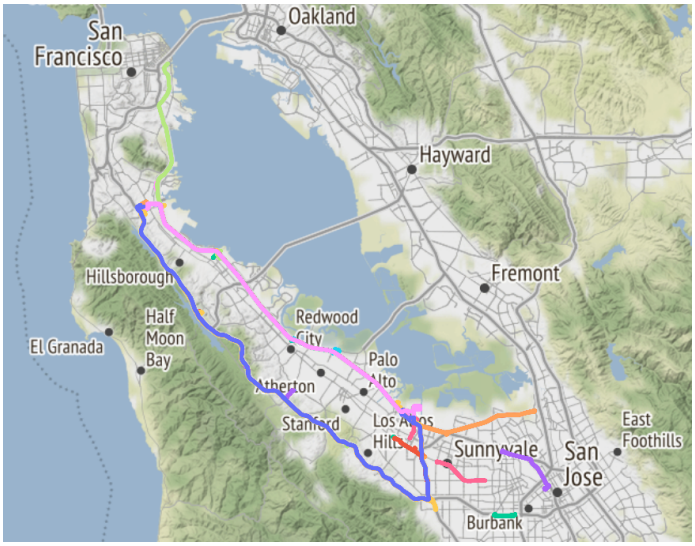

Figure 29. Routes where the datasets were collected, courtesy of Google Decimeter Challenge 2022.

The training datasets consisted of `GnssLogger` files, `RINEX` observation files, ground truth files, and smart phone device's IMU and GNSS data files. The test datasets included the same types of data and followed the same convention as the training dataset, except for the ground truth data that were not provided. The results of test datasets were meant to be used as the prediction of the expected ground truth and were evaluated against the actual custodial ground truth.

5.7.1 Using kNN algorithm

As discussed in Section 2.10.2, using kNN for detecting vehicular roads on given maps can be beneficial for GNSS positioning systems. By extracting relevant features from the map data and using the labeled training data, kNN can leverage spatial data analysis to classify regions as roads or non-roads, making it useful for tasks like map analysis and urban planning. Thus, a kNN model was trained to learn the pathways in order to refine GNSS accuracy by excluding the non-pathways from the positioning process.

In publication **[P6]**, kNN was used to predict the area of the smartphone data collection. This

problem was a classification problem. Hence, the kNN algorithm was used to classify the phone data based on the location where the data was collected. The area was divided into three categories namely: highway, tree-line, and downtown areas according to nature of the environment.

The numbers 1 to 29 represent the collection of the GNSS data of each phone for a particular day. These were then grouped based on the area where the GNSS data was collected (downtown, highway or tree-line). The data was organized in a way such that the phones could be grouped and labeled according to where their data was collected (downtown, highway and tree-line).

All phones were grouped under one of three groups and the groups were then encoded for training (0 = highway , 1 = tree-line, and 2 = downtown) .

The kNN model was trained to classify new data from a new phone into one of the groups or categories (highway, tree-line, or downtown). Afterwards, a RTKLIP PPK configurations was used to process the phone's data based on the classification results.

5.7.2 Using the Kalman fusion algorithm

The dynamic state vector of the fusing Kalman filter mainly comprised the GNSS measured longitudes and latitudes in ECEF coordinates, in addition to the Cartesian velocities of the user, and the IMU (accelerometer) epochs in Cartesian coordinates, as shown in Equation (5.1) (similar to Equation (4.1) from Chapter 4):

$$\mathbf{x} = \begin{bmatrix} p^x & v_x & a_x & p^y & v_y & a_y \end{bmatrix}^T . \tag{5.1}$$

where p^x, p^y are the (longitude, latitude) positions, respectively, gained from GNSS. v_x, v_y are the velocities, and a_x, a_y are the IMU accelerations. Hence, the measurements are p^x, p^y and a_x, a_y. The measurement vector $\mathbf{y_k}$ consisted of the GNSS positioning components and the linear accelerations from IMU.

Similarly, the RTS smoother algorithm worked retroactively to filter the fluctuations and ripples of the vehicle movement by incorporating the output covariance and error residuals into account, as demonstrated in Equations (2.24).

In summary, the steps of applying our proposed GNSS/IMU KF-RTS-ML method proceeded as follows, also found in Figure 30:

1. Data analysis and pre-processing
2. ML based prediction of driving paths using kNN
3. PPK precise positioning techniques to process the GNSS carrier phase
4. GNSS/IMU multisensor fusion integration using KF-RTS algorithms

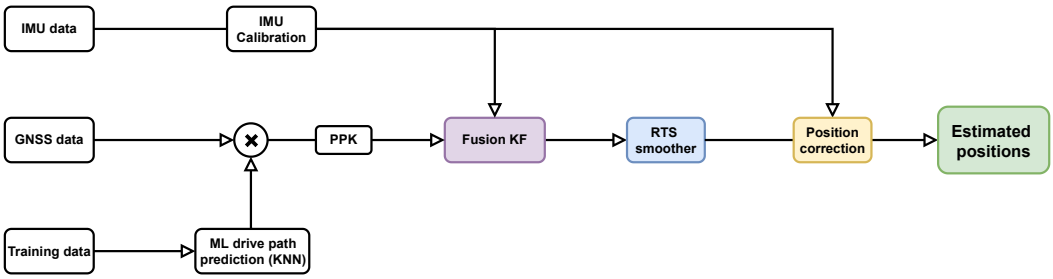

Figure 30. Steps of applying the proposed GNSS/IMU fusion MAP-PPK method.

5.8 Results

The evaluation criteria of GSDC were as follows: "*Submissions are scored on the mean of the 50th and 95th percentile distance errors. For every phone and once per second, the horizontal distance (in meters) is computed between the predicted latitude/longitude and the ground truth latitude/longitude. These distance errors form a distribution from which the 50th and 95th percentile errors are calculated (i.e. the 95th percentile error is the value, in meters, for which 95% of the distance errors are smaller). The 50th and 95th percentile errors are then averaged for each phone. Lastly, the mean of these averaged values is calculated across all phones in the test set.*"

We estimated the location of the smartphone using the carrier phase information of the data, and the evaluation of our method was conducted on the Kaggle platform by comparing against the locally-generated ground truth.

The results from our proposed method showed significant improvements in the positioning accuracy for all road driving scenarios compared to the given WLS solution, as shown in Figure 31.

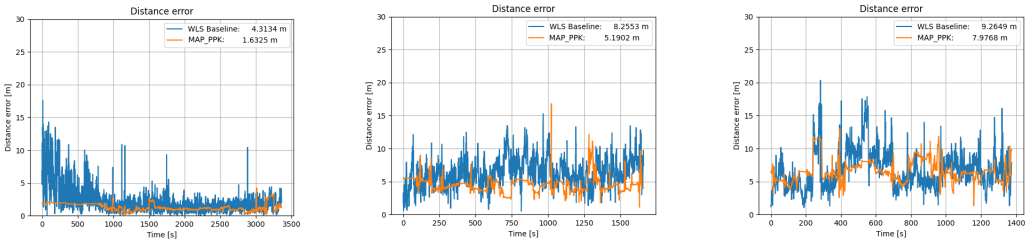

(a) Highway. **(b)** Tree-lined Street. **(c)** Downtown.

Figure 31. Comparison of positioning error between the WLS baseline and the proposed method for each mode of driving paths.

Provided that the actual ground truth datasets were hidden, the results were compared against the next best choice which was the WLS data. Figure 31 shows a significant reduction in positioning errors in favor of our proposed MAP-PPK method when compared with the WLS baseline results in all driving road modes: highway roads, tree-lined and pole-pinned streets, and downtown roads.

By adopting the ML based adaptive PPK positioning techniques on the GSDC test datasets, the mean

accuracy was found to be 2.61 meters for the public score on Kaggle platform. However, after the final evaluation, the private score was evaluated to be **2.29 m** error, which was more enhanced than the original 3-5 m accuracy.

5.8.1 Commentary on the results

GNSS low-cost receivers often have limited channels and computational resources. Therefore, the complexity of the algorithm had to be kept modest. The proposed loosely coupled (GNSS/IMU KF-RTS-ML) method made an acceptable performance in terms of accuracy, robustness, costs, timing, and integrity. Further validations and investigations should be performed to ensure the suitability of the method for real-time applications

In the GSDC 2022 final published results, although the final place of our team "DigiECO_UVA" in the leaderboard was 69th out of 573, our method achieved mean accuracy of **2.291 meters** which awarded our solution a Bronze Medal (Leaderboard, 2022), among others. From this result, it is very convincing that the proposed method (LC-GNSS/IMU/ML using MAP-PPK) can be used to improve the position estimation of smartphones accuracy.

6 LOW EARTH ORBIT SATELLITE BASED POSITIONING

The existing GNSSs are well established and widely used for high-precision outdoor positioning across various consumer segments. They offer global coverage in the most densely populated regions on Earth and they exhibit excellent availability and interoperability, often collaborating with SBAS. However, GNSS systems operate at much higher altitudes, resulting in greater signal degradation from various communications and atmospheric factors. Additionally, the high altitudes limit the signal ability to penetrate indoor spaces due to substantial shadowing effects caused by obstructions. Also, GNSS signals are susceptible to manipulation, making them vulnerable to jamming and spoofing. Therefore, exploring new satellite-based methods to address these GNSS limitations through reliable positioning is a worthwhile endeavor.

In this chapter, the potential of achieving reliable positioning solutions from LEO satellites is discussed to create a new navigation method that mitigates GNSS shortcomings for outdoor applications. The content within is retrieved from publications **[P7]**–**[P10]**. First, the topic was introduced and surveyed in publications **[P7]** and **[P8]**, respectively. Then, a proof of concept for the new method was rendered in publication **[P9]**. Finally, the proposed method was tested and validated using simulated data on real trajectories in publication **[P10]**.

6.1 Introduction to LEO–PNT

In recent years, there has been a noticeable surge in interest surrounding LEO-PNT methods, largely driven by the number of LEO satellites in Earth's orbits. The primary objective of LEO-PNT as a research track is to complement existing GNSS by providing enhanced navigation capabilities in challenging scenarios. This includes autonomous navigation, urban environments, areas with dense forest canopies, and even indoor spaces. Most LEO-PNT techniques typically rely on the deployment of dedicated LEO satellite missions, which can be a costly and resource-intensive endeavor. However, a notable exception to this paradigm is the emergence of MIMO beam ID-based methods, as firstly introduced in publication **[P7]** and discussed in Section 6.2. These innovative techniques enable opportunistic utilization of data transmitted by any available LEO satellite. Enhancing not only the sustainability of space-based exploitation, but also fostering a more adaptive approach to LEO-PNT.

In the past few years, LEO potential in the context of positioning and localization has also started to be investigated, and the LEO-PNT concept has emerged. There are three approaches to the use of LEO constellations for positioning:

1. **SoO approach:** LEO signals as signals of opportunity (SoO). No specific positioning signals are transmitted and the burden of the PNT engine is at the receiver end. Measurements such as: AOA, RSS, or Doppler shifts can be used.
2. **Modified-payload approach:** modification of the LEO transmitter payload to support positioning signalling. GNSS receivers can also be installed onboard the satellites and GNSS-like signals can be rebroadcast in other frequency bands. This can be seen as a "parasitic" solution to LEO signal payloads.
3. **Dedicated LEO-PNT approach:** New LEO-PNT systems with optimized design parameters for positioning and navigation targets (e.g., (Çelikbilek, Saleem, Morales Ferre, Praks, &

Lohan, 2022)).

Dedicated LEO-PNT systems often provide with the highest accuracy among LEO-PNT methods. They require on-board instruments dedicated to providing positioning signals from LEO satellites. Ground users are capable to retrieve GNSS-like observations (pseudoranges and carrier phases) and apply typical GNSS positioning strategies, such as PPP (Ge et al., 2022; M. Li, Xu, Guan, Gao, & Jiang, 2022). Remarkable efforts have been made to develop dedicated LEO-PNT systems by Xona Space System (Rainbow, 2022), the European Space Agency (ESA) (Knight, 2022), CENTISPACE^{TM} (L. Chen et al., 2023), and the indoor navigation from CubeSat technology (INCUBATE) project (INCUBATE, 2022).

SoO opportunistic methods do not involve the transmission of specific PNT messages to users. Consequently, users have no access to precise information regarding satellite orbits and timing. They are often relying on simplified ephemeris data such as two-line elements (TLE) (Farhangian & Landry, 2020; Khalife & Kassas, 2019; Tan, Qin, Cong, & Zhao, 2020). The most common observation is the Doppler shift, providing similar capabilities to the Transit mission (Psiaki, 2021), which was one of the earliest operational satellite-based navigation systems. Presently, numerous studies delve into the potential of opportunistic techniques involving Doppler shifts. The overall accuracy achieved through these methods typically vary within the range of 7 meters to 1000 meters (as discussed in publication **[P8]**), depending on factors such as the estimation procedure employed, the environmental conditions surrounding the receiver, and the extent of satellite constellation coverage.

The new method presented in Section 6.2 can be applied by both dedicated and opportunistic LEO-PNT systems. A preliminary study stated in publications **[P7]** and **[P9]** suggested that LEO satellite beamforming loops should be given unique identifiers (IDs) in the downlink (DL) super-frames to allow users to perform passive positioning. Whereas, the beam IDs can be used as tokens to fetch the satellite ephemeris (time stamped position in orbit), satellite orientation, and massive MIMO (mMIMO) beam pattern information from the satellite vehicle (SV). Subsequently, the beams' footprints (coverage area) on Earth can be estimated, providing a way to perform user multilateration. This positioning method is not dependent on accurate RSS values, time corrections, or other measurements, but it requires dense satellite constellations. It cannot provide precise time information, yet.

6.2 Massive MIMO in the context of LEO–PNT

The introduction of mMIMO antennas in LEO satellites are under deployment. Currently, only few to none of the existing satellite constellations are MIMO-capable, but it is expected that many future LEO constellations are to be equipped with such technology in the following years. Numerous research efforts have been put into this topic due to the merits that it offers, including better throughput, higher capacity, and enhanced quality of service (You et al., 2020).

mMIMO differs from MIMO in terms of the number of onboard antenna elements. mMIMO is implemented by employing 1024 or more antenna elements that are separated by a distance equivalent to half the wavelength (You et al., 2020; Y. Zhang et al., 2021). From an opportunistic perspective, both MIMO and mMIMO signals can be exploited to provide location information based on the beamforming loop IDs. When the number of beams increases as in mMIMO, the positioning resolution is expected to improve.

The congregation of beams from many satellites generates a combined beam footprint that comprises numerous intersections of beams even for a single satellite vehicle. The more satellites there are

illuminating the location of the user terminal (UT) and the smaller the beams are in radius; the smaller the intersections are and the more accurate the positioning estimate is. In each intersection, a particular combination of beam IDs can be detected. By knowing the trajectory and the beam footprint patterns of LEO satellites the vector of beam IDs can be used as the key to extract the position estimates from the time-stamped geo-location information of the beam footprints whenever detected by the UT.

The number of major beams (loops) produced by a single satellite vehicle will depend on the adopted scheme of beamforming in the mMIMO system. Based on the reviewed literature (Ayach, Rajagopal, Abu-Surra, Pi, & Heath, 2014; Molisch et al., 2017; Palacios, Gonzalez-Prelcic, Mosquera, Shimizu, & Wang, 2021), the hybrid beamforming scheme can provide a control over the beam pattern by exploiting the advantages of both analog and digital beamforming schemes. In the method, the mMIMO array is divided into sub-arrays, where each sub-array is connected to a RF chain in order to produce one steerable main beam whose radius is also controllable. For the hybrid beamforming scheme presented in Figure 32, the number of the major beams is proportional to the number of the allocated RF chains.

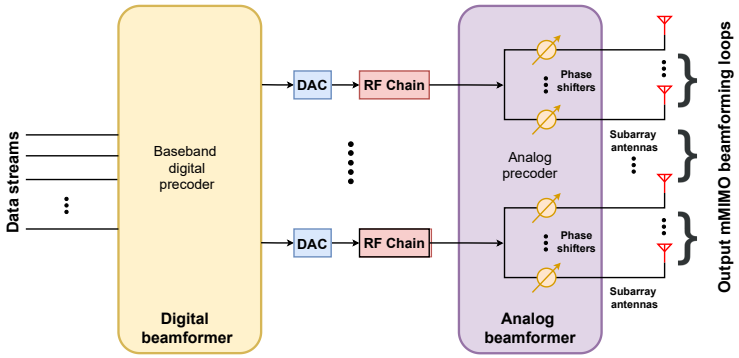

Figure 32. Block diagram showing the scheme of hybrid mMIMO beamforming.

6.3 A new positioning paradigm via LEO–MIMO

This section states the foundations upon which the future implementation of the LEO positioning concept and the research simulation environments are constructed. The main objective is to investigate the suitability of MIMO beamforming loops to be regarded as *geographical pointers*. The identification of those pointers, in addition to the geographical definition of the beam footprints on Earth's surface, shall grant UTs the ability to estimate their positions. The estimation of the UT position is then an optimization task with respect to the vector of the detected beam IDs. In other words, the beams that are incident from LEO satellites will be used as cues to determine the location of the receiver, by solving and optimizing the geometrical problem with known satellite trajectories.

The proposed positioning method requires two types of information datasets: 1) The static datasets that provide fixed information about LEO satellites, e.g., the onboard antenna attributes, the beam patterns, and the beam identifiers. 2) The dynamic datasets that deliver time-stamped information on the location of the satellites and their beams. The detail level of the information on the beams and their *footprints* on Earth can vary. The minimum requirement is to know the locations of the beam

centers (on Earth) for a given time instant. In this study, the beam radii are assumed to be known to the receivers.

When a UT receives signaling (or a handshake) from LEO satellites, it decodes the received frames to find the beam identifiers. With those beam IDs, the UT retrieves the satellite datasets. Based on the geo-location information of the detected beam footprints, the UT is able to multilaterate its own position, as illustrated in Figure 33. Thus, the positioning solution is tangible even with one beam only, however, the congregation of more beams from more LEO satellites shall result in more resolution (i.e. positioning accuracy). Moreover, improved accurate position estimates can be achieved by excluding the undetected footprints, as explained in Section 6.4.3.

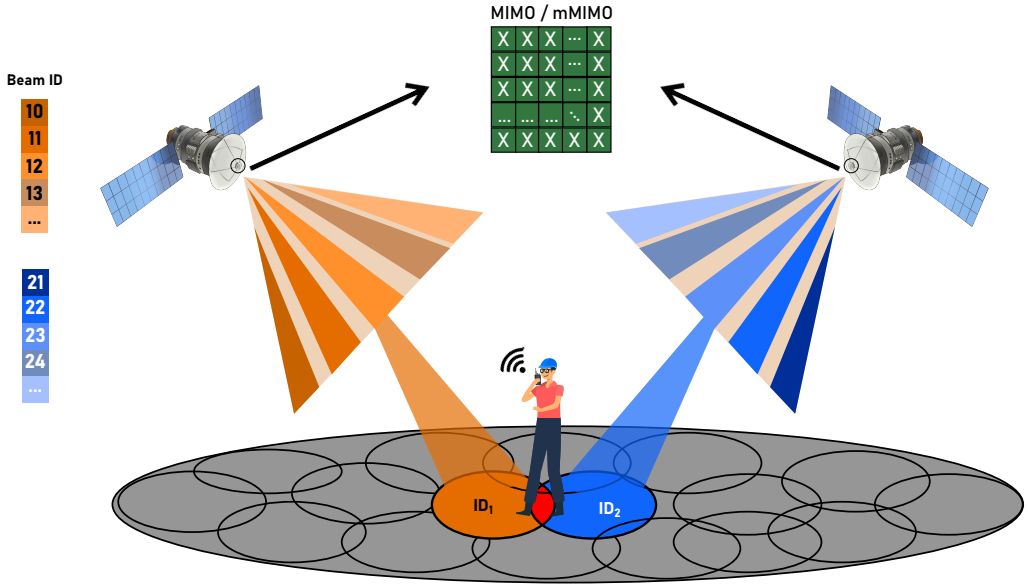

Figure 33. A new LEO-based positioning method from MIMO beam footprints.

The transmitted beam pattern and the geometry between the satellite and the UT infer -to a large extent- the projected shapes of beam footprints. As the positioning concept relies heavily on the information of the beam footprints, essential geometrical and geographical parameters are illustrated in Figure 34. They are, e.g.: the elevation angle, the satellite orbital inclination plane, the beams patterns, and the attributes of the beam conic shape.

In Figure 34, the following aspects are illustrated: (a) Satellite orbital plane inclination with respect to Earth's axis. (b) The satellite mesh coverage in terms of interlocked MIMO beam footprints. (c) MIMO beam geometry is approximated to a conic shape when received on Earth's surface.

The orbital inclination angle and the altitude (see Figure 34a) are the primary attributes to determine the coverage area of a satellite. When it comes to satellite constellations, the objective is to optimize both aspects so that satellites maintain a constant occupation over the regions of interests (ROIs). The transmitted pattern and the elevation angle control the shape of the projected beam footprints (see Figure 34b). The instantaneous orientation of the satellite and Earth's topology also affects the

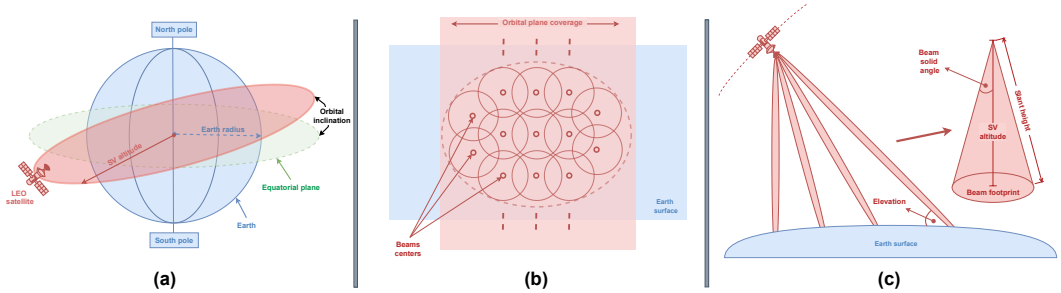

Figure 34. Illustration depicting the satellite-to-Earth geometry.

footprint shape, among other factors. Beamforming parameters and attributes of antennas determine the transmitted pattern, which also can be designed in the form of fixed or steerable circular footprints (Palacios, Gonzalez-Prelcic, Mosquera, Shimizu, & Wang, 2021; Palacios, González-Prelcic, Mosquera, & Shimizu, 2021).

The locations of beam footprints can be predicted once the transmitted patterns and the instantaneous values of the satellite-to-Earth geometry are known. However, the computational complexity increases depending on the required detail level of the footprints and the number of variables involved. Therefore, assuming a fixed pattern and identical beam shapes would ease the computational burden.

6.3.1 Advantages

This novel beam ID-based positioning method provides numerous advantages to the realm of location-based services, research, and applications. Due to its simplified system layout and utilization of opportunistic LEO signals, the beam ID-based method is expected to gain popularity across user segments whenever the technical base requirements are met.

The beam ID-based method offers better SNR or RSS compared to signals from GNSS due to the closer proximity of LEO satellites to Earth. Moreover, it refrains UTs to use any kind of high-sensitive receivers as they will be passively receiving beam IDs (only) without the need for going through the data payloads. This SoO approach can lead to significant reductions in overall costs by diminishing the financial burden associated with sophisticated equipment, as in conventional positioning systems.

Additionally, the beam ID-based approach is resilient towards signal degradation due to path losses and interference. Because the positioning estimation does not require perfect line of sight, it does not require signal reception at certain circumstances. The methodology's performance maintains its robustness even under extreme conditions, ensuring the continuous availability of positioning data. Besides, the system can have good performance in scenarios characterized by unfavorable GDOP profiles, something that is not achievable with GNSS.

6.3.2 Challenges

Intrinsic concerns are expected to challenge the beam ID-based positioning method and impair its operation. For example, the realization of hybrid mMIMO beamforming onboard LEO satellites is

already complicated due to massive antenna elements required to be planted on small-sized LEO satellites, something that may also limit the vehicle's power budget. With optimal designs and suitable telecommunications solutions, the mMIMO link budget can be adjusted to provide the minimum acceptable level of beam coverage to the regions of interest on Earth.

LEO satellites are not owned by a single entity but by several tens of governments and corporations, which shall compromise the interoperability between LEO constellations. Hence, entities who own the mMIMO-equipped LEO satellites should follow with the prescribed technical specifications for their constellation beam footprints in order to allow performing positioning estimations.

Sharing accurate LEO constellation ephemeris and their fixed beam footprint patterns also remains as a major concern, because technical data sharing is not an appealing matter for most private satellite operators. However, it can be granted with the appropriate measures to be taken, also with the expected revenue streams from the corresponding customer segments who are targeted with such a positioning service. To resolve this issue, new independent vendor entities may emerge to bind all LEO constellation operators together in order to handle data sharing and manage the execution and delivery of this positioning service between the users and the operators.

6.4 Technical considerations

As described in Section 6.3, the proposed positioning process is based on the congregation of beams from LEO satellites resulting in inevitable geometrical intersections between all beam patterns that are being received. This leads to solving the positioning estimation problem via geometry algorithms. Figure 35 summarizes the entire positioning process using beam IDs from mMIMO-equipped LEO satellites.

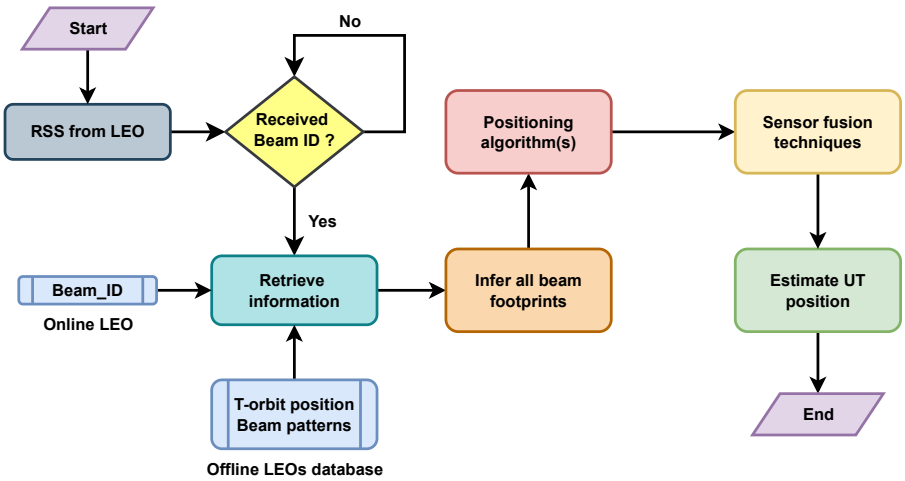

Figure 35. Flowchart of the beam ID-based positioning method.

For the method to be efficient and viable, the beam patterns of LEO satellites should have fixed shapes (known to the users or the positioning engine) and intersect other beams within the same

pattern, like an overlapping mesh shape. Whenever the UT receives LEO-mMIMO satellite communications, it should be able to extract each beam's unique ID. The IDs serve as tokens to fetch more information about the transmitting satellite vehicle, LEO constellation, shape of the beam footprint pattern, timestamped location of the satellite vehicle, and expected beam footprint geographic trajectory on Earth's surface. Eventually, by receiving just one beam ID only from one LEO satellite, the UT can still infer information about its location on Earth with maximum error equivalent to the radius of the received beam footprint.

6.4.1 Transmitter aspects

LEO satellite constellations should be equipped with 1024 or more antenna elements because the best case scenarios is to have more beams per a satellite, which require massive numbers of antenna arrays. Optimally, the transmitted pattern would be fine-tuned to serve the UTs in the desired ROI. This can be achieved by designing the mMIMO codebook and the RF link budget to produce reliable RSS and SNR levels on Earth's surface.

In practice, the skies will bear numerous corporate-owned satellite constellations during the next decade(s), implying that interoperability is not guaranteed. Fortunately, the proposed concept can perform without interoperability as long as the satellite information datasets are kept open access. Corporations can withhold the payload dataframes (e.g. broadband data) from non-subscribers, while allowing any receiver to access the beam IDs during the signaling phase. This will lead to the establishment of positioning systems that utilize most of LEO constellations.

As for the coverage aspects, an optimum LEO satellite constellation was proposed to cover the planet in publication **[P8]**: a minimum of 400 SVs placed at 600 km in altitude, and a minimum of 10 orbital planes inclined at no less than 72°. The same altitude was prescribed in (Caus, Perez-Neira, & Mendez, 2021) to design a beam pattern that has interlocked footprints. The number of major beams produced by a single SV will depend on the adopted scheme of beamforming. According to the reviewed literature (Ayach, Rajagopal, Abu-Surra, Pi, & Heath, 2014; Molisch et al., 2017; Palacios, Gonzalez-Prelcic, Mosquera, Shimizu, & Wang, 2021), the hybrid beamforming scheme is promising in providing control over the beam pattern.

6.4.2 Channel model and user segment

Realistic channel models for mMIMO hybrid beamforming communications were presented in (Khalife & Kassas, 2019; Molisch et al., 2017; Palacios, Gonzalez-Prelcic, Mosquera, Shimizu, & Wang, 2021; Palacios, González-Prelcic, Mosquera, & Shimizu, 2021), whereas in this study, a perfect channel is assumed for simplicity and primarily proving the concept. It is intended to perform more deep studies concerning the telecommunications aspects in future researches. In addition, the user segment (receiver end) is assumed to be a non-MIMO receiver (non-directed receiver pattern) throughout this study.

The most important issue for UT is the ability to read signals from many LEO satellites simultaneously and to fetch their beam IDs. UTs can either use embedded resources or cloud services for positioning. If embedded resources suffice, positioning would be totally passive i.e. UTs would not consume energy for uplink.

6.4.3 Positioning methodology

The positioning methodology is based on: 1) the information on the boundaries of the individual beam footprints, 2) operations of mathematical set, and 3) computation of the center of gravity (CoG) of an area.

The beam footprints form sets of coordinates. The intersection of the sets that represent the detected beams yields the region, inside which the receiver must be located (i.e., the 100% confidence set), simply because the receiver has been able to detect those beams in the first place. By subtracting sets that represent the adjacent undetected beams from the intersection set, the size of the confidence set can be decreased. The two variants of positioning methodology are: **ALG. A**: that utilizes only the detected beams, while **ALG. B**: that uses subtraction to enhance the position estimates.

Upon receiving a LEO satellite signal with a decoded beam ID, the UT starts to search the available open-access databases for the satellite vehicle carrying this beam, and its current location. The same procedure is done with every other beam ID received by the UT. In the end, the UT shall combine all gathered information from all the received beam IDs in order to pinpoint its position on Earth's coordinates.

The chosen way of integrating the positioning information is by assuming that the UT lies at the CoG of the intersection area of all the **detected beams**. This is what was termed as the algorithmic method of "A" or "ALG. A". CoG is based on a simplified presumption that the receiver can be located at any point inside the confidence set with an equal probability. In that case, the CoG of the confidence set can be regarded as an optimal point estimate since it minimizes the sum of the squared errors.

By knowing the whole beam patterns of all received LEO satellites, the information about the absent **undetected beams** can be included in the calculations to omit their geographical footprints from the beam pattern. This leads to a smaller region of intersection than the region resulted from ALG. A and better mean accuracy. Consequently, the algorithmic method "B", or "ALG. B", should outperform ALG. A in terms of precision and accuracy. Figure 36 describes both ALG. A and ALG. B with graphical illustration.

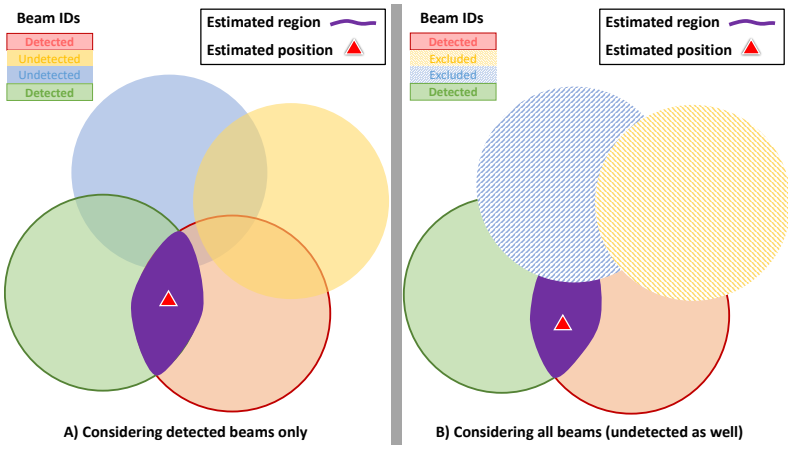

Figure 36. Two positioning method variants to utilize the information of the beam footprints.

Figure 36a shows how **ALG. A** exploit the intersection of the footprints of detected beams to determine the area where the receiver can be located. Figure 36b shows **ALG. B** which considers the nearby undetected beams. Thus, the bounds for the location estimation can be decreased by subtracting the footprints of the undetected beams from the intersection region that was defined by ALG. A.

ALGs A and B can be defined using mathematical sets and set operations, also known as morphology in image processing. Let $D(t)$ and $U(t)$ be the sets of detected and undetected beam IDs, respectively, for time instant t. Moreover, let $\mathbf{c}(i,t)$ be a function that returns the East North (E-N) coordinates of the center of the beam footprint of beam i at time instant t. Similarly, $R(i,t)$ returns the radius of the beam. Mathematical set $A_i(t)$, which includes all locations $\mathbf{x}$ (in E-N coordinates) inside the beam footprint of beam i, can be represented as in Equation (6.1).

$$A_i(t) = \{\mathbf{x} \mid\mid\mid \mathbf{x} - \mathbf{c}(i,t) \mid\mid < R(i,t)\}. \tag{6.1}$$

Now, the intersection $I(t)$ of all $A_i(t)$ of the detected beams is a set of E-N coordinates, i.e., an area, where the UT must be located. The intersection is determined by Equation (6.2).

$$I(t) = \bigcap_{i \in D(t)} A_i(t). \tag{6.2}$$

If the UT was outside the intersection area, it would not detect all the beams in $D(t)$. On the other hand, the UT can be anywhere in $I(t)$, and without any additional information (e.g., signal strength or information of the undetected beams) each location $\mathbf{x}$ in $I(t)$ is equally probable. Therefore, the ideal point estimate for the position of the UT is the CoG of the intersection with uniform mass density. This is the ALG. A, as defined in Equation (6.3).

$$\mathrm{ALG.A}(t) = \frac{\oiint_{\mathbf{x} \in I(t)} \mathbf{x} \mathrm{d}\mathbf{x}}{\oiint_{\mathbf{x} \in I(t)} \mathrm{d}\mathbf{x}}. \tag{6.3}$$

where closed integration is done over the entire area of intersection.

The locations of the undetected beams are utilized to shrink the area of possible UT locations. The footprints of the undetected beams can be subtracted from intersection $I(t)$ used by ALG. A. The shrunk intersection $I_B(t)$ can be obtained by subtracting the union of the undetected beams from the intersection of the detected beams, as given in Equation (6.4).

$$I_B(t) = I(t) - \bigcup_{i \in U(t)} A_i(t). \tag{6.4}$$

Finally, the CoG of set $I_B(t)$ is the output of ALG. B, as given in Equation (6.5).

$$\mathrm{ALG.B}(t) = \frac{\oiint_{\mathbf{x} \in I_B(t)} \mathbf{x} \mathrm{d}\mathbf{x}}{\oiint_{\mathbf{x} \in I_B(t)} \mathrm{d}\mathbf{x}}. \tag{6.5}$$

6.4.4 Positioning algorithms

The positioning techniques carried out by the beam ID-based positioning from LEO satellites (e.g. ALG. A, ALG. B) are not sufficiently accurate or reliable for all positioning applications. Hence, post-processing algorithms are to be used for more precise positioning results.

The rough estimations carried out by ALG B, are imported to a set of algorithms to further refine the final positioning estimations. Some processing steps are done at the local level (per data source e.g. either LEO or IMU) and the global level (sensor data fusion of both LEO/IMU). This strategic approach was undertaken with the primary goal of enhancing the accuracy of positioning estimations, ensuring that the final estimates are more precise and reliable. A bank of algorithms is used to overcome this issue.

The selected post-processing algorithms were: DR, EKF, and RTS, similar to the used algorithmic suit in Chapter 4. The DR algorithm was used as backup in cases of communication loss or data interruptions due to sensor drifts, signal attenuation, or NLOS epoch, to fill the null posterior state based on non-null prior information. The EKF was used as a fusion filter to combine information from the rough LEO positioning estimations carried out by ALG B and inertial information (acceleration data) from IMU. Finally, the RTS smoother was adopted to fine-tune the output trajectory by applying recursive smoothing to the EKF outputs.

6.4.5 Evaluation metrics

To construct a valid assessment on the LEO satellite beam ID-based positioning method, several performance metrics are used. Having the error distributions compiled for most scenarios, the following evaluation metrics are computed numerically: MAE, RMSE, and p95% positioning error. Moreover, the route comparisons in both the x-y coordinates (British national EPSG:27700) and the world's geodetic system (WGS84) of Earth coordinates were sketched, in addition to rendering CDF plots for the real scenario (i.e. Scenario 3). It is believed that those metrics will suffice to verdict the method from the perspectives of: the feasibility to the operator, and to the beneficiary user.

6.5 Simulation setup and attributes

The simulation is done in Matlab (R2022b). The objective is to model beam ID-based positioning and its accuracy with realistic future mega-constellations of LEO satellites. In the simulation, both UTs and satellites move with a temporal resolution of 1 second. The total simulation time is 1,200 seconds, i.e., 20 minutes, which mostly suite the existed computation capabilities.

The simulation model has the following characteristics, simplifications, and presumptions: i) There are several LEO constellations that are launched in sequence. Thus, it is possible to analyze how the accuracy of the positioning method evolves as new constellations with more advanced beamforming capabilities are introduced. ii) The positions of the satellites relative to the UT are calculated using a local planar coordinate system, i.e., the curvature of Earth around the UT is neglected. iii) Each beam has a circular *footprint* on Earth (more specifically, on the plane around the UT), despite varying elevation angles. iv) If the UT is inside a beam footprint, it recognizes the beam ID with a 100% probability. If the UT is outside a beam footprint, it recognizes the beam ID with a 0% probability. v) The UT can read all available beam IDs at the same time, i.e., the satellites and the

beam footprints do not move while reading the beam IDs.

6.5.1 Modelling the beam footprint patterns

A LEO satellite transmits several beams that form a regular beam footprint pattern on Earth. For every satellite from a satellite constellation, all beams have identical radii, R, and the centers of the adjacent beam footprints are separated by $1.5R$, i.e., the adjacent beams partially overlap. Different constellations have different beam footprint radius. When several satellites transmit their beams at the same time, the beam footprint patterns overlap. A schematic example (with a reduced number of beams for clarity) of a combined beam footprint pattern is shown in Figure 37.

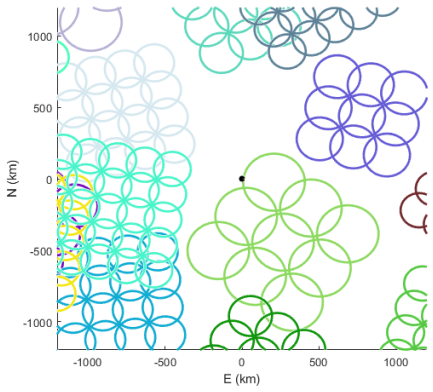

(a) Arbitrary beam footprints from various LEO satellite constellations covering a given region.

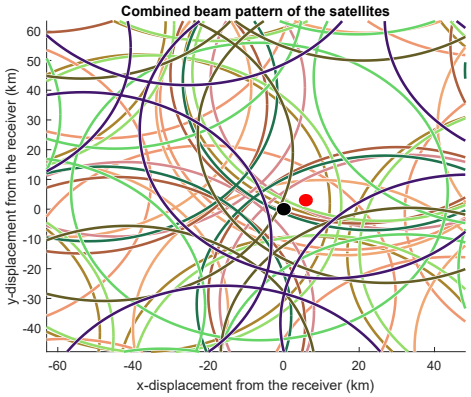

(b) Arbitrary location estimation (red dot) based on detecting the inbound LEO beam IDs by a user receiver (black dot) placed at (0,0).

Figure 37. Illustrating the concept of combined LEO beam footprint patterns.

In more detail, the total beam footprint pattern is computed as follows:

- i) Read the orbital positions (x, y, z) - given in ECEF coordinates - of the satellites for all simulation time steps from h5 files.
- ii) Set the origin of the local East North Up (ENU) coordinate system to the position of the UT at simulation time $t = 0$. Denote that position as: $(\text{lat}_0, \text{lon}_0, h_0)$. In the experiments $h_0 = 0$. Note that if the UT moves during a simulation run, its first position is still the origin of ENU in the setup.
- iii) Convert the orbital positions of the satellites to ENU coordinates, in Matlab, as follows: `[E,N,U] = ecef2enu(x,y,z,lat0,lon0,h0,spheroid)`, where `spheroid = wgs84Ellipsoid` (a Matlab constant).
- iv) Discard beams for which $U < 0$, because they are not located above the UT but below the EN-plane and even at the opposite side of Earth.
- v) Determine the Earth-projections of the satellites by setting $U = 0$ in ENU coordinates.

- vi) Place the beam centers of the footprint patterns symmetrically around the Earth-projection of the satellites (see a random set of beam footprint patterns in Figure 37).
- vii) Finally, rotate the beam footprint patterns in the EN-plane with a satellite-specific random angle $\theta \sim \mathrm{Uniform}(0, 2\pi)$. The rotation is done in homogeneous coordinates around the Earth-projection of the satellite denoted by (E_p, N_p). The new position (E_2, N_2) for beam center (E_1, N_1), is obtained by Equation (6.6).

$$\begin{bmatrix} E_2 \\ N_2 \\ 1 \end{bmatrix} = \mathbf{T} \begin{bmatrix} E_1 \\ N_1 \\ 1 \end{bmatrix}. \tag{6.6}$$

where the transform matrix T is obtained as the product of translation and rotation matrices in Equation (6.7).

$$\begin{bmatrix} 1 & 0 & E_p \\ 0 & 1 & N_p \\ 0 & 0 & 1 \end{bmatrix} \mathbf{T} = \begin{bmatrix} \cos(\theta) & -\sin(\theta) & 0 \\ \sin(\theta) & \cos(\theta) & 0 \\ 0 & 0 & 1 \end{bmatrix} \begin{bmatrix} 1 & 0 & -E_p \\ 0 & 1 & -N_p \\ 0 & 0 & 1 \end{bmatrix}. \tag{6.7}$$

6.5.2 Realization of positioning methodologies

The objective of a positioning technique is to give an optimal position estimate for the UT in the local ENU coordinates. The proposed estimation algorithms use the following measurements:

- i) detected beam IDs
- ii) current simulation time

In simulation, beam detection is simply solved by comparing the beam radius R_i, for beam i, to the distance from the after-rotation beam footprint center (E_i, N_i) to the UT location $(E_{\mathrm{UT}}, N_{\mathrm{UT}})$ as in Equation (6.8).

$$\mathrm{dist}_i = \sqrt{(E_i - E_{\mathrm{UT}})^2 + (N_i - N_{\mathrm{UT}})^2}. \tag{6.8}$$

If $\mathrm{dist}_i < R_i$, beam i is detected. The comparison is done for every beam and every simulation time step. Simulation time is an integer loop index variable.

Based on these measurements, the following information is retrieved:

- iii) all undetected beams that may intersect with the intersection of the detected beams
- iv) the radii of the beam footprints

Step iii) is used to initially reduce the number of beams for the computation of the morphological operations that are computationally expensive. In simulation, the true UT location is known as a

priori information; hence, it is possible to compute the distance to the UT. In simulation, the beams for which the distance to UT is larger than $3R_i$ are discarded.

The intersection of the beams is computed using Matlab polyshapes, which are 2-dimensional polygonal shapes that are defined by vectors of vertex points. The circular beams are thus created using samples from the border of the beam footprints. First, angles from 0 to 2π are sampled uniformly: `rad=linspace(0, 2*pi-(2*pi/samples), samples)`, where `samples=1000`. Second, the coordinates of the border, denoted by `Eb` and `Nb`, are computed. For beam i this is done by: `Eb = R(i)*cos(rad) + E(i)` and `Nb = R(i)*sin(rad) + N(i)`, where `R(i)` is the beam footprint radius and `E(i)` and `N(i)` give the beam center location. Finally, the polyshape struct of the beam footprint is created from the border coordinates as follows: `beam = polyshape(Eb, Nb)`.

The intersection (`IS`) of the beam footprints is computed directly and efficiently from the array of `polyshapes` representing the detected beams: `IS = intersect(beams)`. The output of ALG. A, i.e., the position estimate, is the CoG of the intersection area of the detected beams: `[CoGE,CoGN] = centroid(IS)`. The intersection of several detected beams and its CoG is demonstrated in Figure 38a.

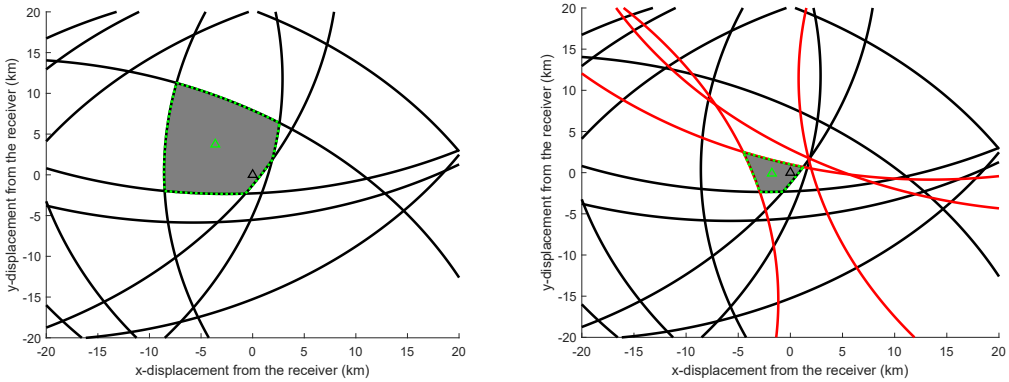

(a) Footprint pattern of only detected beams by the receiver (black triangle) located at (0, 0). The confidence set (gray area) and the estimated user position (green triangle) obtained by **ALG. A**.

(b) The same footprint pattern showing confidence the set and estimated user position by **ALG. B**. Red arcs are those undetected beams that were subtracted from the confidence set.

Figure 38. Effect of beam exclusion on confidence set and positioning accuracy.

When it comes to ALG. B, the undetected beams are subtracted from the intersection as explained in Section 6.4 and demonstrated in Figure 38b. For computational efficiency, subtraction is done iteratively and only for those undetected beams that intersect with the current intersection (`IS`). The implementation of subtracting beam i is as follows:

- i) Find such a vertex of the current intersection that is the nearest to beam center i: `[vertexid,boundaryid,ind] = nearestvertex(IS,E(i),N(i))`.
- ii) Find the respective E-N coordinates of the nearest vertex: `Enear = IS.Vertices(vertexid,1); Nnear = IS.Vertices(vertexid,2)`.

- iii) Compute the Euclidian distance from the nearest vertex to the beam center.
- iv) If the distance is smaller than the radius of the respective undetected beam, create a new polyshape and subtract it from the current intersection to obtain a new current intersection: `IS = subtract(IS, undetectedbeam).`
- v) Repeat steps i-iv until no more undetected beams are available.
- vi) Finally, compute the center of gravity of the residual intersection with function `centroid`.

6.5.3 Generating LEO satellite constellations data

The LEO satellite mega-constellations were reproduced with an in-house simulator tool, named LEO-S9 (LEO simulator with 9 modules). The LEO-S9 tool is flexible to create a variety of space segment scenarios, including diverse dynamics and instruments specific to LEO satellites. The main relevant points simulated with LEO-S9 in this work included the orbit altitude, inclination, velocity, constellation topology, and initial design. The constellation progress with time was reproduced considering the Cowell numerical integration, Earth's gravity, J_2 Oblateness effect, third body attractions, solar radiation, and atmospheric drags. A walker delta topology was selected to keep a symmetric coverage.

The simulation was built by considering the present status and coming developments in LEO satellite missions. Table 7 provides an overview of the primary missions and associated orbit parameters that were considered in this study, and the generation of LEO satellite constellation data.

To assess the performance of the proposed method across various LEO coverage scenarios, simulations for 13 distinct case scenarios were conducted, each denoted as experimental cases 1 through 13. In the initial case, 3000 satellites were simulated, covering a diverse combination of all identified missions. Then, about $\sim$1000 satellites were incrementally added into the simulation for each subsequent case. Notably, experimental case 13 assumed the operation of a total of $\sim$15000 LEO satellites. Each constellation of the 13 generated scenarios has a sufficient coverage to serve the most populated areas of Earth. While this may seem ambitious, it is a foreseeable scenario in the forthcoming years. On the other hand, the test case scenarios are numbered 1–4, to cover three modes of motion: stationary, linear, and nonlinear motion.

Table 7. Status and orbit parameters of the current and planned LEO constellations. Values based on (Pinell, Prol, Bhuiyan, & Praks, 2023).

Mission	Altitude [km]	Inclination [°]	N. Sats.
OrbComm	740 - 875	45, 70, 72	47
Globalstar	1400	52	48
Iridium	625, 720	86	66
Telesat	1015, 1325	51, 98	1671
Kuiper	590 - 630	33, 42, 52	3236
OneWeb	1200	40, 55, 88	6372
Starlink	540 - 570	53, 70, 98	$>$ 10000

The parameters of the generated LEO satellite constellations (number of satellites, number of beams per satellite, the radii of the beams, and the spacial separation of the beams) for motion Scenarios 1–3 are given in Table 8. The adjacent beams centers were separated by $1.5 \times R_{\mathrm{beam}}$ for all constellations, satellites, and beams. This separation value was set in order to impose large-sized beam

intersections needed for the beam ID-based positioning method to have sufficient overlapping of beam congregations. Whereas, the increased overlapping incidents from more beams shall result in better accuracy.

Table 8. LEO satellite mega constellation parameters for motion Scenarios 1–3.

Const.	Sats.	Beams/sat.	R_{beam}
1	3000	3×3	200 km
2	4050	3×3	150 km
3	5040	3×3	140 km
4	6048	4×4	130 km
5	7020	5×5	120 km
6	7992	6×6	110 km
7	9012	7×7	100 km
8	10002	8×8	90 km
9	11052	8×8	80 km
10	12072	8×8	70 km
11	13032	8×8	60 km
12	14004	8×8	50 km
13	15084	8×8	40 km

Based on the illustration shown in Figure 39, the coverage area of a single LEO satellite can be evaluated from Equations (6.9), and (6.10). The coverage area is divided into smaller beamforming loops according to Equation (6.11).

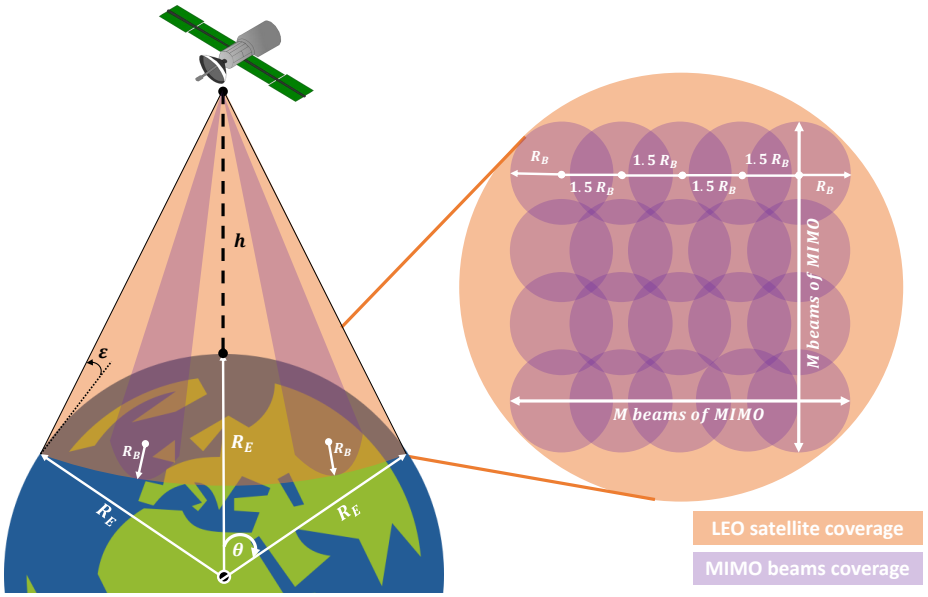

Figure 39. Coverage area of a single LEO satellite with MIMO beams.

First, the coverage geometry is approximated to the relation in Equation (6.9) (Wertz, for Space Technology (U.S.), & (U.S.), 2001).

$$cos(\theta + \epsilon) = \frac{cos(\epsilon)}{1 + \frac{h}{R_E}}, \tag{6.9}$$

whereas θ is the central conic angle in radians measured from Earth's center, ϵ is the elevation angle of the viewing cone of the satellite, h is the altitude of the LEO satellite, and R_E is Earth's radius.

Considering higher and moderate elevation angles (e.g: $45° \leq \epsilon \leq 135°$), therefore, the coverage area A can be evaluated approximately from Equation (6.10). In which, the shape of the LEO satellite coverage area is approximated to be equivalent to the shape of a spherical cap (Harris & Stöcker, 1998), enclosing θ as the central angle.

$$A = 2\pi\, R_E^2\, (1 - cos(\theta)), \tag{6.10}$$

where θ is the central angle, and A is the coverage area approximated as a spherical cap shape.

For MIMO implementation in Figure 39, the radii of beamforming loops can be approximately determined from the evaluated LEO satellite coverage area as in Equation (6.11).

$$A \approx (2R_B + (M - 1) \times 1.5R_B)^2. \tag{6.11}$$

where A is the coverage area, R_B is the beam radius, and M is the squared size of MIMO ($M \times M$).

To summarize, the derived Equation (6.11) is used to determine the required size of MIMO antennas M and the corresponding beam radii R_B, in order to maintain the full coverage from LEO constellations and also facilitate the new positioning methodology.

6.6 Simulation experiments

Each experiment consisted of several simulation runs with changing parameters depending on the objective of the experiment. A simulation run always consisted of 1,200 time steps with a 1-second resolution. The rotation angles of the beam footprints were randomized for each simulation run, but kept constant during that run.

Each simulation run generated a time series of 1,200 seconds (i.e. 20 minutes) with the following data fields: true position in (E, N), estimated position by **ALG. A** in (E, N), estimated position by **ALG. B** in (E, N), positioning error, number of detected beams.

6.6.1 Variation of error metrics

The objective of the first experiment was to evaluate the confidence intervals of the error metrics. It was done by measuring the standard deviation of the error metrics while varying the location of the user terminal. To be precise, the sensitivity of the positioning error to the location of the user terminal was measured. Because the simulation model is computationally heavy, the confidence

intervals were evaluated separately for one set of simulation parameters, in contrast to repeating each experiment several times to obtain their standard deviation estimates individually. The procedure was as follows:

1. Set the location of the UT as well as the origin of the ENU coordinate system to (latitude, longitude) = (37.773972, -122.431297), i.e., in San Francisco, California.
2. Select and combine the first three mega-constellations (see Table 8 for the constellation parameters).
3. Run the simulation (i.e., 1,200 time steps) for both ALGs A and B., and calculate the error metrics.
4. Move the UT by 0.1 degrees, i.e., about 11 km, to North.
5. Repeat 25 times steps 3 and 4.
6. Calculate the standard deviations of MAE, RMSE, and maximum error for ALGs A and B.

6.6.2 Rationale of simulation scenarios

Different use case scenarios were simulated: 1) stationary user terminal, 2) user terminal in slow uniform linear motion, 3) user terminal moving through a pre-defined a route, and 4) repeating Scenario 3 with mMIMO. For each use case, several simulations experiments were performed in order to evaluate the accuracy of the positioning method and algorithms when using realistic future satellite mega-constellations with MIMO capabilities.

As presented in Table 8, the sizes of MIMO elements were randomized but kept under 8×8 for Scenarios 1–3 to simulate the least possible MIMO beamforming patterns from LEO constellations. However, the least best case scenario for MIMO elements is to be mMIMO (e.g. 1,024 antennas at least 32×32).

6.6.3 Scenario 1: stationary user terminal

When the user terminal does not move, it is possible to collect samples from the probability distribution of the true position. As LEO satellites move fast, the beam footprint pattern changes rapidly. Therefore, sampling positions with a 1 Hz rate is expected to give a time series without auto-correlation. If the positioning estimates are unbiased and uncorrelated, the mean value of the samples will converge towards the true position. This will be investigated experimentally using convergence time spans from 1 to 30 seconds.

The procedure is as follows: 1) Set the location of the UT as well as the origin of the ENU coordinate system to (latitude, longitude) = (37.773972, -122.431297), i.e., in San Francisco, California. 2) Select the first mega constellation. 3) Run the simulation for ALGs A and B. 4) Filter the time series of the estimated positions by unweighted sliding average filters of window lengths w = 1, 2, ..., 30, and calculate the error metrics of the filtered time series. 5) Select the next mega-constellation and combine it with the previous ones. 6) Repeat steps 3 to 5 until no more mega-constellations are available.

6.6.4 Scenario 2: slow uniform linear motion

In Scenario 2, the user terminal moves with a constant speed of 1 m/s towards North-East. The initial position is at (latitude, longitude) = (37.773972, -122.431297), i.e., in San Francisco, California. This scenario corresponds, e.g., to a person walking or an autonomous vehicle driving slowly along a straight street. As the movement is easy to predict, it is presumed that the post-processing methods converge effectively towards the correct location.

The procedure is similar to Scenario 1, except that the location of the user terminal is not fixed but a time series of 1,200 values and it is not meaningful to apply a sliding average filter to the time series of the estimated positions.

In more detail, the procedure is as follows: 1) Define the location of the UT as a time series: initial location at (latitude, longitude) = (37.773972, -122.431297) and movement of 1 m/s to North-East. Set the origin of the ENU coordinate system to the initial UT location. 2) Select the first mega constellation. 3) Run the simulation for ALGs A and B. 4) Apply post-processing methods (see Section 6.4.4) to the time series of the estimated positions, and calculate the error metrics of the original and post-processed time series. 5) Select the next mega-constellation and combine it with the previous ones. 6) Repeat steps 3 to 5 until no more mega-constellations are available.

6.6.5 Scenario 3: real nonlinear motion

In Scenario 3, the user terminal moves along the predefined route shown in Figure 50, which is located in San Francisco, California – USA, as all the other experiments for good comparability. The test drive data was retrieved from Google competition 2022 (Howard et al., 2022), as seen in Figure 29. For this dataset, IMU data that was used for sensor fusion tests, was available. Scenario 3 is used to evaluate the beam ID-based positioning method in a use case of real nonlinear movement, including periods of acceleration, deceleration, change of direction, as well as immobility.

The procedure is as follows: 1) Define the location of the UT as a time series using every second sample of the first 2,400 samples, i.e. 1,200 samples from the GSDC data. Set the origin of the ENU coordinate system to the initial UT location with $U = 0$. 2) Select the first mega constellation. 3) Run the simulation for ALGs A and B. 4) Apply post-processing methods (see Section 6.4.4) to the time series of the estimated positions, and calculate the error metrics of the original and post-processed time series. 5) Select the next mega-constellation and combine it with the previous ones. 6) Repeat steps 3 to 5 until all mega-constellations are used.

6.6.6 Scenario 4: real nonlinear motion with mMIMO

This scenario was the repetition and reproduction of Scenario 3 but with mMIMO elements equipped in LEO satellite constellations. In which, the same LEO constellation sizes were used (i.e. 13 constellations with the defined number of satellites per constellation in Table 8), however, the number of beams per satellite and the radii of the beams were changed to mMIMO beam configurations.

To this aim, several denominations of mMIMO-equipped LEO satellite constellations were used, namely Scenarios: 4a, 4b, 4c, 4d, and 4e. Such sub-scenario configurations were set up to study and verify the feasibility of mMIMO beamforming for this positioning method, as demonstrated in Tables 9, 10, 11, 12, and 13.

a) 8 Constellations with minimal mMIMO

Scenario 4a was meant to test the least possible resources of LEO satellites and mMIMO antennas. That is, the minimum requirements for the positioning method to function, which was known by conducting several trials and errors. Consequently, the size of LEO satellite constellations was kept at 8, which means that the total number of LEO satellites in Scenario 4a was the summation of all LEO satellites found in constellations 1–8 (i.e. a total of 52,164 satellites).

As discussed in publication **[P7]** and Section 6.2, the least possible mMIMO configuration was known to contain 1,024 antenna elements, i.e. 32×32. Hence, the mMIMO beam configuration of Scenario 4a was ranged from 32×32 to 46×46 in an ascending order. As for the beam radii, they were approximately calculated from Equations (6.9), (6.10), and (6.11), as shown in Table 9.

Table 9. LEO satellite configurations of Scenario 4A.

Const.	Sats.	Beams/sat.	R_{beam}
1	3000	32×32	40 km
2	4050	34×34	38 km
3	5040	36×36	36 km
4	6048	38×38	34 km
5	7020	40×40	32 km
6	7992	42×42	30 km
7	9012	44×44	28 km
8	10002	46×46	26 km

b) 8 Constellations with maximum mMIMO

In Scenario 4b, the same constellation size of Scenario 4a was used again but with the maximum possible mMIMO antennas configuration of 64×64. It is the size that can be accommodated onboard a small-sized LEO satellite, also it was the size that fitted the processing capabilities of the currently used simulator. The configuration parameters are given in Table 10.

Table 10. LEO satellite configurations of Scenario 4B.

Const.	Sats.	Beams/sat.	R_{beam}
1	3000	64×64	20 km
2	4050	64×64	19 km
3	5040	64×64	18 km
4	6048	64×64	17 km
5	7020	64×64	16 km
6	7992	64×64	15 km
7	9012	64×64	14 km
8	10002	64×64	13 km

c) 9 Constellations with minimal mMIMO

Scenario 4c was designed to test the effect of incrementing the LEO constellation size into 9 constellations, which accommodated a total amount of 63,216 LEO satellites. The mMIMO beam configuration followed the same pattern of Scenario 4a, which started from 32×32 and so forth in an ascending order.The configuration parameters of this scenario are given in Table 11.

Table 11. LEO satellite configurations of Scenario 4C.

Const.	Sats.	Beams/sat.	R_{beam}
1	3000	32×32	40 km
2	4050	34×34	38 km
3	5040	36×36	36 km
4	6048	38×38	34 km
5	7020	40×46	32 km
6	7992	42×42	30 km
7	9012	44×44	28 km
8	10002	46×46	26 km
9	11052	48×48	24 km

d) 11 Constellations with maximum mMIMO

Scenario 4d employed 11 constellations, which accommodated a total amount of 88,320 LEO satellites, and configured with the maximum size of mMIMO beamforming, 64×64. The beam radii were evaluated and presented in Table 12.

Table 12. LEO satellite configurations of Scenario 4D.

Const.	Sats.	Beams/sat.	R_{beam}
1	3000	64×64	20 km
2	4050	64×64	19 km
3	5040	64×64	18 km
4	6048	64×64	17 km
5	7020	64×64	16 km
6	7992	64×64	15 km
7	9012	64×64	14 km
8	10002	64×64	13 km
9	11052	64×64	12 km
10	12072	64×64	11 km
11	13032	64×64	10 km

e) 13 Constellations with maximum mMIMO

Scenario 4e was developed to utilize the maximum available resources of LEO satellite constellations and mMIMO beamforming sizes. In which, the 13 constellations were used to provide 64×64 beams from each of the 117,408 LEO satellites. Hence, the beam radii were computed as given in Table 13.

Table 13. LEO satellite configurations of Scenario 4E.

Const.	Sats.	Beams/sat.	R_{beam}
1	3000	64×64	20 km
2	4050	64×64	19 km
3	5040	64×64	18 km
4	6048	64×64	17 km
5	7020	64×64	16 km
6	7992	64×64	15 km
7	9012	64×64	14 km
8	10002	64×64	13 km
9	11052	64×64	12 km
10	12072	64×64	11 km
11	13032	64×64	10 km
12	14004	64×64	9 km
13	15084	64×64	8 km

6.7 Results and validation

In this section, the output results of all three scenarios were presented and evaluated: 1) the stationary position, 2) the uniform linear motion, and 3) the real vehicle drive test.

6.7.1 Error variations

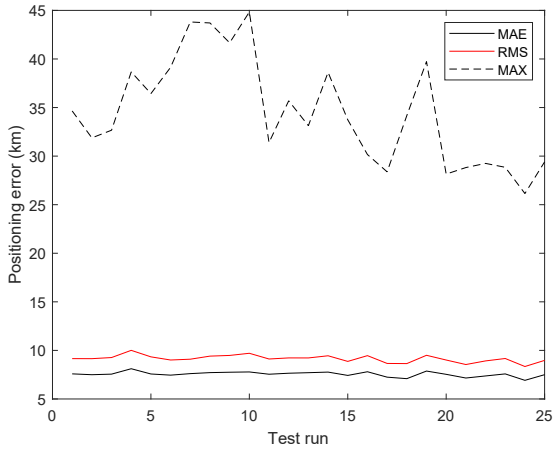

Figure 40. Error metrics in 25 locations for ALG. B. Each UT location is about 11 km from the previous one.

Figure 40 shows the variation of MAE, RMSE, and maximum error during 25 test runs for ALG. B when using the first three mega-constellations. Table 14 gives the sample means and standard

Table 14. Variation of error metrics: sample mean ± standard deviation for MAE, RMSE and maximum error (MAX) in km.

Alg.	Const.	MAE	RMSE	MAX
A	3	14.0 ± 0.52	16.8 ± 0.63	55.65 ± 5.70
A	5	4.71 ± 0.14	5.80 ± 0.18	23.67 ± 3.10
B	3	7.55 ± 0.26	9.15 ± 0.37	34.52 ± 5.49
B	5	2.38 ± 0.08	2.91 ± 0.10	12.32 ± 1.86

Table 15. Relative standard deviation of error metrics.

Alg.	Const.	MAE	RMSE	MAX
A	3	3.71%	3.74%	10.2%
A	5	2.99%	3.15%	13.1%
B	3	3.43%	4.06%	15.9%
B	5	3.23%	3.40%	15.1%

deviations of error metrics with three and five mega-constellations, for ALGs A and B. Table 15 gives the respective relative standard deviations in per cents. Standard deviations estimate the sensitivity of the error metrics with respect to the UT location. They are used to estimate the error margins of the results. It can be concluded that the relative standard deviation of MAE and RMSE is about 3-4% and the relative standard deviation of the maximum error is about 10-16%.

6.7.2 Results of Scenario 1: stationary user terminal

Figure 41 shows raw time series of positioning errors (for ALGs A and B) and the number of detected beams (identical for ALGs A and B), respectively. These demonstrate the amount of variation when the satellites move during a time span of 20 minutes.

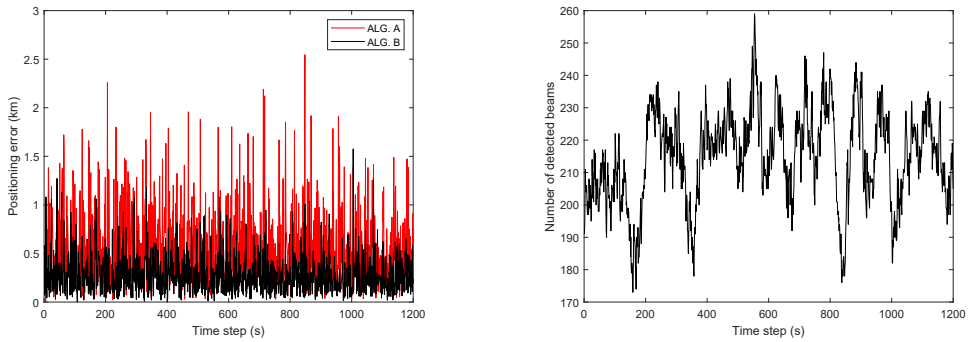

(a) Positioning error vs. time. **(b)** Number of detected beams vs. time.

Figure 41. Error results of Scenario-1 with 13 constellations.

Figure 42 shows how the 60 first samples of the time series of the estimated positions are scattered

around the UT. It can also be seen that the two-dimensional mean values (CoG, center of gravity) of the estimated positions are close to the true position of the UT, which indicates that ALGs A and B give unbiased position estimates. Therefore, it is possible to use several samples and averaging to obtain more accurate position estimates, in case of a stationary UT.

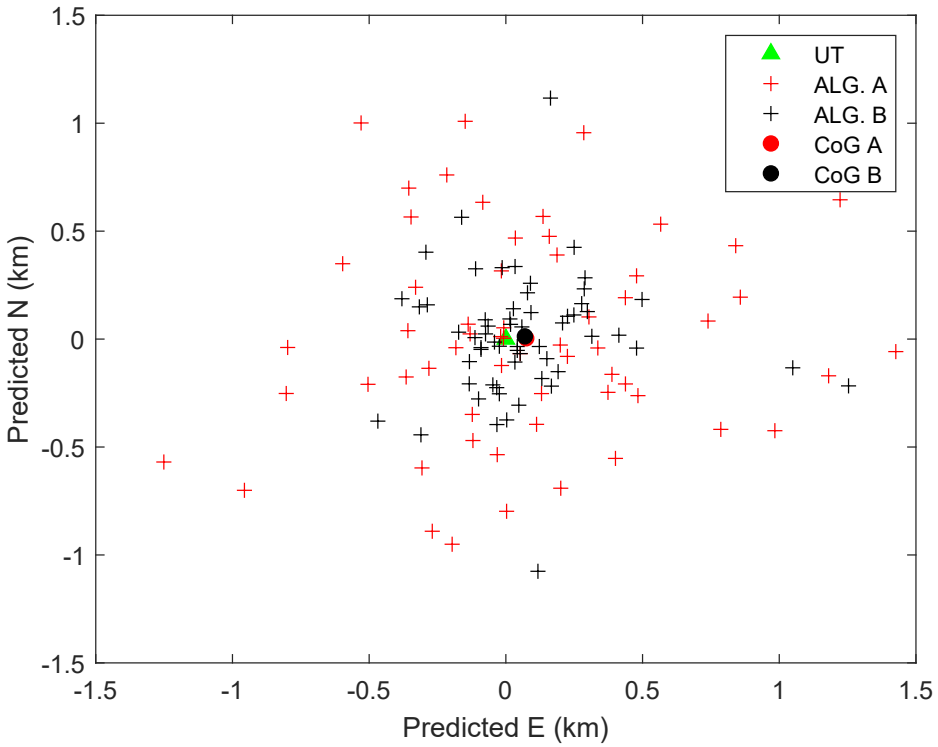

Figure 42. Scattering of the position estimates (N=60) when having 13 constellations.

Figure 43 shows how the RMS positioning error decreases when increasing the length of the sliding averaging filter when using 3 and 13 mega-constellations, respectively. Based on the central limit theorem and the presumption of independent and identically distributed position estimates, it is assumed that the reduction of the RMS error is inversely proportional to the square-root of the window length, as in relation (6.12):

$$\mathrm{RMSE} \propto \frac{1}{\sqrt{w}}, \tag{6.12}$$

where w = window length of the sliding average filter.

To test this hypothesis, the inverse square-root curve was fitted to the data using the least squares method. The visual examination of Figure 43 reveals that the inverse square-root law holds rather accurately when the number of satellites is very large. Thus, the law is applicable when extrapolating positioning errors for longer convergence periods. However, the fitted curve underestimates the reduction of error when the constellation size is not large, as seen in Figure 43.

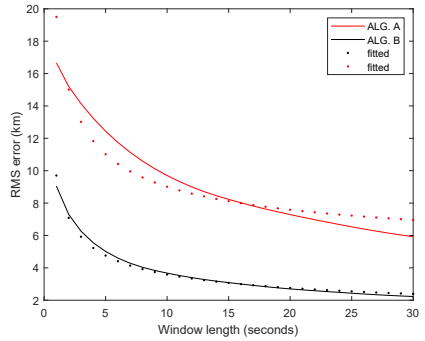

(a) RMS from 3 constellations.

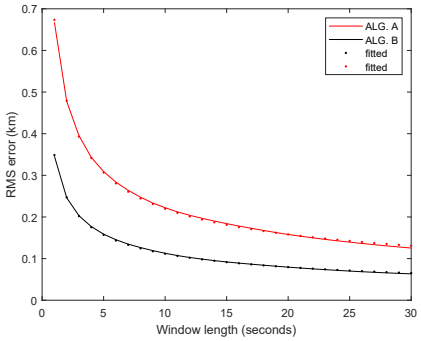

(b) RMS from 13 constellations.

Figure 43. Convergence of RMS error using 3 & 13 constellations.

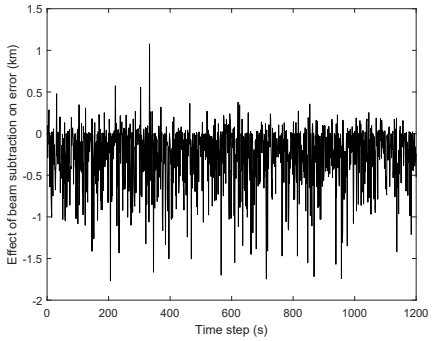

(a) Positioning error affected by beam exclusion (i.e. ALG B).

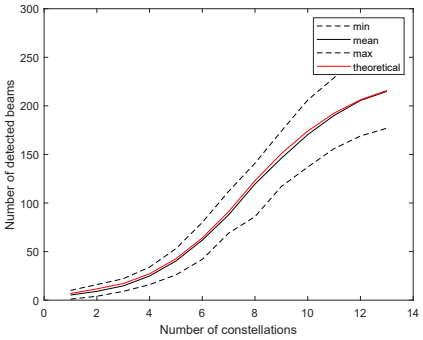

(b) Number of detected beams vs. number of constellations compared to the theoretical value.

Figure 44. Positioning errors and beam exclusion with 13 constellations.

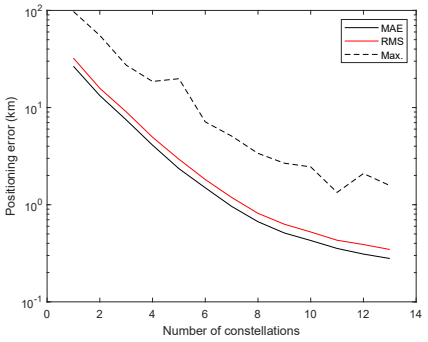

(a) Metrics based on single measurements.

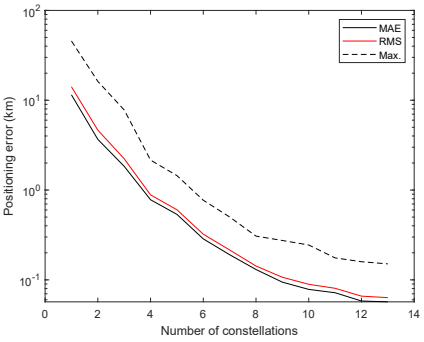

(b) Metrics based on filtering with $w = 13$.

Figure 45. Positioning error (log scale) vs. number of constellations for ALG. B.

The results show that ALG. B provides more accurate position estimates than ALG. A. However, this holds only for the average accuracy. Figure 44 shows the difference between the accuracy of ALGs A and B as a time series, in case of 13 constellations. It demonstrates that ALG. A actually gives quite often better position estimates. The probability that ALG. A gives more accurate estimates than ALG. A is 24.2% in this case. The mean difference of RMS errors between ALGs A and B can be seen, e.g., in Figure 43. In the future, it should be studied if it is possible to utilize the estimates of both algorithms, together with other information, to obtain more accurate position estimates.

The more beams there are congested near the UT, the more accurate positioning is, when keeping other things, such as the size of the beams, unchanged. The number of beams that an UT detects on average (on an arbitrary place on Earth) can be calculated theoretically. It is the ratio of the total area of all beam footprints of available constellations with the habitable area of Earth (510,100,000 km^2). Figure 44 compares the theoretical and simulated values of the number of detected beams. It can be seen that the average value of simulation is well aligned with the theoretical value. It also shows how the number of detected beams increases when adding new constellations to the simulation, according to the mega-constellation model given in Section 6.6.

Finally, Figure 45 shows the positioning errors vs. number of constellations when using single measurements and averaging over 30 seconds, respectively. With all 13 constellations that have totally 117,408 satellites and about 5,908,000 beams, when UT detects on average 215 beams, MAE is about 0.29 km, RMSE is about 0.35 km, and maximum error is about 1.6 km. When averaging 30 measurements, MAE = 0.057 km, RMSE = 0.064 km, and maximum error = 0.152 km.

6.7.3 Results of Scenario 2: slow uniform linear motion

The results of Scenario 2 as found in Figure 46 and Table 16 show very fluctuating raw position estimates in comparison to the straight imaginary route that resembles a person walking in a uniform speed of 1 m/s. Fortunately, the EKF filtering has reduced the positioning error by approximately 80%, and the RTS smoother has further eliminated around 73% of the EKF output error to achieve an overall accuracy of 16.69 meters as MAE. The 95-percentile value of 993 meters is large, but it is mostly due to the first output samples of the filters.

According to Figures 46 and 47, the position estimations gradually converge towards the true location of the UT. A logical explanation for EKF fluctuations in the beginning of time is the convergence time taken by the Kalman gain vector to adapt its weights. Notably, during the preliminary investigations, it was found that a simple sliding average filter (window length, $w = 100$) outperforms EKF in smoothing the outputs of ALG. B estimations. Thus, it signifies the potential to improve the accuracy in the future.

Table 16. Error evaluation of linear motion in Scenario 2.

Method	Const.	MAE [m]	RMSE [m]	p95% [m]
ALG. A	13	508.49	685.91	1179.1
ALG. B	13	241.61	334.28	588.10
EKF	13	47.25	75.02	982.20
EKF-RTS	13	**13.69**	**15.24**	**993.86**

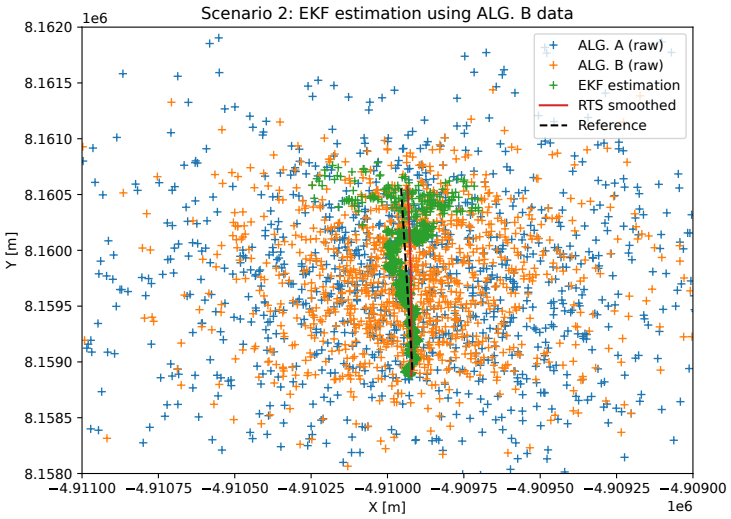

Figure 46. EKF and RTS positioning estimations of a uniform linear motion using ALG. B for Scenario 2.

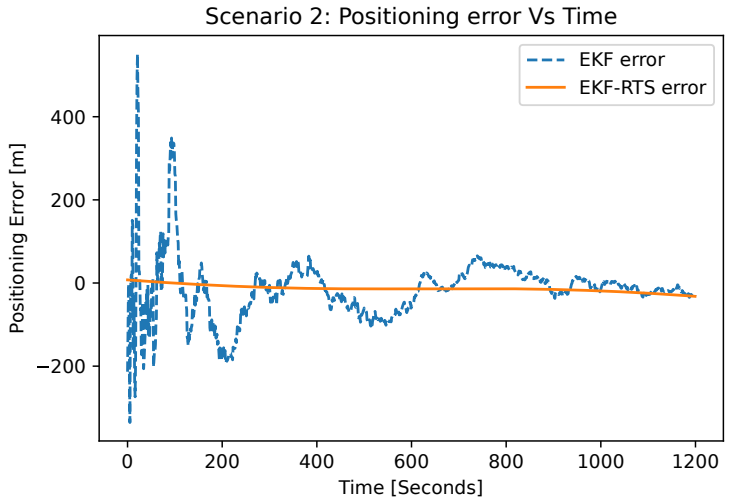

Figure 47. Effect of RTS on EKF error convergence over time in Scenario 2.

6.7.4 Results of Scenario 3: real nonlinear motion

The results of Scenario 3 were very promising and satisfactory to a large extent, as shown in Figures 48, 49, 50, 51, and Table 17.

Primarily, it is clear from trajectory Figures 48 and 50 that the combined EKF-RTS fusion-smoother back-to-back algorithm (using ALG. B) is the most accurate method that is closely following with the ground truth and GNSS with minimal errors. Hence, the applied elementary positioning algorithms after receiving beam IDs (i.e. ALG. A and ALG. B) are not sufficient to conduct precise positioning on their own. In contrast, they constantly require a set of post-processing algorithms, which can be

achieved similar to every other positioning technologies e.g. in GNSS.

The numerical positioning error values in Table 17 and the graphical error plots illustrated in Figures 49 and 51 are confirming the same finding; that the EKF-RTS method outperforms all other algorithms used in this simulation. The CDF curves in Figure 51b imply that the final LEO/IMU positioning estimations are very close to the performance of GNSS in terms of accuracy and precision. However, Figure 51a shows that the best performance of LEO/IMU that can bring it closer to GNSS performance is only achievable using the maximum possible numbers of satellites and constellations, which are already 13 constellations carrying more than 100,000 satellites.

In fact, the simulation of Scenario 3 confirms the early hypothesis in this study; that is the necessity of receiving the maximum available interconnected LEO satellite beams in order to improve the final positioning estimations. The number of received beams in Scenario 3 fluctuated between 172 and 247 beams, with average number of detected beams being = 214.

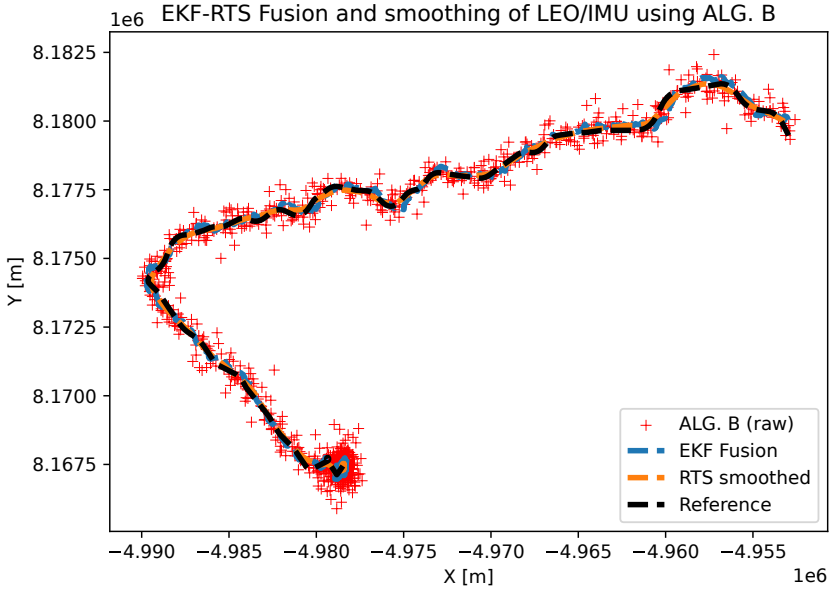

Figure 48. LEO/IMU fusion on ALG. B data in x-y coordinates (British National Grid, EPSG:27700).

Table 17. Error evaluation of LEO/IMU methods vs. GNSS in Scenario 3.

Method	Const.	MAE [m]	RMSE [m]	p95% [m]
ALG. A	13	498.16	683.49	1179.5
ALG. B	13	231.59	317.95	520.06
LEO/IMU EKF	13	104.80	132.00	203.35
LEO/IMU EKF-RTS	13	**66.31**	**83.98**	**142.39**
GNSS only	N/A	**26.63**	**36.42**	**56.60**

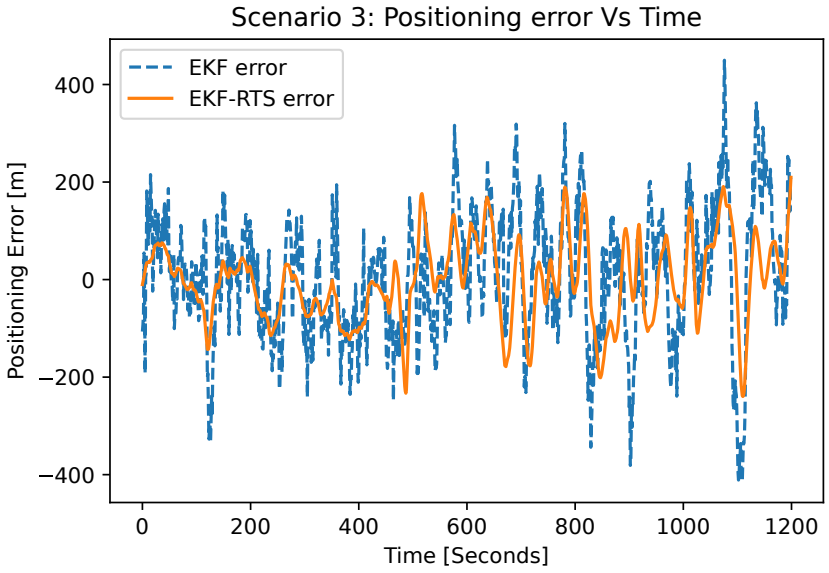

Figure 49. EKF and RTS error convergence over time in Scenario 3.

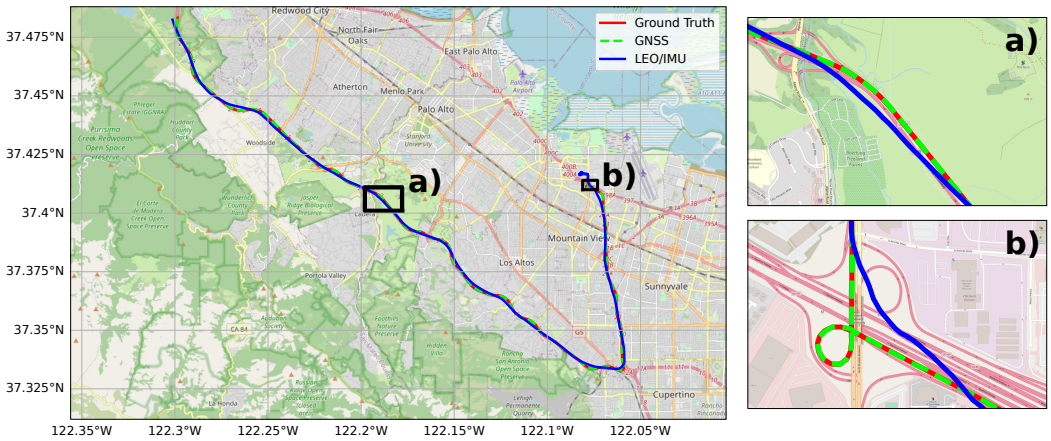

Figure 50. Map trajectory of the smoothed LEO/IMU, GNSS data, and ground truth in California, USA.

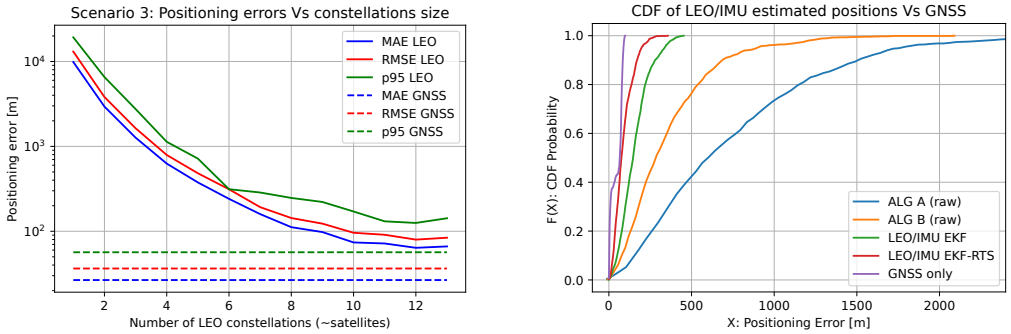

(a) Positioning errors (log scale) of LEO/IMU Vs. GNSS.

(b) Cumulative distribution functions of LEO/IMU methods Vs. GNSS.

Figure 51. Assessment of proposed method LEO/IMU Vs. GNSS, in Scenario 3.

6.7.5 Results of Scenario 4: real nonlinear motion with mMIMO

Tables 18 and 19 show the numerical error results of Scenario 4 (a–e). Figures 52 and 53 demonstrate the error behaviour of all scenario denominations in addition to the rendered route test of Scenario 4E and its conjugate case: Scenario 4E*.

In Table 18, the positioning errors of all sub-scenarios are investigated using MAE, RMSE and p95% metrics to assess the fusion based methods of LEO/IMU EKF-RTS. The best result was found to be Scenario 4E.

In Table 19, the same metrics were used to assess utilizing the raw unprocessed non-fused ALG. B measurements. However in the conjugate version of Scenario 4E (i.e. Scenario 4E*), a simple moving average filter was used to filter the raw ALG. B and show its effect. The best result was found to be Scenario 4E*.

In Figures 52 and 53, clearer views of assessment can be found, graphically. Where the fusion-based method of Scenario 4E already closely matched the accuracy of the raw measurements of Scenario 4E*, and both scenarios outperformed GNSS accuracy with a large margin.

Table 18. Error evaluation of mMIMO IMU fusion vs. GNSS in Scenario 4.

Method	Const.	MIMO	MAE [m]	RMSE [m]	p95% [m]
a) LEO/IMU EKF-RTS	8	$32^2 \rightarrow 46^2$	22.63	29.70	50.84
b) LEO/IMU EKF-RTS	8	64×64	17.65	23.05	36.47
c) LEO/IMU EKF-RTS	9	$32^2 \rightarrow 48^2$	16.86	22.41	32.78
d) LEO/IMU EKF-RTS	11	64×64	11.84	15.46	26.60
e) **LEO/IMU EKF-RTS**	**13**	$\mathbf{64 \times 64}$	**9.90**	**12.71**	**20.97**
GNSS only	N/A	N/A	**26.63**	**36.42**	**56.60**

Table 19. Error evaluation of raw mMIMO data vs. GNSS in Scenario 4.

Method	Const.	MIMO	MAE [m]	RMSE [m]	p95% [m]
a) Raw ALG. B data	8	$32^2 \rightarrow 46^2$	45.84	62.56	101.98
b) Raw ALG. B data	8	64×64	37.17	51.50	82.33
c) Raw ALG. B data	9	$32^2 \rightarrow 48^2$	36.05	48.97	76.28
d) Raw ALG. B data	11	64×64	23.59	32.45	53.20
e) Raw ALG. B data	**13**	$\mathbf{64 \times 64}$	**19.27**	**25.74**	**44.32**
e*) Smoothed ALG. B	**13**	$\mathbf{64 \times 64}$	**9.15**	**11.94**	**19.07**
GNSS only	N/A	N/A	**26.63**	**36.42**	**56.60**

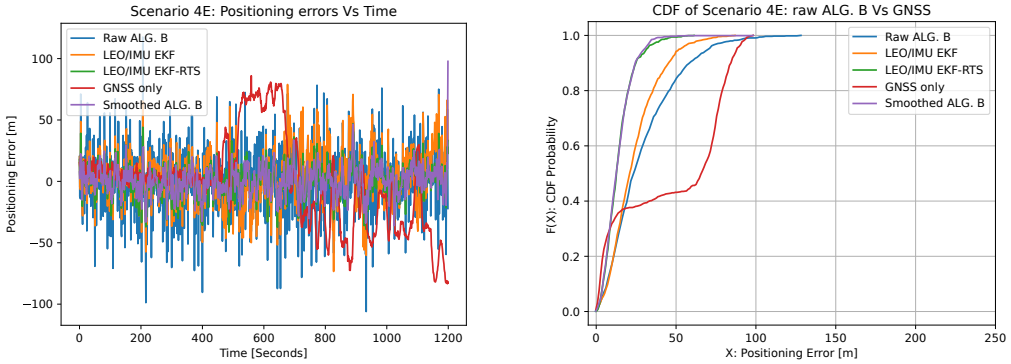

(a) Positioning errors of mMIMO methods Vs. Time.

(b) Cumulative distribution functions of mMIMO methods Vs. GNSS.

Figure 52. Assessment of mMIMO methods Vs. GNSS, in Scenario 4E.

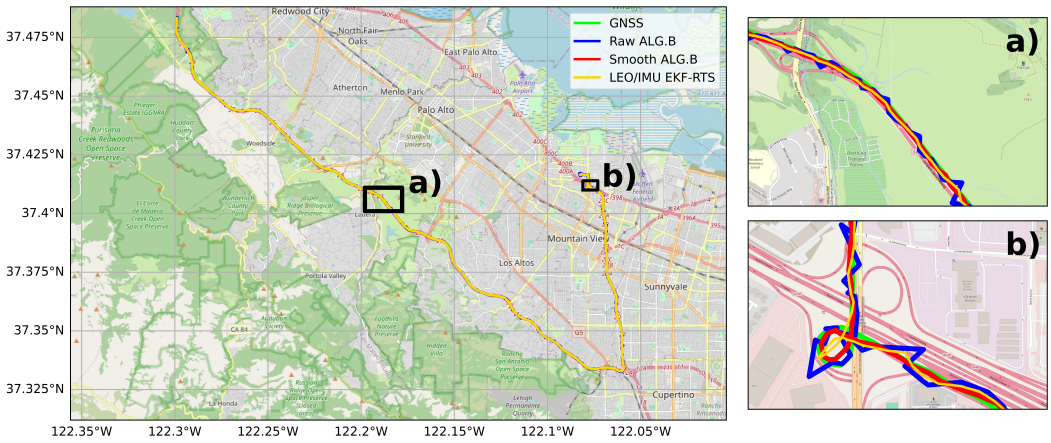

Figure 53. Map trajectory of Scenario 4E: mMIMO data, and GNSS data in California, USA.

6.7.6 Commentary on the results

The results speak volumes, especially for the last scenario(s). First, the error variation results were very noisy when fewer satellite and/or beams were used, which was predictable and expected. In the dynamic motion scenarios, the beam ID-based positioning method showed an acceptable level of accuracy (a handful of kilometers error) as an alternative outdoor positioning method that can help in emergency situations, not as a replacement method to GNSS.

Scenario 3 resembled a real-life situation whereas the method can be used for vague applications that require positioning accuracy of few tens of meters error.

Finally, the results of Scenario 4 were quite interesting and promising since all its denominations were performing better than GNSS in the event of implementing LEO/IMU fusion. The effect of

introducing mMIMO can be seen through the error shift from Figure 51 to Figure 52, where the enhancement in accuracy was significantly proven. By increasing the size of LEO satellite constellations to be mega and the size of MIMO beamforming loops to be massive, the positioning accuracy can be significantly enhanced to a precise accurate level of performance. The fusion-based positioning schemes are still effective with LEO satellites. However, even in the event of no multisensor fusion integration, the proposed method can still perform quite well with raw measurements.

6.8 Discussion

The beam ID-based method is based on mega-constellations of LEO satellites that have MIMO or mMIMO capabilities. The accuracy of the single measurements (i.e. raw ALG. A or ALG. B) is in the order of kilometers when having a few thousands of satellites and minimal MIMO elements (non massive). When the number of satellites exceeds a hundred thousand, positioning errors of a few hundreds of meters can be achieved. Positioning with such errors can be used as a back-up method, e.g., in aviation, search and rescue, and seafaring. However, the experiments showed that by the integration of several measurements or by the fusion of measurements from IMU sensors, the positioning accuracy can be improved significantly. MAE as small as 14 meters was recorded for a slow uniform linear motion when using 13 mega-constellations. With advanced post-processing algorithms, an accuracy closer to GNSS systems is possible.

With a realistic nonlinear motion, the RMSE for LEO/IMU EKF-RTS and for GNSS were approximately 84 m and 36 m, respectively, and MAEs were approximately 66 m and 27 m, respectively. This means that the beam ID-based positioning method is a promising candidate even for nonlinear dynamic motion of vehicles.

Subsequently, when mMIMO capabilities were introduced to LEO satellite constellations, the positioning accuracy of the beam ID-based method outperformed GNSS even with raw non-fusion measurements with MAE/RMSE 9.15m/11.94m compared to 26.6m/36.42m in the GNSS case. This in turn, signals the feasibility of adopting LEO satellites equipped with mMIMO antennas for positioning applications in the future.

There are still many possibilities to further improve the accuracy of the beam ID-based positioning method. Presuming that the signal strength of the beam footprints decreases from the center towards the border in a predictable way it could be measured and used as an additional weighed input. Similarly, other signal quality metrics could be utilized. In the post-processing phase, the number of detected satellites could be used to weigh the raw measurements. This is based on the presumption that the more satellites are detected, the more accurate the position estimate is on average.

The beam ID-based position method has several advantages for sustainability. First, it uses measurements that do not require precise timing or accurate measurements of the signal strengths. Therefore, the required technology at the user segment is expected to be affordable, which promotes social sustainability. Second, the method does not require dedicated satellites to work. This should reduce costs further and save both energy and natural resources. Third, due to the high signal strengths of the LEO satellites and the simple binary measurements (the beam is either detected or not) the method is expected to be tolerant against interference and jamming, especially when fused with the IMU sensor that itself is tolerant to interference as a passive sensor. Hence, the method could guarantee uninterrupted positioning services also in conflict areas. This has several consequences to sustainable development through the uninterrupted operation of numerous autonomous systems that will promote sustainable development in the future.

7 CONCLUSIONS

Precision positioning lies at the core foundation of navigation-based services and location-aware applications, which in turn affects the performance of many smart operations of Industry 4.0, such as: smart logistics and IoT. Depending on: 1) the complexity of the environment, 2) the targeted user segments, 3) the expected outcomes, and 4) the technology required; precise positioning systems can be developed in various configurations, sizes, and shapes.

This article-compilation dissertation was aimed to study the topic of achieving precise positioning estimations that can be held as reliable solutions for smart logistics, both indoors and outdoors. The thesis was poised and focused on the following aspects: 1) building a precise IPS, 2) enhance the current outdoor positioning estimations to be more precise, and 3) develop a new outdoor positioning method that can be reliably used as a back-up to the primary outdoor positioning technology.

7.1 Main findings

In summary, the main findings of this doctoral thesis are listed as follows:

1. UWB systems are suitable low-cost solutions for precise indoor positioning in complex industrial environments.
2. Although UWB can be implemented as a standalone IPS, fusing UWB with other assisting technologies (e.g. inertial sensors) can yield more precision and accuracy.
3. The achieved precise fusion-based UWB positioning estimations for dense indoor environments had a mean accuracy (MAE) of 4.7 cm, an RMSE of 5.5 cm, and a p95% of 9.6 cm, aided by IMU sensors and state-space estimation techniques.
4. GNSS technologies are the most suitable systems for precise outdoor positioning, however, they require continuous enhancements based on the environment of operation.
5. Our enhancements in outdoor vehicular positioning for commercial-grade GNSS receivers in smartphones led to an average accuracy (MAE) of up to 2.29 m, using multisensor fusion, state-space estimation, and machine learning techniques.
6. These results were validated as achieving a Bronze medal rankings in the GNSS positioning estimations at an international competition held by Google in 2022.
7. LEO-PNT is a recently emerging research topic that investigates developing new positioning systems from LEO satellite technologies.
8. A new backup positioning methodology can be developed using LEO satellite mega constellations that are equipped with massive or non-massive MIMO capabilities.
9. The LEO-MIMO positioning method can be entirely passive, which will save significant resources on the receiver-end devices.
10. The simulation experiments showed that our proposed fusion-based LEO beam-based positioning methodology achieved an average accuracy (MAE) of 9.15 m, an RMSE of 11.94 m, and a p95% of 19.07 m, outperforming GNSS in some scenarios.
11. The method was found to be reliable even when using only raw, unprocessed LEO satellite measurements and/or multisensor fusion with IMU.

7.2 Scientific contributions

The main scientific contributions of the dissertation based on the stated findings are as follows:

1) A comprehensive literature review focused on UWB positioning systems, the review that is currently trending among the interested researchers.

The literature review conducted in publication **[P1]** and discussed in Chapter 3 gathered all the state-of-the-art aspects and discussions around UWB indoor positioning technologies. We spent more than 12 months collecting the most recent studies and implementations of UWB-related positioning systems for indoor environments over the preceding five years. This review was designed not only as a step-by-step tutorial for UWB enthusiasts and beginners but also as a reliable academic reference for UWB experts.

2) The development of a precise low-cost IPS that provides accurate navigation solutions to mobile robots and movable assets in dense industrial environments.

A major contribution explained in publications **[P2]**–**[P4]** and discussed in Chapter 4 was achieving centimeter-level accuracy in dense industrial environments, allowing for precise and real-time localization of movable assets. Our approach utilized low-cost technology components to provide affordable positioning solutions for industry and academia. Additionally, we developed a sustainable embedded system to fetch and store positioning estimations from the UWB system, as well as RSS-based systems such as Wi-Fi and BLE. During the development of a precise indoor UWB system, we tested the feasibility of a Wi-Fi RSS positioning system, which was found to be imprecise and inaccurate. Therefore, we recommend the adoption of a fusion-based Wi-Fi RTT approach, and/or a fusion-based BLE positioning system.

3) The enhancement of GNSS vehicular positioning estimations for commercial-grade receivers in smart phones.

Our GNSS contribution, explained in publications **[P5]**–**[P6]** and discussed in Chapter 5, aimed to enhance outdoor vehicular positioning estimations for a variety of smartphone models. Through appropriate algorithmic treatments and multisensor fusion techniques, our solution was able to improve positioning accuracy, achieving a Bronze ranking among precise GNSS solutions in the Google Decimeter Challenge 2022.

4) Another comprehensive literature review focused on LEO satellite positioning systems and LEO-PNT recent research.

The literature review conducted in publications **[P7]**–**[P8]** and discussed in Chapter 6 highlighted the potential of LEO satellite technologies in providing future outdoor positioning solutions. Additionally, the brief review in publication **[P7]** introduced our new LEO-PNT methodology, which harnesses the capabilities of MIMO beamforming to provide an assisting positioning solution for outdoor navigation. The review in publication **[P8]** is currently trending among researchers and enthusiasts interested in LEO-PNT.

5) Coining a new LEO-based positioning methodology that exploits and combines the advantages of LEO satellites and massive MIMO antenna beamforming to achieve precise outdoor positioning estimations using passive signals of opportunity.

Our LEO-PNT contribution, found in publications **[P9]–[P10]** and discussed in Chapter 6, involved investigating, testing, and validating the proposed beam ID-based method that utilizes LEO satellite technologies and massive MIMO capabilities. The method was thoroughly studied and verified in terms of feasibility, effectiveness, and efficiency, and was found to be viable under the prescribed conditions and configurations. The proposed method was submitted by the University of Vaasa as an international patent application on 12/5/2023, and was approved in August 2024.

7.3 Novelties

Our novel proposals in this dissertation can be divided into two categories:

- A) Results-wise
- B) Methodological

For category A, we managed to achieve the most accurate positioning results in the respective environments and setups. Two of these result groups can be regarded as novel:

1. **UWB Indoor Positioning**: Achieving accuracy below 10 centimeters in dense, complicated indoor environments.
2. **LEO-MIMO Outdoor Positioning**: Despite being entirely passive, this method outperformed GNSS results in certain conditions and scenarios.

We believe that both results are scarce in the available literature.

For category B, our proposed LEO-MIMO positioning methodology is believed to be novel. To the best of our knowledge, the utilization of MIMO capabilities in the context of developing outdoor positioning from LEO satellite constellations to achieve precise positioning estimations, as described in Chapter 6, has not been attempted in the available research literature. The anticipated advantages of the proposed LEO-MIMO method are not only substantial but also significant and disruptive to the field of positioning systems, as long as the recommended implementation guidelines are followed.

7.4 Limitations

Although most research limitations were addressed as described throughout this thesis, some inevitable limitations were still encountered. They are listed as follows:

- The scalability issue of UWB systems arises from their low transmission power, resulting in a short range for UWB anchors. The solution involves adding more UWB cells to cover larger areas, which increases resource costs and system complexity.

- Integrating multisensor fusion systems can be quite challenging for real-time applications operating at the nanosecond level. The processing time delays imposed by multiple sensors can lead to further delays as the multisensor scheme becomes more complex.
- Tree-lined roads and highways impose significant shadowing and multipath effects on GNSS signals, which are major concerns for the precision, accuracy, and reliability of autonomous driving vehicles.
- The orbiting speeds of LEO satellites must be harnessed and predicted with high precision, as they can cause significant positioning errors for future LEO-based navigation systems.
- As an established futuristic fact, micro LEO satellite constellations will inadequately serve the functionality of LEO-based positioning systems. In contrast, mega constellations can significantly enhance the performance metrics of LEO-PNT systems.
- LEO satellites that lack MIMO capabilities cannot be considered for our proposed LEO-MIMO positioning methodology. However, they can still be used in application domains that require approximate kilometer-level positioning accuracy.
- MIMO-equipped LEO satellites should be configured to produce massive MIMO beams to enhance positioning accuracy and precision, thereby increasing reliability and integrity.
- The structure of future LEO satellite receivers in handheld devices should accommodate the necessary resources to process massive amounts of MIMO beams simultaneously.

7.5 Future research

For future research, we recommend and plan to carry out the following investigations to fortify and maximize the scientific contributions based on this thesis, as listed below:

1. Testing FGO optimization with UWB multisensor fusion schemes, as many recent studies conclude that FGO algorithms exhibit higher performance indicators in fusion-based systems.
2. For human resource tracking in dense indoor environments, we recommend opting to fusion-based Wi-Fi RTT and/or BLE positioning systems. Since the precision requirements are not very strict, UWB becomes an overqualified solution in such case.
3. Applying map matching along with deep learning techniques for GNSS vehicular positioning is believed to yield more precise positioning estimates.
4. Consider the power RSS levels of LEO satellite signals and incorporate this information into the beam ID-based positioning method. This approach is expected to maximize the resultant precision and accuracy.
5. Preserve more resources by optimizing the simulated number of LEO satellites in the sky, reconfiguring the number of MIMO beams per LEO constellation, and customizing the beam radii and spacing based on the new number of LEO satellites.

REFERENCES

Alarifi, A., Al-Salman, A., Alsaleh, M., Alnafessah, A., Al-Hadhrami, S., Al-Ammar, M., & Al-Khalifa, H. (2016). Ultra Wideband Indoor Positioning Technologies: Analysis and Recent Advances. *Sensors*, *16*(5), 707. https://doi.org/10.3390/s16050707

Aly, H., Basalamah, A., & Youssef, M. (2017, jul). Accurate and energy-efficient gps-less outdoor localization. *ACM Trans. Spatial Algorithms Syst.*, *3*(2).

Angelis, G. D., Moschitta, A., & Carbone, P. (2016, aug). Positioning Techniques in Indoor Environments Based on Stochastic Modeling of UWB Round-Trip-Time Measurements. *IEEE Transactions on Intelligent Transportation Systems*, *17*(8), 2272–2281.

Apple. (2019). *Nearby Interactions with U1*. Retrieved from [2022-01-24]https://www.apple.com/fi/newsroom/2019/09/iphone-11-pro-and-iphone-11 -pro-max-the-most-powerful-and-advanced-smartphones

Apple. (2021). *iPhone 11 Pro and iPhone 11 Pro Max: the most powerful and advanced smartphones.* Retrieved from [2022-01-24]https://developer.apple.com/nearby-interaction/

Asaad, S. M., & Maghdid, H. S. (2022). A comprehensive review of indoor/outdoor localization solutions in iot era: Research challenges and future perspectives. *Computer Networks*, *212*, 109041. https://doi.org/10.1016/j.comnet.2022.109041

Ayach, O. E., Rajagopal, S., Abu-Surra, S., Pi, Z., & Heath, R. W. (2014). Spatially sparse precoding in millimeter wave mimo systems. *IEEE Transactions on Wireless Communications*, *13*(3), 1499-1513.

Barbieri, L., Brambilla, M., Trabattoni, A., Mervic, S., & Nicoli, M. (2021). UWB Localization in a Smart Factory: Augmentation Methods and Experimental Assessment. *IEEE Transactions on Instrumentation and Measurement*, *70*, 1–18. https://doi.org/10.1109/tim.2021.3074403

Bar-Shalom, Y. (1989). Recursive tracking algorithms: from the kalman filter to intelligent trackers for cluttered environment. In *Proceedings. ICCON IEEE international conference on control and applications.* IEEE.

Bar-Shalom, Y., Li, X. R., & Kirubarajan, T. (2001). *Estimation with Applications To Tracking and Navigation*. John Wiley & Sons, Inc.

Bernardini, F., Buffi, A., Fontanelli, D., Macii, D., Magnago, V., Marracci, M.,

... Tellini, B. (2021). Robot-Based Indoor Positioning of UHF-RFID Tags: The SAR Method With Multiple Trajectories. *IEEE Transactions on Instrumentation and Measurement*, *70*, 1–15. https://doi.org/10.1109/tim.2020.3033728

Blazek, J., Jiranek, J., & Bajer, J. (2019, May). Indoor Passive Positioning Technique using Ultra Wide Band Modules. In *2019 International Conference on Military Technologies (ICMT)* (pp. 1–5).

Bongard, J. (2008). Probabilistic robotics. sebastian thrun, wolfram burgard, and dieter fox. (2005, mit press.) 647 pages. *Artificial Life*, *14*(2), 227-229.

Bosch. (2021). *Perfectly keyless.* Retrieved from [2022-01-24]https://www.bosch-mobility-solutions.com/en/solutions/software-and-services/perfectly-keyless/

Carbone, P., Cazzorla, A., Ferrari, P., Flammini, A., Moschitta, A., Rinaldi, S., ... Sisinni, E. (2013, sep). Low Complexity UWB Radios for Precise Wireless Sensor Network Synchronization. *IEEE Transactions on Instrumentation and Measurement*, *62*(9), 2538–2548.

Caus, M., Perez-Neira, A., & Mendez, E. (2021). Smart Beamforming for Direct LEO Satellite Access of Future IoT. *Sensors*, *21*(14).

Ceruzzi, P. E. (2018). Gps. In *Gps* (p. 1-8).

CETECOM. (2019). *Regulatory requirements for Ultra-Wideband technology.* CETECOM™. Retrieved from https://www.cetecom.com/en/news/regulatory-requirements-for-ultra-wideband-technology/

Chen, C.-S. (2017, jan). A non-line-of-sight error mitigation method for location estimation. *International Journal of Distributed Sensor Networks*, *13*(1), 155014771668273.

Chen, L., Lv, F., Yang, Q., Xiong, T., Liu, Y., Yang, Y., ... Jin, Y. (2023). Performance evaluation of centispace navigation augmentation experiment satellites. *Sensors*, *23*(12).

Cheng, C.-H., Kuo, Y.-H., Lam, H., & Petering, M. (2021, apr). Real-Time Location-Positioning Technologies for Managing Cart Operations at a Distribution Facility. *Applied Sciences*, *11*(9), 4049. https://doi.org/10.3390/app11094049

Christ, R. D., & Wernli, R. L. (2014). Chapter 17 - navigational sensors. In R. D. Christ & R. L. Wernli (Eds.), *The rov manual (second edition)* (Second Edition ed., p. 453-475). Oxford: Butterworth-Heinemann. https://doi.org/10.1016/B978-0-08-098288-5.00017-8

Cimdins, M., Schmidt, S. O., & Hellbrück, H. (2020, January).

MAMPI-UWB—Multipath-Assisted Device-Free Localization with Magnitude and Phase Information with UWB Transceivers. *Sensors*, *20*(24), 7090. https://doi.org/10.3390/s20247090

Corbalán, P., Picco, G. P., & Palipana, S. (2019, April). Chorus: UWB Concurrent Transmissions for GPS-like Passive Localization of Countless Targets. In *2019 18th ACM/IEEE International Conference on Information Processing in Sensor Networks (IPSN)* (pp. 133–144).

Dabove, P., Pietra, V. D., Piras, M., Jabbar, A. A., & Kazim, S. A. (2018, apr). Indoor positioning using Ultra-wide band (UWB) technologies: Positioning accuracies and sensors' performances. In *2018 IEEE/ION position location and navigation symposium (PLANS)*. IEEE. https://doi.org/10.1109/plans.2018.8373379

Darbellay, G. A. (1999, nov). An estimator of the mutual information based on a criterion for conditional independence. *Computational Statistics & Data Analysis*, *32*(1), 1–17.

Decawave. (2016). *DW1000 Metrics for Estimation of Non Line Of Sight Operating Conditions* (Vol. 1.1; Tech. Rep.). Author. Retrieved from https://www.decawave.com/wp-content/uploads/2018/10/APS006_Part-3-DW1000-Diagnostics-for-NLOS-Channels_v1.1.pdf

Decawave. (2017). *Mdek1001 kit user manual module development & evaluation kit for the dwm1001*.

Dotlic, I., Connell, A., Ma, H., Clancy, J., & McLaughlin, M. (2017, oct). Angle of arrival estimation using decawave DW1000 integrated circuits. In *2017 14th workshop on positioning navigation and communications (WPNC)*. IEEE. https://doi.org/10.1109/wpnc.2017.8250079

Doucet, A., Gordon, N., & Krishnamurthy, V. (2001). Particle filters for state estimation of jump markov linear systems. *IEEE Transactions on Signal Processing*, *49*(3), 613-624.

Eliko. (2021). *Next-generation location tracking*. Retrieved from [2021-08-30]https://www.eliko.ee/

El-Rabbany, A. (2006). *Introduction to GPS: the Global Positioning System* (2nd ed ed.). Boston, MA: Artech House. Retrieved from https://ieeexplore.ieee.org/document/9106103

Exafore. (2021). *Exafore*. Retrieved from [2021-08-30]https://exafore.com

Faragher, R. (2012, sep). Understanding the Basis of the Kalman Filter Via a Simple and Intuitive Derivation [Lecture Notes]. *IEEE Signal Processing Magazine*, *29*(5),

128–132.

Farhangian, F., & Landry, R. (2020). Multi-constellation software-defined receiver for doppler positioning with leo satellites. *Sensors*, *20*(20).

FCC Federal Register. (2002). *Rules and Regulations of Ultra-Wideband Operation* (Vol. 67; Tech. Rep.). FCC. Retrieved from https://www.govinfo.gov/content/pkg/FR-2002-05-16/pdf/02-11929.pdf

Federal Communications Commission, F. (2002). *Revision of Part 15 of the Commission's Rules Regarding Ultra-Wideband Transmission Systems* (Tech. Rep.). FCC. Retrieved from https://transition.fcc.gov/Bureaus/Engineering_Technology/Orders/2002/fcc02048.pdf

FiRa. (2021). *About FiRa Consortium.* Retrieved from https://www.firaconsortium.org/about/consortium

Fox, V., Hightower, J., Liao, L., Schulz, D., & Borriello, G. (2003, July). Bayesian filtering for location estimation. *IEEE Pervasive Computing*, *2*(3), 24–33.

Fu, G. M., Khider, M., & van Diggelen, F. (2020). Android raw gnss measurement datasets for precise positioning. In *Proceedings of the 33rd international technical meeting of the satellite division of the institute of navigation (ion gnss+2020)* (p. 1925-1937).

Fu, X., & Jia, Y. (2010, oct). An Improvement on Resampling Algorithm of Particle Filters. *IEEE Transactions on Signal Processing*, *58*(10), 5414–5420.

Ge, H., Li, B., Jia, S., Nie, L., Wu, T., Yang, Z., ... Ge, M. (2022). LEO enhanced global navigation satellite system (LeGNSS): progress, opportunities, and challenges. *Geo-spatial Information Science*, *25*(1), 1-13.

GNSS Augmentation - Navipedia. (2024). European Space Agency NaviPedia. Retrieved from [2024-03-04]https://gssc.esa.int/navipedia/index.php/GNSS_Augmentation

Guo, X., Ansari, N., Hu, F., Shao, Y., Elikplim, N. R., & Li, L. (2020). A Survey on Fusion-Based Indoor Positioning. *IEEE Communications Surveys & Tutorials*, *22*(1), 566–594.

Guvenc, I., Chong, C.-C., & Watanabe, F. (2007). NLOS Identification and Mitigation for UWB Localization Systems. In *2007 IEEE wireless communications and networking conference.* IEEE.

Haggenmiller, A., Krogius, M., & Olson, E. (2019). Non-parametric Error Modeling for Ultra-wideband Localization Networks. In *2019 International Conference*

on Robotics and Automation (ICRA) (pp. 2568–2574).

Harmonised European Standard. (2016a). *Short Range Devices (SRD) using Ultra Wide Band technology (UWB); Harmonised Standard covering the essential requirements of article 3.2 of the Directive 2014/53/EU; Part 1: Requirements for Generic UWB applications* (Tech. Rep.). European Telecommunications Standards Institute. Retrieved from https://www.etsi.org/deliver/etsi_en/302000_302099/30206501/02.01.01_60/en_30206501v020101p.pdf

Harmonised European Standard. (2016b). *Short Range Devices (SRD) using Ultra Wide Band technology (UWB); Harmonised Standard covering the essential requirements of article 3.2 of the Directive 2014/53/EU; Part 2: Requirements for UWB location tracking* (Tech. Rep.). European Telecommunications Standards Institute. Retrieved from https://www.etsi.org/deliver/etsi_en/302000_302099/30206502/02.01.01_60/en_30206502v020101p.pdf

Harris, J. W., & Stöcker, H. (1998). *Handbook of Mathematics and Computational Science*. Retrieved from [2024-05-05]https://link.springer.com/book/9780387947464

Hartikainen, J., Solin, A., & Särkkä, S. (2011). *Optimal filtering with Kalman filters and smoothers - a Manual for Matlab toolbox EKF/UKF*. Aalto University.

Helo, P., & Shamsuzzoha, A. (2020, jun). Real-time supply chain—A blockchain architecture for project deliveries. *Robotics and Computer-Integrated Manufacturing*, *63*, 101909. https://doi.org/10.1016/j.rcim.2019.101909

Horsmanheimo, S., Lembo, S., Tuomimaki, L., Huilla, S., Honkamaa, P., Laukkanen, M., & Kemppi, P. (2019, may). Indoor Positioning Platform to Support 5G Location Based Services. In *2019 IEEE international conference on communications workshops (ICC workshops).* IEEE. https://doi.org/10.1109/iccw.2019.8757118

Hostettler, R., & Särkkä, S. (2020). *Lecture notes on basics of sensor fusion*. Aalto University. Retrieved from https://users.aalto.fi/~ssarkka/pub/basics_of_sensor_fusion_2020.pdf

Howard, A., Chow, A., Julian, B., Orendorff, D., Fu, M., Khider, M., & Dane, S. (2022). *Google smartphone decimeter challenge 2022.* Kaggle. Retrieved from https://kaggle.com/competitions/smartphone-decimeter-2022

Humayun, M., Jhanjhi, N., Hamid, B., & Ahmed, G. (2020, jun). Emerging Smart Logistics and Transportation Using IoT and Blockchain. *IEEE Internet of Things Magazine*, *3*(2), 58–62. https://doi.org/10.1109/iotm.0001.1900097

IEEE Computer Society. (2020). IEEE Standard for Low-Rate Wireless Networks–Amendment 1: Enhanced Ultra Wideband (UWB) Physical Layers (PHYs) and

Associated Ranging Techniques. *IEEE Std 802.15.4z-2020 (Amendment to IEEE Std 802.15.4-2020)*, 1-174. https://doi.org/10.1109/IEEESTD.2020.9179124

INCUBATE. (2022). *Project indoor navigation from cubesat technology (INCUBATE).* https://www.incubateproject.org/. ([Online; accessed 12-May-2024])

Indelman, V., Williams, S., Kaess, M., & Dellaert, F. (2012, July). Factor graph based incremental smoothing in inertial navigation systems. In *2012 15th International Conference on Information Fusion* (pp. 2154–2161).

Irene, G., & Rajesh, A. (2018). A Penta-Band Reject Inside Cut Koch Fractal Hexagonal Monopole UWB MIMO Antenna for Portable Devices. *Progress In Electromagnetics Research (PIER C))*, *82*, 225–235. Retrieved from https://www.jpier.org/PIERC/view/18020604/

Issaoui, Y., Khiat, A., Bahnasse, A., & Ouajji, H. (2019). Smart logistics: Study of the application of blockchain technology. *Procedia Computer Science*, *160*, 266–271. https://doi.org/10.1016/j.procs.2019.09.467

Issaoui, Y., Khiat, A., Bahnasse, A., & Ouajji, H. (2020, sep). Toward Smart Logistics: Engineering Insights and Emerging Trends. *Archives of Computational Methods in Engineering*, *28*(4), 3183–3210. https://doi.org/10.1007/s11831-020-09494-2

J. Kulmer, S. Hinteregger, B. Großwindhager, M. Rath, M. S. Bakr, E. Leitinger, & K. Witrisal. (2017, May). Using DecaWave UWB transceivers for high-accuracy multipath-assisted indoor positioning. In *2017 IEEE International Conference on Communications Workshops (ICC Workshops)* (pp. 1239–1245). https://doi.org/10.1109/ICCW.2017.7962828

Jie, C., Shaoshan, C., Yu, L., & Chongyu, R. (2006). Design of integrated navigation system based on information fusion technology for the intelligent transportation system. In *2006 6th international conference on its telecommunications* (p. 1248-1251).

Jiménez Ruiz, A. R., & Seco Granja, F. (2017, aug). Comparing Ubisense, BeSpoon, and DecaWave UWB Location Systems: Indoor Performance Analysis. *IEEE Transactions on Instrumentation and Measurement*, *66*(8), 2106–2117. https://doi.org/10.1109/TIM.2017.2681398

Julier, S., & Uhlmann, J. (2004, mar). Unscented Filtering and Nonlinear Estimation. *Proceedings of the IEEE*, *92*(3), 401–422.

Kalman, R. E. (1960, mar). A New Approach to Linear Filtering and Prediction Problems. *Journal of Basic Engineering*, *82*(1), 35–45.

Kaltiokallio, O., Bocca, M., & Patwari, N. (2012). Follow @grandma: Long-term device-free localization for residential monitoring. In *37th annual ieee conference on local computer networks - workshops* (p. 991-998).

Khalife, J. J., & Kassas, Z. M. (2019). Receiver Design for Doppler Positioning with LEO Satellites. In *Icassp 2019 - 2019 ieee int. conf. on acoustics, speech and signal processing* (p. 5506-5510).

Khodjaev, J., Park, Y., & Malik, A. S. (2009, aug). Survey of NLOS identification and error mitigation problems in UWB-based positioning algorithms for dense environments. *annals of telecommunications - annales des télécommunications*, *65*(5-6), 301–311.

Khurshid, K., & Khokhar, I. A. (2013, aug). Comparison survey of 4G competitors (OFDMA MC CDMA UWB IDMA). In *2013 international conference on aerospace science & engineering (ICASE).* IEEE. https://doi.org/10.1109/icase.2013.6785555

Kitagawa, G. (1998, sep). A Self-Organizing State-Space Model. *Journal of the American Statistical Association*, *93*(443), 1203.

Knight, R. (2022). *ESA Outlines Plans for Demo of LEO PNT Satellites As Part of FutureNAV, Gives Other Updates.* https://insidegnss.com/. ([Online; accessed 15-May-2023])

Krishnan, S., & Santos, R. X. M. (2021). Real-Time Asset Tracking for Smart Manufacturing. In *Intelligent systems reference library* (pp. 25–53). Springer International Publishing. https://doi.org/10.1007/978-3-030-67270-6_2

Kumari, K., & Yadav, S. (2018, 01). Linear regression analysis study. *Journal of the Practice of Cardiovascular Sciences*, *4*, 33.

Leaderboard. (2022). *Leaderboard - google Smartphone Decimeter Challenge 2022*. Retrieved from [2024-02-28]https://kaggle.com/competitions/smartphone-decimeter-2022

Lee, J.-S., Su, Y.-W., & Shen, C.-C. (2007). A Comparative Study of Wireless Protocols: Bluetooth UWB ZigBee and Wi-Fi. In *IECON 2007 - 33rd annual conference of the IEEE industrial electronics society.* IEEE. https://doi.org/10.1109/iecon.2007.4460126

Li, M., Xu, T., Guan, M., Gao, F., & Jiang, N. (2022). LEO-constellation-augmented multi-GNSS real-time PPP for rapid re-convergence in harsh environments. *GPS Solutions*, *26*, 29.

Li, W., Cui, X., & Lu, M. (2018, December). A robust graph optimization realiza-

tion of tightly coupled GNSS/INS integrated navigation system for urban vehicles. *Tsinghua Science and Technology*, *23*(6), 724–732.

Liu, J., Pu, J., Sun, L., & He, Z. (2019). An approach to robust ins/uwb integrated positioning for autonomous indoor mobile robots. *Sensors*, *19*(4). https://doi.org/10.3390/s19040950

Lu, S., Xu, C., Zhong, R. Y., & Wang, L. (2017, jul). A RFID-enabled positioning system in automated guided vehicle for smart factories. *Journal of Manufacturing Systems*, *44*, 179–190. https://doi.org/10.1016/j.jmsy.2017.03.009

Matin, M. (2010, aug). Ultra Wideband Preliminaries. In *Ultra wideband.* Sciyo. https://doi.org/10.5772/10059

Mazhar, F., Khan, M. G., & Sällberg, B. (2017, aug). Precise Indoor Positioning Using UWB: A Review of Methods Algorithms and Implementations. *Wireless Personal Communications*, *97*(3), 4467–4491. https://doi.org/10.1007/s11277-017-4734-x

Miller, L. E. (2003). *Why UWB? A Review of Ultrawideband Technology, Report to NETEX Project Office, DARPA* (Tech. Rep.). National Institute of Standards and Technology (NIST) U.S. Department of Commerce. Retrieved from http://citeseerx.ist.psu.edu/viewdoc/download?doi=10.1.1.76.7051&rep=rep1&type=pdf

Misra, P., & Enge, P. (2011). *Global positioning system: Signals, measurements, and performance*. Ganga-Jamuna Press.

Molisch, A. F., Ratnam, V. V., Han, S., Li, Z., Nguyen, S. L. H., Li, L., & Haneda, K. (2017). Hybrid beamforming for massive mimo: A survey. *IEEE Communications Magazine*, *55*(9), 134-141.

Montenbruck, O., Steigenberger, P., & Hauschild, A. (2014). Broadcast versus precise ephemerides: a multi-gnss perspective. *GPS Solutions*, *19*, 321–333. https://doi.org/10.1007/s10291-014-0390-8

Montoliu, R., Sansano, E., Gascó, A., Belmonte, O., & Caballer, A. (2020, apr). Indoor Positioning for Monitoring Older Adults at Home: Wi-Fi and BLE Technologies in Real Scenarios. *Electronics*, *9*(5), 728. https://doi.org/10.3390/electronics9050728

Morales Ferre, R., Richter, P., De La Fuente, A., & Simona Lohan, E. (2019). In-lab validation of jammer detection and direction finding algorithms for gnss. In *2019 international conference on localization and gnss (icl-gnss)* (p. 1-6).

Morales-Ferre, R., Richter, P., Falletti, E., de la Fuente, A., & Lohan, E. S. (2020). A survey on coping with intentional interference in satellite navigation for manned

and unmanned aircraft. *IEEE Communications Surveys & Tutorials*, *22*(1), 249-291.

Motroni, A., Buffi, A., & Nepa, P. (2021). A Survey on Indoor Vehicle Localization Through RFID Technology. *IEEE Access*, *9*, 17921–17942. https://doi.org/10.1109/access.2021.3052316

Muqaibel, A., Safaai-Jazi, A., & Riad, S. (2004, Feb). Ultra Wideband vs. Narrowband Communications. In *Riyadh international communications & it conference.* Retrieved from https://www.researchgate.net/profile/Ali-Muqaibel/publication/330090948_Ultra_Wideband_vs_Narrowband_Communications/links/5c2ce9ba92851c22a3554edc/Ultra-Wideband-vs-Narrowband-Communications.pdf

Nantee, N., & Sureeyatanapas, P. (2021, mar). The impact of Logistics 4.0 on corporate sustainability: a performance assessment of automated warehouse operations. *Benchmarking: An International Journal*, *ahead-of-print*(ahead-of-print). https://doi.org/10.1108/bij-11-2020-0583

Nekoogar, F. (2005). *Ultra-wideband communications: fundamentals and applications*. Prentice Hall PTR. Retrieved from https://books.google.fi/books/about/Ultra_wideband_Communications.html?id=kAgfAQAAIAAJ&redir_esc=y

NXP. (2022). *Secure Ultra-Wideband (UWB).* Retrieved from [2022-01-24]https://www.nxp.com/products/wireless/secure-ultra-wideband-uwb:UWB-TRIMENSION

Palacios, J., Gonzalez-Prelcic, N., Mosquera, C., Shimizu, T., & Wang, C.-H. (2021). A hybrid beamforming design for massive mimo leo satellite communications. *Front. Space Technol*, *27*.

Palacios, J., González-Prelcic, N., Mosquera, C., & Shimizu, T. (2021). A Dynamic Codebook Design for Analog Beamforming in MIMO LEO Satellite Communications. *arXiv:2111.08655*.

Park, J., Kim, H., Yoon, J., Kim, H., Park, C., & Hong, D. (2021). Development of an ultrasound technology-based indoor-location monitoring service system for worker safety in shipbuilding and offshore industry. *Processes*, *9*(2). https://doi.org/10.3390/pr9020304

Pearl, J. (1987, October). Distributed revision of composite beliefs. *Artificial Intelligence*, *33*(2), 173–215.

Pfeifer, T., & Protzel, P. (2019, May). Expectation-Maximization for Adaptive Mixture Models in Graph Optimization. In *2019 International Conference on Robotics and Automation (ICRA)* (pp. 3151–3157).

Pinell, C., Prol, F., Bhuiyan, M., & Praks, J. (2023). Receiver architectures for positioning with low earth orbit satellite signals: a survey. *EURASIP J. Adv. Signal Process.*, *60*, 2023.

Pittet, S., Renaudin, V., Merminod, B., & Kasser, M. (2008, jun). UWB and MEMS Based Indoor Navigation. *Journal of Navigation*, *61*(3), 369–384.

Pospelova, I. V., Cherepanova, I. V., Bragin, D. S., Sidorov, I. A., Kostyuchenko, E. Y., & Serebryakova, V. N. (2022). The estimation of the potential for using smart-trackers as a part of a medical indoor-positioning system. *Electronics*, *11*(1). https://doi.org/10.3390/electronics11010107

Pozyx. (2021). *Positioning mode.* Retrieved from [2022-03-07]https://docs.pozyx.io/enterprise/Positioning.1224016064.html

Psiaki, M. L. (2021). Navigation using carrier Doppler shift from a LEO constellation: TRANSIT on steroids. *Navigation*, *68*(3), 621-641.

Qorvo. (2020). *Qorvo Completes Acquisition of Decawave.* Retrieved from [2022-01-24]https://www.qorvo.com/newsroom/news/2020/qorvo-completes-acquisition-of-decawave

Rácz-Szabó, A., Ruppert, T., Bántay, L., Löcklin, A., Jakab, L., & Abonyi, J. (2020, nov). Real-Time Locating System in Production Management. *Sensors*, *20*(23), 6766. https://doi.org/10.3390/s20236766

Rainbow, J. (2022). *Lockheed invests in Xona's GPS-alternative constellation.* https://spacenews.com/lockheed-invests-in-xonas-gps-alternative-constellation/. ([Online; accessed 15-May-2023])

Rauch, H. E., Tung, F., & Striebel, C. T. (1965). Maximum likelihood estimates of linear dynamic systems. *AIAA Journal*, *3*(8), 1445-1450.

Ridolfi, M., de Velde, S. V., Steendam, H., & Poorter, E. D. (2018, jun). Analysis of the Scalability of UWB Indoor Localization Solutions for High User Densities. *Sensors*, *18*(6), 1875. https://doi.org/10.3390/s18061875

Ridolfi, M., Vandermeeren, S., Defraye, J., Steendam, H., Gerlo, J., Clercq, D. D., ... Poorter, E. D. (2018, jan). Experimental Evaluation of UWB Indoor Positioning for Sport Postures. *Sensors*, *18*(2), 168. https://doi.org/10.3390/s18010168

Sabath, F., Mokole, E. L., & Samaddar, S. N. (2005). Definition and classification of ultra-wideband signals and devices. *URSI Radio Science Bulletin*, *2005*(313), 12-26.

Samsung. (2019). *Key Industry Players The ASSA ABLOY Group, HID, NXP, Sam-*

sung, Bosch, Sony, LitePoint and TTA Establish FiRa Consortium to Drive Seamless User Experiences Using Ultra-Wideband Technology. Retrieved from [2022-01-24]https://news.samsung.com/global/key-industry-players-the-assa-abloy-group-hid-nxp-samsung-bosch-sony-litepoint-and-tta-establish-fira-consortium-to-drive-seamless-user-experiences-using-ultra-wideband-technology

Santhanam, M. (2011). *UWB TECHNOLOGY AND ITS APPLICATIONS – A SURVEY* (Unpublished master's thesis). School of Engineering, Jönköping University.

Sarkka, S. (2007, sep). On Unscented Kalman Filtering for State Estimation of Continuous-Time Nonlinear Systems. *IEEE Transactions on Automatic Control*, *52*(9), 1631–1641.

Sewio. (2021). *Time Difference of Arrival.* Retrieved from [2021-08-30]https://www.sewio.net/uwb-technology/time-difference-of-arrival/

Shule, W., Almansa, C. M., Queralta, J. P., Zou, Z., & Westerlund, T. (2020). UWB-Based Localization for Multi-UAV Systems and Collaborative Heterogeneous Multi-Robot Systems. *Procedia Computer Science*, *175*, 357–364.

Silvia, Z., Martina, C., Fabio, S., & Alessandro, P. (2018). Ultra Wide Band Indoor Positioning System: analysis and testing of an IPS technology. *IFAC-PapersOnLine*, *51*(11), 1488–1492. https://doi.org/10.1016/j.ifacol.2018.08.292

Si-soo, P. (2021, August). *South Korea's GNSS project to take off with $3.3 billion budget.* Retrieved from [2024-03-04]https://spacenews.com/south-koreas-gnss-project-to-take-off-with-3-3-billion-budget/

Soganci, H., Gezici, S., & Poor, H. (2011, apr). Accurate positioning in ultra-wideband systems. *IEEE Wireless Communications*, *18*(2), 19–27.

Song, Y., & Hsu, L.-T. (2021, January). Tightly coupled integrated navigation system via factor graph for UAV indoor localization. *Aerospace Science and Technology*, *108*, 106370.

Song, Y., Yu, F. R., Zhou, L., Yang, X., & He, Z. (2021, mar). Applications of the Internet of Things (IoT) in Smart Logistics: A Comprehensive Survey. *IEEE Internet of Things Journal*, *8*(6), 4250–4274. https://doi.org/10.1109/jiot.2020.3034385

Srinivas, P., & Kumar, A. (2017). Overview of architecture for gps-ins integration. In *2017 recent developments in control, automation power engineering (rdcape)* (p. 433-438).

Su, K., Jin, S., & Hoque, M. M. (2019). Evaluation of ionospheric delay effects on multi-gnss positioning performance. *Remote Sensing*, *11*(2).

https://doi.org/10.3390/rs11020171

Su, Y., & Fan, Q.-M. (2020). The Green Vehicle Routing Problem From a Smart Logistics Perspective. *IEEE Access*, *8*, 839–846. https://doi.org/10.1109/access.2019.2961701

Sünderhauf, N., & Protzel, P. (2012, March). Towards robust graphical models for GNSS-based localization in urban environments. In *International Multi-Conference on Systems, Signals Devices* (pp. 1–6).

Särkkä, S. (2013). *Bayesian filtering and smoothing*. Cambridge University Press.

Takasu, T., & Yasuda, A. (2009). Development of the low-cost rtk-gps receiver with an open source program package rtklib. In *The international symposium on gps/gnss, jeju, korea.*

Tan, Z., Qin, H., Cong, L., & Zhao, C. (2020). Positioning using iridium satellite signals of opportunity in weak signal environment. *Electronics*, *9*(1).

Tang, X. (2020). Research on Smart Logistics Model Based on Internet of Things Technology. *IEEE Access*, *8*, 151150–151159. https://doi.org/10.1109/access.2020.3016330

Tao, Y., & Zhao, L. (2018, nov). A Novel System for WiFi Radio Map Automatic Adaptation and Indoor Positioning. *IEEE Transactions on Vehicular Technology*, *67*(11), 10683–10692. https://doi.org/10.1109/tvt.2018.2867065

Teunissen, P. J., & Montenbruck, O. (2017). *Springer handbook of global navigation satellite systems* (Vol. XXXI). Springer. Retrieved from https://link.springer.com/book/10.1007/978-3-319-42928-1

Thrun, S., Fox, D., Burgard, W., & Dellaert, F. (2001, may). Robust Monte Carlo localization for mobile robots. *Artificial Intelligence*, *128*(1-2), 99–141.

Tian, Q., Wang, K. I.-K., & Salcic, Z. (2019a, oct). Human Body Shadowing Effect on UWB-Based Ranging System for Pedestrian Tracking. *IEEE Transactions on Instrumentation and Measurement*, *68*(10).

Tian, Q., Wang, K. I.-K., & Salcic, Z. (2019b, may). A Low-Cost INS and UWB Fusion Pedestrian Tracking System. *IEEE Sensors Journal*, *19*(10), 3733–3740.

Tian, Q., Wang, K. I.-K., & Salcic, Z. (2020, apr). An INS and UWB Fusion Approach With Adaptive Ranging Error Mitigation for Pedestrian Tracking. *IEEE Sensors Journal*, *20*(8), 4372–4381. https://doi.org/10.1109/JSEN.2020.2964287

Tim, E. (2021). *Batch processing rtklib solutions with rnx2rtkp and python.*

Retrieved from https://rtklibexplorer.wordpress.com/2022/01/05/batch-processing-rtklib-solutions-with-rnx2rtkp-and-python/

Ullah, I., Shen, Y., Su, X., Esposito, C., & Choi, C. (2020). A Localization Based on Unscented Kalman Filter and Particle Filter Localization Algorithms. *IEEE Access*, *8*, 2233–2246.

Vemula, M., Bugallo, M. F., & Djuric, P. M. (2007, dec). Performance Comparison of Gaussian-Based Filters Using Information Measures. *IEEE Signal Processing Letters*, *14*(12), 1020–1023.

Wang, Y., & Li, X. (2017). The imu/uwb fusion positioning algorithm based on a particle filter. *ISPRS International Journal of Geo-Information*, *6*(8). https://doi.org/10.3390/ijgi6080235

Watson, R. M., & Gross, J. N. (2018). Evaluation of kinematic precise point positioning convergence with an incremental graph optimizer. In *Ieee/ion position, location and navigation symposium (plans)* (p. 589–596).

Wen, W., Pfeifer, T., Bai, X., & Hsu, L.-T. (2021). Factor graph optimization for GNSS/INS integration: A comparison with the extended Kalman filter. *NAVIGATION*, *68*(2), 315–331.

Wertz, J., for Space Technology (U.S.), N. C., & (U.S.), N. R. L. (2001). *Mission geometry: Orbit and constellation design and management : Spacecraft orbit and attitude systems*. Microcosm Press.

Wilzeck, A., Guirao, M. P., & Dimitrov, E. (2018). White Paper on UWB Technology and Regulation. *wiseSense GmbH*.

Woo, S., Jeong, S., Mok, E., Xia, L., Choi, C., Pyeon, M., & Heo, J. (2011). Application of wifi-based indoor positioning system for labor tracking at construction sites: A case study in guangzhou mtr. *Automation in Construction*, *20*(1), 3-13. https://doi.org/10.1016/j.autcon.2010.07.009

Wu, W., Shen, L., Zhao, Z., Li, M., & Huang, G. Q. (2022). Industrial iot and long short-term memory network enabled genetic indoor tracking for factory logistics. *IEEE Transactions on Industrial Informatics*, *PP*(99), 1–1. https://doi.org/10.1109/tii.2022.3146598

Yin, Z., Jiang, X., Yang, Z., Zhao, N., & Chen, Y. (2019, mar). WUB-IP: A High-Precision UWB Positioning Scheme for Indoor Multiuser Applications. *IEEE Systems Journal*, *13*(1), 279–288. https://doi.org/10.1109/jsyst.2017.2766690

You, L., Li, K.-X., Wang, J., Gao, X., Xia, X.-G., & Otterstenx, B. (2020). Leo satellite communications with massive mimo. In *Icc 2020 - 2020 ieee international*

conference on communications (icc) (p. 1-6).

Youssef, M., Mah, M., & Agrawala, A. (2007, September). Challenges: Device-free passive localization for wireless environments. In *Proceedings of the 13th annual ACM international conference on Mobile computing and networking* (pp. 222–229). New York, NY, USA: Association for Computing Machinery.

Zhang, N. (2018). Smart Logistics Path for Cyber-Physical Systems With Internet of Things. *IEEE Access*, *6*, 70808–70819. https://doi.org/10.1109/access.2018.2879966

Zhang, Y., Tan, X., & Zhao, C. (2020, dec). UWB/INS Integrated Pedestrian Positioning for Robust Indoor Environments. *IEEE Sensors Journal*, *20*(23), 14401–14409.

Zhang, Y., Wu, Y., Liu, A., Xia, X., Pan, T., & Liu, X. (2021). Deep learning-based channel prediction for leo satellite massive mimo communication system. *IEEE Wireless Communications Letters*, *10*(8), 1835-1839.

Zhu, L., Spachos, P., Pensini, E., & Plataniotis, K. N. (2021). Deep learning and machine vision for food processing: A survey. *Current Research in Food Science*, *4*, 233-249. https://doi.org/10.1016/j.crfs.2021.03.009

Zhu, N., Marais, J., Bétaille, D., & Berbineau, M. (2018). Gnss position integrity in urban environments: A review of literature. *IEEE Transactions on Intelligent Transportation Systems*, *19*(9), 2762-2778.

Zou, Z. (2011). *Impulse Radio UWB for the Internet-of-Things: A Study on UHF/UWB Hybrid Solution* (Doctoral dissertation, KTH School of Information and Communication Technology). Retrieved from https://www.semanticscholar.org/paper/Impulse-Radio-UWB-for-the-Internet-of-Things-%3A-A-on-Zou/8920dd049f0b31b2aed23f253cc511dccfd5ac28

Çelikbilek, K., Saleem, Z., Morales Ferre, R., Praks, J., & Lohan, E. S. (2022). Survey on optimization methods for leo-satellite-based networks with applications in future autonomous transportation. *Sensors*, *22*(4).

Publication P1

IEEE Access
Multidisciplinary ⋮ Rapid Review ⋮ Open Access Journal

Received March 21, 2022, accepted April 9, 2022, date of publication April 21, 2022, date of current version April 29, 2022.

Digital Object Identifier 10.1109/ACCESS.2022.3169267

Precision Positioning for Smart Logistics Using Ultra-Wideband Technology-Based Indoor Navigation: A Review

MAHMOUD ELSANHOURY[1], (Graduate Student Member, IEEE), PETTERI MÄKELÄ[1,2], JANNE KOLJONEN[1], PETRI VÄLISUO[1], AHM SHAMSUZZOHA[1], TIMO MANTERE[1], MOHAMMED ELMUSRATI[1], (Senior Member, IEEE), AND HEIDI KUUSNIEMI[1,3], (Member, IEEE)

[1]School of Technology and Innovations, University of Vaasa, FI-65200 Vaasa, Finland
[2]Seinäjoki University of Applied Sciences, 60100 Seinäjoki, Finland
[3]National Land Survey, Finnish Geospatial Research Institute, FI-02430 Masala, Finland

Corresponding author: Mahmoud Elsanhoury (mahmoudessam08@gmail.com)

This work was supported in part by the TULEVA Project, in part by the European Regional Fund, European Union, and in part by the University of Vaasa, Finland.

ABSTRACT Logistics is an important driver for the competitiveness of industries and material supply. The development of smart logistics, powered by precise positioning and communication technologies can significantly improve the efficiency of logistics. The emerging technology of ultra-wideband (UWB) precision positioning has attracted significant attention throughout the previous decade owing to its promising capabilities over other radio frequency-based indoor localisation systems. In addition, UWB is characterised by large bandwidth and data rate, short message length, low transmission power and high penetration capability, which are all favourable for indoor positioning applications. However, UWB localisation technology faces several challenges that are somewhat similar to other technologies, such as mitigating errors that originate from non-line-of-sight (NLOS) situations and tackling signal interference in dense environments, and when required to operate in extreme conditions. This paper reviews the most recent advances made in UWB positioning systems over the last five years, with a focus on high-ranking articles. In addition to going through more conventional solutions to UWB challenges, modern solutions, which involve the use of machine learning and sensor data fusion, are discussed. We highlight the most promising findings of the recently implemented and foreseen UWB positioning systems by providing a summary of each reviewed article. Additionally, we address a major challenge that faces the UWB positioning technology: NLOS situations, focusing on some proposed remedies such as multi-sensor fusion and machine learning. As an application, this study introduces how UWB technology promotes smart logistics by offering indoor positioning to improve efficiencies in the delivery of goods from the source to the customer. Furthermore, it demonstrates the benefits of UWB technology for accurate positioning and tracking of both stationary and moving items, and machinery in an indoor logistics environment.

INDEX TERMS Ultra-wideband (UWB), indoor positioning systems (IPS), smart logistics, navigation and localisation, machine learning, sensor fusion.

I. INTRODUCTION

In recent years, the importance of indoor positioning systems (IPS) has been significantly increasing due to the rapid development and popularization of smart devices and technologies. The extensively used technology for positioning is the global navigation satellite systems (GNSSs) that provide reliable outdoor positioning information. However, due to the rather weak signals, their performance in the indoor environment is not sufficient. In addition, indoor surroundings are usually complex and varying in nature due to transferable obstacles that cause variation of signal and noise levels [1]. In such situations, substantial research and development of indoor positioning systems are required with alternative wireless technologies such as Wi-Fi [2], geomagnetic field [3], Bluetooth low energy (BLE) [4], dead-reckoning technique [5], ultra-wideband (UWB), and radio signal tags [6].

The associate editor coordinating the review of this manuscript and approving it for publication was Peng-Yong Kong.

Precise location information of people and assets is a crucial element for Internet of Things (IoT) and smart logistics applications [7]. The various IPS technologies have been widely adopted by researchers and industrial companies during the past decade due to their broad spectrum of applications, including smart logistics [8], tracking medical equipment in healthcare centres [9], tracking individuals in crowded venues [10], ship-building and offshore industry [11], and construction industry [12].

There are numerous indoor localisation technologies with diverse properties. They are often distinguished by positioning accuracy, system robustness, computational power and cost. When compared to indoor positioning technologies using narrowband signals, such as Bluetooth and Wi-Fi, UWB has many advantages [10], [13].

An UWB signal contains different frequency components due to its wide bandwidth, which increases its probability of penetrating obstacles. In addition, because of its low power spectral density, UWB does not interfere with most other radio systems. Because of its short pulse duration, UWB yields high ranging accuracy and good performance under multipath conditions.

Several technologies have been proposed for obtaining a tracking solution in indoor logistics. The selection of an appropriate technology mainly depends on the required precision, number of assets that need to be tracked and speed of the moving assets. Compared to other available technologies, UWB can provide low-cost accurate positioning within few centimetres accuracy; hence, it is frequently used in industrial environments such as smart factory [14], smart logistics [15], [16], warehouse management [17], vehicle localisation [18], robot positioning [19], and smart city [20]. UWB enables simultaneous real-time tracking of objects and provides their localisation despite indoor obstructions due to the advantage of working under non-line-of-sight (NLOS) conditions [21], [22]. UWB technology enables an efficient combination of accuracy, scalability and reliability, which are very crucial in the applications of indoor logistics, such as tracking people and assets, and controlling the automated guided vehicles (AGVs) [23], [24].

Numerous survey articles were presented throughout the past decade with a focus on addressing UWB as an IPS. For example, in 2016, Alarifi *et.al.* [10] published their comprehensive survey paper that presented UWB-IPS technology with new taxonomies as well as analysing the strengths, weaknesses, opportunities, and threats (SWOT) to form a widely acknowledged state-of-the-art review. Similar approach to Alarifi, was presented by Mazhar *et.al.* [25] in 2017. Another survey article that was focused on IPSs in general and UWB in particular was Yassin *et.al.* [26], in which the authors presented a detailed review about the structure and challenges of UWB-IPS compared to other IPS technologies. More surveys are tacitly cited throughout the article and discussed in the relevant sections.

This paper highlights the advances achieved in the realm of UWB localisation during the past half-decade, with a focus on the most recently published literature found from IEEE Xplore, Google Scholar and Crossref platforms. The search terms were limited to ''Ultra Wideband'' AND ''Positioning'' OR ''Localisation'' within the last five years. In addition to the newness of the articles, their selection criteria were based on impact, relevance, higher ranking in the Finnish national system [27], novelty and citation score. However, some older articles were also included due to their importance and the unchanged scientific principles that they describe.

Note that the addressing of UWB throughout this article is intended to review UWB as an IPS rather than a communication system. Hence, we focus on presenting the recent momentum of UWB technology from an IPS design perspective.

Throughout the article, a particular focus was given on applying the UWB technology to deploy indoor positioning in smart logistics systems. For smart logistics, indoor positioning plays an essential role by tracking resources, materials and employees in real-time. This location-based indoor navigation enables logistics providers with asset tracking with reduced search times, process automation and optimisation, increased efficiency and safety for employees [17], [28]. In the case of assets tracking, indoor positioning offers real-time seamless tracking of goods, pallets, vehicles and monitoring of goods' conditions, such as temperature, humidity and dew points. For process automation and optimisation, IPS supports automation through precise geo-based task assignments. By providing precise positioning, IPS provides added safety and security in logistics sites with access authorisations and ensures faster evacuation of employees in case of emergencies [23], [24].

The main contribution of this article is to present the most recent advances in the fast-developing UWB precise positioning technology with a focus on smart logistics applications that can embrace the technology to achieve better system enhancements and optimisations. The availability of new UWB chips at affordable prices has catalyzed the development of new algorithms for new application areas, including machine learning, sensor fusion and collaborative positioning. This article dissects the topic thoroughly down to the basic concepts of localisation and algorithms besides keeping a compact style of summarizing the literature to help researchers and industrial firms cope with the recent advances in UWB technology and its foreseen future.

In addition, a major objective of this review is to provide the researchers, practitioners of smart logistics and related fields with a starting point to understand the potential and limitations of UWB indoor navigation. To the best of our knowledge, other existing reviews have not adopted a similar approach. This article explains the fundamentals of positioning techniques and algorithms not only at the detailed mathematical and algorithmic level but also at the conceptual level. Commercially available equipment is presented, as well. Moreover, numerous articles are summarized in several application-specific tables to easily compare the methods and algorithms in the selected application areas.

Consequently, also readers who do not have previous knowledge of positioning techniques can utilize this article to obtain the basic knowledge of UWB positioning and its use in smart logistics.

The rest of the article is organized as follows: Section II contains a brief review of existing IPSs and presents the role of IPSs in smart logistics. Section III discusses the advantages and challenges of UWB, licensing and regulations, signal attributes, system architecture, and commercial applications. Section IV explains the observables and positioning technologies used with UWB. Section V discusses positioning algorithms, such as least-squares methods, closed-form solutions and various kinds of Bayesian filters. In addition, NLOS identification and mitigation methods are explained. Recent advances in UWB positioning literature is stated in Section VI, whereas advances in sensor fusion techniques are elaborated in Section VII. As the last few years have witnessed a surge on the literature on the adoption of artificial intelligence (AI) solutions, various machine learning (ML) approaches for UWB are discussed in Section VIII. A final discussion on indoor positioning is stated in Section IX, while, the paper is concluded in Section X.

II. INDOOR POSITIONING SYSTEMS

An IPS is a real-time system that uniformly calculates the location of an agent or object, moving or stationary, inside buildings [10], [29]–[31]. An IPS has facilitated numerous navigation applications that require continuous knowledge of the indoor locations of people and objects. It provides assisted navigation for limited-sight and vision-impaired people, tracking of visitors in heavily crowded venues, such as airports and malls, and automated guidance in tourist attractions. Industrial applications use IPSs to ensure precise navigation of industrial robots and accurate positioning of personnel, tools and equipment. Medical applications include monitoring of patients in hospitals and healthcare centres, localisation of crucial medical equipment and enabling navigation for medical robotic assistants [10].

Outdoor positioning has been made feasible owing to GNSSs, such as Global Positioning System (GPS), Galileo, GLONASS and stand-alone cellular positioning systems [31], [32]. However, these systems perform poorly in indoor venues due to the satellite signal deterioration caused by signal attenuation, shadowing and multipath fading imposed by indoor concrete and metallic structures [26], [32]–[34]. Thus, accurate indoor positioning techniques have been proposed to address the deep fading of conventional positioning methods. In addition, hybrid approaches have been proposed to combine multiple indoor and outdoor positioning techniques to mitigate errors and provide more accurate and robust navigation. Numerous indoor positioning techniques can provide positioning accuracy of only a few centimetres as stated in [10], [26], [30]. However, combining multiple indoor positioning techniques requires scrutinised studies to allocate suitable resources for each method and identify the optimal combination as the resource requirements vary from method to method. The optimisation objectives and constraints may concern the energy budget, RF bandwidth budget, infrastructure costs, number of beneficiaries (users) and active time budget.

A. SMART LOGISTICS AND MANUFACTURING

Nowadays, smart logistics is considered a fundamental pillar of Industry 4.0. It enables companies to orchestrate several critical activities, such as demand forecasting, sales planning and inventory management [35], [36]. Smart logistics or 'Logistics 4.0' promotes the acceleration of all logistics processes through planning and controlling with smart tools, technologies and methods. The use of smart technologies helps to gather the necessary information to monitor and control the material flow and for many other purposes. Through intelligent positioning technologies, tools and equipment, global supply and logistics chains are becoming increasingly efficient and effective [37]. Such positioning technologies significantly contribute to end-to-end visibility, improvement in product routing as well as control and replenishment of inventories and mobile assets [38]. A generic supply and logistics chain is displayed in Figure 1, which is divided into inbound and outbound supply and logistics chains.

Smart logistics is considered a fairly complex phenomenon that can be easily applied in geographically dispersed areas for tracking raw materials of the highest quality but lowest cost. Such a phenomenon is generally characterised by the use of new technologies, such as IoT, 5G, sensors, radio frequency identification (RFID) tags, smart products, actuators and intelligent machines [38], [39]. It has the ability, reliability, traceability and authenticity of the information, which are useful to establish intelligent contractual relationships among the stakeholders of the supply chains. Moreover, smart logistics includes considerable potential for improving the logistics process through the application of communication and information technologies at all levels of the value chain. Figure 2 displays the fundamental elements and functionalities of the smart supply and logistics chain, showing that it starts from the supplier and eventually moves forward till the end customer through smart transportation, manufacturing, smart warehousing and smart delivery stages.

Figure 2 also shows that, at each stage in the smart supply and logistics chain, several activities are orchestrated. For instance, at the transportation stage, activities such as traceability of items, location tracking and real-time routing are orchestrated and monitored for smoother operations. Tracking logistics items is an essential issue in today's supply chain and inventory management. In addition, finding items both in indoor and outdoor environments is most critical in any supply chain and logistics management [40]. Due to the trend towards autonomous systems, most logistic systems today are operated without the direct involvement of the workforce to control them. In such a changing environment, smart logistics can be helpful to deliver items through various available precise positioning technologies [41], [42].

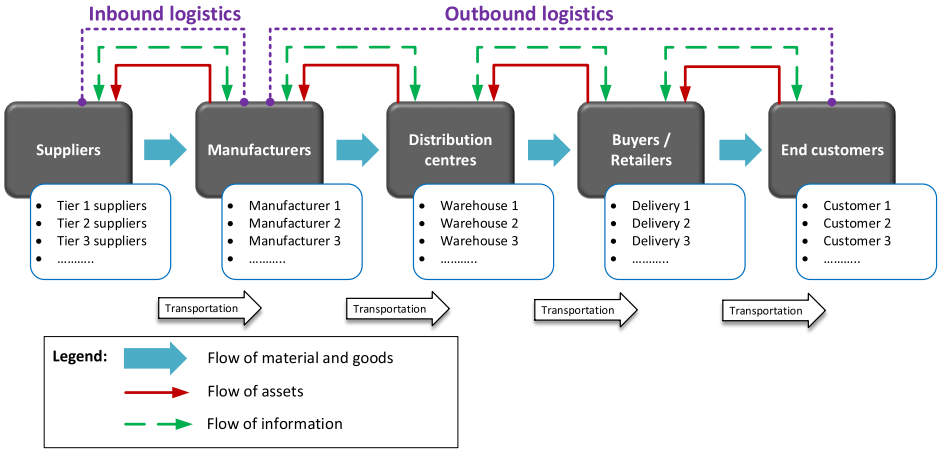

FIGURE 1. Various stakeholders and the flow of material, assets and information in a generic supply and logistics chain.

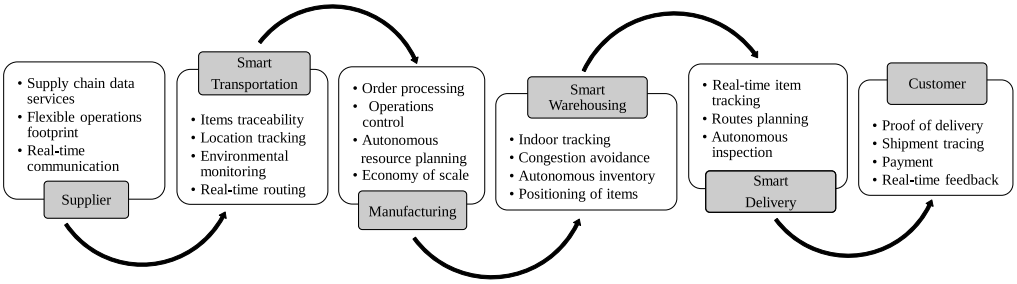

FIGURE 2. Fundamental elements and functionalities of smart supply and logistics chain.

Although several technologies are available to provide outdoor positioning towards logistics items, most of them are not suitable for indoor positioning. In indoor environments, such as warehouses and factory floors, precision positioning of components, parts and products can be achieved through available technologies, such as UWB, Wi-Fi, 5G, 3D imaging, sensors and imaging radio signals [25], [43], [44]. The application of such technologies helps to track indoor logistics items, which can help in minimising the time required to locate items and avoid delays due to the wrong location. A precision positioning technique enables the automatic delivery of goods by using uncrewed intelligent vehicles and aerial vehicles (UAVs) to designated locations while reducing environmental influences.

B. INDOOR POSITIONING SYSTEMS IN SMART LOGISTICS AND MANUFACTURING

Due to the recent advancements in indoor positioning technologies, a growing interest has emerged to utilize location data in logistics and manufacturing. Location data of assets and materials can be used to improve the efficiency, safety and security of manufacturing operations. Real-time tracking of machines and materials yields new possibilities to improve the production processes and follow the material flows. The authors of [45] divided logistics units into six identification layers: (0) raw material (items), (1) package, (2) transport unit, (3) unit load (pallet), (4) container and (5) transportation unit (e.g. truck, ship and train). GNSSs are typically used for tracking containers and transport equipment (two highest layers). However, the smaller cargo units (layers 1-3) are typically handled indoors, which can be tracked using indoor positioning technologies, such as UWB. However, UWB is still a relatively expensive and power-consuming technology, and RFID is a better technology to track the materials and lowest level packages and items.

Real-time location tracking is increasingly attracting global logistics companies due to the need for visibility. Especially, the application of IPSs in logistics and manufacturing

has increased recently [46]. In the case of an indoor environment, such as a warehouse, an IPS contributes to tasks such as minimising the time spent to look for the right pallet, optimising routes and preventing accidents. In the case of smart logistics, companies generally use RFID technology, which can track the inventory and identify goods [42], [47], [48]. However, the limited power source of RFID tags minimises their operational range to a couple of metres. Therefore, they are mainly used for identification rather than positioning purposes. Similarly, Bluetooth and Wi-Fi are also used for indoor positioning, but their operating ranges are no more than 3-5 m [49]. To obtain accurate positioning of logistics items, companies are nowadays exploring UWB-based positioning systems, which enable real-time positioning of goods, assets and people with an accuracy level of 5 to 30 cm. It can provide out-of-the-box localisation with higher ranging accuracy than Wi-Fi or Bluetooth or other active radio solutions [50], [51].

In the case of autonomous robots operating in indoor environments (e.g. warehouses), accurate positioning is essential for navigation. While GNSS-based localisation is unreliable in indoor environments, localisation by UWB technology can accelerate the adoption and ubiquity of distributed robotics systems. Nowadays, UWB-based technology is commonly used in indoor robotic applications from home cleaning to warehouse transportation, including the rapidly emerging autonomous last-mile delivery solutions [46]. In the case of intelligent manufacturing, it is essential to track the parts along the production chain to take the right decisions. Real-time tracking of both stationary and moving parts in the production floor ensures safer operation with a reduced lead time [52], [53]. In addition to parts, it is also essential to track workers' movement on the production floor to enhance operational flexibility. For smart manufacturing, UWB-based location technology is suitable because of its inherent accuracy and reliability [15], [54]. It is considered as the most optimal and accurate approach to ensure indoor localisation [55]. By providing indoor localisation and tracking solutions for vehicles, people and goods, UWB technology promotes increased transparency, safety and productivity in internal logistics on the factory floors [55].

C. PERFORMANCE METRICS OF INDOOR POSITIONING SYSTEMS

The performance of localisation technologies can be assessed using a pyramid-like scheme with system accuracy as the baseline, integrity as the second metric, continuity as the third, and availability as the peak paramount [56]. System accuracy is the degree of conformance of the estimated positioning values to the ground truth. The integrity of localisation systems, as defined by [56], is the trustworthiness of the information provided by the navigation engine. Continuity is the probability of the system to maintain the desired service level within the operation period, while availability is the percentage of time in which the navigation engine is up-running for positioning and can be used by its intended users.

Accuracy of the estimated position is one of the most important performance metrics for indoor positioning systems. Accuracy is often reported as the error distance between the estimated and actual locations, while a location precision is reported in percentages of position information, which is within the distance of accuracy. The most commonly used metrics of accuracy and location precision are the root mean square error (RMSE), the mean absolute error (MAE), the distance root mean square error and circular error probability.

The accuracy of the location estimate depends on the accuracy of individual measurements and the mutual geometry of the tag and anchors. In the time of arrival (TOA) and time difference of arrival (TDOA) methods, the accuracy of the position is expressed as the product of a geometric factor and a range measurement error factor.

In addition to the above mentioned metrics, there are other performance metrics presented in the literature, such as scalability, cost and privacy [10]. The scalability of IPS describes how many tags the system can support per time unit per geographic area. The cost measures the physical limitations and requirements associated with the implementation of a particular technology in terms of technical and financial resources. Money, power consumption and hardware dimensions are examples of cost metrics. Privacy is a concern in network-centric systems, where the location estimation takes place in the server. In the self-positioning model the device estimates its own position, and no one else may know where the device is. Coverage was mentioned as an important parameter [10]; however it can also be considered a property of IPS rather than a performance metric.

D. INDOOR POSITIONING TECHNOLOGIES

IPSs can use various signal technologies, such as radio frequency, infrared, ultrasonic, inertial, optical and electromagnetic [10], [57]. In addition, the positioning system commonly estimates the location of the target device by fusing measurements of two or more signal technologies. The indoor positioning applications have various requirements in terms of the performance metrics. Thus, the technology should be carefully chosen to satisfy these requirements [10]. For example, the navigation systems of AGVs might require highly accurate and reliable position estimates, but the power consumption or price of the sensor mounted in an AGV is not critical. In contrast, low price and power consumption are required from the tags used to locate people and assets in a warehouse, but the accuracy of the position estimate is less critical than that in AGV applications.

Laser triangulation is commonly used in the indoor navigation of AGVs [58]. The laser positioning system uses a laser scanner mounted on top of the vehicle. The laser scans the mirrors mounted at the known locations in the area and measures the angles between the vehicle and device. The vehicle's position is estimated using triangulation with centimetre-level accuracy. Another commonly used approach for AGV navigation is to use light detection and ranging (LiDAR) and inertial motion unit (IMU) measurements [59] or

TABLE 1. Summary of RF-based signal technologies for local positioning systems.

Technology	Accuracy	Typical Range	Method
UWB	2-50 cm	15-50 m	TOA/TDOA trilateration
Wi-Fi RSSI	< 10 m	35 m	Location fingerprinting
Wi-Fi CSI	< 5 m	35 m	Location fingerprinting, AoA
Wi-Fi RTT	> 1 m	35 m	TW-TOA
Bluetooth RSSI	< 5 m	< 50 m	Location fingerprinting
Bluetooth DF	< 1m	< 50 m	AOA, AOD
5G sub-6 GHz	3-10 m	0.5-2 km*	TDOA, TW-TOA, AOA, AOD
5G mmWave	0.2-0.5 m	200 m	TDOA, TW-TOA, AOA, AOD

* Depends on the frequency and the transmit power

image-based (visual) localisation [60] together with simultaneous localisation and mapping (SLAM) algorithms.

However, the laser and vision-based technologies are relatively expensive, and their energy consumption is too high for the tags required in the applications to locate people, materials and assets. In such applications, radio frequency-based signal technologies are commonly used for positioning. An RF signal is used for positioning for the same reasons as it is used for communication. The most important advantages of RF signals are that they can penetrate obstacles and have a wide communication bandwidth. RF-based IPSs use RFID, UWB, wireless local area network (WLAN), Bluetooth or cellular network signals for location estimation [10]. The position can be estimated from the signals of these systems by using proximity information, trilateration, triangulation or location fingerprinting methods. The properties of these systems are summarised in Table 1.

In the case of RFID, the proximity method is generally used. Location fingerprinting, which provides a room-level or couple of metres accuracy, is commonly used with WLAN [61] and Bluetooth [62] received signal strength indicator (RSSI) measurements. RSSI describes only the average attenuation of the signal in the communication channel. More accurate and stable results may be achieved using channel state information (CSI), such as channel impulse response (CIR), which contains more information than a single RSSI value [63]. Some researchers used an antenna array in a Wi-Fi network to estimate CSI, thus, enhancing the accuracy and stability of the fingerprinting positioning system to a few meters [64], [65]. A WLAN signal can also be used for trilateration using the Wi-Fi round trip time (RTT) measurements, referred to as 802.11mc [66]. In Bluetooth direction finding (DF), the target's position is estimated using the triangulation method with the angle of arrival or departure measurements of Bluetooth signals. According to the authors of [67], Bluetooth DF can achieve accurate measurements if not severely affected by multipath interference. Future 5G NR mmWave technology is expected to provide centimetre-level positioning accuracy and one degree orientation accuracy for the device when the TOA, TDOA and angle of arrival (AOA) are used [68].

TABLE 2. Different communication band usage scenarios and their terminology.

Band Type	Fractional Bandwidth B_F	Band Ratio $b_r = \frac{f_h}{f_l}$
Narrowband (NB)	$0.00 < B_F \leq 0.01$	$0.00 < b_r \leq 1.01$
Wideband (WB)	$0.01 < B_F \leq 0.25$	$1.01 < b_r \leq 1.29$
Ultra-Wideband (UWB)	$0.25 < B_F < 2.00$	$b_r \geq 1.29$

UWB is well suited for many positioning applications. In the case of UWB, the position can be estimated with centimetre-level accuracy using triangulation or trilateration positioning methods or both, as discussed in subsequent chapters.

III. UWB POSITIONING

UWB is a wireless short-range radio technology whose communication channel propagates information over a wide spectrum by modulating either a carrier-based waveform or a carrier-less baseband signal in the form of short-width pulses [69]. According to the Federal Communication Commission (FCC) and the International Telecommunication Union (ITU)-R, UWB possesses a spectrum that occupies a bandwidth greater than 20% of the central frequency or has a bandwidth of at least 500 MHz. A UWB RF signal occupies the ultra 500 MHz bandwidth, which facilitates the transmission of large data sizes upon the consumption of lesser energy than other technologies [10], [31], [70]. To differentiate among narrowband (NB), wideband (WB) and UWB, the FCC classification scheme adopts fractional bandwidth calculation, B_F which is a dimensionless frequency-independent indicator, calculated using Equation (1) as follows: [70], [71]

$$B_F = 2\left(\frac{f_h - f_l}{f_h + f_l}\right) \tag{1}$$

where f_h, f_l are the higher and lower frequency bands of the signal, respectively. Hence, the band type is determined using the data shown in Table 2 [70].

In 2002, the FCC described UWB technology as an emerging promising technology that holds great advances for various applications [72], such as imaging systems, ground-penetrating radars (GPRs), wall-imaging systems, medical systems, surveillance systems, vehicular radar systems, communications and measurements systems [73]. UWB can transmit high data rates using tiny pulses of the spectrum spread over wider frequency bands with low PSD, which provides the signal higher penetration capability than most RF waves. Moreover, some types of UWB signals (e.g. impulse radio UWB) do not require sinusoidal carrier waves, which

in turn reduces the power required for transmission. The combined advantages of a UWB signal makes it a prominent candidate for real-time applications, such as 1) tracking and navigation, 2) sensor network communications, 3) ranging and imaging, and 4) extremely high-data-rate short-range communication (e.g. wireless UWB).

Recently, UWB has been widely adopted in personal area networks (PANs), precise indoor positioning, indoor tracking and navigation systems. UWB positioning relies on the unique radio frequency characteristics associated with UWB technology to provide accurate estimates for indoor locations based on the TOA, AOA and TDOA of the signal. The UWB positioning signal takes the form of a low-power short-pulse transmission with large bandwidth [10], [31], [70], making it robust, precise and secure.

A. ADVANTAGES AND CHALLENGES OF UWB COMPARED TO OTHER INDOOR POSITIONING TECHNOLOGIES

1) ADVANTAGES

UWB was first commissioned by the FCC for public use in 2002. Earlier, it was utilized solely by the US military for classified applications [13]. The structure of a UWB signal comprises the transmission of short pulses within large bandwidth ranges between 3.1 and 10.6 GHz, which yields UWB superiority over NB signals. Owing to the large bandwidth and short duty cycle, UWB possesses a larger capacity and higher data rate, which make it a suitable candidate for RF-based IPS implementation. Moreover, UWB lies in the unlicensed spectrum, which can be used by anyone without prior notification. Additionally, the pulse nature of the UWB signal increases its penetration capability. Therefore, UWB tags on mobile targets do not require a direct line of sight (LOS) with its anchors.

However, some scenarios found in dense environments might have negative effects on the UWB signal, causing multipath deterioration and interference with neighbouring frequencies in the spectrum [10]. In addition, the low transmission power can be ineffective in large-sized indoor spaces, as it disallows the signal from travelling to longer distances due to path loss attenuation. Hence, additional UWB anchors are required, which increases costs and complexity [13].

UWB offers numerous benefits over narrowband signals, which widens the range of affected applications. First, UWB is an unlicensed free spectrum that can be used without prior licensing. The UWB spectrum was made free for commercial use in 2002, but before that, it was restricted to military operators, mainly the Department of Defense, for classified applications [13]. UWB has a larger bandwidth than other positioning techniques, ranging from 3.1 to 10.6 GHz [73], [74], which provides it with the superiority in many aspects. For example, based on Shannon's law, the large UWB bandwidth provides large capacity for an RF signal, which implies a high data rate transmission that can support real-time applications, such as instant video streaming [13], [73]. Owing to their large bandwidth, UWB communication

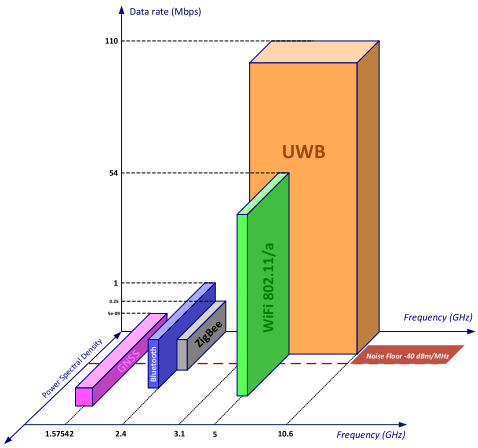

FIGURE 3. Comparison between the attributes of UWB and other various positioning technologies (the dimensions of the shapes are only indicative).

systems are highly robust, operating at higher data rates (110 Mbps) than other RF technologies, making it the highest data rate achieved so far in the precise positioning realm. Another benefit of the large bandwidth is the UWB system's capability of performing in low signal-to-noise-ratio (SNR) communication channels [13], which provides immunity against multipath degradation. The high level of multipath resolution is mainly attributed to the nature of pulse-based RF communication, which occupies the entire bandwidth for each pulse, unlike other carrier-based communications [75], UWB systems do not require a clear LOS, but the UWB communication is perfectly possible under NLOS conditions. However, in positioning applications, NLOS situations might produce erroneous sensor readings, which can disturb the position estimation. Additionally, the short-pulse low-power nature of UWB signals is a major advantage of UWB, making it a suitable candidate for indoor positioning applications, as demonstrated in Figure 3 [26], [76].

Additionally, the UWB signal transmits at low average power due to the short-pulse nature of transmission, submerging it within the noise floor(-40 dBm/MHz), which helps in saving transmitter energy, enhancing the battery life and bestowing resistance against jamming and interception.

2) CHALLENGES

Although UWB technology offers numerous benefits for indoor positioning applications, the technology faces several challenges and drawbacks that affect its performance.

UWB technology is known for its coexistence with other RF systems, but this is not always true. The technical report published by the US National Institute of Standards and Technologies [77] stated that UWB can cause interference to existing nearby RF systems and vice versa. Examples

of the potentially affected RF technologies are the GPS, 3G and WiMAX communication systems [10], [77] due to the misconfiguration of wireless transceiver devices. Many countries have imposed regulations to mitigate the possible interference, which are covered in the following sections.

The low power transmission of UWB is considered an advantage, yet it limits the overall power consumption for the transmitter and receiver. For example, the low-power UWB signal can either travel short distances at a high data rate or long distances at a low data rate [78]; hence, the range of the UWB anchor will be limited. This can only be compensated by using more UWB anchors, which limits the scalability [51], [79] and increases the system complexity and computational load, thus compromising the system accuracy and robustness. Additionally, the processing of wide-band signal usually leads to high power consumption [80]. The high power consumption can be mitigated using a multiband approach in which the signal is split into sub-bands. The sub-band processing method will be briefly discussed in subsection III-C3.

Another advantage that creates a challenging situation is the short pulse nature of UWB signals. The coding of short width pulses requires longer synchronisation times, limiting the data capacity. Moreover, the short-width pulses increase the number of multipath components [77], which also compromises the overall system performance. Researchers have proposed a solution for this issue by devising special schemes and protocols to avoid repeated synchronisation [77]. In addition, the authors of [81] proposed the use of multiple-input multiple-output systems to mitigate the effect of short communications. One last disadvantage of UWB is its limited usage outdoors. According to various countries' regulations, fixed UWB transmitters operating outdoors are not allowed [82], [83], refer to subsection III-B for more details.

B. UWB LICENSING AND REGULATIONS

The UWB bandwidth license is free for indoor applications, yet the regulations for UWB devices are country- or region-specific to define the technical requirements and certification procedures for legal and safe operation [84], and more importantly, to minimise the potential interference to licensed services [69]. These regulations comprise the boundaries and safety limits of the operating frequency, power levels, emissions, energy disruptions, service times and antenna locations. For example, the regulations for UWB devices in the United States are published by FCC in 2002 under the "Code of Federal Regulations Part 15, subpart F" [82], while those in the EU region are issued by the Harmonised European Standard in 2016 (the process started in 2006) under the radio equipment directive "ETSI EN 302 065 – 1 to 5" [83].

Additionally, these official UWB regulations distinguish between the different types and usages of UWB devices, and each type and usage has its own regulation. For example, the FCC has set specific rules for each category of UWB devices and their respective application, such as indoor UWB systems, handheld UWB devices, GPRs and wall imaging systems, surveillance and transportation systems (e.g. UWB on-board aircrafts and UWB installed on rail vehicles) [69].

According to the FCC, the bandwidth of the UWB systems belonging to the indoor and the handheld categories must be kept between 3100 MHz and 10,600 MHz [82]. The indoor UWB systems may not be used outdoors, and they must be designed so that they are capable of operating only indoors. The emissions from UWB devices may not be intentionally directed outside of a building to perform an outside function. Also, the use of outdoor mounted antennas is prohibited. The device may only transmit when sending information to an associated receiver.

An UWB device belonging to the handheld category must be relatively small. These devices are primarily kept in hand while being operated, and they do not employ a fixed infrastructure [82]. Antennas may be mounted only on the handheld UWB device. The use of antennas mounted on outdoor infrastructure is prohibited.

Part 1 of the EU regulation "ETSI EN 302 065" contains requirements for generic UWB applications, and it applies to fixed (indoor only), mobile or portable applications [83]. The UWB transmitter conforming to that document may not be installed at a fixed outdoor location, for use in flying models, aircraft and other forms of aviation. Allowed operation frequency band is from 3.1 to 4.8 GHz and from 6.0 to 9.0 GHz.

Requirements for UWB location tracking are defined in Part 2 of the EU regulation "ETSI EN 302 065". This document covers three types of UWB location tracking system, of which two are applicable for smart logistics applications [85]:

- LT1 systems: These systems, operating in the 6 GHz to 9 GHz region, are intended for general location tracking of people and objects. They operate on an unlicensed basis. The transmitting terminals in these systems are mobile (indoors or outdoors), or fixed (indoors only). Fixed outdoor LT1 transmitters are not permitted.
- LT2 systems: These systems, operating in the 3.1 GHz to 4.8 GHz region, are intended for person and object tracking and industrial applications at well-defined locations. The transmitting terminals in these systems may be located indoors or outdoors, and may be fixed or mobile. They operate at fixed sites and may be subject to registration and authorization.

The regulation documents contain additional points describing the operation peak powers and tabulated emission limits for UWB devices, which vary regionally (e.g. US and EU). Both the ETSI and the FCC regulations allow the use of UWB indoor location tracking, which is very important for many industrial and smart logistics applications. However, the unlicensed outdoor use of UWB is limited to handheld or mobile devices. Because the FCC or LT1 of ETSI do not allow fixed outdoor transmitters, development of UWB outdoor positioning systems becomes difficult. Without transmitting anchors, it is not possible to use TW-TOA and multilateration for position determination. In addition, TDOA scheme with wireless clock synchronization is inapplicable, since

the anchors must transmit synchronization messages to each other. Thus, the only possible way to implement outdoor UWB location system, operating under the provision of FCC or ETSI LT1, is to use TDOA approach with a wired clock synchronization. However, implementing the wired clock synchronization is complex and expensive.

LT2 of ETSI allows the fixed outdoor transmitters in the EU, but the LT2 systems are subject to registration and authorization. In addition, local coordination with possible interference victims has to be performed, and the possible permission would be granted only to a specific site [85]. Currently, developing an UWB-based positioning system for outdoor environment is very difficult.

In June 2020, the fine-ranging alliance (FiRa), the largest UWB consortium, was founded to pave the way for the widespread adoption of UWB-driven applications. Some well-known company members of the FiRa alliance are NXP, Samsung, Qorvo, Qualcomm, Cisco, Apple and BOSCH. The FiRa consortium is committed to providing seamless user experience through secured fine ranging and positioning capabilities of interoperable UWB technologies [86].

C. UWB SIGNAL ATTRIBUTES

The earliest attempt of UWB standardisation within IEEE standards was made by the WiMedia alliance workgroup in IEEE 802.15.3a-2003. This workgroup was responsible for standardising the physical and medium access control (MAC) layers of UWB indoor signals for wireless PANs. The detailed technical aspects of a UWB signal are described in the currently, active UWB standard (802.15.4z-2020), which was developed by the ''LAN/MAN Standards Committee'' of the IEEE Computer Society [87]. UWB signals can be generated using different techniques, the most popular of which is the impulse radio (IR) method. However, there are several other methods that can be adopted in UWB systems. The authors of [69] classified the types of UWB signals into the following six categories:

1) IMPULSE RADIO ULTRA WIDEBAND (IR-UWB)

The IR-UWB modulates the baseband signal through short pulses (order of nanosecond duration each), which have a low duty cycle to transfer information. The frequency spectrum characteristics of IR-UWB can be controlled by varying the pulse shape, phase, amplitude and duration to formulate the spectrum envelope of the signal. IR-UWB can be carrier-based, which requires an external high-frequency sinusoidal carrier signal and a mixer, or carrier-less, which can operate without a local oscillator (LO) in the transceivers, only using the baseband signal. The IR-UWB is typically the most adopted system and is standardised in the IEEE 802.15.4z UWB standard.

2) DIRECT SEQUENCE ULTRA WIDEBAND (DS-UWB)

Direct sequence spread spectrum (DSS) version of the IR-UWB forms the DS-UWB, which treats the signal by a pseudorandom number (PN) code before the amplitude modulation of a train of short pulses. The new bandwidth of the transmitted signal is affected by a spread code, which is typically much higher than the symbol rate at which the chip interval is longer than the pulse width.

3) MULTIBAND ULTRA WIDEBAND (MB-UWB)

The orthogonal frequency division multiplexing (OFDM) version of the IR-UWB can be considered to form the MB-UWB, in which the total bandwidth is divided into multiple frequency sub-bands (minimum 500 MHz each) to occupy the spectrum efficiently. The MB-OFDM approach utilizes the quadrature phase-shift keying (QPSK) modulation with 128 subcarriers and five-band groups containing two or three bands each (14 sub-bands in total). The MB-OFDM recently received approval from ISO/IEC and ETSI.

4) FREQUENCY HOPPING ULTRA WIDEBAND (FH-UWB)

It is a non-conventional carrier-based method in which the transmission occurs through fixed frequency hops over a broad bandwidth and using variant frequency carriers. The hopping sequence is determined by a spreading code or a PN sequence set by the user in which a narrow-band transmission occurs periodically, which can be smaller than (fast hopping), greater than (slow hopping) or equal to the symbol rate. The total spectrum bandwidth is determined by the range of hopping frequencies and not the symbol rate.

5) STEPPED FREQUENCY HOPPING ULTRA WIDEBAND (SFH-UWB)

SFH-UWB is a particular case of FH-UWB, in which the hopping frequencies are selected by the spreading code to form linearly increasing discrete steps until the desired bandwidth is achieved. Then, the hopping frequency is reset to the starting sequence, and the process is repeated.

6) SWEPT FREQUENCY ULTRA WIDEBAND (SF-UWB)

SF-UWB is also known as 'Chirp signalling'. It is the frequency variation of the FH-UWB, in which the carrier frequencies of the UWB waveform are generated by a voltage-controlled oscillator using a continuous variable speed. The symbols are modulated on the slope (chirp) using M-ary modulation and then sent sequentially or superimposed.

D. ARCHITECTURE OF UWB POSITIONING SYSTEM

A typical UWB indoor positioning system includes fixed UWB sensors (anchors), mobile UWB targets (tags), location server and system interface. The location server stores and processes the sensors data, and the system interface (e.g. smartphone, computer or tablet) is for viewing the positioning results, as illustrated in Figure 4. Planar, two-dimensional positioning requires at least three anchors to solve the coordinate equations of the tag, while three-dimensional positioning requires at least four anchors.

Additional optional units can be added to the previous structure to obtain a real-time location system (RTLS). For example, the location server is optional in small-scale

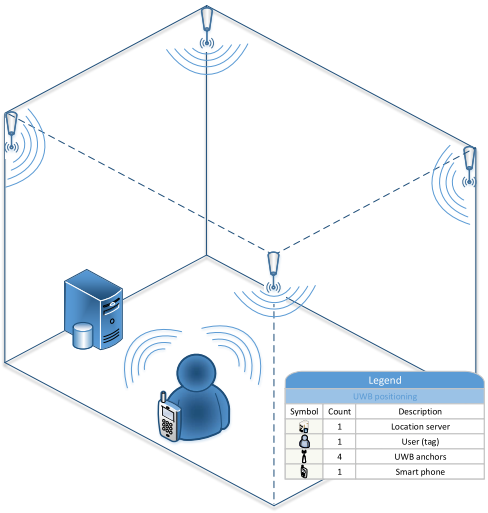

FIGURE 4. Elements of UWB positioning system. User with a tag or mobile phone is located through UWB anchors. The location server can determine the position and provide an API for accessing the location information.

systems but crucial in large-scale systems. There are additional front-end and back-end units for complex indoor environments, such as navigation framework, network gateways, user interface and facilities for IoT integration or other accompanying multi-sensor technologies.

The process of UWB precise positioning commences with relative positioning between the anchors. A single initiator anchor is specified as a reference point or origin (0,0). An auto-positioning feature, such as Decawave's (Qorvo) RTLS application, measures the relative distance between all anchors and thus positions them in the coordinate system. A block diagram depicting an example of a complete process of UWB precise positioning is illustrated in Figure 5.

After fixing the coordinate system, the UWB system starts ranging the mobile UWB tag(s) within the indoor environment before sending the measured raw data to the positioning framework for additional processing. The positioning algorithm, which is pre-specified by the user, uses the raw measurements and a kinematic model to carry out position estimation. Precise position can be achieved by using the UWB system when the ranging method and the positioning algorithm are appropriate to the application and the properties of the environment.

Many applications in various environments require specific NLOS mitigation methods to improve the performance. This article focuses on two NLOS mitigation approaches, multi-sensor fusion and ML algorithms. Both approaches are discussed in detail in section VIII.

In the multi-sensor fusion approach, additional accompanying IPS technology is used to aid the UWB system with a fusion algorithm that fuses data obtained from all sensors based on their weights and shares.

In contrast, the ML approach is designed using large offline data to train a learning algorithm to identify the outlier measurements caused by the NLOS conditions. This approach has its performance metrics as ML algorithms are assessed from the training and testing accuracies. Nevertheless, the overall efficiency of the system is determined by the combined metrics of each phase, in addition to the degree of relevance of the final positioning results to the ground truth.

E. COMMERCIAL PRODUCTS

The growing demand for location-based services in an indoor environment has increased the size of the UWB market during recent years. In addition, the recent advances in UWB technology have provided opportunities for new commercial applications.

The major manufacturers providing UWB chips for open markets are Qorvo and NXP. Qorvo entered the UWB market by acquiring the Irish semiconductor company Decawave in January 2020 [88]. Decawave has been one of the major providers of UWB technology during the past 15 years, along with some other companies, such as Ubisense and BeSpoon [89]. Decawave's UWB technology has been very popular and its chips have been used extensively in research [16], [90]–[93] and commercial IPS [94]–[97].

NXP launched its UWB precision chips in February 2020. Currently, NXP provides Trimension UWB modules for IoT, industrial, mobile and automotive market segments [98]. Trimension UWB modules can be used, for example, like tags or anchors in IPS systems, in mobile devices and in secure car access applications.

One of the most important markets for UWB is mobile phones. In 2019, Apple launched iPhones having an UWB chip called U1 [99]. Samsung released its first high-end mobile phones with UWB technology in 2020. Samsung was one of the founders of the FiRa consortium together with NXP and some other companies [100]. UWB technology provides new opportunities for mobile phone use cases, such as secure access control, location-based services and device-to-device communications. To support third-party application development, Apple has released its ''nearby interaction'' framework for developers and chipset manufacturers building UWB-based applications [101].

The automotive industry is developing UWB applications for secure access control and localisation. For example, Bosch's Perfectly Keyless key management system utilizes UWB in mobile phones for secure access control [102]. The vehicle access and start are controlled via a digital key on a mobile phone and the precise localisation of the phone.

IV. UWB POSITIONING TECHNIQUES

The positioning can be based on either multilateration or multiangulation techniques. When using multiangulation, the position of the unknown tag can be determined from known anchors geometrically by observing the angles of the received

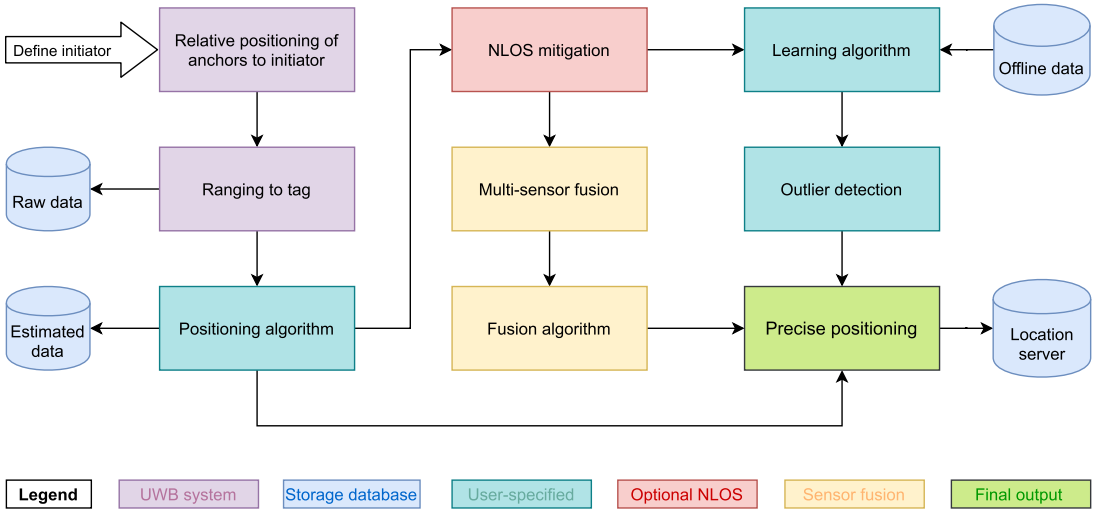

FIGURE 5. Suggested building blocks of the UWB precise positioning process, based on the surveyed UWB literature.

signal either in anchors or in tags. When using multilateration, the ranges between the anchors and tags are obtained by measuring the time of flight (TOF) and multiplying it by the speed of light or by applying a channel attenuation model to the received signal strength (RSS) observations.

In general, the following four active strategies are used for estimating the TOF needed for multilateration:

- TOA: TOA of the signal is measured and subtracted from the known transmission time. The arrival timestamps are obtained by either using a precise clock (synchronous TOA) or by solving them together with the tag position by using at least N+1 anchors, where N is the number of spatial dimensions. The latter method is used in GNSS systems and is known as the pseudorange method. The clock synchronisation accuracy of the sub-nanosecond range is not feasible for moving targets [103], [104], and therefore, the pseudorange method is typically used.
- RTT: The RTT of signal propagation between two objects is measured, and the processing time is reduced to obtain double ToF. This method is also called two-way ranging (TWR) or two-way TOA (TW-TOA). The measurement is repeated between a tag and at least N anchors. This method is sometimes called asynchronous TOA. [105]
- Time of transmission (TOT): The arrival time of the signal sent by a tag is observed by at a minimum of N+1 anchors, and the TOT is solved together with the position of the tag.
- TDOA: The signal sent by the tag is received by at least N+1 anchors, which calculate the time differences of arrival times, avoiding the need for absolute time synchronisation in a tag.

The positioning techniques used with UWB are (1) TOA or TW-TOA; (2) AOA; (3) received signal strength (RSS); (4) TDOA and (5) a hybrid algorithm [10], [104]. The typical UWB system estimates position using a two-step procedure. In the first step, observables related to an unknown position of the tag and known positions of the anchors are determined. Among these, TOA, TDOA, AOA and RSS are given as examples [25], [26]. From these measurements, the RSS is considered the least suitable for use with UWB because its accuracy in an NLOS and a multipath environment is lower than that of time-based methods [104]. In the second step, the position of the tag can be computed using estimation methods such as least-squares (LS) method, Kalman filters (e.g. EKF and UKF) and particle filter (PF). In addition to the previous methods, some recent literature has adopted the AI approach through supervised learning to account for the position estimation in which the raw UWB data are compared with a trained ML model (e.g. support vector machine (SVM)) for predicting the unknown position of the target node [106]. Selecting a suitable positioning technique is vital to the whole precise positioning process as it affects the overall accuracy and defines the system complexity, and hence, the resources' total costs [76]. In this section, we summarise the most widely adopted techniques in the literature, highlighting their methodology, pros and cons.

A. ANGLE OF ARRIVAL

The position of an object can be estimated from the AOA or the angle of departure (AOD) of the signal. Each angle measurement defines a line between the base station and a mobile device. The object's location is determined from the intersection of these lines, as illustrated in Figure 6 a.

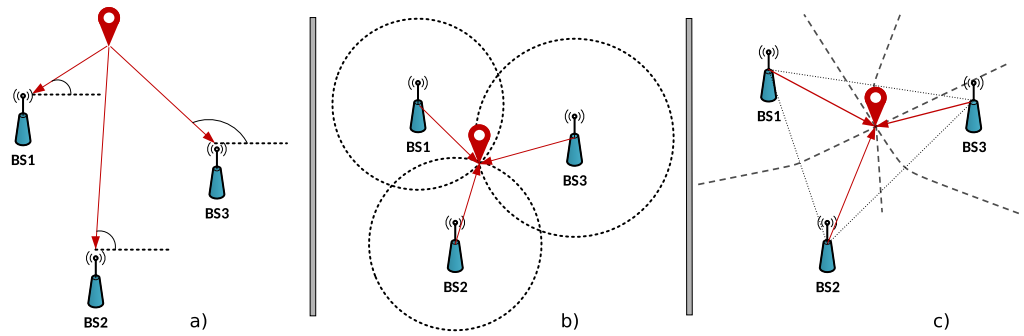

FIGURE 6. Ranging and angulation techniques. a) AOA, b) TOA, TWR and RSS and c) TDOA. In AoA, TOA and TDOA techniques, the tag position is determined from the intersection of the lines, circles and hyperbolas, respectively.

In the AOA method, the tag transmits a signal using a single antenna, and the anchor (base station) receives the signal with multiple antennas arranged in an array. The signal direction is determined from different propagation delays of the signal between multiple antennas of the receiver antenna array and the single transmitter antenna.

In the AOD method, there is a single antenna at the receiver and multiple antennas arranged in an array at the transmitter. Usually, the anchor (beacon) transmits the signal, and the tag receives it. The signal direction is determined from different propagation delays of the signal between multiple antennas of the transmitter antenna array and the single receiving antenna.

The advantage of the AOA (or AOD) observable is that there is no need to time-synchronise the anchor clocks. However, the antennas have to be precisely calibrated to the correct orientation. The AOA can be measured with various techniques, but currently, antenna arrays are mostly used in positioning systems.

There is a significant advantage of using a UWB signal over a narrow band signal in phase difference-based AOA estimation. Due to the short duration of the pulse, the UWB receiver can separate the direct signal from the reflected signal better than the receiver of the NB signal [92].

In UWB-based systems, the AOA measurements are often used together with TOA or TDOA measurements [92]. For instance, the authors of [107] proposed an AOA estimation method for a UWB positioning system using a lower-cost single-anchor system. A centimetre-level UWB positioning system was proposed by [108] using a mono-station TOA/AOA positioning method. In addition, the cell phone applications of Samsung and NXP use both the TOA and AOA observables [109]. The Ubisense positioning system uses both AOA and TDOA measurements, but according to [89], this system is less accurate than the Decawave system, which uses the TOA observable only.

Authors of [110] have developed a TDoA-Based positioning system using a single hotspot. This hotspot consists of anchors placed very close to each other. The tag to be localised is around the hotspot. The system estimates the range and AOA between the hotspot and the tag. According to the authors, the error in AOA estimate is less than 3 degrees when the target is in 15 m distance. The error in the estimated range may be 4 m.

B. TIME OF ARRIVAL

Most of the UWB-based positioning systems use the concept of TOA ranging to determine the user position. This concept is based on measuring the time taken for an RF signal transmitted by an emitter to reach a receiver. The time interval, due to signal propagation delay is multiplied by the speed of light to obtain the distance between the emitter and the receiver.

The TOA technique exploits trilateration to determine the position of the mobile users based on the range from the mobile unit to at least three (3D) anchors at known locations.

In the TOA method, the position is estimated by intersecting circles (2D) or spheres (3D) with radius r_i and centre (x_i, y_i, z_i), as illustrated in Figure 6 b. The radius of the circle r_i is obtained from the propagation delay of the signal. Point (x_i, y_i, z_i) is the known location of the anchor.

The 3D location of the object (x_u, y_u, z_u) can be derived from the set of nonlinear equations as in Equation (2):

$$\rho_i = \sqrt{(x_i - x_u)^2 + (y_i - y_u)^2 + (z_i - z_u)^2} \qquad (2)$$

where i ranges from 1 to 3 and references the base stations at known locations, (x_i, y_i, z_i) denote the i-th base station coordinates in three dimensions and r_i is the range measured from the i-th base station.

The TOA method illustrated above requires the anchors and tags to be accurately synchronised. To avoid the synchronisation requirement, the TWR method can be employed to measure the signal propagation delay. The range between two devices is determined through the two-way exchange of a message and by measuring its arrival time. This method is also known as two-way time-of-arrival (TWR-TOA) or RTT.

The simplest version of the two-way ranging cancels the effect of the clock offset between the terminals, but the clock drifts of the terminals can still cause significant error

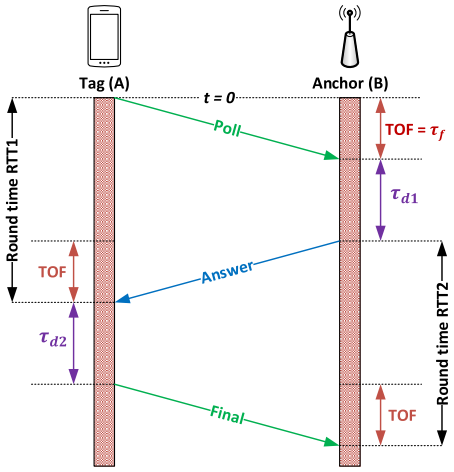

FIGURE 7. Double-sided two-way ranging method to estimate signal flight time cancelling the effects of clock offset and drift.

in the signal flight time estimate. The error caused by the clock drift can be eliminated by making the two-way ranging measurement transaction two times [111]. This method called as double-sided two-way ranging is illustrated in Figure 7, and the TOF of the ranging message is expressed as in Equation (3):

$$\tau_f = \frac{1}{4}\left(\tau_{RTT1} - \tau_{d1} + \tau_{RTT2} - \tau_{d2}\right) \tag{3}$$

where τ_{RTT1} is the RTT measured by the tag, and τ_{RTT2} is that measured by the anchor. The terms τ_{d1} and τ_{d2} are the reply times of the anchor and the tag, respectively. τ_{RTT1} and τ_{d2} are measured using the tag oscillator, and both measurements are biased by the oscillator offset of the tag. Similarly, τ_{RTT2} and τ_{d1} are biased by the oscillator offset of the anchor. Double-sided TWR cancels these oscillator offsets.

C. TIME DIFFERENCE OF ARRIVAL

One method to obtain the signal propagation delay is the TDOA method, which measures the difference in the arrival times of two signals. The anchor clocks must be precisely synchronised, but the tags do not need to be synchronised. The tag position is obtained from the intersection of multiple hyperbolas (Figure 6 c).

The distance difference between the tag and the anchor where the signal arrives first, is expressed as in Equation (4): [112]

$$\begin{aligned} r_{i,1} &= cd_{i,1} = r_i - r_1 \\ &= \sqrt{(x_i - x_u)^2 + (y_i - y_u)^2 + (z_i - z_u)^2} \\ &\quad - \sqrt{(x_1 - x_u)^2 + (y_1 - y_u)^2 + (z_1 - z_u)^2} \end{aligned} \tag{4}$$

where c is the speed of light, $r_{i,1}$ is the distance difference between the first and the ith anchor, r_1 is the distance between the first anchor and the tag and $d_{i,1}$ is the measured TDOA between the first and the ith anchor. Equation (4) defines a set of nonlinear hyperbolic equations whose solution provides the 3D coordinates of the tag.

In principle, the TDoA approach can be implemented in two ways, called as unilateral and multilateral techniques [113], [114]. In the unilateral system, the anchors transmit a signal and the tags measure the TDOA from the received signals. Also, the anchors transmit a signal with different time delays to avoid a signal collision. The unilateral technique has some advantages, such as infinite scalability in the number of tags [115]. As in GNSS, in the unilateral TDOA system the location privacy is preserved, since the position is estimated in the tag. However, in the unilateral architecture the design of the tag is complex and it has high energy consumption [114].

Because of the drawbacks of unilateral approach, most of the UWB-based systems using the TDOA scheme are based on multilateral technique. In multilateral approach the tag sends one message, often called a blink, and the arrival time is then measured by multiple anchors with respect to a common time reference. These arrival times are then sent to a master node or server, which computes the TDOA estimates by subtracting the arrival time of the pivot anchor from those of the other anchors. Thus, the number of TDOA estimates is one less than the number of arrival time measurements.

Even though the multilateral approach is less scalable than unilateral approach, it can still support many more tags than the TW-TOA system. In the multilateral TDOA architecture a tag needs to send only one message per range measurement, while in the TW-TOA scheme, several messages are required [51]. Scheduling techniques are needed to avoid packet collisions in the TW-TOA approach, limiting the number of supported tags. In the TDOA approach, the tags need not to be aware of the anchors, which makes message scheduling easier than in TW-TOA. The authors of [51] investigated the scalability of UWB-based indoor positioning for TDOA and TW-TOA approaches with different MAC protocol combinations. In the mathematical model proposed by the authors, when using a TDOA approach and time division multiple access (TDMA), more than 6000 tags per second can be supported in a single domain shell. The drawback of the TDOA method is that the anchors have to be accurately synchronised. Because the radio signal propagates at the speed of light, 1 ns time offset in the anchor clock would introduce a 30 cm error in the estimated range. Decawave DWM1001 achieves measurement accuracy within 10 cm in the TOA mode, which is equal to 333 ps accuracy in the propagation delay measurement. The synchronisation accuracy must be even better to achieve similar accuracy in the TDOA mode.

The anchors of the UWB-based positioning system can be synchronised either through wires or wirelessly. In wired time synchronisation, the clocks of all anchors are synchronised by means of wires or fibres. In wireless time synchronisation, each anchor has its own clock running independently of

the clocks of the other anchors. The time estimates of the different anchors are synchronised to the common time by sending synchronisation messages.

A time synchronisation mechanism for the TDOA-based UWB positioning system was investigated in [116]. The authors developed a test setup to measure the time synchronisation errors of wired and wireless approaches. The standard deviation of the wireless synchronisation was 400 ps, whereas that of the wired synchronisation was 133 ps. However, the time synchronisation of the anchors might be challenging. Wired clock synchronisation or more stable clocks makes the positioning system complex and expensive. Wireless clock synchronisation techniques lower the range estimation accuracy when unstable clocks are used. Many commercial UWB applications, such as Eliko [97] and Exafore [95], use the TW-TOA approach. Some UWB systems, such as Sewio [96] and Pozyx [94], support both the TDOA and TW-TOA schemes. According to Pozyx, the TW-TOA method provides more accurate position estimates, while TDOA is better suited for large-scale applications, which need multiple tags to be supported.

D. RECEIVED SIGNAL STRENGTH

The measurement of RSS is straightforward and is performed in most radio receivers. RSS decreases as the receiver–transmitter distance increases. This phenomenon can be used to estimate the location of a mobile device from the RSS measurements either by trilateration or location fingerprinting.

Radio signal attenuation is not only affected by the distance between the transmitter and receiver but also by multipath interference and any obstruction on the signal path. Thus, indoor positioning systems seldom compute the object position by using geometric range estimates derived from RSS. Instead, RSS-based indoor positioning systems use location fingerprinting more often. RSS is seldom used with UWB, because using the RSS observable does not completely exploit the benefit of UWB signals [117].

E. PASSIVE POSITIONING

In addition to previous active positioning techniques, location can also be determined by passively monitoring the communication of the UWB network [118] or by special arrangement; where a tag listens passively to the positioning messages sent by the anchors simultaneously [115]. Passive monitoring is not as accurate as active positioning, and the simultaneous positioning message method requires special hardware. Another passive UWB positioning strategy is to use UWB anchors as radars. In this case, the round trip time of the signal sent from the anchor and reflected from the target is measured [93], [119], [120]. Both magnitude and phase of the channel state can be used, in addition to signal reflections from walls. This method is called device-free positioning since it does not require any UWB specific hardware in the target. Passive and device-free methods are still under research. They are not as precise as the active methods and are more sensitive to environmental changes and variation. Thus, they are not discussed further in this review.

V. UWB POSITIONING ALGORITHMS

The position can be estimated from TOA and TDOA observables by using various methods. When the position is estimated using measurements of a single time epoch, it is called static positioning, where the previous or future measurements are not accounted. The most common approach to solve the nonlinear system of equations of TOA and TDOA is to use the iterative LS method. Alternatively, the position can be estimated using closed-form solutions or methods based on likelihoods or probability.

Static positioning is not an optimal solution in most situations, as it does not account for the dynamic state model of the target. In many cases, a Kalman filter and PF provide a better position estimate, as they use the time series of the measurements for computing the current state estimate.

A. ITERATIVE LEAST SQUARES AND CLOSED-FORM SOLUTIONS

The overdetermined and nonlinear system of equations can be solved using the Gauss-Newton algorithm. As the linearisation of this algorithm is based on Taylor-series expansion, it is also called the Taylor algorithm. In this algorithm, the user's position is determined using an iterative process starting from an approximate position.

The true distance between the anchor i and the tag is as described in Equation (5):

$$r_i = \sqrt{(x_i - x_u)^2 + (y_i - y_u)^2 + (z_i - z_u)^2} \tag{5}$$

where (x_i, y_i, z_i) is the position of the i-th anchor and (x_u, y_u, z_u) is the position of the tag. If (x_v, y_v, z_v) is the initial approximate position, let $x_u = x_v + \delta_x$, $y_u = y_v + \delta_y$ and $z_u = z_v + \delta_z$. By linearising Equation (5) using Taylor-series expansion and omitting the second-order and higher terms as in Equations (6)–(10) we have: [121]

$$H\delta = b \tag{6}$$

where

$$\mathbf{b} = \begin{bmatrix} r_1 - r_{v1} \\ r_2 - r_{v2} \\ r_3 - r_{v3} \end{bmatrix}, \quad \mathbf{H} = \begin{bmatrix} a_{x1} & a_{y1} & a_{z1} \\ a_{x2} & a_{y2} & a_{z2} \\ a_{x3} & a_{y3} & a_{z3} \end{bmatrix}, \tag{7}$$

$$\delta = [\delta x_u, \delta y_u, \delta z_u]^T \tag{8}$$

$$a_{xi} = \frac{x_i - x_v}{r_{vi}}, \quad a_{yi} = \frac{y_i - y_v}{r_{vi}}, \; a_{zi} = \frac{z_i - z_v}{r_{vi}} \tag{9}$$

and

$$r_{vi} = \sqrt{(x_i - x_v)^2 + (y_i - y_v)^2 + (z_i - z_v)^2} \tag{10}$$

The LS solution to the position estimation problem is obtained from Equation (11): [121]

$$\delta = (\mathbf{H^T H})^{-1} \mathbf{H^T b} \tag{11}$$

The position of the object (x_u, y_u, z_u) is calculated using an iterative process. In the beginning, the approximated position,

(x_v, y_v, z_v) is set to an initial value. Next, the direction cosine matrix **H** and the predicted-minus-observed range vector **b** are computed. Then, the unknown displacement vector δ is calculated using Equation 8. The iteration process is repeated until the length of the displacement vector does not decrease any further.

The ordinary LS method described above assumes that the error variance in each measurement is the same. The method of weighted LS (WLS) can be used when the error variances of the measurements are not constant. WLS method weights observations by the reciprocal of the error variance $w_i = 1/\sigma_i^2$ for that observation.

The weight matrix is calculated using Equation (12):

$$\mathbf{W} = \begin{bmatrix} \omega_1 & 0 & 0 & 0 \\ 0 & \omega_2 & 0 & 0 \\ \vdots & \vdots & \ddots & \vdots \\ 0 & 0 & \dots & \omega_L \end{bmatrix} \tag{12}$$

The WLS solution is obtained from Equation (13):

$$\Delta\mathbf{x} = (\mathbf{H^T W H})^{-1}\mathbf{H^T W}\Delta\mathbf{p} \tag{13}$$

In addition to the Taylor-series method, several closed-form solution methods have been proposed to solve the set of TOA or TDOA equations. Caffery [122] presented a geometrical interpretation in which straight, rather than circular, lines of positions were used to determine the target device's position. This method is called the linear lines of position (LLOP) method [121], [123] or simply LS method [112]; it does not use linearisation. Another well-known closed-form solution is the Chan algorithm, which estimates the target position from TDOA equations [124].

Many authors have preferred closed-form solutions over the Taylor method [122], [124]. The Taylor-series method has been criticised as it converges towards a local minimum if the initial guess is not close enough to the true position. However, in a GNSS, for example, the Taylor-series method seldom converges towards the minima. The authors of [112] compared the LLOP, Chan algorithm and Taylor-series method and found that the Taylor algorithm provides the best positioning accuracy. A fusion algorithm combining both the Chan and Taylor algorithms can improve the positioning accuracy in the presence of NLOS errors [125].

B. BAYESIAN FILTERS

Recursive Bayesian state estimation, or Bayes filter is an abstract concept for tracking object's position in kinematic case, by combining a dynamic state model with observations. Bayesian filters recursively update the posterior belief to the current state as in Equation (14):

$$\text{Bel}(x_k) = p(x_k | \, y_{0..k-1}), \tag{14}$$

where x_k is the current state and y_k are the observations.

Practical implementations require the definition of dynamic and perceptual models and representation of beliefs. Depending on the implementation, the properties of Bayes filters are different [126]. Some most common implementations are different variations of Kalman Filters, Particle Filter and factor graph optimisation, which are described in the following subsections.

C. KALMAN FILTERS

The Kalman filter algorithm is a recursive estimation method used for predicting the new optimal states in linear state-space systems considering additive white Gaussian noise [127]. The algorithm is based on using a priori knowledge to estimate the posterior states, calculate the Kalman gain and measurement residual caused by the mismatch error and then calculate the new state and covariance vectors and use them as input to the next iteration [127]–[131].

1) EXTENDED KALMAN FILTER

The extended Kalman filter (EKF) is an adapted version of the ordinary linear Kalman filter to estimate states in non-linear dynamic systems [132]. A discrete-time Kalman filter follows two steps: 1) prediction step, where the next state of the system is predicted given the previous measurements fed to the system, and 2) update step, where the current state of the system is estimated given the measurement performed at the active time step [131], [133]. Then, the Kalman filter algorithm is used to satisfy the equations of state-space estimation in Equations (15) as follows:

$$\begin{aligned} x_k &= f(x_{k-1},\ k-1) + q_{k-1} \\ y_k &= h(x_k,\ k) + r_k \end{aligned} \tag{15}$$

whereas x_k and y_k are the state and measurement vectors of the system at time step k and q_{k-1} and r_k are the process and measurement noises at time step *k-1*, where $q_{k-1} \sim N(0, Q_{k-1})$ and $r_k \sim N(0, R_k)$, $f(.)$ and $h(.)$ are the nonlinear functions of model dynamics and measurement, respectively.

In EKF, the state transition matrix **F** and measurement matrix **H** in the linear Kalman filter are replaced by the nonlinear state transition function $f(.)$ and nonlinear measurement function $h(.)$, respectively, to map the algorithm through Gaussian distribution to work under nonlinear conditions. The complete Kalman algorithm for nonlinear systems is demonstrated in Table 3, which is adapted from [131].

Whereas $m_{\bar{k}}$ and $P_{\bar{k}}$ are the predicted mean and covariance of the state, respectively, at time step k before checking the measurement, and m_k and P_k are the estimated mean and covariance of the state at the time step k after checking the measurement. y_k is the measurements vector of the system at the time step k. S_k is the measurement prediction covariance at the time step k. K_k is the filter gain (i.e. the prediction correction coefficient at the time step k). $f(.)$ and $h(.)$ are the nonlinear functions of model dynamics and measurements.

2) UNSCENTED KALMAN FILTER

Unlike EKF, the unscented Kalman filter (UKF) employs the sigma-point Gaussian transformation to map the non-linear state transition function of the system and tends to

TABLE 3. EKF algorithm for nonlinear systems, adapted from [131].

0 Initialization	for $k = 0$ set $\hat{X}_0, P_0^-, Q_0, R_0$	
1 Prediction step	Prior estimate of the state:	$m_k^- = f(m_{k-1}, k-1)$
	Prior estimate of the covariance:	$P_k^- = F_x(m_{k-1}, k-1)P_{k-1}{F_x}^T(m_{k-1}, k-1) + Q_{k-1}$
2 Update step	Measurement residual update:	$V_k = y_k - h(m_k^-, k)$
	Measurement covariance update:	$S_k = H_x(m_k^-, k)\ P_k^-\ {H_x}^T(m_k^-, k) + R_k$
	Kalman gain calculation:	$K_k = P_k^-\ {H_x}^T(m_k^-, k)\ S_k^{-1}$
	Updating the posterior state:	$m_k = m_k^- + K_k V_k$
	Updating the posterior covariance:	$P_k = P_k^- - K_k S_k K_k^T$
	Return to step 1, repeat until k iterations are consumed.	
Output	Estimated state vector: $\hat{X}$	

linearise it through the so-called unscented transform [131], [134], [135]. In other words, while the EKF approximation relies only on one point (the mean), UKF uses more than one point, including the distribution mean. UKF selects additional weighted points (called sigma points) plus the mean for more accurate transformation. This procedure is called the unscented transform. Thus, UKF sometimes outperforms EKF in severely nonlinear systems, whereas EKF performs well in systems with modest nonlinearity [136]. In an ideal case, both EKF and UKF can be used to solve the spatial positioning equation when Newtonian equations of motion are used to form the state transition function and the measurements from motion sensor (e.g. inertial unit, gyroscope or accelerometer) are being filtered. However, various recently proposed approaches use measurements obtained from various sensors to input as the state-transition matrix. The authors in [137]–[139] implemented a fusion positioning method, whereas the state-transition function originates from inertial navigation sensors, such as the inertial measurement unit (IMU) or inertial navigation system (INS), while the measurement function is obtained from UWB sensors. The two streams are fed to EKF/UKF for optimal positioning. The procedures vary from method to method. In some cases EKF is used with multiple anchor readings and a single-observation anchor, whereas another method involves the use of EKF and UKF as a cascaded system to obtain the input parameters of the second filter from the outputs of the first filter. The results showed that the fused UWB, along with the inertial sensor data exhibited improved overall positioning accuracy and system robustness.

Kalman filters also perform well when they coexist with PFs, as in [136], where the authors developed a framework comprising three filters (EKF, UKF and PF) with detailed evaluative metrics. The results showed that the developed structure could be used for numerous purposes besides positioning improvements, such as target tracking and robot localisation. Numerous realisations that involve the use of Kalman algorithms and their variations have been proposed in [22], [34], [51], [136], [140]–[151].

D. PARTICLE FILTERS

Particle Filter (PF) is another realization of Bayes filters for position estimation. PF is a popular choice for positioning because it can be used for solving the DSS shown in Equation (15) without assuming that the dynamic or perceptual models are linear and that the noise is Gaussian. However, it is also possible to implement a PF which assumes Gaussian posterior distribution if a lighter but more restricted version is needed [152]. The reasons for using PF are that the conditions of linearity and Gaussian noise do not hold very often, and linearisation is only possible if the model is well known [152], [153].

PF estimates the posterior belief Bel(x_k) of DSM through a sequential Monte Carlo (SMC) algorithm. The SMC is similar algorithm shown in Table (3), without resorting to linearisation nor Gaussian noise assumption. The posterior distribution can be anything representable by discrete samples (particles). Increasing the number of particles makes it possible to describe more complex distributions, but it also increases the computational cost of the method.

The algorithm is simple to implement, consisting of the following steps:

1) **Initialisation**: N particles are initialised according to the *a priori* knowledge described as probability distribution $p(x_{k-1})$. This distribution can be any suitable empirical distribution which can be presented with particles, or uniform distribution, if more informative distribution is not available.
2) **Estimation loop**
   a) **Predict**: All particles are moved based on the current DSM by sampling new particles, $x_k^i, i \in [1, N]$, from the distribution obtained by convolving the *a priori* distribution with the process model: $\int p(x_k|x_{k-1}, u_k)p(x_{k-1})\mathrm{d}x_{k-1}$. The process model includes also possible inputs, u_k, and process noise.
   b) **Update**: The weights of particles are updated according to the belief of the observations, $w_k^i = p(y_k|x_k^i)$ assuming that the particle, x_k^i, represents

the correct location. Finally the weights are normalized so that their sum is 1.

c) **Resample**: New set of particles is generated by sampling the existing set of particles using their weights so that particles with higher weights are selected more probably than the others.

d) **Estimate**:The position estimate is obtained as a weighted average of the posterior distribution represented by particle locations and weights.

In NLOS conditions, the probability distribution of the position can be multimodal [154], and De Angelis *et al.* showed that ranging, which is based on RTT measurements can be affected by non-Gaussian noise even in LOS situations [143]. Therefore, PF can be more competitive in some realistic indoor environment than LS or EKF.

Many researchers have compared the performance of PFs with classical solutions for UWB-based indoor positioning. Usually, the performance is evaluated by examining the RMS error [155] or more often with the cumulative density function (CDF) of the positioning error in one to three dimensions [143], [148], [156]. These benchmarks show that, in many cases, a PF provides more accurate positioning results than classical methods, but in some cases, spurious errors are also detected when applying a PF (e.g. in the case of a kidnapped robot) [157]

It is also claimed that, instead of using the RMS error, comparing the whole posterior distributions of algorithms is more affective [152]. For example, the posterior distribution provided by a standard PF was assumed to be the most accurate and was compared with the Gaussian posterior distributions provided by EKF, UKF and GPF through Kullback-Leibler divergence and χ^2 information metrics. In this benchmark, the GPF was found to be more accurate in location tracking than EKF or UKF but incurred higher computational cost [152].

In addition to the increased computational cost, the problems identified in applying PF are sample degeneracy and impoverishment caused by the reduction in particle diversity [158]. A PF might also perform poorly in the kidnapped robot case when the robot is suddenly transferred to another location without allowing it to make measurements during the transfer. In this case, there might not be any particle near the actual position of the robot, and the robot might take a long time to find its new location. Counterintuitively, a PF does not also perform well when the measurement noise is too little [159], which is precisely the case in the controlled UWB positioning system. However, many methods have been proposed to overcome these problems. For example, dual MC localisation is a solution for too accurate sensor readings, and the kidnapped robot case can be solved by uniform particle augmentation [159]. Some other improvements are evolved distribution sampling methods [160], particle resetting approach [155], [161] or replacing PF with adapted FIR filter [157]. Zhu *et al.* improved the accuracy of a PF in UWB positioning by using a pre-build error distribution map [162]. At the cost of pre-computation, they gained increased 2D positioning accuracy.

It is relatively easy to fuse information from many sources into the PF estimations to compensate for NLOS issues, for example. Many researchers have fused INS sensors [91], [148], [156], mixing an EKF as a pre-processor of PF information [148]. The PF positioning algorithm can also include other models, such as UWB uncertainty model [91] or a model to predict the UWB signal obstruction caused by a pedestrian's own body [163]. The authors in [164] showed that the inclusion of digital maps into the PF model improved the positioning accuracy. The positioning of the anchor itself can be included in the PF-based positioning system [156].

E. FACTOR GRAPH OPTIMISATION

Factor Graph Optimisation (FGO) is a relatively new positioning algorithm among Bayesian filters. Some earlier publications from 2012 propose using FGO for multipath mitigation of GNSS positioning [165] and for multi-sensor fusion of GPS, IMU and stereo vision [166]. FGO models previous states as nodes and measurements as factors. Like KF and PF, FGO assumes Gaussian noise and utilizes the Bayesian filtering principle for solving the position estimation. The differences are that the FGO does not assume the Markov condition, but it uses information from previous states in addition to utilizing the latest state only. FGO solves the position by optimising the factor graph model with an iterative solver, therefore requiring more resources than KF or PF. However, it is still solvable in real-time, for example, by combining expectation-maximization and nonlinear optimisation methods [167], [168].

Even though FGO shares the unimodal Gaussian model with EKF, it can be more reliable in urban canyon environments for GNSS positioning cases [169]. Recently FGO has raised plenty of interest in positioning research, and it has been also applied to indoor navigation, including UWB positioning [167] and tight coupling of UWB and INS [170]. Besides, FGO can be useful in indoor positioning where multipath propagation causes channel impairments or in complex multi-sensor fusion situations.

F. PARTICLE SWARM OPTIMISATION

Particle Swarm Optimisation (PSO) algorithm belongs to the family of swarm intelligence, which also includes, for example, artificial Bee colony (ABC), Ant colony (AC) and Firefly algorithms. PSO was originally presented by Eberhart and Kennedy [171], [172]. PSO is an iterative global search technique that imitates the social behaviour of the swarm of birds. The algorithm is initialized with a random population of candidate solutions from a D-dimensional search space. Each candidate solution has a position and a velocity, and it is thus described as in Equation (16):

$$(x_i, v_i) = ([x_{i,1}, x_{i,2}, \ldots, x_{i,D}]^T, [v_{i,1}, v_{i,2}, \ldots v_{i,D}]^T) \quad (16)$$

The quality of a solution represented by each particle is estimated by evaluating the loss function $L(x_i)$. The position of the best solution found by a particular particle is stored as the best local solution, $P_{i,\text{best}}$, and the position of the best solution among all particles is stored as global best G_{best}.

In each simulation step, the velocity and the position of each particle are updated according to the formula (17): [126]

$$\begin{cases} v_i^{k+1} = wv_i^k + c_1\xi(P_{i,\text{best}} - x_i^k) + c_2\eta(G_{\text{best}} - x_i^k) \\ x_i^{k+1} = x_i^k + rv_i^k \ , \end{cases} \tag{17}$$

where w is the weight coefficient corresponding to the inertia of the particle, c_1 and c_2 are respectively the self cognition and social knowledge coefficients determining how much the model utilizes local knowledge vs. swarm knowledge. Stochasticity to the model is provided by selecting random variables ξ and η from range [0..1]. Position updating ratio is constrained by a constant factor r.

Some examples of using variations of PSO in positioning are: the use of ensembles of particle swarms to enhance the robustness and accuracy of UWB positioning [173], [174], and [175]. Being a global search strategy, PSO can be useful in finding the global minimum from the search space, but since the UWB positioning problem is often unimodal, simpler optimisation methods are usually more effective. However, in NLOS conditions, for example, the probability of the position can be multimodal [154], then, the global optimisation strategies can be superior in a similar way to PF.

G. NLOS IDENTIFICATION AND MITIGATION

In addition to using PF and PSO algorithms, the robustness of positioning in NLOS conditions can also be increased by specific NLOS identification and mitigation strategies.

Although UWB has several advantages in indoor positioning, it can still suffer from errors caused by NLOS conditions. In an NLOS condition, only the reflected signal is received, while the direct path signal is missing, as shown in Figure 8. The use of reflected signals can cause a significant bias to the position estimate. Various methods have been developed to reduce the inaccuracies imposed by an NLOS condition in UWB-based positioning. The authors in [176] categorised these methods as NLOS identification and NLOS error mitigation techniques. The signal can be identified as an NLOS signal, for example, by analysing the channel statistics parameters, such as mean delay, excess delay, amplitude and SNR. When the faulty observable is identified, it can be excluded from further analysis to improve the positioning accuracy.

Various methods can be used for mitigating NLOS errors, such as outlier detection, PFs, ML and weighted least squares (WLS). The authors in [177] proposed an NLOS identification technique based on multipath channel statistics, such as the kurtosis, the mean excess delay spread and the RMS delay spread. A likelihood ratio test was conducted for LOS and NLOS identification. Smaller weights were assigned to the measurements, which were likely biased. The authors analysed the WLS method, which deployed the likelihood

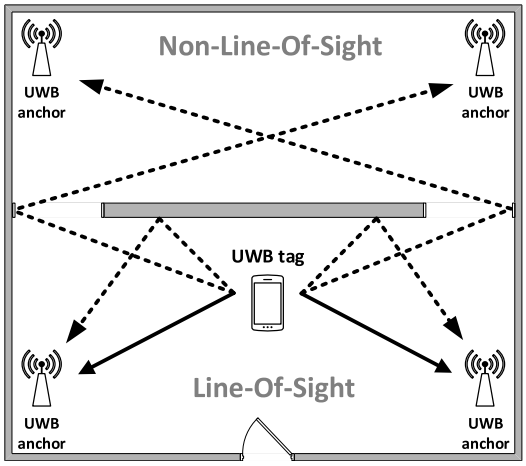

FIGURE 8. NLOS and LOS situations in UWB positioning system. The anchors in the left and right upper corners do not have a LOS connection to the tag, but the signal is received only through reflections, and therefore, the flight time is longer than expected, and the distance estimate fails. The anchors in the lower corners receive the LOS signal first.

functions obtained from the multipath components of the received signal. Recently, ML has been extensively applied for NLOS identification and error mitigation, which is presented in Section VIII-A.

A commercial solution was coined by Decawave (Qorvo) in [178] for systems that contain the DW1000 chips. This embedded resolution comprises the use of additional registers to assign a level of confidence to the received timestamps. Afterwards, it post-processes accumulators to allow the identification of a falsely detected first path, hence, identifying NLOS situations.

VI. RECENT ADVANCES IN UWB POSITIONING LITERATURE

The main contribution of this paper is that it summarises the most recent advances in UWB positioning literature that have spanned the previous five years; hence, we provide a compact summary, as shown in Tables 4–9. The tables categorise each article concerning the publication year, ranging methods used, applied algorithms, whether they use the fusion-based technique and field of application, as well as a summarised description explaining the rationale, methodology and findings for each article. In addition, several other articles are summarised as in-text review outside the table, which can be found in the relevant sections.

VII. ADVANCES IN SENSOR FUSION TECHNIQUES

Sensor fusion is a computational procedure to combine the measurements from multiple sources such that the output information after fusion is maximized [179].

TABLE 4. Summary of UWB literature: General methodology development.

Ref	Year	Ranging method	Algorithm	Multi-sensor	Application	More information
[192]	2020	TOA	LS trilateration	-	General	Improved the UWB positioning accuracy in low SNR situations by proposing a modified leading edge detection algorithm in addition to LS trilateration filtering.
[140]	2020	TW-TOF	KF, MLE	-	2D & 3D positioning	A comparative study employing various signal processing and AI techniques to identify measurement outliers. LOS/NLOS classifiers were investigated in both 2D and 3D localisation.
[173]	2018	TWR, TDOA	ELPSO	-	2D & positioning, 3D	Developed an ensemble learning particle swarm optimisation (ELPSO) method for UWB indoor positioning. The system optimised the positions of 36 tags in which the final estimated values converged after 20 iterations, which outperformed other PSO methods.
[194]	2018	AOD, AOA, TOA, RSS	RiMAX	-	2D & 3D positioning	Developed a novel positioning algorithm using an extension to the RiMAX algorithm and based on the geometrical properties of the propagation path of the UWB signal. The performances of numerous ranging techniques were compared and exploited to achieve channel sounding measurements. The proposed method achieved an overall accuracy of 0.26 m in LOS and 0.90 m in NLOS.
[194]	2019	TOF	TSML-WLS	Wi-Fi	2D & 3D positioning	Investigated the performance of Wi-Fi as an IPS when it cooperated with UWB-IPS. Experimental results showed increased accuracy when Wi-Fi access points were gradually replaced with UWB beacons (20-30 cm per replacement). The proposed hybrid approach achieved an efficient compromise between positioning accuracy and infrastructure costs.
[141]	2020	TW-TOF	KF, MLE	-	2D & 3D positioning	Proposed a real-time indoor positioning system for smart grids by employing UWB as IPS. The proposed framework is based on AI techniques to detect the measurement outliers caused by NLOS conditions and hence improve the positioning accuracy of smart grid components.
[195]	2020	TOA	Trilateration, LSTM	-	2D positioning	Achieved high localisation accuracy (MAE = 0.7 m) by using two LSTM algorithm networks to mitigate the effect of NLOS measurements.
[191]	2019	TOA	PUFIR	INS	2D positioning	Introduced the problem of missing UWB measurements and proposed a fusion with INS augmented by a predictive unbiased finite impulse response (PUFIR) filter. The authors compared its performance with three other filters: KF, an ordinary UFIR and a predictive Kalman filter (PKF). The results showed that the PUFIR filter yielded less RMSE (0.5 m), more robustness than KF and a reliable navigation accuracy (maximum error = 2.28 m) amid missing UWB range measurements.
[189]	2018	TOA	EFIR	INS	2D positioning	Proposed a federated EFIR algorithm to fuse UWB and INS measurements. The real test results showed that the EFIR filter outperformed the conventional federated EKF.
[196]	2020	TOA, TDOA	MLP, CNN	-	2D positioning	Proposed a transfer learning-based UWB NLOS identification scheme for an unmeasured environment. The proposed hybrid method showed better NLOS identification accuracy (98.33 %) at 48 times faster training time than conventional ML algorithms MLP and CNN.
[142]	2020	TOA	SVD-FDCKF	IMU	2D positioning	Proposed an IMU/UWB multi-sensor system using the singular value decomposition federated derivative cubature Kalman filter (SVD)-FDCKF, which continuously corrects the IMU through UWB positioning observables to avoid the accumulation of IMU drift errors in a short time.
[143]	2016	TOA	LS, EKF, PF	-	2D positioning	Simulated the distance measurements using RTT and compared the estimation performance of PF against those of LS and EKF. Results showed that the PF output is more reliable than other algorithms but on account of computational complexity.
[197]	2020	TDOA	WKNN-LSTM	-	2D positioning	The LSTM model was used to predict UWB measurements, which were later used to fix the actual ones. The corrected UWB measurements were fed to the WKNN model, and hence, the localisation was obtained. This method resulted in high precision accuracy of 20 cm.
[125]	2020	TOA	Chan-Taylor	-	3D positioning	The research focuses on mitigating the effect of NLOS error on indoor 3D positioning by achieving RMSE error of 0.2 m.

TABLE 5. Summary of UWB literature: NLOS mitigation and integration with fingerprinting.

Ref	Year	Ranging method	Algorithm	Multi-sensor	Application	More information
[75]	2019	TOA	LSE-Taylor	-	Multi-users in dense environments	Developed waveform division multiple access (WDMA)-based UWB positioning for dense multipath and NLOS environments. The proposed (WUB-IP) method was complemented by a transfer learning approach (SHLA) to mitigate NLOS. The WUP-IP method showed a high precision positioning scheme (RMSE $<$ 2 cm) compared to other methods (RMSE $>$ 10 cm).
[198]	2018	TOA	WLS, IVM	-	NLOS identification	Proposed a novel ML NLOS identification method using WLS and IVM algorithms. The tests showed that IVM had better positioning accuracy (in terms of RMSE and CDF) than RVM and SVM.
[199]	2019	TW-TOF	ECTSRLS	-	NLOS mitigation	Developed an equality constrained Taylor series robust least squares (ECTSRLS) technique followed by a fuzzy comprehensive evaluation (FCE) to mitigate the effects of NLOS situations. The FCE-ECTSRLS method is used for channel identification to select the optimal set of ranges for the position estimation. The experimental results showed that the proposed method outperformed other algorithms by RMSE = 0.602 to 1.063 m.
[200]	2021	AltDS-TWR	LS trilateration	-	Fingerprinting positioning	Presented the Fingerprinting-Assisted UWB-based localisation (FAUL) method to improve the accuracy of UWB localisation in complex indoor environments. FAUL combines fingerprinting and weighted trilateration techniques to reduce the localisation error (accuracy > 95%) when LOS situations are minimal.
[201]	2020	TW-TOF	CNN	-	Fingerprinting positioning	Utilized an ML model (CNN) to improve the accuracy of fingerprinting measurements. The data were divided as 70% for training and 30% for testing, and the CNN method outperformed SVM and random forest algorithms.

TABLE 6. Summary of UWB literature: IoT.

Ref	Year	Ranging method	Algorithm	Multi-sensor	Application	More information
[202]	2018	TOA	LS, CI, TSML	-	IoT	Derived a statistical model based on an LS algorithm to improve the performance of the estimated pairwise distances before forwarding to the localisation algorithms. The method was validated against two algorithms: CI and TSML. The results showed a significant improvement in performance within scenarios of varying geometry, such as IoT scenarios.
[203]	2018	TOA	-	RFID	Industrial + IoT	Highlighted the numerous attempts made to utilize UWB in various environments, including the outer space. Experiments carried out by [208] showed that the UWB/RFID method could achieve up to 4 cm accuracy.
[205]	2017	TOA	Trilateration	RFID	IoT, energy harvesting	Highlighted the characteristics of energy-autonomous tags that can achieve centimetre-level positioning accuracy. The authors demonstrated the UWB-RFID backscatter method, a promising candidate for precise positioning.
[79]	2018	TDOA, TWR	-	-	Tracking in dense environments	Investigated the capability of UWB Decawave DW1000 chip to support numerous tags simultaneously in dense environments. The authors concluded that the proposed method (TDOA-TDMA) can support up to 6171 tags (updates per second), outperforming other combinations of methods.

As sensor technology becomes more sophisticated (and owing to its erroneous nature), multi-sensor fusion has been trending recently. The reliance on multiple measurement devices in positioning applications can result in fewer uncertainties, and greater reliability and accuracy than depending on a single measurement sensor [180]. Numerous tracking systems can be fused with a UWB system to produce more accurate and reliable estimations. Common examples of these systems are GNSSs, inertial navigation systems (INSs), dead reckoning (DR), visual map matching (VMM) and computer vision. The optimal positioning estimations that result from fusing multiple positioning methods follow a unified framework, which is illustrated in Figure 9.

GNSSs (e.g. GPS, GLONASS and Galileo) provide satellite-based positioning estimations for outdoor environments within an acceptable error range. However, the signal suffers from multiple degradation factors, such as multipath fading, path loss and shadowing, which reduce its applicability in indoor positioning applications [147], [181].

INSs are highly reliable positioning systems, as they are not influenced by external factors. However, they accumulate significant errors over time [182], [183]. The main role of

TABLE 7. Summary of UWB literature: Autonomous systems.

Ref	Year	Ranging method	Algorithm	Multi-sensor	Application	More information
[144]	2020	DS-TWR	EKF	DR	AGV control	Proposed a fusion-based UWB/DR localisation technique to achieve 10 cm tracking accuracy for AGVs in harsh industrial environments.
[206]	2020	TOA, TDOA	GD, LS	-	AGV	Developed a low-cost UWB localisation system that provided precise positioning for AGVs using gradient descent and LS algorithms. The proposed method was validated against RTK data, and the result was a robust system capable of localisation both indoors and outdoors.
[183]	2019	TOA	LS, SHFAF	INS	Autonomous robots	Proposed an INS/UWB/SHFAF method to deal with the time-varying noise, which accounts for the positioning errors of indoor autonomous robots. Through simulations and experiments, the proposed method achieved high positioning performance in terms of accuracy and robustness in dense environments.
[186]	2017	TOA	IAKF, AR	INS	Mobile robots	Tested an INS/UWB sensor fusion approach to tackle the problem of accumulated errors for tracking indoor mobile robots in real-time. A 2D kinematic model, improved adaptive Kalman filter (IAKF) algorithm and AR algorithm were used to identify the estimated position outliers. The results showed that IAKF outperformed the KF algorithm with an improved error of 0.24 m.
[136]	2019	TOA	EKF, UKF, PF	-	Robot localisation	Presented and compared the performances of EKF, UKF and PF in positioning mobile robots. The simulation results showed that the PF performed fastest in the low-speed mode (1 m/s), while UKF performed fastest at higher speeds (2-10 m/s).
[147]	2020	TDOA	FKF	GNSS, DR, VMM	Intelligent transportation	Designed the fusion positioning algorithm of GNSS/UWB/DR with a federated Kalman filter (FKF). The results obtained from both the simulation and real vehicle testing showed that the proposed intelligent vehicle localisation accuracy was improved (MAE < 0.88 m). The positioning accuracy could be improved, and an adaptive information distribution coefficient was established based on the FKF.
[207]	2021	TOA	MLKF	-	UAV 3D positioning	Indoor localisation of a fleet of vehicles using UWB. The measurements involved the calculation of inter-vehicle distance, which improved the overall positioning accuracy by 60 percent.
[149]	2018	DS-TWR	EKF	IMU	UAV 3D positioning	Proposed a 3D attitude and pose estimation method for small UAVs involving the use of IMU, UWB and EKF filtering. The best RMSE values achieved for attitude and pose were 1.93° and 0.19 m, respectively.
[208]	2017	TW-TOF	LMA multilateration	-	UAV tracking	Developed a numerical method which involved the use of UWB technology and Levenberg-Marquardt algorithm (LMA) to track and control UAVs. The analysis results showed that an improved accuracy on decimetre order could be achieved for the 3D-positioning of UAVs.
[32]	2020	TOA, TDOA	Cost function	GNSS, LoRa	UAV traffic management	Proposed a high-precision prototype for a UAV traffic management (UTM) system. Besides GPS, the authors used a novel method comprising an IR-calibrated UWB (Decawave) in addition to the LoRa module. The proposed cost function reduced the GPS positioning error from 4.03 to 1.73 cm.

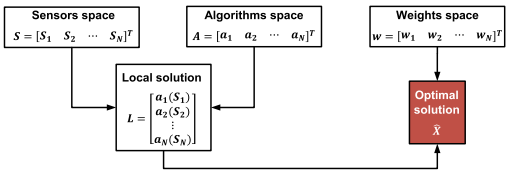

FIGURE 9. Fusion-based positioning framework, adapted from [179], [180].

UWB precise positioning technology is to refine INS errors by tightening the position estimate to the absolute coordinate system, while an INS provides more accurate delta position updates in the short term, making the integrated INS/UWB system more accurate and robust [26], [76]. An IMU differs from an INS as it is not an integrated dynamic system as an INS. However, IMU units are the main building block of an INS [184]. IMUs can still be used independently in fusion-based localisation endeavours, but INSs have recently been widely adopted in positioning systems.

A. SENSOR FUSION POSITIONING IN TRANSPORTATION APPLICATIONS

As cooperative positioning is a crucial element in intelligent transportation systems (ITSs), the authors in [185] developed a cooperative scheme supported by vehicle-to-infrastructure (V2I) communications as a prototype implementation of an

TABLE 8. Summary of UWB literature: Industrial applications.

Ref	Year	Ranging method	Algorithm	Multi-sensor	Application	More information
[34]	2020	TW-TOF	EKF, ESKF	IMU	Coal mine robots	Developed an IMU/UWB-based localisation system to equip CMRs with reliable estimations that improved navigation in underground tunnels. UWB measurements were filtered by EKF, which were federated with IMU measurements through the ESKF algorithm. Small-scale experiments showed improved robustness but less positioning accuracy (RMSE = 0.562 m).
[191]	2019	TDOA, AOA	KF	SINS	Coal mines	Proposed the SINS/UWB method, in which both measurements were fed to a Kalman filter to fuse the estimated position and speed. The results showed that the tightly coupled model and the decision tree model could produce accurate positioning during partial and total node failure situations. The maximum error of the SINS/UWB multimodel method was 0.93 m, accumulated in 327 s.
[149]	2020	ADS-TWR-MTMA	WLM, WLS, KF	IMU	Underground Mines	A numerical analysis using simulation data to validate the impact of using fusion-based method (UWB/IMU) to improve the localisation accuracy in underground Mines.
[209]	2020	TOA	Chan	-	Substation safety monitoring	Investigated the feasibility of a test environment that employs UWB positioning in 500 kV substation operation monitoring. Despite the high costs and shielding problem, the experimental results showed positioning accuracy of 0.15-0.3 m in the UWB substation monitoring environment.
[90]	2017	AOA, TDOA	PF	-	Industrial warehouse	Conducted a comparative study between commercial UWB providers such as BeSpoon, Ubisense and Decawave. The authors concluded that the Decawave system outperformed other systems in terms of reliability and accuracy owing to its advanced antennas.

TABLE 9. Summary of UWB literature: Pedestrian positioning.

Ref	Year	Ranging method	Algorithm	Multi-sensor	Application	More information
[145]	2019	TW-TOF	EKF, K-means	-	Body wearable sensors	Investigated the effect of UWB wearable location with respect to the body on the overall positioning accuracy. The method involved the use of smoothing, filtering and clustering. The experimental results showed that placing the UWB wearable tag on the human chest produced the largest positioning error due to the highest NLOS component, while placing it on the forehead yielded the best accuracy.
[146]	2017	TOA	EKF, EFIR	-	Human localisation	Compared the performances of EKF and EFIR estimators for human localisation based on UWB. The results showed that EFIR performed better than LS and EKF algorithms, with MAE values of 0.19 and 0.54 m for the north and east directions, respectively.
[210]	2017	TOA	PF, ZUPT	IMU	Pedestrian positioning	Proposed a fusion-based method, IMU/UWB, through PF and ZUPT algorithms to achieve precise positioning for pedestrians. The results showed that the proposed method demonstrated high precision under NLOS conditions using fewer particles.
[148]	2020	TOA, TDOA	PF, EKF, ZUPT	INS	Pedestrian tracking	The UWB observables were treated by joint particle filtering, while the INS data were filtered by the ZUPT algorithm. Both UWB and INS errors were loosely fused by EKF, resulting in improved accuracy (MAE = 0.35 m) and better adaptability in robust environments.
[211]	2020	TDOA	SWA	-	Shopping mall	The TDOA ranging technique and sliding window algorithm (SWA) were used to track a moving stroller in a shopping mall down to 20 cm RMSE positioning error.
[51]	2018	TOA	PF, EKF	-	Sports athletes tracking	Investigated the performance of UWB tracking for athletic activities, such as running, walking with varying speeds and accelerations and jumping. The tests involved PF and EKF algorithms, which showed an acceptable accuracy of approximately 20 cm.
[212]	2019	SDS-TWR	-	-	Track indoor cyclists	Studied the feasibility of employing UWB for tracking indoor athletes (cyclists). The authors investigated various configuration setups to conclude the best positioning accuracy, best anchor height in LOS, least energy consumption and the most convenient spot for athletes to mount the mobile UWB tag. The experimental results showed that UWB positioning is viable for tracking indoor cyclists.

ITS. This method comprises a tightly coupled sensor-fused GPS/UWB/INS algorithm built upon an error detection unit, in addition to a robust Kalman filter. The UWB component acts as a refining agent for noisy GPS measurements.

The results showed that the fusion of UWB with GPS/INS improved the overall positioning accuracy of the vehicles down to a sub-metre level with an added pseudo-range gross error in different scenarios (the highest positioning error was 0.78 m) and, thus, increased the system reliability.

In ITSs, various low-cost positioning systems can be fused to improve the overall accuracy and reliability, as demonstrated in [147]. The authors used a federated Kalman filter (FKF) to combine GNSS, UWB, DR and visual map matching (VMM) in one framework, which the authors called an 'intelligent positioning strategy'. VMM is a common method in GNSS positioning, which uses pre-stored maps to correct the fusion error. Three input sources to VMM were propagated: (i) result of GNSS/UWB/DR fusion, (ii) captured images from a vehicle camera and (iii) pre-stored visual map repository, sampled by frame and pose. The integrated GNSS/UWB/DR/VMM strategy was tested in a simulation environment and a real-vehicle test platform on a university campus. The results of both tests showed that the framework improved the accuracy (MAE 0.9 m) and system reliability.

Intelligent logistics (also known as smart logistics) have recently adopted AGV robots which possess key transportation capabilities to maximise the efficiency of logistics traffic. The authors in [139] developed an INS/UWB integrated approach along with an interactive multiple model (IMM) algorithm that involves dual Kalman filters in both LOS and NLOS situations by combining their probabilities through a Markov chain transform. The INS and UWB position errors were fused, and the error covariance was updated using another Kalman filter, which compared the INS measurements against the UWB estimated values. Finally, the Kalman filter yielded the estimated position as the output and proceeded to the weighted fusion step. The results showed that the proposed INS/UWB-IMM method reduced the influence of a LOS/NLOS mixed situation; the average localisation error obtained was 0.2 m.

B. FUSION-BASED POSITIONING IN INDOOR APPLICATIONS

Fusion-based indoor positioning has recently gained significant attention due to advances made in wireless sensor networks, enhancements achieved in positioning technologies and its optimisation capabilities [180]. Another tightly coupled technique was presented by [186], where the authors used an INS/UWB sensor fusion approach to address the problem of accumulated errors in inertial navigation systems, which can localise and track indoor mobile robots in real-time. A 2D kinematic model of a mobile robot was developed for positioning and tracking, in addition to an autoregressive algorithm, to accommodate a third-order error equation for the gyroscope and accelerometer. In addition, an IAKF algorithm was developed, and a covariance matching method was used to identify the estimated position outliers. The results showed that IAKF outperformed the KF algorithm, and the error of the INS/UWB integrated system was improved to 0.24 m, which is an acceptable level for the practical requirements of the system model.

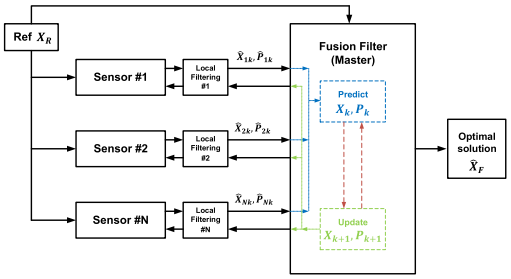

FIGURE 10. Structure of the federated Kalman filters.

The concept of an FKF filter in multi-sensor data fusion has been implemented as a group of sub-filters corresponding to each sensor measurement in addition to the master combining filter, which regularly fuses sensor data to achieve optimal estimations [187], [188]. The concept of federal filters is illustrated in Figure 10. The authors of [189] adopted a federated extended finite impulse response (EFIR) filter as the sub-filter to fuse INS/UWB measurements between the reference nodes and target tag. Another EFIR was used as the master filter to achieve optimal position estimation based on the sub-filter outputs to mitigate the INS error.

The results obtained from [189] showed that the EFIR sub-filter approach was more accurate (RMSE = 0.45 m) and robust than the normal FEKF. In [190], the same authors introduced the problem of missing UWB measurements and proposed the combination of an INS augmented by a predictive unbiased finite impulse response (PUFIR) filter. The performance of the proposed method was compared with those of the other three filters: the Kalman filter, an ordinary UFIR and a PKF. Although the ordinary UFIR filter performed the worst, the PUFIR filter yielded a smaller RMSE (0.5 m) and more robustness than the Kalman filter and yielded reliable navigation accuracy (maximum error = 2.28 m) amid temporary missing UWB range measurements.

The authors of [183] addressed the multipath effect during NLOS situations on a UWB signal in dense, complicated environments for the indoor navigation of autonomous robots. The authors introduced an adaptive filter called Sage-Husa fuzzy adaptive filter (SHFAF) for outlier detection. Such filters assume that the noise is time-varying, especially in an NLOS situation, in contrast to Kalman filters, which assume time-invariant noise. In a SHFAF, noise covariance is estimated by adjusting the innovation weight adaptively, which results in more accurate estimations (88.2% of the time, the positioning error is less than 0.2 m) and enhanced robustness, as demonstrated by the simulation and experimental results.

C. FUSION-BASED POSITIONING IN EXTREME CONDITIONS

GNSS signal is not available in underground mines, and all positioning systems in those conditions are prone to signal deterioration and multipath effects. Being quite tolerant against multipath propagation, UWB positioning has been used in Coal mine robots (CMRs) for precise underground positioning to function in excavation, mining and security control rescue tasks. The authors of [34] developed an IMU/UWB-based localisation system to equip CMRs with reliable Estimations, which can mitigate the navigation uncertainties in underground tunnels. The UWB measurements were propagated into an EKF. Subsequently, its output was federated with IMU measurements through an ESKF to realise six-degree-of-freedom state estimations. The estimates were compared with LiDAR odometry methods. The simulations and small-scale experiments exhibited improved robustness but slightly decreased positioning accuracy for the proposed fusion method ESKF-UWB over EKF-UWB. The authors attributed these results to two reasons: (i) the EKF method did not comprise orientation errors, or (ii) the crawler robot suffered movement vibrations, generating additional IMU noise. This implementation is yet to be investigated on a larger scale.

The strap-down inertial navigation system (SINS) is commonly employed in Chinese coal mines to measure the position and attitude of a shearer on rails; however, it suffers from the accumulation of error drifts over time. Hence, the authors of [191] proposed an integrated SINS/UWB system through a multimodel intelligent fault-tolerant algorithm to refine the positioning errors by switching between a tightly coupled model and a decision tree model based on the working state of UWB anchors. The switching was performed by assessing the ability of all anchor nodes to accurately measure the range between each stationary node and the mobile node. Afterwards, the determined UWB epochs, along with SINS estimations were fed to a Kalman filter to obtain the final position and speed. The results showed that the tightly coupled model could accurately localise the shearer amid partial node failure. In contrast, the decision tree model could produce accurate positioning during total node failure situations. The maximum SINS/UWB multimodel method error was 0.93 m, accumulated in 327 s.

VIII. ADVANCES IN MACHINE LEARNING APPROACHES IN PRECISION POSITIONING

The multilateration techniques directly estimate the position of an agent using distance observables with a direct signal propagation model. The reliability of the estimation can be increased using a dynamic state model, which in addition to current observations, uses the previous positions in estimations as well through Bayesian statistics (e.g. Kalman- and PF-based solutions). These are the most common methods and are particularly functional inside a controlled positioning infrastructure. While plain multilateration and dynamic state models have been the most common methods for positioning estimation, more advanced ML models have become increasingly popular due to their increased calculation capacity and advances in ML methods. They are used for positioning in situations in which simple models do not work efficiently (e.g. due to heavy nonlinearities, abruptly changing conditions, heterogeneous information sources, skewed noise distribution or non-convexity). Typical reasons for using ML are to increase robustness, allow adaptation to changes, implement a collaborative or model-free positioning system, use heterogeneous information sources or select the most useful features for positioning. These methods allow the use of ad hoc observations not originally intended for positioning, such as optical images and RSSs from Wi-Fi base stations. Often traditional positioning algorithms are supplemented with ML methods.

ML methods have been found helpful in many use cases, some of which are listed in the following subsections. Moreover, a summary that describes the properties, strategies and purposes of the reviewed ML algorithms is presented in Table 10.

A. RESOLVING NLOS UNCERTAINTY

UWB systems that are augmented by ML approaches play an important role in resolving NLOS situations. For instance, the basic ML algorithms, such as a *naïve* Bayesian filter and gradient descent algorithms were adopted by [213] and [206], respectively, to address NLOS conditions by recognising measurement outliers, hence improving the overall accuracy. Using large datasets, the authors of [106] proposed a radar system augmented by a multiclass support vector machine algorithm to localise and identify targets by specifying the location within the building rooms, which reduced the uncertainty associated with NLOS. A similar approach with a novel NLOS identification algorithm based on an import vector machine (IVM) algorithm, along with a feature selection strategy was proposed by [198].

The suitable performance of neural network deep-learning approaches have also been rising in dominance in the most recent UWB literature (in a span of the past three years). In [196], the use of a multilayer perceptron, with transfer learning and convolutional neural networks (CNNs) as NLOS classifiers, not only enhanced the overall training accuracy from 44% to 98% but also achieved faster training times than those achieved using CNNs alone in an unmeasured environment. Another neural network approach was presented in [195], where the authors employed a long short-term memory (LSTM) algorithm for predicting the user position based on the received TOA measurements. This LSTM approach resulted in a 7 cm accuracy, which outperformed several other techniques, including the recurrent neural network (RNN) method. The ML methods can be used to increase the robustness of the well-known model-based traditional methods, such as Kalman filter [214].

TABLE 10. Summary of machine learning methods used for positioning.

Algorithm	Purpose	Strategy	Properties	Ref.
Naïve Bayesian filter	NLOS mitigation	Outlier detection	Accuracy in terms of the area under curve (AUC) is 87%	[213]
LS + thresholding	NLOS mitigation	Outlier detection	Penalize the quadratic error (cost function)	[206]
CNN	NLOS mitigation	Outlier detection	Transfer learning, 98% accuracy	[194]
SVM	UWB radar	Venue detection	Correction rate > 95%	[106]
LSTM	Robust positioning	Analysing mean error and hyper-parameters	Mean error 6-7 m, less than with other methods tested	[195]
Multi PF	Adaptive positioning	Change channel model when NLOS is detected	RMS positioning error 20 m in 2000 m field	[215]
Reinforced learning + PF	Adaptive positioning	Change PF mode according to success / failure	Accurate and fast recovery for positioning errors	[216]
PF + ML based data fusion	Collaborative positioning	Peer to peer data fusion	Works during main positioning system outage	[217], [218]
PF + ML autocalibration	Collaborative positioning	Automatic configuration	Autocalibration, adaptive time slot protocol	[220], [221]
Ensemble regression and deep learning	Model-free positioning	Fingerprinting	Based on scanning a map of observables	[224], [225]

B. ADAPTIVE POSITIONING

The parameters of the prediction models can be tuned or changed according to the change in the operating conditions detected by ML models, for example, when an agent moves from outdoors to indoors or the detection of NLOS situations. Some researchers have been able to improve the positioning accuracy by using various dynamic-state models simultaneously and selecting the most suitable model according to the conditions detected by the ML model [215]. Neural networks and reinforced learning methods allow even more flexible adaptation to the changing environment [216].

C. COLLABORATIVE POSITIONING

Collaborative positioning means that agents share information with each other while performing positioning. The solution does not necessarily conform to the preconditions of the static or dynamic state model-based methods, as the noise distribution might be skewed, and the problem might be non-convex. Therefore, traditional optimisation methods might not find the global optimum.

Hoang *et.al.* studied collaborative positioning of vehicles using onboard GNSS, IMU, odometer and UWB for inter-vehicle distance measurement. They formed an ad hoc communication network using the ITS-G5 standard for collaborative positioning [217]. The data fusion was performed using Bayesian frameworks with EKF and PF for pre-processing and data fusion, and they noticed that the PF outperformed the EKF. The experimental result showed that collaborative positioning using vehicle-to-vehicle communication could secure accurate positioning during GNSS outage in some cases [217].

The noise in DGNSS observables is not Gaussian, and the collaborative positioning problem is not convex. Therefore, the ML approach was used to create a cognitive PF for positioning for industrial IoT purposes [218]. They also noticed that if the noise probability distribution of the sensor data can be properly estimated and used in particle weight computation, the positioning accuracy can be further improved.

Infrastructure-free multi-robot localisation using UWB and PF [219]–[221], including functionality for system autocalibration [105], has been extensively studied. Both relative position and orientation of robots can be obtained by attaching several UWB requesters and responders in robots and measuring ranges using TW-TOA [222].

D. MODEL-FREE POSITIONING

In many cases, ML is used for solving problems without pre-defined models, which can be particularly useful when using ad hoc information for positioning. Inside positioning infrastructure, model-based methods are often more efficient than model-free methods. ML learns the model of the problem domain by itself based on the optimal information gain. In addition to positioning itself, ML can also be used for studying the problem and revealing the hidden dependencies between variables. For example, Wi-Fi fingerprint-based positioning is implemented with ML [223]. Nonlinear ensemble regression methods, such as random regression trees and deep learning, can be efficient in this domain [224], [225].

E. DEVELOPMENTS IN MISCELLANEOUS APPLICATIONS

With the rapid development of ML approaches in various sectors, there is a growing need to investigate and analyse ML suitability for localisation applications. In the case of location-based services, ML is growing in popularity as it can produce accurate positioning information for navigational purposes. An ML approach can support the achievement of better positioning performance both outdoors and indoors [226]. This positioning system allows real-time tracking and tracing of goods and enables the optimisation of logistics processes in many application areas [227]. In an indoor warehouse scenario, an ML algorithm allowed, for the first time, a monocular optical positioning application [227].

The authors of [228] proposed a visible light positioning (VLP) algorithm, which is based on ML and works to measure the relative distance between the receiving and transmitting ends of the camera. The combination of VLP systems and dual-function ML algorithms enables an increase in positioning accuracy by reducing the negative effect and eliminating low-intensity reflective signals [229]. In this approach, the position is determined by a proposed triangulation algorithm. The authors of [230] proposed an automated visual positioning system using deep learning, which aids to correctly place a workpiece on a fixture. This approach requires template matching across the image in which the template is compared with the local pixels.

ML methods are also used in fingerprint-based algorithms to enhance the precision and robustness of indoor positioning. The advancement of fingerprint localisation technology is a promising method for indoor positioning in various applications [231]. The authors of [232] developed a fingerprint-based localisation method, which is combined with ML and a heterogeneous feature fusion model. Another promising positioning method is smartphone-based indoor tracking, exploiting opportunistic sensing and machine learning techniques, e.g. SLAM. The SLAM method offers a new intelligent filtering approach to maintain good positioning performance [233].

F. SUMMARY

The research interest towards ML methods in positioning has been continuously increasing during the last five years [234]. ML facilitates the use of more data sources for positioning and development of collaborative positioning schemes, which are too complex for traditional methods. ML plays an important role in developing future location-based services by seamlessly using many available positioning infrastructure and other information sources [234].

IX. DISCUSSION

As UWB is a relatively new standard, the maturity in chip production is rapidly increasing. New accurate and affordable UWB hardware has been recently introduced by Decawave and NXP for industrial applications, and UWB chips are included in recent phone models and other consumer products by the biggest mobile phone manufacturers. This development has made UWB an attractive technology for indoor positioning purposes. Recent UWB positioning systems support decimetre-level accuracy and 60 m distance [105].

Most of the positioning algorithms used with UWB are the same, which have been used for positioning for decades, including multilateration, LS solution, Kalman filtering and particle filtering, but the increased popularity and lowering prices of UWB positioning are also attracting new application areas, solutions and algorithms. While traditional approaches are still optimal for the standard multilateration problem, different ML methods have been proposed to cover special situations, such as the use of heterogeneous data, detection of outliers, mitigation of NLOS situations and automatic adaptation to changing conditions. Automatically calibrated multi-robot positioning systems with collaborative positioning and pose estimation methods have been proposed to assist in controlling industrial robots, drones or cars [159], [235]. Multi-sensor fusion has been studied for increasing the reliability and availability of the positioning service and ML methods to allow seamless roaming between positioning systems and the use of signals of opportunity together with actual positioning observables. Similarly, collaborative positioning can increase the positioning reliability under difficult conditions.

The recent literature in UWB positioning for smart logistics contains adaptation of UWB positioning to many new application areas and increasing the flexibility and reliability using new algorithms.

In the future, low-earth orbit (LEO) satellites can be used to provide an additional mode for both outdoor, and indoor navigation [236]. We intend to implement our proposed positioning system (mobile App), which involves the use of GNSSs, inertial sensors and UWB for smart logistics applications and researching the possibility of using LEO-based positioning observables fused with other available information.

X. CONCLUSION

Due to its versatility, accuracy and robustness, UWB technology is considered an efficient and reliable localisation method for implementing smart logistics. The wide adoption of UWB in location-based services confirms its ability to make an effective compromise among the cost, resource budget and precision. This paper summarises the most recent studies that have adopted UWB in sensitive applications that require high precision positioning in which UWB has successfully reduced the localisation error to a few centimetres. UWB advances for location provision are foreseen to grow as the adoption of this technology in mass-market devices increases via standards and related developments. UWB will likely not only be providing location solutions for special industrial applications but also consumer devices in the future. Moreover, this paper presents a compact review that focuses on using multi-sensor fusion-based systems in specific applications. We highlight the use of inertial sensors, remote sensing devices, visual sensors and other RF-based navigational sensors to achieve seamless navigation under various conditions.

Additionally, we present a higher perspective on the algorithms used for either single-sensor systems or multi-sensor fusion systems, such as Kalman filter, LS, PF, federated filter structure and ML methods. We have designed the architecture of this article to be a compact tutorial for researchers seeking an overall view on UWB positioning technology, aiming to make it a landmark article on the literature track of UWB.

CONFLICT OF INTERESTS

The authors declare no conflict of interests.

ACKNOWLEDGMENT

The authors would like to thank Prof. Miadreza Shafiekhah and the anonymous reviewers for the helpful remarks to further improve the manuscript.

REFERENCES

[1] S. Subedi and J.-Y. Pyun, "A survey of smartphone-based indoor positioning system using RF-based wireless technologies," *Sensors*, vol. 20, no. 24, p. 7230, Dec. 2020. [Online]. Available: https://www.mdpi.com/1424-8220/20/24/7230

[2] D. B. Ninh, J. He, V. T. Trung, and D. P. Huy, "An effective random statistical method for indoor positioning system using WiFi fingerprinting," *Future Gener. Comput. Syst.*, vol. 109, pp. 238–248, Aug. 2020. [Online]. Available: https://www.sciencedirect.com/science/article/pii/S0167739X19324835

[3] C. E. A. Bundak, M. A. A. Rahman, M. K. A. Karim, and N. H. Osman, "Fuzzy rank cluster top k Euclidean distance and triangle based algorithm for magnetic field indoor positioning system," *Alexandria Eng. J.*, vol. 61, no. 5, pp. 3645–3655, May 2022. [Online]. Available: https://www.sciencedirect.com/science/article/pii/S1110016821005883

[4] P. Bencak, D. Hercog, and T. Lerher, "Indoor positioning system based on Bluetooth low energy technology and a nature-inspired optimization algorithm," *Electronics*, vol. 11, no. 3, p. 308, Jan. 2022. [Online]. Available: https://www.mdpi.com/2079-9292/11/3/308

[5] S. Jeong, J. Min, and Y. Park, "Indoor positioning using deep-learning-based pedestrian dead reckoning and optical camera communication," *IEEE Access*, vol. 9, pp. 133725–133734, 2021.

[6] R. Vleugels, B. Van Herbruggen, J. Fontaine, and E. De Poorter, "Ultra-wideband indoor positioning and IMU-based activity recognition for ice hockey analytics," *Sensors*, vol. 21, no. 14, p. 4650, Jul. 2021. [Online]. Available: https://www.mdpi.com/1424-8220/21/14/4650

[7] Y. Song, F. R. Yu, L. Zhou, X. Yang, and Z. He, "Applications of the Internet of Things (IoT) in smart logistics: A comprehensive survey," *IEEE Internet Things J.*, vol. 8, no. 6, pp. 4250–4274, Mar. 2021, doi: 10.1109/jiot.2020.3034385.

[8] W. Wu, L. Shen, Z. Zhao, M. Li, and G. Q. Huang, "Industrial IoT and long short-term memory network enabled genetic indoor tracking for factory logistics," *IEEE Trans. Ind. Informat.*, early access, Jan. 27, 2022, doi: 10.1109/TII.2022.3146598.

[9] I. V. Pospelova, I. V. Cherepanova, D. S. Bragin, I. A. Sidorov, E. Y. Kostyuchenko, and V. N. Serebryakova, "The estimation of the potential for using smart-trackers as a part of a medical indoor-positioning system," *Electronics*, vol. 11, no. 1, p. 107, Dec. 2021. [Online]. Available: https://www.mdpi.com/2079-9292/11/1/107

[10] A. Alarifi, A. Al-Salman, M. Alsaleh, A. Alnafessah, S. Al-Hadhrami, M. Al-Ammar, and H. Al-Khalifa, "Ultra wideband indoor positioning technologies: Analysis and recent advances," *Sensors*, vol. 16, no. 5, p. 707, May 2016, doi: 10.3390/s16050707.

[11] J. Park, H. Kim, J. Yoon, H. Kim, C. Park, and D. Hong, "Development of an ultrasound technology-based indoor-location monitoring service system for worker safety in shipbuilding and offshore industry," *Processes*, vol. 9, no. 2, p. 304, Feb. 2021. [Online]. Available: https://www.mdpi.com/2227-9717/9/2/304

[12] S. Woo, S. Jeong, E. Mok, L. Xia, C. Choi, M. Pyeon, and J. Heo, "Application of WiFi-based indoor positioning system for labor tracking at construction sites: A case study in Guangzhou MTR," *Automat. Construct.*, vol. 20, no. 1, pp. 3–13, Jan. 2011. [Online]. Available: https://www.sciencedirect.com/science/article/pii/S092658051000107X

[13] F. Nekoogar, *Ultra-Wideband Communications: Fundamentals and Applications*. Upper Saddle River, NJ, USA: Prentice-Hall, 2005.

[14] P. Stephan, I. Heck, P. Krau, and G. Frey, "Evaluation of indoor positioning technologies under industrial application conditions in the SmartFactoryKL based on EN ISO 9283," *IFAC Proc. Volumes*, vol. 42, no. 4, pp. 870–875, 2009. [Online]. Available: https://www.sciencedirect.com/science/article/pii/S1474667016339039

[15] S. Krishnan and R. X. M. Santos, "Real-time asset tracking for smart manufacturing," in *Implementing Industry 4.0* (Intelligent Systems Reference Library). Cham, Switzerland: Springer, 2021, pp. 25–53, doi: 10.1007/978-3-030-67270-6_2.

[16] L. Barbieri, M. Brambilla, A. Trabattoni, S. Mervic, and M. Nicoli, "UWB localization in a smart factory: Augmentation methods and experimental assessment," *IEEE Trans. Instrum. Meas.*, vol. 70, pp. 1–18, 2021.

[17] K. Zhao, M. Zhu, B. Xiao, X. Yang, C. Gong, and J. Wu, "Joint RFID and UWB technologies in intelligent warehousing management system," *IEEE Internet Things J.*, vol. 7, no. 12, pp. 11640–11655, Dec. 2020, doi: 10.1109/jiot.2020.2998484.

[18] J. A. Fernandez-Madrigal, E. Cruz-Martin, J. Gonzalez, C. Galindo, and J. L. Blanco, "Application of UWB and GPS technologies for vehicle localization in combined indoor-outdoor environments," in *Proc. 9th Int. Symp. Signal Process. Appl.*, Feb. 2007, pp. 1–4.

[19] Y. Xianjia, L. Qingqing, J. P. Queralta, J. Heikkonen, and T. Westerlund, "Applications of UWB networks and positioning to autonomous robots and industrial systems," in *Proc. 10th Medit. Conf. Embedded Comput. (MECO)*, 2021, pp. 1–6.

[20] D. Minoli and B. Occhiogrosso, "Ultrawideband (UWB) technology for smart cities IoT applications," in *Proc. IEEE Int. Smart Cities Conf. (ISC)*, Sep. 2018, pp. 1–8.

[21] R. S. Kulikov, "Integrated UWB/IMU system for high rate indoor navigation with cm-level accuracy," in *Proc. Moscow Workshop Electron. Netw. Technol. (MWENT)*, Mar. 2018, pp. 1–4, doi: 10.1109/mwent.2018.8337235.

[22] J. Wang, M. Wang, D. Yang, F. Liu, and Z. Wen, "UWB positioning algorithm and accuracy evaluation for different indoor scenes," *Int. J. Image Data Fusion*, vol. 12, pp. 1–23, Jan. 2021, doi: 10.1080/19479832.2020.1864788.

[23] Z.-G. Wu, C.-Y. Lin, H.-W. Chang, and P. T. Lin, "Inline inspection with an industrial robot (IIIR) for mass-customization production line," *Sensors*, vol. 20, no. 11, p. 3008, May 2020, doi: 10.3390/s20113008.

[24] P. T. Lin, C.-A. Liao, and S.-H. Liang, "Probabilistic indoor positioning and navigation (PIPN) of autonomous ground vehicle (AGV) based on wireless measurements," *IEEE Access*, vol. 9, pp. 25200–25207, 2021, doi: 10.1109/access.2021.3057415.

[25] F. Mazhar, M. G. Khan, and B. Sällberg, "Precise indoor positioning using UWB: A review of methods, algorithms and implementations," *Wireless Pers. Commun.*, vol. 97, no. 3, pp. 4467–4491, Aug. 2017, doi: 10.1007/s11277-017-4734-x.

[26] A. Yassin, Y. Nasser, M. Awad, A. Al-Dubai, R. Liu, C. Yuen, R. Raulefs, and E. Aboutanios, "Recent advances in indoor localization: A survey on theoretical approaches and applications," *IEEE Commun. Surveys Tuts.*, vol. 19, no. 2, pp. 1327–1346, 2nd Quart., 2017, doi: 10.1109/comst.2016.2632427.

[27] P. Forum. *Classification Criteria*. Accessed: Jan. 26, 2021. [Online]. Available: https://julkaisufoorumi.fi/en/evaluations/classification-criteria

[28] B. Feng and Q. Ye, "Operations management of smart logistics: A literature review and future research," *Frontiers Eng. Manage.*, vol. 8, no. 3, pp. 344–355, Apr. 2021, doi: 10.1007/s42524-021-0156-2.

[29] L. Zwirello, T. Schipper, M. Harter, and T. Zwick, "UWB localization system for indoor applications: Concept, realization and analysis," *J. Electr. Comput. Eng.*, vol. 2012, pp. 1–11, May 2012, doi: 10.1155/2012/849638.

[30] Y. Gu, A. Lo, and I. Niemegeers, "A survey of indoor positioning systems for wireless personal networks," *IEEE Commun. Surveys Tuts.*, vol. 11, no. 1, pp. 13–32, 1st Quart., 2009, doi: 10.1109/surv.2009.090103.

[31] P. Dabove, V. Di Pietra, M. Piras, A. A. Jabbar, and S. A. Kazim, "Indoor positioning using ultra-wide band (UWB) technologies: Positioning accuracies and sensors' performances," in *Proc. IEEE/ION Position, Location Navigat. Symp. (PLANS)*, Apr. 2018, pp. 175–184, doi: 10.1109/plans.2018.8373379.

[32] Y.-C. Chen, A. I.-C. Lai, and R.-B. Wu, "UWB-assisted high-precision positioning in a UTM prototype," in *Proc. IEEE Topical Conf. Wireless Sensors Sensor Netw. (WiSNeT)*, Jan. 2020, pp. 42–45, doi: 10.1109/wisnet46826.2020.9037604.

[33] A. Poulose, O. S. Eyobu, M. Kim, and D. S. Han, "Localization error analysis of indoor positioning system based on UWB measurements," in *Proc. 11th Int. Conf. Ubiquitous Future Netw. (ICUFN)*, Jul. 2019, pp. 84–88, doi: 10.1109/icufn.2019.8806041.

[34] M. Li, H. Zhu, S. You, and C. Tang, "UWB-based localization system aided with inertial sensor for underground coal mine applications," *IEEE Sensors J.*, vol. 20, no. 12, pp. 6652–6669, Jun. 2020, doi: 10.1109/jsen.2020.2976097.

[35] N. Zhang, "Smart logistics path for cyber-physical systems with Internet of Things," *IEEE Access*, vol. 6, pp. 70808–70819, 2018, doi: 10.1109/access.2018.2879966.

[36] X. Tang, "Research on smart logistics model based on Internet of Things technology," *IEEE Access*, vol. 8, pp. 151150–151159, 2020, doi: 10.1109/access.2020.3016330.

[37] M. Humayun, N. Jhanjhi, B. Hamid, and G. Ahmed, "Emerging smart logistics and transportation using IoT and blockchain," *IEEE Internet Things Mag.*, vol. 3, no. 2, pp. 58–62, Jun. 2020, doi: 10.1109/iotm.0001.1900097.

[38] Y. Issaoui, A. Khiat, A. Bahnasse, and H. Ouajji, "Smart logistics: Study of the application of blockchain technology," *Proc. Comput. Sci.*, vol. 160, pp. 266–271, Jan. 2019, doi: 10.1016/j.procs.2019.09.467.

[39] Y. Su and Q.-M. Fan, "The green vehicle routing problem from a smart logistics perspective," *IEEE Access*, vol. 8, pp. 839–846, 2020, doi: 10.1109/access.2019.2961701.

[40] Y. Issaoui, A. Khiat, A. Bahnasse, and H. Ouajji, "Toward smart logistics: Engineering insights and emerging trends," *Arch. Comput. Methods Eng.*, vol. 28, no. 4, pp. 3183–3210, Sep. 2020, doi: 10.1007/s11831-020-09494-2.

[41] N. Nantee and P. Sureeyatanapas, "The impact of logistics 4.0 on corporate sustainability: A performance assessment of automated warehouse operations," *Benchmarking, Int. J.*, vol. 28, no. 10, pp. 2865–2895, Mar. 2021, doi: 10.1108/bij-11-2020-0583.

[42] S. Lu, C. Xu, R. Y. Zhong, and L. Wang, "A RFID-enabled positioning system in automated guided vehicle for smart factories," *J. Manuf. Syst.*, vol. 44, pp. 179–190, Jul. 2017, doi: 10.1016/j.jmsy.2017.03.009.

[43] Y. Tao and L. Zhao, "A novel system for WiFi radio map automatic adaptation and indoor positioning," *IEEE Trans. Veh. Technol.*, vol. 67, no. 11, pp. 10683–10692, Nov. 2018, doi: 10.1109/tvt.2018.2867065.

[44] S. Horsmanheimo, S. Lembo, L. Tuomimaki, S. Huilla, P. Honkamaa, M. Laukkanen, and P. Kemppi, "Indoor positioning platform to support 5G location based services," in *Proc. IEEE Int. Conf. Commun. Workshops (ICC Workshops)*, May 2019, pp. 1–6, doi: 10.1109/ICCW.2019.8757118.

[45] A. Rácz-Szabó, T. Ruppert, L. Bántay, A. Löcklin, L. Jakab, and J. Abonyi, "Real-time locating system in production management," *Sensors*, vol. 20, no. 23, p. 6766, Nov. 2020, doi: 10.3390/s20236766.

[46] Z. Silvia, C. Martina, S. Fabio, and P. Alessandro, "Ultra wide band indoor positioning system: Analysis and testing of an IPS technology," *IFAC-PapersOnLine*, vol. 51, no. 11, pp. 1488–1492, 2018, doi: 10.1016/j.ifacol.2018.08.292.

[47] A. Motroni, A. Buffi, and P. Nepa, "A survey on indoor vehicle localization through RFID technology," *IEEE Access*, vol. 9, pp. 17921–17942, 2021, doi: 10.1109/access.2021.3052316.

[48] F. Bernardini, A. Buffi, D. Fontanelli, D. Macii, V. Magnago, M. Marracci, A. Motroni, P. Nepa, and B. Tellini, "Robot-based indoor positioning of UHF-RFID tags: The SAR method with multiple trajectories," *IEEE Trans. Instrum. Meas.*, vol. 70, pp. 1–15, 2021, doi: 10.1109/tim.2020.3033728.

[49] R. Montoliu, E. Sansano, A. Gascó, O. Belmonte, and A. Caballer, "Indoor positioning for monitoring older adults at home: Wi-Fi and BLE technologies in real scenarios," *Electronics*, vol. 9, no. 5, p. 728, Apr. 2020, doi: 10.3390/electronics9050728.

[50] Z. Zou, "Impulse radio UWB for the Internet-of-Things: A study on UHF/UWB hybrid solution," Ph.D. dissertation, KTH School Inf. Commun. Technol., Stockholm, Sweden, 2011.

[51] M. Ridolfi, S. Vandermeeren, J. Defraye, H. Steendam, J. Gerlo, D. D. Clercq, J. Hoebeke, and E. D. Poorter, "Experimental evaluation of UWB indoor positioning for sport postures," *Sensors*, vol. 18, no. 1, p. 168, Jan. 2018, doi: 10.3390/s18010168.

[52] P. Helo and A. H. M. Shamsuzzoha, "Real-time supply chain—A blockchain architecture for project deliveries," *Robot. Comput.-Integr. Manuf.*, vol. 63, Jun. 2020, Art. no. 101909, doi: 10.1016/j.rcim.2019.101909.

[53] C.-H. Cheng, Y.-H. Kuo, H. Lam, and M. Petering, "Real-time location-positioning technologies for managing cart operations at a distribution facility," *Appl. Sci.*, vol. 11, no. 9, p. 4049, Apr. 2021, doi: 10.3390/app11094049.

[54] L. Barbieri, M. Brambilla, A. Trabattoni, S. Mervic, and M. Nicoli, "UWB localization in a smart factory: Augmentation methods and experimental assessment," *IEEE Trans. Instrum. Meas.*, vol. 70, pp. 1–18, 2021, doi: 10.1109/tim.2021.3074403.

[55] R. Sonderleittner. (2020). *Why Real-Time Tracking is Part of the Smart Factory*. [Online]. Available: https://www.eliko.ee/why-real-time-tracking-is-part-of-the-smart-factory/

[56] N. Zhu, J. Marais, D. Bétaille, and M. Berbineau, "GNSS position integrity in urban environments: A review of literature," *IEEE Trans. Intell. Transp. Syst.*, vol. 19, no. 9, pp. 2762–2778, Sep. 2018.

[57] K. K. Muthukrishnan, N. Meratnia, and M. Lijding, "FLAVOUR: Friendly location-aware conference assistant with privacy observant architecture," Centre Telematics Inf. Technol. (CTIT), Enschede, The Netherlands, CTIT Tech. Rep., Jun. 2005, nos. 5–28. [Online]. Available: https://ris.utwente.nl/ws/portalfiles/portal/5398270/icsocDemo.pdf

[58] Z. Xu, S. Huang, and J. Ding, "A new positioning method for indoor laser navigation on under-determined condition," in *Proc. 6th Int. Conf. Instrum. Meas., Comput., Commun. Control (IMCCC)*, Jul. 2016, pp. 703–706, doi: 10.1109/imccc.2016.158.

[59] Q. Zou, Q. Sun, L. Chen, B. Nie, and Q. Li, "A comparative analysis of LiDAR SLAM-based indoor navigation for autonomous vehicles," *IEEE Trans. Intell. Transp. Syst.*, early access, Mar. 18, 2021, doi: 10.1109/tits.2021.3063477.

[60] G. Li, X. Liao, H. Huang, S. Song, B. Liu, and Y. Zeng, "Robust stereo visual SLAM for dynamic environments with moving object," *IEEE Access*, vol. 9, pp. 32310–32320, 2021, doi: 10.1109/access.2021.3059866.

[61] V. Honkavirta, T. Perala, S. Ali-Loytty, and R. Piche, "A comparative survey of WLAN location fingerprinting methods," in *Proc. 6th Workshop Positioning, Navigat. Commun.*, Mar. 2009, pp. 243–251, doi: 10.1109/wpnc.2009.4907834.

[62] R. Faragher and R. Harle, "Location fingerprinting with Bluetooth low energy beacons," *IEEE J. Sel. Areas Commun.*, vol. 33, no. 11, pp. 2418–2428, Nov. 2015, doi: 10.1109/jsac.2015.2430281.

[63] F. Zafari, A. Gkelias, and K. K. Leung, "A survey of indoor localization systems and technologies," *IEEE Commun. Surveys Tuts.*, vol. 21, no. 3, pp. 2568–2599, 3rd Quart., 2019.

[64] J. Gjengset, J. Xiong, G. McPhillips, and K. Jamieson, "Phaser: Enabling phased array signal processing on commodity WiFi access points," in *Proc. 20th Annu. Int. Conf. Mobile Comput. Netw. (MobiCom)*. New York, NY, USA: Association for Computing Machinery, Sep. 2014, pp. 153–164, doi: 10.1145/2639108.2639139.

[65] W. Komamiya, S. Tang, and S. Obana, "Precise angle estimation by jointly using spatial/temporal change of channel state information and its application in pedestrian positioning," *IEEE Access*, vol. 9, pp. 59420–59431, 2021.

[66] C. Gentner, M. Ulmschneider, I. Kuehner, and A. Dammann, "WiFi-RTT indoor positioning," in *Proc. IEEE/ION Position, Location Navigat. Symp. (PLANS)*, Apr. 2020, pp. 1029–1035, doi: 10.1109/plans46316.2020.9110232.

[67] L. Botler, M. Spork, K. Diwold, and K. Romer, "Direction finding with UWB and BLE: A comparative study," in *Proc. IEEE 17th Int. Conf. Mobile Ad Hoc Sensor Syst. (MASS)*, Dec. 2020, doi: pp. 44–52, 10.1109/mass50613.2020.00016.

[68] J. Talvitie, M. Koivisto, T. Levanen, M. Valkama, G. Destino, and H. Wymeersch, "High-accuracy joint position and orientation estimation in sparse 5G mmWave channel," in *Proc. IEEE Int. Conf. Commun. (ICC)*, May 2019, pp. 1–7, doi: 10.1109/icc.2019.8761910.

[69] A. Wilzeck, M. P. Guirao, and E. Dimitrov, "White paper on UWB technology and regulation," wiseSense GmbH, Hannover, Germany, Tech. Rep., 2018.

[70] F. Sabath, E. L. Mokole, and S. N. Samaddar, "Definition and classification of ultra-wideband signals and devices," *URSI Radio Sci. Bull.*, vol. 2005, no. 313, pp. 12–26, 2005.

[71] A. Muqaibel, A. Safaai-Jazi, and S. Riad, "Ultra wideband vs. narrowband communications," in *Proc. Riyadh Int. Commun. IT Conf.*, Feb. 2004.

[72] Federal Communications Commission. (2002). *Revision of Part 15 of the Commission's Rules Regarding Ultra-Wideband Transmission Systems*. [Online]. Available: https://transition.fcc.gov/Bureaus/Engineering_Technology/Orders/2002/fcc02048.pdf
[73] M. Matin, "Ultra wideband preliminaries," in *Ultra Wideband*. London, U.K.: IntechOpen, Aug. 2010, doi: 10.5772/10059.
[74] J.-S. Lee, Y.-W. Su, and C.-C. Shen, "A comparative study of wireless protocols: Bluetooth, UWB, ZigBee, and Wi-Fi," in *Proc. 33rd Annu. Conf. IEEE Ind. Electron. Soc. (IECON)*, Nov. 2007, pp. 46–51, doi: 10.1109/iecon.2007.4460126.
[75] Z. Yin, X. Jiang, Z. Yang, N. Zhao, and Y. Chen, "WUB-IP: A high-precision UWB positioning scheme for indoor multiuser applications," *IEEE Syst. J.*, vol. 13, no. 1, pp. 279–288, Mar. 2019, doi: 10.1109/jsyst.2017.2766690.
[76] D. Dardari, A. Conti, U. Ferner, A. Giorgetti, and M. Z. Win, "Ranging with ultrawide bandwidth signals in multipath environments," *Proc. IEEE*, vol. 97, no. 2, pp. 404–426, Feb. 2009, doi: 10.1109/JPROC.2008.2008846.
[77] L. E. Miller, "Why UWB? A review of ultrawideband technology, report to NETEX project office, DARPA," Nat. Inst. Standards Technol. (NIST), U.S. Dept. Commerce, Washington, DC, USA, Tech. Rep., 2003. [Online]. Available: https://citeseerx.ist.psu.edu/viewdoc/download?doi=10.1.1.76.7051&rep=rep1&type=pdf
[78] M. Santhanam, "UWB technology and its applications—A survey," M.S. thesis, School Eng., Jönköping Univ., Jönköping, Sweden, 2011.
[79] M. Ridolfi, S. Van de Velde, H. Steendam, and E. De Poorter, "Analysis of the scalability of UWB indoor localization solutions for high user densities," *Sensors*, vol. 18, no. 6, p. 1875, Jun. 2018, doi: 10.3390/s18061875.
[80] K. Khurshid and I. A. Khokhar, "Comparison survey of 4G competitors (OFDMA, MC CDMA, UWB, IDMA)," in *Proc. Int. Conf. Aerosp. Sci. Eng. (ICASE)*, Aug. 2013, pp. 1–7, doi: 10.1109/icase.2013.6785555.
[81] G. Irene and A. Rajesh, "A penta-band reject inside cut koch fractal hexagonal monopole UWB MIMO antenna for portable devices," *Prog. Electromagn. Res.*, vol. 82, pp. 225–235, 2018. [Online]. Available: https://www.jpier.org/PIERC/view/18020604/
[82] FCC. (2002). *Rules and Regulations of Ultra-Wideband Operation*. [Online]. Available: https://www.govinfo.gov/content/pkg/FR-2002-05-16/pdf/02-11929.pdf#page=5
[83] European Telecommunications Standards Institute. (2016). *Short Range Devices (SRD) Using Ultra Wide Band Technology (UWB); Harmonised Standard Covering the Essential Requirements of Article 3.2 of the Directive 2014/53/EU; Part 1: Requirements for Generic UWB Applications*. [Online]. Available: https://www.etsi.org/deliver/etsi_en/302000_302099/30206501/02.01.01_60/en_30206501v020101p.pdf
[84] (2019). *Regulatory Requirements for Ultra-Wideband Technology*. [Online]. Available: https://www.cetecom.com/en/news/regulatory-requirements-for-ultra-wideb and-technology/
[85] European Telecommunications Standards Institute. (2016). *Short Range Devices (SRD) Using Ultra Wide Band Technology (UWB); Harmonised Standard Covering the Essential Requirements of Article 3.2 of the Directive 2014/53/EU; Part 2: Requirements for UWB Location Tracking*. [Online]. Available: https://www.etsi.org/deliver/etsi_en/302000_302099/30206502/02.01.01_60/en_30206502v020101p.pdf
[86] *About FiRa Consortium*. Accessed: Jun. 1, 2021. [Online]. Available: https://www.firaconsortium.org/about/consortium
[87] *IEEE Standard for Low-Rate Wireless Networks–Amendment 1: Enhanced Ultra Wideband (UWB) Physical Layers (PHYs) and Associated Ranging Techniques*, IEEE Standard 802.15.4z-2020 (Amendment to IEEE Std 802.15.4-2020), 2020, pp. 1–174. [Online]. Available: https://ieeexplore.ieee.org/document/9179124
[88] Qorvo. (2020). *Qorvo Completes Acquisition of Decawave*. [Online]. Available: https://www.qorvo.com/newsroom/news/2020/qorvo-completes-acquisition-of-decawave
[89] A. R. J. Ruiz and F. S. Granja, "Comparing ubisense, bespoon, and decawave UWB location systems: Indoor performance analysis," *IEEE Trans. Instrum. Meas.*, vol. 66, no. 8, pp. 2106–2117, Aug. 2017.
[90] J. Kulmer, S. Hinteregger, B. Grosswindhager, M. Rath, M. S. Bakr, E. Leitinger, and K. Witrisal, "Using DecaWave UWB transceivers for high-accuracy multipath-assisted indoor positioning," in *Proc. IEEE Int. Conf. Commun. Workshops (ICC Workshops)*, May 2017, pp. 1239–1245. [Online]. Available: https://ieeexplore.ieee.org/document/7962828
[91] Q. Tian, K. I.-K. Wang, and Z. Salcic, "An INS and UWB fusion approach with adaptive ranging error mitigation for pedestrian tracking," *IEEE Sensors J.*, vol. 20, no. 8, pp. 4372–4381, Apr. 2020.
[92] I. Dotlic, A. Connell, H. Ma, J. Clancy, and M. McLaughlin, "Angle of arrival estimation using decawave DW1000 integrated circuits," in *Proc. 14th Workshop Positioning, Navigat. Commun. (WPNC)*, Oct. 2017, pp. 1–6, doi: 10.1109/wpnc.2017.8250079.
[93] M. Cimdins, S. O. Schmidt, and H. Hellbrück, "MAMPI-UWB—Multipath-assisted device-free localization with magnitude and phase information with UWB transceivers," *Sensors*, vol. 20, no. 24, p. 7090, Dec. 2020.
[94] Pozyx. (2021). *Positioning Mode*. [Online]. Available: https://docs.pozyx.io/enterprise/Positioning.1224016064.html
[95] (2021). *Exafore*. [Online]. Available: https://exafore.com
[96] Sewio. (2021). *Time Difference of Arrival*. [Online]. Available: https://www.sewio.net/uwb-technology/time-difference-of-arrival/
[97] Eliko. (2021). *Next-Generation Location Tracking*. [Online]. Available: https://www.eliko.ee/
[98] NXP. (2022). *Secure Ultra-Wideband (UWB)*. [Online]. Available: https://www.nxp.com/products/wireless/secure-ultra-wideband-uwb:UWB-TRIMENSION
[99] Apple. (2019). *Nearby Interactions With U1*. [Online]. Available: https://www.apple.com/fi/newsroom/2019/09/iphone-11-pro-and-iphone-11-pro-max-the-most-powerful-and-advanced-smartphones
[100] Samsung. (2019). *Key Industry Players the ASSA ABLOY Group, HID, NXP, Samsung, Bosch, Sony, LitePoint and TTA Establish FiRa Consortium to Drive Seamless User Experiences Using Ultra-Wideband Technology*. [Online]. Available: https://news.samsung.com/global/key-industry-players-the-assa-abloy-group-hid-nxp-samsung-bosch-sony-litepoint-and-tta-establish-fira-consortium-to-drive-seamless-user-experiences-using-ultra-wideband-technology
[101] Apple. (2021). *iPhone 11 Pro and iPhone 11 Pro Max: The Most Powerful and Advanced Smartphones*. [Online]. Available: https://developer.apple.com/nearby-interaction/
[102] Bosch. (2021). *Perfectly Keyless*. [Online]. Available: https://www.bosch-mobility-solutions.com/en/solutions/software-and-services/perfectly-keyless/
[103] P. Carbone, A. Cazzorla, P. Ferrari, A. Flammini, A. Moschitta, S. Rinaldi, T. Sauter, and E. Sisinni, "Low complexity UWB radios for precise wireless sensor network synchronization," *IEEE Trans. Instrum. Meas.*, vol. 62, no. 9, pp. 2538–2548, Sep. 2013, doi: 10.1109/tim.2013.2259101.
[104] H. Soganci, S. Gezici, and H. Poor, "Accurate positioning in ultra-wideband systems," *IEEE Wireless Commun.*, vol. 18, no. 2, pp. 19–27, Apr. 2011, doi: 10.1109/mwc.2011.5751292.
[105] W. Shule, C. M. Almansa, J. P. Queralta, Z. Zou, and T. Westerlund, "UWB-based localization for multi-UAV systems and collaborative heterogeneous multi-robot systems," *Proc. Comput. Sci.*, vol. 175, pp. 357–364, Jan. 2020, doi: 10.1016/j.procs.2020.07.051.
[106] S. P. Rana, M. Dey, H. U. Siddiqui, G. Tiberi, M. Ghavami, and S. Dudley, "UWB localization employing supervised learning method," in *Proc. IEEE 17th Int. Conf. Ubiquitous Wireless Broadband (ICUWB)*, Sep. 2017, pp. 1–5, doi: 10.1109/icuwb.2017.8250971.
[107] H. Zhang, X. Liu, T. A. Gulliver, and X.-R. Cui, "AOA estimation for UWB positioning using a mono-station antenna array," *J. Electron. Inf. Technol.*, vol. 35, no. 8, pp. 2024–2028, Feb. 2014, doi: 10.3724/sp.j.1146.2012.01639.
[108] X. D. Tu, H. Zhang, X. R. Cui, and X. Liu, "An improved mono-station UWB TOA/AOA positioning method," *Appl. Mech. Mater.*, vols. 229–231, pp. 1373–1376, Nov. 2012, doi: 10.4028/www.scientific.net/amm.229-231.1373.
[109] M. Stone. (Jan. 2021). *What is Ultra-Wideband Technology and How Does it Work?* [Online]. Available: https://insights.samsung.com/2021/01/25/what-is-ultra-wideband-and-how-does-it-work-2/
[110] M. Martalo, S. Perri, G. Verdano, F. De Mola, F. Monica, and G. Ferrari, "Improved UWB TDoA-based positioning using a single hotspot for industrial IoT applications," *IEEE Trans. Ind. Informat.*, vol. 18, no. 6, pp. 3915–3925, Jun. 2022.
[111] D. Neirynck, E. Luk, and M. McLaughlin, "An alternative double-sided two-way ranging method," in *Proc. 13th Workshop Positioning, Navigat. Commun. (WPNC)*, Oct. 2016, pp. 1–4, doi: 10.1109/wpnc.2016.7822844.

[112] Y. Cheng and T. Zhou, "UWB indoor positioning algorithm based on TDOA technology," in *Proc. 10th Int. Conf. Inf. Technol. Med. Educ. (ITME)*, Aug. 2019, pp. 777–782, doi: 10.1109/itme.2019.00177.
[113] R. Zandian and U. Witkowski, "Implementation challenges of synchronisation of UWB nodes in TDoA structures," in *Proc. Int. Conf. Indoor Positioning Indoor Navigat. (IPIN)*, Sep. 2018, pp. 1–8.
[114] J. Kolakowski, J. Cichocki, P. Makal, and R. Michnowski, "An ultra-wideband system for vehicle positioning," *Int. J. Electron. Telecommun.*, vol. 56, no. 3, pp. 247–256, Sep. 2010, doi: 10.2478/v10177-010-0032-1.
[115] P. Corbalán, G. P. Picco, and S. Palipana, "Chorus: UWB concurrent transmissions for GPS-like passive localization of countless targets," in *Proc. 18th Int. Conf. Inf. Process. Sensor Netw.*, Apr. 2019, pp. 133–144.
[116] S. Leugner, M. Pelka, and H. Hellbruck, "Comparison of wired and wireless synchronization with clock drift compensation suited for U-TDoA localization," in *Proc. 13th Workshop Positioning, Navigat. Commun. (WPNC)*, Oct. 2016, pp. 1–4, doi: 10.1109/wpnc.2016.7822846.
[117] S. Pittet, V. Renaudin, B. Merminod, and M. Kasser, "UWB and MEMS based indoor navigation," *J. Navigat.*, vol. 61, no. 3, pp. 369–384, Jun. 2008, doi: 10.1017/s0373463308004797.
[118] J. Blazek, J. Jiranek, and J. Bajer, "Indoor passive positioning technique using ultra wide band modules," in *Proc. Int. Conf. Mil. Technol. (ICMT)*, May 2019, pp. 1–5.
[119] M. Youssef, M. Mah, and A. Agrawala, "Challenges: Device-free passive localization for wireless environments," in *Proc. 13th Annu. ACM Int. Conf. Mobile Comput. Netw. (MobiCom)*. New York, NY, USA: Association for Computing Machinery, Sep. 2007, pp. 222–229.
[120] T. J. Daim and R. M. A. Lee, "A weighted least squares consideration for IR-UWB radar based device-free object positioning estimation for indoor environment," *Indonesian J. Electr. Eng. Comput. Sci.*, vol. 15, no. 2, p. 894, Aug. 2019, doi: 10.11591/ijeecs.v15.i2.pp894-901.
[121] C.-S. Chen, "A non-line-of-sight error mitigation method for location estimation," *Int. J. Distrib. Sensor Netw.*, vol. 13, no. 1, Jan. 2017, Art. no. 155014771668273, doi: 10.1177/1550147716682739.
[122] J. J. Caffery, "A new approach to the geometry of TOA location," in *Proc. Veh. Technol. Conf. Fall., IEEE VTS Fall VTC. 52nd Veh. Technol. Conf.*, 2000, pp. 1943–1949, doi: 10.1109/vetecf.2000.886153.
[123] Y. Zhang, J. Ren, and W. Chen, "A ToA-based location algorithm reducing the NLoS error under location-aware networks," in *Proc. 7th Int. Conf. Wireless Commun., Netw. Mobile Comput.*, Sep. 2011, pp. 1–4, doi: 10.1109/wicom.2011.6040577.
[124] Y. T. Chan and K. C. Ho, "A simple and efficient estimator for hyperbolic location," *IEEE Trans. Signal Process.*, vol. 42, no. 8, pp. 1905–1915, Aug. 1994, doi: 10.1109/78.301830.
[125] X. Wang, Z. Huang, F. Zheng, and X. Tian, "The research of indoor three-dimensional positioning algorithm based on ultra-wideband technology," in *Proc. 39th Chin. Control Conf. (CCC)*, Jul. 2020, pp. 5144–5149, doi: 10.23919/ccc50068.2020.9189061.
[126] V. Fox, J. Hightower, L. Liao, D. Schulz, and G. Borriello, "Bayesian filtering for location estimation," *IEEE Pervasive Comput.*, vol. 2, no. 3, pp. 24–33, Jul. 2003.
[127] R. E. Kalman, "A new approach to linear filtering and prediction problems," *J. Fluids Eng.*, vol. 82, no. 1, pp. 35–45, Mar. 1960, doi: 10.1115/1.3662552.
[128] G. A. Darbellay, "An estimator of the mutual information based on a criterion for conditional independence," *Comput. Statist. Data Anal.*, vol. 32, no. 1, pp. 1–17, Nov. 1999, doi: 10.1016/s0167-9473%2899%2900020-1.
[129] G. Schalk and E. C. Leuthardt, "Brain-computer interfaces using electrocorticographic signals," *IEEE Rev. Biomed. Eng.*, vol. 4, pp. 140–154, 2011, doi: 10.1109/rbme.2011.2172408.
[130] R. Faragher, "Understanding the basis of the Kalman filter via a simple and intuitive derivation [lecture notes]," *IEEE Signal Process. Mag.*, vol. 29, no. 5, pp. 128–132, Sep. 2012, doi: 10.1109/msp.2012.2203621.
[131] J. Hartikainen, A. Solin, and S. Särkkä, *Optimal Filtering With Kalman Filters and Smoothers—A Manual for MATLAB Toolbox EKF/UKF*, Aalto Univ., Espoo, Finland, 2011. [Online]. Available: http://citeseerx.ist.psu.edu/viewdoc/summary?doi=10.1.1.331.150
[132] Y. Bar-Shalom, X. R. Li, and T. Kirubarajan, *Estimation With Applications to Tracking and Navigation*. Hoboken, NJ, USA: Wiley, 2001.
[133] Y. Bar-Shalom, "Recursive tracking algorithms: From the Kalman filter to intelligent trackers for cluttered environment," in *Proc. IEEE Int. Conf. Control Appl. (ICCON)*, Apr. 1989, pp. 675–680, doi: 10.1109/iccon.1989.770605.
[134] S. J. Julier and J. K. Uhlmann, "Unscented filtering and nonlinear estimation," *Proc. IEEE*, vol. 92, no. 3, pp. 401–422, Mar. 2004, doi: 10.1109/JPROC.2003.823141.
[135] S. Sarkka, "On unscented Kalman filtering for state estimation of continuous-time nonlinear systems," *IEEE Trans. Autom. Control*, vol. 52, no. 9, pp. 1631–1641, Sep. 2007, doi: 10.1109/TAC.2007.904453.
[136] I. Ullah, Y. Shen, X. Su, C. Esposito, and C. Choi, "A localization based on unscented Kalman filter and particle filter localization algorithms," *IEEE Access*, vol. 8, pp. 2233–2246, 2020, doi: 10.1109/access.2019.2961740.
[137] D. Feng, C. Wang, C. He, Y. Zhuang, and X.-G. Xia, "Kalman-filter-based integration of IMU and UWB for high-accuracy indoor positioning and navigation," *IEEE Internet Things J.*, vol. 7, no. 4, pp. 3133–3146, Apr. 2020, doi: 10.1109/jiot.2020.2965115.
[138] W. You, F. Li, L. Liao, and M. Huang, "Data fusion of UWB and IMU based on unscented Kalman filter for indoor localization of quadrotor UAV," *IEEE Access*, vol. 8, pp. 64971–64981, 2020, doi: 10.1109/access.2020.2985053.
[139] P. Li, Y. Xu, T. Shen, and S. Bi, "INS/UWB integrated AGV localization employing Kalman filter for indoor LOS/NLOS mixed environment," in *Proc. Int. Conf. Adv. Mech. Syst. (ICAMechS)*, Aug. 2019, pp. 294–298, doi: 10.1109/icamechs.2019.8861620.
[140] L. Cheng, Z. Wu, B. Lai, Q. Yang, A. Zhao, and Y. Wang, "Ultra wideband indoor positioning system based on artificial intelligence techniques," in *Proc. IEEE 21st Int. Conf. Inf. Reuse Integr. Data Sci. (IRI)*, Aug. 2020, pp. 438–444, doi: 10.1109/iri49571.2020.00073.
[141] L. Cheng, H. Chang, K. Wang, and Z. Wu, "Real time indoor positioning system for smart grid based on UWB and artificial intelligence techniques," in *Proc. IEEE Conf. Technol. Sustainability (SusTech)*, Apr. 2020, pp. 1–7, doi: 10.1109/sustech47890.2020.9150486.
[142] C. He, C. Tang, and C. Yu, "A federated derivative cubature Kalman filter for IMU-UWB indoor positioning," *Sensors*, vol. 20, no. 12, p. 3514, Jun. 2020, doi: 10.3390/s20123514.
[143] G. De Angelis, A. Moschitta, and P. Carbone, "Positioning techniques in indoor environments based on stochastic modeling of UWB round-trip-time measurements," *IEEE Trans. Intell. Transp. Syst.*, vol. 17, no. 8, pp. 2272–2281, Aug. 2016, doi: 10.1109/tits.2016.2516822.
[144] N. Dwek, M. Birem, K. Geebelen, E. Hostens, A. Mishra, J. Steckel, and R. Yudanto, "Improving the accuracy and robustness of ultra-wideband localization through sensor fusion and outlier detection," *IEEE Robot. Autom. Lett.*, vol. 5, no. 1, pp. 32–39, Jan. 2020, doi: 10.1109/lra.2019.2943821.
[145] T. Otim, L. E. Díez, A. Bahillo, P. Lopez-Iturri, and F. Falcone, "Effects of the body wearable sensor position on the UWB localization accuracy," *Electronics*, vol. 8, no. 11, p. 1351, Nov. 2019, doi: 10.3390/electronics8111351.
[146] Y. Xu, Y. S. Shmaliy, Y. Li, and X. Chen, "UWB-based indoor human localization with time-delayed data using EFIR filtering," *IEEE Access*, vol. 5, pp. 16676–16683, 2017, doi: 10.1109/access.2017.2743213.
[147] B. Zhu, X. Tao, J. Zhao, M. Ke, H. Wang, and W. Deng, "An integrated GNSS/UWB/DR/VMM positioning strategy for intelligent vehicles," *IEEE Trans. Veh. Technol.*, vol. 69, no. 10, pp. 10842–10853, Oct. 2020, doi: 10.1109/tvt.2020.3014516.
[148] Y. Zhang, X. Tan, and C. Zhao, "UWB/INS integrated pedestrian positioning for robust indoor environments," *IEEE Sensors J.*, vol. 20, no. 23, pp. 14401–14409, Dec. 2020, doi: 10.1109/jsen.2020.2998815.
[149] M. Strohmeier, T. Walter, J. Rothe, and S. Montenegro, "Ultra-wideband based pose estimation for small unmanned aerial vehicles," *IEEE Access*, vol. 6, pp. 57526–57535, 2018, doi: 10.1109/access.2018.2873571.
[150] F. Wu and Z. Liu, "Research on UWB/IMU fusion positioning technology in mine," in *Proc. Int. Conf. Intell. Transp., Big Data Smart City (ICITBS)*, Jan. 2020, pp. 934–937, doi: 10.1109/icitbs49701.2020.00207.
[151] H. J. Kim, Y. Xie, H. Yang, C. Lee, and T. L. Song, "An efficient indoor target tracking algorithm using TDOA measurements with applications to ultra-wideband systems," *IEEE Access*, vol. 7, pp. 91435–91445, 2019.
[152] M. Vemula, M. F. Bugallo, and P. M. Djuric, "Performance comparison of Gaussian-based filters using information measures," *IEEE Signal Process. Lett.*, vol. 14, no. 12, pp. 1020–1023, Dec. 2007.
[153] G. Kitagawa, "A self-organizing state-space model," *J. Amer. Stat. Assoc.*, vol. 93, no. 443, p. 1203, Sep. 1998, doi: 10.2307/2669862.
[154] A. Haggenmiller, M. Krogius, and E. Olson, "Non-parametric error modeling for ultra-wideband localization networks," in *Proc. Int. Conf. Robot. Automat. (ICRA)*, May 2019, pp. 2568–2574.
[155] Q. Tian, K. I.-K. Wang, and Z. Salcic, "A resetting approach for INS and UWB sensor fusion using particle filter for pedestrian tracking," *IEEE Trans. Instrum. Meas.*, vol. 69, no. 8, pp. 5914–5921, Aug. 2020.

[156] Q. Tian, K. I.-K. Wang, and Z. Salcic, "A low-cost INS and UWB fusion pedestrian tracking system," *IEEE Sensors J.*, vol. 19, no. 10, pp. 3733–3740, May 15, 2019.
[157] S. Zhao, B. Huang, and F. Liu, "Localization of indoor mobile robot using minimum variance unbiased FIR filter," *IEEE Trans. Autom. Sci. Eng.*, vol. 15, no. 2, pp. 410–419, Apr. 2018.
[158] X. Fu and Y. Jia, "An improvement on resampling algorithm of particle filters," *IEEE Trans. Signal Process.*, vol. 58, no. 10, pp. 5414–5420, Oct. 2010, doi: 10.1109/tsp.2010.2053031.
[159] S. Thrun, D. Fox, W. Burgard, and F. Dellaert, "Robust Monte Carlo localization for mobile robots," *Artif. Intell.*, vol. 128, nos. 1–2, pp. 99–141, May 2001, doi: 10.1016/s0004-3702%2801%2900069-8.
[160] C. Xu, X. Wang, S. Duan, and J. Wan, "Spatial-temporal constrained particle filter for cooperative target tracking," *J. Netw. Comput. Appl.*, vol. 176, Feb. 2021, Art. no. 102913. [Online]. Available: https://www.sciencedirect.com/science/article/pii/S1084804520303726
[161] S. Lenser and M. Veloso, "Sensor resetting localization for poorly modelled mobile robots," in *Proc. Millennium Conf. IEEE Int. Conf. Robot. Automat. Symp. (ICRA)*, Apr. 2000, pp. 1225–1232, doi: 10.1109/robot.2000.844766.
[162] X. Zhu, J. Yi, J. Cheng, and L. He, "Adapted error map based mobile robot UWB indoor positioning," *IEEE Trans. Instrum. Meas.*, vol. 69, no. 9, pp. 6336–6350, Sep. 2020.
[163] Q. Tian, K. I.-K. Wang, and Z. Salcic, "Human body shadowing effect on UWB-based ranging system for pedestrian tracking," *IEEE Trans. Instrum. Meas.*, vol. 68, no. 10, pp. 4028–4037, Oct. 2019.
[164] S. Vandermeeren and H. Steendam, "PDR/UWB based positioning of a shopping cart," *IEEE Sensors J.*, vol. 21, no. 9, pp. 10864–10878, May 2021.
[165] N. Sünderhauf and P. Protzel, "Towards robust graphical models for GNSS-based localization in urban environments," in *Proc. Int. Multi-Conf. Syst., Signals Devices*, Mar. 2012, pp. 1–6.
[166] V. Indelman, S. Williams, M. Kaess, and F. Dellaert, "Factor graph based incremental smoothing in inertial navigation systems," in *Proc. 15th Int. Conf. Inf. Fusion*, Jul. 2012, pp. 2154–2161.
[167] T. Pfeifer and P. Protzel, "Expectation-maximization for adaptive mixture models in graph optimization," in *Proc. Int. Conf. Robot. Automat. (ICRA)*, May 2019, pp. 3151–3157.
[168] W. Wen, T. Pfeifer, X. Bai, and L. Hsu, "Factor graph optimization for GNSS/INS integration: A comparison with the extended Kalman filter," *Navigation*, vol. 68, no. 2, pp. 315–331, Jun. 2021. [Online]. Available: http://onlinelibrary.wiley.com/doi/abs/10.1002/navi.421
[169] W. Li, X. Cui, and M. Lu, "A robust graph optimization realization of tightly coupled GNSS/INS integrated navigation system for urban vehicles," *Tsinghua Sci. Technol.*, vol. 23, no. 6, pp. 724–732, Dec. 2018.
[170] Y. Song and L.-T. Hsu, "Tightly coupled integrated navigation system via factor graph for UAV indoor localization," *Aerosp. Sci. Technol.*, vol. 108, Jan. 2021, Art. no. 106370.
[171] R. Eberhart and J. Kennedy, "A new optimizer using particle swarm theory," in *Proc. 6th Int. Symp. Micro Mach. Hum. Sci. (MHS)*, 1995, pp. 39–43.
[172] J. Kennedy and R. Eberhart, "Particle swarm optimization," in *Proc. Int. Conf. Neural Netw. (ICNN)*, vol. 4, 1995, pp. 1942–1948.
[173] X. Cai, L. Ye, and Q. Zhang, "Ensemble learning particle swarm optimization for real-time UWB indoor localization," *EURASIP J. Wireless Commun. Netw.*, vol. 2018, no. 1, pp. 1–15, May 2018, doi: 10.1186/s13638-018-1135-0.
[174] H. Wu, J. Liu, Z. Dong, and Y. Liu, "A hybrid mobile node localization algorithm based on adaptive MCB-PSO approach in wireless sensor networks," *Wireless Commun. Mobile Comput.*, vol. 2020, Jun. 2020, Art. no. e3845407. [Online]. Available: https://www.hindawi.com/journals/wcmc/2020/3845407/
[175] Y. Wu, S. Ding, Y. Ding, and M. Li, "UWB base station cluster localization for unmanned ground vehicle guidance," *Math. Problems Eng.*, vol. 2021, Apr. 2021, Art. no. e6639574. [Online]. Available: https://www.hindawi.com/journals/mpe/2021/6639574/
[176] J. Khodjaev, Y. Park, and A. S. Malik, "Survey of NLOS identification and error mitigation problems in UWB-based positioning algorithms for dense environments," *Ann. Telecommun.-Annales des Télécommunications.*, vol. 65, nos. 5–6, pp. 301–311, Aug. 2009, doi: 10.1007/s12243-009-0124-z.
[177] I. Guvenc, C.-C. Chong, and F. Watanabe, "NLOS identification and mitigation for UWB localization systems," in *Proc. IEEE Wireless Commun. Netw. Conf.*, Mar. 2007, pp. 1571–1576, doi: 10.1109/wcnc.2007.296.
[178] Decawave. (2016). *DW1000 Metrics for Estimation of Non Line of Sight Operating Conditions*. [Online]. Available: https://www.decawave.com/wp-content/uploads/2018/10/APS006_Part-3-DW1000-Diagnostics-for-NLOS-Channels_v1.1.pdf
[179] M. Elsanhoury, J. Koljonen, P. Välisuo, M. Elmusrati, and H. Kuusniemi, "Survey on recent advances in integrated GNSSs towards seamless navigation using multi-sensor fusion technology," in *Proc. 34th Int. Tech. Meeting Satell. Division Inst. Navigat. (ION GNSS)*, Oct. 2021, pp. 2754–2765, doi: 10.33012/2021.17961.
[180] X. Guo, N. Ansari, F. Hu, Y. Shao, N. R. Elikplim, and L. Li, "A survey on fusion-based indoor positioning," *IEEE Commun. Surveys Tuts.*, vol. 22, no. 1, pp. 566–594, 1st Quart., 2020, doi: 10.1109/comst.2019.2951036.
[181] L. Guanke, Y. Jianan, Y. Wen, and Z. Yanling, "Research on seamless positioning of power wearables based on GPS/UWB combination," in *Proc. IEEE Int. Conf. Comput. Commun. Eng. Technol. (CCET)*, Aug. 2018, pp. 123–127, doi: 10.1109/ccet.2018.8542426.
[182] Y. Wang and X. Li, "The IMU/UWB fusion positioning algorithm based on a particle filter," *ISPRS Int. J. Geo-Inf.*, vol. 6, no. 8, p. 235, Aug. 2017, doi: 10.3390/ijgi6080235.
[183] J. F. Liu, J. X. Pu, L. F. Sun, and Z. S. He, "An approach to robust INS/UWB integrated positioning for autonomous indoor mobile robots," *Sensors*, vol. 19, no. 4, p. 950, Feb. 2019, doi: 10.3390/s19040950.
[184] R. D. Christ and R. L. Wernli, "Navigational Sensors," in *The ROV Manual*. Amsterdam, The Netherlands: Elsevier, 2014, pp. 453–475, doi: 10.1016/b978-0-08-098288-5.00017-8.
[185] J. Wang, Y. Gao, Z. Li, X. Meng, and C. M. Hancock, "A tightly-coupled GPS/INS/UWB cooperative positioning sensors system supported by V2I communication," *Sensors*, vol. 16, no. 7, p. 944, Jun. 2016, doi: 10.3390/s16070944.
[186] Q. Fan, B. Sun, Y. Sun, Y. Wu, and X. Zhuang, "Data fusion for indoor mobile robot positioning based on tightly coupled INS/UWB," *J. Navigat.*, vol. 70, no. 5, pp. 1079–1097, Apr. 2017, doi: 10.1017/s0373463317000194.
[187] J. Kim, G.-I. Jee, and J. G. Lee, "A federated Kalman filter design using a gain fusion algorithm," *IFAC Proc. Volumes*, vol. 31, no. 21, pp. 385–391, Aug. 1998, doi: 10.1016/s1474-6670%2817%2941107-4.
[188] N. A. Carlson and M. P. Berarducci, "Federated Kalman filter simulation results," *Navigation*, vol. 41, no. 3, pp. 297–322, Sep. 1994, doi: 10.1002/j.2161-4296.1994.tb01882.x.
[189] Y. Xu, G. Tian, and X. Chen, "Enhancing INS/UWB integrated position estimation using federated EFIR filtering," *IEEE Access*, vol. 6, pp. 64461–64469, 2018, doi: 10.1109/ACCESS.2018.2878101.
[190] Y. Xu, C. K. Ahn, Y. S. Shmaliy, X. Chen, and L. Bu, "Indoor INS UWB-based human localization with missing data utilizing predictive UFIR filtering," *IEEE/CAA J. Autom. Sinica*, vol. 6, no. 4, pp. 952–960, Jul. 2019, doi: 10.1109/jas.2019.1911570.
[191] H. Yang, T. Luo, W. Li, L. Li, Y. Rao, and C. Luo, "A stable SINS/UWB integrated positioning method of shearer based on the multi-model intelligent switching algorithm," *IEEE Access*, vol. 7, pp. 29128–29138, 2019, doi: 10.1109/access.2019.2898212.
[192] S. Pala, S. Jayan, and D. G. Kurup, "An accurate UWB based localization system using modified leading edge detection algorithm," *Ad Hoc Netw.*, vol. 97, Feb. 2020, Art. no. 102017, doi: 10.1016/j.adhoc.2019.102017.
[193] B. Hanssens, D. Plets, E. Tanghe, C. Oestges, D. P. Gaillot, M. Lienard, T. Li, H. Steendam, L. Martens, and W. Joseph, "An indoor variance-based localization technique utilizing the UWB estimation of geometrical propagation parameters," *IEEE Trans. Antennas Propag.*, vol. 66, no. 5, pp. 2522–2533, May 2018, doi: 10.1109/tap.2018.2810340.
[194] S. Monica and F. Bergenti, "Hybrid indoor localization using WiFi and UWB technologies," *Electronics*, vol. 8, no. 3, p. 334, Mar. 2019, doi: 10.3390/electronics8030334.
[195] A. Poulose and D. S. Han, "UWB indoor localization using deep learning LSTM networks," *Appl. Sci.*, vol. 10, no. 18, p. 6290, Sep. 2020, doi: 10.3390/app10186290.
[196] J. Park, S. Nam, H. Choi, Y. Ko, and Y.-B. Ko, "Improving deep learning-based UWB LOS/NLOS identification with transfer learning: An empirical approach," *Electronics*, vol. 9, no. 10, p. 1714, Oct. 2020, doi: 10.3390/electronics9101714.
[197] H. Wang, X. Wang, Y. Xue, and Y. Jiang, "UWB-based indoor localization using a hybrid WKNN-LSTM algorithm," in *Proc. IEEE 4th Inf. Technol., Netw., Electron. Automat. Control Conf. (ITNEC)*, Jun. 2020, pp. 1720–1725, doi: 10.1109/itnec48623.2020.9085050.

[198] X. Yang, F. Zhao, and T. Chen, "NLOS identification for UWB localization based on import vector machine," *AEU-Int. J. Electron. Commun.*, vol. 87, pp. 128–133, Apr. 2018, doi: 10.1016/j.aeue.2018.02.003.

[199] K. Yu, K. Wen, Y. Li, S. Zhang, and K. Zhang, "A novel NLOS mitigation algorithm for UWB localization in harsh indoor environments," *IEEE Trans. Veh. Technol.*, vol. 68, no. 1, pp. 686–699, Jan. 2019, doi: 10.1109/tvt.2018.2883810.

[200] S. Djosic, I. Stojanovic, M. Jovanovic, T. Nikolic, and G. L. Djordjevic, "Fingerprinting-assisted UWB-based localization technique for complex indoor environments," *Expert Syst. Appl.*, vol. 167, Apr. 2021, Art. no. 114188, doi: 10.1016/j.eswa.2020.114188.

[201] M. Lei, M. Jin, T. Huang, Z. Guo, Q. Wang, Z. Wu, Z. Chen, X. Chen, and J. Zhang, "Ultra-wideband fingerprinting positioning based on convolutional neural network," in *Proc. Int. Conf. Comput., Inf. Telecommun. Syst. (CITS)*, Oct. 2020, pp. 1–5, doi: 10.1109/cits49457.2020.9232628.

[202] S. Monica and G. Ferrari, "Improving UWB-based localization in iot scenarios with statistical models of distance error," *Sensors*, vol. 18, no. 5, p. 1592, May 2018, doi: 10.3390/s18051592.

[203] J. A. del Peral-Rosado *et al.*, "Whitepaper on new localization methods for 5G wireless systems and the Internet-of-Things," COST Action CA15104 (IRACON), IRACON-COST, Ottignies-Louvain-la-Neuve, Belgium, Tech. Rep. COST Action CA15104, 2018. [Online]. Available: http://www.iracon.org/wp-content/uploads/2018/03/IRACON-WP2.pdf

[204] F. Guidi, N. Decarli, D. Dardari, F. Natali, E. Savioli, and M. Bottazzi, "A low complexity scheme for passive UWB-RFID: Proof of concept," *IEEE Commun. Lett.*, vol. 20, no. 4, pp. 676–679, Apr. 2016, doi: 10.1109/lcomm.2016.2530658.

[205] A. Costanzo, D. Dardari, J. Aleksandravicius, N. Decarli, M. Del Prete, D. Fabbri, M. Fantuzzi, A. Guerra, D. Masotti, M. Pizzotti, and A. Romani, "Energy autonomous UWB localization," *IEEE J. Radio Freq. Identif.*, vol. 1, no. 3, pp. 228–244, Sep. 2017, doi: 10.1109/jrfid.2018.2792538.

[206] D. Shi, H. Mi, E. G. Collins, and J. Wu, "An indoor low-cost and high-accuracy localization approach for AGVs," *IEEE Access*, vol. 8, pp. 50085–50090, 2020, doi: 10.1109/access.2020.2980364.

[207] W. Wang, D. Marelli, and M. Fu, "Multiple-vehicle localization using maximum likelihood Kalman filtering and ultra-wideband signals," *IEEE Sensors J.*, vol. 21, no. 4, pp. 4949–4956, Feb. 2021, doi: 10.1109/jsen.2020.3031377.

[208] F. Lazzari, A. Buffi, P. Nepa, and S. Lazzari, "Numerical investigation of an UWB localization technique for unmanned aerial vehicles in outdoor scenarios," *IEEE Sensors J.*, vol. 17, no. 9, pp. 2896–2903, May 2017, doi: 10.1109/jsen.2017.2684817.

[209] J. Zhu, J. Yao, X. Zhu, Z. Li, Y. Ma, and A. Zou, "Research on substation safety monitoring system based on UWB positioning technology," in *Proc. IEEE 3rd Int. Conf. Inf. Syst. Comput. Aided Educ. (ICISCAE)*, Sep. 2020, pp. 332–334, doi: 10.1109/iciscae51034.2020.9236864.

[210] Y. Wang and X. Li, "The IMU/UWB fusion positioning algorithm based on a particle filter," *ISPRS Int. J. Geo-Inf.*, vol. 6, no. 8, p. 235, Aug. 2017, doi: 10.3390/ijgi6080235.

[211] D. Tian and Q. Xiang, "Research on indoor positioning system based on UWB technology," in *Proc. IEEE 5th Inf. Technol. Mechatronics Eng. Conf. (ITOEC)*, Jun. 2020, pp. 662–665, doi: 10.1109/itoec49072.2020.9141707.

[212] K. Minne, N. Macoir, J. Rossey, Q. Van den Brande, S. Lemey, J. Hoebeke, and E. De Poorter, "Experimental evaluation of UWB indoor positioning for indoor track cycling," *Sensors*, vol. 19, no. 9, p. 2041, May 2019, doi: 10.3390/s19092041.

[213] F. Che, A. Ahmed, Q. Z. Ahmed, S. A. R. Zaidi, and M. Z. Shakir, "Machine learning based approach for indoor localization using ultra-wide bandwidth (UWB) system for industrial Internet of Things (IIoT)," in *Proc. Int. Conf. U.K.-China Emerg. Technol. (UCET)*, Aug. 2020, pp. 1–4, doi: 10.1109/ucet51115.2020.9205352.

[214] W. Liu, J. Li, Q. Zeng, F. Guo, R. Wu, and X. Zhang, "An improved robust Kalman filtering strategy for GNSS kinematic positioning considering small cycle slips," *Adv. Space Res.*, vol. 63, no. 9, pp. 2724–2734, May 2019, doi: 10.1016/j.asr.2017.11.041.

[215] N. Xia and M. A. Weitnauer, "TDOA-based mobile localization using particle filter with multiple motion and channel Models," *IEEE Access*, vol. 7, pp. 21057–21066, 2019, doi: 10.1109/access.2019.2897936.

[216] J. L. C. Villacres, Z. Zhao, T. Braun, and Z. Li, "A particle filter-based reinforcement learning approach for reliable wireless indoor positioning," *IEEE J. Sel. Areas Commun.*, vol. 37, no. 11, pp. 2457–2473, Nov. 2019, doi: 10.1109/jsac.2019.2933886.

[217] G. M. Hoang, B. Denis, J. Härri, and D. Slock, "Bayesian fusion of GNSS, ITS-G5 and IR–UWB data for robust cooperative vehicular localization," *Comp. Rendus Phys.*, vol. 20, no. 3, pp. 218–227, Mar. 2019. [Online]. Available: https://www.sciencedirect.com/science/article/pii/S1631070519300246

[218] A. Minetto, A. Gurrieri, and F. Dovis, "A cognitive particle filter for collaborative DGNSS positioning," *IEEE Access*, vol. 8, pp. 194765–194779, 2020.

[219] S. Guler, M. Abdelkader, and J. S. Shamma, "Infrastructure-free multi-robot localization with ultrawideband sensors," in *Proc. Amer. Control Conf. (ACC)*, Jul. 2019, pp. 13–18, doi: 10.23919/acc.2019.8814678.

[220] S. C. Gheorghiu, K. Nagy-Betegh, R. H. Molnar, and R. C. Grammenos, "WALLSY: The UWB and SmartMesh IP enabled wireless ad-hoc low-power localization system," in *Proc. Int. Conf. Localization GNSS (ICL-GNSS)*, Jun. 2021, pp. 1–17, doi: 10.1109/icl-gnss51451.2021.9452247.

[221] A. Chehri, P. Fortier, and P. M. Tardif, "UWB-based sensor networks for localization in mining environments," *Ad Hoc Netw.*, vol. 7, no. 5, pp. 987–1000, Jul. 2009, doi: 10.1016/j.adhoc.2008.08.007.

[222] T.-M. Nguyen, A. Hanif Zaini, C. Wang, K. Guo, and L. Xie, "Robust target-relative localization with ultra-wideband ranging and communication," in *Proc. IEEE Int. Conf. Robot. Autom. (ICRA)*, May 2018, pp. 2312–2319, doi: 10.1109/icra.2018.8460844.

[223] L. Li, X. Guo, N. Ansari, and H. Li, "A hybrid fingerprint quality evaluation model for WiFi localization," *IEEE Internet Things J.*, vol. 6, no. 6, pp. 9829–9840, Dec. 2019, doi: 10.1109/jiot.2019.2932464.

[224] A. H. Salamah, M. Tamazin, M. A. Sharkas, and M. Khedr, "An enhanced WiFi indoor localization system based on machine learning," in *Proc. Int. Conf. Indoor Positioning Indoor Navigat. (IPIN)*, Oct. 2016, pp. 1–8, doi: 10.1109/ipin.2016.7743586.

[225] M. Nowicki and J. Wietrzykowski, "Low-effort place recognition with WiFi fingerprints using deep learning," in *Automation*. Cham, Switzerland: Springer, 2017, pp. 575–584, doi: 10.1007/978-3-319-54042-9_57.

[226] X. Wang and J. Shen, "Machine learning and its applications in visible light communication based indoor positioning," in *Proc. Int. Conf. High Perform. Big Data Intell. Syst. (HPBD&IS)*, May 2019, pp. 274–277, doi: 10.1109/hpbdis.2019.8735490.

[227] C. Loffler, S. Riechel, J. Fischer, and C. Mutschler, "Evaluation criteria for inside-out indoor positioning systems based on machine learning," in *Proc. Int. Conf. Indoor Positioning Indoor Navigat. (IPIN)*, Sep. 2018, pp. 1–8, doi: 10.1109/ipin.2018.8533862.

[228] T. Yuan, Y. Xu, Y. Wang, P. Han, and J. Chen, "A tilt receiver correction method for visible light positioning using machine learning method," *IEEE Photon. J.*, vol. 10, no. 6, pp. 1–12, Dec. 2018, doi: 10.1109/jphot.2018.2880872.

[229] H. Tran and C. Ha, "Improved visible light-based indoor positioning system using machine learning classification and regression," *Appl. Sci.*, vol. 9, no. 6, p. 1048, Mar. 2019, doi: 10.3390/app9061048.

[230] C.-H.-G. Li and Y.-M. Chang, "Automated visual positioning and precision placement of a workpiece using deep learning," *Int. J. Adv. Manuf. Technol.*, vol. 104, nos. 9–12, pp. 4527–4538, Aug. 2019. [Online]. Available: https://www.springerprofessional.de/en/automated-visual-positioning-and-precision-placement-of-a-workpi/17103994

[231] P. Sthapit, H.-S. Gang, and J.-Y. Pyun, "Bluetooth based indoor positioning using machine learning algorithms," in *Proc. IEEE Int. Conf. Consum. Electron.-Asia (ICCE-Asia)*, Jun. 2018, pp. 206–212, doi: 10.1109/icce-asia.2018.8552138.

[232] L. Zhang, N. Xiao, W. Yang, and J. Li, "Advanced heterogeneous feature fusion machine learning models and algorithms for improving indoor localization," *Sensors*, vol. 19, no. 1, p. 125, Jan. 2019, doi: 10.3390/s19010125.

[233] R. M. Faragher and R. K. Harle, "SmartSLAM—An efficient smartphone indoor positioning system exploiting machine learning and opportunistic sensing," in *Proc. 26th Int. Tech. Meeting Satell. Division Inst. Navigat. (ION GNSS)*, Sep. 2013, pp. 1006–1019. [Online]. Available: http://www.ion.org/publications/abstract.cfm?jp=p&articleID=11308

[234] Z. Li, K. Xu, H. Wang, Y. Zhao, X. Wang, and M. Shen, "Machine-learning-based positioning: A survey and future directions," *IEEE Netw.*, vol. 33, no. 3, pp. 96–101, May 2019, doi: 10.1109/mnet.2019.1800366.

[235] I.-H. Li, W.-Y. Wang, C.-Y. Li, J.-Z. Kao, and C.-C. Hsu, "Cloud-based improved Monte Carlo localization algorithm with robust orientation estimation for mobile robots," *Eng. Computations*, vol. 36, no. 1, pp. 178–203, Dec. 2018.

[236] J. J. Khalife and Z. M. Kassas, "Receiver design for Doppler positioning with leo satellites," in *Proc. IEEE Int. Conf. Acoust., Speech Signal Process. (ICASSP)*, May 2019, pp. 5506–5510.

MAHMOUD ELSANHOURY (Graduate Student Member, IEEE) received the B.Sc. degree in telecommunications engineering from Alexandria University, Egypt, in 2013, and the M.Sc. (Tech) degree in telecommunications engineering from the University of Vaasa, Finland, in 2018, where he is currently pursuing the Ph.D. degree in computer science. From 2017 to 2018, he worked as a Research Assistant at the University of Vaasa. In spring 2017, he worked as an Autonomous Robots Lecturer at the Swedish NOVIA University of Applied Sciences. Recently in 2021, he conducted a two-month research visit to American University in Cairo (AUC) to exchange research ideas around UWB and LEO positioning. His current research interests include ubiquitous indoor positioning systems, ultra-wideband (UWB) indoor localization, low-earth orbit (LEO) satellites for positioning, multi-sensor fusion technologies, Kalman filters, and machine learning algorithms.

PETTERI MÄKELÄ received the M.Sc. (Tech) degree in computer science from the Helsinki University of Technology, Finland, in 1994, and the Lic.Sc. (Tech) degree in electrical engineering from the Tampere University of Technology, Finland, in 2008. He is currently pursuing the Ph.D. degree with the University of Vaasa. He worked for more than ten years in product development of GNSS-based systems in industry before establishing a career with the Seinäjoki University of Applied Sciences, Finland. He is also working as a Principal Lecturer with the Seinäjoki University of Applied Sciences. His research interests include positioning technologies, the industrial IoT, and software engineering.

JANNE KOLJONEN was born in Vaasa, Finland, in 1980. He received the M.S. and Ph.D. degrees in automation technology from the University of Vaasa, Finland, in 2004 and 2010, respectively.

He has been working in various research and teaching tasks with the University of Vaasa, since 2002. He is currently working as a Laboratory Engineer and a Program Manager with the University of Vaasa. He has authored more than 40 scientific articles.

PETRI VÄLISUO received the M.Sc. (Tech) degree in computer science from the Tampere University of Technology, Finland, in 1996, and the D.Sc. (Tech) degree in automation technology from the University of Vaasa, Finland, in 2011. He has worked for ten years in telecommunications industry before establishing a research career with the University of Vaasa. He is currently working as an Associate Professor (Tenure Track) of sustainable automation with the School of Technology and Innovation Management, University of Vaasa. He has authored or coauthored 27 peer-reviewed and more than ten other scientific publications. His research interests include ML, the IoT, positioning methods, and other technologies relevant to industrial automation.

AHM SHAMSUZZOHA received the master's degree in mechanical engineering, majoring in energy and environment from the University of Strathclyde, U.K., and the Ph.D. degree in industrial management from the University of Vaasa. He worked as an Assistant Professor at Sultan Qaboos University, Oman, and an Associate Professor at the Shahjalal University of Science and Technology, Bangladesh. He is currently working as an Assistant Professor (Tenure Track) with the Industrial Systems Analytics Program, School of Technology and Innovations and Digital Economy Research Platform, University of Vaasa. He is also involved in many European Union and nationally funded projects in Finland. His research interests include business and entrepreneurship, supply chain and logistics management, energy and environment, blockchain and precision positioning, digitalization, and green innovation.

TIMO MANTERE received the B.Sc. degree in electric power engineering from Vaasa Polytechnic, in 1992, and the M.Sc. degree in economics and business administration and the D.Sc. degree in computer science from the University of Vaasa, in 1996 and 2003, respectively. He is an expert in computer science and automation, mainly researching AI, ML, machine vision, signal processing, and software testing. He is currently working as a University Lecturer and an Associate Professor of computer science and automation systems with the University of Vaasa. He previously worked as a Lecturer at the Lappeenranta University of Technology. He has published approximately 80 scientific papers, articles, and presentations.

MOHAMMED ELMUSRATI (Senior Member, IEEE) received the B.Sc. and M.Sc. degrees (Hons.) in electrical and electronic engineering from the University of Benghazi, Libya, in 1991 and 1995, respectively, and the Licentiate of Science degree (Hons.) in technology and the D.Sc. degree in automation and control engineering from Aalto University, Finland, in 2002 and 2004, respectively.

He is currently a Full Professor of communication, automation, and digitalization at the School of Technology and Innovations, University of Vaasa, Finland. He has more than 145 publications, including articles, books, and book chapters. His research interests include various research topics, including wireless communications, AI, ML, biotechnology, big data analysis, stochastic systems, and game theory.

Dr. Elmusrati is an Active Member in different scientific societies, such as a member of the Society of Industrial and Applied Mathematics (SIAM) and a member of the Finnish Automation Society.

HEIDI KUUSNIEMI (Member, IEEE) received the M.Sc. (Hons.) and Ph.D. degrees in information technology from the Tampere University of Technology, Finland, in 2002 and 2005, respectively. She has more than 18 years of experience in research and development of positioning technologies. In 2016, she was selected as one of the 50 most inspiring technology leaders in Nordic countries. Part of her Ph.D. research was conducted at the Department of Geomatics Engineering, University of Calgary, Canada. She used to be a Visiting Scholar at Stanford University's GPS Laboratory, in 2017. She is currently the Director of the Digital Economy Research Platform and a Professor of computer science at the University of Vaasa, a Research Professor at the Finnish Geospatial Research Institute, National Land Survey of Finland, and an Adjunct Professor of satellite navigation at Tampere University and Aalto University, Finland. She is also active in the 'UN Women in Space' and 'Women in Tech' networks.

Publication P2

Indoor Asset Tracking in Dense Industrial Environments Using Low-cost Wireless Technologies

Mahmoud Elsanhoury[1], Jyri Nieminen[1], Petri Välisuo[1], Akpojoto Siemuri[1], Janne Koljonen[1], Mohammed Elmusrati[1] and Heidi Kuusniemi[1,2]

[1]*University of Vaasa, FI-65200 Vaasa, Finland.*
[2]*National Land Survey, Finnish Geospatial Institute, FI-02430 Masala, Finland.*

Abstract

Location based services are becoming abundant and more reliable in today's world thanks to the technological advancements achieved in the fields of positioning, navigation, and timing. Indoor asset tracking is an essential element of smart automation, warehousing, and manufacturing in industrial environments. Accurate indoor positioning systems (IPSs) exist with heavy financial costs depending on the degree of integrity required, consequently, numerous wireless based systems can be regarded as economical solutions. However, wireless positioning technologies suffer deep channel impairments especially in dense indoor venues that comprise various metallic and concrete structures. In this article, we showcase our work-in-progress research that studies a dense industrial environment in the context of indoor asset tracking. We experiment three potential wireless technologies: Ultra wideband (UWB), Bluetooth low energy (BLE) and Wi-Fi, to render a comparative assessment. Using a Multi-sensor fusion approach, we tend to complement the flaws in one technology with the merits of another, aided by physical quantity sensors like inertial motion units (IMUs). Moreover, we developed a machine learning optimization model to improve the results of the fusion based positioning scheme. The results are to be verified against millimeter-accurate reference measurements, then a seamless positioning scheme for indoor asset tracking can be achieved.

Keywords

Asset tracking, indoor navigation, wireless technologies.

1. Introduction

Modern technologies have transformed human life to new frontiers from individual and industrial perspectives. They facilitated what deemed to be inapplicable implementations from previous decades. Nowadays, new smart systems emerge on annual basis creating new opportunities for manufacturing, warehousing, and logistics.

Prior to the era of internet of things (IoT), indoor positioning and navigation became an important and vital element for Industry 4.0. Indoor positioning systems (IPSs) have seen a

WIPHAL 2023: Work-in-Progress in Hardware and Software for Location Computation, June 06–08, 2023, Castellon, Spain

mahmoud.elsanhoury@uwasa.fi (M. Elsanhoury); jyri.nieminen@uwasa.fi (J. Nieminen); petri.välisuo@uwasa.fi (P. Välisuo); akpojoto.siemuri@uwasa.fi (A. Siemuri); janne.koljonen@uwasa.fi (J. Koljonen); mohammed.elmusrati (M. Elmusrati); heidi.kuusniemi@uwasa.fi (H. Kuusniemi)
0000-0002-9195-4613 (M. Elsanhoury); 0000-0002-9566-6408 (P. Välisuo); 0000-0002-2644-1985 (A. Siemuri); 0000-0001-5834-4437 (J. Koljonen); 0000-0001-9304-6590 (M. Elmusrati); 0000-0002-7551-9531 (H. Kuusniemi)

technological leap and been extensively developed since the commence of the new millennium. Moreover, asset tracking in industrial environments for people, robots, and equipment is highly dependent on reliable indoor positioning systems. Accurate and reliable IPSs come at huge initial and operating costs, consequently, other economical integrated solution have been sought. Radio frequency based technologies are promising solutions that compromise between the cost burden and performance metrics owing to their numerous advantages.

Wireless radio technologies such as ultra-wideband (UWB), Bluetooth low energy (BLE), and Wi-Fi were investigated and adopted by many industrial firms and research institutions [1]. The capabilities of wireless signals allow obstacle penetration in industrial venues, besides providing robust positioning estimations at acceptable levels of accuracy for real-time applications. However, wireless radio-based technologies suffer various channel impairments (e.g. multipath fading and interference), especially in dense environmental conditions which impose fluctuations in their performance as IPSs [2].

In this article, we present our work-in-progress research activities to cover a dense industrial environment (Technobothnia laboratory) in Vaasa, Finland. We aim to devise a reliable indoor positioning system that can support asset tracking of people, equipment, and mobile robots within the given industrial laboratory. Such venue is regularly used by universities, research institutes, regional and local corporations, and others on daily basis. Hence, a seamless positioning system will facilitate and automate numerous processes that benefit many lab visiting segments.

The rest of article is organized as follows: Section 2 describes the role of asset tracking in today's and future applications. Section 3 highlights the most important aspects around indoor positioning technologies, and introduces the potential ones to be adopted in the given context. Section 4 states the merits of utilizing Multi-sensor fusion approach to combine several IPS technologies. Section 5 focus on the role of machine learning algorithms in improving the overall IPS performance metrics. And then the Conclusions section followed by the references section.

2. Asset tracking in industrial venues

As the world approaches the fourth industrial revolution to enter the reign of internet of things (IoT) and everythings (IoE), smart manufacturing and warehousing become mainly dependent on asset tracking. Asset tracking in modern technology era is considered a backbone for smart logistics, smart delivery, smart shipping, and automated manufacturing. Industrial operators strive to keep real-time track of human resources, and robotic equipment especially inside large industrial environments. Challenging as it sounds, reliable asset tracking systems usually require higher levels of sophistication to guarantee the integrity and trustworthiness of the system. Eventually, a reliable asset tracking system could be developed at higher financial costs, in addition to compromising other performance metrics e.g. robustness, availability, scalability, and integrity.

In this article, we investigate some potential wireless technologies that could be adopted as asset tracking systems in the industrial complex of Technobothnia laboratory, Vaasa, Finland. Such dense industrial venue contain large-sized metallic structures comprising wall, tables,

Figure 1: Technobothnia laboratory, a dense industrial environment situated in Vaasa, Finland.

chairs, machines, and tools, besides other materials as concrete walls, wooden structures, etc. as shown in Figure 1.

3. Indoor positioning technologies

Indoor positioning and navigation are essential factors for asset tracking in industrial venues. Prior to building reliable indoor navigation systems, a reliable positioning technology should be identified, investigated and assessed. There exist numerous types of IPSs such as: light-based systems e.g. LASERs, RADAR based systems, ultrasound-based systems e.g. collision avoidance sensors, radio frequency based systems e.g. RFID, ZigBee, Wi-Fi, UWB, BLE, etc. All IPS technologies variate in terms of performance and feasibility, there is no single solution that fits all applications simultaneously, rather, IPS technology adoption is application-wise dependent.

For asset tracking, it is mainly concerned with personnel and robots. The tracking of humans should not necessarily be precise (sub-meter level of accuracy), rather, it is acceptable to get 1–3 meters error as fingerprinting technologies usually provide. However, for mobile robots and movable equipment, precise positioning is very important for real-time tracking due to the sophisticated responsibilities that are carried out by those machines. In this article, we investigate three potential wireless technologies that are fitting with the given environment. We selected UWB as precision positioning technology for robot tracking, in addition to BLE and Wi-Fi for human resources tracking.

3.1. Ultra wideband

UWB emerged as a precise positioning technology that can provide robust sub-meter accuracy suitable for real-time applications and personal area networks (PANs). It is a short range

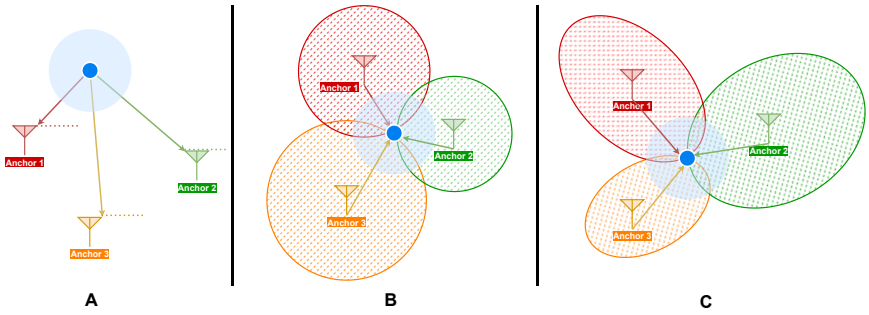

Figure 2: Positioning techniques. a) AoA, b) ToA and RSS and c) TDoA. In AoA, ToA and TDoA techniques, the user position (blue dot) is estimated from the intersection of the lines, circles and hyperbolas, respectively.

communication system with relatively short pulses that can enhance the signal penetration ability into light obstructions [1]. Moreover, UWB has a very large bandwidth (that is the reason for the term "ultra wide") spanning 3.1–10.6 GHz which provide higher capacity and data rates. The power consumption of UWB is relatively lower than most IPS technologies, which leverage the system with longer battery life and less electrical burden [2, 1].

UWB indoor positioning system comprise the use of anchors and tags transceivers, a minimum of three anchors and one tag is required for positioning [2, 1] in order to solve the positioning equations (three unknowns). A positioning technique should be defined and embedded in the system to perform the positioning process. Most commonly used techniques are: angle of arrival (AoA), time of arrival (ToA), time difference of arrival (TDoA), and the received signal strength (RSS) [3, 4]. The working principle differs depending on the positioning technique being used, eventually the positioning solution is obtained after applying selected estimation algorithms based on the formed geometrical shapes between all active anchors and the user tag, as shown in Figure 2.

In UWB, there exist numerous implementations of the mentioned positioning techniques such as: AoA, ToA and TDoA, however, the most commonly used techniques is the ToA. An approximated equation for 2D positioning estimation based on ToA is presented in Equations 1, as follows:

$$d_i = \sqrt{(x_i - x_k)^2 + (y_i - y_k)^2} \tag{1}$$

Where d_i is the measured direct distance between anchor i and the user tag, x_i and y_i are the Cartesian coordinates of the fixed anchor i, and x_k and y_k are the Cartesian coordinates of the estimated user tag x-y position at a given time instant k, where $i = 0, 1, 2, 3, ...$

Some commercial manufacturers develop all techniques in a single UWB chip. Depending on the system vendor and the given environment, UWB range for coverage could reach up to 30 meters, and the positioning accuracy can be within 2–50 centimeters in many cases [1].

3.2. Bluetooth low energy

BLE positioning technology was recently adopted by many IPS vendors for indoor applications e.g. smart homes, and smart logistics. BLE radio frequency system operates in the 2.4 GHz band, with close proximity to the Wi-Fi frequency standards. Moreover, BLE positioning is known with providing less power consumption, and more positioning accuracy in most cases [5].

Similar to UWB, BLE positioning system consists of Bluetooth anchors which in this case are called ”beacons”, in addition to a BLE user tag. However, BLE positioning is most commonly known to be dependent on RSS measurements to infer RSSI (RSS index), which is used to solve the final positioning solution. Translating RSSI into metric distance can be achieved via many approximating formulas, one of the commonly used formula is Equation 2, as follows [5]:

$$B_k = B_0 + 10\alpha log(d_k) + X_\sigma \tag{2}$$

Where B_k is the measured RSSI at a given k time instant, B_0 is the measured RSSI at the reference distance (one meter), α is the medium path loss exponent, d_k is the estimated distance in meter for a given k time instant, and X_σ is a random variable with standard deviation σ that represents a white zero-mean Gaussian noise.

The typical range of BLE technology is estimated to be between 0–25 meters, some researchers stated that BLE range could reach up to 100 meters depending on the density of the covered environment, and the positioning accuracy is within 1–3 meters in most cases [6]

3.3. Wi-Fi

Wi-Fi positioning is -by far- the most widely adopted IPS technology worldwide. Starting from an opportunistic approach, Wi-Fi access points which were primarily installed in indoor venues for Internet coverage, have been used for indoor positioning using RSS information. Later, new Wi-Fi access points were introduced as the old devices were upgraded and leveraged with positioning engines that analyze the sensed wireless signal attributes to provide fingerprinting solutions [7].

Similar to BLE, the working principle of Wi-Fi based positioning is centered around the RSS/RSSI information received from mobile devices and their MAC addresses, then, the positioning algorithms (e.g. Equation 2) provide the most-likely user position estimation [5]. The typical range of Wi-Fi positioning systems depends on the ranges of the utilized access points, also the typical positioning accuracy can be within 1–10 meters depending on the density of the given environment [5].

3.4. Inertial motion systems

Tracking assets in industrial venues requires additional degrees of confidence which can be obtained from retrieving more information about the moving object or person. Consequently, the use of inertial motion units (IMUs) became an effective factor in asset tracking for the extra information layer they provide. IMU sensors are physical-quantity instruments that measure the line and angular accelerations, Euler angles to infer the heading direction, and magnetism due to 3D Cartesian axes.

From a dead reckoning (DR) perspective, IMU lies at the foundation backbone of DR based positioning systems e.g. pedestrian dead reckoning (PDR). In modern IPS technologies, IMUs are most commonly used as an assisting technology to the primary IPS being used, that is, a Multi-sensor fusion approach.

4. Multi-sensor fusion techniques

Multi-sensor fusion is a computational procedure to fuse data from multiple sources in order to enrich the end-result information [8]. The concept of combining multiple IPS technologies has attracted the attention of IPS designers in order to improve the positioning resolution. As every IPS technology has its own merits and drawbacks, Multi-sensor fusion based positioning can be a key solution to minimize the overall IPSs errors. A single IPS technology could be complemented by additional IPS technologies either by loose or tight coupling schemes [9, 10].

Loose coupling integration scheme is obtained by combining the measurements of two or more IPS technologies such that no certain data source is affecting or influencing the measurements from other sources being integrated. Moreover, loose coupling is not dependent on sequencing, hence, any order of data measurements are accepted.

On the contrary, tight coupling scheme comprise the integration of two or more IPS technologies such that some data values are affected and influenced by other data sources being fused. Thus, tight coupling requires proper sequencing of data measurements i.e. place information into suitable order.

An example on loose coupling algorithm that fuses the measurements of UWB and IMU technologies is shown in Equation 3:

$$\mathbf{y} = \begin{bmatrix} d_i = \sqrt{(p_i^x - s_i^x)^2 + (p_i^y - s_i^y)^2} \\ \phi_i = \mathbf{arctan2}(p_i^y - s_i^y / p_i^x - s_i^x) \end{bmatrix} + \begin{bmatrix} n_1 \\ n_2 \end{bmatrix} \tag{3}$$

Where $\mathbf{y}$ is the state-space measurement vector, d_i is the hypotenuse distance from the user to the measuring device, p_i^x and p_i^y denote the positioning states in x-y coordinates at time instant i, s_i^x and s_i^y denote the measured slant distances from UWB sensors in x-y coordinates at time instant i, ϕ_i is the measured heading angle from IMU sensor at time instant i, n_1 and n_2 are the Gaussian noise figures associated with both sensors respectively.

Then, the loosely coupled algorithm (UWB/IMU) proceeds to calculate the predicted state-space estimation of the Multi-sensor fusion solution using the discretized Euler-Maruyama Equation 4 as follows:

$$\begin{bmatrix} p_{i+1}^x \\ p_{i+1}^y \\ \phi_{i+1} \end{bmatrix} = \begin{bmatrix} p_i^x \\ p_i^y \\ \phi_i \end{bmatrix} + \begin{bmatrix} v_i \, cos(\phi_i)\Delta t \\ v_i \, sin(\phi_i)\Delta t \\ \omega_i \Delta t \end{bmatrix} + \begin{bmatrix} e_1 \\ e_2 \\ e_3 \end{bmatrix} \tag{4}$$

Where p_{i+1}^x and p_{i+1}^y are future predictions of the next x-y position, ϕ_{i+1} is the prediction for the next heading (orientation) angle, v_i is the line velocity of the moving object, Δt is the given time step, ω_i denotes the measured angular velocity by IMU, and $e_1\, e_2\, e_3$ are the normalized Gaussian noise vector per each state space estimation respectively.

The main advantage of Multi-sensor fusion approach is to resolve the drawbacks of each IPS technology by integrating with other assisting technologies, also combat the effect of data outliers that are usually caused by systematic errors or non-line-of-sight (NLOS) conditions. Another prominent solution that has been widely adopted to optimize IPS performance in NLOS situations is by using machine learning algorithms.

5. Machine learning optimizations

Outliers are those data points that are significantly different from the rest of the dataset. Inconsistency in data entry or erroneous observations can result in outliers in a dataset. Outliers are usually referred to as abnormal observations which can cause skews in the data distribution.

Although outliers are usually considered erroneous data, they may also carry some important information. Therefore, the outlier detection techniques should cope with the outliers instead of just removing them.

Outlier detection approaches can be classified based on the machine learning algorithms being used. These classifications include clustering-based approaches, classification-based approaches, dimension-reduction-based approaches, and hybrid approaches that combine multiple technologies together [11].

In this paper, we would implement these four classification approaches, then analyze and compare the results in the context of the improvement of the accuracy of indoor positioning.

The planned steps to render the machine learning-based optimization task in our study, are provided as follows:

- Defining the outlier: The data point that is unusual and differs significantly from other data points.
- Outlier detection: We will implement a machine learning model to find whether the training data is polluted by outliers.
- Novelty detection: Investigate if a new unseen observation is an outlier or not. Here, the training data may or may not be polluted with outliers and we are interested in finding whether a new unseen observation is an outlier or not. If that observation is an outlier, we refer to it as a novelty.
- Anomaly detection: We will combine both outlier detection and novelty detection.

All the models used would be trained with a percent of the observed data, then the trained models would be evaluated using the whole (100 % of the) dataset instead of only the remaining percent of the test dataset. This is essential because our task is aimed at differentiating the outlier and normal data from the whole dataset, not just part of it.

The results of the outlier detection process will be evaluated using assessment metrics such as precision, recall, F1 score, and accuracy. Furthermore, we will also evaluate the results by plotting the receiver operating character curve (ROC).

Initial evaluation of the UWB dataset collected can be seen to have very distorted data points compared to the Omron robot data points used as the ground truth. From investigation, we discovered that the data collection synchronization could cause this significant offset in the data points between the UWB and Omron robot. Applying smoothing with the Savitzky-Golay

filter is used to eliminate noise in the UWB signal and improve the smoothness of a signal trend as seen in Figure 3. The filter is used to calculate a polynomial fit of each window based on polynomial degree and window size. Several window sizes were implemented as seen in Table 1. Figure 3 shows the data point route for a window size of 53.

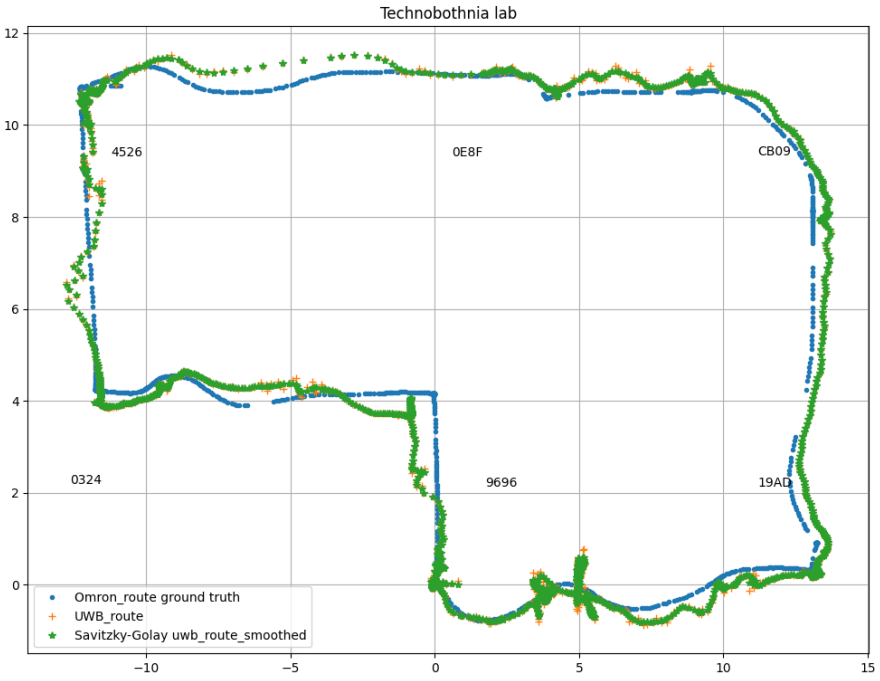

Figure 3: Indoor route in Technobothnia laboratory (Savitzky-Golay filter with a window size of 53).

The error was seen to be significant as a result of the unsynchronized data collection even after applying the Savitzky-Golay filter as seen in Table 1.

Table 1
Mean Square Error (MSE) measurement offset between the UWB route and the Omron ground truth route.

UWB route	Savitzky-Golay Smoothed UWB route			Linear regression
	window size 53	window size 63	window size 93	offset predictor
30.3541	30.3420	30.3390	30.3171	0.5253

Applying a Linear regression (LR) model to the dataset to predict the offset can help improve the error measurement. The LR model was trained on the Omron [x,y] and UWB [x,y] positions

and the offsets between the Omron and UWB data points [diff X and diff Y] were used as the target. The resultant mean square error (MSE) for the LR models is 0.52527 as seen in Table 1.

The initial results look promising and we plan to implement a synchronized data collection procedure to reduce the initial offset before applying outlier detection and offset prediction ML models to improve the position estimation of the proposed indoor positioning system.

6. Integrity of indoor navigation systems

Indoor navigation systems and IPSs need to be assessed against certain performance metrics to guarantee the best quality of service and ensure security against hazardous situations. The integrity of IPSs can be described as the degree of trustworthiness that can be allocated to the received information from a given navigational system [12].

System accuracy is often perceived as the most important metric in IPSs, however, integrity culminates all other performance metrics such as: accuracy, availability, and continuity. Accuracy is the degree of matching of the estimated positioning results to the given ground truth data. And, availability is the up-time duration in which the IPS could be usable. While, continuity is the ability of an IPS to maintain the designed service level during the up-time [8].

In our implementations, we devised a Multi-sensor fusion plan to maintain all previously defined metrics, that is, to achieve an IPS with a high integrity score. In a challenging environment as the given industrial laboratory, keeping the system accuracy, availability and continuity within the desired service levels is very important as it is also very challenging. Furthermore, the hardware part of the ongoing implementation is being backed up with numerous software remedies that comprise minimized cost functions, data cleaning formulas, estimation algorithms, and machine learning optimizations.

7. Conclusions

Seamless indoor navigation is a very crucial element for various smart applications and use cases (e.g. smart logistics and IoT) in industrial and civilian sectors. The designing of integrated IPSs in industrial premises requires some sophisticated modelling for the dense environment in which the IPS is expected to operate. In this article, we briefed the reader about our work-in-progress research to develop an integrated IPS to be used by humans and mobile robots for reliable asset tracking in industrial venues. In addition to the selected potential IPS technologies, we also provided an overall view about our algorithmic toolbox to maintain high degrees of performance and maximize the system integrity.

References

[1] M. Elsanhoury, P. Mäkelä, J. Koljonen, P. Välisuo, A. Shamsuzzoha, T. Mantere, M. Elmusrati, H. Kuusniemi, Precision positioning for smart logistics using ultra-wideband technology-based indoor navigation: A review, IEEE Access 10 (2022) 44413–44445. doi:10.1109/ACCESS.2022.3169267.

[2] A. Alarifi, A. S. Al-Salman, M. Alsaleh, A. Alnafessah, S. Alhadhrami, M. A. Al-Ammar, H. S. Al-Khalifa, Ultra wideband indoor positioning technologies: Analysis and recent advances †, Sensors (Basel, Switzerland) 16 (2016).

[3] S. N. A. Ahmed, Y. Zeng, Uwb positioning accuracy and enhancements, in: TENCON 2017 - 2017 IEEE Region 10 Conference, 2017, pp. 634–638. doi:10.1109/TENCON.2017.8227939.

[4] Z. Silvia, C. Martina, S. Fabio, P. Alessandro, Ultra wide band indoor positioning system: analysis and testing of an ips technology, IFAC-PapersOnLine 51 (2018) 1488–1492. doi:https://doi.org/10.1016/j.ifacol.2018.08.292, 16th IFAC Symposium on Information Control Problems in Manufacturing INCOM 2018.

[5] H. Zou, Z. Chen, H. Jiang, L. Xie, C. J. Spanos, Accurate indoor localization and tracking using mobile phone inertial sensors, wifi and ibeacon, 2017 IEEE International Symposium on Inertial Sensors and Systems (INERTIAL) (2017) 1–4.

[6] Bluetooth location tracking & positioning, 2023. URL: www.inpixon.com/technology/standards/bluetooth-low-energy.

[7] Q. Wang, J. Li, X. Luo, C. Chen, Fusion algorithm of wifi and imu for indoor positioning, in: 2022 3rd International Conference on Information Science, Parallel and Distributed Systems (ISPDS), 2022, pp. 349–354. doi:10.1109/ISPDS56360.2022.9874146.

[8] M. Elsanhoury, J. Koljonen, P. Välisuo, M. Elmusrati, H. Kuusniemi, Survey on recent advances in integrated GNSSs towards seamless navigation using multi-sensor fusion technology, in: Proceedings of the 34th International Technical Meeting of the Satellite Division of The Institute of Navigation (ION GNSS+ 2021), Institute of Navigation, 2021. URL: https://doi.org/10.33012/2021.17961. doi:10.33012/2021.17961.

[9] P. Srinivas, A. Kumar, Overview of architecture for gps-ins integration, in: 2017 Recent Developments in Control, Automation & Power Engineering (RDCAPE), 2017, pp. 433–438. doi:10.1109/RDCAPE.2017.8358310.

[10] Y. Luo, C. Yu, B. Xu, J. Li, G.-J. Tsai, Y. Li, N. El-Sheimy, Assessment of ultra-tightly coupled gnss/ins integration system towards autonomous ground vehicle navigation using smartphone imu, in: 2019 IEEE International Conference on Signal, Information and Data Processing (ICSIDP), 2019, pp. 1–6. doi:10.1109/ICSIDP47821.2019.9173292.

[11] J. Jiang, G. Han, L. liu, L. Shu, M. Guizani, Outlier detection approaches based on machine learning in the internet-of-things, IEEE Wireless Communications 27 (2020) 53–59. doi:10.1109/MWC.001.1900410.

[12] N. Zhu, J. Marais, D. Bétaille, M. Berbineau, Gnss position integrity in urban environments: A review of literature, IEEE Transactions on Intelligent Transportation Systems 19 (2018) 2762–2778. doi:10.1109/TITS.2017.2766768.

Publication P3

2023 13th International Conference on Indoor Positioning and Indoor Navigation (IPIN)

Precise Indoor Positioning System for Mobile Robots via Smoothed UWB/IMU Sensor Fusion

Mahmoud Elsanhoury
Digital Economy Platform
University of Vaasa
Vaasa, Finland
0000-0002-9195-4613
first.lastname@uwasa.fi

Jyri Nieminen
VEBIC Platform
Digital Economy Platform
University of Vaasa
Vaasa, Finland
0009-0001-5477-3792
first.lastname@uwasa.fi

Petri Välisuo
School of Technology and Innovations
Digital Economy Platform
University of Vaasa
Vaasa, Finland
0000-0002-9566-6408
first.lastname@uwasa.fi

Akpojoto Siemuri
Digital Economy Platform
University of Vaasa
Vaasa, Finland
0000-0002-2644-1985
first.lastname@uwasa.fi

Janne Koljonen
School of Technology and Innovations
University of Vaasa
Vaasa, Finland
0000-0001-5834-4437
first.lastname@uwasa.fi

Mohammed Elmusrati
School of Technology and Innovations
University of Vaasa
Vaasa, Finland
0000-0001-9304-6590
first.lastname@uwasa.fi

Heidi Kuusniemi
Digital Economy Platform
School of Technology and Innovations
University of Vaasa
Vaasa, Finland
0000-0002-7551-9531
first.lastname@uwasa.fi

2023 13th International Conference on Indoor Positioning and Indoor Navigation (IPIN) | 979-8-3503-2011-4/23/$31.00 ©2023 IEEE | DOI: 10.1109/IPIN57070.2023.10332542

***Abstract*—Indoor positioning systems (IPSs) are the foundations for all indoor location-based services and applications. In this article, we present a precise and robust IPS using ultra wide-band (UWB) technology fused with an inertial measurement unit (IMU). Both technologies are integrated to account for the non-line-of-sight (NLOS) problems arising in a dense challenging environment found within an industrial laboratory in Finland. Besides the conventional estimation techniques e.g. extended Kalman filter (EKF), we employ the Rauch-Tung-Striebel (RTS) smoothing algorithm in addition to a multivariate regression-based offset compensation method to improve the overall positioning accuracy of the system. The recommended number of distributed UWB anchors versus the coverage area is also discussed and tested in this article. The experiments were held by a patrolling mobile robot with millimeter accuracy, which acted as a ground truth reference to all used algorithms. The positioning estimation results showed a superior performance by the proposed method (UWB/IMU EKF-RTS-LR) with mean accuracy of 4.7 cm, and 9.6 cm for more than 95% of the time.**

***Index Terms*—indoor positioning system (IPS), mobile robots, ultra-wideband (UWB), sensor fusion, inertial motion unit (IMU)**

I. Introduction

Indoor positioning systems (IPSs) play an important role in Industry 4.0 and Internet of Things (IoT) applications. They are the backbone of all indoor navigational and location-based applications found in e.g. smart logistics, asset tracking, smart manufacturing, healthcare applications, smart delivery, etc [1], [2]. However, IPSs face many challenges from various aspects. Primarily, a reliable IPS should achieve an acceptable level in performance metrics such as accuracy, availability, continuity, and integrity [3]. That is why, a reliable IPS usually imposes heavy costs for meeting all metrics to sufficient degrees, especially for certain sensitive applications such as smart manufacturing (e.g. forgery and 3D printing), and healthcare location-based equipment. Moreover, IPSs suffer from discontinuities especially the wireless-based technologies that are highly affected by the impairments of the propagation channel in addition to the blockage and signal denial in some environments, a problem that is very common in the IPS domain.

Fortunately, recent researches affirm that low-cost reliable positioning is feasible by employing one or more assisting resources to aid the primary IPS technology [4]. Thus, a reliable IPS is not necessarily dependent on a single technology, rather, multiple technologies could be fused together to complement the desired performance metrics and achieve reliable positioning estimations.

Sensor fusion is an integration of two or more technologies via computational methodologies that are bound by fusion algorithms such that the output information is maximized [5]. By nature, sensors are prone to systematic errors, biases, and drifts, consequently, sensor fusion methods help in the mitigation of errors as much as possible.

Within the campus of our research institute, the University of Vaasa, lies the reputable industrial venue of Technobothnia, a modern laboratory that serves a minimum of five universities in addition to numerous corporations in the region. This industrial venue consists of several laboratories for all kinds of technical sciences e.g. industrial robotics, smart operations, mobile robots, chemistry labs, heavy-duty 3D printing machines, telecommunications equipment, etc. The visiting traffic is high, hence, an indoor positioning system will be very beneficial to both human operators and robot assets inside the lab. However, the allocated resources are limited to low-cost IPS systems that are based on wireless technologies

2023 13th International Conference on Indoor Positioning and Indoor Navigation (IPIN)

e.g. ultra wide-band (UWB), Wi-Fi, Bluetooth low energy (BLE). An UWB system and an inertial measurement unit (IMU) are selected as the elements of the precise IPS in Technobothnia, with UWB as the primary technology, and IMU as the assisting sensor fusion unit. For later use, Wi-Fi and BLE were considered for future IPSs that shall track assets within 2-3 meters of accuracy.

The fusion of UWB/IMU is abundant in recent IPS literature. Ali *et.al.* showed that the UWB-IMU combination with adaptive Kalman Filter can be used for precision pedestrian positioning even in occasional non line of sight (NLOS) situations [6]. Additional smoothing methods have been shown to improve the precision of the UWB/IMU fusion based positioning in some cases [7]. UWB/IMU positioning can be also fused with many other sensors, such as cellular phone signals, to increase the positioning accuracy and robustness [8]. With fault-tolerant additions, the UWB/IMU combination can be used in demanding mission-critical environments such as coal mines [9], [10]. A more detailed literature review about fusion-based positioning (focusing on UWB/IMU integration) is presented in [2].

The rest of article is organized as follows: Section II describes the main objectives of this research, and the essential embedded elements (software and hardware) to build the IPS system. Section III explains more aspects about the methodology, devices configurations, and the overall setup of the environment. Section IV discusses the output results and provides technical interpretations, evaluations, and commentaries on the applied performance metrics. Followed by a "Conclusion" section to highlight the achievements and potential future work.

II. Fusion Technique

The main objective in this study, is to achieve a reliable IPS with the most possible degree of precision positioning for mobile robots inside the industrial laboratory of Technobothnia, situated in Vaasa - Finland. Since the environment is dense and challenging, the solution had to be through the multisensor fusion technique to keep the overall cost under the budget limits allocated for the IPS. As described in [2], a low-cost system can be built from a single precise wireless technology such as UWB then fused with an assisting technology, that is, IMU to correct the biased, missing, and null values caused by NLOS conditions especially in dense environments. Thus, a loosely-coupled UWB/IMU integrated scheme was implemented as a precise IPS for mobile robots in the selected venue. A floor plan of the experiment area at Technobothnia laboratory is illustrated in Figure 1.

A. Positioning sensors

A Decawave laboratory kit MDEK1001 [11] was utilized to build the UWB positioning system inside our industrial laboratory environment, Technobothnia. Our setup for the MDEK1001 system consisted of one movable tag, and 6 evenly distributed anchors to cover the experimental area of 28x15 squared meters evenly, an additional seventh anchor

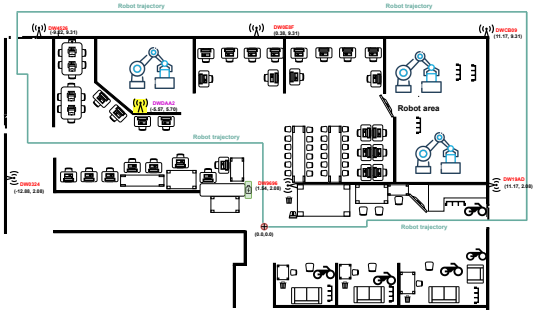

Fig. 1. Floor plan of Technobothnia laboratory with the planned robot trajectory. The highlighted location (yellow) is reserved for the tentative seventh UWB anchor. Battery-like block refers to the robot's docking station.

(DAA2) was inserted at some point to investigate the performance of 6 Vs 7 anchors and the effect of adding more anchors to the setup, which will be discussed in the results sections. The default settings of the Decawave kit are programmed to provide raw distance measurements between the moving tag and a maximum of four anchors (constrains from Decawave) based on the time of arrival (ToA) two-way ranging (TWR) technique, in addition to providing the final EKF estimates of the tag position [11].

Besides, an inertial measurement unit (IMU) sensor Xsens MTi-630 was used to obtain the inertial data of the movable robot such as: orientation, rate of turn, acceleration, and magnetism. The IMU sensor provided another layer of information about the movement of the robot inside the dense environment, thus, accounting for the NLOS situations and helping in inferring the missing data to improve the output fusion-based positioning estimations.

Both UWB and IMU sensors were placed onboard an autonomous mobile robot developed by OMRON (as shown in Figure 2), which possesses numerous positioning sensors such as: LASERs, ultrasound, RADARs, IMU, and LiDARs. The positioning data obtained from the OMRON robot had a millimeter accuracy with a confidence score of more than 90% most of the time (as stated by the built-in robot controller system), hence, it acted as the reference ground truth to our UWB/IMU fusion system.

As shown in Figure 1, a dense industrial environment comprising robots, metallic structures, and concrete materials was selected to test our hypothetical approach for precise indoor fusion-based positioning. The co-ordinal locations of the six UWB anchors are evenly distributed around the venue (area: 28x15 square meters), the seventh UWB anchor highlighted in yellow, was inserted to check the sufficiency of using 6 Vs 7 anchors. The planned robot trajectory was selected to be a multi-modal route i.e. mixed paths of clear and obscured lines of sight (LOS) between the user tag and the fixed anchors, to test the reliability of the system in complex conditions.

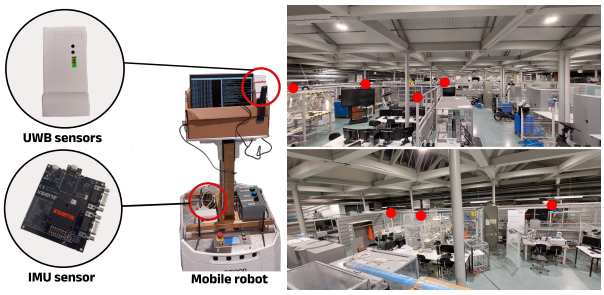

Fig. 2. Embedded elements of the designed IPS showing UWB anchors and tag (Decawave), IMU sensor (XSENS), the fusion software (laptop), and the mobile robot (OMRON). The red dots refer to the locations of fixed UWB anchors, including an additional spot for the tentative seventh anchor.

B. Algorithms

A set of algorithms was selected and applied to sensor readings locally (per sensor) and globally (fusion) in order to achieve more accurate positioning estimations.

1) Dead Reckoning (DR): is widely used in positioning and navigation applications even before the invention of modern localization systems, nowadays the most well-known implementation of DR is the pedestrian dead reckoning (PDR) algorithm which is employed in numerous location-based applications. In this method, we utilized the DR algorithm to fix the blank and null values arriving from UWB sensor readings by incorporating the previous non-null values and the heading angle into the DR estimation of the current missing epoch, as illustrated in Equations (1).

$$\begin{aligned} D_k &= \sqrt{(p^x_{k-2} - p^x_{k-1})^2 + (p^y_{k-2} - p^y_{k-1})^2} \\ \phi_k &= \arctan2\left(\frac{p^y_{k-2} - p^y_{k-1}}{p^x_{k-2} - p^x_{k-1}}\right) \\ p^x_k &= p^x_{k-1} + D_k \cos(\phi_k) \\ p^y_k &= p^y_{k-1} + D_k \sin(\phi_k) \end{aligned} \tag{1}$$

where p^x_k and p^y_k are the x-y positions at time instant k, D_k and ϕ_k are the calculated Euclidean distance and the heading angle from the previous two x-y positions, respectively.

2) Extended Kalman Filter (EKF): is a nonlinear state-space estimation algorithm that is typically used for 2-D and 3-D positioning estimations. In Decawave UWB devices, the system already contains a built-in EKF module that outputs the final filtered data after processing raw ToA measurements from anchors. However, UWB readings are fluctuating around a mean value, which requires further filtration. To this aim, the output positioning values from the Decawave system are fused with the data from the IMU sensor to mitigate the residuals via another layer of EKF Fusion algorithm that combines both information. EKF algorithm proceeds with two steps: the **prediction** step where the prior state mean and covariance are predicted before checking the measurements vector, and the **update** step in which the posterior state mean and covariance are updated after checking the measurements vector. The complete set of formulas employed for the fusion is shown in Equations (2) [12].

$$\begin{aligned} m_k^- &= f(m_{k-1}, k-1) \\ P_k^- &= F_x\, P_{k-1} {F_x}^T + Q_{k-1} \\ V_k &= y_k - h(m_k^-, k) \\ S_k &= H_x\ P_k^-\ {H_x}^T + R_k \\ K_k &= P_k^-\ {H_x}^T\ S_k^{-1} \\ m_k &= m_k^- + K_k V_k \\ P_k &= P_k^- - K_k S_k K_k^T \end{aligned} \tag{2}$$

where $m_{\bar{k}}$ and $P_{\bar{k}}$ are the prior state predicted mean and covariance at time instant k, respectively, m_k and P_k are the posterior state estimated mean and covariance. y_k is the measurements vector at time instant k, and S_k is the measurement prediction covariance. K_k is the filter gain, $f(.)$ and $h(.)$ are the dynamic nonlinear functions of the state-space model and the measurements model, respectively.

For the EKF fusion filter, the state-space vector $\mathbf{x_k}$ comprises the x-y positions, velocities, and accelerations (i.e. 2-D Wiener dynamic model). While, the measurements vector $\mathbf{y_k}$ includes the x-y positions inbound from Decawave devices, the x-y accelerations and the heading angles inbound from the IMU sensor.

3) Rauch-Tung-Striebel (RTS) Smoother: is a Bayesian recursive filter that smoothens the linearized state-space estimates by considering the maximum likelihood of the probability density function (mean and covariance), which are smoothed retroactively [12], [13].

The prior and posterior states estimates $\hat{X}_k|k-1, \hat{X}_k|k$ and their covariances $\hat{P}_k|k-1, \hat{P}_k|k$ which were obtained from the EKF fusion filter are fed to the RTS smoother to calculate the smoothed state estimates $\hat{X}_k|n$, and covariance $\hat{P}_k|n$. The RTS smoother formulas are described in Equations (3) [12], [13].

$$\begin{aligned} \hat{X}_k|_n &= \hat{X}_k|_k + C_k(\hat{X}_{k+1}|_n - \hat{X}_{k+1}|_k) \\ P_k|_n &= P_k|_k + C_k(\hat{X}_{k+1}|_n - \hat{X}_{k+1}|_k) \times C_k^T \end{aligned} \tag{3}$$

where $C_k = P_k|_k F_{k+1}^T P_{k+1}^{-1}|_k$, and $X_k|_k$ is the a-posterior state estimate of time instant k and $X_{k+1}|_k$ is the a-prior state estimate of time instant $k+1$ which also applies to the covariance.

4) Linear Regression (LR) Model: is a statistical method that is used for predictive analysis. It is one of the most common types of supervised machine learning algorithms used to compute the linear relationship between the dependent variable(s) and one or more independent features [14]. Generally, the linear regression function is represented as seen in Equation (4).

$$Y = m + X \times b \tag{4}$$

In the hypothesis function for multivariate linear regression, we assumed that the independent features are the Cartesian [x, y] values of the OMRON robot and UWB respectively, which are represented by X in Equation (4). And, the respective offsets between the OMRON robot (which provides the ground truth data) and UWB represented by Y in Equation (4), is the dependent variable. Assuming there is a linear relationship between X and Y then the offsets can be predicted using Equation (5):

$$y_i = m + \sum_{j=1}^{n} x_{i,j}\beta_j + \epsilon \tag{5}$$

where $i = 1, 2 \ldots n$, and $y_i \in Y$ is the dependent variable, $x_{i,j} \in X$ are the independent variables (multiple inputs, $j = 1, 2 \ldots m$), and ϵ is the prediction error.

The model gets the best regression fit by finding the best m and β_j values where m is the intercept and β_j is the coefficient of $x_{i,j}$. The mean squared error (MSE) is used as the cost (loss) function L, in order to compute the error, which is the difference between the predicted value $\hat{y}$ and the true value y. The loss function $L(\Theta)$ can be written as in Equation (6):

$$L(\Theta) = \frac{1}{n}\sum_{i=1}^{n}(\hat{y_i} - y_i)^2 \tag{6}$$

A flowchart describing the sequence of utilizing all the above-mentioned algorithms is shown in Figure 3.

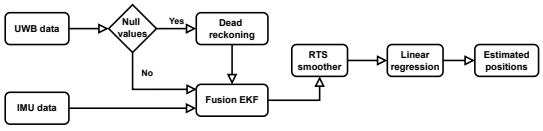

Fig. 3. Sequence of utilized algorithms.

III. Experimental Setup

To set the scene for testing our hypothetical UWB/IMU fusion positioning system in the selected venue, a complete customized embedded system was built that comprises the essential software and hardware peripherals. Then, the devices and the targeted environment were setup for experimentation.

A. Hardware and software

The hardware part consists of a distributed set of six UWB anchors (Decawave) with fixed positions around the coverage area, the IMU sensor (XSENS) mounted on the mobile robot, and the robot itself (OMRON), as shown in Figure 2.

The software part comprises numerous code files that record and communicate real-time data to a storage server. Every sensor point (UWB, IMU, and robot) has a dedicated software scanner that collects the desired tensors of data with the appropriate settings for their units. Afterward, the scanner passes them over to the NodeRed server via web sockets, eventually, they are stored in a local web server which is managed by our institute (i.e. the user), as illustrated in Figure 4.

The Wi-Fi and BLE scanners are already developed but reserved for future use, the focus of this article is centered around UWB/IMU fusion.

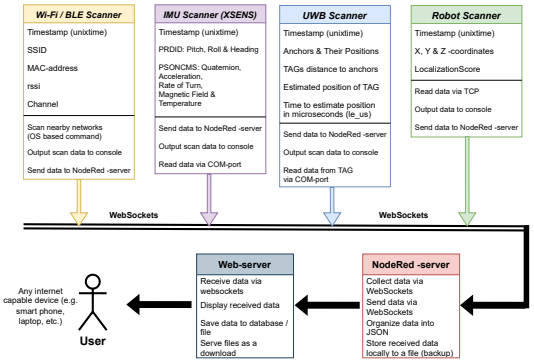

Fig. 4. Block diagram showing the scheme of sensors data collection.

B. Calibration and configuration

All sides of the coverage area including the locations of the fixed UWB anchors were laser-metered using a highly accurate LASER ranger, the measurements were repeated several times till they were sufficiently verified (i.e. standard deviation was $\leq$ 0.01 m). The sensors of the robot were calibrated with localization accuracy exceeding 90% score (as stated by the built-in robot positioning system called "Mobile Runner"), in addition to surveying a new high-detail map of the surrounding environment with updated furniture positions. UWB and IMU sensors were calibrated and configured to produce the appropriate units and positioning output, furthermore, the origin points of all sensors were aligned into a single origin point explicitly marked on the laboratory floor and programmed into sensor configurations. All sensors (UWB, IMU, and robot) were configured to a sample rate of 10 Hz (Ts = 0.1 second).

C. Route design

On the robot's software controller (Mobile Runner), specific routes were designed to allow the robot to patrol the coverage

area in various situations: 1) clear LOS with the robot, 2) poor LOS, 3) visibility through concrete and metal structures, and 4) with the fewest number of anchors (three) visible to the robot. Consequently, six UWB anchor locations were selected to provide evenly distributed coverage to the robot, a seventh location was reserved for a feasibility test.

With all concerns addressed and systems configured, the environment became ready for testing.

IV. Results and discussion

As shown in Figure 5, a dedicated graph for every step (i.e. raw UWB measurements, EKF fusion, RTS smoothing, and LR filtration) is rendered to analyze and assess the proposed method for both configurations scenarios (6 Vs 7 anchors). In addition, a cumulative distribution function (CDF) curve per algorithm is sketched to investigate the performance of the system for longer periods. Moreover, Tables I and II show the mean absolute error (MAE), root mean square error (RMSE), and the 95% percentile values for all algorithms in both scenarios.

TABLE I
Positioning errors [meters] when 6 UWB anchors are used

	UWB	**+Fusion**	**+RTS**	**+LR**
MAE	0.240	0.259	0.232	0.078
RMSE	0.417	0.445	0.389	0.088
p95%	0.278	0.243	0.267	0.141

TABLE II
Positioning errors [meters] when 7 UWB anchors are used

	UWB	**+Fusion**	**+RTS**	**+LR**
MAE	0.221	0.235	0.218	0.047
RMSE	0.323	0.344	0.319	0.055
p95%	0.413	0.340	0.386	0.096

From Figure 5, it is noticeable that the unprocessed UWB measurements are having moderate accuracy with noticeable errors around the start and the stop positions which both have maximum fluctuations in the data, especially from the 6-anchors configuration. Meanwhile, the EKF fusion-based positioning algorithm is performing slightly poorer than the raw UWB data, this remark is also fortified by checking the CDF in the below subplot where the EKF fusion algorithm is found to be the least accurate on the long term without receiving assistance from the RTS smoother algorithm. Consequently, higher accuracy is achieved by backing the EKF fusion algorithm with RTS smoother algorithm, which yielded significantly higher accuracy than the performance of the EKF fusion algorithm, while having slightly higher accuracy than the raw UWB measurements, as also asserted by the numerical values of MAE, RMSE, and p95% in Table I.

The model of LR algorithm was previously trained using positioning data recorded by the OMRON robot from the same environment (but different dataset values), and been used as a training data for the algorithm to both scenarios. Hence, the best positioning accuracy for the 6-anchor configuration is achieved by smoothing the output of the EKF-RTS algorithm with LR algorithm, the procedure that not only helped in improving the performance of the IPS but also achieved significantly precise positioning results as seen from both Figure 5 and Table I. LR filtration step yielded the best positioning accuracy in the 6-anchor configuration data with MAE = 7.8 cm, and RMSE = 8.8 cm compared to the second best records of 23.2 cm (RTS MAE), and 38.9 cm (RTS RMSE), respectively. Furthermore, the long term performance of the UWB/IMU EKF-RTS-LR algorithm is the highest ever in the 6-anchors configuration, by achieving 95% percentile value of 14.1 cm (could have been better if the stationary fluctuations were mitigated) and the most steep curve in the CDF plot, meaning that the LR smoothed solution is the best candidate for continuous accurate navigation services with relatively high standards for an IPS in this dense environment.

On the other hand, the positioning results from the 7-anchor configuration are found to be more promising in most performance metrics as the positioning errors from all methods are more improved than the 6-anchor configuration. Firstly, the EKF fusion continue to perform slightly poorer than the raw UWB measurements and all other algorithms, as seen from the 2nd and 4th subplots of Figure 5, and the values from Table II. Similar to the 6-anchor configuration, the RTS smoothed EKF fusion results are coping with the raw UWB measurements most of the time, but outperform them in few occasions, that is why the CDF curve, MAE, RMSE, and p95% values of both algorithms are nearly identical.

Finally, the ultimate method that comprises UWB/IMU EKF-RTS-LR possesses the best performance metrics in the 7-anchor configuration too, which was an expected behaviour from the algorithm. The LR filtration step had leveraged the overall methodology to achieve MAE = 4.7 cm, and RMSE = 5.5 cm only, which is -by far- the most precise positioning accuracy ever achieved in the Technobothnia lab environment. The second most precise results were -again- from the RTS smoother of MAE = 21.8 cm, and RMSE = 31.9 cm. In addition, the long term performance of the UWB/IMU EKF-RTS-LR algorithm in the 7-anchors configuration is found to be also the highest with p95% = 9.6 cm and the steepest CDF plot among all other algorithms.

In summary, the LR smoothed EKF-RTS fusion algorithm can help to achieve the most precise positioning estimations inside Technobothnia laboratory, since it has demonstrated significantly better MAE, RMSE, and p95% values than all other algorithms, meaning that it does not only have the capability to achieve the most accurate positioning but will also score acceptable levels of continuity, availability and integrity. Thus, the recommended configuration is to cover the given region with 7 UWB anchors aided by the UWB/IMU EKF-RTS-LR algorithm to achieve precise positioning estimations for a mobile robot activity in dense industrial environments as Technobothnia lab, Finland.

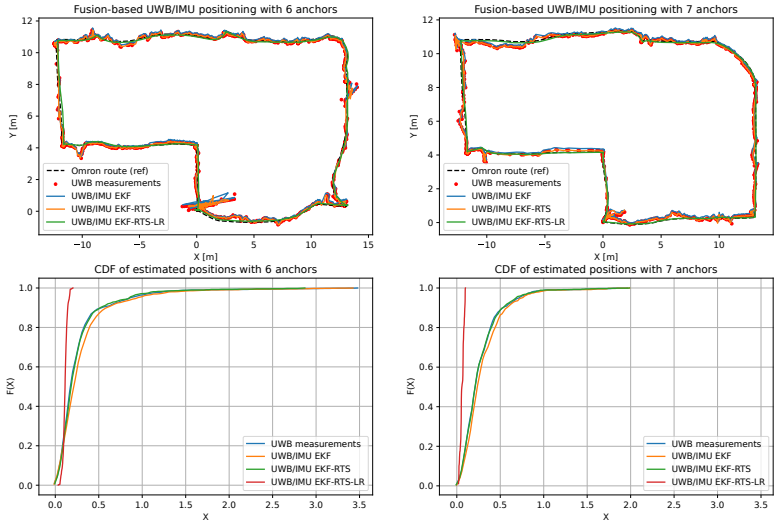

Fig. 5. Plots showing the final positioning results from all utilized algorithms in both configuration scenarios (6 Vs 7 anchors). The lower subplots show the corresponding CDF curves for all algorithms in every scenario.

V. Conclusions

Precise indoor positioning systems are crucial for indoor mobile robot operations especially in dense industrial environments. In this article, we demonstrated our realization of the proposed IPS to provide precise positioning estimations for indoor activities. Through the loosely-coupled multisensor fusion scheme of UWB/IMU technologies and the use of EKF/RTS/LR smoothing algorithms, our method has achieved a positioning accuracy of 9.6 cm across 95% of the time, that is a mean absolute error of 4.7 cm (RMSE = 5.5 cm), using seven UWB anchors to cover a robot operation area of 28x15 square meters in a dense challenging environment. For future work, we aim at investigating more aspects to improve the IPS performance in addition to test RSS-based positioning systems (Wi-Fi and BLE) in the same environment.

Acknowledgment

This work is supported by TULEVA and TosiPaikka projects funds. The corresponding author would like to thank Mrs. Mai Moustafa (Architectural engineer – City of Vaasa) for refurbishing some of the illustrative figures within this article.

References

[1] A. Alarifi, A. Al-Salman, M. Alsaleh, A. Alnafessah, S. Al-Hadhrami, M. Al-Ammar, and H. Al-Khalifa, "Ultra Wideband Indoor Positioning Technologies: Analysis and Recent Advances," *Sensors*, vol. 16, p. 707, may 2016.

[2] M. Elsanhoury, P. Mäkelä, J. Koljonen, P. Välisuo, A. Shamsuzzoha, T. Mantere, M. Elmusrati, and H. Kuusniemi, "Precision positioning for smart logistics using ultra-wideband technology-based indoor navigation: A review," *IEEE Access*, vol. 10, pp. 44413–44445, 2022.

[3] N. Zhu, J. Marais, D. Bétaille, and M. Berbineau, "Gnss position integrity in urban environments: A review of literature," *IEEE Transactions on Intelligent Transportation Systems*, vol. 19, no. 9, pp. 2762–2778, 2018.

[4] X. Guo, N. Ansari, F. Hu, Y. Shao, N. R. Elikplim, and L. Li, "A Survey on Fusion-Based Indoor Positioning," *IEEE Communications Surveys & Tutorials*, vol. 22, no. 1, pp. 566–594, 2020.

[5] M. Elsanhoury, J. Koljonen, P. Välisuo, M. Elmusrati, and H. Kuusniemi, "Survey on recent advances in integrated GNSSs towards seamless navigation using multi-sensor fusion technology," in *Proceedings of the 34th International Technical Meeting of the Satellite Division of The Institute of Navigation (ION GNSS+ 2021)*, Institute of Navigation, Oct. 2021.

[6] R. Ali, R. Liu, A. Nayyar, B. Qureshi, and Z. Cao, "Tightly Coupling Fusion of UWB Ranging and IMU Pedestrian Dead Reckoning for Indoor Localization," *IEEE Access*, vol. 9, pp. 164206–164222, 2021.

[7] D. Feng, C. Wang, C. He, Y. Zhuang, and X.-G. Xia, "Kalman-Filter-Based Integration of IMU and UWB for High-Accuracy Indoor Positioning and Navigation," *IEEE Internet of Things Journal*, vol. 7, pp. 3133–3146, Apr. 2020.

[8] C.-S. Jao, A. A. Abdallah, C. Chen, M.-W. Seo, S. S. Kia, Z. M. Kassas, and A. M. Shkel, "PINDOC: Pedestrian Indoor Navigation System Integrating Deterministic, Opportunistic, and Cooperative Functionalities," *IEEE Sensors Journal*, vol. 22, pp. 14424–14435, July 2022.

[9] H. Yang, T. Luo, W. Li, L. Li, Y. Rao, and C. Luo, "A Stable SINS/UWB Integrated Positioning Method of Shearer Based on the Multi-Model Intelligent Switching Algorithm," *IEEE Access*, vol. 7, pp. 29128–29138, 2019.

[10] M.-G. Li, H. Zhu, S.-Z. You, and C.-Q. Tang, "UWB-Based Localization System Aided With Inertial Sensor for Underground Coal Mine Applications," *IEEE Sensors Journal*, vol. 20, pp. 6652–6669, jun 2020.

[11] Decawave, "Mdek1001 kit user manual module development & evaluation kit for the dwm1001," 2017.

[12] J. Hartikainen, A. Solin, and S. Särkkä, *Optimal filtering with Kalman filters and smoothers - a Manual for Matlab toolbox EKF/UKF*. Aalto University, 2011.

[13] H. E. Rauch, F. Tung, and C. T. Striebel, "Maximum likelihood estimates of linear dynamic systems," *AIAA Journal*, vol. 3, no. 8, pp. 1445–1450, 1965.

[14] K. Kumari and S. Yadav, "Linear regression analysis study," *Journal of the Practice of Cardiovascular Sciences*, vol. 4, p. 33, 01 2018.

Publication P4

Emerging Wireless Technologies for Reliable Indoor Navigation in Industrial Environments

Mahmoud Elsanhoury[1], Akpojoto Siemuri[1], Jyri Nieminen [1], Petri Välisuo[1], Janne Koljonen[1],
Heidi Kuusniemi[1,2], Mohammed S. Elmusrati[1]
[1]*School of Technology and Innovations, University of Vaasa, Finland*
[2] *Finnish Geospatial Research Institute, National Land Survey, Finland*

BIOGRAPHY

Mahmoud Elsanhoury is currently pursuing a doctoral (Ph.D.) degree in computer science and telecommunications engineering at the University of Vaasa, Finland. He received his M.Sc. (tech) degree in telecommunications engineering from Vaasa University in 2018, and his B.Sc. degree in telecommunications engineering from Alexandria University, Egypt in 2013. His current research interests cover ubiquitous indoor positioning systems, ultra-wideband (UWB) indoor localization, low-earth orbit (LEO) satellites for positioning, multisensor fusion technologies, Kalman filters, uncertain stochastic processes, and machine learning algorithms.

Akpojoto Siemuri received his B.Sc.(tech) degree in electrical and computer engineering from the Federal University of Technology Minna, Nigeria in 2010, an M.Sc.(tech) degree in wireless industrial automation with a minor study in industrial management from the University of Vaasa, Finland in 2019. He is currently pursuing a Ph.D. degree in automation technology at the University of Vaasa. From 2018 to 2019, he was a Research Assistant in the Smart Energy Systems Research Platform (SESP) Project at the University of Vaasa, Finland. He is currently a Project Researcher at the University of Vaasa. His research interest includes machine learning, GNSS technologies, smart devices, embedded systems, communication systems, and game theory.

Petri Välisuo is currently working as an Associate Professor (tenure track), in sustainable automation, at the School of Technology and Innovations, University of Vaasa, Finland. He received M.Sc.(tech) degree in computer science from the Tampere University of Technology, Finland, and a D.Sc.(Tech) degree in automation technology from the University of Vaasa, in years 1996 and 2011 respectively. He has authored and co-authored 27 peer-reviewed and more than 10 other scientific publications. His research interests cover machine learning, IoT, positioning methods, and other technologies relevant to industrial automation. He has been working for 10 years in the telecommunication industry before his research career at the University of Vaasa.

Janne Koljonen is a laboratory engineer and degree programme manager at the University of Vaasa, Finland. He has authored more about 50 scientific articles since 2002. He received a Ph.D. degree in automation technology from the University of Vaasa in 2010.

Heidi Kuusniemi is a professor of computer science and director of Digital Economy at the University of Vaasa in Finland. She is also a part-time research professor in satellite navigation at the Finnish Geospatial Research Institute. She has an M.Sc. (Tech.) degree (with distinction) from 2002 and a D.Sc. (Tech.) degree from 2005 in information technology, respectively, from Tampere University of Technology, Finland. She served as a member of the council of natural sciences and technology at the Academy of Finland 2019-2021 and was a member of the scientific advisory committee for GNSS (GSAC) at ESA. Her technical expertise and interests include GNSS reliability and resilience, estimation and data fusion, mobile precision positioning, indoor localization, and PNT in new space.

Mohammed S. Elmusrati is a Full Professor and Head of the Digitalization Unit at the School of Technology and Innovations – University of Vaasa, Finland. He received his B.Sc. (with honors) and M.Sc. (with high honors) degrees in electrical and electronic engineering, from the University of Benghazi, Libya, in 1991 and 1995, respectively, and the Licentiate of Science in Technology (with distinction) and the Doctor of Science in Technology (D.Sc.) degrees in automation and control engineering from Aalto University Finland, in 2002 and 2004, respectively. His research interest includes wireless communications, artificial intelligence, machine learning, biotechnology, big data analysis, stochastic systems, and game theory. Elmusrati has published more than 130 papers, books, and book chapters. Prof. Elmusrati is an active member of different scientific societies such as a Senior Member at IEEE, a Member of the Society of Industrial and Applied Mathematics (SIAM), and a Member of the Finnish Automation Society.

ABSTRACT

Reliable positioning systems are key drivers for location-based services in smart logistics and internet of things (IoT) applications amid the era of Industry 4.0. They are the foundation blocks upon which navigation applications are built for all client segments ranging from public individuals to industrial firms. This research article investigates the existing wireless radio technologies from a low-cost opportunistic perspective to provide precise positioning for dense indoor scenarios. In indoor scenarios, it is a rule of thumb that modern humans spend more than 90% of their time inside buildings, and yet, only a few indoor positioning systems are: less available, more expensive, more disruptable, and/or less accurate. One major reason is that the current indoor positioning technologies are compromising the system performance with other essential metrics such as the overall cost. For instance, the most accurate (millimeter level) indoor positioning technology -so far- is the LASER technology, however, it is massively expensive. On the other hand, some of the existing low-cost positioning technologies for indoor venues are less accurate, besides having other performance drawbacks. One prominent solution for dense indoor situations is Ultra-wideband (UWB) technology, as it provides a positive trade-off between operational costs and system performance. UWB has recently emerged to deliver precise indoor positioning solutions within a centimeter level of accuracy while being a reliable low-cost technology. It is foreseen that UWB will be embedded inside many smartphone models in the near future, some phone manufacturers have already started adopting UWB-chips in 2019 such as Apple and Samsung. Moreover, the FiRa consortium was established by giant founding companies such as Cisco, Google, Samsung, BOSCH, Apple, and Qualcomm, to promote UWB as an indoor positioning technology. Quoting from the FiRa website as follows "UWB is the most effective available technology for delivering accurate ranging and positioning in challenging real-world environments, allowing devices to add real-time spatial context and enabling new user experiences". Previously in 2021, we conducted a thorough review study on UWB, in which we concluded that UWB is an industrial-friendly technology that can provide higher rates of accuracy while maintaining continuous service levels at low costs. In a well-established industrial laboratory in the Ostrobothnia region, Technobothnia, we performed technical experiments to deliver precise UWB positioning for individuals and mobile assets such as autonomous robots. Aided by sensitive inertial motion units (IMUs), the results showed that the UWB precision positioning in a dense challenging environment (i.e. Technobothnia) has been achieved to mean absolute error of **3.7 centimeters** accuracy, and a Wi-Fi positioning accuracy of **4.5 meters**. Our future objective is to further improve the positioning accuracy and reliability to facilitate autonomous operations by mobile robots in the lab. Later, our system will be made open to the public use e.g. for students, visitors, and staff as beneficiaries. Besides UWB technology, there are some additional opportunistic methods that are less accurate (ultra-meter(s) accuracy) however, can be assisted with other multisensor technologies to achieve reliable positioning solutions. The methods that are being investigated are Bluetooth low energy (BLE) and Wi-Fi positioning. The idea is based on the signal-of-opportunity (SOP) paradigm, in which the positioning solution is rendered by measuring one of the radio signal properties, that is, the received signal strength indicator (RSSI). By integrating with IMU sensors, the multisensor combinations BLE/IMU and WiFi/IMU can result in meter-level accuracy, which can be regarded as reliable positioning for certain indoor applications. Moreover, the use of both techniques is foreseen to be sufficient for laboratory mobile activities, as their typical multisensor positioning accuracy can range between 1.5 to 3 meters. The main objective of our proposed method is to refine the achieved positioning accuracy from the multisensor system using a series of algorithmic remedies. First, the positioning solutions are filtered via Bayesian filters to remove the noisy effects and DC offsets. Then, the multisensor scheme is selected as either loose or tight coupling to integrate the IMU readings with the radio-based RSSI estimations and overcome the non-line-of-sight (NLOS) effects. Afterward, the fused solution is treated with recursive Kalman smoothers to further refine the positioning traces, and remove sharpness and stationary effects. The final (optional) step is to apply some machine learning algorithms to adapt navigation routes to the real surroundings based on the collected training data. As a ground truth for all systems and also as training data, an accurate mobile robot is used to bear all sensors together during the experiments. The robot is equipped with LiDARs, ultrasounds, radars, and LASERs that can achieve millimeter accuracy, hence, the data recorded by its sensors are treated as ground truth as well as training data. We also developed an embedded system that synchronizes all data pools together coming from different sensors (UWB – WiFi – BLE – IMU) in the same time frame. In summary, this article studies the indoor navigation opportunities created by existing radio positioning technologies that are tailored for industrial use cases, using multisensor fusion methods for both precise and fingerprinting techniques. A special focus was given to UWB technology as it will be abundant in the near future by embedding smartphones, home appliances, and body wearables with commercial-grade UWB chips, which was already started in 2019. Additionally, we focused on the Wi-Fi based IPS for mobile assets (e.g. robots and humans) that are not necessarily requiring to have precise positioning, few meters of accuracy are becoming sufficient. The existing infrastructure in Technobothnia is currently being customized to embed BLE hardware into the designed IPS, however, the software part has been already implemented. Those RSSI-based indoor positioning methods are becoming trending in large indoor venues (e.g. airports, malls, and train stations) as well as being adopted by major positioning corporations. Consequently, we studied some algorithmic optimization techniques to transform both fingerprinting methods into more accurate reliable techniques. As future research, our proposed methods can be further adapted to be applied for real-time applications, and ensuring that all technologies (including BLE) are functional and up running.

Keywords: Radio technologies, indoor positioning, dense environments, mobile robots, industrial applications.

I. INTRODUCTION

Indoor positioning systems (IPSs) are crucial for Industry 4.0 and Internet of Things (IoT) applications. Several indoor location-based services are dependent on IPSs such in: asset tracking, smart manufacturing and logistics, and so forth [1, 2]. IPSs exist with numerous advantages, yet they face many challenges from multiple sources. In principle, an IPS is assessed for reliability by achieving acceptable levels of performance in the following metrics: accuracy, availability, continuity, and integrity [3]. For this reason, a reliable IPS incur significant costs to compromise all metrics down to sufficient degrees, especially when the application has a high level of sensitivity and low tolerance to errors e.g. healthcare, military, and sophisticated applications. It is abundant that wireless-based IPSs may suffer from signal discontinuities (also known as non-line-of-sight (NLOS)) as the wireless electromagnetic waves are highly prone to channel impairments while propagating in free air, besides the blockage and signal denial in some dense environments.

In addition to the conclusive results from our previous studies found in [2], new researches also support the feasibility of designing a reliable low-cost IPS by integrating multiple technologies together to combat the effect of NLOS situations [4]. Thus, a reliable IPS is not necessarily dependent on a single technology, rather, multiple technologies could be fused together (i.e. multisensor) to realize the desired performance and get better positioning estimations. Multisensor fusion is the integration of two or more technologies using computational paradigms that are implemented by fusion algorithms such that the combined (fused) information is enhanced [5]. Sensors are by-default prone to systematic errors and biases, consequently, multisensor fusion techniques could play an important role in mitigation of errors to the possible minimal.

To this aim, we implemented the essential elements of our proposed IPS inside a real dense environment located on the campus of our research institute (University of Vaasa, Finland), called Technobothnia laboratory. It is a modern laboratory that serves many universities and corporations in the region, as shown in Figure 1. Technobothnia hosts significant visiting traffic owing to the laboratories within, which support various kinds of technical sciences. Consequently, an indoor positioning system will be very beneficial to the movable assets (i.e. humans and robots) who are operating inside the lab.

Figure 1: An indoor aerial view of Technobothnia laboratory, situated in Vaasa, Finland.

Nevertheless, the available resources for positioning inside the lab tend to low-cost IPSs that are based on wireless technologies e.g. ultra wide-band (UWB), Wi-Fi, Bluetooth low energy (BLE). An UWB system and an inertial measurement unit (IMU) are selected as the elements of the precise IPS in Technobothnia, with UWB as the primary technology, and IMU as the assisting sensor fusion unit. Then, Wi-Fi and BLE in addition to an IMU unit were considered for the less accurate (fingerprinting) IPSs that shall track assets within a couple of meters as accuracy. The foundation of UWB and Wi-Fi were implemented successfully to Technobothnia while the BLE hardware infrastructure is still under development to the date of writing those lines. That is, UWB to track assets (e.g. robots and/or humans) within sub-meter level of accuracy, while Wi-Fi to position assets within ultra-meter level of accuracy (i.e. suitable for humans not robots).

The rest of article is organized as follows: Section II states the main approach of this research in addition to the building blocks of the intended IPS systems from software and hardware perspectives. Section III highlights the realized technical actions to obtain the planned IPS e.g. methodology, devices configurations, and the overall setup of the environment. Section IV discusses

the output results and provides some technical interpretations, evaluations, and comments regarding the applied methodologies. The article finalizes with a "Conclusion" section to summarize the results and the achieved IPS performance.

II. DESIGN OF THE FUSION-BASED IPSS

In this section, we describe the whole design aspects of building both UWB and Wi-Fi indoor positioning systems. As described in the introduction, it is the main objective in this research to build two dedicated IPSs that ensure the most possible degree of precision positioning for movable assets (robots using UWB, and humans using Wi-Fi) inside our industrial laboratory of Technobothnia, Finland.

1. Outlines

The dense challenging environment in Technobothnia required a multisensor fusion technique to achieve better accuracy and also keep the overall budget (e.g. costs and time) under the allocated limits for building those IPSs. A low-cost system can be built from a single precise wireless technology such as UWB then fused with an assisting technology [2]. Hence, an IMU could be employed to correct the biased, missing, and null values caused by NLOS conditions especially in dense environments.

To this aim, a loosely-coupled UWB/IMU integrated scheme was implemented as a precise IPS for mobile robots in the selected venue, and another loosely-coupled scheme Wi-Fi/IMU for localizing humans. A floor plan of the experiment area at Technobothnia laboratory is illustrated in Figure 2.

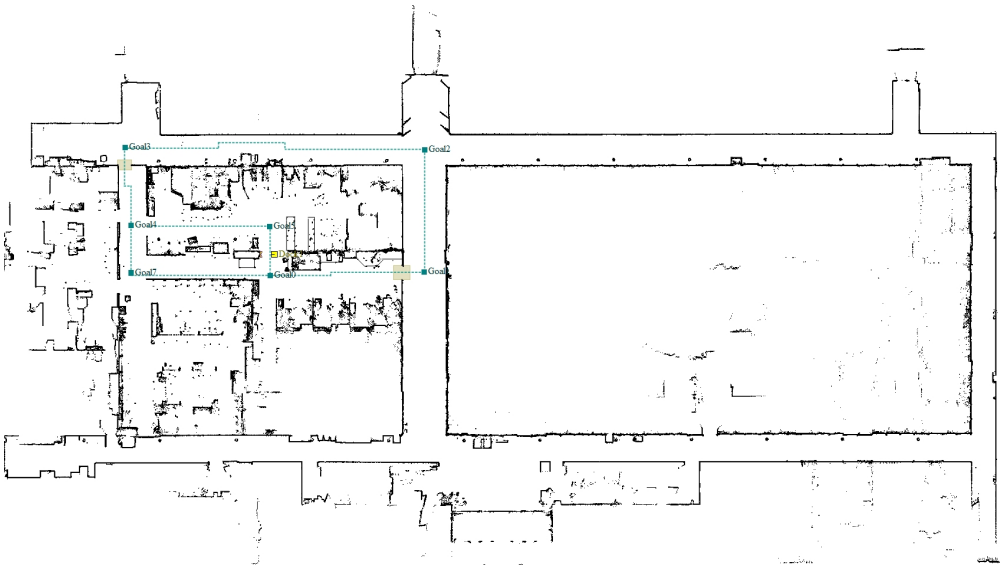

Figure 2: Snapshot from the robot's internal software system showing the floor plan of the whole laboratory building (Technobothnia) after calibrating the map several times. The dense area in the top left-hand corner is our lab area where most technical operations take place.

2. Positioning devices

The testing setup involved patrolling the environment by an autonomous robot whose accuracy is millimeter level, thus can be considered as a source of ground truth data. All other sensors such as: UWB, IMU, and received signal strength indicator (RSSI) scanners (for Wi-Fi and BLE) were mounted on the patrolling robot to get the same route information as the robot.

a). UWB IPS

For UWB, a Decawave laboratory kit MDEK1001 [6] was adopted to represent the UWB IPS inside our industrial laboratory environment, Technobothnia. However, for Wi-Fi IPS we had to interface with the access point devices opportunistically, meaning that we have utilized the existing infrastructure (that was developed by our institute's IT department) by recording

the essential information of the distributed router access points in the area such as: MAC addresses, received signal strength indicator (RSSI), and LASER-measuring their locations to be included in our reference coordinate system (all devices were given the same unified axes and origin point).

In addition, an inertial measurement unit (IMU) sensor Xsens MTi-630 was employed to obtain the inertial data of the user (i.e. the robot) such as: orientation, rate of turn, acceleration, and magnetism. The introduction of IMU sensor provided another layer of information regarding the movement of the robot inside the dense environment. Therefore, IMU helped in accounting for the NLOS situations and inferring the missing data to improve the final positioning estimations.

Our setup for the UWB system consisted of one movable tag (the user), and six evenly distributed anchors to cover the experimental area of 28x15 squared meters evenly, an additional seventh anchor was added to clear the ambiguities of that dense area. The default settings of the Decawave kit are factory-programmed to provide raw distance measurements between the moving tag and a maximum of four anchors (constrains from Decawave) based on the time of arrival (ToA) two-way ranging (TWR) technique, in addition to providing the EKF estimation of the tag position [6].

Both UWB and IMU sensors were placed onboard an autonomous mobile robot developed by OMRON. The robot has several positioning sensors of LASERs, ultrasound, RADARs, IMU, and LiDARs which yield a millimeter accuracy therefore it acted as the reference ground truth to both UWB/IMU and Wi-Fi/IMU fusion systems.

b). Wi-Fi IPS

As mentioned earlier that the Wi-Fi IPS was approached opportunistically. There were six router access points that cover the operation area, we referred to them as: $R_0, R_1, R_2, R_3, R_4, R_5$. We decided to build mathematical models for every router solely, therefore, several RSSI measurements were taken at reference distance of 1m, 3m, 5m, and 10m, those distances were measured using a LASER- ranger. We assumed logarithmic path-loss models to find the relation between the RSSI and the distances from the router. The used formula is found in Equation 1, as follows [7]:

$$B_k = B_0 + 10\alpha log(d_k) + X_\sigma \tag{1}$$

Where B_k is the measured RSSI at a given k time instant, B_0 is the measured RSSI at the reference distance (one meter), α is the medium path loss exponent, d_k is the estimated distance in meter for a given k time instant, and X_σ is a random variable with standard deviation σ that represents a white zero-mean Gaussian noise.

The results of curve-fitting the logarithmic path-loss models provided the values of the characteristic variables (α, B_0) of every router, as shown in Figure 3.

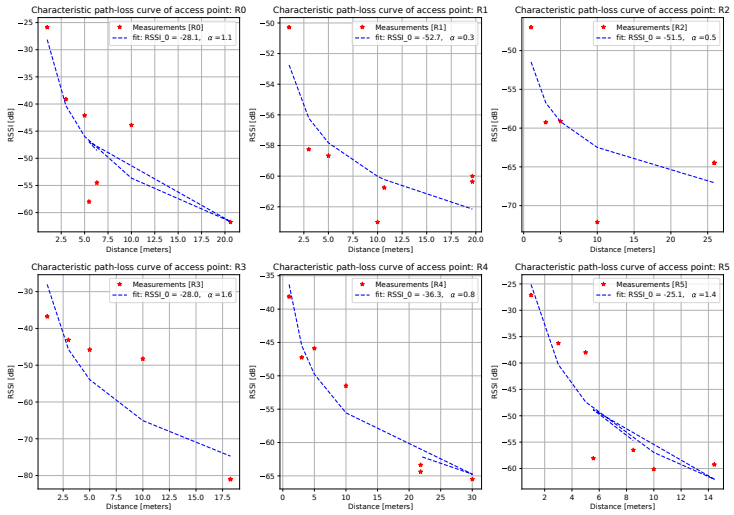

Figure 3: Curve-fitted characteristic path-loss curves of all access points [R0 – R5].

From the curves in Figure 3, it is clear that some routers (especially R_0, R_4, R_5) are having constant RSSI values over several displacements, which means that the RSSI does not change over distance in some cases. This is an important concern in this method, and it is a natural result to being offered some shallow information about the access points. A better approach was to get localization-compatible router brands whose characteristic RSSI vs distance curves are following typical logarithmic relations.

III. EXPERIMENTAL SETUP

In this section, we showcase the prepared setup from software and hardware perspectives that was used for performing robot experiments inside our laboratory.

1. IPS system level design

In order to test our proposed fusion-based IPS systems of UWB/IMU and Wi-Fi/IMU, we deployed a customized embedded system that holds the essential software and hardware elements to carry out the experiments in the selected environment.

The hardware part consists of a distributed set of seven UWB anchors (Decawave) with fixed positions around the coverage area, the IMU sensor (XSENS) mounted on the mobile robot, the laptop recorder was equipped with UWB data logger and RSSI scanner, and the robot itself (OMRON).

The software part was developed using Python and JavaScript to record and communicate real-time data from-to a storage web server. We built the system to bear multiple positioning sensors in the same venue e.g.: robots sensors, UWB anchors, Wi-Fi access points, Bluetooth (future use), and inertial sensors. All sensor points are attached to their corresponding software scanner(s) that records the desired data observables using the appropriate unit settings. Then, all scanners pass the information to the NodeRed server via web sockets, to be stored in a local storage that is interfaced by our team (i.e. the user).

It is worth noting that the BLE software scanner is already developed and up-running but at the moment it has been reserved for future use, as the hardware infrastructure is currently under development. Therefore, the focus of this article will be centered around UWB/IMU and Wi-Fi/IMU fusions.

2. Calibration and configuration

We calibrated the robot's sensors as well as the UWB, IMU and Wi-Fi devices. For the robot, we created a new topology map for the environment and all its furniture, barriers and structures, which was uploaded to the robot's internal storage to mark the boundaries of the experimentation area. IMU sensor was factory-calibrated already. Then for UWB, we calibrated the Decawave anchors to know its covariance error and set the physical coordinates of anchors' locations by the aid of a LASER meter ranger. Same with Wi-Fi access points, we primarily wanted to interface them from system level (by the aid of our IT department), however, we had to work with Wi-Fi access from an opportunistic approach (i.e. deal with them as electromagnetic-wave emitter devices) whose RSSI and MAC information are known. Furthermore, the origin points of all sensors were aligned into a single origin point (0, 0) explicitly marked on the laboratory floor and programmed into sensor configurations. All calibration measurements were taken and recorded several times to ensure maximum stability and accuracy, and devices were configured to 10 Hertz sample rate.

3. Data flow and algorithms

The flow of data was designed to pass from sensor devices to internal data storage called Node-Red via web sockets made specifically to log all sensor data in real-time. Figure 4 illustrates the journey of sensors data in the system to achieve final positioning estimations.

Having all time series data after the web socket reception, the data was fetched to undergo pre-processing and pipe-lining phases. For the Wi-Fi data, the pre-processing step was very complicated since the routers information were interleaved by our IT department for security reasons, thus we had to find out the right MAC addresses information associated with each router, which were not the same as the manufacturer's.

Afterwards, each sensor data that conclude the pre-processing step were referred to a set of additional refining algorithms. In UWB, we replaced the null values by the aid of dead reckoning (DR) algorithm, then propagate the outputs to extended Kalman filter (EKF) fusion, Rauch-Tung-Striebel (RTS) smoother, and linear regression (LR) algorithms. The same sequence applies for Wi-Fi except that the treated Wi-Fi RSSI values are primarily passed through path-loss model in order to be later consumed by a bootstrap Particle filter (PF). Then, the PF estimates the Euclidean distances between the moving user and the fixed Wi-Fi access points with known locations.

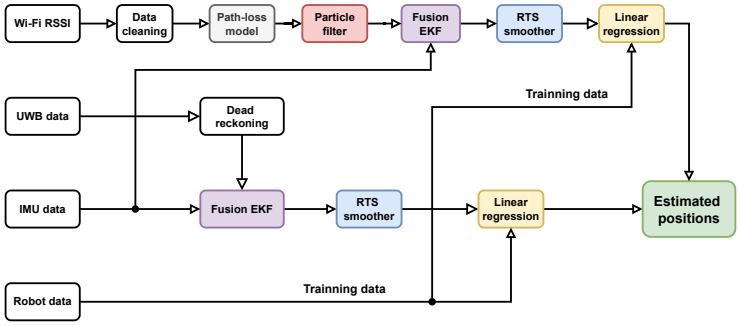

Figure 4: Data flow of measurements and the utilized algorithms to achieve positioning estimations.

4. Route design

On the robot's software controller (Mobile Runner), routes were programmed to allow the robot patrolling the coverage area in mixed situations: 1) clear LOS between the robot and the wireless devices, 2) poor LOS, 3) visibility through concrete and metal structures, and 4) with the fewest number of devices (i.e. three) visible to the robot. The locations of the first six UWB anchors were selected to provide evenly distributed coverage to the robot (e.g. rectangular shape), then a seventh anchor was inserted in the most dense space inside the environment to provide more visibility to the moving robot (UWB tag and RSSI scanners).

IV. RESULTS AND DISCUSSION

After holding several lab experiments in Technobothnia using the described experimental setup and settings, some very promising results emerged from UWB IPS, and some other concerning results emerged from Wi-Fi.

Firstly, UWB plot results are shown in Figure 5. As seen from the figure, the performance of the latest algorithm (LR-UWB/IMU) in the UWB IPS is truly unmatched. As found from the numerical results shown in Table 1, the positioning accuracy of UWB IPS has been achieved between 3.7 – 4.5 centimeters.

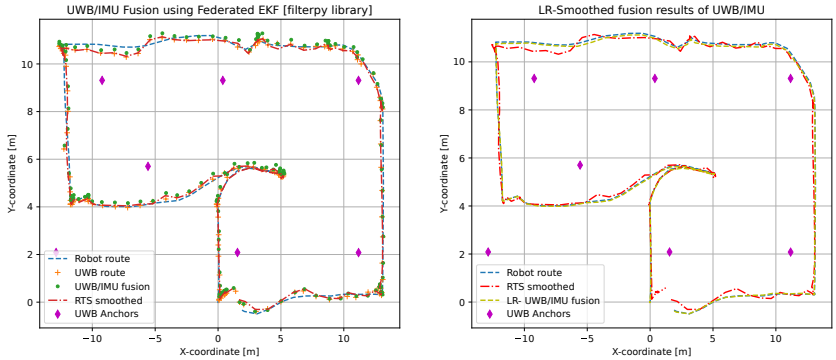

Figure 5: Results of UWB positioning before and after applying Linear Regression algorithm.

On the other hand, the results from Wi-Fi IPS shown in Figure 6 graphically, and Table 2 numerically were clearly erroneous, which was very much expected for various reasons. Only minor improvements occurred before applying the LR algorithm, this means that the performance of machine learning algorithms is a very prominent non-model candidate for reliable indoor positioning.

The sources of Wi-Fi IPS errors could be due to: 1) inconsistent path-loss readings that may be originated from 2) incompatible

Table 1: Positioning errors [in meters] of UWB IPS.

	UWB Kalman Filter	UWB/IMU Fusion	UWB/IMU +RTS	UWB/IMU/RTS +LR
MAE	0.170	0.196	0.169	0.037
RMSE	0.241	0.270	0.240	0.045

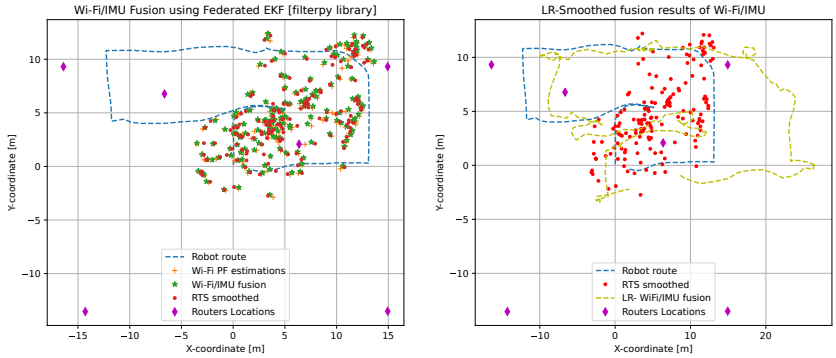

Figure 6: Results of Wi-Fi positioning before and after applying Linear Regression algorithm.

routers for positioning applications, or 3) erroneous software scanner which holds the RSSI values for too long time before refreshing to new readings, 4) the extremely dense environment makes it super-challenging for Wi-Fi positioning in particular. Again, mitigating nearly 30% of the error using LR algorithm is another evidence that machine learning algorithms could be employed as standalone positioning techniques, provided that a proper training process was made.

1. Summary

To summarize what have been achieved in this study, a cumulative distribution function plot was sketched for both UWB IPS and Wi-Fi IPS to note the difference between all utilized methodologies and algorithms from a very high perspective, as shown in Figure 7.

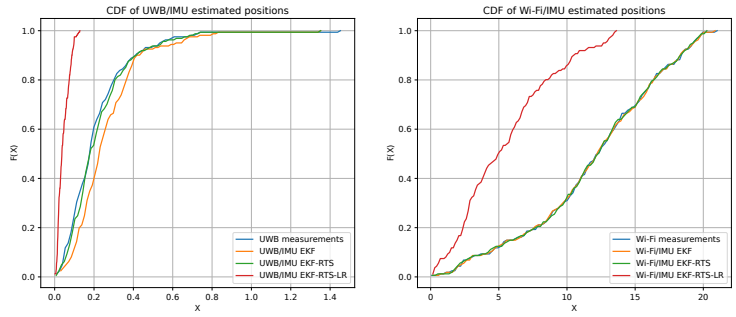

Figure 7: Cumulative distribution function plots for both UWB and Wi-Fi IPSs.

Both red curves in the two plots are having the most steep slope amongst their counterparts, meaning that the LR-smoothed fusion method can yield the best and most accurate results even in dense industrial situations, which is a very fitting solution to combating NLOS conditions. The method is proven to be reliable for both IPSs (UWB and Wi-Fi) to facilitate technical operations with precise location information using UWB/IMU, and ensure an acceptable level of performance for human resources tracking using Wi-Fi/IMU, which could be further improved in the future.

Table 2: Positioning errors [in meters] of Wi-Fi IPS.

	Wi-Fi Particle Filter	**Wi-Fi/IMU Fusion**	**Wi-Fi/IMU +RTS**	**Wi-Fi/IMU/RTS +LR**
MAE	6.862	6.863	6.854	4.515
RMSE	8.304	8.318	8.308	5.812

V. CONCLUSION

Indoor positioning systems are very crucial for navigational and location-aware applications. Building dedicated IPSs in dense industrial environment requires thorough and meticulous investigations to find the appropriate solution for mitigating NLOS effects and achieve reliable positioning estimations. In this article, we illustrated our work in designing two IPSs, precise UWB IPS for tracking indoor mobile robots, and Wi-Fi IPS to localize human resources inside a complex laboratory environment in Finland. Both loosely coupled IPSs with the aid of an IMU sensor have yielded the best positioning results amongst all other techniques, the highest accuracy achieved by UWB was ranging between 3.7 – 4.5 centimeters, while for Wi-Fi it was ranging between 4.5 – 5.8 meters. For future work, we aim to add a BLE IPS which has been already partially implemented in the lab environment, while investigating more improvement techniques to the existing Wi-Fi IPS.

REFERENCES

[1] A. Alarifi, A. Al-Salman, M. Alsaleh, A. Alnafessah, S. Al-Hadhrami, M. Al-Ammar, and H. Al-Khalifa, "Ultra Wideband Indoor Positioning Technologies: Analysis and Recent Advances," *Sensors*, vol. 16, no. 5, p. 707, may 2016.

[2] M. Elsanhoury, P. Mäkelä, J. Koljonen, P. Välisuo, A. Shamsuzzoha, T. Mantere, M. Elmusrati, and H. Kuusniemi, "Precision positioning for smart logistics using ultra-wideband technology-based indoor navigation: A review," *IEEE Access*, vol. 10, pp. 44 413–44 445, 2022.

[3] N. Zhu, J. Marais, D. Bétaille, and M. Berbineau, "Gnss position integrity in urban environments: A review of literature," *IEEE Transactions on Intelligent Transportation Systems*, vol. 19, no. 9, pp. 2762–2778, 2018.

[4] X. Guo, N. Ansari, F. Hu, Y. Shao, N. R. Elikplim, and L. Li, "A Survey on Fusion-Based Indoor Positioning," *IEEE Communications Surveys & Tutorials*, vol. 22, no. 1, pp. 566–594, 2020. [Online]. Available: https://doi.org/10.1109%2Fcomst.2019.2951036

[5] M. Elsanhoury, J. Koljonen, P. Välisuo, M. Elmusrati, and H. Kuusniemi, "Survey on recent advances in integrated GNSSs towards seamless navigation using multi-sensor fusion technology," in *Proceedings of the 34th International Technical Meeting of the Satellite Division of The Institute of Navigation (ION GNSS+ 2021)*. Institute of Navigation, Oct. 2021. [Online]. Available: https://doi.org/10.33012/2021.17961

[6] Decawave, "Mdek1001 kit user manual module development & evaluation kit for the dwm1001," 2017.

[7] H. Zou, Z. Chen, H. Jiang, L. Xie, and C. J. Spanos, "Accurate indoor localization and tracking using mobile phone inertial sensors, wifi and ibeacon," *2017 IEEE International Symposium on Inertial Sensors and Systems (INERTIAL)*, pp. 1–4, 2017.

Publication P5

Survey on Recent Advances in Integrated GNSSs Towards Seamless Navigation Using Multi-Sensor Fusion Technology

Mahmoud Elsanhoury, Janne Koljonen, Petri Välisuo, Mohammed Elmusrati, Heidi Kuusniemi, *University of Vaasa*

BIOGRAPHY

Mahmoud Elsanhoury is a doctoral student majoring telecommunications engineering at the University of Vaasa. He obtained his MSc degree in technology from Vaasa University in 2018, and BSc degree in telecommunications engineering from Alexandria University (Egypt) in 2013. His research interests are ultra-wideband localization, Kalman filters and machine learning algorithms.

Janne Koljonen was born in 1980. He received his M.S. and Ph.D. degrees in automation technology from the University of Vaasa, Finland, in 2004 and 2010, respectively. He has been working with the University of Vaasa since 2002. He is the author of more than 40 scientific articles.

Petri Välisuo is an Associate Professor at the University of Vaasa, Finland. He received MSc. in computer science from Tampere University of Technology and DSc. in automation technology from University of Vaasa, in 1996 and 2011 respectively. He co-authored 27 peer reviewed. His research interests cover machine learning, IoT, and positioning methods.

Mohammed Elmusrati received the D.Sc. degree in Control Engineering from Aalto University -Finland in 2004. Currently, he is a Full Professor in Communication, Automation, and Digitalization at University of Vaasa, Finland. Elmusrati is interested in wireless communications, machine learning, and applications. He has published more than 145 papers, books, and book chapters.

Heidi Kuusniemi is the Director of Digital Economy at University of Vaasa and a Professor at the Finnish Geospatial Research Institute. Possess more than 18 years of experience in research and development of positioning technologies. In 2016, she was selected as one of the 50 most inspiring technology leaders in Nordic countries.

ABSTRACT

During the past few decades, the presence of global navigation satellite systems (GNSSs) such as GPS, GLONASS, Beidou and Galileo has facilitated positioning, navigation and timing (PNT) for various outdoor applications. With the rapid increase in the number of orbiting satellites per GNSS, enhancements in the satellite-based augmentation systems (SBASs) such as EGNOS and WAAS, as well as commissioning new GNSS constellations, the PNT capabilities are maximized to reach new frontiers. Additionally, the recent developments in precise point positioning (PPP) and real time kinematic (RTK) algorithms have provided more feasibility to carrier-phase precision positioning solutions up to the third-dimensional localization. With the rapid growth of internet of things (IoT) applications, seamless navigation becomes very crucial for numerous PNT dependent applications especially in sensitive fields such as safety and industrial applications. Throughout the years, GNSSs have maintained sufficiently acceptable performance in PNT, in RTK and PPP applications however GNSS experienced major challenges in some complicated signal environments. In many scenarios, GNSS signal suffers deterioration due to multipath fading and attenuation in densely obscured environments that comprise stout obstructions. Recently, there has been a growing demand e.g. in the autonomous-things domain in adopting reliable systems that accurately estimate position, velocity and time (PVT) observables. Such demand in many applications also facilitates the retrieval of information about the six degrees of freedom (6-DOF - x, y, z, roll, pitch, and heading) movements of the target anchors. Numerous modern applications are regarded as beneficiaries of precise PNT solutions such as the unmanned aerial vehicles (UAV), the automatic guided vehicles (AGV) and the intelligent transportation system (ITS). Hence, multi-sensor fusion technology has become very vital in seamless navigation systems owing to its complementary capabilities to GNSSs. Fusion-based positioning in multi-sensor technology comprises the use of multiple sensors measurements for further refinement in addition to the primary GNSS, which results in high precision and less erroneous localization. Inertial navigation systems (INSs) and their inertial measurement units (IMUs) are the most commonly used technologies for augmenting GNSS in multi-sensor integrated systems. In this article, we survey the most recent literature on multi-sensor GNSS technology for seamless navigation. We provide an overall perspective for the advantages, the challenges and the recent developments of the fusion-based GNSS navigation realm as well as analyze the gap between scientific advances and commercial offerings. INS/GNSS and IMU/GNSS systems have proven to be very reliable

in GNSS-denied environments where satellite signal degradation is at its peak, that is why both integrated systems are very abundant in the relevant literature. In addition, the light detection and ranging (LiDAR) systems are widely adopted in the literature for its capability to provide 6-DOF to mobile vehicles and autonomous robots. LiDARs are very accurate systems however they are not suitable for low-cost positioning due to the expensive initial costs. Moreover, several other techniques from the radio frequency (RF) spectrum are utilized as multi-sensor systems such as cellular networks, WiFi, ultra-wideband (UWB) and Bluetooth. The cellular-based systems are very suitable for outdoor navigation applications while WiFi-based, UWB-based and Bluetooth-based systems are efficient in indoor positioning systems (IPS). However, to achieve reliable PVT estimations in multi-sensor GNSS navigation, optimal algorithms should be developed to mitigate the estimation errors resulting from non-line-of-sight (NLOS) GNSS situations. Examples of the most commonly used algorithms for trilateration-based positioning are Kalman filters, weighted least square (WLS), particle filters (PF) and many other hybrid algorithms by mixing one or more algorithms together. In this paper, the reviewed articles under study and comparison are presented by highlighting their motivation, the methodology of implementation, the modelling utilized and the performed experiments. Then they are assessed with respect to the published results focusing on achieved accuracy, robustness and overall implementation cost-benefits as performance metrics. Our summarizing survey assesses the most promising, highly ranked and recent articles that comprise insights into the future of GNSS technology with multi-sensor fusion technique.

I. INTRODUCTION

Global navigation satellite systems (GNSSs) is a key element for location-based services (LBS) that are playing an important role in today's smart cities and the futuristic internet-of-things (IoT) applications. With the quantitative and diversative growth of GNSSs constellations, the positioning, navigation and timing (PNT) capabilities were strengthened to new frontiers.

Seamless navigation is mostly demanded in various application where system integrity and reliability are paramount. Conventional GNSS stand-alone methodologies may fail to provide the required seamless navigation thus the researchers developed additional techniques to assist GNSSs, some are illustrated in figure 1.

The integrity of GNSS navigation systems, as defined by [1], is the trustworthiness of the information provided by the navigation engine. Additionally, the performance of GNSSs can be assessed using a pyramid-like scheme with system accuracy as the baseline, integrity as the second metric, continuity as the third, and availability as the peak paramount. System accuracy is the degree of conformance of the estimated positioning values to the ground truth. Continuity is the probability of the system to maintain the desired service level within the operation period while availability is the percentage of time in which the navigation system is usable.

GNSS performs well in non-urban environments mainly due to the user visibility from numerous satellites (more than four) in addition to the satellite-based augmentation system (SBAS) which ensures GNSS integrity, corrections and redundancy. While in urban environments, satellites visibility becomes a challenge hence, additional measures are required to maintain seamless navigation. The two major factors of signal impairments that contribute to the overall error in GNSSs are the multipath components and the non-line-of-sight (NLOS) occurrences. The multipath effects are mitigated via various techniques found in figure 1. Moreover, there exist few methods to combat or compensate the NLOS situations, the most highlighted method among them that provides the best compromise is the use of multi-sensor fusion technologies.

Multi-sensor fusion technology is becoming abundant in the navigation literature due to its many advantages. The use of multiple sensors for navigation can increase the positioning accuracy by mitigating the errors arouse from sensors thus increases the reliability of the system. Moreover, in some cases, multi-sensor fusion implementations can be presented as low-cost system in sensitive applications that require precision by utilizing low-cost multi-sensors however that can be on the account of computational complexity.

In this article, we survey the recent literature on seamless GNSS navigation in the context of multi-sensor fusion technique. After the introductory section, in section II, we provide brief descriptions about the principles of multi-sensor fusion, highlighting the structure of the fusion process, the commonly used sensors and algorithms. In section III, we present the most recent advances in the multi-sensor GNSS literature in a span of the previous five years focusing on the implementations in autonomous driving, pedestrian tracking and GNSS-denied situations. The selection criteria of articles were based on impact, relevance, higher ranking in the Finnish national system [2], novelty and citations score. Nevertheless, some older articles were also included in this review due to their importance and unchanged scientific principles.

II. MULTI-SENSOR FUSION APPROACH

Sensor fusion is a computational procedure to combine the measurements from multiple sources such that the output information after fusion is maximized. The sensor fusion technique is adopted in dynamic systems that require more precision and accuracy due to its capability of mitigating measurements errors which combat environmental impairments, an example is illustrated in figure 2. Moreover, the use of multi-sensors that complements each other (e.g. position and attitude) yields the best possible

Figure 1: Approaches for multipath mitigation in GNSSs (adapted from [1])

results for PNT- based applications.

As sensor technology becomes more sophisticated (and its erroneous nature), multi-sensor fusion has been trending in recent years. In general, the reliance on multiple measurement devices in positioning applications will result in fewer uncertainties and greater reliability and accuracy than depending on a single measurement sensor [3].

The multi-sensors integration architecture may follow three schemes: loosely coupled (LC), tightly coupled (TC) and ultra-tightly coupled (UTC) as described in [4–6]. The LC system is the simplest architecture that provides good redundancy based on the duplicated measurements but requires good satellites visibility (four at least). The TC system can maintain navigation even when satellites visibility is poor (fewer than four) besides having better accuracy and immunity to jamming consequently the TC is widely adopted. In the UTC system, the GNSS receiver tracking loop is aided by a replicated software-defined radio (SDR) receiver that correlates and smooths the error between the received signal and the locally generated one.

1. Structure of the multi-sensor fusion approach

Numerous tracking systems can be fused with GNSSs to provide more accurate and reliable estimations. Common examples of these systems are radars, inertial navigation systems (INSs), inertial measurement units (IMUs), dead reckoning (DR) and computer vision (e.g. cameras). The optimal positioning estimations that result from fusing multiple positioning methods follow a unified framework, which is described in figure 3.

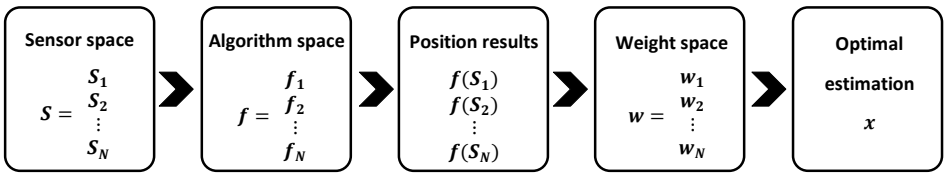

Figure 3: Fusion-based positioning framework (adapted from [3]).

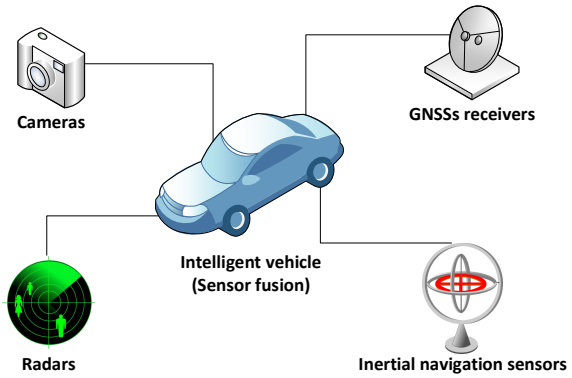

Figure 2: Illustration depicting the elements of multi-sensor system in intelligent vehicles.

In figure 3, the multi-sensor fusion framework comprise *N* sensors and same number of algorithms in which the PNT solution is obtained by solving local sensor data with the respective local algorithm. After that, a master fusion algorithm that comprise the weights vector of each sensor is responsible for fusing all input data to achieve the most optimal solution of the overall fusion-based system.

2. Fusion algorithms

Multi-sensor fusion of multiple technologies requires special algorithms to combine (fuse) all sensors data and produce the unified output estimations. Most commonly used algorithms capable of dealing with redundancy and overdetermined systems are Kalman filters, least squares algorithms and particle filter. Additionally, the algorithmic federation concept is recently trending throughout the recent literature. In this section, we provide a brief overall view about the most common algorithms.

a). Kalman filters

The Kalman filter algorithm is an iterative recursive estimation method to predict the new optimal states in linear state-space systems considering additive white Gaussian noise [7]. The algorithm is based on utilizing the priori knowledge to estimate the posterior states, calculate the Kalman gain and the measurements residual due to the mismatch error then calculate the new state and covariance vectors and use them as input to the next iteration [8–10]. The difference between all types of Kalman filters is showed in figure 4.

Extended Kalman filter (EKF) is an adapted version of the ordinary linear Kalman filter to estimate states in nonlinear dynamic systems [11]. A discrete-time Kalman filter has two steps: 1) prediction step, where the next state of the system is predicted given the previous measurements fed to the system, and 2) update step, where the current state of the system is estimated given the measurement at the active time step [10, 12].

In EKF, the state transition matrix and the measurement matrix in the linear Kalman filter are replaced by the nonlinear state transition function $f(.)$ and nonlinear measurement function $h(.)$ respectively in order to map the algorithm through Gaussian distribution to work in nonlinear conditions.

Unscented Kalman filter (UKF) Unlike EKF, the Unscented Kalman filter (UKF) employs the sigma-point Gaussian transformation to map the nonlinear state transition function of the system and tend to linearize it through the so called the unscented transform [10, 13, 14]. In other words, the UKF uses more than one point including the distribution mean, while EKF approximation relies only on one point, the mean. UKF selects additional weighted points (called sigma points) plus the mean for more accurate transformation. This procedure is called the unscented transform. As a result, UKF sometimes outperforms EKF in severely nonlinear systems, while EKF performs well in systems with modest nonlinearity [15]. There are other sigma-point Kalman filters which are widely adopted such as Cubature Kalman filter (CKF) and Gauss-Hermite Kalman filter (GHKF).

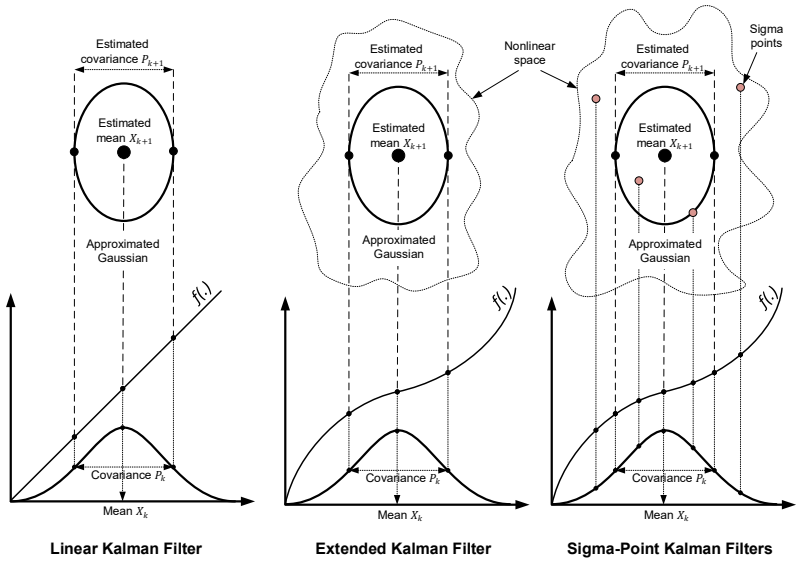

Figure 4: Illustration depicting a comparison between the different types of Kalman filter (adapted from [10]).

b). Particle filters

The position of an observer can be estimated using the discrete state-space model (DSS). In general case the process and measurement functions $f(.)$ and $h(.)$ can be nonlinear and process and measurement noise distributions, q, and, r, non-Gaussian noise sources. The problem of finding a position x_k can be seen as a filtering problem for estimating the posterior probability $p(x_k|y_k)$, which is often assumed to be Gaussian.

A closed form solution can be found only if DSS is linear and q and r are zero mean Gaussian noise sources. In practice these conditions do not hold very often. If the system function is well known, it can be linearized near an operating point and then linear methods be applied [16, 17]. EKF solves a Gaussian posterior estimation by linearization and UKF by using unscented transformation however the standard Particle Filter (PF) provides non-Gaussian posterior estimation iteratively by means of Sequential Monte Carlo (SMC) algorithm. A Gaussian variation of PF (GPF) solves Gaussian posterior distribution using SMC [16].

c). Federated filtering

The federated filtering concept first described by [18] in which the observations of subsystems are estimated locally as first step, then sent for general fusion using a master fusing filter [19]. Kalman filters are widely adopted as fusion filters especially the federated Kalman filtering (FKF) and the federated extended Kalman filter (FEKF) for multiple sensors, as illustrated in figure 5.

Kalman algorithms are the most commonly used filters for federation; ordinary Kalman filter for linear systems, extended (EKF) and unscented(UKF) Kalman filters for nonlinear systems [20].

The algorithmic behavior of FKF follows the state-space matrix equations of: [21]

$$X_{k+1} = \Phi_k X_k + U_k + W_k \tag{1}$$
$$Z_{k+1} = H_{k+1} X_{k+1} + V_{k+1} \tag{2}$$

where X_{k+1} and Z_{k+1} are the iterative global state vector and global measurements vector of the system at time step *k+1*, Φ_k and H_{k+1} are the diagonal state transition matrix and the observation matrix respectively. U_k is the global input matrix, W_k and V_{k+1} are the

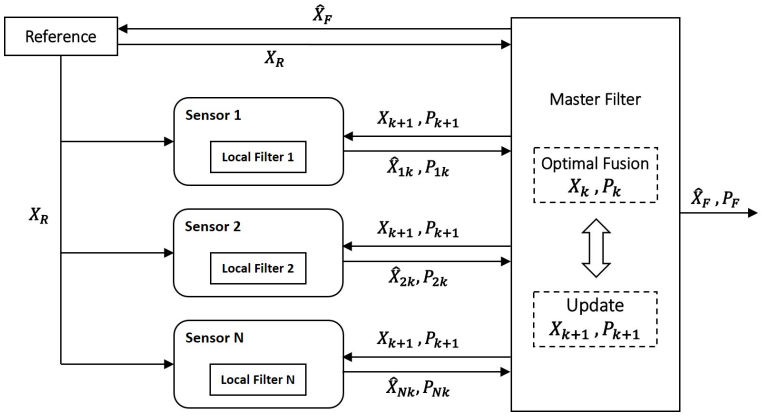

Figure 5: Structure of the federated Kalman filter (FKF).

Gaussian process and measurements noises respectively at time step *k* and *k+1* with covariances Q_k and R_{k+1}.

To obtain the Kalman gain, error residuals (innovation), final estimations for the optimal states and the optimal covariance, the FKF algorithm proceeds with the matrix-form sequence in two steps, as illustrated in table 1.

Moreover, the federated filtering principle can be applied to particle filter (FPF) as in [20, 22, 23] for nonlinear non-Gaussian estimations.

3. Types of commonly used multi-sensors

a). Inertial sensors

Inertial navigation sensors (INSs) are very reliable positioning systems, as they are not influenced by external factors. However, they accumulate significant errors over time [24, 25]. The main role of the primary positioning technology (e.g. GNSS) is to refine INS errors by tightening the position estimate to the absolute coordinate system while INS provides more accurate delta position updates in a short term.

An inertial measurement unit (IMU) differs from INS, as it is not an integrated dynamic system as an INS. However, IMU units are the main building block of INSs [26]. IMUs can still be utilized independently in fusion-based localization endeavors, but INSs have been widely adopted in positioning systems in the recent literature.

Globally, GNSS/INS fusion is a very common implementation due to the numerous advantages of this integration over utilizing each system solely [19]. As described in [4], both systems have complementary data to provide, GNSS estimates the PVT

Table 1: FKF algorithm for nonlinear multi-sensor fusion.

0 Initialization	for $k = 0$ set $\hat{X}_0, P_0^-, Q_0, R_0$
1 Prediction step	Prior estimate of the state: $X_{k+1}^- = \Phi_k X_k + U_k$ Prior estimate of the covariance: $P_{k+1}^- = \Phi_k P_k {\Phi_k}^T + Q_k$
2 Update step	Measurement residual update: $v_{k+1} = Z_{k+1} - H_{k+1} X_{k+1}$ Measurement covariance update: $S_{k+1} = H_{k+1} P_{k+1}^- {H_{k+1}}^T + R_{k+1}$ Kalman gain calculation: $K_{k+1} = P_{k+1}^- {H_{k+1}}^T S_{k+1}^{-1}$ Updating the posterior state: $X_{k+1} = X_{k+1}^- + K_{k+1} v_{k+1}$ Updating the posterior covariance: $P_{k+1} = P_{k+1}^- - K_{k+1} S_{k+1} K_{k+1}^T$ **Return to step 1, repeat until k iterations are consumed.**
Output	Estimated state vector: $\hat{X_F}$

measurements while INS provide the detailed information about the attitude which yield a 6-DOF system. Both systems can be utilized for mutual calibration hence reducing overall error components. The data rate of INS is higher than GNSS which produces better resolution for navigation in addition to exploiting previous features to achieve seamless navigation in GNSS-denied conditions. Consequently, the GNSS/INS multi-sensor fusion is suitable for aerial, terrestrial and extraterrestrial navigation on Earth and in Space.

b). Remote sensing

Remote sensing is the process of mapping the target environment by sending pilot signals and analysing the physical characteristics of the received signals. The pilot signals can be with different wavelengths, frequencies and types. Radars (Radio Detection and Ranging) is one type of remote sensing systems that utilizes low frequency RF signals as pilots, then detects the range of targets by analysing the frequency of the rebounded fraction of the signal. LiDAR (Light Detection and Ranging) is another type of remote sensors that employs high frequency light lasers in the same manner as Radars. Moreover, special types of Cameras can be considered as remote sensing systems when their functionalities are to map the topography of the surroundings, observe the heat maps of territories and so on. Other types of remote sensing can be acoustic like sonar systems, and can be ultra/infra sonic systems depending on the target application.

Radars and LiDARs are very common types of localization techniques that can be standalone systems and also can be used in multi-sensor fusion systems.

III. ADVANCES OF MULTI-SENSOR FUSION

In this section, we present a survey from the most recent literature that focus on the GNSS multi-sensor fusion approach. We highlight the implemented technologies within various applications. As the categorization of the multi-sensor literature is challenging, we present the in-text literature advances as application-based categorization while a summarized tabulation of references is presented from the perspective of quantity, integration and sensor types. The tabulated summary of sources is found in table 2.

Table 2: Summary of surveyed literature.

Dual integration	Triple integration	Quadruple and Quintuple integrations
GNSS/Inertial sensing [27], [28], [29], [5], [30], [31], [6], [32], [33],	GNSS/Inertial sensing/Remote sensing [36], [20], [37]	
GNSS/Remote sensing [34], [35], [36]	GNSS/Inertial sensing/Visual [38], [39], [40], [41],	GNSS/Inertial sensing/Remote sensing/Visual [43], [44], [45]
	GNSS/Inertial sensing/DR [42]	

1. Autonomous Driving and Intelligent Transportation Systems (ITS)

The authors of [36] validated an effective calibration method for the 6-DOF autonomous SLAM vehicles using LIDAR/GPS/IMU technique. The LIDAR error components originated from the deviations of point cloud measurements due to vehicle movement hence calibration became paramount. The GPS/IMU and LIDAR coordinate systems are matched by processing the time synchronization frames of LIDAR point cloud and corrected by the pose from GPS/IMU frame. The measurements of pitch and roll angles in addition to the Z-axis translation had transformed the 3-D positioning problem into 2-D problem. The ground truth data was used to solve the set of linear equations originated from sensors fusion thus obtain the optimal solution. The tests were held in a real vehicle by comparing the 3-D reconstruction results before and after the proposed calibration method. The verification results after calibration showed clearer views and more resolution than the views before calibration that were thicker in contours and more ambiguous.

In [38], the authors utilized triple fusion system GNSS/INS and optical velocity sensors (OVS) in addition to adaptive fault-tolerant fault detection and processing (FDP) algorithm to provide a continuous navigation information. The measurements of GNSS were judged against ground truth data to identify the observation outliers and biases that cross a preset threshold. Outliers were discarded and the biases were fed to the adaptive FDP (with varying covariance) for correction. The comparison

was conducted at three scenarios: clear skies, semi clear skies and totally unclear skies. Moreover, the validation was set to compare between tightly-coupled (TC) and loosely-coupled (LC) triple-fusion GNSS/INS/OVS. The results based on real experiment showed that the TC integration was more accurate the LC integration hence the method was concluded to be suitable for continuous accurate navigation.

Another LC dual-integration method INS/GPS is described in [27], in which the authors utilized an EKF algorithm as a master fusion filter. The conducted simulations on datasets showed that the proposed method achieved better accuracy for attitude, velocity and time also ensured reliability and continuation.

Similar LC approach was developed by [6] using EKF and linear KF estimations to improve the overall accuracy, which was validated via MATLAB simulations.

The authors of [39] proposed a triple-fusion method comprising IMU/GNSS and map matching to integrate the location information of micro-electromechanical systems (MEMs) with commercial road maps. The method was developed to mitigate the uncertainty associated with GNSS positioning hence overcome the problem of lane-detection by providing more accurate location. From algorithmic perspective, the authors used the LC-EKF as the main fusing algorithm also used as a standalone local filter for the tracking step. Additionally, the hidden Markov (HMM) and LS algorithms were used to estimate the vehicle lane by map matching the input road maps using buffered records of the vehicle's poses. Based on real-time experiments in the open-sky scenario, the results showed that the proposed lane determination method achieved 97.14% success rate in detecting the correct lanes.

An UTC architecture was developed by [5] to implement a GNSS/INS integrated system for the navigation of autonomous ground vehicles. The authors compared the performances of the LC-GNSS vector tracking with the GNSS consumer-grade tracking of a smart phone in extreme scenarios. The RTK positioning results validated that the availability of the UTC method was better than other methods but the accuracy should be further improved.

Another UTC architecture is utilized by [31] to combat the nonlinearity introduced by the INS/GPS integration using the unscented particle filter (UPF). The nonlinear measurement equation was formulated using the second-order Taylor expansion of the pseudoranges while the UPF was employed for the dynamic state estimations. Results showed that the proposed method with UPF outperformed the same approach when Kalman filter is used.

Environmental disturbances (e.g. vibrations) can cause error drifts in the attitude measurements hence the issue was studied by [30] using micro electromechanical inertial sensors (MEMS-IMU) and GPS. The authors developed a dual-fusion GPS/MEMS-IMU system with EKF as fusion filter to study the effect of vibrations on attitude. The efficacy and reliability of the proposed method were validated as shown by the results.

Dynamic positioning in urban environments is challenging where GNSS satellites can experience frequent blockages, their carrier-phase reliability decrease or become insufficient in number of usable satellites. Hence, the authors of [28] proposed a TC integration of GNSS/INS sensors to mitigate the error divergence and improve the overall positioning accuracy in complex urban environments. The authors utilized a linear combination of triple-frequency GNSS, proposed an ambiguity fixed observation algorithm to compensate on and round the blocked epochs, and used the nonlinear Cubature Kalman filter (CKF) as the master fusion algorithm. In addition to utilizing two local Kalman filters for the ambiguity resolution and the inertial fusion with GNSS. A test vehicle was used to verify the proposed method. The results of testing several scenarios showed improved accuracies for minimal and maximal number of visible satellites (4 and 11 satellites) ranging from 4.1cm to 67cm for vertical and horizontal directions.

Similar approach (GPS/IMU) was utilized in [29] to mitigate the accumulated errors in IMU caused by the absence of GPS signal. The authors used the vehicle kinematics model (VKM) along with a Kalman filter for the fusion. High efficiency and high precision of the proposed method were validated through simulations.

2. Military Applications

The authors of [41] constructed a hardware-in-the-loop (HIL) simulation to test GNSS/MEMS-IMU system that is fused with fiber optic gyroscope (FOG) resulting in a compound navigation system (CPNS). The proposed GNSS/MIMU/FOG method is aimed at improving the navigation accuracy of smart ammunitions by calibrating the MEMS gyroscope and GPS lag values. The HIL simulations showed that the proposed CPNS had effectively improved the navigation accuracy and significantly reduced the fusion error.

3. Atmospheric Navigation in Space

Fusion-based navigation can solve complex problems for re-usable space crafts during re-entry by enhancing the accuracy of the on-board inertial system, as described in [40]. The authors proposed a triple-integration method INS/Star-tracker/GPS in

which the INS measurements aided both GPS and the star tracker systems to correct the misalignment errors within a unified coordinal frame. Additionally, an EKF algorithm is used as a universal fusing filter to combine all the output estimations after being updated. The simulation results exhibited noticeable improvements in positioning accuracy, orientation accuracy, and overall efficiency.

4. Fusion with Radar systems

To achieve reliable object detection results for remote sensing, GNSS observables can be fused with radar systems to fine-tune the error drifts as in [34]. The authors proposed a theoretical GNSS/SAR approach using omnidirectional GNSS antenna operating at L1 frequency band, C/A code receiver and limited range field of view (FOV). The conducted experiment showed a probability of 0.1% as false alarm while the probability of detection was 95%, the FOV was restricted to 2 Km although theoretically the method should be able to detect objects from 5-8 Km away.

A quintuple-fusion system IMU/GNSS/Radar/Camera/LIDAR was proposed by [44] to provide precise environmental perception capabilities for automated-driving vehicles. The method used a 6-DOF kinematic model to produce PVT estimations which were corrected by the GNSS observations via LC error-state EKF algorithm. The observable measurements of radar, camera and LIDAR enhanced the overall perception of the surrounding environment using an outlier detection of optically impaired data. The conducted results showed that the redundancy of sensor data improved the robustness and the overall accuracy for 2-D and 3-D scenarios. Moreover, the scalability and precision were validated.

5. Pedestrian Tracking

A likelihood detection method was utilized in [20] using FPF approach for tracking in nonlinear non-Gaussian environment. The proposed method was a triple fusion system JIDS/SINS/GPS augmented by FPF algorithm as global fusion filter and local PFs for the three subsystems. After simulating the system, the results showed a high detection rate, low detection time and lower directional RMS values which achieved an improved performance of the fusion-fault tolerance.

6. Unmanned Aerial Vehicles (UAVs)

Ultra Wideband (UWB) is a wireless short-range radio-technology in which its communication channel propagates information over wide spectrum by modulating either a carrier-based waveform or carrier-less baseband signal in the form of short-width pulses [46].

The authors of [36], proposed a high-precision prototype for UAV traffic management (UTM) system. Besides the GPS, the authors utilized a novel method comprising an impulse radio (IR) calibrated UWB (Decawave) in addition to LoRa module. The implemented cost function of the proposed method GPS/UWB had reduced the GPS positioning error from 4.03 to 1.73 cm.

In [45], the authors designed a fusion positioning algorithm of GNSS/UWB/DR/VMM with a federated Kalman filter (FKF). Both the simulation and the results from real vehicle testing showed that the proposed intelligent vehicle localization accuracy was improved (MAE < 0.88 m). The positioning accuracy could be improved adaptive information distribution coefficient was established based on the FKF.

IV. CONCLUSION

Seamless navigation is a very crucial element for many PNT-dependent applications and future IoT implementations. GNSS standalone systems are providing acceptable level of integrity to many technologies especially in open-sky environments. Yet, they are not suitable for precise positioning and seamless navigation due to numerous factors such as: multipath fading, attenuation in dense environments, and signal obstruction in GNSS-denied conditions and urban environments. Multi-sensor fusion technologies are very promising candidates to mitigate positioning errors since they utilize additional navigational sensors that aid GNSSs in providing continuous navigation hence maintain integrity and the desired service level. Numerous applications are beneficiaries of precise multi-sensor fusion systems such as: autonomous self-driving vehicles, UAVs, mobile robots and smart machines. The capabilities of integrated GNSS fusion-based systems are maximized by the added multiple sensors hence meet the requirements of the beneficiary applications. In this survey, we presented a short review of the most recent literature that focus on the developing of dedicated multi-sensor systems in specific applications. We highlighted the use of inertial sensors, remote sensing devices, visual-based sensors, and RF-based navigational sensors to achieve seamless navigation for various scenarios. Moreover, we presented an overall view on the algorithmic implementations of multi-sensor fusion systems such as: Kalman filters, particle filters, and federal filters. We constructed the architecture of this article to be a short supporting tutorial for researchers seeking higher perspective on the GNSS multi-sensor fusion topic. In the future, we intend to design, implement, and develop our proposed fusion-based system that comprise GNSS, inertial sensors, UWB and low-earth orbit satellites (LEO) for seamless navigation.

ACKNOWLEDGEMENTS

This article is part of the TULEVA and INCUBATE projects managed by the Digital Economy platform at the University of Vaasa, Finland.

REFERENCES

[1] N. Zhu, J. Marais, D. Betaille, and M. Berbineau, "GNSS Position Integrity in Urban Environments: A Review of Literature," *IEEE Transactions on Intelligent Transportation Systems*, vol. 19, no. 9, pp. 2762–2778, sep 2018. [Online]. Available: https://doi.org/10.1109%2Ftits.2017.2766768

[2] P. Forum, "Classification criteria." [Online]. Available: https://julkaisufoorumi.fi/en/evaluations/classification-criteria

[3] X. Guo, N. Ansari, F. Hu, Y. Shao, N. R. Elikplim, and L. Li, "A Survey on Fusion-Based Indoor Positioning," *IEEE Communications Surveys & Tutorials*, vol. 22, no. 1, pp. 566–594, 2020. [Online]. Available: https://doi.org/10.1109%2Fcomst.2019.2951036

[4] P. Srinivas and A. Kumar, "Overview of architecture for GPS-INS integration," in *2017 Recent Developments in Control Automation & Power Engineering (RDCAPE)*. IEEE, oct 2017. [Online]. Available: https://doi.org/10.1109%2Frdcape.2017.8358310

[5] Y. Luo, C. Yu, B. Xu, J. Li, G.-J. Tsai, Y. Li, and N. El-Sheimy, "Assessment of Ultra-Tightly Coupled GNSS/INS Integration System towards Autonomous Ground Vehicle Navigation Using Smartphone IMU," in *2019 IEEE International Conference on Signal Information and Data Processing (ICSIDP)*. IEEE, dec 2019. [Online]. Available: https://doi.org/10.1109%2Ficsidp47821.2019.9173292

[6] N. C. Yadav, A. Shanmukha, B. M. Amruth, and Basavaraj, "Development of GPS/INS integration module using Kalman filter," in *2017 International Conference on Algorithms Methodology, Models and Applications in Emerging Technologies (ICAMMAET)*. IEEE, feb 2017. [Online]. Available: https://doi.org/10.1109%2Ficammaet.2017.8186715

[7] R. E. Kalman, "A New Approach to Linear Filtering and Prediction Problems," *Journal of Basic Engineering*, vol. 82, no. 1, pp. 35–45, mar 1960. [Online]. Available: https://doi.org/10.1115%2F1.3662552

[8] R. Faragher, "Understanding the Basis of the Kalman Filter Via a Simple and Intuitive Derivation [Lecture Notes]," *IEEE Signal Processing Magazine*, vol. 29, no. 5, pp. 128–132, sep 2012. [Online]. Available: https://doi.org/10.1109%2Fmsp.2012.2203621

[9] G. A. Darbellay, "An estimator of the mutual information based on a criterion for conditional independence," *Computational Statistics & Data Analysis*, vol. 32, no. 1, pp. 1–17, nov 1999. [Online]. Available: https://doi.org/10.1016%2Fs0167-9473%2899%2900020-1

[10] J. Hartikainen, A. Solin, and S. Särkkä, *Optimal filtering with Kalman filters and smoothers - a Manual for Matlab toolbox EKF/UKF*. Aalto University, 2011.

[11] T. K. Y. Bar-Shalom, X. Rong Li, *Estimation with Applications To Tracking and Navigation*. John Wiley Inc, 2001.

[12] Y. Bar-Shalom, "Recursive tracking algorithms: from the kalman filter to intelligent trackers for cluttered environment," in *Proceedings. ICCON IEEE International Conference on Control and Applications*. IEEE, 1989. [Online]. Available: https://doi.org/10.1109%2Ficcon.1989.770605

[13] S. Julier and J. Uhlmann, "Unscented Filtering and Nonlinear Estimation," *Proceedings of the IEEE*, vol. 92, no. 3, pp. 401–422, mar 2004. [Online]. Available: https://doi.org/10.1109%2Fjproc.2003.823141

[14] S. Sarkka, "On Unscented Kalman Filtering for State Estimation of Continuous-Time Nonlinear Systems," *IEEE Transactions on Automatic Control*, vol. 52, no. 9, pp. 1631–1641, sep 2007. [Online]. Available: https://doi.org/10.1109%2Ftac.2007.904453

[15] I. Ullah, Y. Shen, X. Su, C. Esposito, and C. Choi, "A Localization Based on Unscented Kalman Filter and Particle Filter Localization Algorithms," *IEEE Access*, vol. 8, pp. 2233–2246, 2020. [Online]. Available: https://doi.org/10.1109%2Faccess.2019.2961740

[16] M. Vemula, M. F. Bugallo, and P. M. Djuric, "Performance Comparison of Gaussian-Based Filters Using Information Measures," *IEEE Signal Processing Letters*, vol. 14, no. 12, pp. 1020–1023, dec 2007. [Online]. Available: https://doi.org/10.1109%2Flsp.2007.906214

[17] G. Kitagawa, "A Self-Organizing State-Space Model," *Journal of the American Statistical Association*, vol. 93, no. 443, p. 1203, sep 1998. [Online]. Available: https://doi.org/10.2307%2F2669862

[18] N. A. CARLSON and M. P. BERARDUCCI, "Federated Kalman Filter Simulation Results," *Navigation*, vol. 41, no. 3, pp. 297–322, sep 1994. [Online]. Available: https://doi.org/10.1002%2Fj.2161-4296.1994.tb01882.x

[19] C. Jie, C. Shaoshan, L. Yu, and R. Chongyu, "Design of Integrated Navigation System Based on Information Fusion Technology for the Intelligent Transportation System," in *2006 6th International Conference on ITS Telecommunications*. IEEE, jun 2006. [Online]. Available: https://doi.org/10.1109%2Fitst.2006.288853

[20] L. Ziyu, D. Chenglin, C. Bing, and Y. Xudong, "Application of federated particle filter fusion and fault tolerance in integrated navigation system," in *2017 First International Conference on Electronics Instrumentation & Information Systems (EIIS)*. IEEE, jun 2017. [Online]. Available: https://doi.org/10.1109%2Feiis.2017.8298677

[21] Z. Zhao and J. Zhen, "Federated Kalman filter and its application to GPS/DR integrated navigation system," in *Proceedings of 2011 Cross Strait Quad-Regional Radio Science and Wireless Technology Conference*. IEEE, jul 2011. [Online]. Available: https://doi.org/10.1109%2Fcsqrwc.2011.6037047

[22] Z. Y. Li, Y. Liu, P. Zhu, and C. Ying, "Federated Particle Filter Technology Based on JIDS/SINS/GPS Integrated Navigation System," *Applied Mechanics and Materials*, vol. 347-350, pp. 1544–1548, aug 2013. [Online]. Available: https://doi.org/10.4028%2Fwww.scientific.net%2Famm.347-350.1544

[23] L. Meng and L. Jia-hong, "A Federated particle filtering algorithm based on EKPF," in *2011 International Conference on Electric Information and Control Engineering*. IEEE, apr 2011. [Online]. Available: https://doi.org/10.1109%2Ficeice.2011.5778115

[24] Y. Wang and X. Li, "The IMU/UWB Fusion Positioning Algorithm Based on a Particle Filter," *ISPRS International Journal of Geo-Information*, vol. 6, no. 8, p. 235, aug 2017. [Online]. Available: https://doi.org/10.3390%2Fijgi6080235

[25] J. Liu, J. Pu, L. Sun, and Z. He, "An Approach to Robust INS/UWB Integrated Positioning for Autonomous Indoor Mobile Robots," *Sensors*, vol. 19, no. 4, p. 950, feb 2019. [Online]. Available: https://doi.org/10.3390%2Fs19040950

[26] R. D. Christ and R. L. Wernli, "Navigational Sensors," in *The ROV Manual*. Elsevier, 2014, pp. 453–475. [Online]. Available: https://doi.org/10.1016%2Fb978-0-08-098288-5.00017-8

[27] D. M.G. and A. Arun, "Analysis of INS Parameters and Error Reduction by Integrating GPS and INS Signals," in *2018 International Conference on Design Innovations for 3Cs Compute Communicate Control (ICDI3C)*. IEEE, apr 2018. [Online]. Available: https://doi.org/10.1109%2Ficdi3c.2018.00013

[28] F. Ye, S. Pan, W. Gao, H. Wang, G. Liu, C. Ma, and Y. Wang, "An Improved Single-Epoch GNSS/INS Positioning Method for Urban Canyon Environment Based on Real-Time DISB Estimation," *IEEE Access*, vol. 8, pp. 227 566–227 578, 2020. [Online]. Available: https://doi.org/10.1109%2Faccess.2020.3044197

[29] S. ZHOU, P. ZHAO, and J. JIN, "Cascaded GPS/IMU Integrated Positioning System Based on Vehicle Kinematics Model," in *2020 Chinese Control And Decision Conference (CCDC)*. IEEE, aug 2020. [Online]. Available: https://doi.org/10.1109%2Fccdc49329.2020.9164392

[30] Z. Li and Y. Tang, "Attitude Determination for Land Vehicles Based on Low Cost GPS/MEMS-IMU," in *2018 Eighth International Conference on Instrumentation & Measurement Computer, Communication and Control (IMCCC)*. IEEE, jul 2018. [Online]. Available: https://doi.org/10.1109%2Fimccc.2018.00311

[31] J. X. Ren, J. L. Zi, H. Y. Guan, and J. Li, "Design of an Ultra-Tightly Coupled Integrated INS/GPS Navigation System Based on UPF," in *2020 27th Saint Petersburg International Conference on Integrated Navigation Systems (ICINS)*. IEEE, may 2020. [Online]. Available: https://doi.org/10.23919%2Ficins43215.2020.9133853

[32] K. Park, W. Kim, and J. Seo, "Effects of Initial Attitude Estimation Errors on Loosely Coupled Smartphone GPS/IMU Integration System," in *2020 20th International Conference on Control, Automation and Systems (ICCAS)*, Oct. 2020, pp. 800–803, iSSN: 2642-3901.

[33] M. Crabolu, M. Giuberti, and G. Bellusci, "Electrically integrated miniature motion tracking module with multiple external GNSS receiver support," in *2018 DGON Inertial Sensors and Systems (ISS)*, Sep. 2018, pp. 1–13, iSSN: 2377-3480.

[34] Y. Zheng, Y. Yang, and W. Chen, "Analysis of radar sensing coverage of a passive GNSS-based SAR system," in *2017 International Conference on Localization and GNSS (ICL-GNSS)*. IEEE, jun 2017. [Online]. Available: https://doi.org/10.1109%2Ficl-gnss.2017.8376246

[35] D. Perea-Strom, A. Morell, J. Toledo, and L. Acosta, "GNSS Integration in the Localization System of an Autonomous Vehicle Based on Particle Weighting," *IEEE Sensors Journal*, vol. 20, no. 6, pp. 3314–3323, Mar. 2020.

[36] C. Chen, G. Xiong, Z. Zhang, J. Gong, J. Qi, and C. Wang, "3D LiDAR-GPS/IMU Calibration Based on Hand-Eye Calibration Model for Unmanned Vehicle," in *2020 3rd International Conference on Unmanned Systems (ICUS)*. IEEE, nov 2020. [Online]. Available: https://doi.org/10.1109%2Ficus50048.2020.9274947

[37] Q. Xu, X. Li, and C.-Y. Chan, "Enhancing Localization Accuracy of MEMS-INS/GPS/In-Vehicle Sensors Integration During GPS Outages," *IEEE Transactions on Instrumentation and Measurement*, vol. 67, no. 8, pp. 1966–1978, Aug. 2018.

[38] W. Jiang, D. Liu, B. Cai, C. Rizos, J. Wang, and W. Shangguan, "A Fault-Tolerant Tightly Coupled GNSS/INS/OVS Integration Vehicle Navigation System Based on an FDP Algorithm," *IEEE Transactions on Vehicular Technology*, vol. 68, no. 7, pp. 6365–6378, jul 2019. [Online]. Available: https://doi.org/10.1109%2Ftvt.2019.2916852

[39] M. M. Atia, A. R. Hilal, C. Stellings, E. Hartwell, J. Toonstra, W. B. Miners, and O. A. Basir, "A Low-Cost Lane-Determination System Using GNSS/IMU Fusion and HMM-Based Multistage Map Matching," *IEEE Transactions on Intelligent Transportation Systems*, vol. 18, no. 11, pp. 3027–3037, nov 2017. [Online]. Available: https://doi.org/10.1109%2Ftits.2017.2672541

[40] J. Wu and W. Wang, "An On-Orbit Initial Alignment Method for Reusable Spacecraft with INS Star Sensor and GPS," in *2018 Eighth International Conference on Instrumentation & Measurement Computer, Communication and Control (IMCCC)*. IEEE, jul 2018. [Online]. Available: https://doi.org/10.1109%2Fimccc.2018.00226

[41] X. Cai, C. Zhang, Y. Yang, S. Gao, J. Lu, and R. Zhang, "Data Fusion Method of Measurement Lag Compensation for Multirate MIMU/FOG/GNSS Compound Navigation," *IEEE Sensors Journal*, vol. 20, no. 9, pp. 5048–5060, may 2020. [Online]. Available: https://doi.org/10.1109%2Fjsen.2020.2966926

[42] W. J. Park, J. H. Lee, C. H. Kang, M. H. Seo, S. Y. Park, J. Y. Yeo, J. W. Song, and C. G. Park, "Low Cost MEMS-IMU Based DR/GPS Integrated System in Urban Environment," in *2018 18th International Conference on Control, Automation and Systems (ICCAS)*, Oct. 2018, pp. 767–771.

[43] S. Guo, B. He, C. Feng, H. Liu, F. Yin, X. Zhang, X. Mu, T. Li, and T. Yan, "Fault Tolerant Multi-Sensor Federated Filter for AUV Integrated Navigation," in *2019 IEEE Underwater Technology (UT)*, Apr. 2019, pp. 1–4, iSSN: 2573-3796.

[44] Y. Liang, S. Muller, D. Schwendner, D. Rolle, D. Ganesch, and I. Schaffer, "A Scalable Framework for Robust Vehicle State Estimation with a Fusion of a Low-Cost IMU the GNSS Radar a Camera and Lidar," in *2020 IEEE/RSJ International Conference on Intelligent Robots and Systems (IROS)*. IEEE, oct 2020. [Online]. Available: https://doi.org/10.1109%2Firos45743.2020.9341419

[45] B. Zhu, X. Tao, J. Zhao, M. Ke, H. Wang, and W. Deng, "An Integrated GNSS/UWB/DR/VMM Positioning Strategy for Intelligent Vehicles," *IEEE Transactions on Vehicular Technology*, vol. 69, no. 10, pp. 10 842–10 853, oct 2020. [Online]. Available: https://doi.org/10.1109%2Ftvt.2020.3014516

[46] A. Wilzeck, M. P. Guirao, and E. Dimitrov, "White Paper on UWB Technology and Regulation," *wiseSense GmbH*, 2018.

Publication P6

PEER REVIEWED

Application of Machine Learning to GNSS/IMU Integration for High Precision Positioning on Smartphones

Akpojoto Siemuri[1], Mahmoud Elsanhoury[1], Petri Välisuo[1], Heidi Kuusniemi[1,2], Mohammed S. Elmusrati[1]
[1] *School of Technology and Innovations, University of Vaasa, Finland*
[2] *Finnish Geospatial Research Institute, National Land Survey, Finland*

BIOGRAPHY

Akpojoto Siemuri received his B.Sc.(tech) degree in electrical and computer engineering from Federal University of Technology Minna, Nigeria in 2010, a M.Sc.(tech) degree in wireless industrial automation with a minor study in industrial management from the University of Vaasa, Finland in 2019. He is currently pursuing a Ph.D. degree in automation technology at the University of Vaasa. From 2018 to 2019, he was a Research Assistant in the Smart Energy Systems Research Platform (SESP) Project at the University of Vaasa, Finland. He is currently a Project Researcher in Digital Economy Research Platform, University of Vaasa. His research interest includes machine learning, GNSS technologies, smart devices, embedded systems, communication systems, and game theory.

Mahmoud Elsanhoury is currently pursuing the doctoral (Ph.D) degree in computer science and telecommunications engineering at the University of Vaasa, Finland. He received his M.Sc. (tech) degree in telecommunications engineering from Vaasa University in 2018, and the B.Sc. degree in telecommunications engineering from Alexandria University, Egypt in 2013. His current research interests cover ubiquitous indoor positioning systems, ultra-wideband (UWB) indoor localization, low-earth orbit (LEO) satellites for positioning, multisensor fusion technologies, Kalman filters, uncertain stochastic processes and machine learning algorithms.

Petri Välisuo is currently working as an Associate Professor (tenure track), sustainable automation, in the School of Technology and Innovation Management of University of Vaasa, Finland. He received M.Sc.(tech) degree in computer science from the Tampere University of Technology, Finland, and D.Sc.(tech) degree in automation technology from University of Vaasa, in years 1996 and 2011 respectively. He has authored and co-authored 27 peer reviewed and more than 10 other scientific publications. His research interests cover machine learning, IoT, positioning methods and other technologies relevant to industrial automation. He has been working 10 years in telecommunication industry before the research career at the University of Vaasa.

Dr. Heidi Kuusniemi is a professor in computer science and director of Digital Economy at the University of Vaasa in Finland. She is also a part-time research professor in satellite navigation at the Finnish Geospatial Research Institute. She has a M.Sc. (Tech.) degree (with distinction) from 2002 and a D.Sc. (Tech.) degree from 2005 in information technology, respectively, from Tampere University of Technology, Finland. She served as a member of the council of natural sciences and technology at the Academy of Finland 2019-2021 and was a member of the scientific advisory committee for GNSS (GSAC) at ESA. Her technical expertise and interests include GNSS reliability and resilience, estimation and data fusion, mobile precision positioning, indoor localization and PNT in new space.

Prof. Mohammed S. Elmusrati received his B.Sc. (with honors) and M.Sc. (with high honors) degrees in electrical and electronic engineering, University of Benghazi, Libya, in 1991 and 1995, respectively, and the Licentiate of Science in technology (with distinction) and the Doctor of Science in Technology (D.Sc.) degrees in automation and control engineering from Aalto University Finland, in 2002 and 2004, respectively. Currently, he is Full Professor and Head of the Digitalization Unit at the School of Technology and Innovations – University of Vaasa, Finland. His research interest includes wireless communications, artificial intelligence, machine learning, biotechnology, big data analysis, stochastic systems, and game theory. Elmusrati has published more than 130 papers, books, and book chapters. Prof. Elmusrati is an active member in different scientific societies such as Senior Member at IEEE, Member at Society of Industrial and Applied Mathematics (SIAM), and Member at Finnish Automation Society.

 https://doi.org/10.33012/2022.18375

ABSTRACT

This paper describes our solution for the Google smartphone decimeter challenge (GSDC), which was held from May to August 2022. The GSDC is a competition for improving positioning accuracy of smartphones. The global navigation satellite system (GNSS) data from smartphones have lower signal levels and higher noise in GNSS observations compared to commercial GNSS receivers. Therefore, it is difficult to directly apply the existing GNSS high-precision positioning methods like precise point positioning (PPP) and real-time kinematic (RTK). The smartphones used to collect the raw GNSS data have multi-constellation, dual-frequency GNSS receivers, and Inertial Measurement Unit (IMU) sensors. Multi-sensor fusion technology has become very prominent for seamless navigation systems due to its complementary capabilities to GNSS positioning. In this work, we developed a machine learning (ML) based adaptive positioning approach to estimate the positions of the smartphone by utilizing post-processed kinematic (PPK) precise positioning techniques to process the GNSS datasets. The ML model is used to predict the driving paths (highways, tree-lined streets, or downtown areas). Depending on the predicted driving path, PPK technique uses the carrier phase to compute the user position using differential corrections from known GNSS base stations. We then use of the Rauch–Tung–Striebel (RTS) smoother, which consists of a forward pass Kalman Filter (KF) and a backward recursion smoother to achieve a loosely coupled integration of GNSS and IMU measurements for positioning estimation of the smartphone. We refer to this method as LC-GNSS/IMU/ML using ML based adaptive positioning (MAP) real-time kinematic (RTK) post-processing algorithm (MAP RTK). This method is validated using reference data from GNSS survey-grade receivers provided with the training datasets. The final validation of this proposed method is done on Kaggle.com, the host of the GSDC competition. Using the proposed method, we estimated the location of the smartphone and tackled the competition. The final public score was 2.61 m, while the final private score was 2.29 m.

Keywords - Adaptive positioning; Machine Learning; Kalman Filter; Rauch–Tung–Striebel smoother; Inertial Measurement Units; Global Navigation Satellite Systems; Post-processed kinematic; Smartphones

I. INTRODUCTION

Multi-constellation global navigation satellite systems (GNSS) provide benefits such as the availability of more visible satellites that can be used to improve user positioning performance [1]. This is useful in challenging environments where GNSS signals could be partially or totally blocked and are affected by multi-path reflections, for example, in urban areas or places with dense foliage, this becomes very useful. Accuracy greater than 100 meters in the worst non-line-of-sight condition can improve to between 5 meters and sub-meter depending on the technique used for data collection and the receiver used (survey-grade or low-cost receivers). In 2016, the Android operating system released an application program interface to access raw GNSS measurement data from GNSS installed in smartphones [2]. As a result, high-precision positioning at the decimeter and centimeter levels on smartphones has attracted much attention [3, 4]. There have been growing interests in the use of low-cost receivers and GNSS chipsets on smartphones for positioning applications. However, they do not provide very precise accuracy as the high grade (survey-grade receivers), especially due to antenna constraints. Differential correction, a data collection technique, can be used to remove errors in GNSS data created by selective availability, ionospheric delay, tropospheric delay, and ephemeris errors. There are other factors that lead to error in positioning, such as multi-path propagation which causes ranging measurement errors [5]. Other factors (less correctable) that create an error in GNSS data include the large distance between the rover and the base station (about 10 mm degradation with every kilometer away from the base station when differential correction is considered), low SNR (signal to noise ratio), and low satellite elevation [5].

GNSS provides raw signals, which the GNSS chipsets in smartphones use to compute a position. Code phase utilization is one processing technique that gathers data via a C/A (coarse acquisition) code receiver, which uses the information contained in the satellite signals (aka the pseudo-random code) to calculate positions. After differential correction, this processing technique can result in 1-5 meter accuracy. Carrier phase utilization is another processing technique that gathers data via a carrier phase receiver, which uses the radio signal (aka carrier signal) to calculate positions. The carrier signal, which has a much higher frequency than the pseudo-random code, is more accurate than using the pseudo-random code alone. After differential correction, this processing technique can result in sub-meter accuracy depending on the GNSS receiver. The data used in this paper is from the Google smartphone decimeter challenge (GSDC). In GSDC, each dataset includes raw GNSS measurements collected in the US San Francisco Bay and other areas by several Android smartphone devices, together with the ground truth trajectories collected by high-grade GNSS and inertial navigation unit (IMU) integration system for reference.

Another point of interest is how machine learning (ML) can be used to improve the positioning of smartphones. ML is a very powerful tool in processing time-series data, as it can be applied in learning time-dependent patterns across multiple models. It is useful in analyzing hidden and unknown patterns and information in GNSS data. GNSS is a source of affordable big data useful for ML exploitation. Also, data storage and the growth of less expensive and more powerful processing capabilities have propelled the growth of ML [6]. The aim of using ML is not to generate an explicit formula for the distribution of the data; however, it is used to train an algorithm to detect the relationships between the features of a data set, directly from the data.

In this paper, we describe our solution used in this competition in which there were over 571 teams from all over the world

working on high-precision positioning of smartphones.

II. STRATEGY

Real-time kinematic (RTK)-GNSS technique, which is usually used for high-precision positioning, is difficult to implement in smartphones due to limitations of their antennas. This is because it is difficult to solve the integer ambiguities in the carrier phase measurements using smartphone antenna. Even in an open-sky environment with an accuracy of 3 m it is still difficult to reach decimeter level since there is a lot of noise and outliers in the observations. Therefore, a robust position estimation method is needed. In our work, we still attempt to make use of RTK-GNSS technique or in our case, post-processed kinematic (PPK) positioning techniques to process the GNSS datasets. A ML model is used to predict the driving paths (highways, tree-lined streets, or downtown areas) for adaptive positioning using PPK. In the PPK technique, the carrier phase is used to compute the user position making use of differential corrections. We then implement loosely coupled integration of GNSS and IMU measurements for position estimation, using Kalman filter (KF) algorithm and Rauch–Tung–Striebel (RTS) smoother. The initial results show improvements in the positioning accuracy. GNSS low-cost receivers often have limited channels and computational resources, therefore, the complexity of the algorithm had to be kept modest. Further validations will be performed to ensure the integrity of the proposed loosely coupled GNSS/IMU/ML (LC-GNSS/IMU/ML) method.

The steps or approach taken are as follows:

1. Data Analysis and Preparation
2. ML based prediction of driving path
3. PPK precise positioning techniques to process the GNSS datasets
4. GNSS/IMU integration making use of KF/RTS-based method

III. DATA ANALYSIS AND PREPARATION

The performance of smartphones satellite observation indicates that they cannot track satellites stably, also they can only observe a small number of satellites continuously with dual-frequency signals. Furthermore, the quality of the satellites observed by smartphones generally have a low carrier-to-noise ratio (C/NR) [7]. Multipath is another factor that significantly impaired the positioning accuracy of smartphones. Therefore, we first analyze the GNSS data of smartphones provided by GSDC to understand the observation quality of GNSS data.

At the ION GNSS+ 2022, Google released a total of 206 traces in the challenge, whose collection process is described in a paper published in the proceedings of ION GNSS+ 2020 [2]. The data were released twice, first the training data and next was the test data. The training datasets consisted of GnssLogger files, RINEX observation files, ground truth files, and device IMU/GNSS data files (GNSS intermediate values derived from raw GNSS measurements, provided for convenience). The test datasets include the same types of data and follow the same convention as the training dataset, except for the ground truth data that are not provided. The results of test datasets will be used as the prediction of the expected ground truth and will be evaluated using the unreleased ground truth. In both the training and test datasets, the derived values can be used to compute a corrected pseudorange which is a closer approximation to the geometric range from the phone to the satellite.

The driving paths of the provided GNSS data can be classified into three main categories: highways, tree-lined streets, or downtown areas. The train dataset ground truth track is shown in Figure 1. These pools of GNSS and IMU datasets collected from smartphones can be useful in developing high precision GNSS positioning using the accompanied high accuracy ground truth from high-grade GNSS receivers. Table 1 shows an overview of the weighted least square (WLS) positioning results, provided by the competition organizer for three categories of driving environments. The smartphone observed pseudorange is much noisier compared to commercial GNSS receiver, and GNSS code positioning using only pseudorange has limited positioning accuracy.

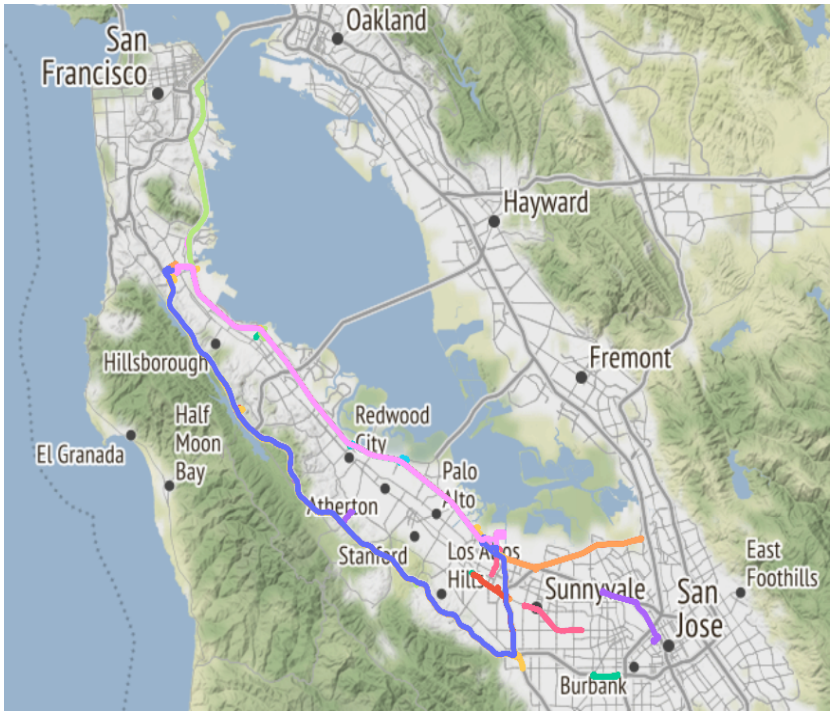

Figure 1: Driving trajectories included in training and some test data provided by GSDC.

The driving trajectories or paths are from the training data reference positions (ground truth) of the training data. Some new driving paths were included in the test data that are not present in the training data.

Table 1: Horizontal positioning error of the WLS baseline position in each driving path

Path	Highway	Tree-lined Street	Semi-Downtown
WLS baseline score	**4.3134 [m]**	**8.2553 [m]**	**8.0413 [m]**

IV. RELATED RESEARCHES

Precise point positioning using carrier phase measurements has been actively studied in the GNSS field. In [8] precise point positioning using carrier phase measurements with graph optimization is implemented and compared with Kalman filter based implementation. The use of RTK position estimation combined with IMU and other sensors have been studied [9, 10]. These papers showed an improvement in positioning accuracy compared to least-squares-based positioning. GNSS position estimation is highly dependent on the environment where the GNSS receiver is operating (open sky or urban canoys). In [3], the area of data collection was considered during position estimation. This paper is unique because it uses ML to predict the driving path of the data for an adaptive RTK position estimation. The Rauch–Tung–Striebel (RTS) smoother is used to achieve a loosely coupled integration of the GNSS carrier-phase and IMU measurements for positioning estimation in the smartphone.

V. PROPOSED METHOD

1. ML based Adaptive processing

Machine learning (ML) is applied to improve the positioning estimation of the KF/RTS-based GNSS/IMU integration using the ground truth data provided with GSDC training datasets. These ground truth data were collected using high-end survey-grade GNSS receivers. The driving paths of the provided GNSS data can be classified into three categories: highways (open sky) with line-of-sight (LOS), tree-lined streets, and downtown areas with multi-path/Non-LOS (NLOS). The training dataset is used to train the ML model to predict the driving paths. Different approaches has to be used in different areas. Especially in the downtown area where multipath signals caused by reflections and diffractions can significantly degrade the GNSS observations. Based on the predicted driving path, different PPK configurations are used to process the data for improved solutions. Parameters such as elevation angle of the satellite, C/NR, etc are considered based on the predicted driving path. This is done because GNSS measurements are easily disturbed by external influence such as multi-path which can be experienced in tree-lined streets, and downtown areas.

2. PPK precise positioning techniques

Real-time kinematic positioning (RTK) is the application of surveying to correct for common errors in current satellite navigation (GNSS) systems. It uses carrier phase measurements and the information content of the signal and relies reference station or interpolated virtual station to provide real-time corrections, which can give up to centimetre-level accuracy. In our case we use the post-process kinematic (PPK) for position estimation since the data is not collected in real-time. After the prediction of the driving path using the ML model, the data are then processed using PPK precise positioning techniques. The way the data is processed depends on the predicted driving path. First, we convert each phone GNSSLogger raw data file into a RINEX file that can then be processed with RTKLIBS programs [11]. RTKPOST [11] was first used to get an understanding of a couple of datasets and the right configurations to used to get a good PPK solution. Afterward, we batch process all of the data sets to get the position estimation. In the PPK technique, carrier phase data is used to compute the user position. The use of PPK requires differential correction, therefore some base observation were used to download raw observation data for the appropriate dates and times from some nearby CORS stations using NOAA National Geodetic Survey website. The SLAC, P222, and VDCY stations are used because they were reasonably close to all of the data collection rides. The satellite broadcast navigation data (BRDM files) for each data set was also downloaded from the International GNSS Service website including the clock navigation data, and satellite precise orbits [12]. These are used during the post-processing of the GNSS data.

3. Hardware clock bias

In GSDC dataset there are a couple of data sets that have corrupted carrier phase measurements. The initial RTKLIB solutions for these datasets are quite poor and are typicaly worse compared to the included Google baseline solutions which uses the WLS for pseudo-range measurements. These data sets can be identified by the *HardwareClockDiscontinuityCount* field in the raw Androiod log files [13]. If the final value in this field is larger than the initial value, then the carrier phase measurements will be corrupted by the clock discontinuities. The log files of the datasets are scanned using an algorithm to identify any with greater than one discontinuity[12]. The solutions for the listed dataset use the robust WLS solution in place of the poor RTK solutions [14].

4. GNSS/IMU integration using RTS smoothing algorithm

The Inertial Measurement Unit (IMU) is frequently used in robotics, vehicles, and, of course, in mobile phones. An IMU is usually made up of an accelerometer, gyroscope, and magnetometer. Tactical grade IMU is fully calibrated compared to low-cost ones which come with some factory calibrations stored in the IMU registers. The calibration only covers the scaling factors of each axes. The accelerometer measures the acceleration of a movement, the gyroscope measures the angular speed of the sensor, and the magnetometer measures the Earth's local magnetic field direction and magnitude.

Sensor fusion also referred to as data fusion, information fusion, or multi-sensor data fusion is used in the fusion of data from the accelerometer, magnetometer, and gyroscope. The fusion is performed to obtain position estimates and mitigate overall errors. Kalman filter is used for IMU and data fusion whereas numerical integration is required to obtain the position estimates. Basically, accelerometer values are fed to a dynamic model where they were numerically time-integrated twice to get the position, with the discretization and linearization (approximation) phases. The angular velocities measured from the gyroscope can be integrated with respect to time used to obtain the pitch and roll angles, which are later employed in the dynamic model to serve in the general state vector as fine-tuning values for the IMU localization.

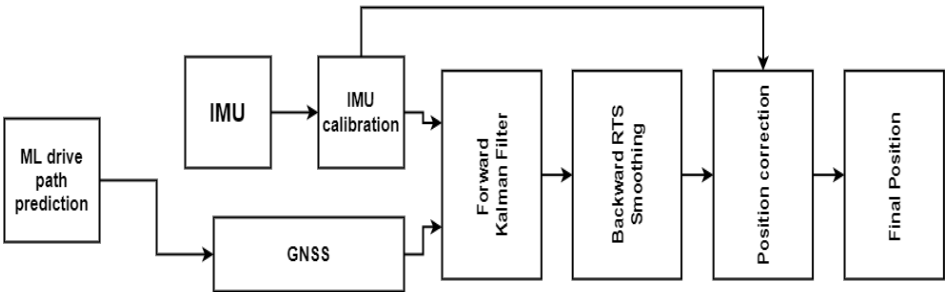

Figure 2: The flow diagram of MAP RTK post-processing algorithm.

GNSS measurements are easily disturbed by external influence such as multipath but the integration of GNSS with IMU is beneficial as the advantages and disadvantages of GNSS and IMU complement each other to enable accurate measurements in challenging areas. They are three types of IMU and GNSS integration namely, loosely coupled, tightly coupled, and ultra-tight coupled integration [15]. In this research we used the loosely coupled integration with KF/RTS, to integrate GPS and IMU in one system. We use the acceleration measured by IMU for inertial navigation calculation to get the data of position. We use them together with the information of GNSS for integration. The result is used as a prior observation of Kalman filtering while the covariance matrix and state transition matrix gained from forward Kalman filtering process is used for the reverse RTS smooth to the state estimate. The Rauch–Tung–Striebel (RTS) smoother, consists of a forward pass Kalman Filter (KF) and a backward recursion smoother to achieve the loosely coupled integration of GNSS and IMU measurements for positioning estimation in the smartphone. The forward classical Kalman filter is used to estimate the state of each moment, while the backward filter is to obtain more accurate state estimate on the basis of forward filter [16]. The flow diagram of MAP RTK post-processing algorithm is shown in Figure 2.

The state vector of the Kalman filter comprises both GNSS (longitute, latitude) and IMU (accelerometer) epochs, as follows in equation 1:

$$\mathbf{x} = [p^x \quad v_x \quad a_x \quad p^y \quad v_y \quad a_y]^T \tag{1}$$

where p^x, p^y are the (longitude, latitude) positions gained from GNSS. v_x, v_y are the non-measured speeds, and a_x, a_y are the IMU accelerations, respectively. Hence, the measurements are p^x, p^y and a_x, a_y. This makes the attributes of Kalman filter as follows in equation 2:

$$\mathbf{H} = \begin{bmatrix} 1 & 0 & 0 & 0 & 0 & 0 \\ 0 & 0 & 1 & 0 & 0 & 0 \\ 0 & 0 & 0 & 1 & 0 & 0 \\ 0 & 0 & 0 & 0 & 0 & 1 \end{bmatrix} \tag{2}$$

The Newtonian equations of motion for predicting the iterative position, velocity and acceleration are:

$$x_{k+1} = x_k + \Delta t \dot{x}_k + \frac{\Delta t^2}{2} \ddot{x}_k + \frac{\Delta t^3}{6} \dddot{x}_k$$

$$\dot{x}_{k+1} = \dot{x}_k + \Delta t \ddot{x}_k + \frac{\Delta t^2}{2} \dddot{x}_k$$

$$\ddot{x}_{k+1} = \ddot{x}_k + \Delta t . \dddot{x}_k$$

Where Δt is the time step, the state transition F matrix becomes:

$$\mathbf{F} = \begin{bmatrix} 1 & \Delta t & \frac{\Delta t^2}{2} & 0 & 0 & 0 \\ 0 & 1 & \Delta t & 0 & 0 & 0 \\ 0 & 0 & 1 & 0 & 0 & 0 \\ 0 & 0 & 0 & 1 & \Delta t & \frac{\Delta t^2}{2} \\ 0 & 0 & 0 & 0 & 1 & \Delta t \\ 0 & 0 & 0 & 0 & 0 & 1 \end{bmatrix} \tag{3}$$

The Kalman algorithm proceeds as follows:

$$\begin{aligned} \mathbf{x_{k+1}} &= \mathbf{F_k x_k} + Q_k \\ \mathbf{y_k} &= \mathbf{H_k x_k} + R_k \end{aligned} \tag{4}$$

where Q_k, R_k are the process and measurements covariance matrices, and x_{k+1} and y_k are the new states update and the generated measurements update, respectively.

These filtered a-priori and a-posteriori state estimates $\hat{X}_k|k-1, \hat{X}_k|k$ and the covariances $\hat{P}_k|k-1, \hat{P}_k|k$ are saved for use in the backwards pass (for retrodiction). The smoothed state estimates $\hat{X}_k|n$, and covariances $\hat{P}_k|n$ are computed for the backward pass. The below recursive equations are used starting from the last time step and proceeding backwards in time [17].

$$\hat{X}_k|_n = \hat{X}_k|_k + C_k(\hat{X}_{k+1}|_n - \hat{X}_{k+1}|_k) \tag{5}$$

$$P_k|_n = P_k|_k + C_k(\hat{X}_{k+1}|_n - \hat{X}_{k+1}|_k) \times C_k^T \tag{6}$$

where $C_k = P_k|_k F_{k+1}^T P_{k+1}^{-1}|_k$

$X_k|_k$ is the a-posteriori state estimate of timestep k and $X_{k+1}|_k$ is the a-priori state estimate of timestep $k+1$ which also applies to the covariance.

VI. EXPERIMENTS

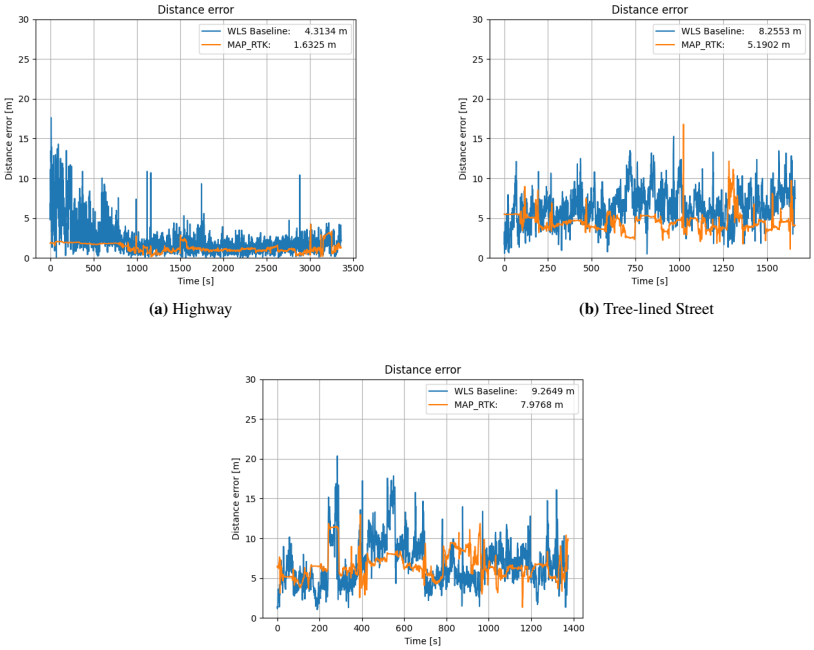

(a) Highway

(b) Tree-lined Street

(c) Downtown

Figure 3: Comparison of positioning error between the WLS baseline and proposed method for each driving paths

The proposed method was evaluated using reference locations provided with the training dataset. In our studies, we made use of the carrier phase information of the data. The results of our model compared to the WLS solutions provided for the GSDC with respect to the ground truth is shown below. We can see an improvement in the estimated position for the respective driving paths as shown in Figure 3.

VII. RESULTS

We estimated the location of the smartphone and made evaluation of our method on the Kaggle platform. In our studies, we used the carrier phase information of the data. As a starting point, using GNSS only solution, initial results using our ML adaptive PPK positioning techniques on the 36 GSDC test datasets gave an accuracy of 2.62 meters for the public score on Kaggle platform. After the loosely coupled integration of the IMU sensor with GNSS navigation solutions, the score became 2.29 meters. From this result, we have shown that the proposed method (LC-GNSS/IMU/ML using MAP RTK) can be used to improve the position estimation of smartphones with relatively high accuracy.

VIII. CONCLUSION

Global Navigation Satellite System (GNSS) provides raw signals, which the GNSS chipsets in smartphones use to compute a position. The positioning accuracy provided by mobile phones is about 3-5 meters of positioning accuracy. This may be useful in some applications but in many cases, this can create a "jumpy" experience for many mobility applications relying on localization. In this paper, we employ a new LC-GNSS/IMU/ML method which makes use of the MAP RTK post-processing algorithm to process carrier-phase information, IMU sensors to improve the position estimates of smartphones. The results obtained show improvements in the positioning accuracy. Using the proposed method, we estimated the location of the smartphone and tackled the competition. The final public score was 2.61 m, while the final private score was 2.29 m. GNSS low-cost receivers and smartphones often have limited channels and computational resources, therefore, the complexity of the algorithm had to be kept modest. Further validations will be performed to ensure the integrity of the proposed method. In the future, we will look into factor graph and robust outlier detection for improvement of our solution.

ACKNOWLEDGEMENTS

The authors would like to acknowledge Google for providing the datasets used in this study and give credits to some kaggle.com notebooks adapted in this study as referenced in this paper.

REFERENCES

[1] P. Huang, C. Rizos, and C. Roberts, "Machine learning algorithm to forecast ionospheric time delays using global navigation satellite system observations," *GPS Solutions*, vol. 22, pp. 221–231, 2018. [Online]. Available: https://doi.org/10.1007/s10291-018-0776-0

[2] G. M. Fu, M. Khider, and F. van Diggelen, "Android raw gnss measurement datasets for precise positioning," in *Proceedings of the 33rd International Technical Meeting of the Satellite Division of The Institute of Navigation (ION GNSS+2020)*, September 2020, pp. 1925–1937.

[3] T. Suzuki, "First place award winner of the smartphone decimeter challenge: Global optimization of position and velocity by factor graph optimization," in *Proceedings of the 34th International Technical Meeting of the Satellite Division of The Institute of Navigation (ION GNSS+2021)*, September 2021, pp. 2974–2985.

[4] X. Zhang, X. Tao, F. Zhu, X. Shi, and F. Wang, "Quality assessment of gnss observations from an android n smartphone and positioning performance analysis using time-differenced filtering approach," in *Gps Solutions*, vol. 22, 2018, pp. 1–11.

[5] K. Elliott D. and H. Christopher J., *Understanding GPS/GNSS: Principles and Applications*. Artech House, 2017.

[6] A. Siemuri, H. Kuusniemi, M. S. Elmusrati, P. Välisuo, and A. Shamsuzzoha, "Machine learning utilization in GNSS—use cases, challenges and future applications," in *2021 International Conference on Localization and GNSS (ICL-GNSS)*, 2021, pp. 1–6.

[7] K. Zhang, F. Jiao, and J. Li, "The assessment of gnss measurements from android smartphones," in *China Satellite Navigation Conference, Springer*, vol. 22, 2018, p. 147–157.

[8] R. M. Watson and J. N. Gross, "Evaluation of kinematic precise point positioning convergence with an incremental graph optimizer," in *IEEE/ION Position, Location and Navigation Symposium (PLANS)*, 2018, p. 589–596.

[9] D. Chen and G. X. Gao, "Probabilistic graphical fusion of lidar, gps, and 3d building maps for urban uav navigation," in

Navigation, Journal of the Institute of Navigation, vol. 66, 2019, p. 151–168.

[10] W. Li, X. Cui, and M. Lu, "A robust graph optimization realization of tightly coupled gnss/ins integrated navigation system for urban vehicles," in *Tsinghua Science and Technology*, vol. 23, no. 6, 2018, p. 724–732.

[11] T. Takasu and A. Yasuda, "Development of the low-cost rtk-gps receiver with an open source program package rtklib," in *The International Symposium on GPS/GNSS, Jeju, Korea*, 2009.

[12] E. Tim. (2021) Batch processing rtklib solutions with rnx2rtkp and python. [Online]. Available: https://rtklibexplorer.wordpress.com/2022/01/05/batch-processing-rtklib-solutions-with-rnx2rtkp-and-python/

[13] G. Developers. (2022) Gnss clock. [Online]. Available: https://developer.android.com/reference/android/location/GnssClock

[14] taroz1461. (2022) Carrier smoothing + robust wls + kalman smoother. [Online]. Available: https://www.kaggle.com/code/taroz1461/carrier-smoothing-robust-wls-kalman-smoother

[15] Cahyadi, Mokhamad Nur and Rwabudandi, Irene, "Integration of GNSS-IMU for increasing the observation accuracy in condensed areas (infrastructure and forest canopies)," *E3S Web Conf.*, vol. 94, p. 03015, 2019. [Online]. Available: https://doi.org/10.1051/e3sconf/20199403015

[16] S. Tian, C. Jiabin, S. Chunlei, and Y. Huan, "The application of r-t-s smoothing algorithm in the post-processing of the integrated navigation," in *2017 29th Chinese Control And Decision Conference (CCDC)*, 2017, pp. 197–201.

[17] H. E. RAUCH, F. TUNG, and C. T. STRIEBEL, "Maximum likelihood estimates of linear dynamic systems," *AIAA Journal*, vol. 3, no. 8, pp. 1445–1450, 1965. [Online]. Available: https://doi.org/10.2514/3.3166

Publication P7

Is LEO-based positioning with mega-constellations the answer for future equal-access localization?

Ruben Morales Ferre, *Member, IEEE,* Elena Simona Lohan, *Senior Member, IEEE,*
Heidi Kuusniemi, *Member, IEEE,* Jaan Praks, *Senior Member, IEEE,* Sanna Kaasalainen, *Member, IEEE,*
Christina Pinell, *Student Member, IEEE,* and Mahmoud Elsanhoury *Student Member, IEEE*

***Abstract*—Capital expenditures and indoor challenges are two of the main obstacles towards equal-access positioning services worldwide. Global Navigation Satellite Systems (GNSS) are not well functioning indoors and in some outdoor challenging scenarios, such dense forest canopies, or hilly terrains rich in vegetation, due, for example, to multipaths and low carrier-to-noise ratios. Terrestrial solutions can be nowadays used to complement GNSS, but they are typically costly to deploy with high coverage and do not offer equal access, for example in some low-revenue countries, in regions forbidding wireless 5G access due to health concerns, or in areas hard to reach with terrestrial infrastructure, such as deep jungle, desert areas with sandy dunes, or deep valleys/deep canyons. As many Low Earth Orbit (LEO) mega-constellations are emerging and their satellites are significantly closer to Earth than GNSS satellites, solutions based on LEO could complement GNSS. LEO-based communications are expected to be widespread in the next decade, and they will offer a global and-easy-to-access infrastructure, with the main costs to the end user coming from the receiver equipment. It is our assumption that future wireless receivers will support the integration of terrestrial and satellite infrastructure, and thus, the LEO-based positioning tasks could be mainly implemented as software adds-on on existing future receivers. Nevertheless, a closer proximity to Earth does not automatically mean stronger received signals or acceptable positioning accuracy, especially when the carrier frequencies of the new LEO signals are higher than those in GNSS. In here, we present a feasibility study of LEO-based equal-access localization, by looking at the current opportunities, benefits, and challenges of LEO mega-constellations used as signals of opportunities (SoO). We show that there is an unharnessed-yet potential of future LEO mega-constellations for equal-access localization, although several challenges are still to be overcome.**

I. Introduction

Position, Navigation, and Timing (PNT) services are mainly offered by GNSS with signals broadcast by satellites in Medium Earth Orbits (MEO). GNSS offer continuous, global, and free-of-charge positioning outdoors, with accuracies ranging from few meters to sub-meter levels. Despite being a successful technology for many applications, GNSS share some weaknesses, including the followings: i) accurate indoor localization solutions are not currently available due to weak-signal reception; ii) performance is poor in dense-urban canyons, areas with tunnels and areas dense foliage/trees, due to heavy multipath reflections and attenuation; iii) launching new MEO satellites for improved navigation capabilities has a long time-to-market and an expensive development cycle.

Our paper offers a feasibility study of the potential usage of LEO satellites mega-constellations for equal-access localization, by summarizing the opportunities provided by LEO signals, the unsolved challenges, as well as solutions to address these challenges. An illustrative scenario is also included, to compare LEO and MEO indoor coverage in terms of received Carrier-to-Noise ratio (C/N_0) and Geometric Dilution of Precision (GDOP), which are two known and widely used metrics in navigation community [1], [2].

II. Landscape of LEO mega constellations

Current LEO satellite constellations are meant for three main applications: i) enhanced mobile broadband applications (e.g., Starlink, Kuiper, OneWeb, ...); ii) Internet of Things applications and narrow-band communications (e.g., Astrocast, Myriota, ...); and iii) Earth Observation and surveillance applications (e.g., ICEYE, Satellogic, ...). Typically, LEO mega-constellations - with thousands of satellites each - are focusing on the first category, while the other two categories rely on few hundreds of satellites per constellation.

The future sky will support tens of thousands of LEO satellites [3], where one of its main benefits for positioning will be an increased visibility of satellites on Earth. While none of the above-mentioned constellations are specifically designed with positioning targets in mind, their wireless signals can be used as SoO for computing the PNT solution. SoO is a well-established concept for using wireless signal for something else than its initial purpose [4]. However, it has not been thoroughly investigated in the context of LEO positioning.

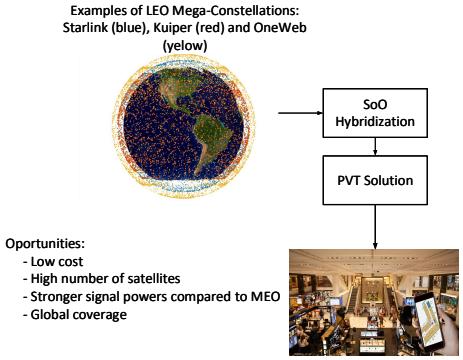

Fig. 1: Concept of LEO mega-constellations potential as SoO.

An illustrative block diagram of LEO constellations as SoO is shown in Fig. 1, with three of the existing LEO mega-constellations plotted as examples. The captured signals can be processed via a SoO-hybridization unit, operating with time, Doppler, or time-Doppler measurements. If the LEO satellite position is known, the PNT solution can be then formed via multilateration, in a similar manner as GNSS operations. Additional synchronization tasks might be necessary when LEO signals are not synchronized between them.

One can think about LEO SoO in three dimensions: i) time domain, harnessing the various LEO waveforms, transmitted at various frequencies/bandwidths; ii) angle/spatial domain; iii) Doppler/frequency domain, exploiting the high orbital speeds of the LEO satellites and the rich frequency spectrum. Most LEO satellites will be equipped with multi-antenna arrays, enabling beamforming [3] and spatio-temporal 'fingerprints' of antenna beams [5]. E.g., most signals coming from LEO constellations operate in Ku, K, or Ka frequency bands, namely at 12-40 GHz, where path losses are about 10-30 dB higher compared to L-band MEO GNSS. Higher carrier frequencies also increase the path losses, due atmospheric attenuation. Nevertheless, LEO satellites are functioning in orbits between 10 and 115 times closer to the Earth, which makes the overall path losses to be with up with 30 dB smaller than for a MEO signal operating at the same frequency. Thus, the opposite path-loss effects of higher carrier frequencies but closer proximity to Earth need careful investigation.

Another potential benefit of LEO as SoO for positioning is related to the capital expenditures (capex) to invest in a new positioning system. Such capex costs are three-fold: the infrastructure costs, usually the highest among the three parts, the receiver/user equipment costs, and the service/maintenance cost. Assuming that the existing infrastructures can be used at little/no cost, then LEO signals would have a clear cost advantage over other terrestrial localization solutions,e.g., relying on WiFi, Ultra-Wide Band (UWB), Bluetooth Low Energy (BLE), or cellular/5G-based positioning which require dense or ultra-dense infrastructure for a reasonable coverage. A thorough survey of existing indoor positioning techniques can be found in [6], yet all the methods surveyed rely on available indoor infrastructure, such as WiFi/BLE access points or some other form of Internet access.

In order to enable the access equality and to cover also regions with limited resources and lack of terrestrial wireless infrastructure, the use of signals coming from satellites offering global coverage is a very promising solution. In particular, 5G-based positioning would require significant investments in 5G infrastructure relying on dense and ultra-dense networks for good coverage especially with mm-wave signals. LEO mega constellations are, at the same time able to offer global coverage as well as shifting the burden of infrastructure costs from the end user to the system manufacturer, since the user will only require a receiver compatible with the considered frequency bands. LEO business models are still in the definition phase, with many proposals shifting the main revenue sources from customers/end-users to the investors. The main remaining costs for a LEO-based positioning would come from the receiver costs, where receiver processing should include the PNT computation based on one or several LEO mega-constellation signals. Receiver aspects in LEO-based positioning are further addressed in Section III.

Several challenges are still to be overcome towards the full potential of LEO as SoO. First, we address scenarios by comparing MEO and LEO capabilities in Section III and we detail the design aspects in the receiver processing part, with a focus also on the innovative concept of Multiple Input Multiple Output (MIMO) beamforming for positioning. Then we discuss the opportunities, challenges, and possible solutions for LEO-based indoor navigation (Section IV).

III. Example scenarios and design considerations

In order to analyze the LEO potential as SoO, several aspects need to be tackled. Few of these aspects are addressed in the next sub-sections, namely: i) an analysis of performance metrics in terms of C/N_0, number of visible satellites, and satellite geometry under a realistic indoor Non Line of Sight (NLOS) scenario; ii) a discussion on the receiver-design aspects in LEO-based signal processing; and iii) a brief description of the innovative concept of massive MIMO-based processing for positioning.

A. LEO potential - a case study

This sub-section presents a comparison of LEO and MEO-based performance metrics in terms of positioning. Two performance metrics were selected for this purpose: the indoor received C/N_0 and GDOP [1]. We used Starlink, Oneweb, and Kuiper as representatives of LEO constellations, operating at 12-20 GHz (Ku/K bands), and Galileo and GPS as representative of MEO constellations, operating at 1.575 GHz (L-band). In addition, the average number of visible satellites per Earth point and per constellation is also shown. The considered MEO GNSS constellations are at about 20000-23000 km altitude, while the LEO constellations are at altitudes of about 600 km, 1200 km and 300-600 km for Kuiper, Oneweb and Starlink, respectively. The C/N_0 is a well known metric in navigation community, referring at the signal-to-noise ratio in the desired bandwidth and thus measured in dB-Hz units; it basically measures how well a signal could be acquired and further processed indoors; the higher C/N_0, the better the acquisition. GDOP is a measure of how good the geometry of the satellites position is and readers can find its detailed definition for example in [1]; the smaller the GDOP, the better the geometry, and thus the better the positioning accuracy.

Fig. 2 gives a comparative example of the average C/N_0 in indoor and outdoor scenarios at 10^4 random user Earth locations for LEO/MEO signals. The path-loss simulator was based on the QuaDRiGa framework [7], which includes antenna-gain modeling, atmospheric delays, and multipath propagation. The constellation-orbit simulator relies on the MATLAB Satellite-Communications toolbox. The considered scenario is a dense urban scenario, with NLOS propagation. For comparative purposes, also the results for an outdoor scenario are shown. Each scenario consist on ten NLOS components. The scenario layout contains buildings up to 60 m height. The indoor receiver is considered to be at 10 m inside a building. The

three selected LEO mega-constellations in Fig. 2 use Ku/K frequency bands ($12-20$ GHz), while GNSS constellations use L band (1.575 GHz). It is to be noted that some of the future LEO systems will use even higher carrier frequencies, moving towards the mmWave ranges. In Fig. 2, the LEO power reception is higher compared with MEO, showing better potential than GNSS for indoor reception. In this analysis, the Effective Isotropic Radiated Powers (EIRPs) for each satellite in the constellations were set to 59 dBm, 59 dBm,69.5 dBm,65 dBm and 69.1 dBm for Galileo, GPS, Kuiper, Oneweb, and Starlink, respectively. Outdoors, LEO C/N_0 levels are between 32-43 dBHz (Starlink has the highest C/N_0 due to the its lower orbital altitude, followed closely by Kuiper), while the C/N_0s for the considered MEO constellations are about 25-27 dBHz. Indoors, the gap between LEO and MEO C/N_0 is slightly lower than outdoors, but still noticeable: the received C/N_0 is about 17 dBHz and 16-19 dBHz for LEO and MEO, respectively. Therefore LEO constellations show a gain of up to 18 dB outdoors and up to 5 dB indoors. Fig. 2 also shows the mean number of satellites in view $\overline{\#Sat}$ for each one of the selected constellations indoors (those satellites with a higher or equal elevation to 10° from the specific user position and with a received power higher than the receiver sensitivity set to -150 dBm, which is a typical PNT receiver sensitivity). No specific antenna pattern was taken into account, as information about antenna patterns on-board LEO satellites is currently not available in public domain, but we have adopted a mathematical model of elevation-based angle-of-service for the beamforming part. For MEO constellations, the average number of satellites in view indoors is about 2, while for LEO this number is considerably bigger, showing a better coverage and excellent potential for multilateration (i.e., combining signals from multiple satellites to form a PNT solution): about 73, 694, and 344 for Kuiper, Oneweb and Starlink, respectively. In the constellation simulations we used the total planned number of satellites for each LEO mega-constellations, which are 7774, 47844, and 34408 for Kuiper, Oneweb and Starlink, respectively.

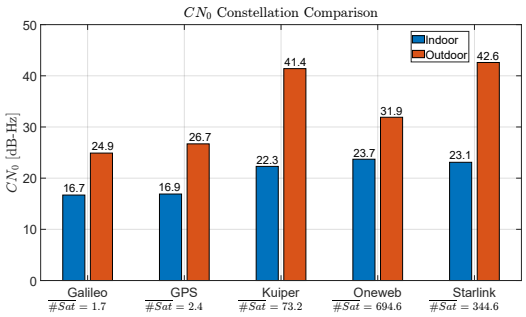

Fig. 2: Illustrative example of C/N_0 indoors for LEO vs MEO constellations.

Fig. 3 shows the GDOP comparison in the case of joint processing of multiple constellations: the comparison is between a combination of three LEO constellations (upper plot in Fig. 3) and a combination of four MEO constellations (bottom plot in Fig. 3). The total number of satellites on sky for the current four MEO constellations (Galileo, Glonass, GPS, and Beidou) is 111 and the total number of satellites expected to be launched on sky in the next five years for the three considered LEO constellations (OneWeb, Kuiper, and Starlink) is 44732. The results in Fig. 3 show that joint processing of LEO signals is able to achieve a GDOP-level significantly lower than 1, and on average 2.5 times lower than MEO. Additionally, we have also calculated the average number of satellites per Earth point: by combining only three LEO mega-constellations, one can get an average number of satellites in view of 2658 satellites, while the average number for the combined four GNSS systems is 35. The significant amount of visible future LEO satellites per Earth point can be a rich source of novel positioning methods, besides the traditional code and Doppler positioning, e.g., via Machine Learning (ML) based on beam patterns, as addressed in sub-section III-C.

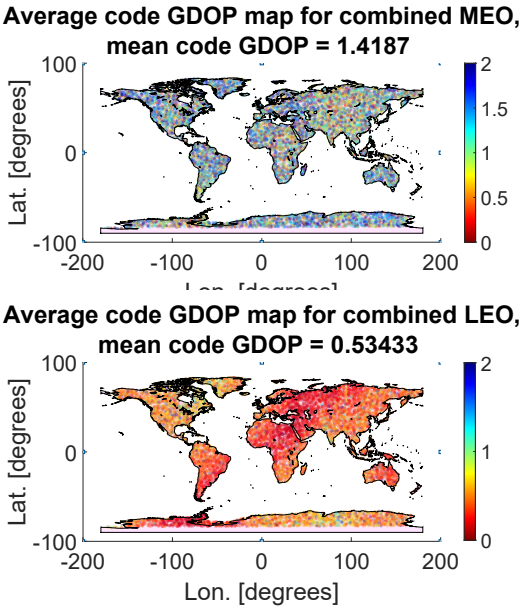

Fig. 3: GDOP for combined MEO GNSS (GPS, Galileo, BeiDou, and Glonass, upper plot) and LEO (Kuiper, Oneweb, and Starlink, lower plot).

B. Receiver processing

One of the main issues in the receiver design for opportunistic navigation using LEO satellites is the absence of user positioning parameters in the transmitted signal. Instead of relying on such a broadcast, as it is the case with MEO GNSS, additional sources are used to obtain missing positioning information. If the Doppler shift of the LEO satellite carrier signal is to be used for positioning, the receiver's positioning computation algorithm needs to be designed in a different

manner than MEO GNSS receivers, to measure, combine, and process the Doppler shifts of all LEO visible satellites. Such receiver algorithm would also need to account for the unknown clock drift between the satellite clock and receiver clock, as well as for the unknown position and velocity of each visible satellite. Common solutions are to obtain the satellite's state from the Two Line Element (TLE) files, likely to be available in open access, but the satellite position accuracy via TLE is typically poor and solutions to overcome this error source are needed. Furthermore, additional sensors such as altimeters or inertial navigation sensors may provide user altitude information. The computation of position and clock drift may be done, e.g., by using extended Kalman filter [8].

External information may be integrated within a LEO receiver if a Software Defined Radio (SDR) is used. This is part of the appeal of opportunistic navigation, because the components may be Commercial-off-the-shelf (COTS). As shown in previous sub-section, LEO signals tend to have a greater C/N_0 and a better GDOP than MEO signals and these are appealing features to support LEO-based opportunistic navigation at the receiver end. Further details may be found in [8], [2] and references therein. The higher-frequencies LEO constellations will require better performing electronics in order to handle the faster changing signal. This typically comes at a higher cost. Moreover, larger bandwidth is available at higher carrier frequency bands compared to GNSS L-band. A larger bandwidth requires more complex and more costly band-pass filters at the receiver front-end. Alternatively, sub-band or filter-bank-based processing can be studied. The larger bandwidth in LEO may be an advantage if information of the signal characteristics are known and thus it could be exploited for navigation, as wider bandwidths ensure higher accuracies in time-based positioning. Multiple frequencies will also provide challenges for antenna design.

C. Massive MIMO for LEO-based positioning

The implementation of Massive MIMO (mMIMO) in LEO satellites has not started yet as the topic is still under research [9], [10]. However, the introduction of mMIMO beamforming can leverage LEO satellites not only for the regular satellite-Earth communications but also as SoO for positioning. The concept of mMIMO is implemented by the usage of multiple antenna arrays (1000 or more antenna elements), separated by a distance equivalent to half the wavelength, instead of utilizing single antenna systems, hence exploiting the multi-paths. This setup has numerous advantages which can enhance the LEO-based localization. The use of spatially multiplexed antennas improves the uplink and downlink throughputs, as it increases the capacity, quality of service, and the data rate of the channel link [9]. One of the main advantages of the beamforming is the extension of the coverage area on Earth per each LEO satellite by using space-time block coding which maximizes the number of user terminals, as shown in Fig. 4. This beamforming concept can be additionally used in the context of positioning, in order to derive certain patterns of beams that are visible only in a certain point of the Earth at a certain time. By combining ML algorithms with such beamforming information, one could also create beamforming-based positioning, a new concept that remains to be investigated. Additionally, the use of numerous antennas in beamforming helps in focusing the energy, thus it improves the efficiency and decreases the susceptibility to jamming and interference.

As a potential challenge, the mMIMO use in LEO satellites comes at higher costs, as they require advanced resources for the signal processing both at the transmitter and the receiver side, in order to be able to solve complex algorithms in the software segment of the system. In addition, complex electronic components are needed at satellite side to control the massive number of antennas in the hardware segment. Consequently, the power budget of mMIMO receivers can be limited due to the large power demand of mMIMO ML processing. This imposes technical limitations and additional costs on the consumer-level receiver devices which could be overcome at long-term with the advent of zero-energy devices (i.e., devices that harness the energy from the environment and interfering signals and are able to self recharge the batteries).

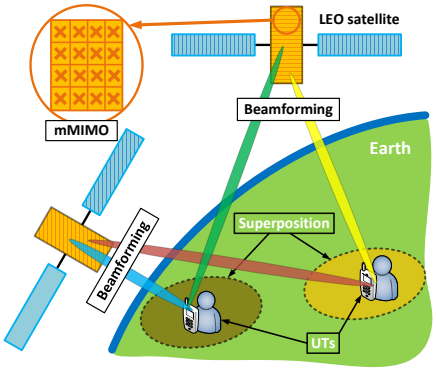

Fig. 4: Principle of mMIMO-beamforming use in LEO satellites.

IV. Challenges, Opportunities, and Solutions towards Equal Access to Seamless PNT Services

Seamless PNT services refer to location-based services relying on both indoor and outdoor localization. While GNSS can solve the outdoor access in most areas nowadays, some challenging outdoor scenarios such as regions with heavy vegetation and/or hilly terrains, as well as indoor scenarios still need equal-access positioning services. Challenges towards such an equality of access are, for example, the cost or difficulty of building adequate and dense-enough terrestrial infrastructure, the desire to preserve a natural habitat or a greenfield untouched by infrastructure, and the scenarios where current GNSS solutions fail to offer a robust enough positioning, due to various types of intentional or unintentional interference. In terms of positioning, the main differences between indoors and outdoors are: i) lower received signal strengths indoors due to wall absorption, signal scattering, and multipath propagation;

ii) multipath-rich environments and absence of Line of Sight (LOS) propagation; and iii) fast-changing propagation scenarios due to people movements, doors closing and opening, changes in furniture, etc. A significant limitation towards equal access to location-based services is the access to infrastructure, such as WiFi/BLE/UWB/cellular access points, or other infrastructure. Infrastructure-less positioning solutions, such as magnetic-field based positioning, can carry a hidden cost of creating and maintaining training databases, as such methods typically rely on offline data collection for training ML algorithms. The alternative could be the use of universally accessible signals, such as those coming from satellite systems with wide Earth coverage. Both MEO GNSS and LEO mega constellations have currently excellent coverage outdoors [1] and even higher coverage is expected in the next 5-10 years with the future LEO constellations.

When focusing on indoor location-based services, security of the solution is of utmost importance. MEO GNSS is currently addressing security features through dedicated authenticated signals, e.g., through the Galileo Open Service Navigation Message Authentication (OSNMA). LEO systems support also various authentication mechanisms, such as physical layer security [11], [12] or through the use of ML [13], which are promising also in the context of positioning.

An additional challenge is the tradeoff between the number of satellites and achieved coverage, as it takes several LEO satellites on orbit to match the footprint of one MEO satellite. This challenge is easily overcome by the huge total number of LEO satellites to be launched on sky in the next few years [1]. Another challenge is that smaller satellites and cheaper transmitters in LEO systems result in less stable clocks, higher clock inaccuracies, higher phase noises and I/Q imbalances, and higher non-linearities of the components than in MEO, which pose additional constraints on the LEO-based PNT. Nevertheless, such hardware inaccuracies enable physical-layer-based authentication, such as Radio Frequency fingerprinting (RFF) [12] or ML algorithms [13] that use the hardware imperfections of each satellite transmitter as a modality to identify if a transmitter is genuine or not.

A summary of challenges, opportunities, and solutions are listed in Table I.

V. LEO MEGA-CONSTELLATIONS AND BUSINESS MODELS

The emergence of LEO mega-constellations are making satellite connectivity 2.0 successful. Large LEO-based satellite internet constellations need careful cost planning to ensure long-term viability - including low-cost spacecraft manufacturing, launch, ground and user equipment. The mega-constellations show signs of truly transforming both the business-to-consumer and business-to-business communications markets, reaching both the hard-to-reach consumers as well as the masses and related services. The worldwide pandemic has also significantly increased the demand for internet connectivity, strengthening the economic viability of satellite internet via LEO.

The positioning market is already forecast to grow dramatically according to various market reports, such as those provided by ReportLinker/MarketandMarket reports from $2019-2020$. Ubiquitous localization as side products of the connectivity service offered by the mega-constellations would likely cause an even larger increase in innovation from developers/start-ups, driving the market further. The strength of LEO constellations providing PNT is that the service can be designed to meet the specific needs of the markets, providing a market-driven solution rather than retrofitting legacy systems [14]. As a weakness, [14] mentions that such a business case can then likely not be closed, due to the fact that a dedicated system will be very expensive and thus economically less attractive. However, a hosted payload on the mega-constellations that are already planned to be launched is a very promising approach.

VI. SUMMARIZING DISCUSSIONS AND CONCLUSIONS

Modern LEO mega constellations can bring performance and energy efficiency to a next level if re-purposed for the indoor positioning as SoO, by exploiting, code, Doppler, and beam-based measurements from space. The high number of LEO satellites and their proximity to Earth, as well as easier support for authentication/security signals are features in favour of LEO, but their use of large carrier frequencies (e.g., 12 MHz or higher) can act as deterrents by introducing additional path losses and indoor penetration losses. A big advantage of LEO mega constellations as SoO for localization lies in their potential zero-cost worldwide equal access to signals from space, which would remove the need of a specific indoor infrastructure and would rely on tailored SDRs. The target performance criteria for positioning should be framed as a multi-dimensional problem of reaching accurate positioning, high coverage, and high energy efficiency, while still preserving the original communications targets for which LEO mega-constellations were launched (e.g., high throughput and low latency in communications) as well as ensuring full security and privacy to the end users. If some of the future LEO mega-constellations will also host GNSS transceivers on-board, additional hybrid LEO-GNSS solutions could be envisaged, with on-board GNSS transceivers offering synchronization information, clock bias corrections, as well as assisted data, such as atmospheric corrections. Data fusion and hybridization solutions can rely on classical algorithms such as Kalman and particle filtering or can make use of the advances in ML field and remain a topic of future investigation. Robust and accurate positioning using LEO mega-constellations can leverage new approaches compared to the traditional trilateration, especially when combining code-Doppler measurements. To cope with less stable clocks and challenges in precisely locating the satellites, mathematical and computational methods traditionally applied in other contexts could be extended to find fast, accurate, and robust solutions for the multilateration problem. The multi-beamforming capacity of future LEO satellites also offer the promise of fingerprinting-based positioning, where combinations of beams from various satellites will carry a unique imprint on Earth and could be identified through ML algorithms. Studies regarding the requirements on the beam width limits to ensure the best location fingerprinting capabilities are currently missing from the existing literature and remain the topic of future investigations.

Opportunities	**Challenges**	**Solutions**
Lower cost to build and launch than MEO satellites	Current orbital planes/orbit altitudes not optimized for PNT	A combination of Doppler, angle, RFF & code-based positioning could harness best the capabilities of LEO SoO. With the advent of future wireless devices supporting the integration of terrestrial and satellite signals at the receiver side, additional localization tasks could be implemented as software adds-ons. Waveform specificity of LEO signals could be circumvented via non-time-based localization solutions.
Large number of satellites from various LEO mega-constellations	LEO constellations are not typically synchronized or built to be inter-operable; code-based positioning approaches may be challenging	Hybridizing Doppler-based and angle-based positioning from all available constellations; on-board GNSS receivers to help synchronization issues between LEO satellites; co-design of LEO services for increased interoperability
High dynamics and higher satellite speeds may enable better Doppler-based positioning than MEO satellites	Ephemeris broadcast to meet the positioning targets may be hindered by proprietary restrictions; Doppler/carrier-phase ambiguities must be solved	Blind Doppler estimation and multi-system positioning to deal with ambiguities and incomplete information; simultaneous transmitter-receiver location through geometrical modeling
Global coverage, increased visibility	Minimum four satellites per Earth position must be visible; global coverage so far has been optimized for single-satellite visibility for communication purposes only	Combining the signals coming from various mega-constellations
Potentially lower path losses than with MEO satellites due to closer proximity to Earth	Indoor additional losses need careful modeling/mitigation	Beamforming/multi-antenna LEO capabilities could be used for enhanced multipath mitigation
Rich transmitter-hardware features due to imperfections of the transmitter payload chain (power amplifiers, mixers, etc.) to serve as authentication/security features	Time-based positioning methods are more challenging if clock inaccuracies are high	Doppler/angle-based positioning to compensate for time-based estimation inaccuracies or replace completely the timing-based estimates for low-cost receivers supporting only certain waveforms
Narrowband modulations to enable lower-energy receiver processing, e.g., due to faster acquisition times, and better link budgets than the wideband modulations used in MEO GNSS	Time-based positioning accuracy increases with higher available bandwidth; narrowband modulations may not reach high time-delay estimation accuracy	Time/code-based positioning complemented with angle/Doppler-based positioning, by taking advantage of high satellite speeds and rich beamforming structures; ML-based positioning can also be envisaged with the rich spatial data from LEO
Possibility of introducing authentication and encryption signals, unconstrained by legacy MEO signals	Authorized access may be limited by the LEO service provider	Physical layer authentication mechanisms such as RFF/ML may complement the signals with authorized use

TABLE I: Opportunities, challenges, and solutions for LEO mega-constellations as future SoO for equal-access localization.

In conclusions, LEO mega-constellation carry a yet-to-be-explored potential for equal-access indoor navigation, especially in remote/un-populated areas with indoor dwellings and factories, where current indoor-positioning solutions are not affordable. Thousands of LEO satellites belonging to various mega constellations will span over the Earth within the next few years, offering worldwide wireless signals at low-to-moderate costs to the end users equipped with a LEO receiver. The main capex costs of the ground and sky infrastructure are to be covered by the LEO-systems manufacturers, and their main revenue source is likely to come from communication-based services, such as mobile broadband or IoT applications. At the same time, a niche research domain, is the use of such LEO signals as SoO for indoor positioning, where low-to-moderate cost receivers can be designed to capture LEO signals on various nearby carrier frequencies and apply code, Doppler, angle, and beam-based positioning algorithms to locate the users indoors.

ACKNOWLEDGMENT

This work was supported by Jane and Aatos Erko Foundation and by Teknologiateollisuus 100-year Foundation (INCUBATE) and by Academy of Finland (ULTRA).

REFERENCES

[1] R. M. Ferre and E. S. Lohan, "Comparison of MEO, LEO, and terrestrial IoT configurations in terms of GDOP and achievable positioning accuracies," *IEEE Journal of Radio Frequency Identification*, 2021.

[2] T. G. Reid, A. M. Neish, T. Walter, and P. K. Enge, "Broadband leo constellations for navigation," *NAVIGATION*, vol. 65, no. 2, pp. 205–220, 2018.

[3] M. Y. Abdelsadek, H. Yanikomeroglu, and G. K. Kurt, "Future Ultra-Dense LEO Satellite Networks: A Cell-Free Massive MIMO Approach," in *2021 IEEE International Conference on Communications Workshops (ICC Workshops)*, pp. 1–6, 2021.
[4] S. H. Yueh, R. Shah, X. Xu, B. Stiles, and X. Bosch-Lluis, "A satellite synthetic aperture radar concept using p-band signals of opportunity," *IEEE Journal of Selected Topics in Applied Earth Observations and Remote Sensing*, vol. 14, pp. 2796–2816, 2021.
[5] S. Balakrishnan, S. Gupta, A. Bhuyan, P. Wang, D. Koutsonikolas, and Z. Sun, "Physical layer identification based on spatial–temporal beam features for millimeter-wave wireless networks," *IEEE Transactions on Information Forensics and Security*, vol. 15, pp. 1831–1845, 2020.
[6] B. Jang and H. Kim, "Indoor positioning technologies without offline fingerprinting map: A survey," *IEEE Communications Surveys Tutorials*, vol. 21, no. 1, pp. 508–525, 2019.
[7] S. Jaeckel, L. Raschkowski, K. Börner, and L. Thiele, "Quadriga: A 3-d multi-cell channel model with time evolution for enabling virtual field trials," *IEEE Transactions on Antennas and Propagation*, vol. 62, no. 6, pp. 3242–3256, 2014.
[8] J. J. Khalife and Z. M. Kassas, "Receiver design for doppler positioning with leo satellites," in *ICASSP 2019 - 2019 IEEE Int. Conf. on Acoustics, Speech and Signal Processing*, pp. 5506–5510, 2019.
[9] L. You, K.-X. Li, J. Wang, X. Gao, X.-G. Xia, and B. Otterstenx, "LEO Satellite Communications with Massive MIMO," in *ICC 2020 - 2020 IEEE International Conference on Communications (ICC)*, pp. 1–6, June 2020.
[10] Y. Zhang, Y. Wu, A. Liu, X. Xia, T. Pan, and X. Liu, "Deep Learning-Based Channel Prediction for LEO Satellite Massive MIMO Communication System," *IEEE Wireless Communications Letters*, vol. 10, Aug. 2021.
[11] A. Vázquez-Castro and M. Hayashi, "Physical layer security for rf satellite channels in the finite-length regime," *IEEE Transactions on Information Forensics and Security*, vol. 14, no. 4, pp. 981–993, 2019.
[12] J. Zhang, R. Woods, M. Sandell, M. Valkama, A. Marshall, and J. Cavallaro, "Radio frequency fingerprint identification for narrowband systems, modelling and classification," *IEEE Transactions on Information Forensics and Security*, vol. 16, pp. 3974–3987, 2021.
[13] P. V. R. Ferreira, R. Paffenroth, A. M. Wyglinski, T. M. Hackett, S. G. Bilen, R. C. Reinhart, and D. J. Mortensen, "Reinforcement Learning for Satellite Communications: From LEO to Deep Space Operations," *IEEE Communications Magazine*, vol. 57, no. 5, pp. 70–75, 2019.
[14] Catapult, "Routes to Market Report, Satellite Technologies for Indoor Positioning and Navigation (IPIN) Systems," *Innovate UK reports*, 2020. Accessed 15.09.2021.

R. Morales-Ferre is a PhD student pursuing a double PhD degree at Tampere University and Universitat Autonoma de Barcelona. His research interests include satellite-based navigation, GNSS security and integrity, signal processing with applications to communications and navigation, positioning with alternative positioning methods such as cellular 4G LTE/5G, and array signal processing.

E.S. Lohan is a Professor at Tampere University and a Visiting Professor at Universitat Autonoma de Barcelona and the leader of TLTPOS research group on Signal processing for wireless positioning at TAU. Her research interests include satellite-based navigation, indoor positioning, and RF convergence. She is currently coordinating a MSCA European Joint Doctorate network, A-WEAR, with 17 international units.

H. Kuusniemi is the director of the multi-disciplinary research platform Digital Economy at the University of Vaasa, professor in computer science, and part-time research professor in satellite navigation at the Finnish Geospatial Research Institute (FGI) of the National Land Survey.

J. Praaks is an Assistant Professor at the Aalto university. His main research interests include hyperspectral remote sensing and multi-payload cubesats.

S. Kaasalainen is a professor and head of Department of navigation and positioning at the FGI of the National Land Survey. Her research interests are resilient PNT, situational awareness, and optical sensors. She also has research experience in remote sensing, sensor development, and astronomy.

C. Pinell is a Masters student in the Space Science and Technology program working for the FGI.

M. Elsanhoury is currently pursuing the Ph.D degree in computer science at the University of Vaasa, Finland. He received his M.Sc. (tech) degree in telecommunications engineering from Vaasa University in 2018, and the B.Sc. degree from Alexandria University, Egypt in 2013. His current research interest covers: ubiquitous indoor positioning, fusion-based UWB positioning, LEO satellites positioning, Kalman filters, and machine learning algorithms.

Publication P8

SPECIAL SECTION ON POSITIONING AND NAVIGATION IN CHALLENGING ENVIRONMENTS

IEEE Access
Multidisciplinary | Rapid Review | Open Access Journal

Received 5 July 2022, accepted 16 July 2022, date of publication 26 July 2022, date of current version 15 August 2022.

Digital Object Identifier 10.1109/ACCESS.2022.3194050

SURVEY

Position, Navigation, and Timing (PNT) Through Low Earth Orbit (LEO) Satellites: A Survey on Current Status, Challenges, and Opportunities

F. S. PROL[1], R. MORALES FERRE[2], Z. SALEEM[3], (Graduate Student Member, IEEE), P. VÄLISUO[4], C. PINELL[1], E. S. LOHAN[2], (Senior Member, IEEE), M. ELSANHOURY[4], (Graduate Student Member, IEEE), M. ELMUSRATI[4], (Senior Member, IEEE), S. ISLAM[1], K. ÇELIKBILEK[2], K. SELVAN[4], J. YLIAHO[5], K. RUTLEDGE[4], A. OJALA[6], L. FERRANTI[3,4], J. PRAKS[3], (Member, IEEE), M. Z. H. BHUIYAN[1], S. KAASALAINEN[1], AND H. KUUSNIEMI[1,4,5], (Member, IEEE)

[1]Department of Navigation and Positioning, Finnish Geospatial Research Institute (FGI), National Land Survey of Finland (NLS), 02150 Espoo, Finland
[2]Faculty of Information Technology and Communication Sciences, Electrical Engineering Unit, Tampere University, 33720 Tampere, Finland
[3]Department of Radio Science and Engineering, Aalto University, 02150 Espoo, Finland
[4]School of Technology and Innovation, University of Vaasa, 65101 Vaasa, Finland
[5]Digital Economy Research Platform, University of Vaasa, 65101 Vaasa, Finland
[6]School of Marketing and Communication, University of Vaasa, 65101 Vaasa, Finland

Corresponding author: E. S. Lohan (elena-simona.lohan@tuni.fi)

This work was supported in part by the INdoor Navigation from CUBesAT Technology (INCUBATE) Project through the Technology Industries of Finland Centennial Foundation, and in part by the Jane and Aatos Erko Foundation (JAES).

ABSTRACT More and more satellites are populating the sky nowadays in the Low Earth orbits (LEO). Most of the targeted applications are related to broadband and narrowband communications, Earth observation, synthetic aperture radar, and internet-of-Things (IoT) connectivity. In addition to these targeted applications, there is yet-to-be-harnessed potential for LEO and positioning, navigation, and timing (PNT) systems, or what is nowadays referred to as LEO-PNT. No commercial LEO-PNT solutions currently exist and there is no unified research on LEO-PNT concepts. Our survey aims to fill the gaps in knowledge regarding what a LEO-PNT system entails, its technical design steps and challenges, what physical layer parameters are viable solutions, what tools can be used for a LEO-PNT design (e.g., optimisation steps, hardware and software simulators, etc.), the existing models of wireless channels for satellite-to-ground and ground-to-satellite propagation, and the commercial prospects of a future LEO-PNT system. A comprehensive and multidisciplinary survey is provided by a team of authors with complementary expertise in wireless communications, signal processing, navigation and tracking, physics, machine learning, Earth observation, remote sensing, digital economy, and business models.

INDEX TERMS Constellation design, low earth orbit positioning, navigation and timing, LEO business models, receiver optimisation, satellite-to-ground channel models.

I. INTRODUCTION AND MOTIVATION

Investments within the space industry have shifted in the past decade from the Medium Earth Orbit (MEO) satellite-based constellations and applications to Low Earth Orbit (LEO) satellite-based ones. Several LEO systems currently offer a wide range of services, ranging from broadband connectivity (e.g., Iridium, OneWeb, and Starlink) and Internet of Things (IoT) applications (e.g., Hiber, Myriota, etc.) to Earth observation and synthetic aperture radar (EO-SAR) applications (e.g., Iceye, HawkEye, etc.). LEO-based signals have already created a paradigm shift in the field of communication and sensing applications. There is now a worldwide research effort towards a similar paradigm shift in positioning

The associate editor coordinating the review of this manuscript and approving it for publication was Kegen Yu.

applications, i.e., the LEO positioning, navigation, and timing (LEO-PNT) concept [1]–[4].

Traditional satellite-based positioning systems rely on MEO [5] and Geostationary Earth Orbit (GEO) satellite systems, such as the US Navstar GPS (Global Positioning System), the European Galileo, the Russian GLONASS (Globalnaya Navigazionnaya Sputnikovaya Sistema), and the Chinese Beidou, as well as on augmented satellite systems [6], [7] such as the European Geostationary Navigation Overlay Service (EGNOS) in Europe, the GPS-Aided Geo-Augmented Navigation system (GAGAN) in India, or the Wide Area Augmentation System (WAAS)/Canadian WAAS (CWAAS) in the North American continent. Strictly speaking, MEO orbits start at around 2,000 km above sea level and range up to 35,786 km, while GEO orbits are placed at exactly 35,786 km above sea level. However, all satellite-based navigation systems from MEO and GEO nowadays have orbits at least 19,100 km above sea level, which makes their signals reach Earth with a high attenuation due to inherent distance-based path losses during the satellite-to-ground wireless signal propagation.

The first LEO satellites were launched more than 50 years ago and it was only in the 1980*s* that Iridium [8] was launched as a global system for low-latency narrowband communications. Later on, LEO-based broadband constellations, such as OneWeb, Starlink, and Kuiper [9] emerged and aimed to offer high-capacity wireless connectivity globally, especially in remote areas that are hard to access via a terrestrial infrastructure.

In the past few years, LEO potential in the context of positioning and localization has also started to be investigated, and the LEO-PNT concept has emerged. There are three approaches to the use of LEO constellations for positioning:

1) **SoO approach:** LEO signals as signals of opportunity (SoO). No specific positioning signals are transmitted and the burden of the PNT engine is at the receiver end. Measurements such as angle of arrival (AOA), received signal strength (RSS), or Doppler shifts can be used.
2) **Modified-payload approach:** modification of the LEO transmitter payload to support positioning signalling. Global navigation satellite system GNSS) receivers can also be installed onboard the satellites and GNSS-like signals can be rebroadcast in other frequency bands. This can be seen as a ''piggybacking'' solution to LEO signal payloads.
3) **New LEO-PNT approach:** Novel LEO-PNT systems with optimised design parameters for positioning and navigation targets (e.g., [10]).

Our paper addresses several aspects of implementing a LEO-PNT system. The main goal is to find the viable instruments and techniques to be used, possible gains in comparison to classic GNSS, and the overall capability of LEO-PNT systems depending on distinct positioning approaches. Our main contributions are:

- Comprehensive survey of LEO-based positioning systems, methods, and algorithms;
- Unified view of the various signal design considerations;
- Overviewing the parameters of existing and planned LEO constellations;
- Literature review on the various satellite-to-ground and ground-to-satellite channel effects and channel models;
- Presenting state-of-the-art positioning algorithms that can be tailored for LEO-PNT systems;
- Review of the main simulation tools for LEO-based positioning and sensing;
- Perspective on future commercial endeavours in LEO-based services.

Table 1 provides an overview of related surveys in the existing literature and how they compare with the work in our survey. Three manners of addressing a certain topic were identified: i) those who give a full picture of the topic in a self-contained manner; ii) those who partially address a certain topic and are not self-contained; and iii) those who do not address a particular topic but still have relevant material related to other LEO research topics.

As shown in Table 1 our work differs from previous literature by offering a comprehensive view of the three LEO segments (space, ground, and user) as well as of the commercial perspective on LEO-PNT solutions. The next sections comprise first an overview of solutions existing at each of the four segments. Each section ends with a summary of relevant features in the context of the three LEO-PNT approaches (SoO, modified payload, and new LEO-PNT). For the sake of clarity, signal design was treated as a separate section even if it belongs to the space segment.

II. SIGNAL DESIGN CONSIDERATIONS

This section gives a comprehensive overview of the signal design aspects of LEO signals. We discuss the methodology for choosing carrier frequencies and bandwidths and review the possible modulation and channel coding methods. Finally, we address the questions of multiple access (i.e., how different LEO satellites are sharing the wireless channel) and beam forming (i.e., multi-element antenna arrays onboard the satellites and signals sent in directional beams towards the target users).

A. CARRIER FREQUENCY AND BANDWIDTH CHOICES

The frequencies used for satellite communications, navigation, and sensing or Earth-Observation (EO) applications are generally chosen from those that are favourable in terms of power efficiency, minimal propagation distortions and attenuation (e.g., minimal path losses), and reduced noise and interference (e.g., low amount of interference to existing wireless systems sharing the same frequency bands). In addition, the frequency regulations of the International Telecommunication Union's Radiocommunication Bureau (ITU-R) and of individual nations must be obeyed. These conditions force the operation into the frequency regions with best trade-offs. Table 2 shows a summary of the main frequency bands currently used in satellite communications, as well as the

TABLE 1. Related surveys on LEO and the literature, and comparison with our survey.

Reference	LEO Space Segment					LEO Ground Segment		LEO User Segment			Commercial Perspectives
	Signal Design	Constellations	Satellite Communication	Small Satellite Platforms	LEO POD	Architecture	Optimisation	Channel Effects	LEO-PNT Receivers	Positioning Algorithms	
[10]	○	◗	○	○	○	○	●	○	○	○	○
[11]	○	○	●	◗	○	○	○	○	○	○	○
[12]	○	○	●	◗	○	○	○	○	○	○	◗
[13]	○	○	●	○	○	○	○	○	○	○	○
[14]	○	○	●	○	○	○	○	●	○	○	○
[15]	○	◗	●	○	○	○	○	●	○	○	○
[16], [17]	○	●	●	○	◗	○	○	●	●	●	◗
[18]	○	○	○	●	○	○	○	○	○	○	●
[19]	○	○	○	◗	○	○	○	○	○	○	●
[20]	○	◗	●	●	○	●	○	○	○	○	○
[21]	○	●	○	○	○	○	○	○	○	○	◗
[22]	○	●	○	●	○	○	○	○	○	○	●
[23]	○	○	○	○	○	○	○	○	○	○	●
[24]	○	●	○	●	○	○	○	○	○	●	○
[25]	○	●	●	○	○	○	○	○	○	○	●
[26]	◗	●	●	○	○	○	○	○	○	○	○
[27]	○	○	○	○	●	○	○	○	○	○	○
[28]	○	○	○	○	●	○	○	○	○	○	○
Current survey	●	●	●	●	●	●	◗	●	●	●	●

● – topic addressed in detail/self-contained, ◗ – topic partially addressed (i.e., not self contained, requires additional readings for deep understanding), ○ – topic not addressed

TABLE 2. Frequency bands for satellite constellations with typical usage.

Frequency Band	Frequency	Typical Usage	Constellation Examples	Orbits
UFH	0.3-3 GHz	IoT;	Myriota; Hiber	LEO
L-Band	1-2 GHz	PNT; Communications	GPS; Galileo; Iridium	MEO; LEO
S-Band	2-4 GHz	Communications; Earth observation	Inmarsat; Helios Wire	GEO; LEO
C-Band	4-8 GHz	Communications; Satellite TV	Eutelsat; Telesat	LEO
X-Band	8-12 GHz	Military; Weather monitoring	BlackSky Global	LEO
Ku-Band	12-18 GHz	Communications; TV; Broadband services	OneWeb; StarLink	LEO
K-Band	18-26 GHz	Short-range applications	N/A	N/A
Ka-Band	26.5-40 GHz	TV; Broadband services	Starlink; Kuiper; Teledesic; Viasat	LEO; GEO
Q-Band	33-50 GHz	Communications; Radio astronomy; Gateway links	Jupiter-3; BlueWalker-3	LEO
V-Band	40-75 GHz	Communications; Broadband services	OneWeb; Starlink;	LEO

encountered trade-offs. In addition to LEO satellite orbits, GEO and MEO orbits are also included. Table 2 summarises the IEEE band designation, frequency range, typical usage, examples of constellations that use those frequencies, and the typical orbits (LEO, MEO, or GEO) whose satellite signals are using those frequency bands.

Figure 1 shows the frequency bands listed in Table 2 in terms of the trade-offs in antenna size, spectrum bandwidth, throughput, atmospheric fading, and band usage. There is a clear trade-off between most of these parameters. For instance, maximum theoretical throughput is achieved with higher carrier frequencies due to their ability to support better multiple-antenna-array processing and larger antenna arrays. But then again, the atmospheric attenuation and other path losses are stronger at higher carrier frequencies, and thus the ranges/coverage areas are smaller.

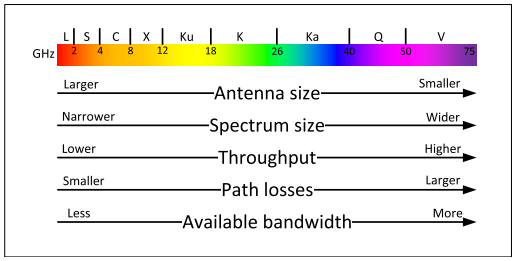

FIGURE 1. Frequency bands with respect to antenna size, spectrum size, throughput, atmospheric fading and usage.

According to Figure 1, there is no clear winner in terms of the frequency band to use in a specific LEO satellite-based application. So the final selection must take into account the regulatory aspects, as well as the cost (e.g., of antenna design). Most LEO systems operate in Ku and Ka bands, and the emerging LEO systems tend to move into higher frequency (Q/V bands). While the carrier frequency of the current LEO systems is mainly used for SoO positioning, new LEO-PNT systems can benefit from carrier frequencies above 5 GHz. Although it may be necessary to keep the

frequency below 12 GHz (C and X bands) to keep path losses at moderate levels, the 5 GHz spectrum would provide less inter-system interference because it is less used.

SoO and modified-payload approaches rely on bandwidths used for communications, widely varying between narrow bandwidths, such as 30 kHz for Blacksky Global, and ultra high bandwidths, such as 100 MHz for Kuiper, 250 MHz for OneWeb, 40 – 400 MHz for Iceye, and 600 MHz for Capella Space.

In code- or code/Doppler-based positioning, the time-based estimation accuracy is known to be proportional to the signal bandwidth. The higher the bandwidth, the more accurate the timing estimation. Therefore, bandwidths of the order of 10 to 100 MHz are recommended. The tradeoff is between the positioning accuracy, the receiver complexity, and the contiguous spectrum availability. If only Doppler-based measurements are used, lower bandwidths are enough to transmit the navigation data. In GNSS systems, bandwidths of up to 1 MHz are recommended. The higher end is suitable for code division multiple access or orthogonal frequency division multiple access, and the lower ends (few tens of kHz) are suitable for time- or frequency- division multiple access.

B. MODULATION CHOICES

The modulation schemes should take into account the purpose of the satellite system, facing a main tradeoff between cost and performance. Throughputs are important in broadband communication. However, in particular to positioning, reliability of the transmissions is more important than maximum achievable throughput, so that high and ultra-high data rates are not needed. For instance, GNSS L1 rate is 50 bits per second and Galileo E1 rate is 250 symbols per second. Hence, low-order modulation methods, along with low-rate channel codes with high error-correction capabilities, are preferable over higher-order modulation schemes with high-rate forward error correction (FEC) codes [26]. When a LEO system has the dual purpose of communication and positioning, the criteria for the best modulation and coding should include both positioning and communication metrics (e.g., reliability, throughput, spectral and energy efficiency).

The vast majority of the available or planned LEO systems rely on digital modulations. For this reason, we overview the available digital modulations and do not focus on analog ones. Tables 3 and 4 list the main available modulation techniques for LEO signals, grouped into linear (Table 3) and non-linear modulation (Table 4), respectively. Advantages and disadvantages are discussed for each modulation family, and examples of LEO constellations employing some modulations are also given. In some cases, the same system (e.g., Starlink, Oneweb) appears as an example under several modulation types; this means that a certain system can use more than one modulation type.

In linear-modulation techniques, such as those listed in Table 3, the principle of superposition applies, meaning that linear superposition of inputs is seen as linear superposition of outputs; also, if the input is scaled by a certain factor, the output of the modulator is scaled by exactly the same factor. Non-linear modulation techniques do not fulfil this superposition principle. They usually have a lower spectral efficiency than linear modulation techniques, but they may have a slightly better robustness to Doppler error.

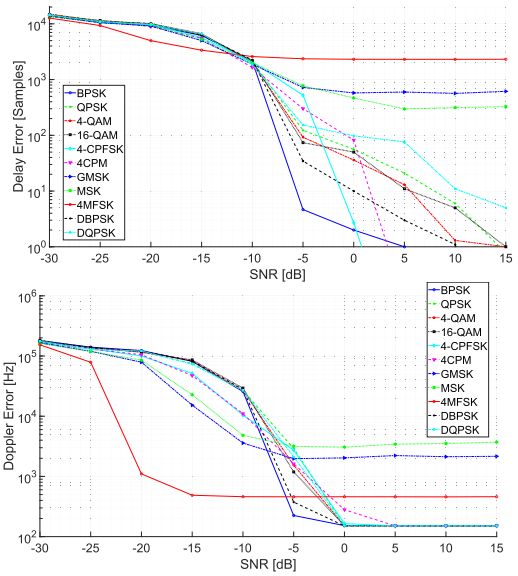

FIGURE 2. Performance of various modulations considering time and frequency measurements.

Most LEO constellations use low-order linear BPSK or QPSK modulations (e.g., Globalstar Iridium Next, OneWeb, RapidEye). A few medium and small-sized constellations also use nonlinear low order modulations, such as GMSK (e.g., Myriota). A few mega-constellations aiming at ultra broadband communications have opted for high-order modulations, such as M-QAM with M up to 64 in Starlink and 64-APSK for Telesat.

Figure 2 shows the performance of 11 different linear and non-linear modulations listed in Table 3 and Table 4 in a scenario with multipath. We clearly observe that any of the considered modulation performs equally well with both time and frequency measurements. Phase (e.g., BPSK, QPSK, or CPM) modulations typically behave better measuring the delay, while frequency modulations (e.g., MFSK, GMSK) typically behave better with frequent measurements. Although the low-order BPSK/QPSK or GMSK modulations seem more appropriate for LEO-PNT, the BPSK modulation is more suitable for time-based positioning due to its linearity and simplicity, while GMSK is more suitable for Doppler-based positioning as it is more robust to Doppler errors.

C. CHANNEL-CODING CHOICES

Channel coding is employed to protect wireless signals against channel errors. It relies on redundancies added to the signal, and therefore it increases the transmitted symbol

TABLE 3. Summary of linear modulation techniques and their applicability to LEO signals.

	Modulation Type	Advantages	Disadvantages	Description and Examples	Ref.
Linear	M-ary Amplitude Shift Keying (M-ASK) and On-Off Keying (OOK)	High bandwidth efficiency. Simple receiver design and inexpensive.	Rather inefficient and susceptible to channel interferences (noise affects the amplitude). Non-constant envelope; it needs highly linear power amplifiers.	Binary ASK is also called OOK. This modulation changes the amplitude of the carrier according to the signal to be transmitted. Currently not in use for LEO signals.	[29]–[31]
	M-ary Phase Shift Keying (M-PSK) (e.g., BPSK, QPSK, etc.)	Efficiency is high and it is less susceptible to channel errors compared to M-FSK and M-ASK.	Side lobes interfere with adjacent carriers.	This modulation changes the phase of the analog carrier to transmit the data. Examples: Starlink uplink (BPSK), OneWeb (QPSK, 8-PSK), Hawkeye (BPSK, QPSK).	[32]
	M-ary Amplitude and Phase-Shift Keying (M-APSK)	Low peak-to-average power ratio (PAPR). Better spectral efficiency than M-PSK and better resistance to channel distortions than M-QAM.	Modulation/demodulation has higher complexity than stand-alone M-ASK/M-PSK, and it requires optimisation.	It is a generalisation of M-ASK and M-PSK, and it can be considered as a superclass of M-QAM, as it includes M-QAM cases, plus cases where all symbols are either all real or all imaginary. Examples: Planet Labs (16-APSK), Telesat (64-APSK), Oneweb (256-APSK), Viasat (32- and 64-APSK).	[32]–[34]
	M-ary Quadrature Amplitude Modulation (M-QAM)	Better data-carrying capacity than M-ASK and M-PSK. Supports high data rates. High spectral efficiency and low symbol distortion.	It is susceptible to noise (especially for high-order modulations).	Higher M means higher spectral efficiency. Examples: Starlink, OneWeb (16-QAM).	[32]

TABLE 4. Summary of nonlinear modulation techniques and their applicability to LEO signals.

	Modulation Type	Advantages	Disadvantages	Description	Ref.
Non-linear	Symmetry chirp spread spectrum (SCS)	Reduces the cross-correlation level caused by Doppler shifts. Smaller cross-correlation than chirp spread spectrum (CSS) with similar autocorrelation gain.	Lower performance than CSS in terms of interference.	The waveform is divided into subsections and a different (but symmetric with respect to the bandwidth) chirp rate is applied to each subsection.	[35], [36]
	Asymmetry chirp signal (ACS)	Keeps good auto-correlation compared with SCS and has better cross-relation than SCS in time and frequency domains.	Varying the effective wavelength λ_{eff} may increase the positioning accuracy.	It is a type of revised SCS in which the λ_{eff} is varying (in contrast with SCS, which has constant λ_{eff}).	[37]
	Chirp Spread Spectrum (CSS)	Can be used both as modulation and multiple access scheme.	CSS modulation cannot be directly applied to satellite constellations due to large cross-correlation.	Data between different users is distinguished by using different values for the start frequency of chirp signals.	[37], [38]
	Differential encoded QPSK (DEQPSK)	More robust to Doppler effects than QPSK; can remove the phase ambiguities specific to QPSK.	Complex Tx/Rx.	It employs a single-stage differential modulation. Example: Iridium.	[39]
	Double differential MPSK (DDMPSK)	Robust to Doppler effects.	Complexity of the Tx/Rx.	It employs a two-stage differential modulation by which the Doppler effect due to satellite orbiting motion is nullified.	[40]
	Frequency shift keying (FSK)	FSK Tx and Rx implementations are simple. Less susceptible to errors and interference than ASK because interference is often confined to a specific frequency.	Bandwidth efficiency is not as high as with ASK.	It shifts the frequency of the carrier to modulate the data.	[41]
	Gaussian filtered minimum shift keying (GMSK)	There are no phase discontinuities. Side lobes in the spectral density are low, which produces less interference and uses the spectrum better. Excellent power efficiency due to a constant envelope.	Main lobe is narrower than using MSK modulation. Filtering can cause inter-symbol interference. A higher power level than QPSK.	It is a modified minimum shift keying (MSK) modulation where the phase is filtered through a Gaussian filter to smooth the transitions from one point to the next in the constellation. This decreases the side lobes power. Example: Myriota.	[42]

rate; in other words, the spectral efficiency decreases. Consequently, higher-order channel codes are more wasteful of bandwidth resources, while offering better protection against channel errors compared to lower-order channel codes. Table 5 lists the main available channel-coding techniques, compares them in terms of advantages and disadvantages, and lists some examples used in current and planned LEO systems.

A numerical comparison of four main channel coding techniques, namely convolutional, Turbo, LDPC, and polar codes

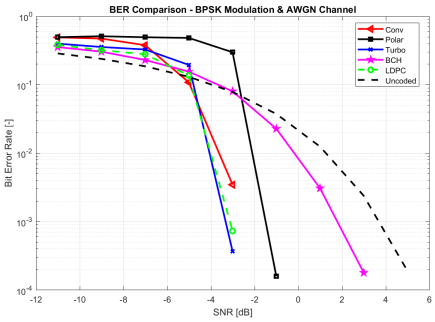

FIGURE 3. Comparison of various channel-coding techniques for a BPSK-modulated signal.

was provided in [47] with BPSK modulations. It was shown that the best performance at low signal-to-noise ratios is achieved with simple convolutional codes, while Turbo coding gives the best performance at moderate and high signal-to-noise ratios. Following the approach in [47], we have also selected five channel-coding types from Table 5, and compared them in Fig. 3 for a BPSK-modulated signal of 20 MHz bandwidth and 10 GHz carrier frequency. The uncoded bit error rate is also shown as a benchmark. The best performance is achieved with Turbo, convolutional, and LDPC channel coding. The convolutional coding offers the lowest decoding delay and lowest complexity among the three, followed by Turbo coding.

Based on Table 5, the numerical analysis from [47], and our numerical results, convolutional coding seems more suitable for LEO-PNT systems targeting low complexity and delay-sensitive receivers. On the other hand, turbo coding is advisable for high-grade delays-tolerant receivers.

D. MULTIPLE-ACCESS CHOICES

Three types of measurements can be used for positioning purposes: Doppler, pseudorange, and carrier phase. If the carrier phase is used, the signal must be continuous [48]. For this reason, multiple access methodologies such as time division multiple access (TDMA) are not applicable for satellite positioning because transmissions are split into different time slots and the transmissions are not continuous.

If the transmitted signal is continuous, a delay lock loop (DLL) and a frequency lock loop (FLL) can be used to obtain the pseudorange and Doppler-shift measurements, respectively [49]. On the contrary, if the signal is not continuous, open loop estimation techniques must be used. Neither space division multiple access (SDMA) nor polarisation division multiple access (PDMA) are applicable because a receiver should get transmissions from at least four satellites to calculate the 3D position. SDMA by itself cannot provide more than a single satellite or, otherwise the signal transmissions would interfere with each other. PDMA is only able to provide two satellite transmissions at a time using two different polarizations (i.e., horizontal and vertical). Therefore, the only options are frequency division multiple access (FDMA), code division multiple access (CDMA), and orthogonal frequency division multiple access (OFDMA).

FDMA and OFDMA are more sensitive to Doppler shifts, which, combined with the fact that LEO constellations suffer more Doppler shifts than those at higher altitudes, makes FDMA and OFDMA not advisable if positioning is based on Doppler/frequency measurements.

E. BEAMFORMING ASPECTS

Beamforming via LEO satellites is typically needed to increase the satellite footprint or Earth coverage area. In order to serve as many users/devices on Earth as possible with sufficient quality of service, multiple input, multiple output (MIMO) approaches have been proposed to be used both onboard LEO satellites and on user devices [50], [51]. Various antenna array structures have been proposed, such as interlaced triangular lattice antenna arrays [52] or multi-beam phased arrays [53], [54]. The current general understanding is that a large number of beams will be supported at the satellite side, the ground station side, or both. This enables beam-based multiplexing and possibly beam-based positioning, a concept not yet investigated, but listed as a potential future research direction in [55].

F. SUMMARY OF SIGNAL-DESIGN CONSIDERATIONS

We contemplate four main topics for signal design consideration: modulation, channel coding, multiple access scheme, and beamforming. The outcome is that the modulation scheme of a dedicated LEO-PNT system will not need to support high rates of data. For this reason, low-order modulations are the most promising for PNT purposes, but so far there is no clear preference for linear or non-linear ones. Non-linear modulations are more robust to Doppler shifts, but additional research is needed to fully understand the trade-offs between modulation complexity of implementation and its robustness to various channel impairments. The same applies to channel coding. The chosen channel coding scheme will need to achieve an acceptable trade-off between computational and spectral efficiency, where low-complexity channel coding solutions (e.g. convolutional coding) will most likely be enough for reaching LEO-PNT targets. The most likely candidates for multiple access schemes are CDMA and OFDMA, although further analysis is needed to be able to choose among them. The sensitivity of OFDMA with respect to Doppler shifts is a critical aspect and one that may make CDMA techniques more suitable than OFDMA techniques for dedicated LEO-PNT system. Finally, the future PNT-system can benefit from the latest advances in MIMO, increasing even further the performance of the system and enabling novel positioning solutions such as fingerprinting based on beam patterns.

Table 6 summarises the signal design considerations when comparing distinct positioning approaches. The most flexible, but also the most costly, is the new LEO-PNT approach, designed from scratch only with navigation targets in mind. The most rigid, but the least expensive, is the SoO approach,

TABLE 5. Main coding techniques and their suitability for LEO signals.

Coding Technique	Advantages	Disadvantages	Description and examples	Ref.
Block codes	It is the easiest and simplest technique to detect and correct errors. Error probability is reduced.	The information cannot be extracted until the whole code is received. The entire block must be retr smitted in the case of an error. Transmission bandwidth requirement is high, and extra bits reduces bit rate.	Coding and redundancy are implemented at block level. Memory-less between consecutive blocks. Both hard and soft decoding are possible on the receiver side.	[43]
Cyclic redundancy check (CRC)	Very efficient decoding methods due to very rich algebraic structure.	Are meant for simple error detection, not for error correction.	A type of block code in which any arbitrary cyclic shift of any valid code word yields another valid code word. Some examples of CRC codes are Reed-Solomon (RS), and Bose-Chaudhuri-Hocquenghem (BCH).	[44]
Convolutional codes	Better performance than block codes. Best for very large data streams. More energy efficient than block codes when you have large streams of data	Computational complexity increases exponentially with the length of the code.	Coding also done at block level, but with memory between consecutive blocks. Both hard and soft decoding are possible on receiver side, although Viterbi soft decoding is typically used.	[43]
Fountain codes	Performance close to Shannon limit.	Not need to know the rate of packet loss.	Rateless codes that allow recovery of the original message through the reception of any subset of the packets (or "drops"), as long as the number of packets received is higher than the size of the original message.	[45]
Low-density parity check (LDPC)	Efficient iterative decoding with reasonable complexity. Performance close to capacity.	The encoding complexity is higher than for turbo codes. Iterative LDPC decoding typically requires many more iterations than iterative turbo decoding, which may lead to a higher latency.	Special case of block codes with sparse structure for parity check. Examples: Amazon Kuiper.	[43], [46]
Polar codes	Maximum performance is equal to capacity.	The coding is optimized for a specific SNR. Operating at different SNR points requires different code designs	Special case of block codes with capacity-achieving properties. They are based on the channel polarization phenomenon.	[43]
Trellis codes	The data rate can be increased without increasing the bandwidth by transmitting more information per symbol. The information content of the symbol is increased by increasing the number of possible symbol values.	For high spectral efficiencies a high-rate convolutional code is required. Bigger noise sensitivity in the large symbol alphabet	A combination of coding and modulation in which the idea is to build redundancy such that symbol alphabet design depends on the code rate. Soft decoding is typically deployed.	[43]
Turbo codes	Performance close to Shannon limit.	High latency due to interleaving and iterative decoding. High decoding complexity.	Two or more interleaved convolutional codes, commonly in parallel. An interleaver allows for efficient iterative decoding at RX.	[43]

where existing LEO signals is used without any dedicated design at the transmitter side. The middle-ground solution is the modified-payload approach, where the navigation payload is added on-board of LEO satellites with some parameters, such as the multiple access and beamforming, dictated or limited by the initial design of the satellites.

III. SPACE SEGMENT

The space segment is composed of a constellation of satellites transmitting RF signals to users. The main elements of interest to materialise the space segment are the satellite platform, onboard instruments, and constellation design. This section provides details about these elements, including viable options of instruments and techniques to be considered in the upcoming LEO-PNT systems. Additionally, orbit optimisation and cost estimation are discussed with particular interest to the navigation systems.

A. PLATFORM AND ONBOARD INSTRUMENTS

In the following subsections, we present considerations about the satellite platform and the navigation payload. To analyse

TABLE 6. Recommended choices for three alternatives of a LEO-PNT. Some (e.g., new LEO-PNT) have much more flexibility than others in setting the signal parameters.

	SoO	Modified Payload	New LEO-PNT
Carrier Frequency	defined by the SoO system; most usual in Ka/Ku band, see Table 2	defined by the LEO system where navigation payload is added; most usual in Ka/Ku band	$5-12$ GHz as a tradeoff between low interference with existing systems and low path losses
Bandwidth	defined by the SoO system; most usually above 100 MHz to support communication needs	defined by the LEO system where navigation payload is added; navigation payload may need a smaller bandwidth than its communication counterpart	maximum 1 MHz is enough for systems relying on Doppler-based positioning; $10-100$ MHz recommended for systems relying on code- or code/Doppler-based positioning.
Modulation	defined by the SoO system; most common modulations are PSK and MSK	can be defined by the LEO system where navigation payload is added or can use a simple modulation (e.g., BPSK) for the navigation payload	determined by minimising the non-desired effects for positioning
Channel coding	defined by the SoO system; most common channel-coding schemes in use are the convolutional codes	can be defined by the LEO system where navigation payload is added, same as for a SoO, or can use a simple channel coding for low complexity (e.g., convolutional coding) for the navigation payload	convolutional coding for low-complexity delay-sensitive receivers and Turbo coding for high-grade delays-tolerant receivers.
Multiple access	defined by the SoO system; most common multiple-access schemes in existing LEO systems are low-order modulations, such as BPSK, QPSK, and GMSK	mainly defined by the LEO system where navigation payload is added. it might differ with respect the original SoO system with some limitations	determined by the LEO-PNT system configuration. The only limitation is the compatibility and/or hardware
Beamforming	defined by the SoO system	defined by the LEO system where navigation payload is added, same as for a SoO	no beamforming or transmitter with large main-beam antennas for wide coverage on Earth

the navigation payload, we selected onboard antenna and clocks since they have the strongest impact on the cost and accuracy of a LEO-PNT system.

1) PLATFORM CONSIDERATIONS

Satellite platforms are the structures in which the payload and all scientific instruments are mounted. Basic subsystems of a small satellite platform include command and data handling (CDH), attitude and orbit control system (AOCS), electric power system (EPS), thermal control system (TCS), mechanical structure (STR), and telemetry, tracking, and command (TTC) [56], [57]. These subsystems are briefly described in [18], [20], [56], [58]–[60] and [61].

The efficiency and quality of the subsystems mainly depend on the weight the platform can carry. Despite heavier platforms have great benefits, they usually require dedicated launches for injecting the satellite's mass into the required orbit. These dedicated launches slow down the whole mission implementation and, foremost, increases considerably the total cost of the mission. Dedicated launches can cost over €10 million Euros. On the other hand, smaller satellites can be carried as a secondary payload, providing significant cost reduction. According to the metrics provided by [62] at the moment this work is conducted, the launch of microsat platforms with 6U is about €300,000, being 1U equals to $10 \times 10 \times 10$ cm. To demonstrate the importance of the launch, and indirectly the platform mass, to the total cost of a satellite mission, [62] shows a rough approximation of $\textit{total cost} = 3.5(\textit{launch cost})$.

As demonstrated later in this section, dedicated LEO-PNT systems will require the materialisation of hundreds of satellites. In this scenario, small satellites seems to be the most feasible option for dedicated systems. We therefore present Table 7 as the main possible options of platforms in upcoming LEO-PNT systems. A major drawback of these small satellite platforms, however, is the power consumption. There are intrinsic limitations in the small satellites since they cannot support high consumption power requirements. Hence, dedicated studies are necessary to define the best platform given the power consumption requirements of the payload. Onboard clocks and antenna can be considered as the main equipment to increase the payload size and power consumption. The next subsections, therefore, present a discussion of possible clock and antenna options for LEO-PNT systems.

2) ANTENNA DESIGN

The satellite antenna is highly influenced by the following criteria [63]: the frequency band used during the transmissions (L-band, C-band, Ku-band, etc.), the maximum radiated power, power consumption, the size of the satellite, and the desired coverage per satellite. Classical GNSS systems based on MEO satellite use patch and quadrifilar helix antennas. However, this may not be an option for the upcoming LEO satellites. To indicate a few possible options, we present the most frequently used antenna types for space applications in LEO heights.

- **Wire Antennas** comprise monopoles, dipoles, helical antennas, and Yagi–Uda arrays [63]. These antennas are kept folded and are deployed after launching, since they are typically placed externally. Wire antennas are especially common for high frequency (HF), very HF (VHF), and ultra HF (UHF) applications, where the wavelength is longer. These antennas are easy to build and provide good radiation efficiency within a relatively small volume at a contained price.
- **Reflector Antennas** offer high gain, high directivity, and good resolution, but they come with increased mechanical complexity. These antennas are external and deployed after launching. Reflector antennas are typically used with C-, X-, Ku-, and Ka/K-bands [11], [63]. Moreover, they can be used in multi-band and multi-beam applications. The main drawbacks of these antennas are that are typically bulky (especially at low frequency) and heavy, which make difficult to integrate in small-sized satellites [11]. To partially solve this issue, inflatable reflector antennas were proposed by the authors in [64]. These antennas are folded during launch and deployed after reaching orbit.
- **Reflectarray Antenna** is a planar array of reflective elements illuminated by a feed [65]. Since their structure is flat, they can be easily integrated in small satellites. These antenna types, given their contained size, are typically used for high frequency band applications (e.g., C-band and above).

TABLE 7. Small satellite platforms [59], [61].

Small Satellites	Mass [kg]
Cubesat	$\leq$ 1.33 kg per U
Picosat	$\leq$ 1
Nanosat	1 – 10
Microsat	11 – 100
Minisat	101 – 500

- **Membrane Antennas** are thin, fabric-based antennas, which can fold during launch and can fit into small satellites [66]. Membrane antennas are typically used for frequencies ranging from UHF to K-band [67].
- **Horn Antenna** is a rectangular or, more commonly, circular piece of a waveguide [68], broader at the open end. Horn antennas are especially useful at high frequency bands, from K-band onwards [66], but can also be used at lower frequency bands.
- **Patch Antennas** are one of the most used antennas because they are easy to fabricate, have a low profile and low cost, and are easy to integrate [69]. Patch antennas are typically used in S- C- and X-bands, providing a typical gain ranging from 4.8 to 30.5 dBi [11].

3) CLOCK ON BOARD

Space-based navigation systems rely on stable atomic clocks to define a space-time reference frame. They serve applications worldwide since space systems allow the synchronisation of electronic devices in the ground over large regions. A major challenge is the need for stable and continuous frequencies. In the case of GNSS, if the clock time is not sufficiently stable, or if its frequency drifts are unpredictable, the pseudoranges accumulate significant errors. Assuming that a 1 m precision is needed in the pseudorange measurements, 3 ns timing uncertainty is required for signals travelling at the speed of light. Maintaining 3 ns timing uncertainty for one day requires a frequency stability of [3ns/86400s]=3.5×10^{-14}, which is achievable with atomic clocks but not with other kinds of clocks [16]. A detailed analysis of several clock performances is provided by [70].

MEO satellite-based navigation clocks are made by passive hydrogen maser and rubidium atomic frequency standards, which rely upon lamps and magnetic state selectors. Considerable research has shown the benefits of replacing discharge lamps for optical pumping and laser-driving systems; however, these state-of-the-art clocks remain on the ground [16]. Alternative proposals have been made to use more stable atomic clocks in future space missions. As shown by [71], two-way lasers, or microwave links, could be used to synchronise highly stable clocks in space. Indeed, lasers have higher spectral purity and brightness than lamps, and enable atomic clocks with better stability and accuracy, but at the expense of complexity, reliability, and cost. Additionally, optical atomic clocks can achieve better stability and accuracy, but they are much more complex and are not currently robust enough for navigation systems. The future optical atomic clocks are likely to find their way into space navigation missions.

The atomic clocks used nowadays as references for PNT applications are too large and consume too much power for use in small LEO payloads. To overcome this issue, recent advances in Photonics and microelectromechanical systems (MEMS) have shown the possibility of creating low-power and small-volume atomic clocks. Zhang *et al.* [72], for instance, developed a low-power, miniaturized atomic clock system with a cesium gas cell by using laser and advanced complementary metal-oxide semiconductor (CMOS) circuits. The prototype achieved a long-term Allan deviation of 2.2×10^{-12} (10^5s) stability and a short-term Allan deviation below 8.4×10^{-11} (1s) stability.

Another solution to the high volume and power consumption of stable atomic clocks is to adapt heterogeneous clock systems and exploit the reference time from a GNSS receiver onboard a LEO satellite. In this regard, Van Buren *et al.* [73] designed an architecture that uses a single-crystal oscillator, one or more chip scale atomic clocks (CSACs), and a spaceborne GPS receiver. This heterogeneous group of oscillators is combined in order to discipline the crystal oscillator and obtain overall system stability for timeframes ranging from less than a second to several days.

In addition to the natural presence of noises and instabilities, clocks in orbit experience relativistic frequency shifts. The relativistic effects need to be considered since the frequency of a clock tick on a satellite differ from those of a clock on the ground, mainly because satellite clocks are moving much faster than clocks on the ground, and they experience a much lower gravitational force. A formulation often used to consider the relativity in precise GNSS positioning is:

$$\tau = -2(\mathbf{r} \cdot \mathbf{v})/c^2 \tag{1}$$

where $\mathbf{r}$ and $\mathbf{v}$ are the satellite position and velocity vectors, respectively. As discussed by [74], the approximations conducted to derive equation (1) are nearly negligible at the altitude of a GNSS satellite orbit; however, a more appropriate formulation can provide markedly better results at the LEO satellite altitudes. The numerical integrations proposed in [74] better consider the Earth's gravitational potential. Despite the heavier implementation requirements, the numerical integration of the periodic relativistic effects may take the place of equation (1) in LEO-PNT navigation systems.

B. CONSTELLATION DESIGN

Constellations are composed of multiple satellites deployed in various orbital planes to accomplish the requisite coverage for a common application. The orbital planes within the constellation are separated by the right ascension angles relative to a reference plane, and are deployed based on orbital parameters. The orbital parameters include altitude, inclination, eccentricity, number of orbital planes, and number of satellites per plane. Figure 4 highlights the principal parameters for a constellation design.

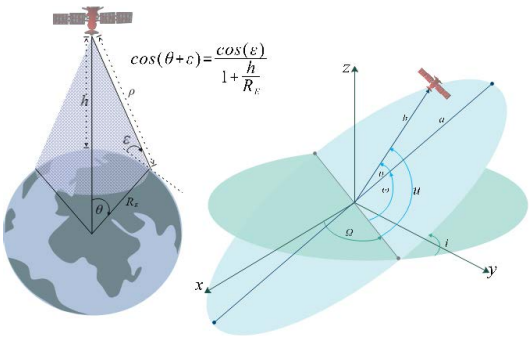

FIGURE 4. Coverage geometry and orbital parameters: ϵ is the elevation angle of the viewing cone of the satellite, h is the satellite altitude, R_E is the Earth's radius, and θ is the central angle of coverage. Semi-major axis a, eccentricity e, inclination i, argument of perigee ω, right ascension of the ascending node (RAAN) Ω, and mean anomaly M are the orbital parameters [75], [76].

To define the best design for a specific application, the orbital parameters need to be optimised accordingly to the mission requirements. In dedicated LEO-PNT systems, the constellation design keeping a continuous 4-fold with global coverage (minimum of 4 satellites in view at any time and location) is the main requirement. The minimum number of satellites required for a 4-fold global coverage can be found as [75]:

$$N_{minsv} = \frac{4K}{1-\cos(\theta)} \tag{2}$$

where $K = 1, 2, \ldots$ is the k-th fold coverage desired in the constellation ($K = 4$ in our analysis).

The minimum number of orbital planes to achieve global coverage is computed as [77], [78]:

$$N_{minPlane} = \frac{360}{2\theta} \tag{3}$$

where θ corresponds to the cap angle (in degrees).

Finally, the minimum orbit inclination to satisfy full global coverage can be computed as [79]:

$$i_{min} = \max(\Phi_{max} - \theta, 0), \tag{4}$$

where i_{min} is the minimum inclination angle (in degrees), Φ_{max} is defined as $max(|\phi_l|, \phi_u)$, with ϕ_l and ϕ_u being the minimum and maximum latitudes comprising the desired coverage area, respectively.

Figure 5 shows simulations of the minimum number of satellites to achieve 4-fold coverage, as well as the minimum number of orbital planes and orbit inclination to achieve global coverage. Assuming an orbit altitude of 600 km, for instance, we can extract from Figure 5 that the minimum required number of satellites is 400, the minimum number of orbital planes is 10, and the minimum inclination is 75°. We can observe that the number of satellites and planes decreases as the altitude increase, i.e., higher altitudes provide better coverage. Nevertheless, the distribution shows an asymptotic pattern, in which no relevant improvements

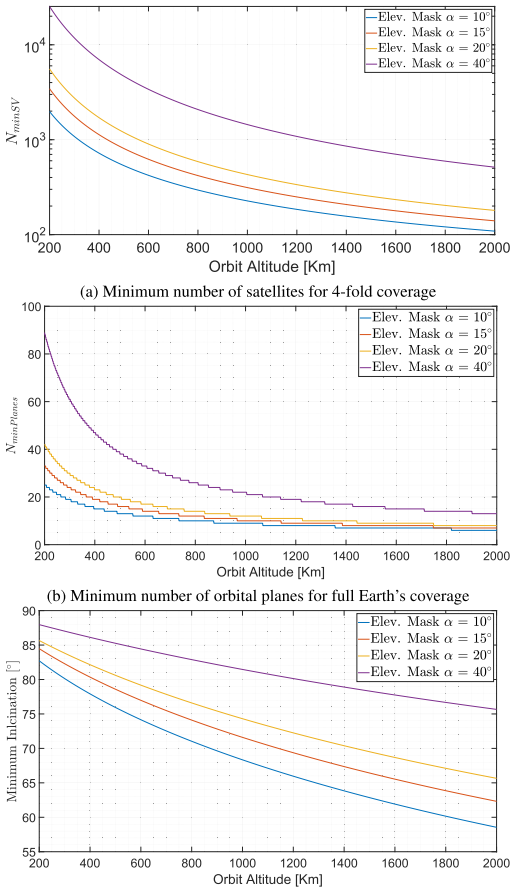

(a) Minimum number of satellites for 4-fold coverage

(b) Minimum number of orbital planes for full Earth's coverage

(c) Minimum orbit inclination for full Earth's coverage

FIGURE 5. Minimum number of satellites in orbit for 4-fold coverage, minimum number of orbital planes, and minimum inclination for full global coverage as a function of orbit altitude.

in the number of satellites and planes are obtained above 1000 km. Therefore, altitudes around 500-1000 km are reasonable regions to deploy the LEO satellite, which also keep a reasonable balance between path losses and drag forces due to the Earth's attraction, as shown in Figure 6.

In addition to the orbital parameters, the constellation design also comprises a topology selection with the primary objective to maximise efficiency while minimising overall system costs [80]. Figure 7 shows visual examples of constellations with distinct topology and at different altitudes, inclinations, and number of orbital planes. The Walker delta is usually the preferred topology by GNSS systems since they keep a symmetric coverage by the user in the ground. However, other options do exist, as presented in the following ([81] and [75]):

- **Street of Coverage**: Street-of-coverage (SoC) constellations consist of satellites in orbital planes with the same altitude and inclination. The coverage is determined by

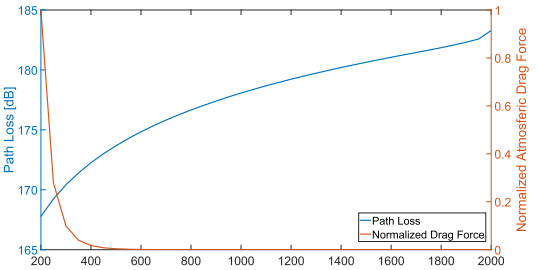

FIGURE 6. Typical path loss and drag force experienced by a satellite orbiting at different altitudes. Transmitted effective isotropic radiated power is set to 69dBm.

the number of satellites, the phase distribution within the plane, and the plane separations. The distribution of orbital planes in SoC is nonsymmetric [75], [76].

- **Draim Constellation**: Draim constellations employ elliptical orbital planes with the same period and inclination. In this configuration, a broad range of orbital parameters can be used, providing wider constellation design options. Compared to constellations with circular or near-circular orbits, elliptical orbits require fewer satellites for coverage.
- **Flower Constellation**: Flower constellations are defined in a rotating frame of reference [82]. Most flower configurations are symmetric, with satellites having the same semi-major axis, eccentricity, inclination, and argument of perigee. The distribution in orbits is acquired through variations in mean anomaly and RAAN. Flower constellation configurations exist in 2D [83] and 3D lattice flower [84] and in 2D and 3D necklace flower [85], [86]. Flower constellations are more complicated to implement, but provide better coverage.

Despite many LEO constellations use the Walker pattern, geodetic positioning is a secondary application in the current LEO constellations. Today's LEO constellations are mainly used as SoO, hence there are no navigation requirements to the constellation design. A few options of already developed constellations typically used in SoO positioning are shown in Table 8. These LEO constellations, including Globalstar, Orbcomm, Iridium, and Iridium NEXT, were first developed for communications; however, as shown later in Section VI, they have found great applicability in SoO positioning.

C. SUMMARY OF SPACE SEGMENT CONSIDERATIONS

We have discussed aspects such as antenna type, clock on board, and available satellite platforms. In this regard, the most likely antenna type to be used will be influenced by the operating carrier frequency. For low or relatively low carrier frequencies (e.g., VHF, UHF, L-band, S-band), larger antenna types will be needed. Antenna types in these bands are typically wire, patch, and slot antennas. On the contrary, at higher frequency bands (e.g., Ku-band, K/Ka-band) reflectors and reflect-arrays antennas are typically used. Since antenna sizes and weights rather vary, dedicated studies are required to define the proper platform type depending on the wanted carrier frequency.

TABLE 8. Fully-deployed LEO Constellations with Global Coverage [25], [58], [88]–[91].

Name	# N_P	# Sat	i [deg]	h [km]	m_{sat} [kg]	Services
Globalstar	8	48	45	1414	700	Voice, Data
Orbcomm	4	50	45	825	172	IoT, M2M
Iridium	6	66	86.5	780	689	Voice, Data
Iridium NEXT	6	66	87	780	860	Voice, Data

As for satellite clocks, instrument size and power consumption by highly stable atomic clocks are the biggest challenges. Recent advances show the possibility of creating miniaturized atomic clock systems with a cesium gas cell and advanced CMOS circuits. Another prominent solution guides us in the direction of exploiting the time reference of GNSS receivers onboard a LEO satellite. In this way, it is possible to synchronise a heterogeneous group of oscillators and obtain overall clock stability. Despite these efforts, state-of-the-art optical pumping and laser-driving clock systems are still on the ground, so that atomic clocks using lamps and magnetic state selectors are still the only ones used for time reference in PNT applications. The relativistic effects on the clocks also need special attention since the formulations used today for GNSS positioning require non-negligible approximations. In this regard, we observed in the literature that numerical integration considering Earth's gravitational potential provides remarkable improvements for the altitudes of LEO satellites.

Regarding the constellation design, our investigation has shown that Walker delta seems to be the most straightforward choice for the constellation topology, despite other options do exist. In addition, we have observed that several options of constellation parameters can be adopted to optimise a dedicated LEO-PNT system. Table 9 summarises the constellation parameters computed based on our simulations. We mainly highlight the results obtained for the dedicated LEO-PNT systems, which needs to keep a continuous 4-fold with global coverage. From Table 9, we notice that around 400 satellites are necessary for new LEO-PNT systems. With this number of satellites on mind, and knowing that the total mission cost is equal to 3.5 times the launch cost for a six-year lifetime, we can conclude that €1 billion is a realistic mission cost to implement a dedicated LEO-PNT system, which is a significant reduction when compared to MEO-PNT systems. Galileo, for instance, had an estimated cost of €10 billion.

IV. GROUND SEGMENT

The ground segment deals with the maintenance tasks of the satellite system. It involves ground-stations to perform the precise orbit determination, ephemeris computation, clock corrections estimation, and periodic updates of the satellite messages and other parameters. This section discusses the

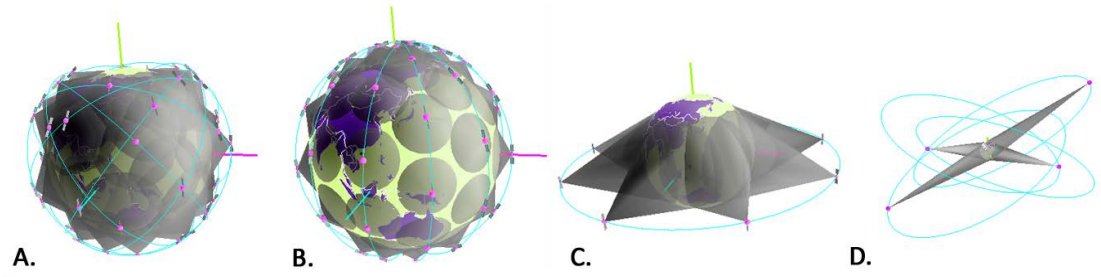

FIGURE 7. Visualization of constellations created with *SaVi* [87]: *A.* Walker constellation with 8 orbital planes and 6 satellites per plane at a 53-degree inclination. *B.* Walker star constellation with 6 polar orbital planes having 11 satellites per plane. *C.* MEO Constellation satellites distributed evenly in the orbital plane *D.* Draim constellation of 4 satellites.

main aspects of the ground segment that may differ from those in classical GNSS.

A. GROUND STATIONS OPTIMISATION

The ground segment is composed by ground stations strategically located worldwide to track, monitor, and communicate with the satellite system. Unlike MEO or GEO systems, LEO orbit and clock determinations can be made independently of ground stations since LEO satellites can carry spaceborne GNSS receivers. However, few studies focus on optimisation of the LEO ground segment. The ground stations optimisation primarily deals with the determination of the optimal number and placement of ground stations to obtain the best performance at monitoring, management, and control of satellites. Since this issue is not specific to LEO satellite systems from an optimisation point of view, we review studies based on MEO and GEO satellite systems.

Some of the most common metrics and techniques for obtaining the best location for a ground station are summarised in Table 10. The example studies share similarities in their metrics and evaluations. As main metrics the optimisation, [92] considers signal availability level, number of visible satellites, geometric dilution of precision (GDOP), scintillation fade depth, ionospheric delay, and rainfall attenuation. In case of [93], ground station network optimisation is studied with particular interest in the effect of rain attenuation on system availability. The key factors identified in the optimisation problem include satellite availability, ground station switching strategies and the number of ground stations on the network. Additionally, the work in [94] has defined the 'quadruple coverage' as the main metric, i.e., at least four ground stations are observed by the same satellite.

Due to the inherent gains of LEO satellites, metrics that depend on the geometry and signal-to-noise ratios may become the primary options for ground stations optimisation in LEO-PNT systems. The approaches proposed by [49], [95], and [92] are highlighted here due to the GDOP and satellite visibility dependency. Other common metrics, such as cost estimations, coverage, and atmospheric delays, are also often discussed, but they rarely share common models in different studies, and are therefore not considered as options.

TABLE 9. Orbital altitude, total number of planes, total number of satellites and orbit altitude to keep requirements of LEO-PNT systems.

	SoO	Modified Payload	New LEO-PNT
Orbit altitude	Is determined by non-navigation requirements whose transmissions are used as SoO.	Is determined by by a mix between non-navigation and navigation requirements.	500-1000km
Number of satellites			around 400
Number of orbital planes			$\geq$10
Orbit inclination			>75°

B. PRECISE ORBIT DETERMINATION

The traditional satellite orbit determination for LEO is conducted with ground stations and onboard receivers of the Doppler Orbitography and Radio-positioning Integrated by Satellite (DORIS) instrument system. An antenna mounted on the satellite points towards Earth to receive radio signals from the ground stations. The frequency shift caused by the Doppler effect is used to determine the distance between the ground stations and LEO satellites. A major product of the DORIS observations is the precise orbit determination with particular reference to altimetry and remote sensing.

Another relevant technology for precise orbit determination is satellite laser ranging (SLR). Despite the original application of SLR instruments being the derivation of geodetic parameters, they have great capabilities for precise orbit determination due to the high precision of the range measurements. In SLR, ground stations are continuously emitting laser pulses in the optical spectrum, and the LEO satellites are equipped with retro-reflectors to reflect the laser pulse. The basic observation is twice the laser time of flight between the ground station and a satellite. Due to the highly precise measurements, SLR is one of the main means of external validation of precise orbit determination (POD).

After the first assessment of space-borne GPS receivers onboard the Topex/Poseidon mission [98], GNSS became a well-established tracking system to provide LEO position, velocity, and time. The LEO orbit determination can be simply obtained by GNSS with single point positioning (SPP), where the solution relies on GNSS broadcast ephemerides and single-frequency pseudorange observations. As an advantage, the GNSS measurements observed on board the

TABLE 10. Examples of metrics used in ground segment optimisation problems.

Metric	Mathematical Formulations	Parameter Explanations	Reference
Carrier-to-noise ratio (C/N_0)	$C/N_{0_{db-Hz}} = 10\log_{10}(\frac{P_{carrier}}{P_{noise}})$	P is the power of the signal or noise, for the same system bandwidth and equivalent times	[49]
Geometric dilution of precision ($GDOP$)	$\Delta y = (H^T H)^{-1} H^T \Delta x$ $GDOP = \sqrt{tr\,(H^T H)^{-1}}$	Δy is the position offset H is the satellite geometry matrix Δx is the net error in the pseudorange value $tr(.)$ refers to the trace operator	[92], [95]
Link outage probability (LOP)	$LOP = \sum_{i=0}^{M-1} \binom{N}{i} A_i \times (1 - A_{N-i})$	M is the smallest number of required ground stations N is the total number of ground stations A_i is the availability of ground station i	[93], [96]
Rainfall attenuation (ITU-R Model)	$\gamma_R = kR^\alpha$	γ_R is the specific attenuation R is the rain rate k and α are frequency-based coefficients	[97]

satellite are sufficient for the LEO orbit determination. However, the precision of a few metres in dynamic solutions can pose a crucial issue to LEO-PNT navigation systems. A more sophisticated solution often incorporates precise GNSS products, carrier phase measurements, and dual-frequency data. The basic measurements are the zero-difference or double-difference observations. Zero-difference observation refers to the raw phase and pseudorange observations, as in precise point positioning (PPP). Double-difference approaches, on the other hand, use double-difference GNSS observations between the LEO satellite and ground stations or other LEO satellites. Following the continuous progress of GNSS technologies, the satellite-borne GNSS technique based on zero- or double-differences has gradually become the primary method of precise orbit determination for many satellite missions.

Most LEO missions carry out POD solutions offline, after downloading GNSS measurements and auxiliary data by the processing center on the ground. This latency depends on the time required for the downlink process and the time required to generate precise GNSS orbit and clock products. For a LEO-based navigation system that relies on spaceborne GNSS receivers, the latency of this downlink transmission and GNSS products generation can add a crucial burden to the real-time users, so that the LEO positioning technique must be selected according to the particular application of the satellite mission. A high-accuracy solution is based on hybrid systems utilising both GNSS and non-GNSS data. These hybrid solutions combine the best of both techniques, but they increase the time latency. On the other hand, a technique that has gained attention in recent years [99] is the use of precise GNSS algorithms with broadcast ephemerides. The GNSS-POD with broadcast ephemerides allows precise positioning without the need for complementary ground-to-space links, thus reducing the latency issue.

Among the positioning techniques to determine the satellite orbit, three typical solutions are: 1) kinematic, 2) dynamic, and 3) reduced-dynamic. The kinematic approach relies purely on geometrical determinations of the 3D coordinates. The LEO position is obtained epoch by epoch with no motion constraints. The main products are the coordinates, ambiguities, and receiver clocks. In the dynamic solution, the satellite orbit is constrained to a force model described by an equation of motion. The dynamic determinations are therefore governed by physical laws to represent a time-dependent orbit in which the quality depends on the gravitational and non-gravitational force models. The reduced-dynamic technique combines the kinematic and dynamic techniques by introducing a stochastic process in the representation of the trajectory. The residual of the estimations is adjusted within the orbit determination to help the compensation of remaining force model deficiencies [100]. Most often, empirical accelerations are included in the system in the radial, along-track, and cross-track (RAC) directions.

Table 11 provides an overview of the main POD options to be considered by the ground segment of a LEO-PNT system. It provides the type of input data (DORIS, SLR, or GNSS) as well as the positioning strategy, obtained solutions and overall accuracy level.

C. EPHEMERIDES

Defining the ephemerides that satisfy accuracy requirements for geodetic positioning is one of the most critical prerequisites of a LEO-PNT system. In SoO approaches, two-line elements (TLEs) are typically used to list a set of orbital elements and describe the LEO orbit with roughly approximations. In case of dedicated LEO-PNT systems, more accurate orbital descriptions are required.

Broadcast ephemeris models have been developed mainly for MEO and GEO satellites. Dedicated MEO-PNT systems typically uses ephemeris models based on Keplerian orbital elements [108]. They are broadcast to the user as legacy messages embedded in the system signal and can describe MEO satellites with an approximated user range error of 0.5 m [109]. This performance relies on the model fit errors, orbit determination and propagation errors.

Unlike MEO and GEO, the LEO satellites are much closer to the Earth. Therefore, they are affected to a greater extent by gravity and atmospheric drag forces. The legacy broadcast ephemeris models are therefore not capable of describing these complex orbital dynamics. Meng *et al.* [110], for instance, developed a broadcast model that takes into account the Keplerian elements being singular in some cases due to small eccentricities of the LEO orbits. The best results with this method were obtained using 22 Keplerian parameters in contrast to 16 in the legacy messages. The use of 16 parameters provided a user range error of around 4 to 18 m in LEO satellites at 800 km, while more coefficients could improve

the accuracy to the cm-level. In addition, the legacy messages of MEO orbit are described by arcs of two hours length. However, the authors in [110]–[112] have found reasonable accuracy only when describing LEO orbits with 20 to 30 min arc lengths.

Despite broadcast ephemeris are the most traditional way to compute the satellite orbit in navigation systems, the best efforts allow the provision of more precise products. The International GNSS Service (IGS) analysis centers provide ephemeris in the form of GNSS precise products. They allow precise orbit determination for the level of a few centimeters in near real time. Similar approaches can be conducted for LEO satellites, which may be relevant for applications requiring precise geodetic solutions. Current MEO GNSS satellites distribute precise orbital coordinates with a time resolution of 15 minutes. The best time step to distribute LEO precise products to users is not yet fully known.

D. SUMMARY OF GROUND SEGMENT CONSIDERATIONS

The most common metrics for obtaining the best location for a ground station were identified as signal availability level, number of visible satellites, GDOP, scintillation fade depth, ionospheric delay, and signal attenuation. Due to the proximity and speed of LEO satellites, metrics that depend on geometry and signal-to-noise ratios have been highlighted as the options with the best benefits in LEO-PNT systems.

There is no clear standard of how the ground segment should perform the POD of LEO satellites. A clear trend however is observed for techniques using onboard GNSS receivers. The most straightforward GNSS solution tends to use reduced-dynamic model, least-squares solvers, dual frequency signals with zero-difference phase and code observations. This can allow a 5 cm-level accuracy, which is a reasonable accuracy to develop broadcast ephemeris models.

In SoO approaches, TLE is the main ephemeris used for the orbit description, which are known to provide rough approximations of the satellites. In dedicated LEO-PNT approaches, more accurate models are required. However, instead of the broadcast ephemeris used in classical GNSS systems, the most recent advances show the necessity of dedicated ephemeris models. A viable option is to adapt the Keplerian-based ephemeris model used in GPS to incorporate more complex orbital dynamics. To this end, 22 Keplerian parameters with 20 to 30 min arc lengths can provide reasonable results in LEO satellites, in contrast to 16 parameters with 2 hours arc lengths of the legacy broadcast messages. Another option is to distribute precise products like IGS, so no Keplerian elements are broadcast. In such cases, more accurate solutions are expected, but the best time step to distribute the LEO coordinates is not yet fully known.

V. CHANNEL EFFECTS

Various channel effects can produce signal reflection, loss, refraction, diffraction, and polarisation shifts in LEO satellites. We summarise in this section the main channel effects that require different mitigation approaches from those used in classic GNSS.

A. PHASE WIND-UP EFFECT

Because of the electromagnetic nature of circularly polarised waves, antenna rotation on the transmitter or receiver side causes a phase variation. This phase variation, known as a phase wind-up, is reflected as a direct variation in the range measurements provided by the carrier phase. An antenna rotation of 360° generates an apparent range increase by a wavelength in the carrier phase. The impact of phase wind-up over GNSS L1 measurements refers to an error of about 0.19 m, so that phase wind-up must be corrected in precise solutions. At higher frequencies, the phase wind-up is smaller and, depending on the chosen frequency, can even be neglected for certain applications. The impact of neglecting the phase wind-up in precise positioning of LEO satellites using GNSS as transmitter has been pointed out in [113]; but to our knowledge, there is no discussion related to the phase wind-up originated by LEO satellite rotations, when the LEO satellites are the signal transmitter. In principle, faster panel rotations are expected for LEO satellites, resulting from the higher orbital speed.

B. IONOSPHERIC EFFECTS

The Earth's ionosphere is composed of positive ions and free electrons formed in the atmosphere [114], mainly by the ionization of neutral gases due to solar radiation. The number of electrically charged particles is large enough to cause refraction over several bands of RF signals. The ionosphere refers to the region between 50 to ∼2,000 km above the Earth's surface. Above the ionosphere, the electron density is low but still high enough to cause a significant refraction of the RF signals crossing a large portion of this layer, which is known as the plasmasphere.

Typical PNT receivers are designed to measure the propagation time of an RF signal. As the RF signal propagates through the ionosphere, it bends due to refraction effects, resulting in a longer time for the receiver to track the signal. This time delay is commonly referred as the ionospheric delay.

Since the ionosphere is a dispersive medium [115], [116], the RF signal propagates with distinct phase and group velocities. The refractive index is therefore applicable in two distinct formulations to represent the ionospheric delay over the RF signal (in metres):

$$I_g = \frac{40.3}{f^2}\int_s^r n_e ds \quad I_p = -\frac{40.3}{f^2}\int_s^r n_e ds \tag{5}$$

with I_g and I_p being the ionospheric group and phase delay, n_e the electron density, f the signal frequency, and $\int_s^r ds$ the geometric distance between the receiver r and satellite s.

As shown in equation (5), the ionospheric delay is proportional to the electron density and inversely proportional to the signal frequency. Higher frequencies are less affected by the ionospheric refractivity. In case of GPS L1 frequency,

TABLE 11. Survey of the LEO POD studies, including the POD method, accuracy and solution.

Ref.	Input Data	Positioning Strategy	Solution Obtained	Achieved Accuracy
[28]	Dual-frequency precise ephemerid GPS	POD using zero-difference observations in the GPS High-precision Orbit Determination Software Tools (GHOST)	Reduced-dynamic: position, velocity, atmospheric drag, solar radiation pressure, RAC accelerations, receiver clock, ambiguities; kinematic: position	reduced-dynamic: 2 cm kinematic: 4-5 cm
[99]	Dual-frequency broadcast ephemerid GPS, Galileo, Beidou	Real-time POD using zero-difference observations	Position, velocity, atmospheric drag, solar radiation pressure, RAC accelerations, receiver clock, ambiguities	8-10 cm
[101]	Dual-frequency broadcast ephemerid GPS	Real-time POD using zero-difference observations and pseudo-ambiguity	Position, velocity, atmospheric drag, solar radiation pressure, RAC accelerations, receiver clock, ambiguities	20–40 cm (position) 0.2–0.4 mm/s (velocity)
[102]	Dual-frequency precise ephemerid GPS	POD combining GPS and DORIS	Position, velocity, atmospheric drag, RAC accelerations, receiver clock, ambiguities	1.66-3.16 cm
[103]	Dual-frequency precise ephemerid simulated data	PPP aided by Keplerian elements	Position, velocity, gravity perturbation, three-body perturbation, atmospheric damping, solar pressure, and others	15 cm (position) 0.18 mm/s (velocity)
[104]	Doppler SLR normal point	Dynamic orbit determination to express forces acting on the satellite based on the Cowell numerical integration	Position, velocity, atmospheric drag, solar radiation pressure, RAC accelerations	DORIS-only: 7.69 cm SLR-only: 11.96 cm
[105]	Dual-frequency precise ephemerid GPS	POD using zero-difference observations POD using double-difference observations	Position, velocity, atmospheric drag, solar radiation pressure, RAC accelerations, receiver clock, ambiguities	zero-difference: 1-2.5 cm double-difference: 0.68-6.8 mm
[106]	Dual-frequency precise ephemerid GPS	POD using zero-difference observations in the PANDA software	Position, velocity, atmospheric drag, solar radiation pressure, RAC accelerations, receiver clock, ambiguities	2-10 cm
[107]	Dual-frequency real-time JPL eph. GPS	POD using zero-difference observations	Position, velocity, atmospheric drag, solar radiation pressure, RAC accelerations, receiver clock, ambiguities, and orbit manoeuvres	10-20 cm
[108]	SLR normal point	Dynamic orbit determination with the Cowell numerical integration in the GEODYN II software	Position, velocity, atmospheric drag	around 10 m (post-fit residuals)

for instance, the ionosphere can cause errors up to 15 m in the zenith direction [117]. The consideration of the ionospheric delay is therefore crucial for accurate positioning.

Several ionospheric models have been developed in the past decades to properly describe electron density for PNT applications with single-frequency systems. Traditional ionospheric models for real-time PNT applications are the Klobuchar model [118], currently used in GPS, the NeQuick [119], used by Galileo, and the BeiDou global broadcast ionospheric delay correction model [120]. Additionally, since 1998, the IGS is providing global ionospheric maps (GIMs) for more precise applications [121]. To date, the precision of the ionospheric delay estimation from the IGS remains around 1-2 metres [122]. The ionospheric delay provided by two-dimensional GIMs is counted from the ground up to the GNSS satellite height of around 20,000 km. Due to the topside ionosphere and plasmasphere, which represents 10% - 60% of the total ionospheric delay [123], the GIMs are not directly applicable in LEO-PNT systems. On these systems, the ionospheric delay will only affect the region up to the LEO orbit height and, hence, dedicated ionospheric models are necessary for single-frequency solutions.

In the case of sub-metre requirements, the use of isolated ionospheric models may not be sufficient. In such cases, PNT technology is more suitable if developed with two or more frequencies. Then, by means of a linear combination of the phase (or group) delays between the frequencies, it is possible to eliminate the first-order effects of the ionosphere. The first-order effect refers to approximately 99% of the refractivity [124]. The remaining effects of higher order can reach tens of centimetres. In GNSS applications, the higher-order effects can be eliminated by 3D ionospheric models to less than a few millimetres [124], so that similar ionospheric models can be adapted for use in the LEO-PNT technologies.

Diffractive effects pose a greater challenge to PNT technologies than ionospheric delays. As the signal's plane waves cross the ionosphere, small-scale irregularities in the electron density scatter the signal and result in rapid fluctuations of both phase and amplitude [125]. Interference patterns are then observed on the ground, inducing uncertainties in tracking loops due to multiple signal paths. The main effects observed on a receiver are associated with fading events, cycle slips, and loss of lock. Summing up all the challenges, the PNT system can completely fail to provide continuous operation during intense ionospheric scintillation, which occurs mainly at low and high latitudes during high solar activity. There are several studies on characterisation and mitigation of ionospheric scintillation in GNSS positioning (see [126] and references therein), but scintillation is still a limiting factor for sub-decimetre applications or for truly continuous operation. Any GNSS user at tropical or high-latitudes is particularly vulnerable to a positioning disruption during high solar activity.

The dependence of RF signals on ionospheric scintillation can be represented by [127]:

$$\sigma_{\phi}^{La} = \frac{f_{Lb}}{f_{La}} \sigma_{\phi}^{Lb} \quad S_4^{La} = \left(\frac{f_{Lb}}{f_{La}}\right)^{1.5} S_4^{Lb} \tag{6}$$

where σ_ϕ and S_4 stand for the phase and amplitude, respectively, of most common scintillation indexes, and *La* and *Lb* represent two L-band signals following the rule $f_{La} > f_{Lb}$.

Building on equation (6), we can understand that the higher the frequency, the lower the expected scintillation impact over the RF signals. This rule was validated in [128], showing that lower GPS frequencies (L2 and L5) suffer more intense scintillation than L1. Moreover, according to equation (6), for 2 GHz LEO-PNT system the effects of ionospheric scintillation are reduced by approximately 20% to 30% in comparison to GPS L1. For this reason, there is a great opportunity for the upcoming LEO-PNT systems to mitigate the ionospheric scintillations by increasing the signal frequency.

C. TROPOSPHERIC EFFECTS

The troposphere, often described as the neutral part of the Earth's atmosphere, is the closest atmospheric layer to the Earth's surface. The troposphere is stratified up to an altitude of about 50 km, where the refractive index is always greater than one. In consequence, tropospheric delays are expected in signals emitted by satellites on low Earth orbits. Variations in tropospheric delay depend on temperature, atmospheric pressure, humidity, and water vapor. This delay also depends on the receiver's geographic location as well as the satellite elevation angle relative to the receiver.

In terms of LEO-PNT systems, identical empirical models currently used in GNSS can be used for frequencies below 15 GHz. A possible gain is related to decorrelation of the troposphere during the estimation process. Indeed, the line of sight changes much faster for LEO transmitters than MEO ones. This geometric gain may greatly impact the time required to estimate the wet part of the tropospheric delay. Past studies [129], [130] have already observed the benefits of using LEO satellites to improve the PNT convergence time, but no studies have been developed so far to assess the time gain in the troposphere estimation.

D. TERRESTRIAL EFFECTS

LEO constellations can offer higher signal power than MEO. Nonetheless, signal quality and power are reduced by multipath effects when non-line-of-sight (NLoS) propagation dominates. Outdoor multipath may be dealt with in a similar way to classic GNSS systems. However, given the possibility of indoor positioning, we discuss the transmission of RF signals into buildings and introduce satellite-to-indoor channel models developed in this environment.

Unlike the reception of GNSS signals outdoors, where the line of sight (LoS) propagation dominates the communications between satellites and end user, indoor reception includes additional local interactions of materials and signals on spatial scales ranging from just a few metres to hundreds of metres. The smaller spatial scales allow direct experimentation with a building's system response to excitation by externally applied electromagnetic radiation. The use of the channel impulse response method has been central to several measurement and modelling activities [132], [133].

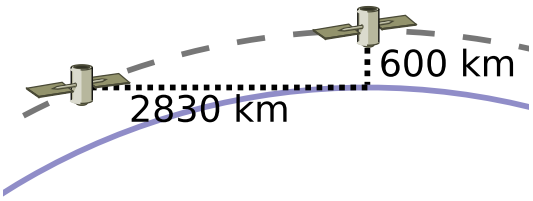

FIGURE 8. Two LEO satellites (altitude 600 km), one at nadir and the other near the horizon relative to a single receiver location on the ground. In this situation, the increased free space attenuation is approximately 13dB taking these two distances into consideration.

Results from observation and analysis activities have demonstrated that:

1) Indoor received signals vary as a function of the azimuthal and polar/altitude angles associated with the transmitter/receiver geometry [134], see Figure 8, and building materials (Figure 9).
2) Signal-level fluctuations can be as high as 30 dB over periods of several hundred milliseconds within various locations in a single room [135].
3) There is "diffuse" multipath activity with contributions of 20 to 35 wave fronts and associated delays up to 100 ns relative to the LoS signal [136].
4) Multipath delays indoors are smaller than those observed from the outdoor environment.

As shown in Figure 10, electromagnetic waves from LEO antennas travel a few hundred kilometres along the LoS. Waves may hit the different objects on earth (buildings, trees, cars, etc.) and propagate into different directions due to scattering, diffraction, and reflections. Furthermore, waves can penetrate the building roof or walls, resulting in losses that depend on the construction material (Figure 9). In general, wave propagation indoors will be mainly in the form of multipath, and the impulse response of multipath wireless channels can be modelled as [137]:

$$h(t;\tau) = \sum_i \alpha_i(t)\, e^{-j\theta_i(t)} \delta((t - \tau_i(t))) \tag{7}$$

The summation is performed over the waves' path components. Each path has its specific gain α_i, angle θ_i, and delay τ_i. Due to the associated uncertainty, it is convenient to consider the parameters of the channel impulse response as random processes. The signal strength usually decreases inversely with the distance between the transmitter and receiver (in free space, the power gain obeys an inverse square law). However, due to the multipath environment, it could easily be shown that the power attenuation with distance can be higher than 2, and is usually between 3 and 5 or even more.

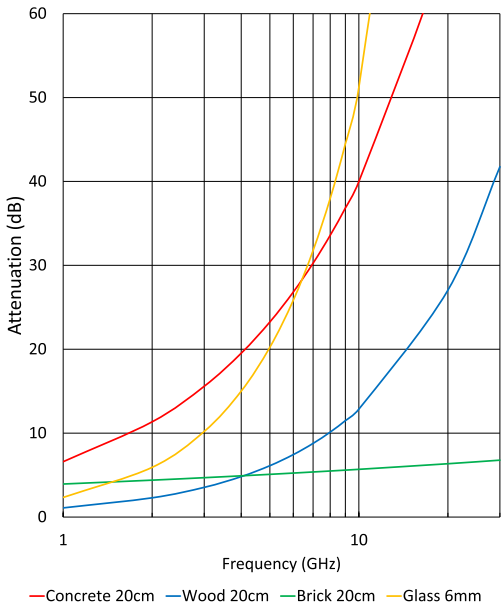

FIGURE 9. RF signal attenuation caused by absorption characteristics of common building materials (as a function of wavelength, GHz). [131].

In some exceptional indoor scenarios, the power-law factor may be less than 2; this is known as the waveguide effect, but a power-law factor of 3 to 4 is more common in indoor applications. In a real environment, the channel model depends on a vast number of factors. Hence, it is infeasible to find an accurate deterministic model that could be used to express the general channel model, and therefore it is more realistic to use a stochastic model to express the multipath channel uncertainties. The models best known for this purpose are the Rician, Rayleigh, and Nakagami-m channel models.

The Rician channel model is used for a strong LoS beam beside multipath components, as shown in Figure 10. When the LEO satellite is on a small horizontal angle, the electromagnetic wave might propagate indoors with a strong LoS path through the windows. On the other hand, the Rayleigh channel is a useful model in a rich multipath environment without a dominant LoS path. The Nakagami-m channel is a scalable model that is capable of modelling a wide class of fading channel conditions, and it fits the empirical data well [138].

Generally speaking, the received signal power can be modelled with

$$P_r = \frac{G_{rt}\sigma\eta}{d^{\alpha}}P_t \tag{8}$$

where P_r and P_t are the received and transmitted power respectively, G_{rt} is the multiplication of transmitter and receiver antenna gains, d is the distance between the transmitter and receiver, and σ is the shadowing losses. Shadowing can be modelled as a random process with log-normal

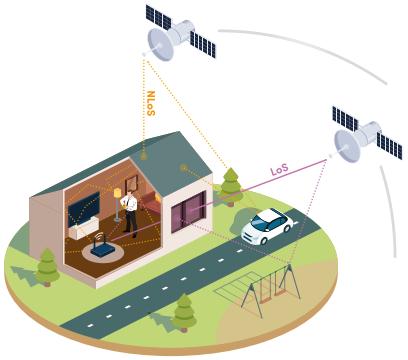

FIGURE 10. Conceptual depiction of LoS and NLoS signals propagating from LEO satellites to an indoor environment.

distribution, but passed through a narrow band linear filter. Shadowing represents slow losses such as those caused by entering buildings or being behind a big object. On the other hand, η represents a small-scale fading (i.e., fast-changing received signal characteristic due to small changes in the receiver location). The small-scale factor generally results from multipath. It can be modelled as the square of a random process (Rayleigh, Rician, or Nakagami-m) passed through a linear filter representing the Doppler filter (i.e., it creates the duration period of the time correlation due to the Doppler spread), and α is the exponent factor of the distance power decay.

E. SUMMARY OF CHANNEL EFFECTS CONSIDERATIONS

We first identified that faster antenna rotations are expected in LEO satellites than in MEO orbits. As a result, phase wind-up effects will likely produce fast artificial range variations, which can be mitigated by the adoption of lower wavelengths. We also find that most ionospheric models for GNSS positioning do account the ionospheric delay from the ground up to approximately 20,200 km. There is a large region between approximately 800 and 20,200 km of the extra ionospheric content in such models, which requires dedicated ionospheric models for single-frequency systems. Another point is that ionospheric scintillation has been one of the main barriers to achieving sub-decimeter accuracy for precise GNSS positioning. Therefore, there is a great opportunity for upcoming LEO-PNT systems to mitigate ionospheric scintillation by increasing signal frequency. New LEO-PNT systems can also provide a significant means for mitigating the tropospheric effects. Due to the faster speed of LEO compared to MEO satellites, the spatial-temporal decorrelation of the tropospheric delay estimation is better achieved as the line of sight geometry changes faster. LEO-PNT systems can also provide several benefits for indoor positioning. Given the close proximity to the Earth, LEO signals are received indoors at a higher power. But the carrier frequency plays an important

TABLE 12. Impact of channel effects over a LEO-PNT system using SoO, modified payload, or new LEO-PNT.

	SoO	Modified Payload	New LEO-PNT
Phase Wind-Up	negligible	depends on system frequency. Centimetre error on L-band.	depends on system frequency. Centimetre error on L-band.
Ionospheric Refraction	negligible	depends on system frequency. Metric error on L-band	depends on system frequency. Metric error on L-band.
Ionospheric Scintillation	impact not investigated, but depends on system frequency	impact not investigated, but depends on system frequency	depends on system frequency. Loss of lock and metric error on L-band.
Tropospheric Effects	negligible	Metric error	Metric error
Multipath	Depends on AoA. Can reach several hundred Hertz.	1/4 of wavelength. Centimetre error on L-band.	1/4 of wavelength. Centimetre error on L-band.

role, since higher frequency bands suffer from a higher attenuation, especially indoors. The trade-offs between higher path losses due to increased carrier frequencies and smaller path losses due to close proximity to Earth need to be carefully investigated.

Table 12 summarises the current general understanding of the impact of signal channel effects in the case of SoO, modified payloads or new dedicated signals.

VI. USER SEGMENT

The user segment consists of RF receivers and antennas that receive PNT signals, process the measurements, and provide solutions. From a wide range of users, this section focuses on the PNT user segment.

A. RECEIVER CONSIDERATIONS

A general navigation receiver architecture, comprises a radio front-end and components for processing base band signals and navigation data. Initial signal reception and conversion into a digitized sample is performed in the radio front-end. The remaining components of the radio front-end amplify the signal above the noise, and downconvert it to an intermediate frequency (IF). The analog to digital converter and signal processing chain completes the receiver. To form a general understanding of LEO-PNT receivers, this section is separated into two parts: receiver design for 1) a LEO system that is dedicated to PNT, and 2) a Doppler measurement-based system.

1) DEDICATED SYSTEMS

A dedicated LEO-PNT system contains navigation parameters embedded in the RF signal. The receiver is responsible for decoding the navigation messages in a customized device. Dedicated LEO-PNT systems do not yet exist globally, but there are aspirations in this direction. Satelles [139] and Xona Space System [140] are two examples of companies that serve as guides to the necessary assumptions for a dedicated LEO-PNT user receiver. Receiver assumptions are concerned with signal design, as decoding a signal is a user receiver's task. A reasonable option is to follow the design of a GNSS signal since we can benefit from the vast expertise in this field. A dedicated signal such as this is composed of a minimum of two frequencies and three layers. As previously mentioned, two frequencies allow for ionospheric corrections. Three layers refer to the carrier wave, code and data modulations superimposed on it.

Accuracy is the key advantage of a dedicated system over an opportunistic one. Xona Space Systems plans to use this to their advantage and develop a LEO-PNT service, called Xona Pulsar, for the high-reliability sector of autonomous vehicles. Three aspects determine the accuracy gain of a dedicated LEO-PNT signal compared with an exclusive carrier positioning method: the code gain, the transmitted data, such as ephemeris, and the timing reference:

1) *Code* refers to known modulation onto the carrier wave identifying the specific transmitting satellite. A local replica of this signal is reproduced in the user receiver for correlation between the two signals. Acquisition and tracking of weaker signals are enabled by correlation. This is known as code gain. Such higher acquisition sensitivity benefits pseudorange measurements in a weak signal environment. An example of this is the satellite time and location (STL) service by Satelles. STL is hosted on Iridium satellites, and its significance lies in the adjustments to the transmitted signal. The beginning of the STL transmission is marked by the STL burst. Performing correlation with this burst enables even weaker signals to be detected within the user receiver [139]. In a 13-floor building, the STL code gain results in a C/N_0 between 35 and 55 dB-Hz, compared to GNSS in an unobstructed environment [141]. The STL burst is the functional equivalent of PRN code in GNSS.
2) *Data* refers to the information transmitted in the signal. In the case of GNSS, this is the navigation message, or ephemeris. A dedicated LEO-PNT system would also need to transmit such navigational information to perform precision positioning measurements. The navigation parameters need to be adjusted specifically to the LEO environment, with likely additions of new parameters. The user receiver must then be adjusted to the respective symbol duration and pass on the parameters to the navigation filter.
3) *Pseudorange* measurements rely on high-precision timing and frequency information. GNSS satellites contain highly accurate, and expensive atomic clocks for their timing broadcasts. A GNSS receiver can be used to provide an external timing reference. However, if the LEO-PNT system is to be independent of GNSS, and no atomic clock timing broadcasts are available, other timing references are needed. Satelles compared temperature compensated crystal oscillators (TCXOs), oven-controlled crystal oscillators (OCXOs), and a rubidium disciplined clock [139]. It was concluded that OCXOs result in a better timing output than TCXOs, and rubidium clocks perform best out of the three. A compact rubidium clock was shown to achieve sub-500 ns maximum time interval error (MTIE). That is

the maximum error within a seven-day time interval without further ground corrections. An OCXO with ground-station-issued corrections obtained sub-100 ns. Ultimately, user receiver precision requirements determine whether a rubidium clock is necessary or a cheaper OCXO will suffice.

There is a significant change in LoS for a LEO satellite near the horizon compared to its zenith position. The shortest LoS is between the satellite's zenith position and the user receiver. Thus, the least path loss and highest received signal power are obtained for a LoS satellite. This might be considered in the user receiver as a setting in the SDR of high angles in the elevation mask [142].

2) DOPPLER LEO-PNT

In Doppler LEO-PNT systems, COTS components are frequently used in combination with signals of opportunity (SoO). Thus, an additional element for frequency downconversion may be required when using K-band frequencies. In addition to downconversion, the most significant differences between LEO-PNT and GNSS are in the positioning framework, assumptions concerning navigation parameters, and the implementation of the acquisition and tracking loops. There is no need to use correlators, as SoO contains no code signal to be replicated and matched in a user receiver. An ephemeris message is not decoded either. Furthermore, the most suitable receiver architecture is based on the requirements of the user environment.

The final positioning solution is obtained by a navigation filter. Extended Kalman filters (EKFs) are common, and they are explored further in Section VI-C, along with other positioning solutions. However, it is necessary to know which navigation information is missing to substitute it accordingly. This is done by adjusting the acquisition and tracking loops, as well as using additional measurement components, such as altimeters. Tracking loops in Doppler positioning generally lay out of the PLL [143], or they are implemented based on a Kalman filter [144], [145]. The former type of tracking loop is commonly used in combination with a known signal structure. The latter type may be adjusted to also track customized navigation observable based on signals of publicly unknown structure [144].

A positioning framework based solely on Doppler measurements is presented by [146]. The state of the user receiver is determined by three spatial components, three velocity components, clock offset, and clock drift. Thus, the user receiver requires eight processing channels to perform eight simultaneous carrier Doppler shift measurements. A carrier Doppler shift measurement accuracy of $0.01\,\mathrm{m\,s^{-1}}$ in terms of equivalent range-rate accuracy needs to be achieved to obtain positioning solutions comparable to GNSS [146]. However, timing accuracy is still stated to be the most challenging aspect.

Due to the lack of ephemeris data in the Doppler positioning method, the satellite's status is generally obtained by feeding the receiver and navigation filter by public TLE files [145]. The vertical resolution of Doppler measurements is poor, but the accuracy can be improved with altimeters [144]. Another common addition is an inertial measurement unit (IMU) or an inertial navigation system (INS) [1]. These may also be used for velocity measurements of a dynamic user receiver.

Propagation errors caused by the ionosphere and troposphere are typically neglected for simplicity. The order of magnitude of these errors is significantly smaller than the velocity errors of TLE files, but the effects are noticeable in the positioning accuracy.

Further errors are introduced by receiver and transmitter clocks. Appropriate models for their behaviour are, therefore, necessary. A common simplified method is using white Gaussian noise errors with constant clock drift with known variance. The timing or frequency reference used in the receiver determines the accuracy of the actual clock state. Timing accuracy on the order of milliseconds is realistic [146], making this the critical accuracy aspect for receiver considerations using Doppler positioning. However, if the satellite has access to precise atomic clock timing and sends frequent updates, it is possible to ease the accuracy requirements in the user receiver clock [147].

Another consideration is the number of tracking and processing channels. Using multiple constellation signals, it might be favourable to implement several independent channels requiring multiple user radio front-ends. The bandwidth is dependent on the respective signal frequency too. The Doppler shift of a LEO signal varies significantly during an overhead pass, such that a broad bandwidth commonly needs to be sampled [144]. Devices that collect the samples and perform such post-processing are shown in [1] and [144].

The user environment determines the priorities in the receiver architecture. A weak signal environment may require a focus on acquisition sensitivity through targeted improvements to the acquisition loop [148]. Moreover, a LEO receiver may be used to aid a GNSS receiver's acquisition search space [149]. Both of these approaches likely focus on processing low frequencies, such as L-band or lower, as they are less attenuated by obstructions compared to high frequencies, such as K-bands [146]. The advantage of K-band frequencies lies in the signal transmissions of LEO mega-constellations. Their vast numbers of satellites may be able to provide consistent global signal availability. To benefit from this, a user receiver may require additional downconversion in the radio front-end [144].

Table 13 summarises Doppler-LEO-PNT receiver configurations with simulated and experimental user positioning results. Common to all of them is a customised SDR approach. The simulated accuracy results outperform the real-scenario user positioning partially because of simplified conditions of the simulations. More satellites are assumed to be available for measurements, and more precise knowledge of satellite states is presumed. Initial experiments with multiple Starlink satellites support a trend towards higher

accuracy. The best user positioning performance, with an accuracy around 7.7 m, is obtained using six Starlink satellites, an altimeter, and a customised SDR setup [144].

B. PNT TECHNIQUES

There are several techniques to obtain PNT solutions after the received data is processed. SoO techniques are mostly applied using single receiver stations with configurations and accuracy levels already mentioned in Table 13. This section focuses on dedicated LEO-PNT approaches. For the sake of simplicity, we categorise the distinct PNT techniques into two types: using one or multiple receiver stations.

1) PNT TECHNIQUES WITH ONE RECEIVER STATION

Single-receiver PNT techniques have received increased attention due to their simplicity for users, who need only one receiver. Two popular techniques used in GNSS are single point positioning (SPP) and precise point positioning (PPP).

SPP is the basic GNSS mode. It is based on single-frequency pseudorange observations, broadcast ephemeris, and simple correction models for the ionosphere and troposphere. This is the usual method for civil GNSS applications, reaching an accuracy of a few metres. Santerre *et al.* [152], for instance, achieved an accuracy of 5 to 20 meters in a challenging urban environment. LEO-PNT systems aiming for similar accuracy with SPP require a dedicated signal for the generation of pseudoranges, in addition to a dedicated broadcast ephemeris and embedded ionospheric model.

The main drivers for PPP are the carrier phase measurements, aided by precise models to describe satellite orbit, clocks, troposphere, ionosphere, and terrestrial effects. Since the carrier phase has an accuracy of a few millimetres, the PPP accuracy depends on external models, which encompass orbital errors, clock errors, channel effects, receiver errors, and terrestrial effects. For GNSS, real-time and post-processed products are continuously provided to properly mitigate these systematic errors. Such products are generated through the best efforts of an international community sharing open data processed by a series of institutes that maintains global and regional GNSS networks. The computations to produce relevant products are coordinated by the IGS analysis centers. PPP can achieve an accuracy of a few centimetres. To provide this robust position solution with PPP, a LEO-PNT system needs to provide similar precise products, which calls for worldwide cooperation.

SPP and PPP can be applied using distinct measurement combinations to benefit from the internal signal proprieties. PPP approaches solely using single-frequency (SF) measurements may provide metric solutions [153]. For more accurate PPP, SF combinations often help the solver, despite the existence of cm-level SF-PPP when using robust ionospheric models [122]. In dual-frequency (DF) systems, cm-level PPP solutions are possible using a mix of linear combinations in the estimation process [154], such as ionospheric-free, wide-lane, narrow-lane and Geometry-free combinations.

Usually, standalone GPS allows a stable PPP solution after 30 to 60 minutes. LEO-PNT technologies, however, can improve real-time PPP and convergence time by several minutes when aided by GNSS [129], [130]. In the most recent LEO-PNT simulations [129], [130], PPP convergence time dramatically shortened to about 6 minutes when using only LEO satellites. Even faster, 3 minute convergence time was feasible when using a LEO constellation-augmented by classic GNSS. All solutions were in the cm-level, demonstrating the great benefits of LEO satellites to PPP techniques.

2) PNT TECHNIQUES WITH MULTIPLE RECEIVER STATIONS

PNT techniques with multiple receiver stations often require one or a few base stations with known coordinates for the determination of unknown coordinates of the target receiver stations (rover stations). There are two major methods: 1) computing differential corrections or 2) forming measurement combinations relative to a base station.

1) **differential positioning**: point positioning is first performed for the base station to compute corrections. Then, another point positioning is applied to the rover station. The rover's point positioning is improved by the corrections computed for the base station, reaching an accuracy that depends on how far they are apart. Assuming that the rover is close enough to the base, similar errors are expected between the stations. This is called differential GNSS (DGNSS) and it is applied in GNSS to obtain dm-level accuracy [155], [156] without the need of external precise models and products. The technique can be further improved with the virtual reference station (VRS) concept [157].
2) **relative positioning**: the main idea is to transform measurements of the distance between transmitter and receiver into distances between the base and rover stations, the so-called baselines. Relative positioning offers advantages over single-receiver PNT techniques. The baselines are formed using measurement combinations of single-difference (SD) and double-difference (DD) to eliminate several errors intrinsic to the measurements. The basic assumption is that two receivers are simultaneously observing the same satellites. By subtracting the corresponding pseudorange (or phase) measurements between the receivers and/or satellites, clock errors, atmospheric effects, phase wind-up and the initial non-integer part of the phase bias are eliminated/mitigated. The DD combination is the most preferable observable in GNSS positioning techniques aiming to solve phase biases. It benefits from noise and error mitigation of the original measurements, being the main driver of several state-of-the-art GNSS software solutions, such as BERNESE [158], which provides millimetre-level solutions.

To our knowledge, there are no simulations to assess the performance of PNT techniques with multiple receivers for the upcoming LEO-PNT systems. However, we expect that

TABLE 13. Survey of user receivers in Doppler positioning. Ephemeris is obtained via TLEs in all references, except [150]. The accuracy is stated in the user positioning root mean square error (RMSE).

Receiver Configuration	User Velocity	Constellation	Measurement	Estimator	Accuracy in m	Ref.
Equipped with an altimeter	Static	Orbcomm	Pseudorange rate	EKF	11.38 (2D, simulated) , 358 (2D, experimental), (both including height info.)	[145]
Equipped with INS	Dynamic	Globalstar, Orbcomm, Iridium, Starlink	Pseudorange rate	EKF	10.5 (simulated GOI), 10.1 (simulated Starlink)	[151]
Equipped with INS	Dynamic	Orbcomm	Pseudorange rate	EKF	416.5 (experimental)	[151]
KF-loops in SDR	Static	Starlink	Carrier phase	Least Square	7.7 including height info. (2D), 25.9 without height info. (2D), 33.5 without height info. (2D) (all experimental)	[144]
Multi-constellation switching mode	Static	Iridium, Orbcomm	Pseudorange rate	EKF	177.1 (3D, experimental), 132 (2D, experimental)	[143]
Quadratic square accumulating Doppler Shift	Static	Iridium	Doppler-shift	Least Square	400 (3D, experimental), 163/ 198 including height info. (2D, experimental)	[148]
Equipped with INS	Dynamic	Iridium	Pseudorange and range rate	KF	200 m to 1 km (simulated)	[1]
Mobile receiver and base station	Dynamic	Globalstar, Orbcomm, Iridium, Starlink	Differential Doppler measurement with AOA	KF	100 m within 2 km of base station (simulated)	[150]

satellite clocks can be eliminated in the DD formation, so that a looser design can be defined in the space segment. As a counterpart, the user needs at least two receivers in the field campaigns. Therefore, higher costs are expected on the user side. To mitigate user cost, the ground segment must be implemented with several reference stations to serve as base stations with known coordinates, which is already the case for GNSS. The maintenance of the DGNSS or DD receiver networks is a responsibility of national and international institutes. They maintain continuously operating reference stations (CORS) by combining the efforts of hundreds of government, academic, and private organizations. The cost to implement a similar worldwide service, while a great impediment to applying strategies similar to GNSS and obtaining the most precise PNT solutions, is still doable.

C. PNT ESTIMATORS

Even though LEO satellites have the potential for complementary PNT services, the current LEO satellites are not optimal for PNT. They can be smaller and of lower quality than MEO satellites. The lack of actual LEO-PNT satellites favours using SoO in addition to navigation signals. Some obstacles can be mitigated with more advanced estimation algorithms to select and fuse LEO signals and additional information. This subsection reviews the estimation and optimisation algorithms for LEO PNT: LS, Kalman Filters (KF), Particle Filters (PF), Factor Graphs (FG) and Particle Swarm Optimisation (PSO).

1) LEAST SQUARES

The LS method is simple, computationally efficient, and therefore useful for LEO satellite positioning problems. Because the LS solution is not robust against erroneous data, it is crucial to detect and remove incorrect observations before using them. The standard method in the GNSS domain is the receiver autonomous integrity monitoring (RAIM) algorithm. In LEO positioning, some more advanced techniques have been developed. For example, an unsupervised clustering method for removing NLOS signals was used before solving the terminal position with LS [159].

2) KALMAN FILTER

Many Doppler-based LEO positioning solutions have been developed based on KF reaching close to 10 m accuracy [144], [145], [176]. They often combine Doppler observations of SoO with IMU values [177].

- **Extended Kalman Filter** (EKF): Kalman algorithm is an iterative recursive filtering method for predicting optimal states in linear state-space systems considering additive white Gaussian noise [164]. The algorithm proceeds by utilising prior knowledge to estimate the posterior states, calculate the Kalman gain, and determine the residual error due to the mismatch between the generated ground truth and the measurements. Then the new state mean and covariance vectors are calculated and fed to the next iteration [165]–[167]. An extended Kalman filter is a non-linearly approximated version of the ordinary linear Kalman filter to estimate states in nonlinear dynamic systems [168], as illustrated in Figure 11. In EKF, the state transition and the measurement matrices from the linear Kalman filter are replaced by non-linear state transition functions $f(.)$ and non-linear measurement function $h(.)$, respectively, to map the algorithm through Gaussian distribution to work in non-linear conditions.
- **Unscented Kalman filter** (UKF): UKF employs the sigma point transformation to model the non-linear state transition function of the system and linearize it via the unscented transform [167], [169]. The UKF algorithm utilises additional points besides the distribution mean, while EKF approximation relies only on one point, the mean. UKF selects these weighted points (i.e., the sigma points) plus the mean for better mapping the non-linear space. This procedure is called the unscented transform. There are other sigma point Kalman filters, such as Cubature (CKF).

TABLE 14. Positioning estimators summary.

Algorithm	Accuracy	Speed	Properties	Ref.
Iterative LS	high	moderate	static, iterative, can converge to local minimum	[49], [160]
Direct LS	moderate	high	static, partly iterative	[161]–[163]
wLS / ML	high	moderate	static, iterative, flexible, can converge to local minimum	[49], [160]
KF	moderate	high	dynamic, linear, recursive, parametric	[164]–[167]
EKF	moderate	high	dynamic, recursive, parametric	[168]
UKF	moderate	high	dynamic, recursive, parametric	[167], [169]
PF	moderate	moderate	dynamic, recursive, non-parametric	[170], [171]
FGO	high	low	dynamic, iterative parametric	[172], [173]
PSO	high	low	static, iterative, non-parametric, global optimisation	[174], [175]

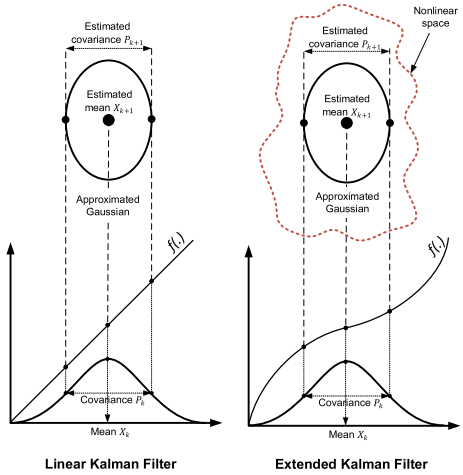

FIGURE 11. Illustration depicting EKF approximation for non-linear systems, adapted from [178].

3) PARTICLE FILTER (PF)

PF models the posterior distribution of the location with a swarm of discrete samples, known as particles. The particle cloud can represent many kinds of distributions, and the noise models related to observations and dynamic state model can also be arbitrary [179]. The basic implementations of PF have certain limitations, but there are many advanced versions, described for example by Elfring et.al [171]. PF has been used for LEO carrier tracking [180] and RADAR-based object tracking applications [181]. The flexible noise model makes the PF applicable to LEO positioning problems.

4) FACTOR GRAPH (FG)

Factor graph is one of the newest Bayesian filtering methods. Unlike with a Kalman filter, all past states can be used to calculate the maximum posterior probability iteratively. In the FGO model, the joint distribution is factorised as multiplication of marginal distributions, which can be represented graphically as a factor graph. The previous navigation and sensor calibration states are represented as nodes, and the edges are the sensor observations represented as factors. The iterative solution utilising previous states and observations improves the accuracy and robustness of the position estimate at the cost of additional computational resources. Real-time solution is still possible if the sampling frequency is not too high [173], [182]. Some early publications have found FG useful in mitigating multipath effects [183] and for sensor fusion combining GPS, IMU, and stereo vision [184]. Even though there are few examples using FG for LEO satellite navigation, the flexibility and additional accuracy of FGs make them potentially attractive. Since FGs are often used in simultaneous location and mapping (SLAM) applications, they are particularly suitable for simultaneous tracking and navigation (STAN), where the uncertain orbit of LEO satellite is refined while carrying out positioning.

5) GLOBAL OPTIMISATION METHODS

Particle swarm optimisation (PSO), originally introduced in [185] and [174], is a global optimisation strategy, i.e., it strives for finding the global optimum in possibly non-linear, non-convex search space. PSO can be used for solving the static positioning problem when local optima can cause problems; otherwise, iterative LS is more efficient. The PSO method as such cannot utilise the dynamic model, but it is sometimes combined with dynamic methods such as PF [175]. PSO has been applied in the LEO navigation domain to satellite selection [186] and faulty signal avoidance [187].

6) SENSOR FUSION

Fusion-based positioning methods combine the measurements of multiple sensors to further refine the PNT solution, maximising the information content, mitigating the sources of errors and thus reaching higher precision [178]. The main steps of sensor fusion are described in Figure 12, where data from a group of sensors are locally processed using their corresponding solvers (algorithms), then the output is weighed and later combined with other sensors (fused) globally using the proper fusion scheme to produce the final optimal solution.

Sensor fusion as a computational procedure can take the architecture of three distinct fusion schemes: a) loosely

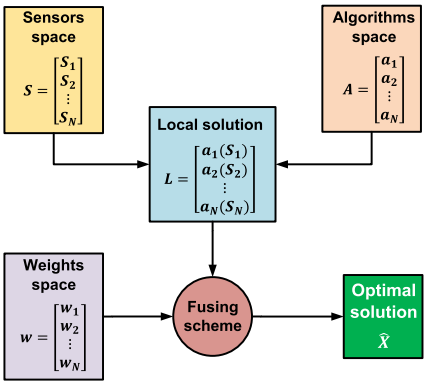

FIGURE 12. Sensor fusion framework, adapted from [178], [188].

coupled (LC), b) tightly coupled (TC), and c) ultra tightly coupled (UTC). As stated by [189], in GNSS, LC is the simplest type among the three architectures that provides the essential redundancy based on the duplicated information in situations of good visibility (four satellites) to achieve high accuracy. TC is widely adopted because it provides better accuracy and is less susceptible to jamming, in addition to maintaining navigation in situations of poor visibility (fewer than four satellites). While in UTC, the tracking loop of GNSSs is assisted with an accompanying SDR loop that matches and smooths between the locally generated signal and the actual received signal.

LEO satellites have great potential to benefit from sensor fusion with other technologies to leverage PNT-based applications. The fusion of LEO positioning data with other assisting positioning technologies would exploit the link budgets of existing LEO constellations to provide PNT data at no additional cost or complication to onboard hardware technology. As the conceptual proposal released by [190] states, it is possible to get low-cost PNT solutions using the existing broadband LEO satellites in orbit, such as the Starlink constellation, by fusion with GNSS. The authors concluded that the resources of the Starlink constellation, which already enable coverage to most of the world's population ($< 60°$ latitude), could be reallocated to consume 0.8% of downlink capacity, 0.36% of energy capacity, and a negligible percentage of uplink capacity to sacrifice an increase of approximately 0.1 dB in maximum pointing loss.

Another concept is the STAN framework [191]. It is a LEO-based method in a realistic simulation environment to localise an unmanned aerial vehicle (UAV) where GNSS signal is denied, by interfacing with the Globalstar, Iridium, Orbcomm, and Starlink constellations. Unlike GNSS, which periodically send information about their clock offsets and current location, the STAN framework tracks the LEO satellite states by exploiting their signals to determine their pseudoranges and Doppler measurements, then feeds the drawn data to the vehicle's onboard inertial navigation sensors (INS). The optimal fusion estimation is then performed via EKF to localise the UAV. Simulation results showed an absolute error of 9.9 m and an RMSE of 10.5 m with Globalstar, Iridium, and Orbcomm, while with Starlink the LEO/INS method achieved an error of 9.8 m and RMSE of 10.1 m.

The introduction of massive multiple-input multiple-output (mMIMO) concept into LEO-PNT is recently discussed by [55], [192], [193]. The concept comprises the use of massive arrays of beamforming antennas hence exploiting the multipath. This setup has numerous advantages which can enhance the LEO-based localization, especially in the inevitable events of superposition where the UT is spotted by multiple beamformed loops. In addition, mMIMO is capable of extending the coverage area on Earth per each LEO satellite by adopting space-time block coding which maximizes the number of beneficiary UTs.

D. SUMMARY OF USER SEGMENT CONSIDERATIONS

We have found potential in the development of PNT receivers as the whole LEO-based positioning sector is developing at a fast pace. However, there is still a distinction between high versus low accuracy. Signals of opportunity receivers require lower complexity than dedicated LEO-PNT solutions, at the cost of providing lower positioning performance, as their main tasks are offering good communication and sensing performance, rather than good positioning performance. Dedicated LEO-PNT systems, on the other hand, are more accurate, but limited in providing only PNT (and possibly sensing) applications. The accuracy discrepancy is getting smaller as more commercial efforts are filling this market and providing better satellite visibility and higher coverage on Earth. However, the best way to compete with GNSS technology is still uncertain, but is leaning towards working in cooperation with it rather than as a competitive solution. The PPP solution appears to be the most benefited among the GNSS techniques, but simulations are still required to assess the LEO-PNT systems when using multiple ground stations. Regarding estimators, LC is the simplest type of sensor fusion that provides the necessary redundancy based on the duplicated information, while TC is less susceptible to jamming and tolerates poor coverage better. The STAN methods may be beneficial for LEO PNT when the orbits are not as accurate as in the case of GNSS.

VII. SIMULATION EXAMPLES

Several simulator manufacturers offer LEO satellite simulation options. This section provides an overview of the main hardware and software simulators.

A. HARDWARE SIMULATORS

The hardware-based LEO simulators are a prime example of tools to facilitate LEO-PNT development. They are space segment-based, which means that they can simulate GNSS measurements of receivers onboard LEO satellites. Ground segment-based simulators using LEO satellites as

transmitters, on the other hand, are rare according to the authors' knowledge.

- **Spirent simulator**: Spirent simulators are commonly used to simulate GNSS signals from various constellations and receiver configurations. Although most simulators are designed primarily for MEO-based GNSS signal generation considering the receiver on the ground, the Spirent GSS9000 series can simulate receivers onboard LEO satellites by describing the LEO trajectory with high dynamic motion and ultra-low latency. For example, GSS9000 can simulate relative velocities of 120 km/s, including one or two versatile RF outputs. The user can use both RF outputs at the same time: one to generate available GNSS signals, and the other to generate novel PNT signals replaying in-phase & quadrature (IQ) data in conjunction with the GNSS simulator.
- **LabSat SatGen**: even though SatGen is a software simulator, it requires a LabSat device to play the simulated data as RF signals. SatGen software enables users to generate IQ data depending on their trajectory, which can be replayed on the Labsat GNSS simulator. Researchers can utilize SatGen to build a scenario that simulates extremely high dynamic situations, allowing them to test receiver performance onboard LEO satellites.

B. SOFTWARE SIMULATORS

Various commercial or open-access software simulators currently exist for LEO modelling at different architectural levels, but none of the current ones are providing a full-chain solution, to the best of the authors' knowledge. According to the segment in the propagation chain, we can divide these software simulators into several subsections:

1) SPACE-SEGMENT SIMULATORS

- **MATLAB**: for modelling the satellite orbits and 3D coordinates motion, we can use the MATLAB Satellite Communications Toolbox (introduced in release 2020a). This toolbox contains useful functions to model and propagate satellite orbits and constellations, visualise the propagated orbits, and analyse line-of-sight access between satellites and ground stations. For propagating the orbits, different perturbation models can be used: two-body (assumes the Earth is a sphere and no perturbations besides gravity), SGP4 (taking into consideration Earth oblateness and atmospheric drag) and SDP4 (which, besides the perturbations considered by SGP4, additionally includes solar and lunar gravity). MATLAB Satellite Communications Toolbox model both 3D position and velocity, which is useful for Doppler-based measurements.
- **poliastro**: poliastro is an open source Python library that allows the simulation of astrodynamics and orbital mechanics, with a focus on ease of use, speed, and quick visualisation. Several useful functions can be utilised to perform the computation of classical orbital elements, numerical orbit propagation, and orbital manoeuvres. The orbit propagation can be computed considering a two-body force, gravitational effects due to Earth oblateness, atmospheric drag, and several propagators, such as the Cowell numerical integration.
- **STK**: System Tool Kit (STK) by Analytical Graphics is a software simulation tool for analysing land, sea, air, and space assets within a high-fidelity environment model and time-dynamic three-dimensional simulation. It enables the modelling, analysis, and interaction of mission objects and targets. STK is widely used in aerospace applications for the analysis of satellites, orbits, and space environment. It supports multiple satellite and constellation missions. Additionally, it enables access calculations for ground stations and areas of interest. STK provides real-time 2D and 3D visualisation from the land, sea, air, and space components using high-resolution terrain, imagery, and RF environment. Advanced modules include satellite subsystem modelling, space environment effects, and conjunction analysis [194].
- **GMAT**: The General Mission Analysis Tool (GMAT) is a free and open source software application developed by NASA in collaboration with public and private contributors, as well as industry. It is a multi-mission space mission design, optimisation, and navigation software package that supports missions ranging from low Earth orbit to lunar, libration points, and deep space. It contains orbit propagators, spacecraft models, and thruster models. It facilitates analysis by generating reports and plots. The GMAT tool is widely used to support missions, educate students, and conduct outreach [195], [196].
- **SaVoir**: SaVoir by Taitus Software is a multi-satellite swath planner initially developed for the European Space Agency to aid in rapidly evaluating acquisition opportunities with a satellite and sensor combination across any region of interest. This application displays Earth and other celestial bodies in 2D and 3D, as well as a vast number of images of the Earth's surface with current or expected clouds. The initial set of orbits and models for major remote sensing satellites and constellations that has already been integrated can be updated online. Multiple earth orbiting satellites can be simulated in near real time [197]–[199].
- **Savi**: SaVi is a cross-platform, open source software program for analysis and visualisation of satellite constellations. Satellite orbits can be created and analysed in two and three dimensions. The software enables the user to monitor satellite coverage for Earth-orbiting satellites. The software includes a variety of existing satellite constellations, including Iridium, Globalstar, GPS, and Galileo. [87], [198].

2) WIRELESS CHANNEL SIMULATORS

- **QuaDRiGa**: One option for modelling a realistic wireless channel is by using the QuaDRiGa [200], [201] framework. QuaDRiGa is a MATLAB-based software developed by Fraunhofer HHI that enables modelling wireless channels by generating realistic radio channel impulse responses for system-level simulations. It is very flexible, allowing different simulation layouts by modifying some variables. QuaDRiGa offers a wide operating range (carrier frequencies comprised between 0.5 GHz and 100 GHz) for the simulations. In addition, QuaDriga offers the possibility to modify the transmitter and receiver position, orientation, and movement profile (with specific focus on satellite orbit propagation). Additionally the antenna type to be used in both receiver and transmitter can be selected among a few options, or or a customised. The specific channel models for satellite application are downlink oriented [202]. QuaDRiGa framework contains the following ready-to-use downlink specific channel scenarios: rural, sub-urban, urban, dense urban, and as LoS and NLoS propagation conditions. Each of these scenarios contains specific features (e.g., number of multipath and scattering object's size) according to its nature.

3) GROUND- AND USER-SEGMENT SIMULATORS

The authors are not aware of any commercial or open source simulators in the existing literature to simulate LEO-PNT dedicated or opportunistic signals; however, some works have recently developed their own techniques: [27], [130], [203], [204].

VIII. COMMERCIAL PERSPECTIVES

To form an understanding of commercial endeavours for the upcoming LEO-PNT systems, business model typology can be used. They help to understand the whole ecosystem where the firms work and how they create value for other firms as well as end users. The business model can be applied, including four components [205]. The first component is ''product/service'', that refers to how a firm is using LEO-PNT-enabled technologies to provide new services. As an example, the US start-up company Satelles provides PNT-based services complementary to the GNSS to allow better performance quality and operational resilience. Their services can be used to increase safeguarding time stamps in trading or using satellite time and location (STL) when GNSS signals are disrupted or manipulated. The second component,''value network'', refers to the key actors (firms, authorities, customers, partners, etc.) enabling LEO-PNT services. Satelles has several partners in their value network that together enable the implementation of the services. These partners include solution providers and original equipment manufacturers incorporating STL technology. The third component, ''value delivery'', demonstrates how value is delivered to and between various actors in the value network. In the case of Satelles, the value is delivered through partners to end users, such as data centers and teleoperators. The fourth component, ''revenue model'', shows how the value that a firm offers to end users, customers, and partners, can generate financial income. The Satelles' revenue model is based on the services they provide for customers and end users.

As accurate PNT is a key requirement for a variety of markets and industries, upstream and downstream firms are currently launched or planned, such as Satelles, Future Navigation, and Xona Space Systems [19]. The upstream market in the new space industry is typically considered to include hardware manufacturing firms, whereas the downstream segment typically includes data analytic service providers [206]. Based on these two segments, the overall GNSS market is rapidly evolving. Currently, the business models for PNT services largely depend on the existing GNSS systems. Since LEO-PNT system developments are moving at a fast pace, new business models for both start-ups and established firms in upstream as well as downstream markets are expected in the near future.

IX. CONCLUSION

In this survey, several requirements to build a new LEO-PNT system have been analysed. An extensive literature review has shown considerations to implement the signal design, space segment, ground segment, and user segment. Advantages and drawbacks of various instruments and techniques were discussed in order to detect possible options to materialise LEO-based navigation systems. Our investigation has not led to a clear recommendation of preferable options in every single aspect of the LEO-PNT system since there are very few works that have provided simulations in the current literature. Future simulations are therefore required to define optimal signal designs, constellations, atmospheric models, and PNT techniques. Nevertheless, dedicated LEO-PNT systems, as adopted by Xona Space Systems, are a viable option to bring relevant gains to the current PNT solutions and lead to innovative business models for both start-ups and established companies.

We have also analysed relevant material of the current stage and future direction in LEO-PNT systems. The rapid evolution in the space segment has led to a significant reduction of cost in the launch, deployment and maintenance of small satellites. At the same time, the literature review over simulation results have shown that GNSS technologies, which are now exclusively based on MEO and GEO satellites, can be improved by LEO satellites in terms of geometry and signal reception power. These are important measures for improving urban and indoors navigation, setting LEO-PNT as a possible solution to solve current challenges in the field of navigation, positioning and timing.

REFERENCES

[1] H. Benzerrouk, Q. Nguyen, F. Xiaoxing, A. Amrhar, A. V. Nebylov, and R. Landry, ''Alternative PNT based on iridium next LEO satellites Doppler/INS integrated navigation system,'' in *Proc. 26th Saint Petersburg Int. Conf. Integr. Navigat. Syst. (ICINS)*, May 2019, pp. 1–10.

[2] A. Nardin, F. Dovis, and J. A. Fraire, "Empowering the tracking performance of LEO PNT by means of meta-signals," in *Proc. IEEE Int. Conf. Wireless for Space Extreme Environments (WiSEE)*, Oct. 2020, pp. 153–158.

[3] R. Morales-Ferre, E. S. Lohan, G. Falco, and E. Falletti, "GDOP-based analysis of suitability of LEO constellations for future satellite-based positioning," in *Proc. IEEE Int. Conf. Wireless Space Extreme Environments (WiSEE)*, Oct. 2020, pp. 147–152.

[4] D. Egea-Roca, J. A. López-Salcedo, G. Seco-Granados, and E. Falletti, "Comparison of several signal designs based on chirp spread spectrum (CSS) modulation for a LEO PNT system," in *Proc. 34th Int. Tech. Meeting Satell. Division Inst. Navigat. (ION GNSS+)*, Oct. 2021.

[5] C. Fernandez-Prades, L. L. Presti, and E. Falletti, "Satellite radiolocalization from GPS to GNSS and beyond: Novel technologies and applications for civil mass market," *Proc. IEEE*, vol. 99, no. 11, pp. 1882–1904, Nov. 2011.

[6] E. A. Bretz, "Precision navigation in European skies," *IEEE Spectr.*, vol. 40, no. 9, p. 16, Sep. 2003.

[7] Y.-F. Tsai and K.-S. Low, "Performance assessment on expanding SBAS service areas of GAGAN and MSAS to Singapore region," in *Proc. IEEE/ION Position, Location Navigat. Symp. (PLANS)*, May 2014, pp. 686–691.

[8] J. L. Grubb, "The traveler's dream come true (satellite personal communication)," *IEEE Commun. Mag.*, vol. 29, no. 11, pp. 48–51, Nov. 1991.

[9] O. B. Osoro and E. J. Oughton, "A techno-economic framework for satellite networks applied to low Earth orbit constellations: Assessing starlink, oneweb and kuiper," *IEEE Access*, vol. 9, pp. 141611–141625, 2021.

[10] K. Çelikbilek, Z. Saleem, R. Morales Ferre, J. Praks, and E. S. Lohan, "Survey on optimization methods for LEO-satellite-based networks with applications in future autonomous transportation," *Sensors*, vol. 22, no. 4, p. 1421, Feb. 2022.

[11] S. Abulgasem, F. Tubbal, R. Raad, P. I. Theoharis, S. Lu, and S. Iranmanesh, "Antenna designs for CubeSats: A review," *IEEE Access*, vol. 9, pp. 45289–45324, 2021.

[12] A. H. Lokman, P. J. Soh, S. N. Azemi, H. Lago, S. K. Podilchak, S. Chalermwisutkul, M. F. Jamlos, A. A. Al-Hadi, P. Akkaraekthalin, and S. Gao, "A review of antennas for picosatellite applications," *Int. J. Antennas Propag.*, vol. 2017, Apr. 2017, Art. no. 4940656.

[13] R. Rajan, R. Vedanayagi, and S. Renukadevi, "Antenna designs for amateur band low Earth orbit (LEO) satellites—A review," *Int. J. Res. Eng. Appl. Manage.*, vol. 4, no. 5, pp. 245–259, Sep. 2018.

[14] P. Petropoulou, E. T. Michailidis, A. D. Panagopoulos, and A. G. Kanatas, "Radio propagation channel measurements for multi-antenna satellite communication systems: A survey," *IEEE Antennas Propag. Mag.*, vol. 56, no. 6, pp. 102–122, Dec. 2014.

[15] O. Kodheli, E. Lagunas, N. Maturo, S. K. Sharma, B. Shankar, J. F. M. Montoya, J. C. M. Duncan, D. Spano, S. Chatzinotas, S. Kisseleff, J. Querol, L. Lei, T. X. Vu, and G. Goussetis, "Satellite communications in the new space era: A survey and future challenges," *IEEE Commun. Surveys Tuts.*, vol. 23, no. 1, pp. 70–109, 4th Quart., 2021.

[16] T. G. Reid, T. Walter, P. K. Enge, D. Lawrence, H. S. Cobb, G. Gutt, M. O'Connor, and D. Whelan, "Navigation from low earth orbit: Part 1: Concept, current capability, and future promise," in *Position, Navigation, and Timing Technologies in the 21st Century: Integrated Satellite Navigation, Sensor Systems, and Civil Applications*, vol. 2. Wiley, 2020, pp. 1359–1379, doi: 10.1002/9781119458555.ch43a.

[17] Z. Z. M. Kassas, *Navigation From Low-Earth Orbit*. Hoboken, NJ, USA: Wiley, 2021, pp. 1381–1412.

[18] J. Bouwmeester, and J. Guo, "Survey of worldwide pico- and nanosatellite missions, distributions and subsystem technology," *Acta Astron*, vol. 67, nos. 7–8, pp. 854–862, 2010.

[19] E. Kulu, "Satellite constellations-2021 industry survey and trends," in *Proc. 35th Annu. Small Satell. Conf.*, 2021, pp. 1–20.

[20] F. Davoli, C. Kourogiorgas, M. Marchese, A. Panagopoulos, and F. Patrone, "Small satellites and cubesats: Survey of structures, architectures, and protocols," *Int. J. Satell. Commun. Netw.*, vol. 37, no. 4, pp. 343–359, Jul./Aug. 2019.

[21] G. Curzi, D. Modenini, and P. Tortora, "Large constellations of small satellites: A survey of near future challenges and missions," *Aerospace*, vol. 7, no. 9, p. 133, Sep. 2020.

[22] R. S. Jakhu and J. N. Pelton, *Small Satellites and Large Commercial Satellite Constellations*. Cham, Switzerland: Springer, 2017, pp. 357–378.

[23] G. Denis, D. Alary, X. Pasco, N. Pisot, D. Texier, and S. Toulza, "From new space to big space: How commercial space dream is becoming a reality," *Acta Astronautica*, vol. 166, pp. 431–443, Jan. 2020.

[24] H. Ge, B. Li, S. Jia, L. Nie, T. Wu, Z. Yang, J. Shang, Y. Zheng, and M. Ge, "LEO enhanced global navigation satellite system (LeGNSS): Progress, opportunities, and challenges," *Geo-Spatial Inf. Sci.*, vol. 25, no. 1, pp. 1–13, Jan. 2022.

[25] S. Liu, Z. Gao, Y. Wu, D. W. Kwan Ng, X. Gao, K.-K. Wong, S. Chatzinotas, and B. Ottersten, "LEO satellite constellations for 5G and beyond: How will they reshape vertical domains?" *IEEE Commun. Mag.*, vol. 59, no. 7, pp. 30–36, Jul. 2021.

[26] N. Saeed, A. Elzanaty, H. Almorad, H. Dahrouj, T. Y. Al-Naffouri, and M.-S. Alouini, "CubeSat communications: Recent advances and future challenges," *IEEE Commun. Surveys Tuts.*, vol. 22, no. 3, pp. 1839–1862, 3rd Quart., 2020.

[27] X. Li, Z. Jiang, F. Ma, H. Lv, Y. Yuan, and X. Li, "LEO precise orbit determination with inter-satellite links," *Remote Sens.*, vol. 11, no. 18, p. 2117, Sep. 2019.

[28] J. van den IJssel, J. Encarnação, E. Doornbos, and P. Visser, "Precise science orbits for the Swarm satellite constellation," *Adv. Space Res.*, vol. 56, no. 6, pp. 1042–1055, Sep. 2015.

[29] I. Gorbatyy, "Particularities of the amplitude shift keying signal spectrum calculation," in *Proc. Int. Conf. 'Modern Problems Radio Eng., Telecommun. Comput. Sci.' (TCSET)*, 2008, pp. 475–476.

[30] F. Xiong, "M-ary amplitude shift keying OFDM system," *IEEE Trans. Commun.*, vol. 51, no. 10, pp. 1638–1642, Oct. 2003.

[31] T. Anfray, A. Mottet, J.-J. Bonnefois, R. Cousty, S. Mariojouls, A. Laurent, H. Porte, J. Hulin, W. Atitallah, J. Hauden, T. Schmitt, and P. Berceau, "Assessment of the performance of DPSK and OOK modulations at 25 Gb/s for satellite-based optical communications," in *Proc. IEEE Int. Conf. Space Opt. Syst. Appl. (ICSOS)*, Oct. 2019, pp. 1–6.

[32] I. D. Portillo, B. G. Cameron, and E. F. Crawley, "A technical comparison of three low earth orbit satellite constellation systems to provide global broadband," *Acta Astronautica*, vol. 159, pp. 123–135, Jun. 2019.

[33] P. Ferrand, M. Maso, and V. Bioglio, "High-rate regular APSK constellations," *IEEE Trans. Commun.*, vol. 67, no. 3, pp. 2015–2023, Mar. 2019.

[34] K. P. Liolis, R. D. Gaudenzi, N. Alagha, A. Martinez, and A. G. I. Fàbregas, "Amplitude phase shift keying constellation design and its applications to satellite digital video broadcasting," in *Digital video*, F. D. Rango, Ed. Rijeka, Croatia: IntechOpen, 2010, ch. 20.

[35] Y. Qian, L. Ma, and X. Liang, "Symmetry chirp spread spectrum modulation used in LEO satellite Internet of Things," *IEEE Commun. Lett.*, vol. 22, no. 11, pp. 2230–2233, Nov. 2018.

[36] A. Roy, H. B. Nemade, and R. Bhattacharjee, "Symmetry chirp modulation waveform design for LEO satellite IoT communication," *IEEE Commun. Lett.*, vol. 23, no. 10, pp. 1836–1839, Oct. 2019.

[37] Y. Qian, L. Ma, and X. Liang, "The performance of chirp signal used in LEO satellite Internet of Things," *IEEE Commun. Lett.*, vol. 23, no. 8, pp. 1319–1322, Aug. 2019.

[38] T. Wu, D. Qu, and G. Zhang, "Research on Lora adaptability in the LEO satellites Internet of Things," in *Proc. 15th Int. Wireless Commun. Mobile Comput. Conf. (IWCMC)*, Jun. 2019, pp. 131–135.

[39] M. K. Simon, "On the bit-error probability of differentially encoded QPSK and offset QPSK in the presence of carrier synchronization," *IEEE Trans. Commun.*, vol. 54, no. 5, pp. 806–812, May 2006.

[40] M. N. Pachery and M. R. Bhatnagar, "Double differential modulation for LEO-based land mobile satellite communication," *IEEE Trans. Aerosp. Electron. Syst.*, vol. 56, no. 4, pp. 3339–3346, Aug. 2020.

[41] H. Ezzat, A. Hassan, and M. El-Soudani, "M-ary continuous phase frequency shift keying transmissions through nonlinear channels in additive Gaussian noise and cochannel interferences," in *Proc. Int. Zurich Seminar Digit. Commun., Electron. Circuits Syst. Commun.*, Mar. 1990, pp. 495–511.

[42] M. Rahmani and B. G. Family, "Design and implementation of a GMSK baseband modem for UHF radio modem," in *Proc. Int. Power Syst. Conf. (PSC)*, Dec. 2019, pp. 33–36.

[43] T. Venugopal and S. Radhika, "A survey on channel coding in wireless networks," in *Proc. Int. Conf. Commun. Signal Process. (ICCSP)*, Jul. 2020, pp. 0784–0789.

[44] J. Jin Kong and K. K. Parhi, "Interleaved cyclic redundancy check (CRC) code," in *Proc. 37th Asilomar Conf. Signals, Syst. Comput.*, vol. 2, Nov. 2003, pp. 2137–2141.

[45] D. J. C. MacKay, "Fountain codes," *IEE Proc. Commun.*, vol. 152, no. 6, pp. 1062–1068, Dec. 2005.

[46] R. G. Gallager, "Low-density parity-check codes," *IRE Trans. Inf. Theory*, vol. 8, no. 1, pp. 21–28, Jan. 1962.
[47] B. Tahir, S. Schwarz, and M. Rupp, "BER comparison between convolutional, turbo, LDPC, and polar codes," in *Proc. 24th Int. Conf. Telecommun. (ICT)*, May 2017, pp. 1–7.
[48] L. Wang, Z. Lü, X. Tang, K. Zhang, and F. Wang, "LEO-augmented GNSS based on communication navigation integrated signal," *Sensors*, vol. 19, no. 21, p. 4700, Oct. 2019.
[49] E. D. Kaplan and C. J. Hegarty, Eds., *Understanding GPS: Principles and Applications*, 2 ed. Norwood, MA, USA: Artech House, 2006.
[50] P. Angeletti and R. De Gaudenzi, "A pragmatic approach to massive MIMO for broadband communication satellites," *IEEE Access*, vol. 8, pp. 132212–132236, 2020.
[51] M. Caus, A. Perez-Neira, and E. Mendez, "Smart beamforming for direct LEO satellite access of future IoT," *Sensors*, vol. 21, no. 14, p. 4877, Jul. 2021.
[52] B. Falkner, H. Zhou, A. Mehta, and A. Modigliana, "Flat panel interlaced shared aperture antenna array for LEO Ka-band high throughput satellite communication applications," in *Proc. IEEE Int. Symp. Antennas Propag. USNC-URSI Radio Sci. Meeting (APS/URSI)*, Dec. 2021, pp. 777–778.
[53] G. He, X. Gao, L. Sun, and R. Zhang, "A review of multibeam phased array antennas as LEO satellite constellation ground station," *IEEE Access*, vol. 9, pp. 147142–147154, 2021.
[54] K. Y. Zhong, Y. J. Cheng, H. N. Yang, and B. Zheng, "LEO satellite multi-beam coverage area division and beamforming method," *IEEE Antennas Wireless Propag. Lett.*, vol. 20, no. 11, pp. 2115–2119, Nov. 2021.
[55] R. M. Ferre, E. S. Lohan, H. Kuusniemi, J. Praks, S. Kaasalainen, C. Pinell, and M. Elsanhoury, "Is LEO-based positioning with mega-constellations the answer for future equal access localization?" *IEEE Commun. Mag.*, vol. 60, no. 6, pp. 40–46, Jun. 2022.
[56] C. D. Brown, *Elements of Spacecraft Design*. Reston, VA, USA: American Institute of Aeronautics and Astronautics, Jan. 2002.
[57] P. Fortescue, G. Swinerd, and J. Stark, *Spacecraft Systems Engineering*. Hoboken, NJ, USA: Wiley, 2011.
[58] T. P. Garrison, M. Ince, J. Pizzicaroli, and P. A. Swan, "Systems engineering trades for the IRIDIUM constellation," *J. Spacecraft Rockets*, vol. 34, no. 5, pp. 675–680, Sep. 1997.
[59] T. Wekerle, J. B. Pessoa Filho, L. E. V. L. D. Costa, and L. G. Trabasso, "Status and trends of smallsats and their launch vehicles—An up-to-date review," *J. Aerosp. Technol. Manage.*, vol. 9, no. 3, pp. 269–286, 2017.
[60] R. A. de Carvalho, J. Estela, and M. Langer, *Nanosatellites: Space and Ground Technologies, Operations and Economics*. Hoboken, NJ, USA: Wiley, 2020.
[61] B. Yost, S. Weston, G. Benavides, F. Krage, J. Hines, S. Mauro, S. Etchey, K. O'Neill, and B. Braun, "State-of-the-art small spacecraft technology," NASA, Washington, DC, USA, Tech. Rep. NASA/TP-20210021263, 2021.
[62] J. D. Liddle, A. P. Holt, S. J. Jason, K. A. O'Donnell, and E. J. Stevens, "Space science with cubesats and nanosatellites," *Nature Astron.*, vol. 4, no. 11, pp. 1026–1030, Nov. 2020.
[63] S. K. Rao, "Advanced antenna technologies for satellite communications payloads," *IEEE Trans. Antennas Propag.*, vol. 63, no. 4, pp. 1205–1217, Apr. 2015.
[64] A. Babuscia, B. Corbin, M. Knapp, R. Jensen-Clem, M. Van de Loo, and S. Seager, "Inflatable antenna for cubesats: Motivation for development and antenna design," *Acta Astronautica*, vol. 91, pp. 322–332, Oct. 2013.
[65] R. Florencio, J. A. Encinar, R. R. Boix, V. Losada, and G. Toso, "Reflectarray antennas for dual polarization and broadband telecom satellite applications," *IEEE Trans. Antennas Propag.*, vol. 63, no. 4, pp. 1234–1246, Apr. 2015.
[66] Y. Rahmat-Samii, V. Manohar, and J. M. Kovitz, "For satellites, think small, dream big: A review of recent antenna developments for cubesats," *IEEE Antennas Propag. Mag.*, vol. 59, no. 2, pp. 22–30, Apr. 2017.
[67] P. A. Warren, J. W. Steinbeck, R. J. Minelli, and C. H. Mueller, "Large, deployable S-band antenna for a 6U cubesat," in *Proc. 29th AIAA/USU Conf. Small Satell.*, 2015, pp. 1–7.
[68] T. M. Braun, *Satellite Communications Payload and System*. Hoboken, NJ, USA: Wiley, 2021.
[69] P. Li, J. Liang, and X. Chen, "Study of printed elliptical/circular slot antennas for ultrawideband applications," *IEEE Trans. Antennas Propag.*, vol. 54, no. 6, pp. 1670–1675, Jun. 2006.
[70] F. J. Gonzalez Martinez, "Performance of new GNSS satellite clocks," Ph.D. thesis, Karlsruher Institut für Technologie, Fakultät für Bauingenieur-, Geo- und Umweltwissenschaften (BGU), Karlsruhe, Germany, 2014.
[71] P. Berceau, M. Taylor, J. Kahn, and L. Hollberg, "Space-time reference with an optical link," *Classical Quantum Gravity*, vol. 33, no. 13, Jul. 2016, Art. no. 135007.
[72] H. Zhang, H. Herdian, A. T. Narayanan, A. Shirane, M. Suzuki, K. Harasaka, K. Adachi, S. Yanagimachi, and K. Okada, "29.4 ultra-low-power atomic clock for satellite constellation with 2.2×10^{-12} long-term Allan deviation using cesium coherent population trapping," in *IEEE Int. Solid-State Circuits Conf. (ISSCC) Dig. Tech. Papers*, Feb. 2019, pp. 462–464.
[73] D. Van Buren, P. Axelrad, and S. Palo, "Design of a high-stability heterogeneous clock system for small satellites in LEO," *GPS Solutions*, vol. 25, no. 3, p. 105, Jul. 2021.
[74] K. M. Larson, N. Ashby, C. Hackman, and W. Bertiger, "An assessment of relativistic effects for low Earth orbiters: The GRACE satellites," *Metrologia*, vol. 44, no. 6, pp. 484–490, Nov. 2007.
[75] J. Wertz, *Mission Geometry: Orbit and Constellation Design and Management: Spacecraft Orbit and Attitude Systems*. Portland, OR, USA: Microcosm Press, 2001.
[76] V. A. Chobotov, *Orbital Mechanics*, 3rd ed. Reston, VA, USA: American Institute of Aeronautics and Astronautics, Jan. 2002.
[77] D. Beste, "Design of satellite constellations for optimal continuous coverage," *IEEE Trans. Aerosp. Electron. Syst.*, vol. AES-14, no. 3, pp. 466–473, May 1978.
[78] B. Gavish and J. Kalvenes, "The impact of satellite altitude on the performance of LEOS based communication systems," *Wireless Netw.*, vol. 4, pp. 119–213, Feb. 1998.
[79] G. Dai, X. Chen, M. Wang, E. Fernández, T. N. Nguyen, and G. Reinelt, "Analysis of satellite constellations for the continuous coverage of ground regions," *J. Spacecraft Rockets*, vol. 54, no. 6, pp. 1294–1303, Nov. 2017.
[80] E. Lansard, E. Frayssinhes, and J.-L. Palmade, "Global design of satellite constellations: A multi-criteria performance comparison of classical Walker patterns and new design patterns," *Acta Astronautica*, vol. 42, no. 9, pp. 555–564, May 1998.
[81] T. J. Lang and W. S. Adams, "A comparison of satellite constellations for continuous global coverage," in *Mission Design & Implementation of Satellite Constellations* (Space Technology Proceedings). The Netherlands: Springer, 1998, pp. 51–62.
[82] D. Mortari, M. P. Wilkins, and C. Bruccoleri, "The flower constellations," *J. Astron. Sci.*, vol. 52, nos. 1–2, pp. 107–127, Mar. 2004.
[83] M. E. Avendaño, J. J. Davis, and D. Mortari, "The 2-D lattice theory of flower constellations," *Celestial Mech. Dyn. Astron.*, vol. 116, no. 4, pp. 325–337, Aug. 2013.
[84] J. J. Davis, M. E. Avendaño, and D. Mortari, "The 3-D lattice theory of flower constellations," *Celestial Mech. Dyn. Astron.*, vol. 116, no. 4, pp. 339–356, Aug. 2013.
[85] D. Arnas, D. Casanova, E. Tresaco, and D. Mortari, "3-dimensional necklace flower constellations," *Celestial Mech. Dyn. Astron.*, vol. 129, no. 4, pp. 433–448, Dec. 2017.
[86] D. Arnas, D. Casanova, and E. Tresaco, "2D necklace flower constellations," *Acta Astronautica*, vol. 142, pp. 18–28, Jan. 2018.
[87] L. Wood, "SaVi: Satellite constellation visualization," 2022, *arXiv:1204.3265*.
[88] L. Globalstar, "Description of the globalstar system," Globalstar, Covington, LA, USA, Tech. Rep. GS-TR-94-0001, 2000.
[89] Globalstar. (2016). *Terrestrial Use of the 2473–2495 MHz Band for Low-Power Mobile Broadband Networks; Amendments to Rules for the Ancillary Terrestrial Component of Mobile Satellite Service Systemsystem, Attachment a: Technical Information to Supplement Schedule*. Accessed: Dec. 20, 2021. [Online]. Available: https://docs.fcc.gov/public/attachments/FCC-16-181A1.pdf
[90] M. J. Evans and T. D. Maclay, "Mission design of the orbcomm constellation," in *Mission Design Implement. Satell. Constellations*, J. C. van der Ha, Ed. Amsterdam, The Netherlands: Springer, 1997, pp. 103–112.
[91] O. Gupta, "Iridium NEXT SensorPODs: Global access for your scientific payloads," in *Proc. AIAA/USU Conf. Small Satell.*, 2011, pp. 1–5.
[92] A. A. M. Shah Sadman and M. Hossam-E-Haider, "Study of GNSS parameters and environmental factors over Bangladesh intended for selecting ideal ground station location for SBAS," in *Proc. 2nd Global Conf. Advancement Technol. (GCAT)*, Oct. 2021, pp. 1–6.
[93] A. Cornejo, S. Landeros-Ayala, J. M. Matias, and R. Martinez, "Applying learning methods to optimize the ground segment for HTS systems," in *Proc. IEEE 11th Latin Amer. Symp. Circuits Syst. (LASCAS)*, Feb. 2020, pp. 1–4.

[94] X. Liu, Y. Ge, C. Zhao, B. Li, and R. Zhou, "A study on global monitoring station optimization deployment method based on navigation satellite quadruple observing coverage," in *Proc. Int. Conf. Commun., Inf. Syst. Comput. Eng. (CISCE)*, May 2021, pp. 394–399.
[95] C.-S. Chen, Y.-J. Chiu, C.-T. Lee, and J.-M. Lin, "Calculation of weighted geometric dilution of precision," *J. Appl. Math.*, vol. 2013, Oct. 2013, Art. no. 953048.
[96] C. Fuchs and F. Moll, "Ground station network optimization for space-to-ground optical communication links," *IEEE/OSA J. Opt. Commun. Netw.*, vol. 7, no. 12, pp. 1148–1159, Dec. 2015.
[97] *Specific Attenuation Model for Rain for Use in Prediction Methods*, document P.2040-2 (09/2021), ITU Recommendation, International Telecommunication Union, United Nations, 2021.
[98] T. P. Yunck, W. I. Bertiger, S. C. Wu, Y. E. Bar-Sever, E. J. Christensen, B. J. Haines, S. M. Lichten, R. J. Muellerschoen, Y. Vigue, and P. Willis, "First assessment of GPS-based reduced dynamic orbit determination on TOPEX/Poseidon," *Geophys. Res. Lett.*, vol. 21, no. 7, pp. 541–544, Apr. 1994.
[99] A. Hauschild and O. Montenbruck, "Precise real-time navigation of LEO satellites using GNSS broadcast ephemerides," *Navigation*, vol. 68, no. 2, pp. 419–432, 2021.
[100] D. Arnold, O. Montenbruck, S. Hackel, and K. Sośnica, "Satellite laser ranging to low Earth orbiters: Orbit and network validation," *J. Geodesy*, vol. 93, no. 11, pp. 2315–2334, Nov. 2019.
[101] F. Wang, X. Gong, J. Sang, and X. Zhang, "A novel method for precise onboard real-time orbit determination with a standalone GPS receiver," *Sensors*, vol. 15, no. 12, pp. 30403–30418, Dec. 2015.
[102] Y. Zhao, F. Yu, and N. Xu, "PPP augmentation and real-time precise orbit determination for LEO satellites," in *Proc. 36th Chin. Control Conf. (CCC)*, Jul. 2017, pp. 5937–5941.
[103] Q. Kong, J. Guo, Y. Sun, C. Zhao, and C. Chen, "Centimeter-level precise orbit determination for the HY-2A satellite using DORIS and SLR tracking data," *Acta Geophys.*, vol. 65, pp. 1–12, Jan. 2017.
[104] D. Gu, B. Ju, J. Liu, and J. Tu, "Enhanced GPS-based GRACE baseline determination by using a new strategy for ambiguity resolution and relative phase center variation corrections," *Acta Astronautica*, vol. 138, pp. 176–184, Sep. 2017.
[105] Z. Qile, L. Jingnan, and G. Maorong, "High precision orbit determination of CHAMP satellite," *Geo-Spatial Inf. Sci.*, vol. 9, no. 3, pp. 180–186, Jan. 2006.
[106] Y. T. Yoon, M. Eineder, N. Yague-Martinez, and O. Montenbruck, "TerraSAR-X precise trajectory estimation and quality assessment," *IEEE Trans. Geosci. Remote Sens.*, vol. 47, no. 6, pp. 1859–1868, Jun. 2009.
[107] Y.-R. Kim, E. Park, D. Kucharski, H.-C. Lim, and B. Kim, "The challenge of precise orbit determination for STSAT-2C using extremely sparse SLR data," *Adv. Space Res.*, vol. 57, no. 5, pp. 1159–1176, Mar. 2016.
[108] P. Steigenberger, O. Montenbruck, and U. Hessels, "Performance evaluation of the early CNAV navigation message," *Navigation*, vol. 62, no. 3, pp. 219–228, Sep. 2015.
[109] O. Montenbruck, P. Steigenberger, and A. Hauschild, "Broadcast versus precise ephemerides: A multi-GNSS perspective," *GPS Solutions*, vol. 19, no. 2, pp. 321–333, 2015.
[110] L. Meng, J. Chen, J. Wang, and Y. Zhang, "Broadcast ephemerides for LEO augmentation satellites based on nonsingular elements," *GPS Solutions*, vol. 25, no. 4, p. 129, Oct. 2021.
[111] X. Xie, T. Geng, Q. Zhao, X. Liu, Q. Zhang, and J. Liu, "Design and validation of broadcast ephemeris for low Earth orbit satellites," *GPS Solutions*, vol. 22, no. 2, p. 54, Apr. 2018.
[112] X. Guo, L. Wang, W. Fu, Y. Suo, R. Chen, and H. Sun, "An optimal design of the broadcast ephemeris for LEO navigation augmentation systems," *Geo-Spatial Inf. Sci.*, vol. 25, no. 1, pp. 34–46, 2022.
[113] J. Yuan, S. Zhou, X. Hu, L. Yang, J. Cao, K. Li, and M. Liao, "Impact of attitude model, phase wind-up and phase center variation on precise orbit and clock offset determination of GRACE-FO and centispace-1," *Remote Sens.*, vol. 13, no. 13, p. 2636, Jul. 2021.
[114] K. Davies, Ed., *Ionospheric Radio*. London, U.K.: P. Peregrinus on Behalf of the Institution of Electrical Engineers, 1990.
[115] E. V. Appleton, "Wireless studies of the ionosphere," *Inst. Elect. Eng. Proc. Wireless Inst.*, vol. 7, no. 21, pp. 257–265, Sep. 1932.
[116] D. R. Hartree, "The propagation of electromagnetic waves in a refracting medium in a magnetic field," *Math. Proc. Cambridge Phil. Soc.*, vol. 27, no. 1, pp. 143–162, Jan. 1931.
[117] L. Marini-Pereira, L. F. D. Lourenço, J. Sousasantos, A. O. Moraes, and S. Pullen, "Regional ionospheric delay mapping for low-latitude environments," *Radio Sci.*, vol. 55, no. 12, pp. 1–12, Dec. 2020.
[118] J. Klobuchar, "Ionospheric time-delay algorithm for single-frequency GPS users," *IEEE Trans. Aerosp. Electron. Syst.*, vol. AES-23, no. 3, pp. 325–331, May 1987.
[119] B. Nava, P. Coïsson, and S. Radicella, "A new version of the NeQuick ionosphere electron density model," *J. Atmos. Sol.-Terr. Phys.*, vol. 70, no. 15, pp. 1856–1862, Dec. 2008.
[120] Y. Yuan, N. Wang, Z. Li, and X. Huo, "The BeiDou global broadcast ionospheric delay correction model (BDGIM) and its preliminary performance evaluation results," *Navigation*, vol. 66, no. 1, pp. 55–69, Jan. 2019.
[121] M. Hernàndez-Pajares, J. M. Juan, J. Sanz, R. Orus, A. Garcia-Rigo, J. Feltens, A. Komjathy, S. C. Schaer, and A. Krankowski, "The IGS VTEC maps: A reliable source of ionospheric information since 1998," *J. Geodesy*, vol. 83, no. 3, pp. 263–275, Mar. 2009.
[122] F. dos Santos Prol, P. de Oliveira Camargo, J. F. G. Monico, and M. T. de Assis Honorato Muella, "Assessment of a TEC calibration procedure by single-frequency PPP," *GPS Solutions*, vol. 22, p. 35, Apr. 2018.
[123] F. S. Prol, M. M. Hoque, and A. A. Ferreira, "Plasmasphere and topside ionosphere reconstruction using METOP satellite data during geomagnetic storms," *J. Space Weather Space Climate*, vol. 11, p. 5, Jan. 2021.
[124] Z. G. Elmas, M. Aquino, H. A. Marques, and J. F. G. Monico, "Higher order ionospheric effects in gnss positioning in the European region," *Ann. Geophys.*, vol. 29, pp. 1383–1399, Jan. 2011.
[125] A. W. Wernik, J. A. Secan, and E. J. Fremouw, "Ionospheric irregularities and scintillation," *Adv. Space Res.*, vol. 31, no. 4, pp. 971–981, 2003.
[126] N. Linty, A. Minetto, F. Dovis, and L. Spogli, "Effects of phase scintillation on the GNSS positioning error during the September 2017 storm at Svalbard," *Space Weather*, vol. 16, no. 9, pp. 1317–1329, 2018.
[127] E. J. Fremouw, R. L. Leadabrand, R. C. Livingston, M. D. Cousins, C. L. Rino, B. C. Fair, and R. A. Long, "Early results from the DNA wideband satellite experiment-complex-signal scintillation," *Radio Sci.*, vol. 13, no. 1, pp. 167–187, Jan. 1978.
[128] A. O. Moraes, E. Costa, M. A. Abdu, F. S. Rodrigues, E. R. de Paula, K. Oliveira, and W. J. A. Perrella, "The variability of low-latitude ionospheric amplitude and phase scintillation detected by a triple-frequency GPS receiver," *Radio Sci.*, vol. 52, no. 4, pp. 439–460, Apr. 2017.
[129] B. Li, H. Ge, M. Ge, L. Nie, Y. Shen, and H. Schuh, "LEO enhanced global navigation satellite system (LeGNSS) for real-time precise positioning services," *Adv. Space Res.*, vol. 63, no. 1, pp. 73–93, Jan. 2019.
[130] H. Ge, B. Li, L. Nie, M. Ge, and H. Schuh, "LEO constellation optimization for LEO enhanced global navigation satellite system (LeGNSS)," *Adv. Space Res.*, vol. 66, no. 3, pp. 520–532, Aug. 2020.
[131] *ITU Recommendation P.2040: Effects of Building Materials and Structures on Radiowave Propagation Above About 100 MHz*, document P.2040-2 (09/2021), ITU Recommendation, International Telecommunication Union, United Nations, 2021.
[132] Z. Bodnaar, Z. Herczku, J. Bearces, I. Papp, F. Som, B. G. Molnaar, and I. Frigyes, "A detailed experimental study of the LEO satellite to indoor channel characteristics," *Int. J. Wireless Inf. Netw.*, vol. 6, no. 2, pp. 79–91, 1999.
[133] A. Tkac and V. Wieser, "Channel estimation using measurement of channel impulse response," in *Proc. ELEKTRO*, May 2014, pp. 113–117.
[134] S. Lien, F. Choy, and M. Cherniakov, "Outdoor-to-indoor propagation modelling for LEO satellite communication systems," in *Proc. IEEE IEEE Region Annu. Conf. Speech Image Technol. Comput. Telecommun. (TENCON)*, vol. 1, Dec. 1997, pp. 105–108.
[135] T. Jost, W. Wang, U.-C. Fiebig, and F. Pérez-Fontán, "A wideband satellite-to-indoor channel model for navigation applications," *IEEE Trans. Antennas Propag.*, vol. 62, no. 10, pp. 5307–5320, Oct. 2014.
[136] T. Jost, W. Wang, A. Dammann, U.-C. Fiebig, M. Walter, and F. Schubert, "Satellite-to-indoor broadband channel measurements at 1.51 GHz and 5.2 GHz," in *Proc. 3rd Eur. Conf. Antennas Propag.*, Mar. 2009, pp. 2236–2240.
[137] H. Koivo and M. Elmusrati, *Systems Engineering in Wireless Communications*. Hoboken, NJ, USA: Wiley, 2009.
[138] M. Nakagami, "The *m*-distribution—A general formula of intensity distribution of rapid fading," in *Statistical Methods in Radio Wave Propagation*, W. Hoffman, Ed. New York, NY, USA: Pergamon, 1960, pp. 3–36.
[139] G. Gutt, D. Lawrence, S. Cobb, and M. O'Connor, "Recent PNT improvements and test results based on low Earth orbit satellites," in *Proc. Int. Tech. Meeting Inst. Navigat.*, Reston, VA, USA, Feb. 2018, pp. 570–577.
[140] T. G. R. Reid, B. Chan, A. Goel, K. Gunning, B. Manning, J. Martin, A. Neish, A. Perkins, and P. Tarantino, "Satellite navigation for the age of autonomy," in *Proc. IEEE/ION Position, Location Navigat. Symp. (PLANS)*, Apr. 2020, pp. 342–352.

[141] Y. T. J. Morton, F. Diggelen, J. J. Spilker, B. W. Parkinson, S. Lo, and G. Gao, Eds., *Position, Navigation, and Timing Technologies in the 21st Century*, vol. 1. Hoboken, NJ, USA: Wiley, 2020.
[142] L. Wang, R. Chen, D. Li, G. Zhang, X. Shen, B. Yu, C. Wu, S. Xie, P. Zhang, M. Li, and Y. Pan, "Initial assessment of the LEO based navigation signal augmentation system from luojia-1A satellite," *Sensors*, vol. 18, no. 11, p. 3919, Nov. 2018.
[143] F. Farhangian and R. Landry, "Multi-constellation software-defined receiver for Doppler positioning with LEO satellites," *Sensors*, vol. 20, no. 20, p. 5866, Oct. 2020.
[144] J. Khalife, M. Neinavaie, and Z. Z. Kassas, "The first carrier phase tracking and positioning results with starlink LEO satellite signals," *IEEE Trans. Aerosp. Electron. Syst.*, vol. 58, no. 2, pp. 1487–1491, Apr. 2022.
[145] J. J. Khalife and Z. M. Kassas, "Receiver design for Doppler positioning with LEO satellites," in *Proc. IEEE Int. Conf. Acoust., Speech Signal Process. (ICASSP)*, May 2019, pp. 5506–5510.
[146] M. L. Psiaki, "Navigation using carrier Doppler shift from a LEO constellation: TRANSIT on steroids," *Navigation*, vol. 68, no. 3, pp. 621–641, Sep. 2021.
[147] P. A. Iannucci and T. E. Humphreys, "Economical fused LEO GNSS," in *Proc. IEEE/ION Position, Location Navigat. Symp. (PLANS)*, Apr. 2020, pp. 426–443.
[148] Z. Tan, H. Qin, L. Cong, and C. Zhao, "Positioning using IRIDIUM satellite signals of opportunity in weak signal environment," *Electronics*, vol. 9, no. 1, p. 37, Dec. 2019.
[149] L. Cheng, Y. Dai, W. Guo, and J. Zheng, "Structure and performance analysis of signal acquisition and Doppler tracking in LEO augmented GNSS receiver," *Sensors*, vol. 21, no. 2, p. 525, Jan. 2021.
[150] S. Thompson, S. Martin, and D. Bevly, "Single differenced Doppler positioning with low Earth orbit signals of opportunity and angle of arrival estimation," in *Proc. Int. Tech. Meeting Inst. Navigat.*, Feb. 2021, pp. 497–509.
[151] Z. M. Kassas, J. J. Khalife, and J. J. Morales, "New-age satellite-based navigation–STAN: Simultaneous tracking and navigation with LEO satellite signals," *Inside GNSS Mag.*, vol. 14, no. 4, pp. 56–65, 2019.
[152] R. Santerre, L. Pan, C. Cai, and J. Zhu, "Single point positioning using GPS, GLONASS and BeiDou satellites," *Positioning*, vol. 5, no. 4, pp. 107–114, 2014.
[153] K. Su, S. Jin, and M. Hoque, "Evaluation of ionospheric delay effects on multi-GNSS positioning performance," *Remote Sens.*, vol. 11, no. 2, p. 171, Jan. 2019.
[154] J. Geng, Q. Wen, Q. Zhang, G. Li, and K. Zhang, "GNSS observable-specific phase biases for all-frequency PPP ambiguity resolution," *J. Geodesy*, vol. 96, no. 2, p. 11, Feb. 2022.
[155] M. Bakuła, "Network code DGPS positioning and reliable estimation of position accuracy," *Surv. Rev.*, vol. 42, no. 315, pp. 82–91, Jan. 2010.
[156] D. Alves, L. Dalbelo, J. Monico, and M. Shimabukuro, "First Brazilian real time network DGPS through the internet: Development, application and availability analyses," *J. Geodetic Sci.*, vol. 2, no. 1, pp. 1–7, Jan. 2012.
[157] D. B. M. Alves and J. F. G. Monico, "GPS/VRS positioning using atmospheric modeling," *GPS Solutions*, vol. 15, no. 3, pp. 253–261, Jul. 2011.
[158] L. García-Asenjo, S. Baselga, C. Atkins, and P. Garrigues, "Development of a submillimetric GNSS-based distance meter for length metrology," *Sensors*, vol. 21, no. 4, p. 1145, Feb. 2021.
[159] F. Zhu, T. Ba, Y. Zhang, X. Gao, and J. Wang, "Terminal location method with NLOS exclusion based on unsupervised learning in 5G-LEO satellite communication systems," *Int. J. Satell. Commun. Netw.*, vol. 38, no. 5, pp. 425–436, 2020. [Online]. Available: https://onlinelibrary.wiley.com/doi/pdf/10.1002/sat.1346
[160] J. Yan, C. C. J. M. Tiberius, G. J. M. Janssen, P. J. G. Teunissen, and G. Bellusci, "Review of range-based positioning algorithms," *IEEE Aerosp. Electron. Syst. Mag.*, vol. 28, no. 8, pp. 2–27, Aug. 2013.
[161] Y. T. Chan and K. C. Ho, "A simple and efficient estimator for hyperbolic location," *IEEE Trans. Signal Process.*, vol. 42, no. 8, pp. 1905–1915, Aug. 1994.
[162] G. Shen, R. Zetik, and R. S. Thoma, "Performance comparison of TOA and TDOA based location estimation algorithms in LOS environment," in *Proc. 5th Workshop Positioning, Navigat. Commun.*, Mar. 2008, pp. 71–78.
[163] J. Yan, C. C. J. M. Tiberius, P. J. G. Teunissen, G. Bellusci, and G. J. M. Janssen, "A framework for low complexity least-squares localization with high accuracy," *IEEE Trans. Signal Process.*, vol. 58, no. 9, pp. 4836–4847, Sep. 2010.
[164] R. E. Kalman, "A new approach to linear filtering and prediction problems," *J. Basic Eng.*, vol. 82, no.1, pp. 35–45, May 1960.
[165] R. Faragher, "Understanding the basis of the Kalman filter via a simple and intuitive derivation [lecture notes]," *IEEE Signal Process. Mag.*, vol. 29, no. 5, pp. 128–132, Sep. 2012.
[166] Y. Bar-Shalom, "Recursive tracking algorithms: From the Kalman filter to intelligent trackers for cluttered environment," in *Proc. IEEE Int. Conf. Control Appl. (ICCON)*, Apr. 1989, pp. 675–680.
[167] J. Hartikainen, A. Solin, and S. Särkkä, *Optimal Filtering With Kalman Filters and Smoothers—A Manual for MATLAB Toolbox EKF/UKF*. Espoo, Finland: Aalto Univ., 2011.
[168] Y. Bar-Shalom, X. R. Li, and T. Kirubarajan, *Estimation With Applications to Tracking and Navigation*. Hoboken, NJ, USA: Wiley, 2001.
[169] S. J. Julier and J. K. Uhlmann, "Unscented filtering and nonlinear estimation," *Proc. IEEE*, vol. 92, no. 3, pp. 401–422, Mar. 2004.
[170] F. Gustafsson, F. Gunnarsson, N. Bergman, U. Forssell, J. Jansson, R. Karlsson, and P.-J. Nordlund, "Particle filters for positioning, navigation, and tracking," *IEEE Trans. Signal Process.*, vol. 50, no. 2, pp. 425–437, Feb. 2002.
[171] J. Elfring, E. Torta, and R. van de Molengraft, "Particle filters: A hands-on tutorial," *Sensors*, vol. 21, no. 2, p. 438, Jan. 2021.
[172] V. Indelman, S. Williams, M. Kaess, and F. Dellaert, "Information fusion in navigation systems via factor graph based incremental smoothing," *Robot. Auto. Syst.*, vol. 61, no. 8, pp. 721–738, Aug. 2013.
[173] T. Pfeifer and P. Protzel, "Expectation-maximization for adaptive mixture models in graph optimization," in *Proc. Int. Conf. Robot. Autom. (ICRA)*, May 2019, pp. 3151–3157.
[174] J. Kennedy and R. Eberhart, "Particle swarm optimization," in *Proc. Int. Conf. Neural Netw. (ICNN)*, vol. 4, Nov./Dec. 1995, pp. 1942–1948.
[175] H. Wu, J. Liu, Z. Dong, and Y. Liu, "A hybrid mobile node localization algorithm based on adaptive MCB-PSO approach in wireless sensor networks," *Wireless Commun. Mobile Comput.*, vol. 2020, pp. 1–17, Jun. 2020, Art. no. e3845407.
[176] M. Neinavaie, J. Khalife, and Z. M. Kassas, "Acquisition, Doppler tracking, and positioning with starlink LEO satellites: First results," *IEEE Trans. Aerosp. Electron. Syst.*, vol. 58, no. 3, pp. 2606–2610, Jun. 2022.
[177] F. Farhangian, H. Benzerrouk, and R. Landry, "Opportunistic in-flight INS alignment using LEO satellites and a rotatory IMU platform," *Aerospace*, vol. 8, no. 10, p. 280, Sep. 2021.
[178] M. Elsanhoury, J. Koljonen, P. Välisuo, M. Elmusrati, and H. Kuusniemi, "Survey on recent advances in integrated GNSSs towards seamless navigation using multi-sensor fusion technology," in *Proc. 34th Int. Tech. Meeting Satell. Division Inst. Navigat. (ION GNSS+)*, Sep. 2021, pp. 2754–2765.
[179] M. Vemula, M. F. Bugallo, and P. M. Djuric, "Performance comparison of Gaussian-based filters using information measures," *IEEE Signal Process. Lett.*, vol. 14, no. 12, pp. 1020–1023, Dec. 2007.
[180] Z. Luan, Z. Li, and Y. Li, "Research on carrier tracking algorithm of low earth orbit satellite based on particle filter," *Proc. SPIE*, vol. 11373, pp. 839–846, Jan. 2020.
[181] R. Awadhiya, "Particle filter based track before detect method for space surveillance radars," in *Proc. IEEE Radar Conf. (RadarConf)*, Mar. 2022, pp. 1–6.
[182] W. Wen, T. Pfeifer, X. Bai, and L. T. Hsu, "Factor graph optimization for GNSS/INS integration: A comparison with the extended Kalman filter," *J. Inst. Navigat.*, vol. 68, no. 2, pp. 315–331, 2020.
[183] N. Sunderhauf and P. Protzel, "Towards robust graphical models for GNSS-based localization in urban environments," in *Proc. Int. Multi-Conf. Syst., Sygnals Devices*, Mar. 2012, pp. 1–6.
[184] V. Indelman, S. Williams, M. Kaess, and F. Dellaert, "Factor graph based incremental smoothing in inertial navigation systems," in *Proc. 15th Int. Conf. Inf. Fusion*, Jul. 2012, pp. 2154–2161.
[185] R. Eberhart and J. Kennedy, "A new optimizer using particle swarm theory," in *Proc. 6th Int. Symp. Micro Mach. Hum. Sci. (MHS)*, 1995, pp. 39–43.
[186] D. Zhao, C. Cai, and L. Li, "A binary discrete particle swarm optimization satellite selection algorithm with a queen informant for multi-GNSS continuous positioning," *Adv. Space Res.*, vol. 68, no. 9, pp. 3521–3530, Nov. 2021.
[187] E. Wang, C. Jia, G. Tong, P. Qu, X. Lan, and T. Pang, "Fault detection and isolation in GPS receiver autonomous integrity monitoring based on chaos particle swarm optimization-particle filter algorithm," *Adv. Space Res.*, vol. 61, no. 5, pp. 1260–1272, Mar. 2018.

[188] X. Guo, N. Ansari, F. Hu, Y. Shao, N. R. Elikplim, and L. Li, "A survey on fusion-based indoor positioning," *IEEE Commun. Surveys Tuts.*, vol. 22, no. 1, pp. 566–594, 1st Quart., 2020.
[189] P. Srinivas and A. Kumar, "Overview of architecture for GPS-INS integration," in *Proc. Recent Develop. Control, Autom. Power Eng. (RDCAPE)*, Oct. 2017, pp. 433–438.
[190] P. A. Iannucci and T. E. Humphreys, "Fused low-earth-orbit GNSS," *IEEE Trans. Aerosp. Electron. Syst.*, Jun. 6, 2022, doi: 10.1109/TAES.2022.3180000.
[191] Z. Kassas, J. Morales, and J. Khalife, "New-age satellite-based navigation STAN: Simultaneous tracking and navigation with leo satellite signals," *Inside GNSS*, vol. 14, no. 4, 2019.
[192] L. You, K.-X. Li, J. Wang, X. Gao, X.-G. Xia, and B. Ottersten, "Massive MIMO transmission for LEO satellite communications," *IEEE J. Sel. Areas Commun.*, vol. 38, no. 8, pp. 1851–1865, Aug. 2020.
[193] Y. Zhang, Y. Wu, A. Liu, X. Xia, T. Pan, and X. Liu, "Deep learning-based channel prediction for LEO satellite massive MIMO communication system," *IEEE Wireless Commun. Lett.*, vol. 10, no. 8, pp. 1835–1839, Aug. 2021.
[194] *Systems Tool Kit (STK) by AGI*, Analytical Graphics, (AGI), Exton, PA, USA, 2022.
[195] S. P. Hughes, "General mission analysis tool (GMAT)," NASA, Washington, DC, USA, Tech. Rep., 2016.
[196] D. J. Conway and S. P. Hughes, "The general mission analysis tool (GMAT): Current features and adding custom functionality," in *Proc. Int. Conf. Astrodyn. Tools Techn. (ICATT)*, 2010, pp. 1–8.
[197] J. Galán-Vioque, R. Vázquez, E. Carrizosa, C. Vera, F. Perea, and F. Martín, "Towards a visual tool for swath acquisition planning in multiple-mission EoSs," in *Proc. IWPSS Workshop*, 2011, pp. 1–8.
[198] P. Truchly and J. Cervienka, "Simple visualization tool for analysis of satellite orbits and constellations," in *Proc. Int. Conf. Emerg. eLearning Technol. Appl. (ICETA)*, Nov. 2016, pp. 359–364, doi: 10.1109/ICETA.2016.7802101.
[199] *SaVoir Multi-Satellite Swath Planner*, Taitus Software, Rome, Italy, 2022.
[200] S. Jaeckel, L. Raschkowski, K. Börner, and L. Thiele, "QuaDRiGa: A 3-D multi-cell channel model with time evolution for enabling virtual field trials," *IEEE Trans. Antennas Propag.*, vol. 62, no. 6, pp. 3242–3256, Jun. 2014.
[201] S. Jaeckel, L. Raschkowski, K. Börner, and L. Thiele, "QuaDRiGa: A 3-D multi-cell channel model with time evolution for enabling virtual field trials," *IEEE Trans. Antennas Propag.*, vol. 62, no. 6, pp. 3242–3256, 2014, doi: 10.1109/TAP.2014.2310220.
[202] S. Jaeckel, L. Raschkowski, and L. Thieley, "A 5G-NR satellite extension for the QuaDRiGa channel model," in *Proc. Joint Eur. Conf. Netw. Commun. 6G Summit (EuCNC/6G Summit)*, Jun. 2022, pp. 142–147.
[203] X. Ren, J. Zhang, J. Chen, and X. Zhang, "Global ionospheric modeling using multi-GNSS and upcoming LEO constellations: Two methods and comparison," *IEEE Trans. Geosci. Remote Sens.*, vol. 60, pp. 1–15, 2022.
[204] S. Xiong, F. Ma, X. Ren, J. Chen, and X. Zhang, "LEO constellation-augmented multi-GNSS for 3D water vapor tomography," *Remote Sens.*, vol. 13, no. 16, p. 3056, Aug. 2021.
[205] A. Ojala, "Business models and opportunity creation: How IT entrepreneurs create and develop business models under uncertainty," *Inf. Syst. J.*, vol. 26, no. 5, pp. 451–476, Sep. 2016.
[206] M. Vidmar, A. Rosiello, and O. Golra, "Resilience of new space firms in the United Kingdom during the early stages of COVID-19 crisis: The case for strategic agility," *New Space*, vol. 8, no. 4, pp. 172–178, Dec. 2020.

F. S. PROL received the Ph.D. degree in cartographic sciences from São Paulo State University (UNESP), Brazil, with a focus on geodetic remote sensing and geodetic positioning, in 2019. He has been working at the Finnish Geospatial Research Institute (FGI), since 2021. His research interests include ionospheric modeling, GNSS positioning, and data assimilation.

R. MORALES FERRE received the B.Sc. degree in telecommunication systems engineering and the M.Sc. degree in telecommunication engineering from the Universitat Autonoma de Barcelona (UAB), in 2016 and 2018, respectively. He is currently pursuing the double Ph.D. degree with Tampere University (TAU) and UAB. He worked as a Research Assistant with the Signal Processing for Communications & Navigation (SPCOMNAV) Group, UAB, until 2018. In 2018, he received a TAU rector's grant, which partially finances his Ph.D. studies. He is also involved as a Ph.D. Researcher in EU and Academy of Finland funded projects. His current research interests include GNSS security and integrity, signal processing with applications to communications and navigation, and positioning by means of GNSS and alternative positioning methods, such as cellular networks or LEO constellations and array signal processing.

Z. SALEEM (Graduate Student Member, IEEE) received the bachelor's degree in mechatronics engineering from NUST, Pakistan, and the double master's degree in space science and technology with space robotics as a major from Erasmus Mundus Program, Aalto University, Finland, and the Luleå University of Technology, Sweden. She is currently pursuing the Ph.D. degree with the School of Electrical Engineering, Aalto University, working on distributed space systems. Her area of expertises are guidance, navigation, and control with experience across aerospace and robotics.

P. VÄLISUO received the M.Sc. (Tech.) degree in computer science from the Tampere University of Technology, Finland, in 1996, and the D.Sc. (Tech.) degree in automation technology from the University of Vaasa, Finland, in 2011. He has worked for ten year's in telecommunications industry before establishing a research career with the University of Vaasa, where he is currently working as an Associate Professor (a tenure Track), sustainable automation with the School of Technology and Innovation Management. He has authored and coauthored 27 peer-reviewed and more than ten other scientific publications. His research interests include ML, the IoT, positioning methods, and other technologies relevant to industrial automation.

C. PINELL received the B.Sc. degree in physics from the University of Bonn, Germany, in 2018, and the double M.Sc. (Tech.) degree in space science and technology from Aalto University, Finland, and the Luleå University of Technology, Sweden, in 2021. She is currently conducting research at the Finnish Geospatial Research Institute (FGI). Her research interests include space science and instrumentation, resilient PNT, and receiver technologies.

E. S. LOHAN (Senior Member, IEEE) received the M.Sc. degree in electrical engineering from the Polytechnics University of Bucharest, Romania, in 1997, the D.E.A. degree (French equivalent of master) in econometrics with the Ecole Polytechnique, Paris, France, in 1998, and the Ph.D. degree in telecommunications from the Tampere University of Technology, in 2003. She is currently a Professor at Tampere University (TAU), Finland, where she is also a Professor at the Electrical Engineering Unit, and the Coordinator of the MSCA EU "A-WEAR" network. Her current research interests include GNSS, LEO-PNT, wireless location techniques, wearable computing, and privacy-aware positioning solutions.

M. ELSANHOURY (Graduate Student Member, IEEE) received the B.Sc. degree in telecommunications engineering from Alexandria University, Egypt, in 2013, and the M.Sc. (Tech.) degree in telecommunications engineering from the University of Vaasa, Finland, in 2018, where he is currently pursuing the Ph.D. degree in computer science. From 2017 to 2018, he worked as a Research Assistant at the University of Vaasa. In Spring 2017, he worked as an Autonomous Robots Lecturer at the Swedish NOVIA University of Applied Sciences. Recently in 2021, he conducted a two-month research visit to American University in Cairo (AUC) to exchange research ideas around UWB and LEO positioning. His current research interests include ubiquitous indoor positioning systems, ultra-wideband (UWB) indoor localization, low-earth orbit (LEO) satellites for positioning, multi-sensor fusion technologies, Kalman filters, and machine learning algorithms.

M. ELMUSRATI (Senior Member, IEEE) received the B.Sc. and M.Sc. degrees (Hons.) in electrical and electronic engineering from the University of Benghazi, Libya, in 1991 and 1995, respectively, and the Licentiate of Science degree (Hons.) in technology and the Doctor of Science (D.Sc.) degree in automation and control engineering (technology) from Aalto University, Finland, in 2002 and 2004, respectively. Currently, he is a Full Professor in communication, automation, and digitalization at the School of Technology and Innovations—University of Vaasa, Finland. He has published about 150 papers, books, and book chapters. His research interests include wireless communications, artificial intelligence, machine learning, biotechnology, big data analysis, stochastic systems, and game theory. He is an Active Member in different scientific societies, such as a member of the Society of Industrial and Applied Mathematics (SIAM) and a member of Finnish Automation Society.

S. ISLAM received the M.Sc. (Tech.) degree (Hons.) from Tampere University (TAU), Finland, in 2019, where he is currently pursuing the Ph.D. degree. He is also a Research Scientist at the Finnish Geospatial Research Institute (FGI-NLS). He is a member of the Resilient Position, Navigation, and Timing Group, Department of Navigation and Positioning, FGI-NLS. He is involved in research projects on GNSS receiver development and validation, timing algorithms, maritime navigation, LEO-PNT, GNSS jamming, and spoofing. He is one of the key people in the implementation of the GPS L5 solution in FGI-GSRx. His research interests include GNSS signal processing, resilient software-defined radio (SDR) development, satellite-based augmentation systems (SBAS), and 5G new radio (NR).

K. ÇELIKBILEK received the B.Sc. (Tech.) degree in electrical and electronics engineering from Bilkent University, in 2018, and the M.Sc. (Tech.) degree in robotics and artificial intelligence from Tampere University, in 2020, where he is currently pursuing the Ph.D. degree in computing and electrical engineering. His research interests include deep learning, reinforcement learning, multi-objective optimization, satellite communication, and robotics.

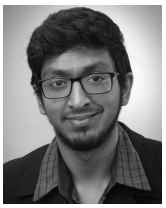

K. SELVAN received the B.S. degree in electronics and communication engineering from Anna University, India, in 2012, and the M.S. degree in communications and systems engineering from the University of Vaasa, Finland, in 2020, where he is currently pursuing the Ph.D. degree in automation technology. From 2018 to 2020, he was a Research Assistant at Digital Economy Research Platform, University of Vaasa, where he is currently a Project Researcher at Digital Economy Research Platform. His research interests include GNSS technologies, LEO-PNT, satellite-data analysis, machine learning, satellite communication, and smart devices.

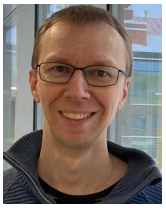

J. YLIAHO received the M.Sc. (Tech.) degree in electrical engineering from the Tampere University of Technology, in 2008. He is currently pursuing the Ph.D. degree with the University of Vaasa, Finland. He is also a Laboratory Engineer with the University of Vaasa. His current research interests include space-based signals of opportunity for PNT and related projects at Digital Economy Research Platform, University of Vaasa.

K. RUTLEDGE received the B.A. and B.S. degrees in environmental and biological sciences from Lenoir-Rhyne University, Hickory, NC, USA, in 1978, and the M.Sc. degree in marine systems ecology and biostatistics from Old Dominion University, Norfolk, VA, USA, in 1982. He is currently the Research Program Manager of Space and the Project Manager of Digital Economy Research Platform, University of Vaasa, Vaasa, Finland. He has been working with atmospheric acoustics, satellite instrument algorithm development and surface observation systems as a NASA Contractor in the USA. He worked as a Site Scientist for several surface observation networks, including NASA's AERONET, MPLNET, and the WMO's baseline surface radiation network. This work included instrumenting an offshore observation platform to support components of NASA's Clouds and the Earth's Radiant Energy System program (in the ocean environment). Recently, he has developed or help develop projects associated with wind, ice and space in Scandinavia.

A. OJALA received the Ph.D. degree in economics from the University of Jyväskylä. He is currently a Professor in international business with the School of Marketing and Communication, University of Vaasa, Finland. He is also an Adjunct Professor in software business at Tampere University, Finland. His articles have been published in *Information Systems Journal*, *Journal of World Business*, *Journal of Systems and Software*, *Journal of Cleaner Production*, IEEE SOFTWARE, *IT Professional*, and among other academic venues. His research interests include global digital business, international entrepreneurship, and business models.

L. FERRANTI received the B.Sc. (Tech.) and M.Sc. (Tech.) degrees in electrical engineering from the Tampere University of Technology, in 2018 and 2019, respectively. He is currently pursuing the Ph.D. degree in computer science with the University of Vaasa. His current research interests include computational mathematics and its applications to engineering domains and applying algebraic geometry methods to positioning problems.

J. PRAKS (Member, IEEE) received the B.Sc. degree in physics from the University of Tartu, Estonia, in 1996, and the D.Sc. (Tech.) degree in space technology and remote sensing from Aalto University, Espoo, Finland, in 2012. He is currently an Assistant Professor in electrical engineering with the Department of Electronics and Nanoengineering, School of Electrical Engineering, Aalto University. He has been working with microwave remote sensing, scattering modeling, microwave radiometry, hyperspectral imaging and with advanced SAR techniques, such as polarimetry, interferometry, polarimetric interferometry, and tomography. One of most visited topic in his research is remote sensing of boreal forest. Since 2009, he has been taken interest in emerging nanosatellite technology. He led project which produced two first Finnish satellites. He has been involved also in spinning off several companies in the field of satellite remote sensing. His research team is a member or the Finnish Centre of Excellence in Research of Sustainable Space and he is a Principal Investigator of several small satellite missions. He is an Active Member of scientific community, a member of Finnish National Committee of COSPAR, the Chairperson of Finnish National Committee of URSI, and the chair and the co-chair of many national and international conferences.

M. Z. H. BHUIYAN is currently a Research Professor at the Department of Navigation and Positioning, Finnish Geospatial Research Institute. He has been also working as a Technical Expert of the EU Agency for the Space Program (EUSPA) in H2020 project reviewing and proposal evaluation. His research interests include multi-GNSS receiver development, PNT robustness and resilience, and seamless positioning. He is actively involved in teaching GNSS related courses in Finnish universities and other training schools.

S. KAASALAINEN is currently a Professor and the Head of the Department of Navigation and Positioning, FGI of the National Land Survey. Her research interests include resilient PNT, situational awareness, and optical sensors. She also has research experience in Lidar remote sensing, sensor development, and astronomy.

H. KUUSNIEMI (Member, IEEE) received the M.Sc. degree (Hons.) in information technology and the Ph.D. degree from the Tampere University of Technology, Finland, in 2002 and 2005, respectively. She is currently the Director of the Digital Economy Research Platform and a Professor in computer science at the University of Vaasa, a Research Professor at the Finnish Geospatial Research Institute, National Land Survey of Finland, and an Adjunct Professor in satellite navigation at Tampere University and Aalto University, Finland. She has more than 20 year's of experience in research and development of positioning technologies and has held many significant positions of trust and expertise in the global scientific navigation community. Part of her Ph.D. research was conducted at the Department of Geomatics Engineering, University of Calgary, Canada. She was a member of the Research Council for Natural Sciences and Engineering at the Academy of Finland (2019–2021) and a Visiting Scholar at the GPS Laboratory, Stanford University, in 2017. Her research interests include global navigation satellite systems, especially reliability, estimation and data fusion, mobile precision positioning with applications, indoor localization, and opportunities of PNT in new space.

Publication P9

A Novel Beam-Based Positioning Paradigm Via Opportunistic Signal of Future Massive MIMO LEO Satellite Constellations

Mahmoud Elsanhoury, Janne Koljonen, Mohammed Elmusrati, and Heidi Kuusniemi

***Abstract*—Mega constellations of low Earth orbit satellites are expected to communicate through massive multiple-input multiple-output (mMIMO) channels. This paper proposes a novel positioning paradigm that utilizes the mMIMO communication as signal-of-opportunity. By identifying beams during the signaling phase of transmission and by having open access satellite information datasets, the receiver will become capable of solving its position geometrically. We investigated the method's accuracy in simulation, and the first results encourage to study the topic further. In the subsequent research, theoretical studies, more accurate simulation models, and more sophisticated positioning algorithms are to be studied in order to enrich this new localization methodology.**

***Index Terms*—LEO satellites, massive MIMO, beamforming, 5G signals, positioning and navigation, GNSS.**

I. Introduction

Earth's sky is getting occupied by numerous low Earth orbit (LEO) satellites forming mega constellations that are expected to be several tens of thousands in population by 2030. Major corporations are to provide broadband internet connection to uncovered or signal-denied areas, and navigation applications for civilian and military uses. Signal-of-opportunity (SoO or SOP) aspects of LEO satellite links have emerged as a new research track that aims at exploiting the huge overhead satellite-Earth communications traffic to provide navigational and positioning solutions [1].

In this article, a new positioning paradigm is proposed. The method relies on identifying massive multiple-input multiple-output (mMIMO) beams amid the signaling phase of communication. The identifiers of the detected beams are used to solve position of the user terminal (UT) based on the satellite-to-Earth geometry of the beams. The proposed positioning method is not dependent on accurate received signal strength (RSS) values, nor time corrections, or other measurements. Therefore, it has potential to provide world-wide robust and low-cost positioning services. Originally, the proposed method was briefly discussed in our previous article [2]. To our best knowledge, the method is novel and it has not been discussed earlier in the scientific literature.

This introduction continues by briefly reviewing the state-of-the-art (SOTA) of the LEO–mMIMO and LEO–PNT (positioning-navigation-timing) topics, so that it is possible to understand and evaluate the proposed positioning method and its value in academic and practical terms. Section II discusses the foundations of the proposed beam-based positioning concept. Section III introduces the simulation setup. Section IV presents the results. In section V, we discuss the results as for the prospects to implement the method. Finally, Section VI concludes the article and suggests future research topics to support the development of the proposed paradigm.

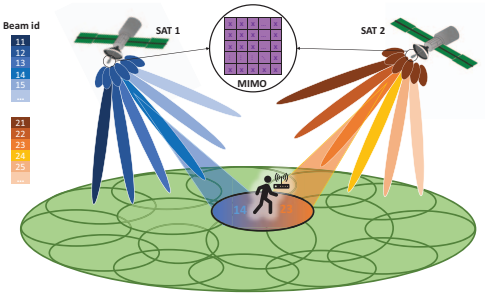

Fig. 1. Schematic of satellite beam footprints illuminating the area of a receiver. The beam colors indicate unique identifiers, which in this illustration is composed of two digits: the first is the satellite ID, and the second is the beam ID.

A. MIMO beamforming for positioning

LEO satellites are to be equipped with mMIMO antennas, which consist of over 1,000 elements. As discussed in Ferre et al. [2], mMIMO shall bring significant advantages to both LEO satellite link and SoO-based positioning. As for the satellite-Earth communications link, mMIMO provides higher channel capacity, increases the number of user terminals (UTs), and improves the uplink and downlink (UL/DL) throughput.

As illustrated in Figure 1, the satellite beamforming loops are to be given unique identifiers (IDs) in the DL super-frames. Hence, the UT can identify a beam once it is located within its footprint. The beam IDs can be used as tokens to fetch the satellite ephemeris (timestamped position in orbit), satellite orientation, and mMIMO beam pattern information either from the satellite vehicle (SV) itself or from external databases available for positioning applications. Subsequently, the beams footprint (coverage area) on Earth can be estimated. An algorithm how to solve the position of the UT is introduction in Section II-D in more detail.

Achieving LEO–PNT can have two approaches, either via SoO or by designing new LEO constellations with a dedicated PNT capability. Our proposed LEO beam-based positioning

979-8-3503-8078-1/24/$31.00 ©2024 IEEE

concept is compatible with both approaches provided that the SVs are equipped with mMIMO beamforming elements and having open access to particular satellite information datasets. Unlike GNSSs, the proposed method can cope with poor geometrical dilution of precision (GDOP) situations where all satellites are nearly overhead.

B. SOTA in LEO–mMIMO

Palacios et al. [3], [4] addressed a hybrid beamforming approach to simulate mMIMO beamforming codebook for LEO DL communications.The hypothetical mega LEO constellation consisted of 4,399 SVs placed at 1,300 km in altitude and having 83 orbital planes inclined at 53°. The SVs had 60×72 mMIMO antenna elements. The beam footprints were rendered as a circular-shaped lattice, where each beam spanned a radius of 66 km.

You et al. [5] proposed a fusion-based mMIMO algorithm to efficiently schedule UT groups. Statistical channel state information (sCSI) was used to maximize the UL/DL throughput. Another adoption of CSI to implement LEO–mMIMO via deep learning is presented in [6].

Caus et al. [7] proposed a resource sharing beamforming scheme for LEO satellites placed at 600 km in altitude. The channel capacity was increased by generating narrow directed beamforming loops towards the UTs with 24×24 antenna elements. Hence, a minimal inter-user interference was achieved also both the signal-to-noise ratio (SNR) and signal-interference-to-noise ratio (SINR) were enhanced by repeating the beamformer patterns.

C. SOTA in LEO–PNT

Global navigation satellite systems (GNSS) are an established method for outdoor precision positioning. However, GNSSs operate at high altitudes ranging from approximately 20000 to 24000 km above the Earth's surface, which results in higher signal degradation and path losses, compared to LEO satellites. Therefore, GNSS positioning performs poorly in indoor venues. Because GNSS signals are highly prone to alteration, GNSS positioning is vulnerable to jamming and spoofing [8].

Because LEO satellites orbit at much lower altitudes (below 2000 km) than the GNSS satellites, their signals have less degradation and better penetration capabilities. Those merits led to the emergence of a recent research track that discusses the adoption of LEO satellites in PNT applications [1].

Sabbagh et al. [9] tested a hypothesis based on pseudoranges obtained from carrier phase observables via a single LEO–UT system. Extended Kalman filter (EKF) algorithm was used to filter the two-line element (TLE) data of both satellites, which led to bestowing a localization ability on the receiver's end.

Khalife et al. [10] devised a receiver design and a framework for LEO–PNT using Doppler frequency measurements of two existing LEO satellites. The proposed framework was able to localize the UT with a root-mean-square error of 360 meters during 60 seconds of convergence time.

For a comprehensive literature review dedicated for the LEO–PNT topic see Prol et al. [1].

II. Proposed positioning method

This section states the foundations upon which the future implementation of the positioning concept and the research simulation environments will be built. The main objective in this article is to investigate the suitability of mMIMO beamforming loops to be regarded as *geographical pointers*. The identification of those pointers, in addition to the geographical definition of the beam footprints on Earth's surface, grant UTs the ability to estimate their positions. The estimation of the UT position is then an optimization task with respect to the vector of the detected beam IDs.

The proposed positioning method requires two types of information datasets: 1) The static datasets provide fixed information about LEO satellites, e.g., the onboard antenna attributes, the beam patterns, and the beam identifiers. 2) The dynamic datasets deliver time-stamped information on the location of the satellites and their beams. The detail level of the information on the beams and their *footprints* on Earth can vary. The minimum requirement is to know the locations of the beam centers (on Earth) for a given time instant. In this study, we assume additionally that the beam radii are known.

When a UT receives signaling (or handshake) from LEO satellites, it decodes the received frames to find the beam identifiers. With the IDs the UT retrieves the satellite datasets. Based on the geo-location information of the detected beam footprints, the UT is able to multilaterate its own position. More accurate position estimates can be achieved by excluding the undetected footprints as explained in Section II-D.

A. Satellite-to-Earth geometry

The transmitted beam pattern and the geometry between the satellite and the UT infer – to large extent – the projected shapes of beam footprints. As the positioning concept relies heavily on the information on the beam footprints, essential geometrical and geographical parameters are illustrated in Figure 2. They are, e.g., the elevation angle, the satellite orbital inclination plane, the beams patterns, and the attributes of the beam conic shape.

The orbital inclination angle and the altitude (see Figure 2a) are the primary attributes to determine the coverage area of a satellite. When it comes to satellite constellations, the objective is to optimize both aspects so that satellites maintain a constant occupation over the regions of interest (ROI). The transmitted pattern and the elevation angle control the shape of the projected beam footprints (see Figure 2b). The instantaneous orientation of the satellite and Earth's topology also affects the footprint shape, among other factors. Beamforming parameters and attributes of antennas determine the transmitted pattern, which also can be designed in the form of fixed or steerable circular footprints [3], [4].

The locations of beam footprints can be predicted once the transmitted patterns and the instantaneous values of the satellite-to-Earth geometry are known. However, the computational complexity increases depending on the required detail level of the footprints and the number of variables involved.

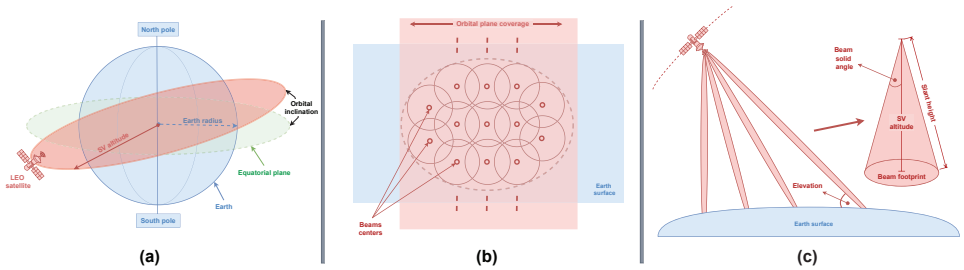

Fig. 2. Illustration depicting the satellite-to-Earth geometry. (a) Satellite orbital plane inclination with respect to Earth's axis. (b) The satellite mesh coverage in terms of interlocked mMIMO beam footprints. (c) mMIMO beam geometry is approximated to a conic shape when received on Earth's surface.

Therefore, assuming fixed pattern and identical beam shapes would ease the computational burden.

B. Transmitter technical aspects

Each LEO satellite within a constellation should be equipped with a minimum of 1024 or more antenna elements in order to achieve a mMIMO status. However, in the conducted preliminary simulations we limited the maximum number of beams per a satellite to 8×8 for computational simplicity. Optimally, the transmitted pattern would be fine-tuned to serve the UTs in the desired ROI. This can be achieved by designing the mMIMO codebook and the RF link budget to produce reliable RSS and SNR levels on Earth's surface.

In practice, the skies will bear numerous corporate-owned satellite constellations, implying that interoperability is not guaranteed. Fortunately, the proposed concept can perform without interoperability as long as the satellite information datasets are kept open access. Corporations can withhold the payload dataframes (e.g. broadband data) from non-subscribers, while allowing any receiver to access the beam IDs during the signaling phase. This will lead to the establishment of positioning systems that utilize most of LEO constellations.

As for the coverage aspects, an optimum LEO satellite constellation to cover the planet was proposed in [1]: a minimum of 400 SVs placed at 600 km in altitude, and a minimum of 10 orbital planes inclined at no less than 72°. The same altitude was prescribed in [7] to design a beam pattern that has interlocked footprints. The number of major beams produced by a single SV will depend on the adopted scheme of beamforming. According to the reviewed literature [3], [11], [12], the hybrid beamforming scheme is promising in providing control over the beam pattern.

C. Channel model and user segment

Realistic channel models for mMIMO hybrid beamforming communications were presented in [3], [4], [10], [11], whereas in this paper, we assume a perfect wireless channel (i.e. has the highest signal to noise ratio) for simplicity. In addition, the user segment (receiver end) is assumed to be non-MIMO receiver (non-directed receiver pattern) throughout the article.

The most important issue for UT is the ability to read signals from many LEO satellites and fetch the beam IDs simultaneously. Then, UTs can either use embedded resources or cloud services for positioning. If embedded resources suffice, positioning would be totally passive i.e. UTs would not consume energy for uplink. Each incident satellite beam will have its own broadcast channel with specific allocated frequency and code. Thus, when the signal is decoded by the receiver, the beam ID will be retrieved solely and not necessarily decoding the whole signal frame. That will save much processing time and battery power for handheld UT devices. However, in some cases when the processing power in some UT devices is restrained, the decode-able number of beams could be limited to certain thresholds in order to avoid overruns (i.e. decode n beams only).

D. Positioning algorithm

The positioning algorithm is based on: 1) the information on the boundaries of the individual beam footprints, 2) operations of mathematical set, and 3) computation of the center of gravity (CoG) of an area.

The beam footprints form sets of coordinates. The intersection of the sets that represent the detected beams yields the region, inside which the receiver must be located (i.e., the 100% confidence set), simply because the receiver has been able to detect those beams in the first place. By subtracting sets that represent the adjacent undetected beams from the intersection set, the size of the confidence set can be decreased. Figure 3 demonstrates the basic principles of the positioning algorithm and its two variants: **ALG. A** utilizes only the detected beams, while **ALG. B** uses subtraction to enhance the position estimates.

A reasonable presumption is that the receiver can be at any point inside the confidence set with an equal probability. In that case, the CoG of the confidence set can be regarded as an optimal point estimate since it minimizes the sum of the squared errors.

ALG. A and ALG. B can be defined mathematically as in Equations 1 and 2, where the integration is done over the entire areas of intersection $I_A(t)$ and $I_B(t)$, respectively.

$$\mathrm{CoG_A} = \mathrm{ALG.A}(t) = \frac{\iint_{\mathbf{x}\in I_A(t)} \mathbf{x}\mathrm{d}\mathbf{x}}{\iint_{\mathbf{x}\in I_A(t)} \mathrm{d}\mathbf{x}} \quad (1)$$

$$\mathrm{CoG_B} = \mathrm{ALG.B}(t) = \frac{\iint_{\mathbf{x}\in I_B(t)} \mathbf{x}\mathrm{d}\mathbf{x}}{\iint_{\mathbf{x}\in I_B(t)} \mathrm{d}\mathbf{x}} \quad (2)$$

III. Simulation experiments

The objectives of the simulation are: 1) to estimate the distribution of the positioning error for an arbitrary time instant, 2) to find the relationship between the error metrics and the number of detected beams, and 3) to compare ALGs. A and B in terms of positioning accuracy.

The experiments are based on the following simplifying assumptions: 1) All satellite beam patterns and 2) all beam footprints are mutually identical, 3) the beam footprints are circular in shape, and 4) the beams are detected either with 100% or 0% probabilities in cases of being illuminated or not illuminated by the beam, respectively.

Each satellite has a regular 8×8 grid of beams. Note that increasing the number of beams above this limit does not incur any effect on the positioning error distributions in this simulation settings. The beam radius is 50 km, and the beam centers are separated by 75 km (i.e. 1.5x the radius).

Figure 3 shows a sample of the combined beam pattern with 10 satellites and how the UT position is solved in case of ALGs. A and B. Note how the beam boundaries divide the region into numerous sub-regions (i.e. confidence sets) that vary in size and shape. The positioning error distribution differs depending on the location of sub-region, time instant, and the varying shape of the combined beam pattern. Hence, a large sample size is needed in order to obtain a reliable estimate of the error distribution.

The fundamental steps to obtain a single positioning error sample are as follows: 1) Obtain a randomized combined beam pattern. 2a) Compare the 2D Euclidean distances between the UT and the beam centers (d) to the beam radius (R). If $d \leq R$, mark the respective beam as detected. 2b) In case of ALG. B, mark beams, for which $R < d < 3R$, as undetected, 3) Describe the borders of the detected beams as coordinate vectors (we used 1,000 points per beam). 4a) Find the intersection area (i.e. confidence set) of the detected beams. 4b) In case of ALG. B, apply the following steps i–ii iteratively for all undetected beams: i) Compute the minimum distance d_{min} from the current confidence set to the beam center. ii) If $d_{min} < R$, update the current confidence set by subtracting the undetected beam. 5) Compute the CoG of the confidence set. We implemented the simulation in MATLAB using the `polyshape` library to describe the borders of the beam footprints.

Finally, the estimation of the positioning error distribution is done by obtaining $N = 500$ samples of positioning errors while randomly rotating the satellites and shifting their positions above the UT. The actual number of detected beams is recorded for each sample, because it varies from sample to sample. From the error distribution, three evaluation metrics are computed: maximum error, root-mean-square error (RMSE), and mean absolute error (MAE).

IV. Simulation results

The results show that ALG. B enables error reduction by over 40% in comparison to ALG. A, when the number of detected beams (D) grows larger than 15. With fewer beams, the advantage diminishes but is still significant. With 50 satellites overhead the UT, D = 73.4, on average. The error metrics for ALG. B were: max. error = 2.5 km, RMSE = 0.52 km, and MAE = 0.41 km. These values can be compared to the beam radius (50 km). Hence, the average error around 1% and the maximum error below 5% of the beam radius demonstrate the potential of the proposed positioning concept and algorithm. With 100 satellites, the respective figures are: D = 146.9, max. error = 1.90 km, RMSE = 0.273, and MAE = 0.22 km.

The results also show that the RMSE and MAE are proportional to $1/D$, for both ALGs. A and B. Conceptually, the explanation is as follows: having other factors fixed, $1/D$ is proportional to the average distance between the adjacent beams, which correlates to the average distance from UT to the nearest beam boundaries, which in turn correlates to the positioning error. As a conclusion, positioning errors can be effectively decreased further by increasing the number of satellites and illuminating beams .

V. Discussion

The novel beam-based positioning method is simple in design and uses LEO signals that have higher SNR/RSS in comparison to GNSS signals. These issues bring immediate benefits. The UTs are not required to perform high-precision measurements, which should, together with the SoO nature, yield lower costs. The new paradigm is potentially more tolerant against path losses and interference than GNSS due to the privileged wireless communications attributes e.g. proximity to Earth, higher SNR, etc. In addition, it performs well in poor GDOP profiles unlike GNSSs that require perfect GDOP to function properly.

Positioning accuracy is naturally a key metric in any location-based technology. According to the simulation results position errors around MAE = 0.7 km are to be reached with the following settings: 44,000 mMIMO LEO satellites, each having a 8×8 beam pattern with an average radius of 50 km per beam. As Earth area is 510,100,000 km^2, each point on Earth would be illuminated by 30 satellites and 43.4 beams, on average. In practice, corporate-owned constellations are optimised to serve the most-populated regions, hence, positioning errors around 100–200 m could be achieved in some areas. At the same time, reliable positioning services with reasonable accuracy can be provided world wide, even in the GNSS-denied regions.

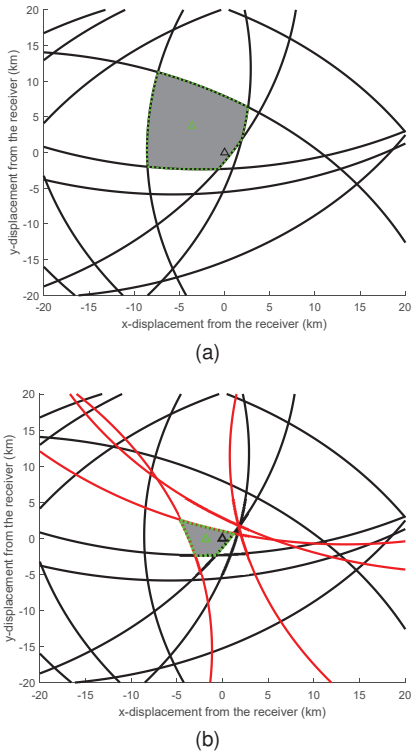

Fig. 3. (a) The resultant footprint pattern of the detected beams with 10 satellites overhead the receiver (black triangle) located at (0, 0). The confidence set (gray area in this case is $I_A(t)$) and the estimated UT position (green triangle) obtained by **ALG. A**. (b) Confidence set $I_B(t)$ and estimated UT position by **ALG. B**. Red arcs are those undetected beams that were subtracted from the confidence set.

With more sophisticated positioning algorithms that utilize RSS measurements and sequential position estimates, and with hybrid positioning methods, even better accuracy levels are possible. Already the first simulation results assert that the beam-based positioning method is worthy of further pursuit.

Provided that the essential satellite information datasets are kept as open access, the positioning systems can utilize most of the LEO constellations for the best possible accuracy. Positioning services could be run, for instance, by private operators that collect the satellite information datasets and provide positioning solutions as cloud services or as stand-alone software. We estimate that the concept could be harnessed to commercial use in less than 10 years from now.

VI. Conclusion

LEO satellites are to be equipped with mMIMO in the near future. Introducing the beam-based positioning paradigm marks the advent of a new research topic that is concerned with exploiting 5G beamforming features of LEO satellites' communications to infer UT position in Earth's coordinates. Considering the passive SoO nature of the proposed method, the simulation results (MAE = 0.22 km with 100 satellites) are considered very promising, as positioning is possible even in poor GDOP situations. Furthermore, the proposed method does not require high-accuracy measurements at the receiver side, thus reducing costs and sensitivity to interference. As future work, more sophisticated simulation environment will be built to model mMIMO beamforming components, the communication channel, and various sources of noise and interference. In addition, LEO satellite orbits and realistic mega constellations will be modelled. Additional positioning algorithms will be developed and analyzed for enhanced accuracy and reliability.

VII. Acknowledgement

This work was supported by the Jane and Aatos Erkko Foundation and by the Teknologiateollisuus 100-year Foundation (INCUBATE project). The proposed ideas within this article are currently under the process of IPR patenting (Finnish patent application number: 20235545).

References

[1] F. S. Prol, R. M. Ferre, Z. Saleem, P. Välisuo, C. Pinell, E. S. Lohan, M. Elsanhoury, M. Elmusrati, S. Islam, K. Çelikbilek, K. Selvan, J. Yliaho, K. Rutledge, A. Ojala, L. Ferranti, J. Praks, M. Z. H. Bhuiyan, S. Kaasalainen, and H. Kuusniemi, "Position, Navigation, and Timing (PNT) Through Low Earth Orbit (LEO) Satellites: A Survey on Current Status, Challenges, and Opportunities," *IEEE Access*, vol. 10, pp. 83 971–84 002, 2022.

[2] R. M. Ferre, E. S. Lohan, H. Kuusniemi, J. Praks, S. Kaasalainen, C. Pinell, and M. Elsanhoury, "Is LEO-Based Positioning with Mega-Constellations the Answer for Future Equal Access Localization?" *IEEE Communications Magazine*, vol. 60, no. 6, pp. 40–46, 2022.

[3] J. Palacios, N. Gonzalez-Prelcic, C. Mosquera, T. Shimizu, and C.-H. Wang, "A Hybrid Beamforming Design for Massive MIMO LEO Satellite Communications," *Front. Space Technol*, vol. 27, 2021.

[4] J. Palacios, N. González-Prelcic, C. Mosquera, and T. Shimizu, "A Dynamic Codebook Design for Analog Beamforming in MIMO LEO Satellite Communications," *arXiv:2111.08655*, 2021.

[5] L. You, K.-X. Li, J. Wang, X. Gao, X.-G. Xia, and B. Ottersten, "Massive MIMO Transmission for LEO Satellite Communications," *IEEE Journal on Selected Areas in Communications*, vol. 38, no. 8, pp. 1851–1865, 2020.

[6] Y. Zhang, Y. Wu, A. Liu, X. Xia, T. Pan, and X. Liu, "Deep Learning-Based Channel Prediction for LEO Satellite Massive MIMO Communication System," *IEEE Wireless Communications Letters*, vol. 10, no. 8, pp. 1835–1839, 2021.

[7] M. Caus, A. Perez-Neira, and E. Mendez, "Smart Beamforming for Direct LEO Satellite Access of Future IoT," *Sensors*, vol. 21, no. 14, 2021.

[8] M. Orabi, J. Khalife, and Z. M. Kassas, "Opportunistic Navigation with Doppler Measurements from Iridium Next and Orbcomm LEO Satellites," in *2021 IEEE Aerospace Conference (50100)*, 2021, pp. 1–9.

[9] R. Sabbagh and Z. M. Kassas, "Observability Analysis of Receiver Localization via Pseudorange Measurements From a Single LEO Satellite," *IEEE Control Systems Letters*, vol. 7, pp. 571–576, 2023.

[10] J. J. Khalife and Z. M. Kassas, "Receiver Design for Doppler Positioning with LEO Satellites," in *ICASSP 2019 - 2019 IEEE Int. Conf. on Acoustics, Speech and Signal Processing*, 2019, pp. 5506–5510.

[11] A. F. Molisch, V. V. Ratnam, S. Han, Z. Li, S. L. H. Nguyen, L. Li, and K. Haneda, "Hybrid Beamforming for Massive MIMO: A Survey," *IEEE Communications Magazine*, vol. 55, no. 9, pp. 134–141, 2017.

[12] O. E. Ayach, S. Rajagopal, S. Abu-Surra, Z. Pi, and R. W. Heath, "Spatially Sparse Precoding in Millimeter Wave MIMO Systems," *IEEE Transactions on Wireless Communications*, vol. 13, no. 3, pp. 1499–1513, 2014.

Publication P10

IEEE TRANSACTIONS ON GEOSCIENCE AND REMOTE SENSING , VOL. XX, NO. XX, NOVEMBER 2024 1

MIMO Beam ID-Based Positioning Method With Low Earth Orbit Satellite Mega-Constellations

Mahmoud Elsanhoury, *Graduate Student Member, IEEE,* Janne Koljonen, Fabricio S. Prol, Mohammed S. Elmusrati, *Senior Member, IEEE*, and Heidi Kuusniemi, *Member, IEEE*

***Abstract*—Satellite-based positioning methods provided the world with reliable location information coverage that led to various navigation applications and services. While existing global navigation satellite systems (GNSS) offer high-precision outdoor positioning, they are prone to interception, spoofing and jamming, which are concerning vulnerabilities. The menace of GNSS jamming is escalating, posing substantial risks to various critical systems reliant on precise positioning, such as in-flight navigation and health systems. New positioning methods dependent on low Earth orbit (LEO) satellites have been trending recently under positioning, navigation, and timing (PNT) research topic. As LEO satellites are orbiting at lower altitudes and are massive in numbers, they are foreseen to have less signal degradation, higher service availability and improved signal reception on Earth. In this article, we propose a new satellite-based positioning method using the multiple-input multiple-output (MIMO) beamforming antennas installed onboard upcoming LEO satellite constellations. Our proposed positioning technology serves as both a supplement and a potential substitute in the event of severe intentional jamming, offering enhanced resilience and reliability. The core idea is to use the received satellite beam identifiers as geographical pointers that enable the users to infer their position on Earth using LEO satellite ephemeris and the beam pattern shape with no complicated timing required. The article evaluates this novel beam-based positioning method through simulation setups, realistic LEO constellation data, and probabilistic positioning models. Also, discussing its feasibility and potential implications, emphasizing on the dynamics of space-based positioning and navigation. The obtained results are encouraging and satisfactory, especially with real scenarios that have been achieved by fusing the LEO satellite positioning data with the inertial motion data of a moving vehicle, resulting in a mean absolute error of 9.15 meters, and a 95-percentile error of 19.07 meters.**

***Index Terms*—MIMO, LEO-PNT, beamforming, LEO satellites, navigation, positioning, GNSS.**

I. Introduction

THE skies of Earth are experiencing growing congestion with low Earth orbit (LEO) satellites, forming mega constellations expected to exceed tens of thousands within a few years. Significant cost reductions in LEO satellite design and rocket launches have prompted major corporations to plan the deployment of thousands of satellites into orbit to establish a sustainable presence in the skies and new space economy to emerge. These LEO satellites are primarily developed to extend broadband internet coverage to rural and signal-deprived areas while also supporting navigation applications for general purposes. A new avenue of research, known as the Signal-of-Opportunity (SoO or SOP), seeks to leverage the substantial satellite-Earth communications traffic from LEO satellites to provide navigational and positioning solutions.

Existing global navigation satellite systems (GNSSs), such as GPS, GLONASS, Beidou and Galileo, are widely utilized for high-precision outdoor positioning across various consumer segments. They offer global coverage in the most densely populated regions on Earth and exhibit excellent availability and interoperability, often collaborating with space-based augmentation systems (SBAS) like WAAS and EGNOS. However, GNSS systems operate at much higher altitudes, ranging from medium Earth orbits (MEO) to geostationary Earth orbits (GEO), situated between 2,000 to 35,000 kilometers above sea level. These elevated altitudes result in greater signal degradation due to various factors, first and foremost suffering from atmospheric effects. Additionally, the high altitudes limit the signal ability to penetrate indoor spaces due to substantial shadowing effects caused by obstructions. Furthermore, GNSS signals are susceptible to manipulation, making them vulnerable to jamming and spoofing. Therefore, exploring new satellite-based methods to address these GNSS limitations through SoO positioning is a worthwhile endeavor.

In recent years, there has been a noticeable surge in interest surrounding LEO-PNT methods [1], largely driven by the number of LEO satellites in our skies. The primary objective of LEO-PNT is to complement existing GNSS by providing enhanced navigation capabilities in challenging scenarios. This includes autonomous navigation, urban environments, areas with dense forest canopies, and even indoor spaces. Most LEO-PNT techniques typically rely on the deployment of dedicated LEO satellite missions, which can be a costly and resource-intensive endeavor. However, a notable exception to this paradigm is the emergence of multiple-input multiple-output (MIMO) beam ID-based methods. These innovative techniques enable opportunistic utilization of data transmitted by any available LEO satellite, enhancing, not only the sustainability of space-based exploitation, but also fostering a more adaptive approach to LEO-PNT.

In this article, we evaluate and discuss the feasibility of the novel beam-based positioning method from multiple-input multiple-output (MIMO) antennas onboard LEO satellites. The innovation lies within utilizing the beamforming loops incident

Manuscript received xx October 2023; revised xx January 2024; accepted xx February 2024. Date of publication xx August 2024; date of current version xx September 2024.

Mahmoud Elsanhoury, Janne Koljonen, Mohammed S. Elmusrati, and Heidi Kuusniemi are with the School of Technology and Innovations, University of Vaasa, FI-65200, Finland (e-mail: firstname.surname@uwasa.fi). Fabricio S. Prol and Heidi Kuusniemi are with the Finnish Geospatial Research Institute (FGI) of the National Land Survey, Finland (e-mail: firstname.lastname@nls.fi).

from MIMO-equipped LEO satellites to provide location information for user terminals (UT) on Earth. The beam identifiers (ID) and the satellite-to-Earth geometry information are used to obtain estimates of the user position amid the signaling phase of the wireless communications link between the space segment and the user segment. The proposed positioning method does not rely on received signal strength (RSS), time offsets, or other measurements, and it is expected to be quite insensitive to many signals degradation and alterations. Therefore, it has potential to provide a world-wide robust and low-cost positioning services that are sufficiently accurate for many purposes. However, the concept does not yet provide timing information.

The rest of paper is organized as follows: in Section II, we glance over the state-of-the-art and recent trends in both LEO–PNT and massive MIMO (mMIMO) topics, in order to address our bridging idea that combines both aspects. Section III discusses the elements of the proposed beam ID-based positioning concept from technical realization perspective. Section IV shows how the concept has been implemented and evaluated in a simulation test-bed from feasibility point of view. Section V highlights the experimental setup and the generated LEO satellite constellations data. Section VI contains the rendered results (plots and numerical assessments) using definitive performance metrics and studying the asymptotic behaviour of error. In Section VII, we discuss and comment on the results as for the prospects to implement the concept in the future. Finally, Section VIII summarizes the findings and foresees future work.

II. Research foundations

In this section, we briefly introduce the basics and the advancements of the two main pillar topics of our proposed positioning method: 1) recent LEO-PNT positioning paradigms, and 2) the use of mMIMO in LEO satellites and how they can be exploited for outdoor positioning. In addition, we state the potential advantages and challenges of the proposed concept.

A. On LEO-PNT methods

Dedicated LEO-PNT systems often provide with the highest accuracy among LEO-PNT methods. They require on-board instruments dedicated to providing positioning signals from LEO satellites. Ground users are capable to retrieve GNSS-like observations (pseudoranges and carrier phases) and apply typical GNSS positioning strategies, such as precise point positioning (PPP) [2], [3]. Remarkable efforts have been made to develop dedicated LEO-PNT systems by Xona Space System [4], the European Space Agency (ESA) [5], CENTISPACE^{TM} [6], and the indoor navigation from CubeSat technology (INCUBATE) project [7].

Opportunistic methods do not involve the transmission of specific PNT messages to users. Consequently, users have no access to precise information regarding satellite orbits and timing, often relying on simplified ephemeris data such as two-line elements (TLE) [8]–[10]. The most common observation is the Doppler shift, providing similar capabilities to the Transit mission [11], which was one of the earliest operational satellite-based navigation systems. Presently, numerous studies delve into the potential of opportunistic techniques involving Doppler shifts. The overall accuracy achieved through these methods typically vary within the range of 7 meters to 1000 meters [12], depending on factors including the estimation procedure employed, the environmental conditions surrounding the receiver, and the extent of satellite constellation coverage.

The method presented in this work can be applied by both dedicated and opportunistic LEO-PNT systems. As discussed in our preliminary study [13], the satellite beamforming loops are given unique identifiers (IDs) in the DL super-frames. The beam IDs are used as tokens to fetch the satellite ephemeris (time stamped position in orbit), satellite orientation, and mMIMO beam pattern information from the satellite vehicle (SV). Subsequently, the beams' footprints (coverage area) on Earth are estimated, providing a way to perform user trilateration. This positioning method is not dependent on accurate RSS values, time corrections, or other measurements, but it requires dense satellite constellations.

B. MIMO antennas in LEO satellites

The introduction of MIMO and mMIMO antennas in LEO satellites are under deployment. Currently, only few to none of the existing satellite constellations are MIMO-capable, but it is expected that one to many of future LEO constellations are to be equipped with such technology in the following years. Numerous research efforts have been put into this topic due to the merits that it offers, including better throughput, higher capacity, and enhanced quality of service [14].

mMIMO differs from MIMO in terms of the number of onboard antenna elements. mMIMO is implemented by employing 1024 or more antenna elements that are separated by a distance equivalent to half the wavelength [14]. From an opportunistic perspective, both MIMO and mMIMO signals can be exploited to provide location information based on the beamforming loop identifiers (IDs). When the number of beams increases as in mMIMO, the positioning resolution is expected to be improved.

The congregation of beams from many satellites generates a combined beam footprint that comprises numerous intersections of beams even for a single satellite vehicle. The more satellites there are illuminating the location of the UT and the smaller the beams are in radius; the smaller the intersections are and the more accurate the positioning estimate is. In each intersection, a particular combination of beam IDs can be detected. By knowing the trajectory and the beam footprint patterns of LEO satellites the vector of beam IDs can be used as the key to extract the position estimates from the time-stamped geo-location information of the beam footprints whenever detected by the UT.

The number of major beams (loops) produced by a single satellite vehicle will depend on the adopted scheme of beamforming in the mMIMO system. Based on the reviewed literature [15]–[17], the hybrid beamforming scheme can provide a control over the beam pattern by exploiting the advantages of both analog and digital beamforming schemes. In the method, the mMIMO array is divided into sub-arrays, where each sub-array is connected to an RF chain in order to produce one

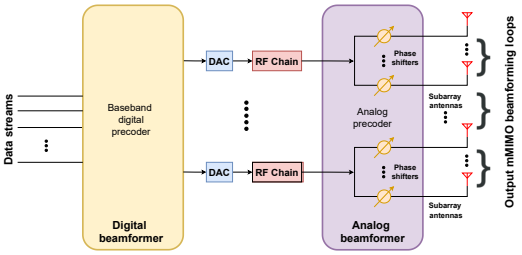

Fig. 1. Block diagram depicting the hybrid beamforming scheme of mMIMO.

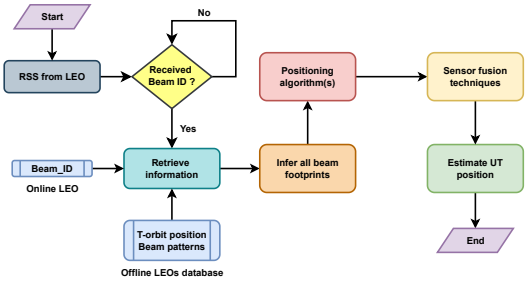

Fig. 2. Stages of the beam ID-based positioning method.

steerable main beam whose radius is also controllable. For the hybrid beamforming scheme presented in Figure 1, the number of the major beams is proportional to the number of the allocated RF chains.

C. Potential Advantages

Our novel beam ID-based positioning method provides numerous advantages to the realm of location-based services, research, and applications. Due to its simple system layout and utilization of opportunistic LEO signals, the beam ID-based method is expected to gain popularity across user segments whenever the technical base requirements are met.

The beam ID-based method offers better Signal-to-Noise Ratio (SNR) or RSS compared to signals from GNSS due to the closer proximity of LEO satellites to Earth. Moreover, it refrains UTs to use any kind of high-sensitive receivers as they will be passively receiving beam IDs (only) without the need for going through the data payloads. This SoO approach can lead to significant reductions in overall costs by diminishing the financial burden associated with sophisticated equipment as in conventional positioning systems.

Additionally, the beam ID-based approach is resilient towards signal degradation due to path losses and interference. Because the positioning estimation does not require perfect line of sight, it does not require signal reception at certain circumstances. The methodology's performance maintains its robustness even under adverse conditions, ensuring the continual availability of positioning data. Besides, the system can have good performance in scenarios characterized by unfavorable Geometric Dilution of Precision (GDOP) profiles, something that is not achievable with GNSS.

D. Challenges

Intrinsic concerns are expected to challenge the beam ID-based positioning method and impair its operation. For example, the realization of hybrid MIMO beamforming onboard LEO satellites is already complicated due to large amount of antenna elements required to be planted on small-sized LEO satellites, something that may also limit the vehicle's power budget. With optimal designs and suitable telecommunications solutions, the mMIMO link budget can be adjusted to provide the minimum acceptable level of beam coverage to the regions of interest on Earth.

Besides, LEO satellites are not owned by a single entity, rather, several tens of governments and corporations, which shall jeopardize the interoperability between LEO constellations. Hence, entities who own the mMIMO-equipped LEO satellites should follow with the prescribed technical aspects for their constellation beam footprints in order to be capable of performing positioning estimations.

Sharing accurate LEO constellation ephemeris and their fixed beam footprint patterns also remains as a major concern, because technical data sharing is not an appealing matter for most private satellite operators. However, it can be granted with the appropriate measures to be taken, also with the expected revenue streams from the corresponding customer segments who are targeted with such a positioning service. To resolve this issue, new independent vendor entities may emerge to bind all LEO constellation operators together in order to handle data sharing and manage the execution and delivery of this positioning service between the users and the operators.

III. Technical Considerations

Prior to constructing the simulation model, we aim to provide a comprehensive overview of the technical aspects of the LEO-mMIMO beam ID-based positioning method. This involves offering a detailed perspective of both the spatial and user segments. Figure 2 summarizes the entire positioning process using beam IDs from mMIMO-equipped LEO satellites.

A. Beam ID-based positioning method

As described in Section II, the proposed positioning process is based on the congregation of beams from LEO satellites resulting in inevitable geometrical intersections between all beam patterns that are being received, which leads to solving the positioning estimation problem via geometry algorithms.

For the method to be efficient and viable, the beam patterns of LEO satellites should have fixed shapes (known to the users or the positioning engine) and intersect other beams within the same pattern, like an overlapping mesh shape. Then, whenever the UT receives LEO-mMIMO satellite communications, it should be able to extract each beam's unique ID. The IDs serve as tokens to fetch more information about the transmitting satellite vehicle, LEO constellation, shape of the beam

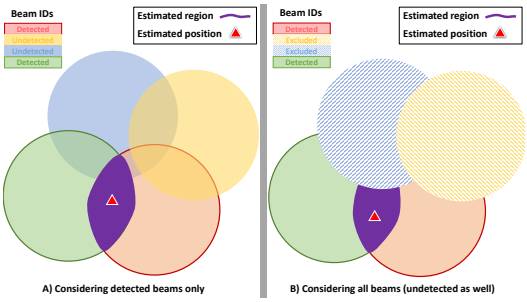

Fig. 3. Two positioning algorithm variants to utilize the information of the beam footprints: (left) **ALG. A:** The intersection of the footprints of detected beams determines the area where the receiver can be located. (right) **ALG. B:** Considering the nearby undetected beams, the bounds for the location estimation can be decreased by subtracting the footprints of the undetected beams from the intersection of ALG. A.

footprint pattern, timestamped location of the satellite vehicle, and expected beam footprint geographic trajectory on Earth's surface. Eventually, by receiving just one beam ID only from one LEO satellite, the UT can still infer information about its location on Earth with errors (kilometers) equivalent to the radius of the received beam footprint.

B. Positioning algorithms

Upon receiving a LEO satellite signal with a decoded beam ID, the UT starts to search the available open-access databases for the satellite vehicle carrying this beam, and its live location. The same procedure is done with every other beam ID received by the UT. In the end, the UT shall combine all gathered information from all the received beam IDs in order to pinpoint its position on Earth's coordinates. The chosen way of integrating the positioning information is by assuming that the UT lies at the center of gravity (CoG) of the intersection area of all the **detected beams**. This is what we call the "A" algorithm or "ALG. A".

By knowing the whole beam patterns of all received LEO satellites, the information about the absent **undetected beams** can be included in the calculations to omit their geographical footprints from the beam pattern. This leads to a smaller region of intersection than the region resulted from ALG. A and better mean accuracy. Figure 3 describes both ALG. A and ALG. B with graphical illustration.

ALGs A and B can be defined using mathematical sets and set operations, also known as morphology in image processing. Let $D(t)$ and $U(t)$ be the sets of detected and undetected beam IDs, respectively, for time instant t. Moreover, let $\mathbf{c}(i,t)$ be a function that returns the East North (E-N) coordinates of the center of the beam footprint of beam i at time instant t. Similarly, $R(i,t)$ returns the radius of the beam. Mathematical set $A_i(t)$, which includes all locations $\mathbf{x}$ (in E-N coordinates) inside the beam footprint of beam i, can be represented as in Equation 1.

$$A_i(t) = \{\mathbf{x} \mid\mid \mathbf{x} - \mathbf{c}(i,t) \mid\mid < R(i,t)\} \tag{1}$$

Now, intersection $I(t)$ of all $A_i(t)$ of the detected beams is a set of E-N coordinates, i.e., an area, where the UT must be located. The intersection is determined by Equation 2.

$$I(t) = \bigcap_{i \in D(t)} A_i(t) \tag{2}$$

If the UT was outside the intersection area, it would not detect all the beams in $D(t)$. On the other hand, the UT can be anywhere in $I(t)$, and without any additional information (e.g., signal strength or information of the undetected beams) each location $\mathbf{x}$ in $I(t)$ is equally probable. Therefore, the ideal point estimate for the position of the UT is the CoG of the intersection with uniform mass density. This is the ALG. A, as defined in Equation 3.

$$\text{ALG.A}(t) = \frac{\iint_{\mathbf{x} \in I(t)} \mathbf{x} \mathrm{d}\mathbf{x}}{\iint_{\mathbf{x} \in I(t)} \mathrm{d}\mathbf{x}} \tag{3}$$

where integration is done over the entire area of intersection.

The locations of the undetected beams are utilized to shrink the area of possible UT locations. The footprints of the undetected beams can be subtracted from intersection $I(t)$ used for Alg. A. The shrunk intersection $I_B(t)$ can be obtained by subtracting the union of the undetected beams from the intersection of the detected beams, as given in Equation 4.

$$I_B(t) = I(t) - \bigcup_{i \in U(t)} A_i(t) \tag{4}$$

Finally, the CoG of set $I_B(t)$ is the output of ALG. B, as given in Equation 5.

$$\text{ALG.B}(t) = \frac{\iint_{\mathbf{x} \in I_B(t)} \mathbf{x} \mathrm{d}\mathbf{x}}{\iint_{\mathbf{x} \in I_B(t)} \mathrm{d}\mathbf{x}} \tag{5}$$

C. Post-processing algorithms

The positioning techniques carried out by the beam ID-based positioning from LEO satellites (e.g. ALG. A, ALG. B) are not sufficiently accurate or reliable for positioning applications. Hence, post-processing algorithms are to be used for more precise positioning results.

The rough estimations carried out by ALG B, are imported to a set of algorithms to further refine the final positioning estimations. Some processing steps are done at the local level (per data source e.g. either LEO or IMU) and the global level (sensor data fusion of both LEO/IMU). This strategic approach was undertaken with the primary goal of enhancing the accuracy of positioning estimations, ensuring that the final estimates are more precise and reliable. A bank of algorithms is used to overcome this issue.

1) Dead Reckoning (DR): in cases of communication loss or data interruptions (due to sensor drifts, signal attenuation or NLOS), the dead reckoning (DR) algorithm can be employed to fill the null posterior state based on non-null prior information. DR is widely used in positioning and navigation applications even before the advent of contemporary localization systems. Equations (6) illustrate DR in mathematical notation.

$$
\begin{aligned}
D_k &= \sqrt{(p^x_{k-2} - p^x_{k-1})^2 + (p^y_{k-2} - p^y_{k-1})^2} \\
\phi_k &= \arctan2\left(\frac{p^y_{k-2} - p^y_{k-1}}{p^x_{k-2} - p^x_{k-1}}\right) \\
p^x_k &= p^x_{k-1} + D_k \cos(\phi_k) \\
p^y_k &= p^y_{k-1} + D_k \sin(\phi_k)
\end{aligned} \tag{6}
$$

where k is the time instant, p^x_k and p^y_k are the x-y positions, D_k and ϕ_k are the evaluated Euclidean distance and the heading angle, respectively.

2) Extended Kalman Filter (EKF): is a nonlinear state-space estimation technique commonly employed for 2-D and 3-D positioning estimations through conducting two steps: the state prediction step, and the state update step. EKF mathematical procedures [18] are presented in Equations (7).

$$
\begin{aligned}
m^-_k &= f(m_{k-1}, k-1) \\
P^-_k &= F_x\, P_{k-1} {F_x}^T + Q_{k-1} \\
V_k &= y_k - h(m^-_k, k) \\
S_k &= H_x\, P^-_k\, {H_x}^T + R_k \\
K_k &= P^-_k\, {H_x}^T\, S^{-1}_k \\
m_k &= m^-_k + K_k V_k \\
P_k &= P^-_k - K_k S_k K^T_k
\end{aligned} \tag{7}
$$

where $m_{\bar{k}}$ and $P_{\bar{k}}$ are the iterative predicted state mean and covariance, respectively, m_k and P_k are the posterior state estimated mean and covariance, respectively. y_k is the input measurements vector, and S_k is the measurement prediction covariance. K_k is the filter gain, $f(.)$ and $h(.)$ are the system dynamic functions of the state-space model and the measurements model, respectively. In case of LEO/IMU multi-sensor fusion, the state-space vector $\mathbf{x}_k$ comprises the predicted x-y positions, velocities, and accelerations (i.e. a 2-D Wiener dynamic model), while the measurements vector $\mathbf{y}_k$ includes the measurements from LEO satellites (ALG. B). However, the rest of motion kinematics (accelerations and heading angles) are inbound from the IMU sensor, as shown in Equations (8).

$$
\begin{aligned}
\mathbf{x_k} &= \mathbf{F_k x_k} + Q_k \\
\mathbf{y_k} &= \mathbf{H_k x_k} + R_k
\end{aligned} \tag{8}
$$

3) Rauch-Tung-Striebel (RTS) Smoother: is a Bayesian recursive filter that enhances the linearized state-space estimates by retrospectively smoothing the probability density function's maximum likelihood (mean and covariance) [18], [19]. The prior and posterior state estimates $\hat{X}_k|k-1, \hat{X}_k|k$ and their covariances $\hat{P}_k|k-1, \hat{P}_k|k$, which were obtained from the previous filtering (e.g. EKF filtering) are fed to the RTS smoother to calculate the smoothed state estimates $\hat{X}_k|n$ and covariance $\hat{P}_k|n$. The RTS smoother formulas from [18], [19] are described in Equations (9).

$$
\begin{aligned}
\hat{X}_k|_n &= \hat{X}_k|_k + C_k(\hat{X}_{k+1}|_n - \hat{X}_{k+1}|_k) \\
P_k|_n &= P_k|_k + C_k(\hat{X}_{k+1}|_n - \hat{X}_{k+1}|_k) \times C^T_k
\end{aligned} \tag{9}
$$

where $C_k = P_k|_k F^T_{k+1} P^{-1}_{k+1}|_k$, and $X_k|_k$ is the a-posterior state estimate of time instant k and $X_{k+1}|_k$ is the a priori state estimate of time instant $k+1$ which also applies to the covariance. In summary, the sequence of algorithmic realization starts with applying ALG. B on the received LEO satellite beam IDs, and whenever a loss of measurements occurs then DR is activated. Then, the output of the previous steps is fed to a state-space filtering algorithm such as: EKF, and, afterwards, an RTS smoother is used to refine the final positioning estimations.

D. Evaluation metrics

To construct a valid assessment on the LEO satellite beam ID-based positioning method, several performance metrics are used. Having the error distributions compiled for most scenarios, the following evaluation metrics are computed numerically: mean absolute error (MAE), root-mean-square error (RMSE), and the 95-percentile (p95%) positioning error. Moreover, we sketch the route comparisons in both the x-y coordinates (British national EPSG:27700) and the world's geodetic system (WGS84) of Earth coordinates, in addition to rendering a cumulative distribution function (CDF) plots for the real scenario (i.e. scenario 3). We believe that those metrics will suffice to verdict the method from both the feasibility to the operator and the beneficiary user perspectives.

IV. Simulation model

The simulation is done in Matlab (R2022b). The objective is to model beam ID-based positioning and its accuracy with realistic future mega-constellations of LEO satellites. In the simulation, both UTs and the satellites move with a temporal resolution of 1 second. The total simulation time is 1,200 seconds, i.e., 20 minutes.

The simulation model has the following characteristics, simplifications, and presumptions: i) There are several LEO constellations that are launched in sequence. Thus, it is possible to analyze how the accuracy of the positioning method evolves as new constellations with more advanced beamforming capabilities are introduced. ii) The positions of the satellites relative to the UT are calculated using a local planar coordinate system, i.e., the curvature of Earth around the UT is neglected. iii) Each beam has a circular *footprint* on Earth (more specifically, on the plane around the UT), despite varying elevation angles. iv) If the UT is inside a beam footprint, it recognizes the beam ID with a 100% probability. If the UT is outside a beam footprint, it recognizes the beam ID with a 0% probability. v) The UT can read all available beam IDs at the same time, i.e., the satellites and the beam footprints do not move while reading the beam IDs.

A. Modeling beam footprint patterns

A LEO satellite transmits several beams that form a regular beam footprint pattern on Earth. For every satellite from a satellite constellation, all beams have identical radii, R, and the centers of the adjacent beam footprints are separated by $1.5R$, i.e., the adjacent beams partially overlap. Different

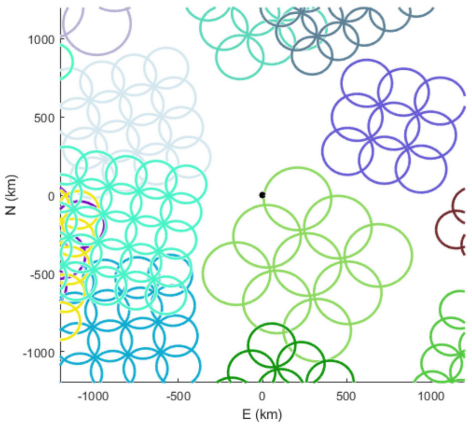

Fig. 4. Randomly selected beam footprint patterns from constellations 1-5 (see Table II for the beam pattern parameters of corresponding constellations).

constellations have different beam footprint radius. When several satellites transmit their beams at the same time, the beam footprint patterns overlap. A schematic example (with a reduced number of beams for clarity) of a combined beam footprint pattern is shown in Figure 4.

In more detail, the total beam footprint pattern is computed as follows: i) Read the orbital positions (x, y, z) - given in Earth-centered Earth-fixed (ECEF) coordinates - of the satellites for all simulation time steps from h5 files. ii) Set the origin of the local ENU coordinate system to the position of the UT at simulation time $t = 0$. Denote that position as: $(\mathrm{lat}_0, \mathrm{lon}_0, h_0)$. In our experiments $h_0 = 0$. Note that if the UT moves during a simulation run, its first position is still the origin of ENU in our setup. iii) Convert the orbital positions of the satellites to ENU coordinates, in Matlab, as follows: `[E,N,U] = ecef2enu(x,y,z,lat0,lon0,h0,spheroid)`, where `spheroid = wgs84Ellipsoid` (a Matlab constant). iv) Discard beams for which $U < 0$, because they are not located above the UT but below the EN-plane and even at the opposite side of Earth. v) Determine the Earth-projections of the satellites by setting $U = 0$ in ENU coordinates. vi) Place the beam centers of the footprint patterns symmetrically around the Earth-projection of the satellites (see a random set of beam footprint patterns in Figure 4). vii) Finally, rotate the beam footprint patterns in the EN-plane with a satellite-specific random angle $\theta \sim \mathrm{Uniform}(0, 2\pi)$. The rotation is done in homogeneous coordinates around the Earth-projection of the satellite denoted by (E_p, N_p). The new position (E_2, N_2) for beam center (E_1, N_1), is obtained by Equation 10.

$$\begin{pmatrix} E_2 \\ N_2 \\ 1 \end{pmatrix} = \mathbf{T} \begin{pmatrix} E_1 \\ N_1 \\ 1 \end{pmatrix} \tag{10}$$

where the transform matrix T is obtained as the product of translation and rotation matrices in Equation 11.

$$\begin{pmatrix} 1 & 0 & E_p \\ 0 & 1 & N_p \\ 0 & 0 & 1 \end{pmatrix} \mathbf{T} = \begin{pmatrix} \cos(\theta) & -\sin(\theta) & 0 \\ \sin(\theta) & \cos(\theta) & 0 \\ 0 & 0 & 1 \end{pmatrix} \begin{pmatrix} 1 & 0 & -E_p \\ 0 & 1 & -N_p \\ 0 & 0 & 1 \end{pmatrix}. \tag{11}$$

B. Implementation of the positioning algorithms

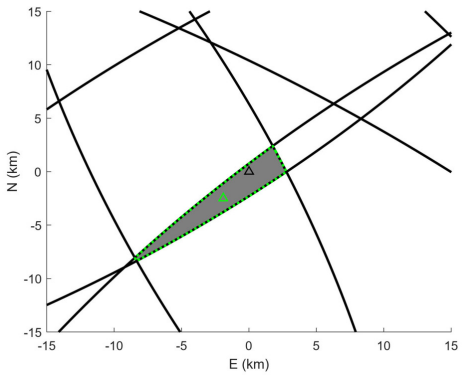

Fig. 5. An example from the simulation how the intersection of the detected beams limits the possible location of the UT (black triangle). The green triangle shows the CoG of the intersection.

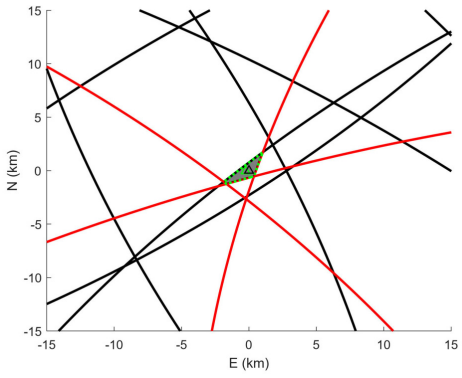

Fig. 6. The same situation as in Figure 5, but the borders of the undetected beams (red arcs) are used to further limit the possible location of the UT.

The objective of a positioning algorithm is to give an optimal position estimate for the UT in the local ENU coordinates. The proposed estimation algorithms use the following measurements: i) detected beam IDs, ii) current simulation time. In simulation, beam detection is simply solved by comparing the beam radius R_i, for beam i, to the distance from the after-rotation beam footprint center (E_i, N_i) to the UT location $(E_{\mathrm{UT}}, N_{\mathrm{UT}})$

$$\mathrm{dist}_i = \sqrt{(E_i - E_{\mathrm{UT}})^2 + (N_i - N_{\mathrm{UT}})^2}.$$

If $\mathrm{dist}_i < R_i$, beam i is detected. The comparison is done for every beam and every simulation time step. Simulation time is an integer loop index variable.

Based on these measurements the following information is retrieved: iii) all undetected beams that may intersect with the intersection of the detected beams and iv) the radii of the beam footprints. Step iii) is used to preliminary reduce the number of beams for the computation of the morphological operations that are computationally expensive. In simulation, the true UT location is known a priori; hence, it is possible to compute the distance to the UT $\mathrm{dist_i}$. In our simulation, beams, for which the distance to UT is larger than $3R_i$ are discarded.

The intersection of the beams is computed using Matlab polyshapes, which are 2-dimensional polygonal shapes that are defined by vectors of vertex points. The circular beams are thus created using samples from the border of the beam footprints. First, angles from 0 to 2π are sampled uniformly: `rad=linspace(0, 2*pi-(2*pi/samples), samples)`, where `samples=1000`. Second, the coordinates of the border, denoted by `Eb` and `Nb`, are computed. For beam i this is done by: `Eb = R(i)*cos(rad) + E(i)` and `Nb = R(i)*sin(rad) + N(i)`, where `R(i)` is the beam footprint radius and `E(i)` and `N(i)` give the beam center location. Finally, the polyshape struct of the beam footprint is created from the border coordinates as follows: `beam = polyshape(Eb, Nb)`.

The intersection (`IS`) of the beam footprints is computed directly and efficiently from the array of polyshapes representing the detected beams: `IS = intersect(beams)`. The output of ALG. A, i.e., the position estimate, is the CoG of the intersection area of the detected beams: `[CoGE,CoGN] = centroid(IS)`. The intersection of several detected beams and its CoG is demonstrated in Figure 5.

When it comes to ALG. B, undetected beams are subtracted from the intersection as explained in Section III and demonstrated in Figure 6. For computational efficiency, subtraction is done iteratively and only for those undetected beams that intersect with the current intersection (`IS`). The implementation of subtracting beam i is as follows: i) Find such a vertex of the current intersection that is the nearest to beam center i: `[vertexid,boundaryid,ind] = nearestvertex(IS,E(i),N(i))`. ii) Find the respective E-N coordinates of the nearest vertex: `Enear = IS.Vertices(vertexid,1); Nnear = IS.Vertices(vertexid,2)`. iii) Compute the Euclidian distance from the nearest vertex to the beam center. iv) If the distance is smaller than the radius of the respective undetected beam, create a new polyshape and subtract it from the current intersection to obtain a new current intersection: `IS = subtract(IS,undetectedbeam)`. v) Repeat steps i-iv until no more undetected beams are available. vi) Finally, compute the center of gravity of the residual intersection with function `centroid`.

C. Satellite mega-constellations

The satellite mega-constellations were reproduced with an in-house simulator tool, named LEO-S9 (LEO simulator with 9 modules). The LEO-S9 tool is flexible to create a variety of space segment scenarios, including diverse dynamics and instruments specific to LEO satellites. The main relevant points simulated with LEO-S9 in this work included the orbit altitude, inclination, velocity, constellation topology, and initial design. The constellation progress with time was reproduced considering the Cowell numerical integration, Earth's gravity, J_2 oblateness effect, third body attractions, solar radiation, and atmospheric drags. A walker delta topology was selected to keep a symmetric coverage.

The simulation was built by considering the present status and coming developments in LEO satellite missions. Table I provides an overview of the primary missions and associated orbit parameters that were considered in this study, and the generation of LEO satellite constellation data.

To assess the performance of the proposed method across various LEO coverage scenarios, simulations for 13 distinct case scenarios were conducted, each denoted as experimental cases 1 through 13. In the initial case, 3000 satellites were simulated, covering a diverse combination of all identified missions. Then, about $\sim$1000 additional satellites were incrementally included into the simulation for each subsequent case. Notably, experimental case 13 assumed the operation of a total of $\sim$15000 LEO satellites. Meaning that every constellation of the 13 generated scenarios is enough to cover the most populated areas of Earth. While this may seem ambitious, it is a foreseeable scenario in the forthcoming years. On the other hand, the test case scenarios are numbered 1–4, to cover three modes of motion: stationary, linear, and nonlinear motion.

TABLE I
STATUS AND ORBIT PARAMETERS OF THE CURRENT AND PLANNED LEO CONSTELLATIONS. VALUES BASED ON [20]

Mission	Altitude [km]	Inclination [°]	N. Sats.
OrbComm	740 - 875	45, 70, 72	47
Globalstar	1400	52	48
Iridium	625, 720	86	66
Telesat	1015, 1325	51, 98	1671
Kuiper	590 - 630	33, 42, 52	3236
OneWeb	1200	40, 55, 88	6372
Starlink	540 - 570	53, 70, 98	$>$ 10000

The parameters of the generated LEO satellite constellations (number of satellites, number of beams per satellite, the radii of the beams, and the spacial separation of the beams) for motion Scenarios 1–3 are given in Table II. The adjacent beams centers were separated by $1.5 \times R_{\mathrm{beam}}$ for all constellations, satellites, and beams. This separation value was set in order to impose large-sized beam intersections needed for the beam ID-based positioning method to have sufficient overlapping of beam congregations. Whereas, the increased overlapping incidents from more beams shall result in better accuracy.

Based on the illustration shown in Figure 7, the coverage area of a single LEO satellite can be evaluated from Equations (12), and (13). Then, the coverage area is divided into smaller beamforming loops according to Equation (14).

TABLE II
LEO SATELLITE MEGA CONSTELLATION PARAMETERS FOR MOTION SCENARIOS 1–3

Const.	Sats.	Beams/sat.	R_{beam}
1	3000	3×3	200 km
2	4050	3×3	150 km
3	5040	3×3	140 km
4	6048	4×4	130 km
5	7020	5×5	120 km
6	7992	6×6	110 km
7	9012	7×7	100 km
8	10002	8×8	90 km
9	11052	8×8	80 km
10	12072	8×8	70 km
11	13032	8×8	60 km
12	14004	8×8	50 km
13	15084	8×8	40 km

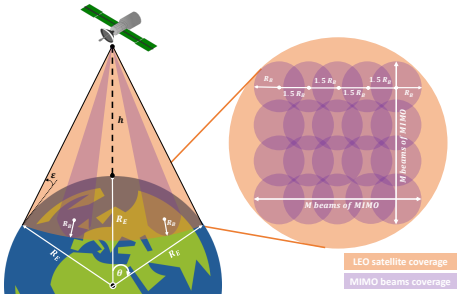

Fig. 7. Coverage area of a single LEO satellite with MIMO beams

First, the coverage geometry is approximated to the relation in Equation (12) [21].

$$cos(\theta + \epsilon) = \frac{cos(\epsilon)}{1 + \frac{h}{R_E}} \tag{12}$$

whereas θ is the central conic angle in radians measured from Earth's center, ϵ is the elevation angle of the viewing cone of the satellite, h is the altitude of the LEO satellite, and R_E is Earth's radius.

Considering higher and moderate elevation angles (e.g: $45° \leq \epsilon \leq 135°$), therefore, the coverage area A can be evaluated approximately from Equation (13). In which, the shape of the LEO satellite coverage area is approximated to be equivalent to the shape of a spherical cap [22], enclosing θ as the central angle.

$$A = 2\pi\, R_E^2\, (1 - cos(\theta)) \tag{13}$$

where θ is the central angle, and A is the coverage area approximated as a spherical cap shape.

Afterwards, for MIMO implementation considering Figure 7, the radii of beamforming loops can be approximately determined from the evaluated LEO satellite coverage area as in Equation (14).

$$A \approx (2R_B + (M-1) \times 1.5R_B)^2 \tag{14}$$

where A is the coverage area, R_B is the beam radius, and M is the squared size of MIMO ($M \times M$).

V. SIMULATION EXPERIMENTS

Three use case scenarios were simulated: 1) stationary user terminal, 2) user terminal in slow uniform linear motion, 3) user terminal moving through a pre-defined a route. For each use case, several simulations experiments were performed in order to evaluate the accuracy of the positioning method and algorithms when using realistic future satellite mega-constellations with MIMO capabilities. Each experiment consisted of several simulation runs with changing parameters depending on the objective of the experiment. A simulation run always consisted of 1,200 time steps with a 1-second resolution. The rotation angles of the beam footprints were randomized for each simulation run, but kept constant during that run.

Each simulation run generated a time series of 1,200 seconds with the following data fields: true position in (E, N), estimated position by ALG. A in (E, N), estimated position by ALG. B in (E, N), positioning error, number of detected beams. The parameters of the satellite constellations (number of satellites, number of beams per satellite, the radii of the beams, and the spacial separation of the beams) are given in Table II. The adjacent beams centers are separated by $2 \times R_{\text{beam}}$ for all constellations, satellites, and beams.

A. Variation of error metrics

The objective of the first experiment is to evaluate the confidence intervals of the error metrics. It is done by measuring the standard deviation of the error metrics while varying the location of the user terminal. To be precise we measure here the sensitivity of the positioning error to the location of the user terminal. Because the simulation model is heavy to compute, the confidence intervals are evaluated separately for one set of simulation parameters, in contrast to repeating each experiment several times to obtain their standard deviation estimates individually.

The procedure is a follows: 1) Set the location of the UT as well as the origin of the ENU coordinate system to (latitude, longitude) = (37.773972, -122.431297), i.e., in San Francisco, California. 2) Select and combine the first three mega-constellations (see Table II for the constellation parameters). 3) Run the simulation (i.e., 1,200 time steps) for both ALGs A and B. and calculate the error metrics. 4) Move the UT by 0.1 degrees, i.e., about 11 km, to North. 5) Repeat 25 times steps 3 and 4 . 6) Calculate the standard deviations of MAE, RMSE, and maximum error for ALGs A and B.

B. Use case scenario 1: stationary user terminal

When the user terminal does not move, it is possible to collect samples from the probability distribution of the true position. As LEO satellites move fast, the beam footprint pattern changes rapidly. Therefore, sampling positions with a 1 Hz rate is expected to give a time series without auto-correlation. If the positioning estimates are unbiased and uncorrelated, the mean value of the samples will converge towards the true position. This will be investigated experimentally using convergence time spans from 1 to 30 seconds.

The procedure is as follows: 1) Set the location of the UT as well as the origin of the ENU coordinate system to (latitude, longitude) = (37.773972, -122.431297), i.e., in San Francisco, California. 2) Select the first mega constellation. 3) Run the simulation for ALGs A and B. 4) Filter the time series of the estimated positions by unweighted sliding average filters of window lengths w = 1, 2, ..., 30, and calculate the error metrics of the filtered time series. 5) Select the next mega-constellation and combine it with the previous ones. 6) Repeat steps 3 to 5 until no more mega-constellations are available.

C. Use case scenario 2: slow uniform linear motion

In scenario 2, the user terminal moves with a constant speed of 1 m/s towards North-East. The initial position is at (latitude, longitude) = (37.773972, -122.431297), i.e., in San Francisco, California. This scenario corresponds, e.g., to a person walking or an autonomous vehicle driving slowly along a straight street. As the movement is easy to predict, it is presumed that the post-processing methods converge effectively towards the correct location.

The procedure is similar to scenario 1, except that the location of the user terminal is not fixed but a time series of 1,200 values and it is not meaningful to apply a sliding average filter to the time series of the estimated positions.

The procedure is as follows: 1) Define the location of the UT as a time series: initial location at (latitude, longitude) = (37.773972, -122.431297) and movement of 1 m/s to North-East. Set the origin of the ENU coordinate system to the initial UT location. 2) Select the first mega constellation. 3) Run the simulation for ALGs A and B. 4) Apply post-processing methods (see Section III-C) to the time series of the estimated positions, and calculate the error metrics of the original and post-processed time series. 5) Select the next mega-constellation and combine it with the previous ones. 6) Repeat steps 3 to 5 until no more mega-constellations are available.

D. Use case scenario 3: realistic nonlinear motion

In scenario 3, the user terminal moves along the predefined route shown in Figure 22, which is located in San Francisco, California, as all the other experiments for good comparability. The data is from Google GNSS competition 2022 [23]. For this dataset we also have IMU data that can be used for sensor fusion tests. Scenario 3 is used to evaluate our positioning method in a use case of realistic nonlinear movement, including periods of acceleration, deceleration, change of direction, as well as immobility.

The procedure is as follows: 1) Define the location of the UT as a time series using the every second sample of the first 2,400 samples, i.e. first 1,200 samples of the Google GNSS competition 2022 data. Set the origin of the ENU coordinate system to the initial UT location with $U = 0$. 2) Select the first mega constellation. 3) Run the simulation for ALGs A and B. 4) Apply post-processing methods (see Section III-C) to the time series of the estimated positions, and calculate the error metrics of the original and post-processed time series. 5) Select the next mega-constellation and combine it with the previous ones. 6) Repeat steps 3 to 5 until all mega-constellations are used.

E. Use case scenario 4: real nonlinear motion with mMIMO

This scenario was the repetition and reproduction of Scenario 3 but with mMIMO elements equipped in LEO satellite constellations. In which, the same LEO constellation sizes were used (i.e. 13 constellations with the defined number of satellites per constellation in Table II), however, the number of beams per satellite and the radii of the beams were changed to mMIMO beam configurations.

To this aim, several denominations of mMIMO-equipped LEO satellite constellations were used, namely Scenarios: 4a, 4b, 4c, 4d, and 4e. Such sub-scenario configurations were setup to study and verify the feasibility of mMIMO beamforming for this positioning method, as demonstrated in Tables III, IV, V, VI, and VII.

a) 8 Constellations with least mMIMO:

Scenario 4a was meant to test the least possible resources of LEO satellites and MIMO antennas, that is, the minimum requirements for the positioning method to function, known by conducting several trials and errors. Consequently, the size of LEO satellite constellations was kept at 8, which means that the total number of LEO satellites in Scenario 4a was the summation of all LEO satellites found in constellations 1–8 (i.e. a total of 52,164 satellites).

As discussed in [14], the least possible mMIMO configuration was known to contain 1,024 antenna elements, i.e. 32×32. Hence, the mMIMO beam configuration of Scenario 4a was ranged from 32×32 to 46×46 in an ascending order, by incrementing with a factor of 2 in each iteration. As for the beam radii, they were approximately calculated from Equations (12), (13), and (14), as shown in Table III.

TABLE III
LEO SATELLITE CONFIGURATIONS OF SCENARIO 4A

Const.	Sats.	Beams/sat.	R_{beam}
1	3000	32×32	40 km
2	4050	34×34	38 km
3	5040	36×36	36 km
4	6048	38×38	34 km
5	7020	40×40	32 km
6	7992	42×42	30 km
7	9012	44×44	28 km
8	10002	46×46	26 km

b) 8 Constellations with maximum mMIMO:

In Scenario 4b, the same constellation size of Scenario 4a was used again but with the maximum possible mMIMO antennas configuration of 64×64. It is the size that can be accommodated onboard a small-sized LEO satellite, also it was the size that fitted the processing requirements of the currently used simulator. Then, the beam radii were evaluated as shown in Table IV.

c) 9 Constellations with least mMIMO:

Scenario 4c was designed to test the effect of incrementing the LEO constellation size into 9 constellations, which accommodated a total amount of 63,216 LEO satellites. The mMIMO beam configuration followed the same pattern of Scenario 4a,

TABLE IV
LEO SATELLITE CONFIGURATIONS OF SCENARIO 4B

Const.	Sats.	Beams/sat.	R_{beam}
1	3000	64×64	20 km
2	4050	64×64	19 km
3	5040	64×64	18 km
4	6048	64×64	17 km
5	7020	64×64	16 km
6	7992	64×64	15 km
7	9012	64×64	14 km
8	10002	64×64	13 km

which started from 32×32 and so forth in an ascending order. Hence the beam radii of this scenario were given in Table V.

TABLE V
LEO SATELLITE CONFIGURATIONS OF SCENARIO 4C

Const.	Sats.	Beams/sat.	R_{beam}
1	3000	32×32	40 km
2	4050	34×34	38 km
3	5040	36×36	36 km
4	6048	38×38	34 km
5	7020	40×46	32 km
6	7992	42×42	30 km
7	9012	44×44	28 km
8	10002	46×46	26 km
9	11052	48×48	24 km

d) 11 Constellations with maximum mMIMO:

Scenario 4d employed 11 constellations, which accommodated a total amount of 88,320 LEO satellites, and configured with the maximum size of mMIMO beamforming, 64×64. The beam radii were evaluated and presented in Table VI.

TABLE VI
LEO SATELLITE CONFIGURATIONS OF SCENARIO 4D

Const.	Sats.	Beams/sat.	R_{beam}
1	3000	64×64	20 km
2	4050	64×64	19 km
3	5040	64×64	18 km
4	6048	64×64	17 km
5	7020	64×64	16 km
6	7992	64×64	15 km
7	9012	64×64	14 km
8	10002	64×64	13 km
9	11052	64×64	12 km
10	12072	64×64	11 km
11	13032	64×64	10 km

e) 13 Constellations with maximum mMIMO:

Scenario 4e was developed to utilize the maximum available resources of LEO satellite constellations and mMIMO beamforming sizes. In which, the 13 constellations were used to provide 64×64 beams from each of the 117,408 LEO satellites. Hence, the beam radii were computed as given in Table VII.

VI. RESULTS

In this section we present and evaluate the output results of all three scenarios: the stationary position, the uniform linear motion, and the real vehicle drive test.

TABLE VII
LEO SATELLITE CONFIGURATIONS OF SCENARIO 4E

Const.	Sats.	Beams/sat.	R_{beam}
1	3000	64×64	20 km
2	4050	64×64	19 km
3	5040	64×64	18 km
4	6048	64×64	17 km
5	7020	64×64	16 km
6	7992	64×64	15 km
7	9012	64×64	14 km
8	10002	64×64	13 km
9	11052	64×64	12 km
10	12072	64×64	11 km
11	13032	64×64	10 km
12	14004	64×64	9 km
13	15084	64×64	8 km

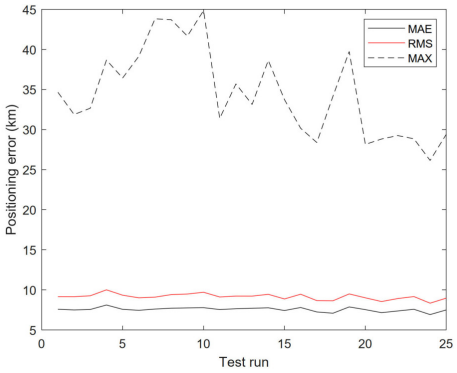

Fig. 8. Error metrics in 25 locations for ALG. B. Each UT location is about 11 km from the previous one.

A. Variation of error metrics

Figure 8 shows the variation of MAE, RMSE, and maximum error during 25 test runs for ALG. B when using the first three mega-constellations. Table VIII gives the sample means and standard deviations of error metrics with three and five mega-constellations, for ALGs A and B. Table IX gives the respective relative standard deviations in per cents. Standard deviations estimate the sensitivity of the error metrics with respect to the UT location. They are used to estimate the error margins of the results. It can be concluded that the relative standard deviation of MAE and RMSE is about 3-4% and the relative standard deviation of the maximum error is about 10-16%.

B. Use case scenario 1: stationary user terminal

Figures 9 and 10 show raw time series of positioning errors (for ALGs A and B) and the number of detected beams (identical for ALGs A and B), respectively. These demonstrate the amount of variation when the satellites move during a time span of 20 minutes.

Figure 11 shows how the 60 first samples of the time series of the estimated positions are scattered around the UT. It can also be seen that the two-dimensional mean values (CoG,

TABLE VIII
VARIATION OF ERROR METRICS: SAMPLE MEAN ± STANDARD DEVIATION FOR MAE, RMSE AND MAXIMUM ERROR (MAX) IN KM.

Alg.	Const.	MAE	RMSE	MAX
A	3	14.0 ± 0.52	16.8 ± 0.63	55.65 ± 5.70
A	5	4.71 ± 0.14	5.80 ± 0.18	23.67 ± 3.10
B	3	7.55 ± 0.26	9.15 ± 0.37	34.52 ± 5.49
B	5	2.38 ± 0.08	2.91 ± 0.10	12.32 ± 1.86

TABLE IX
RELATIVE STANDARD DEVIATION OF ERROR METRICS.

Alg.	Const.	MAE	RMSE	MAX
A	3	3.71%	3.74%	10.2%
A	5	2.99%	3.15%	13.1%
B	3	3.43%	4.06%	15.9%
B	5	3.23%	3.40%	15.1%

center of gravity) of the estimated positions are close to the true position of the UT, which indicates that ALGs A and B give unbiased position estimates. Therefore, it is possible to use several samples and averaging to obtain more accurate position estimates, in case of a stationary UT.

Figures 12 and 13 show how the RMS positioning error decreases when increasing the length of the sliding averaging filter when using 3 and 13 mega-constellations, respectively. Based on the central limit theorem and the presumption of independent and identically distributed position estimates, we further assume that the reduction of the RMS error is inversely proportional to the square-root of the window length:

$$\mathrm{RMSE} \propto \frac{1}{\sqrt{w}}$$

where w = window length of sliding average filter.

To test this hypothesis we fit the inverse square-root curve to the data with the least squares method. The visual examination of Figures 12 and 13 reveals that the inverse square-root law holds rather accurately when the number of satellites is very large. Thus, the law is applicable when extrapolating positioning errors for longer convergence periods. However, the fitted curve underestimates the reduction of error when the constellation size is not large, as seen in Figure 12.

The results show that ALG. B gives more accurate position estimates than ALG. A. However, this holds only for the average accuracy. Figure 14 shows the difference between the accuracy of ALGs A and B as a time series, in case of 13 constellations. It demonstrates that ALG. A actually gives quite often better position estimates. The probability that ALG. A gives more accurate estimates than ALG. A is 24.2% in this case. The mean difference of RMS errors between ALGs A and B can be seen, e.g., in 13. In the future, it should be studied if it is possible to utilize the estimates of both algorithms, together with other information, to obtain more accurate position estimates.

The more beams there are congested near the UT, the more accurate positioning is, when keeping other things, such as the size of the beams, unchanged. The number of beams that an UT detects on average (on an arbitrary place on Earth) can be calculated theoretically. It is the ratio of the total area of all beam footprints of available constellations with the area of

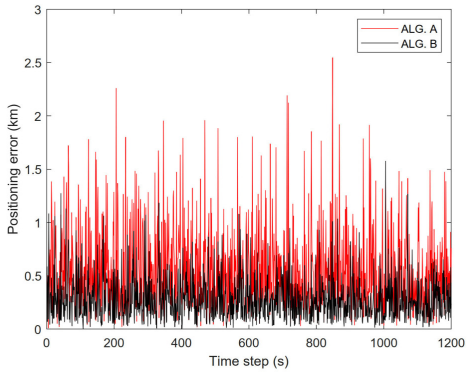

Fig. 9. Positioning error vs. time with 13 constellations.

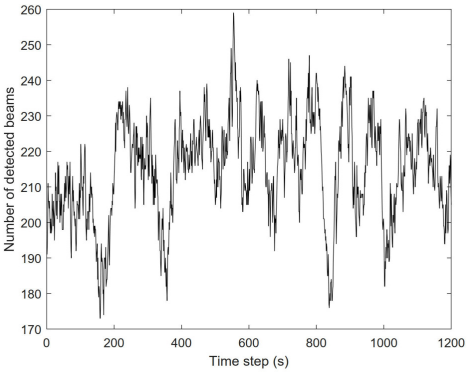

Fig. 10. Number of detected beams vs. time with 13 constellations.

Earth (510,100,000 km^2). Figure 15 compares the theoretical and simulated values of the number of detected beams. It can be seen that the average value of simulation is well aligned with the theoretical value. It also shows how the number of detected beams increases when adding new constellations to the simulation, according to our mega-constellation model given in Section V.

Finally, Figures 16 and 17 show position error vs. number of constellations when using single measurements and averaging over 30 seconds, respectively. With all 13 constellations that have totally 117,408 satellites and about 5,908,000 beams, when UT detects on average 215 beams, MAE is about 0.29 km, RMSE is about 0.35 km, and maximum error is about 1.6 km. When averaging 30 measurements, MAE = 0.057 km, RMSE = 0.064 km, and maximum error = 0.152 km.

C. Use case scenario 2: slow uniform linear motion

The results of scenario 2 as found in Figure 18 and Table X show very fluctuating raw position estimates in comparison to the straight imaginary route that resembles a person walking

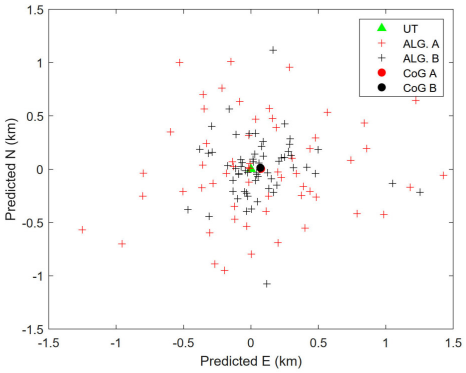

Fig. 11. Scattering of the position estimates (N=60) when having 13 constellations.

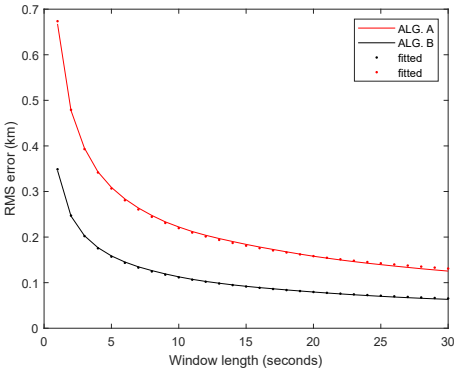

Fig. 13. Convergence of RMS error when having 13 constellations.

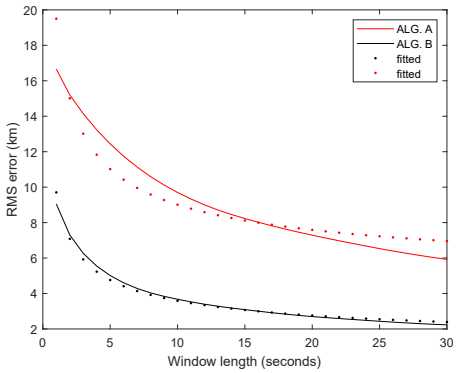

Fig. 12. Convergence of RMS error when having 3 constellations.

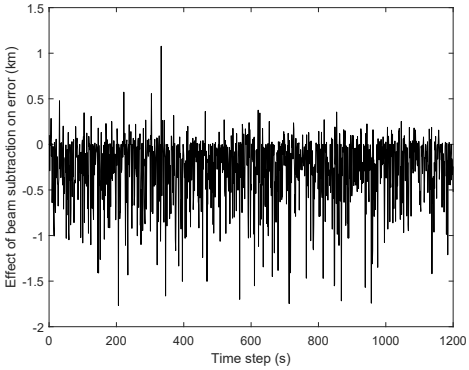

Fig. 14. Difference of position errors between ALGs A and B when having 13 mega-constellations. ALG. B gives more accurate estimates on average.

in a uniform speed of 1 m/s. Fortunately, the EKF filtering has reduced the positioning error by approximately 80%, and the RTS smoother has further eliminated around 73% of the EKF output error to achieve an overall accuracy of 16.69 meters as MAE. The 95-percentile value of 993 meters is large, but it is mostly due to the first output samples of the filters. According to Figures 18 and 19, the position estimations gradually converge towards the true location of the UT. It is unclear why the EKF outputs fluctuate heavily. Notably, during our investigations we found that a simple sliding average filter (window length, $w = 100$) outperforms EKF in smoothing the outputs of ALG. B estimations. Thus, it signifies the potential to improve the accuracy in the future.

D. Use case scenario 3: realistic nonlinear motion

The results of scenario 3 are very promising and satisfactory to a large extent, as shown in Figures 20, 21, 22, 23, 24, and Table XI.

Primarily, it is clear from trajectory Figures 20 and 22 that the combined EKF-RTS fusion-smoother back-to-back algorithm (using ALG. B) is the most accurate method that is closely following with the ground truth and GNSS with minimal errors. Hence, the applied elementary positioning algorithms after receiving beam IDs (i.e. ALG. A and ALG. B) are not sufficient for conducting a reliable satellite-based positioning on their own, rather, they constantly require a set of post-processing algorithm, similar to every other positioning technologies e.g. in GNSS.

The numerical positioning error values in Table XI and

TABLE X
ERROR EVALUATION OF LINEAR MOTION (SCENARIO 2).

Method	Const.	MAE [m]	RMSE [m]	p95% [m]
ALG. A	13	508.49	685.91	1179.1
ALG. B	13	241.61	334.28	588.10
EKF	13	47.25	75.02	982.20
EKF-RTS	13	**13.69**	**15.24**	**993.86**

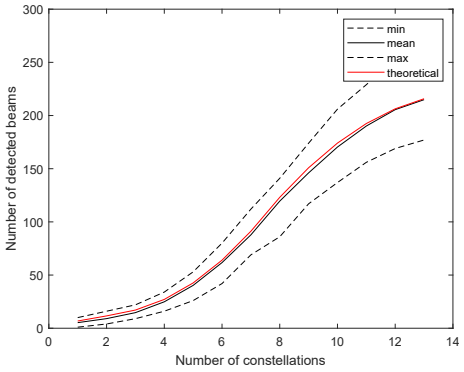

Fig. 15. Number of detected beams vs. number of constellations. Comparison to the theoretical value.

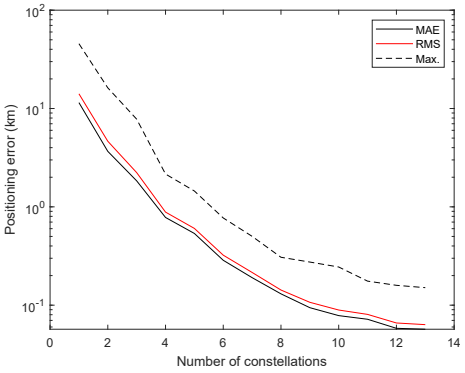

Fig. 17. Positioning error (log scale) vs. number of constellations for ALG. B. Metrics based on filtering with $w = 13$.

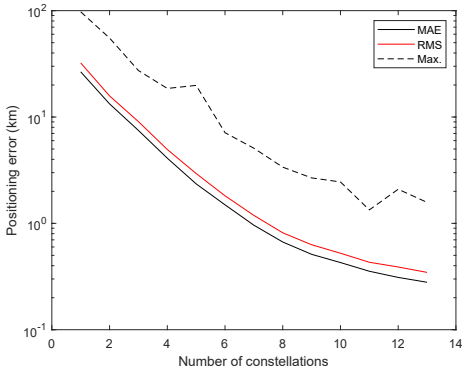

Fig. 16. Positioning error (log scale) vs. number of constellations for ALG. B. Metrics based on single measurements.

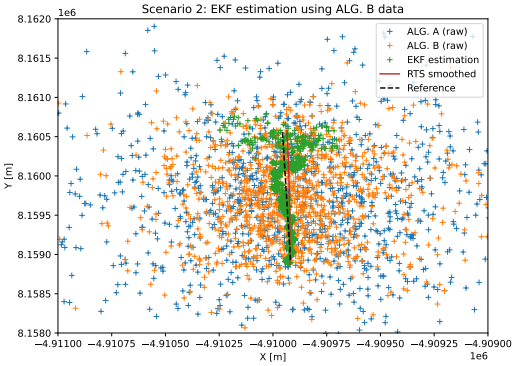

Fig. 18. Scenario 2: EKF and RTS positioning estimations of a uniform linear motion using ALG. B.

the graphical error plots illustrated in Figures 21 and 23 are confirming the same finding; that the EKF-RTS method outperforms all other algorithms used in this simulation. The CDF curves in Figure 24 imply that the final LEO/IMU positioning estimations are very close to the performance of GNSS in terms of accuracy and precision. However, Figure 23 shows that the best performance of LEO/IMU that can bring it closer to GNSS performance is only achievable using the maximum possible numbers of satellites and constellations, which are already 13 constellations carrying more than 100,000 satellites.

In fact, the simulation of scenario 3 confirms the early hypothesis in this study; that is the necessity of receiving the maximum available interconnected LEO satellite beams in order to improve the final positioning estimations. The number of received beams in scenario 3 fluctuated between 172 and 247 beams, with average number of detected beams = 214.

E. Use case scenario 4: realistic nonlinear motion with mMIMO

Tables XII and XIII show the numerical error results of Scenario 4 (a–e). Figures 25, 26, and 27 demonstrate the error behaviour of all Scenario 4 denominations in addition to the rendered route test of Scenario 4E and its conjugate Scenario 4E*.

In Table XII, the positioning errors of all sub-scenarios were investigated using MAE, RMSE and p95% metrics to assess the fusion based methods of LEO/IMU EKF-RTS. The best result was found to be Scenario 4E.

While in Table XIII, the same metrics were used to assess utilizing the raw unprocessed non-fused ALG. B measurements. However in the conjugate version of Scenario 4E (i.e. Scenario 4E*), a simple moving average filter was used to filter the raw ALG. B and show its effect. The best result was found to be Scenario 4E*.

From Figures 26 and 27, clearer views of assessment can be found, graphically. Where the fusion-based method of

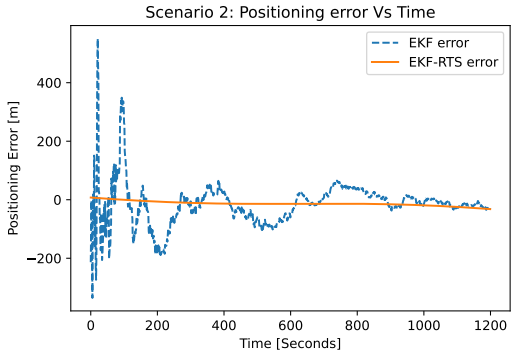

Fig. 19. EKF and RTS error convergence over time in scenario 2.

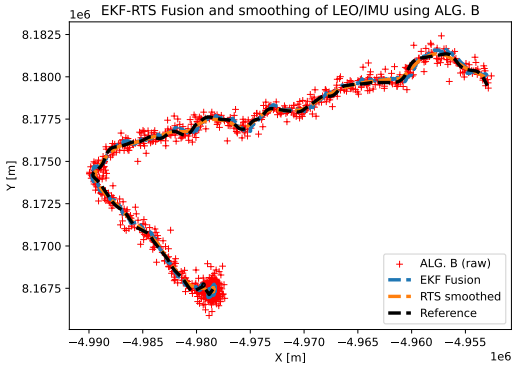

Fig. 20. LEO/IMU fusion using EKF and EKF-RTS on ALG. B data in x-y coordinates.

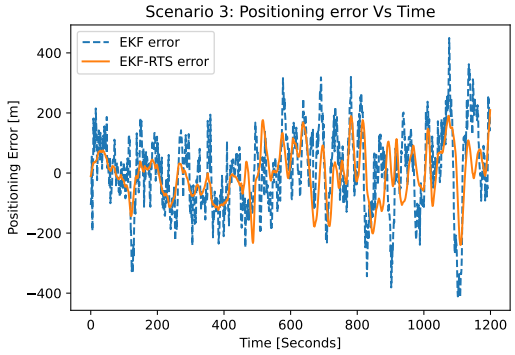

Fig. 21. EKF and RTS error convergence over time in scenario 3.

TABLE XI
ERROR EVALUATION OF LEO/IMU METHODS VS. GNSS

Method	Const.	MAE [m]	RMSE [m]	p95% [m]
ALG. A	13	498.16	683.49	1179.5
ALG. B	13	231.59	317.95	520.06
LEO/IMU EKF	13	104.80	132.00	203.35
LEO/IMU EKF-RTS	13	**66.31**	**83.98**	**142.39**
GNSS only	N/A	**26.63**	**36.42**	**56.60**

Scenario 4E already closely matched the accuracy of the raw measurements of Scenario 4E*, and both scenarios outperformed GNSS accuracy.

TABLE XII
ERROR EVALUATION OF MMIMO IMU FUSION VS. GNSS IN SCENARIO 4

Method	Const.	MIMO	MAE [m]	RMSE [m]	p95% [m]
a) LEO/IMU EKF-RTS	8	$32^2 \rightarrow 46^2$	22.63	29.70	50.84
b) LEO/IMU EKF-RTS	8	64×64	17.65	23.05	36.47
c) LEO/IMU EKF-RTS	9	$32^2 \rightarrow 48^2$	16.86	22.41	32.78
d) LEO/IMU EKF-RTS	11	64×64	11.84	15.46	26.60
e) **LEO/IMU EKF-RTS**	**13**	$\mathbf{64 \times 64}$	**9.90**	**12.71**	**20.97**
GNSS only	N/A	N/A	**26.63**	**36.42**	**56.60**

TABLE XIII
ERROR EVALUATION OF RAW MMIMO DATA VS. GNSS IN SCENARIO 4

Method	Const.	MIMO	MAE [m]	RMSE [m]	p95% [m]
a) Raw ALG. B data	8	$32^2 \rightarrow 46^2$	45.84	62.56	101.98
b) Raw ALG. B data	8	64×64	37.17	51.50	82.33
c) Raw ALG. B data	9	$32^2 \rightarrow 48^2$	36.05	48.97	76.28
d) Raw ALG. B data	11	64×64	23.59	32.45	53.20
e) Raw ALG. B data	**13**	$\mathbf{64 \times 64}$	**19.27**	**25.74**	**44.32**
e*) Smoothed ALG. B	**13**	$\mathbf{64 \times 64}$	**9.15**	**11.94**	**19.07**
GNSS only	N/A	N/A	**26.63**	**36.42**	**56.60**

VII. DISCUSSION

The beam ID-based method is based on mega-constellations of LEO satellites with mMIMO capabilities. The accuracy of the single measurements (or raw ALGs. A or B) is in the order of kilometers when having a few thousands of satellites. When the number of satellites exceeds a hundred thousand, positioning errors of a few hundreds of meters can be achieved. Positioning with such errors can be used as back-up method, e.g., in aviation and seafaring. However, our experiments showed that by the integration of several measurements or by the fusion of the raw measurements with IMU sensors, the positioning accuracy can be improved significantly. MAE as small as 14 meters was recorded for a slow uniform linear motion scenario 2 when using 13 mega-constellations. With advanced post-processing algorithms, an accuracy closer to GNSS systems is possible. In scenario 3, with a realistic nonlinear motion, the RMSEs for LEO/IMU EKF-RTS and for GNSS were approximately 84 m and 36 m, respectively, and MAEs were approximately 66 m and 27 m, respectively. Meaning that the beam ID-based positioning method is a promising candidate even for nonlinear dynamic motion of vehicles.

Finally, the results of Scenario 4 were quite interesting and promising since all its denominations were performing better than GNSS in the event of implementing LEO/IMU fusion. The effect of introducing mMIMO can be seen through the error shift from Figure 24 to Figure 25, where the enhancement

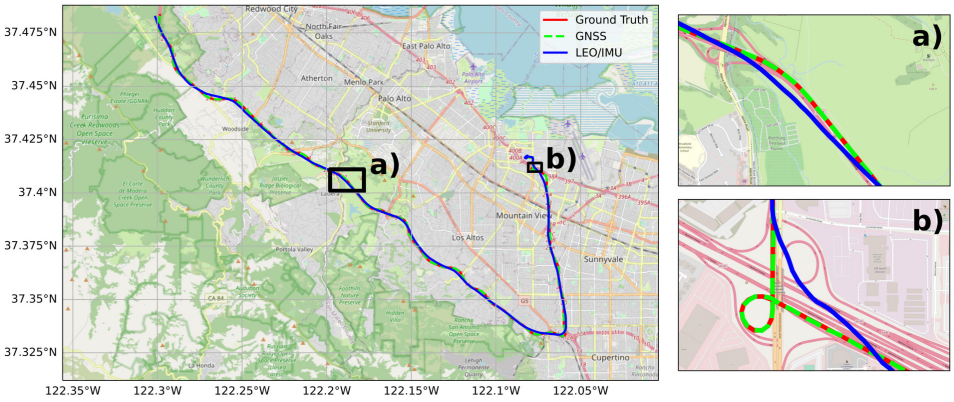

Fig. 22. Map trajectory of smoothed LEO/IMU, GNSS, and ground truth in California, USA. The dataset is a courtesy of Google decimeter challenge 2022.

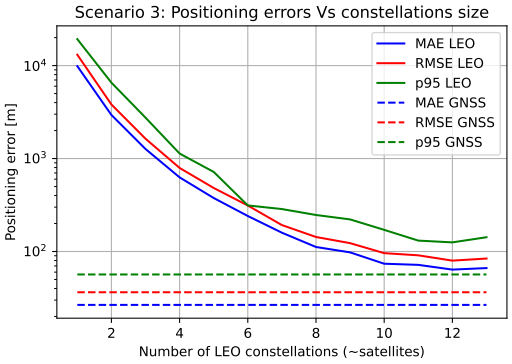

Fig. 23. Positioning errors (log scale) of LEO/IMU EKF-RTS and GNSS vs. number of LEO satellite constellations used.

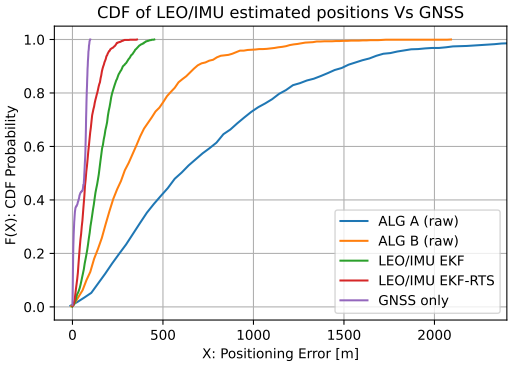

Fig. 24. Cumulative distribution functions of LEO/IMU methods and GNSS.

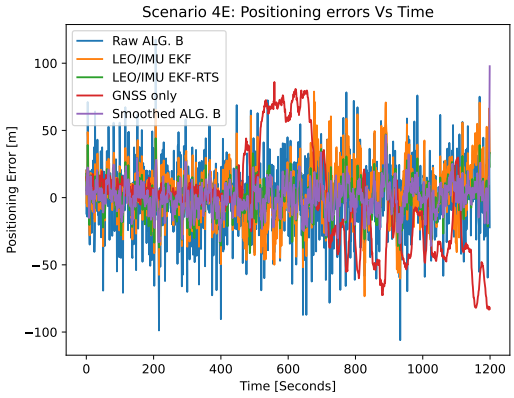

Fig. 25. Positioning errors of mMIMO methods Vs. Time

in accuracy was significantly proven. By increasing the size of LEO satellite constellations to be mega and the size of MIMO beamforming loops to be massive, the positioning accuracy can be significantly enhanced to a precise accurate level of performance. The fusion-based positioning schemes are still effective with LEO satellites, however, even in the event of no multisensor fusion integration, the proposed method can still perform quite well with raw measurements.

There are possibilities to further improve the accuracy of the beam ID-based positioning method. Presuming that the signal strength of the beam footprints decreases from the center towards the border in a predictable way it could be measured and used as an additional weighed input. Similarly, other signal quality metrics could be utilized. In the post-processing phase, the number of detected satellites could be used to weigh the raw measurements. This is based on the presumption that the more satellites are detected, the more accurate the position estimate is on average.

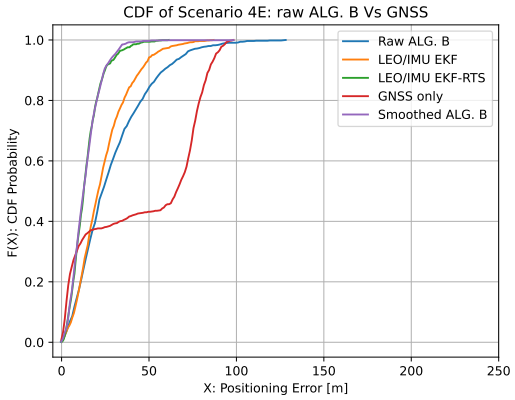

Fig. 26. Cumulative distribution functions of mMIMO methods Vs. GNSS

The beam ID-based position method has several advantages for sustainability. First, it uses measurements that do not require precise timing or accurate measurements of the signal strengths. Therefore, the required technology at the user segment is expected to be affordable, which promotes social sustainability. Second, the method does not require dedicated satellites to work. This should reduce costs further and save both energy and natural resources. Third, due to the high signal strengths of the LEO satellites and the simple binary measurements (beam is either detected or not) the method is expected to be tolerant other interference and jamming, especially when fused with the IMU sensor that itself is tolerant to interference as a passive sensor. Hence, the method could guarantee uninterrupted positioning services also in conflict areas. This has several consequences to sustainable development through the uninterrupted operation of numerous autonomous systems that will promote sustainable development in the future.

VIII. Conclusion

Massive MIMO antenna arrays are expected to equip LEO satellites due to their numerous advantages from the perspectives of telecommunication and positioning technologies. In this article, we presented our novel beam ID-based positioning method that uses the identifications of mMIMO beamforming loops that are incident from LEO satellite constellations. Through known geolocations of the beam footprint patterns and light-weight algorithmic treatment, the location of the user terminal on Earth's surface can be determined, even by receiving beam(s) from one LEO satellite only in case of extreme conditions. We also developed an algorithm that utilizes the absent undetected beams for improved accuracy. The quality of positioning is substantially improved by increasing the number of LEO satellites in the skies, which in turn increases the amount of received beams. A detailed simulation environment was designed to comprise realistic LEO satellite constellation data and real-world navigation datasets. The conducted simulations showed a satisfactory level of performance for the fusion scheme that integrated LEO satellites data and IMU measurements. With the help of EKF-RTS filters, the LEO/IMU fusion technique has achieved the best positioning estimations that came closer to the performance of GNSS in terms of accuracy and precision. The MAE of the LEO/IMU EKF-RTS method is evaluated at 9.15 meters, while the 95-percentile error in the long term was 19.07 meters. In the simulation, owing to the demanding computing power needs, we capped the number of MIMO beamforming loops per a satellite at 8×8 for Scenarios 1–3. Nevertheless, we explored larger antenna configurations in Scenario 4 such as 64×64, yielded more positioning accuracy as MAE = 9.15 meters and p95% = 19.07 meters, which is technically feasible in the next generation of LEO satellites. As a future work, more refinements and model sophistication can be added to the simulation environment to improve the performance and integrity of the method. In addition, more research on positioning and post-processing algorithms is needed in order to reduce the number of LEO satellites required for conducting accurate UT positioning. In fact, the method has many potential benefits as for sustainability and commercialization, those aspects should be addressed, verified and quantified in future studies.

Acknowledgment

This work was supported by the Jane and Aatos Erkko Foundation and by the Teknologiateollisuus 100-year Foundation (INCUBATE project). The proposed ideas within this article are currently under the process of IPR patenting (Finnish patent application number: 20235545).

References

[1] F. S. Prol, R. M. Ferre, Z. Saleem, P. Välisuo, C. Pinell, E. S. Lohan, M. Elsanhoury, M. Elmusrati, S. Islam, K. Çelikbilek, K. Selvan, J. Yliaho, K. Rutledge, A. Ojala, L. Ferranti, J. Praks, M. Z. H. Bhuiyan, S. Kaasalainen, and H. Kuusniemi, "Position, navigation, and timing (pnt) through low earth orbit (leo) satellites: A survey on current status, challenges, and opportunities," *IEEE Access*, vol. 10, pp. 83971–84002, 2022.

[2] H. Ge, B. Li, S. Jia, L. Nie, T. Wu, Z. Yang, J. Shang, Y. Zheng, and M. Ge, "LEO enhanced global navigation satellite system (LeGNSS): progress, opportunities, and challenges," *Geo-spatial Information Science*, vol. 25, no. 1, pp. 1–13, 2022.

[3] M. Li, T. Xu, M. Guan, F. Gao, and N. Jiang, "LEO-constellation-augmented multi-GNSS real-time PPP for rapid re-convergence in harsh environments," *GPS Solutions*, vol. 26, p. 29, 2022.

[4] J. Rainbow, "Lockheed invests in Xona's GPS-alternative constellation." https://spacenews.com/lockheed-invests-in-xonas-gps-alternative-constellation/, 2022. [Online; accessed 15-May-2023].

[5] R. Knight, "ESA Outlines Plans for Demo of LEO PNT Satellites As Part of FutureNAV, Gives Other Updates." https://insidegnss.com/, 2022. [Online; accessed 15-May-2023].

[6] L. Chen, F. Lv, Q. Yang, T. Xiong, Y. Liu, Y. Yang, H. Pan, S. Wang, M. Liu, R. He, D. Zheng, L. Zhang, and Y. Jin, "Performance evaluation of centispace navigation augmentation experiment satellites," *Sensors*, vol. 23, no. 12, 2023.

[7] "Project indoor navigation from cubesat technology (INCUBATE)." https://www.incubateproject.org/. [Online; accessed 15-May-2023].

[8] J. J. Khalife and Z. M. Kassas, "Receiver design for doppler positioning with leo satellites," in *ICASSP 2019 - 2019 IEEE International Conference on Acoustics, Speech and Signal Processing (ICASSP)*, pp. 5506–5510, 2019.

[9] F. Farhangian and R. Landry, "Multi-constellation software-defined receiver for doppler positioning with leo satellites," *Sensors*, vol. 20, no. 20, 2020.

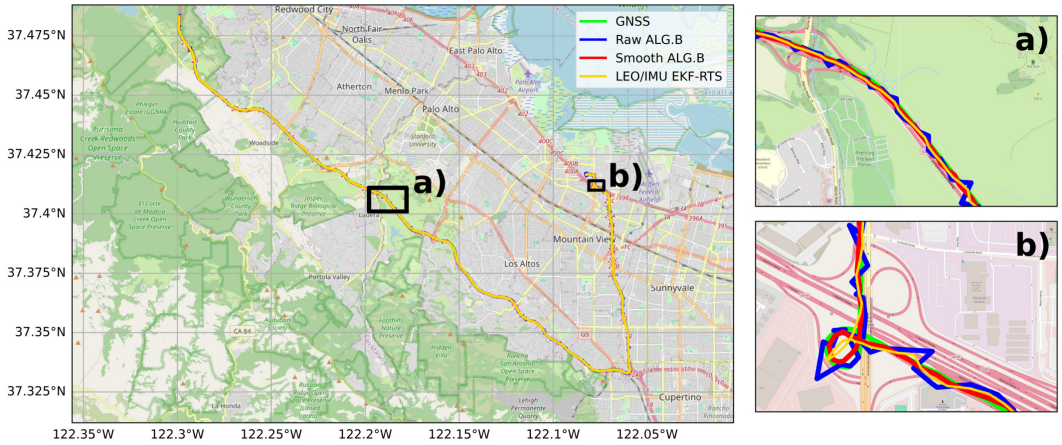

Fig. 27. Map trajectory of Scenario 4E: mMIMO data, and GNSS data in California, USA

[10] Z. Tan, H. Qin, L. Cong, and C. Zhao, "Positioning using iridium satellite signals of opportunity in weak signal environment," *Electronics*, vol. 9, no. 1, 2020.

[11] M. L. Psiaki, "Navigation using carrier Doppler shift from a LEO constellation: TRANSIT on steroids," *Navigation*, vol. 68, no. 3, pp. 621–641, 2021.

[12] F. S. Prol, S. Kaasalainen, E. S. Lohan, M. Z. H. Bhuiyan, J. Praks, and H. Kuusniemi, "Simulations using leo-pnt systems: A brief survey," in *2023 IEEE/ION Position, Location and Navigation Symposium (PLANS)*, pp. 381–387, 2023.

[13] M. Elsanhoury, J. Koljonen, M. Elmusrati, and H. Kuusniemi, "A Novel Beam-Based Positioning Paradigm Via Opportunistic Signal of Future Massive MIMO LEO Satellite Constellations," *Techrxiv*, 2023.

[14] R. M. Ferre, E. S. Lohan, H. Kuusniemi, J. Praks, S. Kaasalainen, C. Pinell, and M. Elsanhoury, "Is leo-based positioning with mega-constellations the answer for future equal access localization?," *IEEE Communications Magazine*, vol. 60, no. 6, pp. 40–46, 2022.

[15] J. Palacios, N. Gonzalez-Prelcic, C. Mosquera, T. Shimizu, and C.-H. Wang, "A hybrid beamforming design for massive mimo leo satellite communications," *Front. Space Technol*, vol. 27, 2021.

[16] A. F. Molisch, V. V. Ratnam, S. Han, Z. Li, S. L. H. Nguyen, L. Li, and K. Haneda, "Hybrid beamforming for massive mimo: A survey," *IEEE Communications Magazine*, vol. 55, no. 9, pp. 134–141, 2017.

[17] O. E. Ayach, S. Rajagopal, S. Abu-Surra, Z. Pi, and R. W. Heath, "Spatially sparse precoding in millimeter wave mimo systems," *IEEE Transactions on Wireless Communications*, vol. 13, no. 3, pp. 1499–1513, 2014.

[18] J. Hartikainen, A. Solin, and S. Särkkä, *Optimal filtering with Kalman filters and smoothers - a Manual for Matlab toolbox EKF/UKF*. Aalto University, 2011.

[19] H. E. Rauch, F. Tung, and C. T. Striebel, "Maximum likelihood estimates of linear dynamic systems," *AIAA Journal*, vol. 3, no. 8, pp. 1445–1450, 1965.

[20] C. Pinell, F. Prol, M. Bhuiyan, and J. Praks, "Receiver architectures for positioning with low earth orbit satellite signals: a survey," *EURASIP J. Adv. Signal Process.*, vol. 60, p. 2023, 2023.

[21] J. Wertz, N. C. for Space Technology (U.S.), and N. R. L. (U.S.), *Mission Geometry: Orbit and Constellation Design and Management : Spacecraft Orbit and Attitude Systems*. Space technology library, Microcosm Press, 2001.

[22] J. W. Harris and H. Stöcker, *Handbook of Mathematics and Computational Science*. Springer New York, NY, 1998.

[23] A. Howard, A. Chow, B. Julian, D. Orendorff, M. Fu, M. Khider, and S. Dane, "Google smartphone decimeter challenge 2022," 2022.